

# Unquenched Charmonium and Beyond

Zi-Yue Bai<sup>1a,b,c,d</sup>, Dian-Yong Chen<sup>1e,b</sup>, Qi Huang<sup>1f,b</sup>, Xiang Liu<sup>1a,b,c,d,\*</sup>, Si-Qiang Luo<sup>1a,b,d</sup>, Jun-Zhang Wang<sup>1g,b</sup>

(Lanzhou Group)

<sup>a</sup>School of Physical Science and Technology, Lanzhou University, Lanzhou 730000, China

<sup>b</sup>Lanzhou Center for Theoretical Physics, Key Laboratory of Theoretical Physics of Gansu Province, Key Laboratory of Quantum Theory and Applications of MoE, Gansu Provincial Research Center for Basic Disciplines of Quantum Physics, Lanzhou University, Lanzhou 730000, China

<sup>c</sup>MoE Frontiers Science Center for Rare Isotopes, Lanzhou University, Lanzhou 730000, China

<sup>d</sup>Research Center for Hadron and CSR Physics, Lanzhou University & Institute of Modern Physics of CAS, Lanzhou 730000, China

<sup>e</sup>School of Physics, Southeast University, Nanjing 210094, China

<sup>f</sup>School of Physics and Technology, Nanjing Normal University, Nanjing 210023, China

<sup>g</sup>Department of Physics, Chongqing University, Chongqing 401331, China

---

## Abstract

The year 2024 marked the 50th anniversary of the discovery of the  $J/\psi$  particle, which unveiled the charm quark and the charmonium spectrum, instigating the "November Revolution" in particle physics. This discovery catalyzed the development of quenched potential models, most notably the Cornell model, which provided a foundational quantitative description of the hadronic spectrum. However, the landscape of hadron spectroscopy has been profoundly transformed since the turn of the 21st century with the observation of numerous charmonium-like states, such as  $X(3872)$ , which exhibit properties starkly at odds with quenched model predictions. These discrepancies, exemplified by the "X(3872) low-mass puzzle" and the "Y problem" associated with vector states like  $Y(4260)$ , underscore the critical limitations of the quenched approximation and signal the necessity for a new theoretical paradigm. This review synthesizes recent advances in hadronic spectroscopy, arguing that the unquenched picture, which incorporates coupled-channel effects such as hadronic loops, is essential for a unified description of these new states and associated anomalies. We demonstrate how unquenched effects provide compelling solutions to long-standing puzzles in charmonium decays (e.g., the " $\rho\pi$  puzzle" and anomalous dipion transitions), predict and explain the existence of exotic charged states like  $Z_c(3900)$  and  $Z_b(10610)$  via mechanisms such as Initial Single Pion Emission, and offer a framework for understanding interactions between charmonia and with nucleons. Furthermore, we emphasize the universality of unquenched effects, extending their application to bottomonium and light-flavor sectors. As experimental precision continues to improve, we advocate for the systematic development of unquenched hadronic spectroscopy, which heralds a new era of high-precision theoretical and experimental studies, moving decisively beyond the quenched approximation to achieve a more complete understanding of non-perturbative behavior of the strong interaction.

**Keywords:** Charmonium, Unquenched effect, Hadronic loop mechanism, Coupled-channel effect, Nonperturbative behavior of strong interaction, Bottomonium, Light flavor vector mesons

---

## Contents

<b>1</b>	<b>Introduction</b>	<b>3</b>
<b>2</b>	<b>Anomalous decay behaviors of charmonia and hadronic loop mechanism</b>	<b>6</b>
2.1	Phenomenology . . . . .	6

---

<sup>1</sup>These authors equally contribute to this work and are listed in alphabetical order.

\*Corresponding author

Email address: xiangliu@lzu.edu.cn (Xiang Liu)

2.1.1	$\rho\pi$ puzzle	6
2.1.2	Large non- $D\bar{D}$ decays of $\psi(3770)$	8
2.1.3	Anomalous transitions in high-lying heavy quarkonia	9
2.2	Hadronic loop mechanism	10
2.2.1	Decoding the $\rho\pi$ puzzle through the hadronic loop mechanism	11
2.2.2	Large non- $D\bar{D}$ decays of $\psi(3770)$	13
2.2.3	Anomalous transitions in high-lying heavy quarkonia	15
2.3	Other applications of hadronic loop mechanism	19
<b>3</b>	<b>Low-mass puzzle of <math>X(3872)</math> and the construction of <math>2P</math> charmonia</b>	<b>20</b>
3.1	Low-mass puzzle in new hadronic states	20
3.2	The role of coupled-channel effects in alleviating the $X(3872)$ low-mass puzzle	23
3.3	$X(3915)$ and $Z(3930)$ as $2P$ charmonium states	26
3.3.1	Initial research	26
3.3.2	Anomalous small mass gap between $X(3915)$ and $Z(3930)$	28
3.3.3	Anomalous large the branching ratio for the $X(3915) \rightarrow J/\psi\omega$ decay	30
3.3.4	Unexpected disappear of $X(3915)$ in $\gamma\gamma \rightarrow D\bar{D}$	31
3.3.5	The experimental measurement of $B \rightarrow KD\bar{D}$ from the LHCb Collaboration	33
<b>4</b>	<b><math>Y</math> Problem and its solution</b>	<b>34</b>
4.1	$Y(4260)$ and its evolving interpretations	35
4.1.1	Experimental timeline and key results	35
4.1.2	Resonant explanations and confronted difficulties	36
4.1.3	Non-resonant picture: concept and applications	37
4.2	From quenched to unquenched: the evolution of charmonium potential models	41
4.2.1	1978: The Cornell potential—establishing the quenched framework	41
4.2.2	1995: From lattice QCD to the screened potential—a step toward unquenching	41
4.2.3	2014: Mass gaps and a prediction—evidence for a narrow charmonium state near 4.2 GeV	43
4.3	2017: Precise data reveal more charmonium-like $Y$ structures—the $Y$ problem	46
4.4	Toward a unified theoretical framework for the $Y$ problem	52
4.4.1	Non-resonant interference revisited: killing $Y(4320)$ and $Y(4390)$ and confirming $Y(4220)$ as a genuine resonance	52
4.4.2	$Y(4220)$ as a scaling point to reconstruct $J/\psi$ family within the unquenched picture	53
4.4.3	The $4S$ - $3D$ mixing scheme in charmonium	56
4.4.4	The vector charmonium mass spectrum in the unquenched picture for the 4–4.5 GeV region	58
4.4.5	Are these $Y$ states around 4.6 GeV from $e^+e^-$ annihilation higher charmonia?	58
4.4.6	Accumulating experimental evidence	61
4.5	Coupled-channel analysis for key charmonium(-like) states	62
4.5.1	$S$ - $D$ mixing scheme induced by the coupled-channel mechanism	62
4.5.2	Coherent coupled-channel description of near-threshold structures: $\psi(3770)$ , $G(3900)$ , $R(3760)$ , $R(3780)$ , and $R(3810)$	66
<b>5</b>	<b>The initial single pion emission mechanism: explaining charged <math>Z_b</math> and predicting charmonium-like charged <math>Z_c/Z_{cs}</math></b>	<b>68</b>
5.1	Anomalous phenomena related to $\Upsilon(10860)$	69
5.1.1	Experimental observation of $\Upsilon(10860)$	69
5.1.2	Theoretical interpretations of $\Upsilon(10860)$ : bottomonium vs tetraquark	70
5.1.3	Puzzles in the dipion invariant mass distributions and $\cos\theta$ distributions.	71
5.1.4	Charged bottomoniumlike structures $Z_b(10610)$ and $Z_b(10650)$	73
5.1.5	Role of $Z_b(10610)$ and $Z_b(10650)$ in solving the puzzles of the process $\Upsilon(5S) \rightarrow \Upsilon(2S)\pi^+\pi^-$	74
5.2	Initial single pion emission mechanism	76
5.2.1	Charged $Z_b$ states and the proposal of the initial single pion emission mechanism	76

5.2.2	Prediction of charmonium-like charged $Z_c$ structure . . . . .	78
5.2.3	Experimental observations of the $Z_c$ structures . . . . .	80
5.2.4	Reproduce $Z_c(3900)$ in the $\pi^\pm J/\psi$ invariant mass spectra of $e^+e^- \rightarrow \pi^+\pi^- J/\psi$ at $\sqrt{s} = 4.260$ GeV . . . . .	82
5.2.5	Reproduce the enhancement structures in the $\pi^\pm\psi(3686)$ invariant mass spectra of $e^+e^- \rightarrow \pi^+\pi^-\psi(3686)$ . . . . .	83
5.3	Initial single chiral particle emission mechanism and the predicted $Z_{cS}$ structures . . . . .	86
5.3.1	Prediction of isoscalar partner of $Z_c$ . . . . .	87
5.3.2	Predictions of charged $Z_{cS}$ structures . . . . .	87
5.3.3	Experimental searches for $Z_{cS}$ structures . . . . .	88
<b>6</b>	<b>Interaction between hadrons involved in charmonia</b> . . . . .	<b>90</b>
6.1	Experimental observation of di- $J/\psi$ invariant mass spectrum from $pp$ collisions . . . . .	90
6.2	Theoretical status and challenges in identifying genuine multiquark states . . . . .	94
6.3	Employing scattering between charmonia to understand these observed enhancements in the di- $J/\psi$ invariant mass spectrum . . . . .	96
6.4	Exploration on microscopic mechanism of the interaction between charmonia . . . . .	100
6.5	Lattice QCD result of interactions involved in fully heavy hadrons . . . . .	105
<b>7</b>	<b>Extension to <math>\Upsilon</math> family and light flavor vector mesonic states</b> . . . . .	<b>108</b>
7.1	Universality of vector mesonic structures in $e^+e^-$ annihilation . . . . .	108
7.2	Higher bottomonia in the unquenched picture . . . . .	108
7.2.1	Higher bottomonium . . . . .	108
7.2.2	Anomalous hidden-bottom decay phenomena of several high-lying bottomonia . . . . .	112
7.2.3	A global description of the anomalous bottomonium decays via the hadronic loop mechanism . . . . .	113
7.2.4	A consistent assignment of $\Upsilon(10753)$ into the bottomonium family . . . . .	120
7.3	Construction of light-flavor vector mesons around the 2 GeV mass region . . . . .	126
7.3.1	Status of light-flavor meson spectroscopy . . . . .	126
7.3.2	The unquenched spectrum of light vector meson and their contribution in the cross sections of the $e^+e^-$ annihilations into open-strange channels . . . . .	127
7.3.3	Unified description of the cross sections for more relevant reaction processes within the support of the unquenched spectroscopy . . . . .	129
<b>8</b>	<b>Summary</b> . . . . .	<b>139</b>

## 1. Introduction

In the recently passed year of 2024, the academic community worldwide celebrated the 50th anniversary of the discovery of the  $J/\psi$  particle [1, 2]. This major breakthrough, hailed as the "November Revolution" of particle physics [3, 4], not only confirmed the existence of the charm quark—the fourth flavor quark proposed by the GIM mechanism [5] to suppress flavor-changing neutral currents (FCNCs)—but also revealed a new family of hadrons: charmonium. Over the decade following the discovery of the  $J/\psi$  particle, most of the charmonium states listed in the Particle Data Group (PDG)'s Review of Particle Physics (RPP) were gradually established through experiments.

New discoveries often provide crucial opportunities for theoretical advancement. In the 1950s, with the construction of particle accelerators, a large number of light flavor hadrons were discovered. Against this background, SU(3) symmetry was proposed as a theoretical framework for classifying hadrons [6, 7, 8, 9], becoming a milestone in the development of particle physics and marking the beginning of the first phase of hadronic spectroscopy research. This is a classic example of experimental phenomena driving theoretical breakthroughs.

A similar situation emerged with the observation of charmonium states beginning in 1974. The distinctive mass spectrum of charmonium inspired the Cornell group to propose the famous Cornell potential model [10, 11, 12], which combines a linear potential and a Coulomb potential described by  $V(r) = ar + b/r$ , thereby achieving for the first time a quantitative description of the hadronic spectrum. It should be noted that the Cornell potential is a typical quenched

approximation model. For low-lying hadronic states, such models can adequately address certain specific problems in spectroscopy. Subsequently, inspired by the Cornell model, various potential models were developed, including the high-precision Godfrey-Isgur (GI) model [13], further advancing the description of the hadronic spectrum. However, after 1986, no new charmonium states were reported experimentally, and hadronic spectroscopy entered a period of relative inactivity.

Since the beginning of the 21st century, with the continuous accumulation of experimental data, many new hadronic states have been discovered, particularly the charmonium-like XYZ states [14, 15, 16, 17, 18, 19, 20, 21, 22, 23, 24, 25, 26, 27, 28, 29, 30, 31]. These discoveries signify the arrival of a revival in hadronic physics, continuing to this day. Based on past experience, we have reason to expect that these new phenomena will drive further theoretical breakthroughs. These developments are closely related to a deeper understanding of the non-perturbative behavior of the strong interaction—one of the core challenges in modern particle physics.

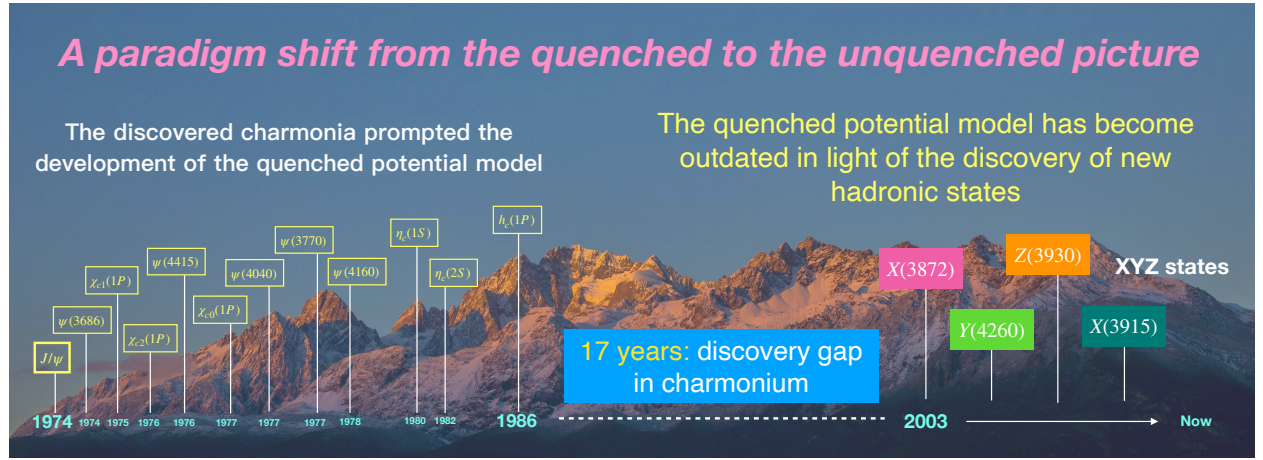


Figure 1: A paradigm shift from the quenched to the unquenched picture.

In 2003, the BaBar Collaboration, through studying the  $B \rightarrow KJ/\psi\pi^+\pi^-$  decay process, first reported the charmonium-like state  $X(3872)$  [32]. Like a stone thrown into a calm lake, the discovery of  $X(3872)$  stirred widespread and far-reaching research waves, promoting extensive exploration of hidden-charm hadronic matter over the past two decades. The charmonium states discussed in this review fall within this category. Comparing the mass of  $\chi_{c1}(2P)$  predicted by quenched potential models [10, 11, 12, 13] with the actual mass of  $X(3872)$  reveals a significant discrepancy, known as the " $X(3872)$  low-mass puzzle." In fact, this puzzle is not limited to  $X(3872)$ ; it also appears in other new hadronic states such as  $D_{s0}(2317)$  [33],  $D_{s1}(2460)$  [34], and  $\Lambda_c(2940)$  [35]. One explanatory approach involves introducing exotic hadronic structures like multiquark states [14, 19, 21, 20, 23, 25, 26, 27, 28]. Subsequently, the theoretical community gradually recognized that quenched models were insufficient to describe these new states, and the development of unquenched models significantly alleviated these mass discrepancy issues [36, 37, 38, 39, 40, 41, 42, 43, 44, 44, 45, 46, 47, 48]. Additionally,  $X(3915)$  [49] and  $Z(3930)$  [50], produced via the  $\gamma\gamma$  fusion process, have also been included in the candidate list for  $2P$  charmonium. This review will use the establishment of  $2P$  charmonium as a main thread to systematically introduce recent advances in unquenched charmonium research.

The charmonium-like state  $Y(4260)$  is a particularly striking example among these new discoveries, and its study benefited from advances in initial state radiation (ISR) technology. The BaBar Collaboration first observed  $Y(4260)$  in the cross sections for the  $e^+e^- \rightarrow J/\psi\pi^+\pi^-$  process [51]. Subsequently, BaBar Collaboration reported the observation of  $Y(4360)$  in the  $e^+e^- \rightarrow \psi(3686)\pi^+\pi^-$  process [52]. This state was later confirmed by the Belle collaboration, as well as another state,  $Y(4660)$  [53]. Near 4.6 GeV, Belle Collaboration also discovered another state  $Y(4630)$  through the  $e^+e^- \rightarrow \Lambda_c\bar{\Lambda}_c$  process [54]. With more precise data, the BESIII Collaboration reanalyzed  $e^+e^- \rightarrow J/\psi\pi^+\pi^-$  in 2017 and proposed that  $Y(4260)$  should be resolved into two substructures,  $Y(4220)$  and  $Y(4320)$  [55]. Furthermore,  $Y(4220)$  and  $Y(4390)$  were observed in the  $e^+e^- \rightarrow h_c\pi^+\pi^-$  process [56]. The challenge of understanding these  $Y$  states constitutes the so-called " $Y$  problem"—a term first appearing in the BESIII white paper [57]. Although

early attempts interpreted them as exotic hadronic states, comprehensively understanding so many  $Y$  states remains highly challenging. This review will introduce a unified theoretical framework based on the unquenched charmonium picture, incorporating interference effects and an  $S$ - $D$  mixing scheme to provide a solution to the " $Y$  problem." It is worth mentioning that this framework can be naturally extended to the study of bottomonium and light flavor vector meson states in  $e^+e^-$  annihilation, demonstrating its universality.

Unquenched effects also play a key role in understanding the anomalous decay behaviors of low-lying charmonia. For example, the " $\rho\pi$  puzzle" in the decays of  $J/\psi$  and  $\psi(3686)$  to light flavor meson pairs clearly violates expectations based on the "12% rule" [58]. In 2006, the hadronic loop mechanism—a direct manifestation of unquenched effects—was first introduced to study  $J/\psi \rightarrow P + V$  decays (where  $P$  and  $V$  represent light pseudoscalar and vector mesons, respectively) [59]. This mechanism was later extended to understand anomalous decays of other charmonia, such as  $\psi(3770)$  [60, 61, 62] and  $\chi_{cJ}(1P)$  ( $J = 0, 1, 2$ ) [63, 64, 65, 66]. Notable cases include the large non- $D\bar{D}$  decay branching fraction of  $\psi(3770)$  observed by the CLEO-c [67] and BES Collaborations [68, 69, 70, 71], and the unexpectedly large branching fractions of  $\chi_{cJ}(1P)$  in the  $\gamma V$  [72, 73] and  $VV$  [74, 75] decay channels.

Beyond anomalous decay widths, the dipion invariant mass spectrum of  $\psi(3770) \rightarrow J/\psi\pi^+\pi^-$  [76] could not be explained by quenched models such as QCD multipole expansion [77]. Introducing an intermediate  $D\bar{D}$  hadronic loop connecting the initial state  $\psi(3770)$  and the final state  $J/\psi\pi^+\pi^-$  successfully reproduced the dipion invariant mass distribution. A similar approach was also applied to describe the dipion spectra in bottomonium decays such as  $\Upsilon(4S) \rightarrow \Upsilon(nS)\pi^+\pi^-$ , where a  $B\bar{B}$  hadronic loop must be introduced [78]. These results provide compelling evidence for the importance of unquenched effects.

The anomalous decays of  $\Upsilon(10860) \rightarrow \Upsilon(nS)\pi^+\pi^-$  ( $n = 1, 2, 3$ ) and  $\Upsilon(10860) \rightarrow h_b(mP)\pi^+\pi^-$  ( $m = 1, 2$ ), reported by the Belle Collaboration [79, 80], further promoted the introduction of hadronic loop contributions. In particular, the discovery of two charged bottomonium-like structures,  $Z_b(10610)$  and  $Z_b(10650)$ , led to the proposal of the initial single pion emission (ISPE) mechanism [81]. This mechanism successfully explained the  $Z_b$  states appearing near the  $B\bar{B}^*$  and  $B^*\bar{B}^*$  thresholds in the  $\Upsilon(nS)\pi^\pm$ , ( $n = 1, 2, 3$ ) and  $h_b(mP)\pi^\pm$ , ( $m = 1, 2$ ) invariant mass spectra. The ISPE mechanism is essentially a manifestation of the hadronic loop mechanism, a typical unquenched effect.

The ISPE mechanism can also be extended to the hidden-charm dipion decays of highly excited charmonium and charmonium-like  $Y$  states, predicting charged charmonium-like structures near the  $D\bar{D}^*$  and  $D^*\bar{D}^*$  thresholds in the final states such as  $J/\psi\pi^\pm$ ,  $\psi(3686)\pi^\pm$ , and  $h_c\pi^\pm$  [82]. In 2013, the BESIII Collaboration observed  $Z_c(3900)$  [83], a discovery later selected as one of the highlights of the year by Physics magazine, a publication of the American Physical Society. This review will summarize these advances, highlighting the critical role of unquenched effects.

In recent years, the LHCb, CMS, and ATLAS Collaborations have observed enhanced structures in the invariant mass spectra of double  $J/\psi$  and  $J/\psi\psi(3686)$  produced in  $pp$  collisions [84, 85, 86, 87, 88, 89, 90]. Understanding these new phenomena is closely related to interactions between charmonia. Within the unquenched picture, charmonium states are strongly coupled to charmed meson pairs. Therefore, hadronic loops composed of charmed mesons may provide a mechanism for charmonium interactions.

With advances in computing power, lattice QCD studies have effectively derived the interaction potentials between charmonia (such as  $J/\psi$  and  $\eta_c$ ) and nucleons ( $N$ ) [91]. These results provide important basis for testing related theoretical schemes, which propose that unquenched charmonia may interact with nucleons through charmed meson loops—a mechanism similar to charmonium-charmonium interactions. This framework can also be applied to study interactions between fully heavy hadrons, such as the recently investigated  $\Omega_{QQQ}$ - $\Omega_{QQQ}$  interaction via lattice QCD [92]. This review will introduce the latest progress in this field.

As the title indicates, "beyond" is a key theme of this review, emphasizing that unquenched effects are not limited to charmonium. As discussed in Section 7, this effect equally applies to bottomonium and light vector meson states, possessing universal significance.

Over the past two decades, numerous new hadronic states and related phenomena have been discovered. Through collaborative efforts between theorists and experimentalists, hadronic spectroscopy research has entered a new developmental stage, marking the advent of the "era of high-precision hadronic spectroscopy." What defines high-precision hadronic spectroscopy? It is reflected not only in the improvement of experimental measurement accuracy but also in the advancement of theoretical prediction precision. How can we further enhance the accuracy of theoretical predictions? We believe it is essential to vigorously promote unquenched hadronic spectroscopy research. This review uses charmonium as an example to demonstrate the importance of unquenched effects from multiple perspectives (see Fig. 1). Clearly, this effect is universally present in all hadrons.

In the 1970s and 1980s, the discovery of numerous charmonium states drove the development of quenched models, represented by the Cornell potential. Entering the 21st century, with the continuous emergence of new charmonium-like hadronic states, hadronic physics has stepped into a new phase where quenched models can no longer meet the demands of contemporary research. As we celebrate the 50th anniversary of the discovery of the  $J/\psi$  particle, we also witness the end of one era and the beginning of another—the era of high-precision hadronic spectroscopy characterized by unquenched effects. This new era is undoubtedly full of challenges and significant opportunities.

## 2. Anomalous decay behaviors of charmonia and hadronic loop mechanism

### 2.1. Phenomenology

#### 2.1.1. $\rho\pi$ puzzle

In perturbative QCD, the dominant hadronic decay width of charmonium states, which proceeds primarily via three-gluon annihilation, is proportional to their leptonic width, with both quantities depending on the square of the wave function at the origin [93]. This leads to a simple scaling law between the hadronic branching fractions of the ground state  $J/\psi$  and its first radial excitation  $\psi(3686)$ . Specifically, for any hadronic final state  $h$ , one expects [94]

$$Q_h \equiv \frac{BR(\psi(3686) \rightarrow h)}{BR(J/\psi \rightarrow h)} \simeq \frac{BR(\psi(3686) \rightarrow e^+e^-)}{BR(J/\psi \rightarrow e^+e^-)} = \frac{(7.94 \pm 0.22) \times 10^{-3}}{(5.971 \pm 0.032) \times 10^{-2}} = (13.3 \pm 0.4)\%. \quad (1)$$

Experimentally, the ratio of leptonic branching fractions is about 12%, which gives rise to the so-called "12% rule". This rule implies that the hadronic decay patterns of  $\psi(3686)$  should resemble those of  $J/\psi$ , with an overall suppression factor of roughly 0.12.

The "12% rule" is reasonably well satisfied for most hadronic channels. However, striking violations are observed in certain exclusive decay modes, most notably in the  $\rho\pi$  and  $K^+K^*(892)^- + \text{c.c.}$  final states. These are dominant decay modes of  $J/\psi$  but are strongly suppressed in  $\psi(3686)$ , with branching fractions more than two orders of magnitude below the expectation [58, 94]

$$Q_{\rho\pi} = \frac{\mathcal{B}(\psi(3686) \rightarrow \rho\pi)}{\mathcal{B}(J/\psi \rightarrow \rho\pi)} = \frac{(3.2 \pm 1.2) \times 10^{-5}}{(1.88 \pm 0.12) \times 10^{-2}} \simeq 0.2\%,$$

$$Q_{K^+K^*(892)^- + \text{c.c.}} = \frac{\mathcal{B}(\psi(3686) \rightarrow K^+K^*(892)^- + \text{c.c.})}{\mathcal{B}(J/\psi \rightarrow K^+K^*(892)^- + \text{c.c.})} = \frac{(2.9 \pm 0.4) \times 10^{-5}}{(6.0_{-1.0}^{+0.8}) \times 10^{-3}} \simeq 0.5\%. \quad (2)$$

Many other vector-pseudoscalar ( $VP$ ) channels show similar suppression, as summarized in Table 1. This dramatic suppression, observed experimentally and in stark contrast to the "12% rule", constitutes the longstanding " $\rho\pi$  puzzle" in charmonium physics.

The " $\rho\pi$  puzzle" points to the involvement of additional nonperturbative QCD effects and has motivated a wide range of theoretical efforts to account for this anomaly. Hou and Soni proposed a  $J/\psi$ -glueball mixing mechanism to explain the enhancement of the  $J/\psi \rightarrow \rho\pi$  and  $K\bar{K}^*(892) + \text{c.c.}$  decays [95]. Brodsky, Lepage, and Tuan suggested that these decays proceed via an intermediate glueball [96]. Brodsky and Karliner argued that the  $J/\psi$  decays could be enhanced through quark rearrangement mechanisms involving  $|\bar{q}q\bar{c}c\rangle$  Fock components present in light vector mesons, while the corresponding  $\psi(3686)$  decays are suppressed due to the node in its radial wave function [97]. Feldmann and Kroll further investigated these enhancements through the mixing of the  $J/\psi$  with light-quark states, notably  $\omega$  and  $\phi$  [98]. Clavelli and Intemann proposed a vector-meson-mixing model involving the  $\rho$ ,  $\omega$ ,  $\phi$ , and  $J/\psi$ , while Guo et al. suggested the molecular components in the  $J/\psi$  [99], which yields sizable hadronic decay modes of the  $J/\psi$  [100]. In addition, Li, Bugg, and Zou introduced the final-state interactions (FSI) as an explanation, demonstrating that the  $a_2\rho$  loop contribution can enhance the decay rate of  $J/\psi \rightarrow \rho\pi$  [101]. Collectively, these frameworks focus on resolving the " $\rho\pi$  puzzle" by enhancing the  $J/\psi$  decay rates, while the following approaches instead emphasize the suppression of  $\psi(3686)$  decays.

Suzuki suggested that the coupling of  $\psi(3686)$  to virtual charmed-meson pairs could generate an amplitude destructively interfering with the perturbative QCD  $\psi(3686) \rightarrow 3g$  process, thereby suppressing specific channels like  $\rho\pi$  and  $K\bar{K}^*(892) + \text{c.c.}$  [102, 103]. Rosner introduced a  $2S-1D$  mixing scheme, wherein the  $\psi(1D)$  contribution destructively interferes with that of  $\psi(3686)$  in these channels [104]. Gérard and Weyers proposed that the three-gluon decay

Table 1: Measured branching ratios of  $\psi(3686)$  and  $J/\psi$  decays into two-light-meson final states  $h'$  [94]. The corresponding ratios  $Q_{h'}$  and their qualitative deviations from the perturbative-QCD 12% rule are listed, showing cases of strong suppression, enhancement, or consistency with the expectation.

$h'$	$\mathcal{B}(\psi(3686) \rightarrow h')$	$\mathcal{B}(J/\psi \rightarrow h')$	Ratio $Q_{h'}$ (%)	Expected $\sim 12\%$ ?
$\rho\pi$	$(3.2 \pm 1.2) \times 10^{-5}$	$(1.88 \pm 0.12) \times 10^{-2}$	$0.2 \pm 0.1$	Strong Suppression
$K^+ K^*(892)^- + \text{c.c.}$	$(2.9 \pm 0.4) \times 10^{-3}$	$(6.0^{+0.8}_{-1.0}) \times 10^{-1}$	$0.5^{+0.1}_{-0.2}$	Strong Suppression
$\bar{K}^0 K^*(892)^0 + \text{c.c.}$	$(1.09 \pm 0.20) \times 10^{-4}$	$(4.2 \pm 0.4) \times 10^{-3}$	$2.6 \pm 0.6$	Suppression
$\phi\eta'$	$(1.54 \pm 0.20) \times 10^{-5}$	$(4.6 \pm 0.5) \times 10^{-4}$	$3.3 \pm 0.6$	Suppression
$\phi\eta$	$(3.10 \pm 0.31) \times 10^{-5}$	$(7.4 \pm 0.6) \times 10^{-4}$	$4.2 \pm 1.0$	Suppression
$\rho a_2(1320)$	$(2.6 \pm 0.9) \times 10^{-4}$	$(1.09 \pm 0.22) \times 10^{-2}$	$2.4 \pm 1.0$	Suppression
$\omega f_2(1270)$	$(2.2 \pm 0.4) \times 10^{-4}$	$(4.3 \pm 0.6) \times 10^{-3}$	$5.1 \pm 1.2$	Suppression
$\omega\pi^0$	$(2.1 \pm 0.6) \times 10^{-5}$	$(4.5 \pm 0.5) \times 10^{-4}$	$4.7 \pm 1.5$	Suppression
$\pi^+\pi^-$	$(7.8 \pm 2.6) \times 10^{-6}$	$(1.47 \pm 0.14) \times 10^{-4}$	$5.3 \pm 1.9$	Suppression
$K^+K^-$	$(7.5 \pm 0.5) \times 10^{-5}$	$(3.06 \pm 0.05) \times 10^{-4}$	$24.5 \pm 1.7$	Enhancement
$K_S^0 K_L^0$	$(5.34 \pm 0.33) \times 10^{-5}$	$(1.95 \pm 0.11) \times 10^{-4}$	$27.4 \pm 2.3$	Enhancement
$b_1(1235)^0\pi^0$	$(2.4 \pm 0.6) \times 10^{-4}$	$(2.3 \pm 0.6) \times 10^{-3}$	$10.4 \pm 3.8$	Consistency
$\rho\eta$	$(2.2 \pm 0.6) \times 10^{-5}$	$(1.93 \pm 0.23) \times 10^{-4}$	$11.4 \pm 3.4$	Consistency
$\rho\eta'$	$(1.9^{+1.7}_{-1.2}) \times 10^{-5}$	$(8.1 \pm 0.8) \times 10^{-5}$	$23.5^{+21.2}_{-15.0}$	Consistency (Large error)
$\phi f_1(1285)$	$(3.0 \pm 1.3) \times 10^{-5}$	$(2.6 \pm 0.5) \times 10^{-4}$	$11.5 \pm 5.5$	Consistency
$\omega\eta'$	$(3.2^{+2.5}_{-2.1}) \times 10^{-5}$	$(1.89 \pm 0.18) \times 10^{-4}$	$16.9^{+13.4}_{-11.3}$	Consistency (Large error)
$b_1(1235)^\pm\pi^\mp$	$(4.0 \pm 0.6) \times 10^{-4}$	$(3.0 \pm 0.5) \times 10^{-3}$	$13.3 \pm 3.0$	Consistency

of  $\psi(3686)$  is absent or suppressed by treating  $J/\psi$  and  $\psi(3686)$  as orthogonal states, with  $\psi(3686)$  decays proceeding mainly through a two-step process involving an intermediate  $h_c(1^{+-})$  state [105]. Conversely, Chen and Braaten argued that these decays are dominated by higher color-octet Fock states, attributing the suppression of  $\psi(3686)$  to an additional dynamical effect related to the small mass gap between  $\psi(3686)$  and the  $D\bar{D}$  threshold [106]. Other proposed mechanisms include the sequential fragmentation model by Karl and Roberts [107], the hindered M1 transition scenario by Pinsky [108], the exponential falloff of hadronic form factors within a nonrelativistic quark model suggested by Chaichian and Törnqvist [109].

In fact, under the unquenched picture, the hadronic loop mechanism also offers a potential explanation for the “ $\rho\pi$ ” puzzle, which will be introduced in detail later.

### 2.1.2. Large non- $D\bar{D}$ decays of $\psi(3770)$

Before discussing the non- $D\bar{D}$  decays of  $\psi(3770)$ , we first briefly review the Okubo–Zweig–Iizuka (OZI) rule, which plays a crucial role in understanding the suppression of such decay processes. The OZI rule, a consequence of an empirical observation, was independently proposed in the 1960s by Okubo [110], Zweig [9, 111], and Iizuka [112]. It states that a decay process involving disconnected quark lines between the initial and final states is strongly suppressed relative to one in which these lines are connected. This rule successfully explained several anomalies encountered in the 1960s in the study of short-lived particles. For instance, certain decay modes expected to occur frequently were found to have significantly smaller widths than predicted, such as  $\phi \rightarrow \pi^+\pi^-\pi^0$  [14, 94, 113, 114].

Furthermore, the OZI rule naturally accounts for a striking feature observed in heavy quarkonium spectroscopy. States below the open-flavored meson-pair threshold typically possess narrow widths, whereas those above the threshold exhibit much broader widths. This behavior arises because the decays of the ground and low-lying states (such as  $J/\psi$ ,  $\psi(3686)$ , and  $\Upsilon(nS)$  with  $(n = 1, 2, 3)$ ) are OZI-suppressed, leading to small total widths. In contrast, for states above the threshold, OZI-allowed strong decay channels become accessible, resulting in a dramatic increase—sometimes by several orders of magnitude—in their total widths. Consequently, for heavy quarkonia above the threshold, OZI-allowed decay modes overwhelmingly dominate.

Since the  $\psi(3770)$  mass lies just above the  $D\bar{D}$  threshold, conventional theoretical expectations predict that it should predominantly decay into  $D\bar{D}$  pairs, with the non- $D\bar{D}$  decay channels suppressed by the OZI rule. However, experimental measurements have revealed a surprisingly large non- $D\bar{D}$  branching fraction. Before 2005, the branching ratio for  $\psi(3770) \rightarrow \text{non-}D\bar{D}$  was reported as  $(10.9 \pm 6.9 \pm 9.2)\%$  [115], with subsequent measurements by the BESII Collaboration yielding values of  $(16.4 \pm 7.3 \pm 4.2)\%$  [68],  $(14.5 \pm 1.7 \pm 5.8)\%$  [69],  $(13.4 \pm 5.0 \pm 3.6)\%$  [70], and  $(15.1 \pm 5.6 \pm 1.8)\%$  [71]. Notably, the CLEO Collaboration reported a branching fraction of  $\mathcal{B}(\psi(3770) \rightarrow D\bar{D}) = (100.3 \pm 1.4^{+4.8}_{-6.6})\%$  [67], further deepening the puzzle.

These experimental results, indicating a non- $D\bar{D}$  branching ratio of approximately 10% to 15%, are significantly larger than theoretical expectations. Meanwhile, the exclusive non- $D\bar{D}$  decay modes of  $\psi(3770)$  listed by the PDG [94]—such as  $J/\psi\eta$ ,  $J/\psi\pi\pi$ ,  $\phi\eta$ , and  $\gamma\chi_{cJ}$  ( $J = 0, 1$ )—sum to a branching fraction of less than 2%, insufficient to account for the observed discrepancy. The unexpectedly large non- $D\bar{D}$  decay rate of  $\psi(3770)$  has therefore long stood as a significant puzzle in understanding its decay dynamics, motivating extensive experimental and theoretical investigations over the past two decades.

Theoretical efforts to resolve the  $\psi(3770)$  non- $D\bar{D}$  decay puzzle have been extensive [116, 77, 117, 118, 119, 120, 121, 104, 122, 123, 124, 125, 62, 60, 61, 126, 126]. Kuang and Yan studied the hidden-charm decay  $\psi(3770) \rightarrow J/\psi\pi\pi$  within the framework of QCD multipole expansion [77], finding results consistent with the corresponding exclusive experimental measurements [94]. He, Fan, and Zhao investigated the decay  $\psi(3770) \rightarrow \text{light hadrons}$  and, by including color-octet contributions, obtained  $\Gamma(\psi(3770) \rightarrow \text{light hadrons}) = 467^{+338}_{-187}$  keV, corresponding to a total non- $D\bar{D}$  branching fraction of about 5% [125].

Given that the dominant decay mode of  $\psi(3770)$  is  $D\bar{D}$ , the hadronic loop mechanism was proposed as a possible pathway for  $\psi(3770)$  to access non- $D\bar{D}$  final states [62, 60, 61]. Theoretical estimates for the  $VP$  final states vary considerably, ranging from 0.2–1.1% [62, 60] to (0.04 – 0.17)% or (3.38 – 5.23)% [61], depending on the input parameters. These results suggest that accounting for hadronic loop effects can substantially mitigate the discrepancy between theoretical predictions and experimental observations [60]. Later, we will come back to this point.

### 2.1.3. Anomalous transitions in high-lying heavy quarkonia

For a charmonium state  $\psi$  decaying into two light mesons  $h_1$  and  $h_2$ , perturbative QCD predicts that the branching ratio behaves asymptotically as

$$\mathcal{B}[\psi(\lambda) \rightarrow h_1(\lambda_1)h_2(\lambda_2)] \sim \left( \frac{\Lambda_{\text{QCD}}^2}{m_c^2} \right)^{|\lambda_1+\lambda_2|+2}, \quad (3)$$

where  $\lambda$ ,  $\lambda_1$ , and  $\lambda_2$  denote the helicities of the respective mesons. It is evident that the leading contribution arises when  $\lambda_1 + \lambda_2 = 0$ , while configurations violating this condition are power-suppressed. This phenomenon is known as the helicity selection rule [127]. The rule can equivalently be expressed in terms of the naturalness quantum number,  $\sigma \equiv P(-1)^J$ , as  $\sigma(\psi) = \sigma(h_1)\sigma(h_2)$ , where  $P$  and  $J$  are the parity and spin of the corresponding meson. The helicity selection rule has been widely applied in analyzing exclusive decay processes of heavy quarkonia. In Refs. [98, 127, 128], specific examples of helicity-allowed and helicity-suppressed decay modes are explicitly discussed. However, with the accumulation of experimental data, an increasing number of observations have revealed substantial deviations from the rule's predictions. For instance, the well-known  $J/\psi \rightarrow VP$  decay mentioned earlier, as well as the  $\eta_c \rightarrow VV$  process, should be strongly suppressed according to the rule, yet they constitute important decay channels of the  $J/\psi$  and  $\eta_c$ , respectively [94].

For the processes  $\chi_{cJ} \rightarrow VV$ , the decay of  $\chi_{c1}$  violates the helicity selection rule, whereas those of  $\chi_{c0}$  and  $\chi_{c2}$  do not. Consequently, the decays of  $\chi_{c1}$  into two light vector mesons are expected to be strongly suppressed compared with the corresponding decays of  $\chi_{c0}$  and  $\chi_{c2}$ . In addition,  $\chi_{c1} \rightarrow \omega\phi$  is a double-OZI-suppressed process. Therefore, the branching ratios of the channels  $\chi_{c1} \rightarrow \phi\phi$ ,  $\omega\omega$ , and  $\omega\phi$  are expected to be small, making them difficult to observe experimentally, especially in the case of  $\chi_{c1} \rightarrow \omega\phi$ . However, in 2011, the BESIII Collaboration reported the first observations of  $\chi_{c1} \rightarrow \phi\phi$ ,  $\omega\omega$ , and  $\omega\phi$ , with the corresponding branching ratios measured to be  $(4.4 \pm 0.3 \pm 0.5) \times 10^{-4}$ ,  $(6.0 \pm 0.3 \pm 0.7) \times 10^{-4}$ , and  $(2.2 \pm 0.6 \pm 0.2) \times 10^{-5}$ , respectively [75]. These sizable branching fractions, comparable to those of  $\chi_{c0}$  and  $\chi_{c2}$ , indicate the presence of significant nonperturbative contributions.

For the decay  $\psi(3770) \rightarrow J/\psi\pi^+\pi^-$ , the dipion invariant mass spectrum distribution has been measured experimentally [76]. A clear discrepancy is evident when comparing these data with theoretical predictions based on the QCD multipole expansion (a quenched method) [77], as shown in Fig. 2. A similar discrepancy has been reported for the decay  $\Upsilon(4S) \rightarrow \Upsilon(nS)\pi^+\pi^-$  ( $n = 1, 2$ ), where the measured dipion invariant mass spectrum distributions also cannot be described by the QCD multipole expansion approach [129, 130, 131], as shown in Fig. 103. Both the  $\psi(3770)$  and  $\Upsilon(4S)$  are heavy quarkonia with masses above the open-flavor thresholds ( $D\bar{D}$  and  $B\bar{B}$ , respectively). Therefore, effects beyond the quenched approximation must be considered [78].

Anomalies have also been observed in the radiative decays of heavy quarkonia. In particular, the radiative transitions  $J/\psi \rightarrow \gamma\eta_c$  and  $\psi' \rightarrow \gamma\eta_c^{(\prime)}$  are expected to be dominantly governed by magnetic dipole (M1) transitions, which involve a quark spin flip in the conventional  $q\bar{q}$  picture. However, as studied in Ref. [132], both the NR model and the GI model exhibit significant discrepancies in their predictions for these M1 transitions when compared with the experimental data [94]. Specifically, for  $J/\psi \rightarrow \gamma\eta_c$ , the predicted partial decay widths are approximately a factor of two larger than the measured value, while for  $\psi' \rightarrow \gamma\eta_c$ , the theoretical predictions exceed the experimental results by nearly an order of magnitude (see Table 4 for details).

Besides, Gao, Zhang, and Chao studied the radiative decays of charmonia  $J/\psi$  and  $\chi_{cJ}$  into light mesons within the framework of perturbative QCD, performing a complete numerical calculation of the quark-gluon loop diagrams [133]. Their theoretical results for  $J/\psi \rightarrow \gamma\eta$  and  $\gamma\eta'$  are in good agreement with the experimental data. Moreover, they predicted the branching ratios of  $\chi_{c1} \rightarrow \gamma\rho^0$ ,  $\gamma\omega$ , and  $\gamma\phi$  to be  $1.4 \times 10^{-5}$ ,  $1.6 \times 10^{-6}$ , and  $3.6 \times 10^{-6}$ , respectively. Nevertheless, the corresponding measurements reported by the CLEO Collaboration are  $(2.43 \pm 0.19 \pm 0.22) \times 10^{-4}$ ,  $(8.5 \pm 1.5 \pm 1.2) \times 10^{-5}$ , and  $(1.28 \pm 0.76 \pm 0.15) \times 10^{-5}$  [72], which are about an order of magnitude larger than the theoretical predictions. Furthermore, the measured branching ratios for the radiative decay processes  $h_b(1P) \rightarrow \eta_b(1S)\gamma$ ,  $h_b(2P) \rightarrow \eta_b(1S)\gamma$ , and  $h_b(2P) \rightarrow \eta_b(2S)\gamma$  [134] are found to be larger than the corresponding theoretical expectations by a factor of about 1.2–2.5 [135].

These deviations indicate that additional unquenched effects may play an important role in these radiative decay processes.

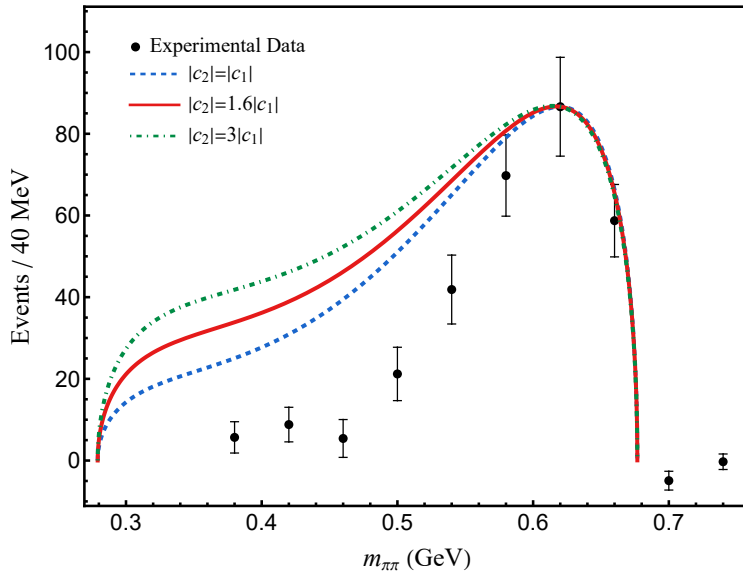


Figure 2: Comparison of the dipion invariant-mass distribution between the experimental measurement [76] and the result from the QCD multipole expansion [77]. The  $2S-1D$  mixing angle is taken as  $\theta_{2S-1D} = -10^\circ$ , and several representative values of  $|c_1|$  and  $|c_2|$  suggested in Ref. [77] are illustrated.

## 2.2. Hadronic loop mechanism

In prior studies [11, 136, 137, 138, 101, 139, 140, 103, 141, 142, 143, 144, 145, 146, 147, 148, 149], the limitations of the quenched approximation for charmonium physics were recognized. For instance, Kuang attempted to extend the QCD multipole expansion method by incorporating coupled-channel effects [143]. However, progress in this direction remained limited, primarily due to constraints imposed by the experimental data available at the time. The situation began to change around 2006, when the observations of anomalous behaviors in certain charmonium states [150, 151, 115, 74, 67, 68, 69, 70, 71, 72, 75, 73], as mentioned above, motivated theorists to re-examine this issue. This renewed effort involved introducing the hadronic loop mechanism [59, 152, 62, 60, 61, 63, 64, 65, 152] into the description of heavy quarkonium transitions.

A key aspect of the perturbative QCD framework is that heavy quarkonium annihilation into gluons occurs at short distances on the order of  $r \sim 1/m_Q$ , where the strong coupling constant  $\alpha_s(m_Q)$  is sufficiently small to justify a perturbative expansion. However, for high-lying charmonia and bottomonia, their spatial radii increase. For sufficiently excited states, these radii can even exceed the interaction range of the soft gluon field. In such cases, long-distance contribution may become significant, potentially violating the power-counting rules of perturbative QCD [153, 154]. Another contributing factor is that, although the charm quark is heavy, its mass may still be insufficient to fully satisfy the requirements of a reliable perturbative QCD treatment, thereby undermining the validity of the perturbative framework [64]. When strong interactions occur at long distances, the momentum transfer is small, and the running coupling constant of QCD becomes large. Consequently, perturbative QCD is no longer applicable. Thus, long-distance contributions constitute an important reason for the failure of rules deduced from perturbative QCD.

By taking the  $J/\psi \rightarrow VP$  decay as an example, we may explicitly illustrate this issue. The decays of  $J/\psi \rightarrow \rho\pi$  and other  $VP$  final states are OZI-suppressed. The corresponding diagrams for  $J/\psi$  decays into  $VP$  via three-gluon annihilation are shown in Fig. 3, where Fig. 3(a) represents the single-OZI-suppressed (SOZI) process and Fig. 3(b) corresponds to the double-OZI-suppressed (DOZI) process. In the SOZI process, the quark lines between the initial and final states are disconnected once, whereas in the DOZI process they are disconnected twice.

There exists a long-distance contribution to the  $J/\psi \rightarrow VP$  decay, as illustrated at the quark level in Fig. 4. However, it is difficult to directly evaluate such a process at the quark level using quantum field theory due to the nonperturbative nature of strong interactions in the low-energy regime. Therefore, a phenomenological approach must be developed to quantitatively describe this process.

At the hadron level, the long-distance contribution to the  $J/\psi \rightarrow VP$  decay can be described equivalently. In

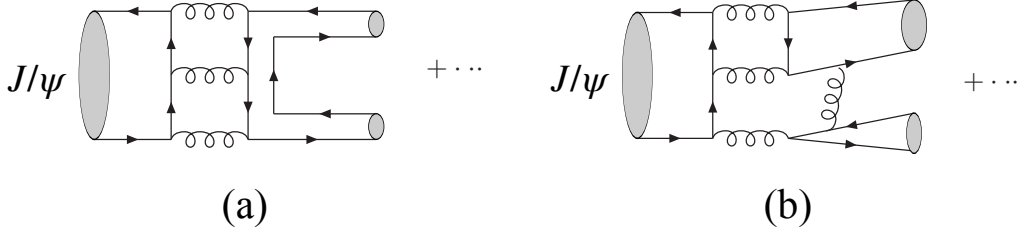


Figure 3: Quark-level short-distance contribution for the  $J/\psi \rightarrow VP$  decay. Here, (a) and (b) represent the single-OZI-suppressed (SOZI) and double-OZI-suppressed (DOZI) processes for the decays of  $J/\psi \rightarrow VP$ , respectively. Figure adapted from Ref. [59].

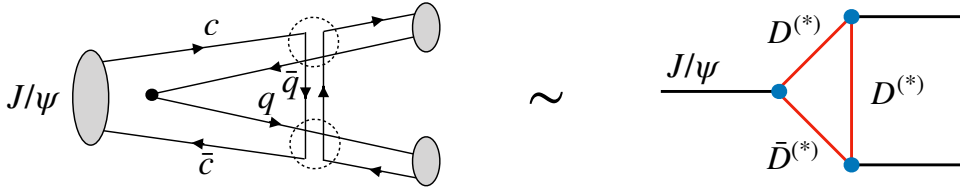


Figure 4: Quark-level (left) and hadron level (right) long-distance contribution for the  $J/\psi \rightarrow VP$  decay. The left figure adapted from Ref. [59].

this framework, the  $J/\psi$  meson first dissociates into two virtual charmed mesons, which then interact via the exchange of another charmed meson carrying appropriate charge, flavor, spin, and isospin quantum numbers. Thus, charmed-meson hadronic loops serve as a bridge connecting the initial and final states, as shown in Fig. 4. It is a phenomenological framework known as the hadronic loop mechanism, which provides a tractable method for calculating non-perturbative, long-distance effects in hadronic transitions.

Focusing on a general transition  $A \rightarrow BC$  mediated by a hadronic loop composed of hadrons  $M_i$  ( $i = 1, 2, 3$ ), the process involves three interaction vertices  $V_j$  ( $j = 1, 2, 3$ ), which can be described using an effective Lagrangian approach. Consequently, the decay amplitude can be expressed as

$$\begin{array}{c}
 \begin{array}{c}
 \text{---} A \text{---} \text{---} V_1 \text{---} M_1 \text{---} V_2 \text{---} B \text{---} \\
 \text{---} V_3 \text{---} M_2 \text{---} V_3 \text{---} C \text{---} \\
 \text{---} M_3 \text{---}
 \end{array}
 \end{array}
 : \quad \mathcal{M}_{A \rightarrow BC} = \int \frac{d^4 q}{(2\pi)^4} \frac{i}{q_{M_1}^2 - m_{M_1}^2} \frac{i}{q_{M_2}^2 - m_{M_2}^2} \frac{i}{q_{M_3}^2 - m_{M_3}^2} \times \mathcal{V}_1 \mathcal{V}_2 \mathcal{V}_3 \times \mathcal{F}\mathcal{F}, \quad (4)$$

where  $\mathcal{F}\mathcal{F}$  denotes a monopole or dipole form factor. This form factor is introduced primarily to account for the off-shell effects of the exchanged hadron in the subprocess  $M_1 + M_2 \rightarrow B + C$ , and to incorporate the internal structure effects of the exchanged meson. Additionally,  $\mathcal{F}\mathcal{F}$  serves to suppress high-momentum contributions and regularize the ultraviolet divergence of the loop integral, analogous to the role of a Pauli-Villars regulator.

In the following three subsections, we illustrate how the hadronic loop mechanism plays a crucial role in addressing several long-standing puzzles in quarkonium physics: the  $\rho\pi$  puzzle in  $J/\psi \rightarrow VP$  decays, the unexpectedly large non- $D\bar{D}$  decay width of the  $\psi(3770)$ , and anomalous transitions among high-lying heavy quarkonia. It should be emphasized that the hadronic loop mechanism effectively embodies the coupled-channel effect, thereby representing a physically motivated and universal unquenched picture of these processes.

### 2.2.1. Decoding the $\rho\pi$ puzzle through the hadronic loop mechanism

The  $J/\psi$  decays into a vector ( $V$ ) and a pseudoscalar ( $P$ ) meson provide a critical testing ground for understanding the interplay between perturbative and nonperturbative QCD dynamics. The widely discussed “ $\rho\pi$  puzzle”—the significant suppression of  $J/\psi \rightarrow \rho\pi$  relative to naive perturbative QCD expectations—highlights the importance of nonperturbative mechanisms. A coherent description requires the inclusion of both the short-distance OZI-suppressed

three-gluon annihilation, and the long-distance hadronic loop effects. Since the former cannot be reliably calculated *ab initio*, it is treated via a phenomenological effective coupling  $|\mathcal{G}_S^{PV}|$ , which is assumed universal across all  $J/\psi \rightarrow PV$  channels due to the flavor-blind nature of gluon interactions.

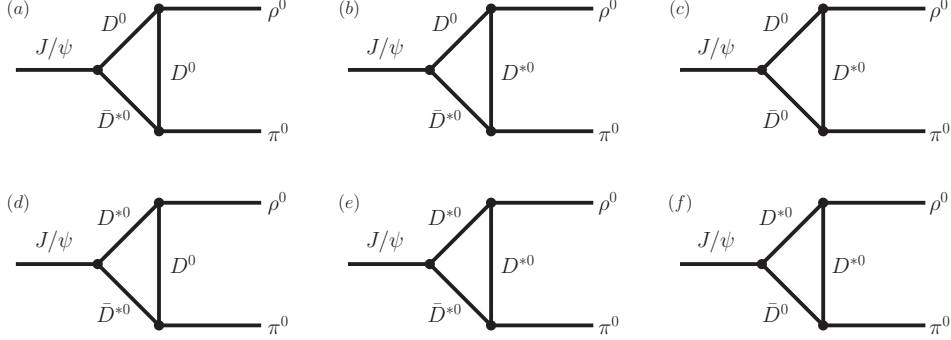


Figure 5: Feynman diagrams for  $J/\psi \rightarrow \rho^0\pi^0$  via  $D^{(*)}$ -meson loops. Diagrams (a)–(f) involve neutral charmed mesons; charged-meson loops follow by replacement  $D^{(*)0} \rightarrow D^{(*)\pm}$ . Adapted from Ref. [59].

The dominant long-distance contribution is modeled by the hadronic loop mechanism, where the  $J/\psi$  couples to the final state via virtual intermediate charmed mesons ( $D^{(*)}$ ,  $D_s^{(*)}$ ). In Fig. 5, the contribution of the hadronic loop mechanism to  $J/\psi \rightarrow \rho^0\pi^0$  is illustrated as an example. The total transition amplitude for a channel  $J/\psi \rightarrow VP$  can be expressed in a compact Lorentz structure [59]:

$$\mathcal{M}^{PV} = \mathcal{G}^{PV} \varepsilon_{\mu\nu\alpha\beta} \epsilon_{J/\psi}^\mu \epsilon_V^{*\nu} p_3^\alpha p_4^\beta, \quad (5)$$

where the effective coupling  $\mathcal{G}^{PV}$  encapsulates contributions from both the short-distance ( $\mathcal{G}_S^{PV}$ ) and long-distance ( $\mathcal{G}_H^{PV}(\alpha)$ ) processes:

$$\mathcal{G}^{PV} = \mathcal{G}_S^{PV} \beta^{PV} + \mathcal{G}_H^{PV}(\alpha). \quad (6)$$

Here,  $\beta^{PV}$  are the SU(3) flavor factors obtained from  $\text{Tr}(PV)$ , and  $\alpha$  is a dimensionless parameter governing the hadronic form factor cutoff,  $\Lambda(m_i) = m_i + \alpha\Lambda_{\text{QCD}}$  ( $\Lambda_{\text{QCD}} = 220$  MeV). The loop amplitudes  $\mathcal{G}_H^{PV}(\alpha)$  are calculated explicitly via Feynman diagrams involving  $D^{(*)}$  loops (for light non-strange final states) or  $D_s^{(*)}$  loops (for final states involving strangeness). A monopole form factor,  $\mathcal{F}(m_i, q^2) = (\Lambda^2 - m_i^2)/(\Lambda^2 - q^2)$ , is employed to regulate the loop integrals and account for the off-shell effects of the exchanged mesons, where  $\Lambda$  plays a role analogous to the cutoffs used in the Pauli–Villars renormalization scheme.

The model is constrained using the experimental branching ratios for two reference channels:  $J/\psi \rightarrow \rho^0\pi^0$  and  $J/\psi \rightarrow K^{*+}K^- + \text{c.c.}$ . A global fit yields the parameter values:  $\alpha = 0.13$ ,  $|\mathcal{G}_S^{PV}| = 4.51 \times 10^{-3} \text{ GeV}^{-1}$ . With these parameters fixed, predictions are made for all other  $J/\psi \rightarrow PV$  channels. The results, summarized in Table 2, reveal several key insights:

- The hadronic loop contribution is *sizable*, comparable in magnitude to the short-distance OZI amplitude.
- A *destructive interference* between the two amplitudes is essential to reproduce the observed branching ratios, particularly for the suppressed  $\rho\pi$  channel.
- The predictions for channels such as  $\phi\eta$ ,  $\phi\eta'$ , and  $\omega\eta'$  show satisfactory agreement with experimental data, validating the model’s consistency.

Ref. [152] also pointed out that the hadronic loop effect is important for understanding the “ $\rho\pi$  puzzle”. In that work, the authors investigated the long-distance hadronic loop effects to the decays of  $J/\psi(\psi') \rightarrow VP$ , together with the short-distance contributions, and the electromagnetic (EM) transition amplitudes which dominate the isospin-violating channels. By fixing the relevant parameters with the experimental data for  $J/\psi, \psi' \rightarrow \rho\pi$  and  $K^*\bar{K} + \text{c.c.}$ ,

Table 2: Comparison between the calculated results and experimental data. The first two decay modes are used to fix the parameters  $\alpha$  and  $|\mathcal{G}_S^{PV}|$ . The table is adapted from Ref. [59].

Decay mode	$\rho^0\pi^0$	$K^{*+}K^- + \text{c.c.}$	$\phi\eta$	$\phi\eta'$	$\omega\eta$	$\omega\eta'$
$BR \times 10^{-3}$ (Experiment) [155]	$4.2 \pm 0.5$	$5.0 \pm 0.4$	$0.65 \pm 0.07$	$0.33 \pm 0.04$	$1.58 \pm 0.16$	$0.167 \pm 0.025$
$\mathcal{G}^{PV}(10^{-3} \text{ GeV}^{-1})$	$2.08 \pm 0.25$	$1.65 \pm 0.26$	$0.89 \pm 0.096$	$0.71 \pm 0.086$	$1.27 \pm 0.13$	$0.46 \pm 0.069$
$\mathcal{G}_H^{PV}(10^{-3} \text{ GeV}^{-1})$ (Theory)	6.59	6.16	3.55	5.13	5.46	4.07
$\mathcal{G}^{PV}(10^{-3} \text{ GeV}^{-1})$ (Theory)	2.08 (fitting)	1.65 (fitting)	0.92	0.62	0.95	0.40
BR ( $\times 10^{-3}$ ) (Theory)	4.2 (fitting)	5.0 (fitting)	0.70	0.25	0.86	0.14

they reached a similar conclusion: the destructive interference between the long-distance charmed-meson loops and the short-distance amplitudes in  $\psi'$  decays leads to the observed deviations from the “12% rule”. Ref. [152] further suggested that the hadronic loop mechanism constitutes a general nonperturbative effect in the charmonium energy region and may be involved in an even wider range of decay modes.

In conclusion, the combined framework incorporating both the short-distance three-gluon annihilation and the long-distance hadronic loop mechanism provides a consistent and quantitative description of the  $J/\psi/\psi' \rightarrow VP$  decays. The significant interference between the short-distance three-gluon and long-distance hadronic-loop amplitudes offers a compelling explanation for the long-standing “ $\rho\pi$  puzzle”, underscoring the critical role of nonperturbative charmed-meson loops in charmonium decays.

### 2.2.2. Large non- $D\bar{D}$ decays of $\psi(3770)$

The unexpectedly large non- $D\bar{D}$  decay rates observed for  $\psi(3770)$  indicate the presence of additional mechanisms. Among the possible explanations, the hadronic loop mechanism has been regarded as a plausible non-perturbative contribution capable of accounting for these anomalously large non- $D\bar{D}$  decay modes.

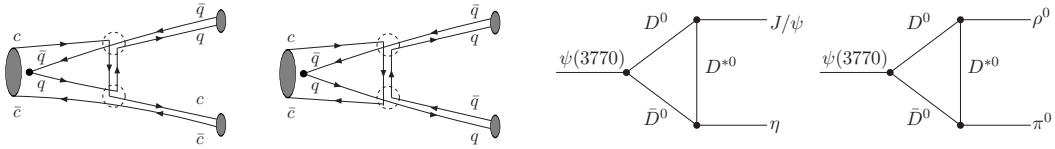


Figure 6: Quark- and hadron-level Feynman diagrams illustrating the hadronic loop transitions  $\psi(3770) \rightarrow J/\psi\eta$  and  $\psi(3770) \rightarrow \rho^0\pi^0$ . Figure adapted from Ref. [60].

The large non- $D\bar{D}$  decays of  $\psi(3770)$  include both hidden-charm and light-hadron (L–H) decay channels. The corresponding Feynman diagrams in the hadronic loop framework are shown in Fig. 6, with the left panel depicting the quark level and the right panel the hadron level. In this mechanism,  $\psi(3770)$  first couples to an intermediate pair of charmed mesons,  $D\bar{D}$ , which subsequently convert into the final states via a charmed meson exchange [60]. It should be noted that since the mass of  $\psi(3770)$  lies above the  $D\bar{D}$  threshold, the intermediate  $D\bar{D}$  pair can go on-shell and become real. Consequently, the hadronic loop effect in this case is also referred to as final-state interaction (FSI). The absorptive part of the decay amplitudes for  $\psi(3770) \rightarrow D(k_1) + \bar{D}(k_2) \rightarrow J/\psi(k_3) + \eta(k_4)$  and  $\psi(3770) \rightarrow D(k_1) + \bar{D}(k_2) \rightarrow \mathbb{V}(k_3) + \mathbb{P}(k_4)$  corresponding to Fig. 6 are given by [60]

$$\begin{aligned}
A_{J/\psi\eta} &= \mathcal{G}_{J/\psi\eta} \mathcal{Q}_{J/\psi\eta} \frac{|\mathbf{p}|}{32\pi^2 M_\psi} \int d\Omega \left[ i g_{\psi D\bar{D}}(k_1 - k_2) \cdot \epsilon_\psi \right] \left[ i g_{J/\psi D\bar{D}^*} \epsilon_{\kappa\xi\lambda\tau} \epsilon_{J/\psi}^{*\kappa} (-i k_1^\xi)(i q^\tau) \right] \left[ g_{D^* D \mathbb{P}}(i k_{4\mu}) \right] \\
&\times \frac{i}{q^2 - m_{D^*}^2} \left( -g^{\mu\lambda} + \frac{q^\mu q^\lambda}{m_{D^*}^2} \right) \mathcal{F}^2 \left[ m_{D^*}^2, q^2 \right], \tag{7}
\end{aligned}$$

and

$$\begin{aligned}
A_{\text{PV}} &= \mathcal{G}_{\text{PV}} Q_{\text{PV}} \frac{|\mathbf{p}|}{32\pi^2 M_\psi} \int d\Omega \left[ i g_{\psi D\bar{D}}(k_1 - k_2) \cdot \epsilon_\psi \right] \left[ -2i f_{D^* D\bar{V}} \epsilon_{\kappa\xi\tau\lambda} (i k_3^\kappa) \epsilon_V^{*\xi} (-ik_1^\tau - iq^\tau) \right] \left[ g_{D^* D\bar{P}}(i k_{4\mu}) \right] \\
&\times \left( -g^{\mu\lambda} + \frac{q^\mu q^\lambda}{m_{D^*}^2} \right) \frac{i}{q^2 - m_{D^*}^2} \mathcal{F}^2 \left[ m_{D^*}^2, q^2 \right], \tag{8}
\end{aligned}$$

respectively, where  $\mathcal{F}^2 \left[ m_{D^*}^2, q^2 \right]$  denotes the monopole form factor. The full decay amplitude is ultimately obtained via the dispersion relation technique [60, 156, 157, 158, 159, 160].

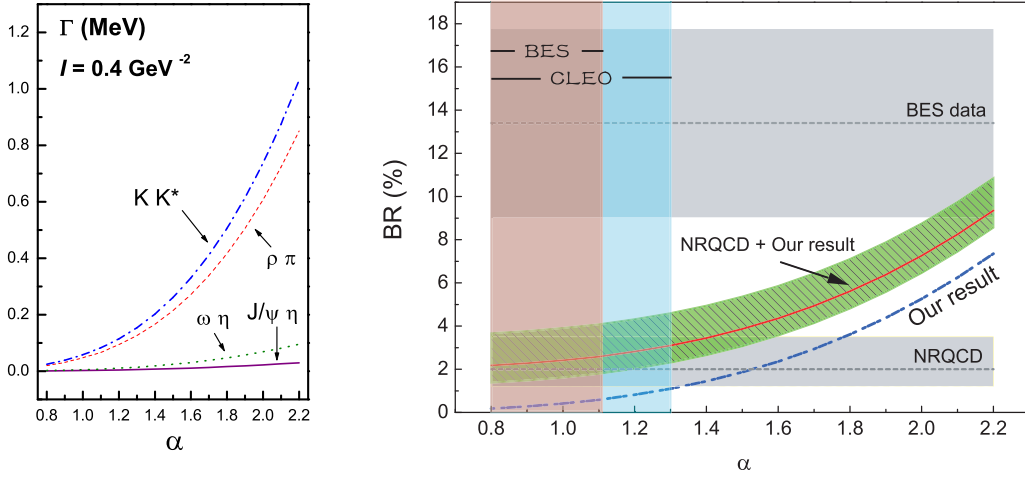


Figure 7: Left panel: The decay widths for the non- $D\bar{D}$  channels of  $\psi(3770)$  on the dependence of parameter  $\alpha$ . Right panel: a comparison of the branching ratios predicted by the hadronic loop mechanism (blue dash-dotted line) with the BES measurement of the excess non- $D\bar{D}$  component in inclusive  $\psi(3770)$  decays (dashed line with shaded band), as well as with the NRQCD prediction for  $\psi(3770) \rightarrow \rho\pi$  obtained via the color-octet mechanism and calculated up to next-to-leading order (dash-dotted line with shaded band) [125]. In the right panel, the red line with the green shaded band denotes the total prediction that includes both the NLO NRQCD contribution and the hadronic loop effect. The green band represents the uncertainty range estimated in Ref. [125]. The orange and light-blue shaded regions indicate the allowed ranges of  $\alpha$  inferred from the BES [161] and CLEO [162] measurements of  $\psi(3770) \rightarrow \rho\pi$ , respectively. Figure adapted from Ref. [60].

The  $\alpha$  parameter, introduced in the form factors, has been constrained to the ranges of  $0.8 < \alpha < 1.1$  and  $0.8 < \alpha < 1.3$ , based on the BES [161] and CLEO measurements [162] of  $BR(\psi(3770) \rightarrow \rho\pi)$ , respectively [60]. Within these ranges, the predicted branching fraction for  $\psi(3770) \rightarrow \text{non-}D\bar{D}$  arising from the hadronic loop mechanism is estimated to be  $\mathcal{B}_{\text{non-}D\bar{D}}^{\text{Hadronic Loop}} = (0.2\text{--}1.1)\%$ , as shown in Fig. 7. When combined with the NRQCD contribution, the total non- $D\bar{D}$  branching ratio can reach a maximum value of approximately 4.6%.

More comprehensive analyses has been presented, incorporating both the long-distance  $t$ -channel and  $s$ -channel hadronic loop contributions (see Fig. 8), together with the short-distance SOZI contribution [62] and EM contribution [61], to the decay processes of  $\psi(3770) \rightarrow VP$ . The total decay amplitude can be expressed as [62]

$$\mathcal{M}_{fi} = \mathcal{M}^L + e^{i\delta} \mathcal{M}^{\text{SOZI}} \equiv i \left( g_L + e^{i\delta} g_S \mathcal{F}_S(\vec{p}_V) \right) \epsilon_{\alpha\beta\mu\nu} P_\psi^\alpha \epsilon_\psi^\beta P_V^\mu \epsilon_V^{*\nu} / M_{\psi(3770)}. \tag{9}$$

Here, an exponential form factor,  $\mathcal{F}_S^2(\vec{p}_V) \equiv \exp(-\vec{p}_V^2/8\beta^2)$  with  $\beta = 0.5$  GeV, is applied to depicting the flavor-blind SOZI transition [163, 164, 61, 62]. The  $s$ -channel contributions are evaluated within the on-shell approximation, while the  $t$ -channel contributions follow similar treatment as in Ref. [60] discussed above, where the parameter  $\alpha$  is determined either by the measured branching ratio  $BR(\psi(3770) \rightarrow J/\psi\eta) = (9.0 \pm 4.0) \times 10^{-4}$  [165, 61, 62] or from the  $\psi(3686)$  decays [62].

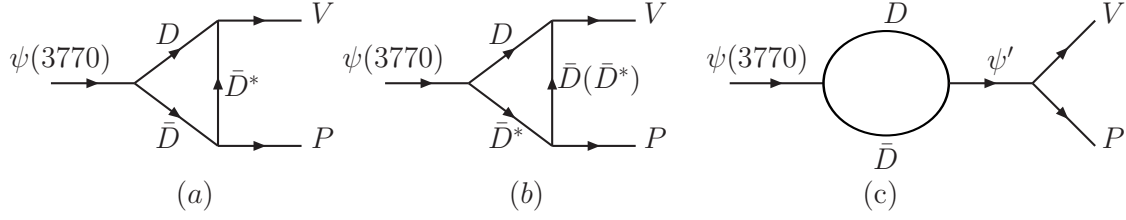


Figure 8:  $t$ -channel (a, b) and  $s$ -channel (c) hadronic loop of  $\psi(3770) \rightarrow VP$ . Figure adapted from Ref. [62].

Both Refs. [62] and [61] find that the  $t$ -channel transitions appear to play a dominant role in the  $\psi(3770) \rightarrow VP$  decays, whereas the  $s$ -channel and EM contributions are generally small and negligible. Ref. [62] obtained the total branching ratio of about 0.64% for all non- $D\bar{D}$   $VP$  channels of  $\psi(3770)$ , consistent with the result of (0.2–1.1)% calculated in Ref. [60]. In Ref. [61], the first scenario yields a total branching ratio in the range of (0.04–0.17)%, which is close to the results of Refs. [60, 62], while the second scenario leads to a substantially larger value of (3.38–5.23)%.

In summary, even with the inclusion of color-octet contributions, the NRQCD prediction for the branching ratio of  $\psi(3770) \rightarrow \text{non-}D\bar{D}$ , calculated up to next-to-leading order, still fails to reproduce the BES data [125], as shown in Fig. 7. The hadronic loop mechanism is expected to play an essential role. When the hadronic loop effects are incorporated, the discrepancy between theoretical predictions and experimental measurements is substantially reduced.

### 2.2.3. Anomalous transitions in high-lying heavy quarkonia

2.2.3.1.  $\chi_{c1} \rightarrow VV$ . The observations of  $\chi_{c1} \rightarrow VV$  processes [74, 75], which exhibit pronounced violations of the helicity selection rule [127, 128], together with the sizable discrepancies between the measured branching ratios of  $\chi_{c1} \rightarrow \gamma V$  [72, 73] and the corresponding pQCD predictions [133], provide compelling evidence for the presence of nonperturbative effects. As shown below, these issues can be naturally understood by incorporating the long-distance hadronic loop contributions.

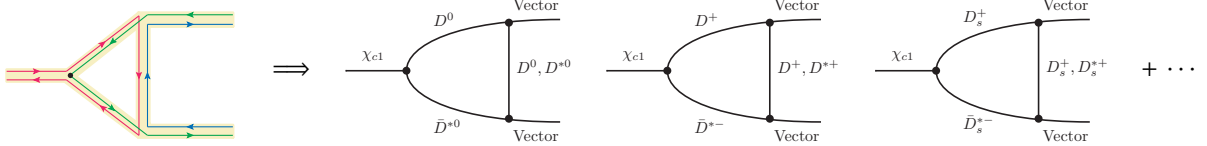


Figure 9: Hadronic loop contributions to  $\chi_{c1} \rightarrow VV$  at the quark and hadron levels. The ellipsis indicates additional hadron level diagrams obtained via the charge-conjugation operation  $D_{(s)}^{(*)} \rightleftharpoons \bar{D}_{(s)}^{(*)}$ . Figure adapted from Ref. [63]

The processes  $\chi_{c1} \rightarrow VV$  proceed via the hadronic loop mechanism as illustrated in Fig. 9,  $\chi_{c1}$  first dissociates into a pair of virtual charmed mesons,  $D_{(s)}\bar{D}_{(s)}^* + \text{H.c.}$ , through an  $S$ -wave coupling. The intermediate charmed mesons then transition into two on-shell light vector mesons by exchanging an appropriate charmed meson. Through this mechanism at long distance, the decays of  $\chi_{c1} \rightarrow VV$  can evade the helicity selection rule. In addition, an  $\omega$ - $\phi$  mixing scheme

$$\begin{pmatrix} |\phi^P\rangle \\ |\omega^P\rangle \end{pmatrix} = \begin{pmatrix} \cos\theta & \sin\theta \\ -\sin\theta & \cos\theta \end{pmatrix} \begin{pmatrix} |\phi^I\rangle \\ |\omega^I\rangle \end{pmatrix} \quad (10)$$

is introduced to prevent the DOZI amplitude of  $\chi_{c1} \rightarrow \omega\phi$  from vanishing. In this scheme,  $|\phi^P\rangle$  ( $|\omega^P\rangle$ ) and  $|\phi^I\rangle$  ( $|\omega^I\rangle$ ) denote the physical states and the ideally mixed states, respectively, and the mixing angle  $\theta = (3.4 \pm 0.2)^\circ$  is suggested [166, 167, 168, 63].

The amplitudes corresponding to pseudoscalar and vector charmed meson exchange, as depicted in Fig. 9, can be

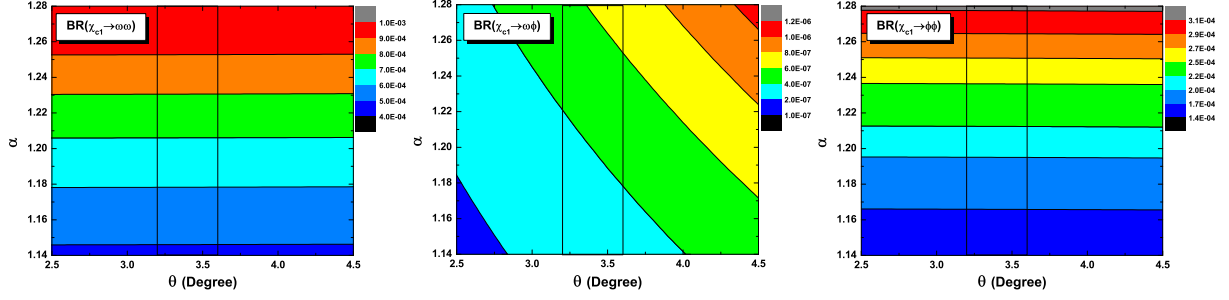


Figure 10: Contour plots showing the dependence of  $BR(\chi_{c1} \rightarrow \omega\omega)$ ,  $BR(\chi_{c1} \rightarrow \phi\phi)$ , and  $BR(\chi_{c1} \rightarrow \omega\phi)$  on the parameters  $\theta$  and  $\alpha$ . The region between the two vertical solid lines denotes the range allowed by the  $1\sigma$  uncertainty of the mixing angle  $\theta$ . The figure is adapted from Ref. [63].

written as [63]

$$\begin{aligned} \mathcal{M}^{(P)} = & \int \frac{d^4q}{(2\pi)^4} [ig_{\chi_{c1}\mathcal{D}\mathcal{D}^*}\epsilon_\sigma] [-ig_{\mathcal{D}\mathcal{D}^*V}(p_1+q) \cdot \epsilon_3^*] [2if_{\mathcal{D}^*\mathcal{D}^*V}\epsilon_{\mu\nu\alpha\beta}p_4^\mu\epsilon_4^{*\nu}(q^\alpha - p_2^\alpha)] \\ & \times \frac{i}{p_1^2 - m_{\mathcal{D}}^2} \frac{i}{p_2^2 - m_{\mathcal{D}^*}^2} \left( -g^{\sigma\beta} + \frac{p_2^\sigma p_2^\beta}{m_{\mathcal{D}^*}^2} \right) \frac{i}{q^2 - m_{\mathcal{D}}^2} \mathcal{F}^2(q^2, m_{\mathcal{D}}^2), \end{aligned} \quad (11)$$

and

$$\begin{aligned} \mathcal{M}^{(V)} = & \int \frac{d^4q}{(2\pi)^4} [ig_{\chi_{c1}\mathcal{D}\mathcal{D}^*}\epsilon_\sigma] [2if_{\mathcal{D}^*\mathcal{D}^*V}\epsilon_{\mu\nu\alpha\beta}p_3^\mu\epsilon_3^{*\nu}(p_1^\alpha + q^\alpha)] \\ & \times [ig_{\mathcal{D}^*\mathcal{D}^*V}(q-p_2) \cdot \epsilon_4^*g_{\lambda\kappa} - 4if_{\mathcal{D}^*\mathcal{D}^*V}(p_{4\kappa}\epsilon_{4\lambda}^* - p_{4\lambda}\epsilon_{4\kappa}^*)] \\ & \times \frac{i}{p_1^2 - m_{\mathcal{D}}^2} \frac{i}{p_2^2 - m_{\mathcal{D}^*}^2} \left( -g^{\sigma\kappa} + \frac{p_2^\sigma p_2^\kappa}{m_{\mathcal{D}^*}^2} \right) \frac{i}{q^2 - m_{\mathcal{D}^*}^2} \left( -g^{\beta\lambda} + \frac{q^\beta q^\lambda}{m_{\mathcal{D}^*}^2} \right) \mathcal{F}^2(q^2, m_{\mathcal{D}^*}^2), \end{aligned} \quad (12)$$

respectively, in which the dipole form factor  $\mathcal{F}^2(q^2, m_E^2)$  is adopted. The  $\alpha$  parameter introduced in the form factor is constrained into the range of  $\alpha = 1.14 \sim 1.28$ , by reproducing the measured branching ratio of  $BR[\chi_{c1} \rightarrow K^{*0}\bar{K}^{*0}] = (1.67 \pm 0.32 \pm 0.31) \times 10^{-3}$  [74]. With this constraint, the branching ratios for  $\chi_{c1} \rightarrow \omega\omega$ ,  $\phi\phi$ , and  $\omega\phi$  can be predicted. The results are summarized in Table 3, along with the subsequently measured decay branching ratios. The dependence of the calculated branching ratios on the parameter  $\alpha$  and the  $\omega$ - $\phi$  mixing angle  $\theta$  is illustrated in Fig. 10.

Table 3: Predicted ranges of the branching ratios for  $\chi_{c1} \rightarrow VV$  within the hadronic loop framework in Refs. [63] and [64], shown together with the subsequently measured decay branching ratios.

Channel	Ref. [63]	Ref. [64]	Experimental value
$K^{*0}\bar{K}^{*0}$	$(1.1 \sim 2.3) \times 10^{-3}$	$(1.2 \sim 2.0) \times 10^{-3}$	$(1.67 \pm 0.32 \pm 0.31) \times 10^{-3}$ [74]
$\chi_{c1} \rightarrow VV$			
$\omega\omega$	$(4.8 \sim 10.4) \times 10^{-4}$	$(8.7 \sim 18.0) \times 10^{-4}$	$(6.0 \pm 0.3 \pm 0.7) \times 10^{-4}$ [75]
$\phi\phi$	$(1.5 \sim 3.2) \times 10^{-4}$	$(2.7 \sim 4.6) \times 10^{-4}$	$(4.4 \pm 0.3 \pm 0.5) \times 10^{-4}$ [75]
$\omega\phi$	$(2.5 \sim 6.9) \times 10^{-7}$	...	$(2.2 \pm 0.6 \pm 0.2) \times 10^{-5}$ [75]
$\rho\rho$	...	$(2.6 \sim 5.4) \times 10^{-3}$	...
$K^{*0}\bar{K}^0 + \text{c.c.}$	...	$(4.0 \sim 6.7) \times 10^{-5}$	...
$\chi_{c2} \rightarrow VP$			
$K^{*+}K^- + \text{c.c.}$	...	$(4.0 \sim 6.7) \times 10^{-5}$	...
$\rho^+\pi^- + \text{c.c.}$	...	$(1.2 \sim 2.0) \times 10^{-7}$	...

Ref. [64] also studies the  $\chi_{c1} \rightarrow VV$  channels, and in addition, presents an analysis of the  $\chi_{c2} \rightarrow VP$  decays (see these diagrams in Fig. 11), both of them violate the helicity selection rule. The calculations employ procedures similar to those of Ref. [63] discussed above, and the corresponding numerical results are summarized in Table 3.

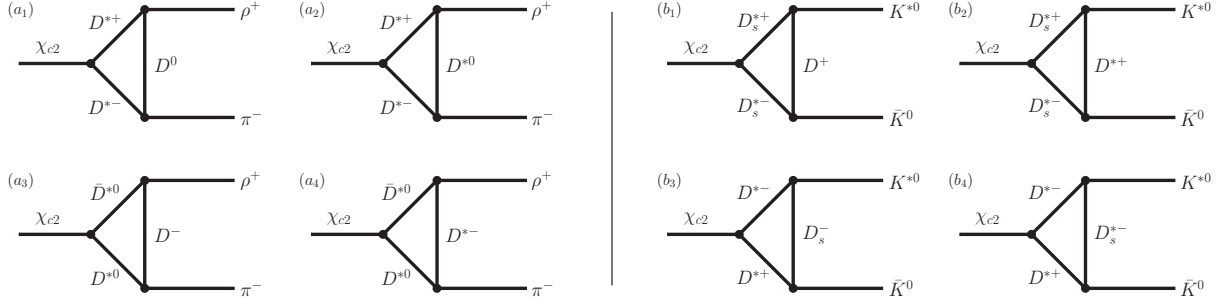


Figure 11: Hadronic loop diagrams illustrating the long-distance contributions of  $\chi_{c2} \rightarrow \rho^+ \pi^-$  (left panel) and  $K^{*0} \bar{K}^0$  (right panel) as studied in Ref. [64]. The diagrams for  $\chi_{c2} \rightarrow \rho^- \pi^+$  and  $\bar{K}^{*0} K^0$  are implicated.

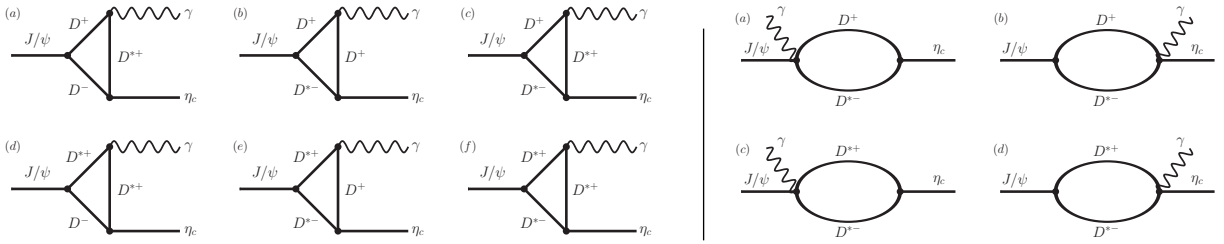


Figure 12: Feynman diagrams for the  $J/\psi \rightarrow \gamma \eta_c$  process in the hadronic loop mechanism. The left panel shows the triangle diagram contributions, while the right panel shows the contact terms. Similar diagrams also occur in  $\psi' \rightarrow \gamma \eta_c$  and  $\gamma \eta_c'$  [170].

From Table 3, we see that the predicted branching ratios for  $\chi_{c1} \rightarrow \omega \omega$  and  $\chi_{c1} \rightarrow \phi \phi$  in Refs. [63, 64] are close, and both are comparable to the subsequently measured values. This indicates that the long-distance hadronic loop mechanism provides a reasonable explanation for the evasion of the helicity selection rule. Furthermore, the  $\omega$ - $\phi$  mixing scheme may offer a possible source for the DOZI forbidden process  $\chi_{c1} \rightarrow \omega \phi$ , as the corresponding branching ratio increases rapidly with the mixing angle  $\theta$ , as shown in Fig. 10. However, with the currently adopted value  $\theta = (3.4 \pm 0.2)^\circ$  [63], the calculated branching ratio remains about two orders of magnitude smaller than the experimental measurement, suggesting that further investigation is required. The predicted branching ratio for  $\chi_{c2} \rightarrow K^* \bar{K} + \text{c.c.}$  is at the level of  $10^{-5}$ , indicating that this decay mode may be observable in future experiments.

**2.2.3.2. Radiative decays.** In Refs. [169, 170], Li and Zhao showed that hadronic loop effects provide explicit corrections to the M1 transition amplitudes. Their interference with the conventional M1 amplitudes can naturally explain the discrepancies between the GI model predictions and the experimental measurements for the  $J/\psi$  and  $\psi' \rightarrow \gamma \eta_c$  transitions. The total amplitude can be parameterized as [170]

$$\mathcal{M}_{fi} = (g_{V\gamma P} + \tilde{g}_{tri} e^{i\delta}) \epsilon_{\alpha\beta\mu\nu} p_\gamma^\alpha \epsilon_\gamma^\beta p_i^\mu \epsilon_i^\nu, \quad (13)$$

where the first term represents the M1 transition amplitude, while the second denotes the charm-meson loop contributions. In Ref. [170], a destructive phase  $\delta = \pi$  is adopted, since the M1 transition amplitude in the quenched quark model has overestimated the experimental data.

The concrete diagrams for  $J/\psi \rightarrow \gamma \eta_c$  and  $\psi' \rightarrow \gamma \eta_c^{(\prime)}$  via hadronic loops are shown in Fig. 12. As discussed in Ref. [170], the contact diagrams (right panel of Fig. 12) do not contribute to the transition matrix elements in the effective Lagrangian approach. Therefore, it is sufficient to concentrate on the triangle diagrams (left panel of Fig. 12).

The explicit transition amplitude for the first triangle diagram shown in the left panel of Fig. 12 can be written as

$$\mathcal{M}_T^{(a)} = (i^3) \int \frac{d^4 p_2}{(2\pi)^4} [g_{\psi DD} \epsilon_\psi^\rho (p_{1\rho} - p_{3\rho})] [-g_{\eta_c D^* D} (p_{f\sigma} + p_{3\sigma})] [-e_{GD^* D \gamma} \epsilon_{\alpha\beta\mu\nu} p_\gamma^\alpha \epsilon_\gamma^{*\beta} p_2^\mu] \quad (14)$$

$$\times \frac{i}{p_1^2 - m_1^2} \frac{i(-g^{\nu\sigma} + p_2^\nu p_2^\sigma / m_2^2)}{p_2^2 - m_2^2} \frac{i}{p_3^2 - m_3^2} \mathcal{F}(m_2, p_2^2), \quad (15)$$

where  $\mathcal{F}(m_2, p_2^2)$  is the dipole form factor. The amplitudes for the remaining triangle diagrams can be obtained analogously.

With the destructive phase  $\delta = \pi$ , the parameter  $\alpha = 0.98 \pm 0.27$  [170] is fixed by combining the GI model result [132] with the hadronic loop mechanism so as to reproduce the experimental partial width  $\Gamma_{\text{exp}}(J/\psi \rightarrow \gamma\eta_c) = (1.58 \pm 0.37) \text{ keV}$  [171]. The same values of  $\alpha$  and  $\delta$  are subsequently used to predict the partial widths of  $\psi' \rightarrow \gamma\eta_c$  and  $\psi(3770) \rightarrow \gamma\eta_c$  and  $\gamma\eta'_c$ , as shown in Table 4.

Table 4: Radiative partial decay widths from different mechanisms.  $\Gamma_{\text{M1}}^{\text{NR}}$  and  $\Gamma_{\text{M1}}^{\text{GI}}$  denote the M1 transition widths obtained in the NR and GI quark models, respectively [132].  $\Gamma_{\text{IML}}$  represents the contributions from the intermediate meson loop (IML) transitions shown in Fig. 12, while  $\Gamma_{\text{all}}$  denotes the coherent results including both the M1 transition amplitude from GI model and the IML contributions. The experimental values are taken from the PDG [171] and the measurements reported by the BESIII [172] and CLEO [173] Collaborations. The LQCD results are also listed for comparison [174]. The Table is adapted from Ref. [170].

Initial meson	$J/\psi(1^3S_1)$	$\psi'(2^3S_1)$		$\psi''(1^3D_1)$	
Final meson	$\eta_c(1^1S_0)$	$\eta'_c(2^1S_0)$	$\eta_c(1^1S_0)$	$\eta'_c(2^1S_0)$	$\eta_c(1^1S_0)$
$\Gamma_{\text{M1}}^{\text{NR}}$ (keV)	2.9	0.21	9.7	...	...
$\Gamma_{\text{M1}}^{\text{GI}}$ (keV)	2.4	0.17	9.6	...	...
$\Gamma_{\text{IML}}$ (keV)	$0.08^{+0.13}_{-0.06}$	$0.02^{+0.02}_{-0.01}$	$2.78^{+5.73}_{-1.96}$	$1.82^{+1.95}_{-1.19}$	$17.14^{+22.93}_{-12.03}$
$\Gamma_{\text{all}}$ (keV)	$1.58^{+0.37}_{-0.37}$	$0.08^{+0.03}_{-0.03}$	$2.05^{+2.65}_{-1.75}$	$1.82^{+1.95}_{-1.19}$	$17.14^{+22.93}_{-12.03}$
$\Gamma_{\text{exp}}$ (keV)	$1.58 \pm 0.37$ [171]	$0.143 \pm 0.027 \pm 0.092$ [172]	$0.97 \pm 0.14$ [173]	...	...
$\Gamma_{\text{LQCD}}$ (keV)	$2.51 \pm 0.08$	...	$0.4 \pm 0.8$	...	$10 \pm 11$

As shown in Table 4, the inclusion of unquenched hadronic loop contributions, which destructively interfere with the M1 amplitude, effectively suppresses the M1 transition strength. Consequently, the predicted partial widths for  $\psi' \rightarrow \gamma\eta_c$  ( $\gamma\eta'_c$ ) are consistent with the experimental measurements. Moreover, the hadronic loop effects in  $\psi' \rightarrow \gamma\eta_c$  ( $\gamma\eta'_c$ ) are much more significant than those in  $J/\psi \rightarrow \gamma\eta_c$  and become comparable to the M1 contributions. This behavior highlights the necessity of the unquenched quark model scenario, especially for transitions occurring near open-charm thresholds.

Furthermore, the hadronic loop contributions to the  $\psi(3770) \rightarrow \gamma\eta_c$  ( $\gamma\eta'_c$ ) transitions are predicted to be of the same order of magnitude as the quenched LQCD result [174]. This suggests that the interference between the quenched and unquenched amplitudes may play an important role in the  $\psi(3770)$  radiative decays. Such an interplay is closely related to the non- $D\bar{D}$  decays of  $\psi(3770)$ .

For the radiative decays  $\chi_{c1} \rightarrow \gamma V$ , the typical quark-level and hadron-level Feynman diagrams within the hadronic loop mechanism are illustrated in Fig. 13. The transition element can be written as [65]

$$\mathcal{M}[\chi_{c1} \rightarrow \gamma V] = \sum_i \langle \gamma V | \mathcal{H}^{(2)} | i \rangle \langle i | \mathcal{H}^{(1)} | \chi_{c1} \rangle, \quad (16)$$

in which  $\mathcal{H}^{(1)}$  denotes the interaction between  $\chi_{c1}$  and  $D\bar{D}^* + \text{H.c.}$ , while  $\mathcal{H}^{(2)}$  describes the transition  $D\bar{D}^* + \text{H.c.} \rightarrow \gamma V$  mediated by the exchange of an appropriate charmed meson.

In Fig. 14, the  $\alpha$ -dependence of the branching ratios for  $\chi_{c1} \rightarrow \gamma\rho^0, \gamma\omega, \gamma\phi$  are presented. For comparison with the experimental measurements [72], the theoretical predictions shown here include both the hadronic loop contributions obtained in Ref. [65] and the pQCD estimation calculated in Ref. [133].

As shown in Fig. 14, an overlap exists between the numerical results obtained in Ref. [64] and the experimental data reported by CLEO. The corresponding  $\alpha$  ranges for  $\chi_{c1} \rightarrow \gamma\rho^0, \gamma\omega, \gamma\phi$  are  $2.18 < \alpha < 2.35, 2.06 < \alpha < 2.28,$  and  $1.16 < \alpha < 2.77,$  respectively, all of which lie within a reasonable parameter space. Notably, a common  $\alpha$  range of  $2.18 < \alpha < 2.28$  is found for all three radiative decay channels. Thus, the hadronic loop mechanism can serve as the underlying source that reduces the discrepancy between the pQCD calculations and the experimental measurements for  $\chi_{c1} \rightarrow \gamma V$ .

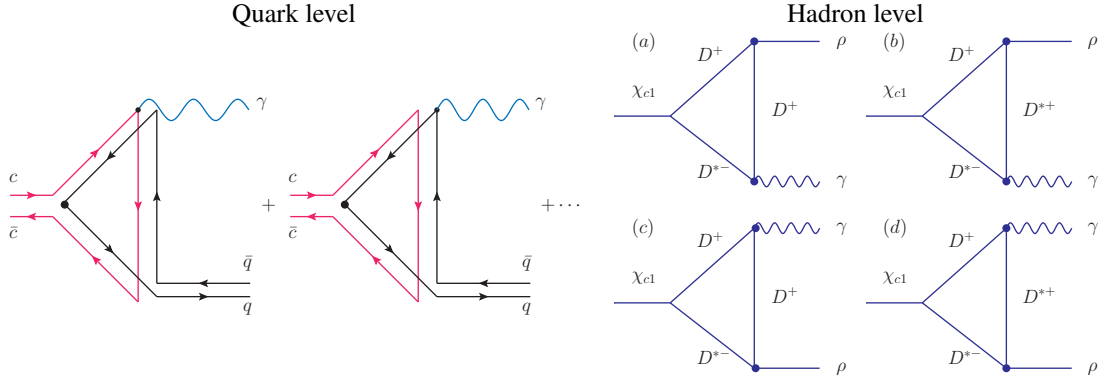


Figure 13: The left panel shows the typical quark level diagrams that describe the hadronic loop contributions to the processes  $\chi_{c1} \rightarrow \gamma V$ , while the right panel illustrates the corresponding hadronic level schematic diagram for  $\chi_{c1} \rightarrow \gamma \rho^0$ . The red and black lines represent the charm and light quarks, respectively. The photon can be emitted either from the charm-quark line or from the light-quark line. By applying the charge-conjugation transformation  $D^{(*)+} \rightleftharpoons D^{(*)0}$  and  $D^{(*)-} \rightleftharpoons \bar{D}^{(*)0}$ , the rest two diagrams for  $\chi_{c1} \rightarrow D\bar{D}^* + \text{H.c.} \rightarrow \gamma \rho^0$  can be obtained from diagrams (a) and (d). Figure adapted from Ref. [65].

Chen, Liu, and Matsuki have emphasized that hadronic loop effects also play a significant role in the radiative transitions  $h_b(nP) \rightarrow \gamma \eta_b(mS)$  ( $n, m = 1, 2$ ) in the bottomonium sector [175]. Their results indicate that the contributions from hadronic loops can naturally account for the discrepancies between experimental measurements [134] and earlier quenched theoretical predictions [135].

In summary, the long-distance hadronic loop mechanism provides a natural explanation for processes that violate the helicity selection rule, such as  $\chi_{c1} \rightarrow VV$ , and reconciles the significant discrepancies between quenched theoretical predictions and experimental measurements in several radiative transitions, including  $J/\psi(\psi') \rightarrow \gamma \eta_c(\gamma \eta'_c)$ ,  $\chi_{c1} \rightarrow \gamma V$ , and  $h_b(nP) \rightarrow \gamma \eta_b(mS)$ . Experimental searches for promising channels, such as  $\chi_{c2} \rightarrow K^* \bar{K} + \text{c.c.}$  and  $\psi(3770) \rightarrow \gamma \eta_c(\gamma \eta'_c)$ , would be particularly valuable for confirming the presence of this mechanism.

### 2.3. Other applications of hadronic loop mechanism

Based on the preceding analysis, the introduction of a hadronic loop composed of charm mesons can effectively link the initial charmonium state with the final-state particles, providing an explanation for the anomalous charmonium decay phenomena observed experimentally. This mechanism clearly reflects the unquenched effect, whereby the initial charmonium couples to a charm meson pair following the OZI rule—a typical manifestation of coupled-channel dynamics.

In heavy-flavor physics, the decays of  $B$  mesons have drawn considerable interest. While the pQCD factorization framework offers a valuable approach, it remains applicable only to certain typical processes and exhibits notable limitations [176, 177, 178, 179, 180, 181, 182, 183, 184, 185]. Consequently, achieving quantitative descriptions of a broader range of  $B$ -meson decay modes continues to pose a significant challenge.

To address such challenges, alternative non-perturbative mechanisms such as final-state interactions (FSI) have been introduced. As discussed in Ref. [186, 187, 188], the FSI mechanism can be employed to study  $B$ -meson decays. In this approach, one first identifies experimentally well-measured main decay channels of the  $B$  meson to constrain the weak interaction vertex. The resulting on-shell intermediate mesonic states then rescatter via strong interactions into the observed final state. It is worth noting that, while both the FSI and the hadronic loop mechanisms utilize hadronic loops to connect initial and final configurations, their physical origins differ: the hadronic loop mechanism emerges from intrinsic coupled-channel effects, whereas FSI describes post-weak-decay rescattering.

In recent years, the FSI framework has found broad application—for example, in exploring additional sources of  $CP$  violation in  $B_c$  meson decays [189], investigating  $D$  meson decays and related  $CP$  puzzles [190, 191, 192, 193, 194, 195, 196, 197], analyzing  $\Lambda_c$  decays [198, 199, 200], studying dominant decay processes and  $CP$  violation in  $\Lambda_b$  decays [201, 202, 203], and assisting in the identification of the double-charm baryon  $\Xi_{cc}(3620)$  [204, 205, 206, 207, 208].

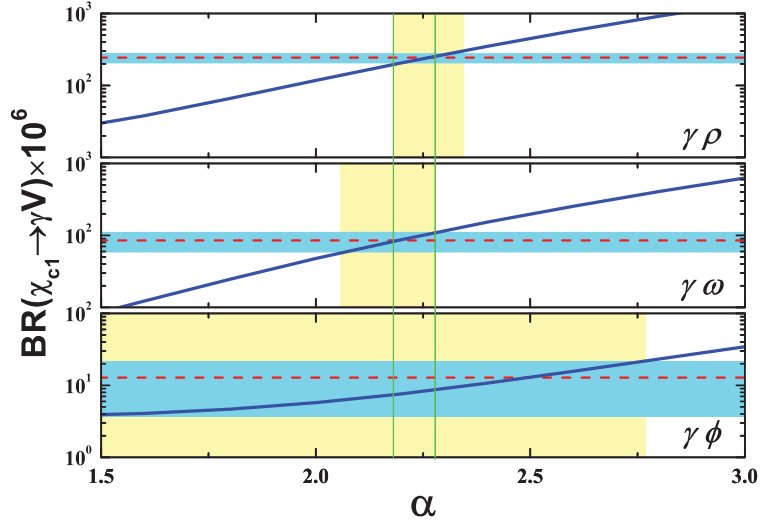


Figure 14: The branching ratios of  $\chi_{c1} \rightarrow \gamma\rho^0, \gamma\omega, \gamma\phi$  as functions of the parameter  $\alpha$ . The red dashed lines with blue bands represent the experimental measurements [72], while the blue solid curves denote the theoretical predictions incorporating both the hadronic loop contribution and the pQCD calculation [133]. The vertical yellow bands indicate the regions where the theoretical results overlap with the corresponding experimental data. Within the same  $\alpha$  interval marked by the two green vertical lines, the obtained branching ratios are consistent with the measurements.

Notably, FSI has also been applied to charmonium(-like) production in  $B$ -meson decays (see Refs. [186, 187, 209, 210, 211]), including processes such as  $B \rightarrow K + \chi_{cJ}$ . In these cases, the initial  $B$  meson decays via the weak interaction into a charmed meson pair, which then transforms into a final-state charmonium and a kaon through charm meson exchange. This transition is facilitated by the coupled-channel mechanism linking the charmonium to charmed mesons. It is important to emphasize that, within the conventional pQCD factorization approach, decays of the type  $B \rightarrow \text{charmonium} + K$  are forbidden; however, the inclusion of hadronic loop or FSI mechanisms renders such processes viable.

Additionally, the hadronic loop mechanism has also been applied in the past two decades to study the strong decays of the observed charmonium-like  $XYZ$  states [212, 213, 214, 215, 216, 217, 218, 219, 220, 221, 222, 223, 224, 225, 226, 227, 228, 229, 230, 231, 232, 233, 234, 235, 236, 237, 238, 239, 126, 240], shedding light on their properties.

### 3. Low-mass puzzle of $X(3872)$ and the construction of $2P$ charmonia

#### 3.1. Low-mass puzzle in new hadronic states

Since 2003, with the accumulation of experimental data, an increasing number of new hadronic states have been reported. Thus, 2003 marks a renaissance in hadron spectroscopy. Interested readers may consult the review articles [241, 16, 242, 19, 17, 18, 21, 22, 23, 24, 243, 26, 27, 244, 245, 28, 29, 246, 247, 248] for further details. These abundant observations have not only stimulated extensive discussions on exotic hadronic states, including multi-quark configurations, but also provided opportunities to refine existing theoretical models and frameworks. Over the past two decades, we have witnessed these new advances.

Among these newly observed hadronic states, several typical states—such as  $D_{s0}^*(2317)$ ,  $D'_{s1}(2460)$ ,  $X(3872)$ , and  $\Lambda_c(2940)$ —have attracted widespread attentions within the research community due to the emergence of a low-mass puzzle associated with their properties. In the following, we first introduce their experimental observations individually, and then summarize the nature of this low-mass puzzle:

- $D_{s0}^*(2317)$  and  $D'_{s1}(2460)$ : In 2003, the BaBar Collaboration observed a new charmed-strange state,  $D_{s0}^*(2317)$ , in the  $D_s^+\pi^0$  channel [33]. Its mass was measured to be  $m = 2316.8 \pm 0.4$  MeV for  $D_s^+ \rightarrow K^+K^-\pi^+$  and

$m = 2317.6 \pm 1.3$  MeV for  $D_s^+ \rightarrow K^+ K^- \pi^+ \pi^0$ , and the width was measured as  $\Gamma \lesssim 10$  MeV. Subsequent experiments, including those by the CLEO, Belle, BESIII, and BaBar collaborations, confirmed its existence [249, 250, 34, 251, 252, 253]. If  $D_{s0}^*(2317)$  is classified within the charmed-strange meson family, a significant discrepancy arises: its mass is approximately 180 MeV lower than the prediction of quenched models such as the GI model [13]. This discrepancy provides the main motivation for introducing exotic multi-quark interpretations [254, 255, 256, 257, 258, 259, 260, 261, 262].

Later, the CLEO Collaboration also reported a new charmed-strange state,  $D_{s1}'(2460)$ , in the  $D_s^{*+} \pi^0$  channel, with mass and width  $m = 2463.4 \pm 1.7(\text{stat}) \pm 1.0(\text{syst})$  MeV and  $\Gamma < 7$  MeV at 90% C.L. [34]. A similar low-mass phenomenon also exists for this state, as its mass is about 80 MeV below the prediction of the GI model [13], a representative quenched approach.

- $X(3872)$ : Here, we introduce the charmonium-like state  $X(3872)$ , a prominent figure among the newly observed hadronic states. The Belle Collaboration first observed  $X(3872)$  in the  $J/\psi \pi^+ \pi^-$  channel of the decay  $B \rightarrow K J/\psi \pi^+ \pi^-$  [32]. The measured mass and width are  $m = 3872.0 \pm 0.6(\text{stat}) \pm 0.5(\text{syst})$  MeV and  $\Gamma < 2.3$  MeV at 90% C.L., respectively. A clear discrepancy exists between the mass of  $X(3872)$  and the theoretical prediction for the charmonium state  $\chi_{c1}(2P)$  from Ref. [13], i.e., the experimental mass is about 80 MeV below the calculation in Ref. [13], presenting another instance of the low-mass puzzle.

Given that  $X(3872)$  lies very close to the  $D\bar{D}^*$  threshold, a hadronic molecular interpretation has been proposed to resolve this discrepancy [263, 264, 265, 266, 267, 268, 269, 270, 271, 272, 273, 274, 275, 276]. In the following section, we will illustrate how coupled-channel effects—a characteristic unquenched mechanism—play a crucial role in addressing this issue.

- $\Lambda_c(2940)$ : Besides the mesonic states mentioned above, the low-mass puzzle also occurs in the baryonic sector, as exemplified by  $\Lambda_c(2940)$ . This state was first reported by the BaBar Collaboration in the  $D^0 p$  channel [35] and later confirmed by the Belle Collaboration via the  $\Sigma_c(2455)\pi$  invariant mass spectrum [277]. In 2017, the LHCb Collaboration further analyzed  $\Lambda_c(2940)$  in the decay  $\Lambda_b^0 \rightarrow D^0 p \pi^-$  and suggested its most likely spin-parity to be  $3/2^-$  [278]. If it is interpreted as a conventional charm baryon, the mass of  $\Lambda_c(2940)$  is about 60–100 MeV lower than the values predicted by theoretical studies [279, 280, 281, 282, 283, 284, 285].
- In fact, this low-mass puzzle phenomenon extends across multiple systems, including heavy-light mesons, heavy quarkonia, and singly heavy-flavor baryons. Turning to the spectroscopy of light-flavor hadrons, we note that  $\Lambda(1405)$  also exhibits a low-mass phenomenon [36].

In Figs. 15-16, we compare the experimental masses with theoretical results of  $D_{s0}^*(2317)$ ,  $D_{s1}'(2460)$ ,  $X(3872)$ , and  $\Lambda_c(2940)$ .

The low-mass puzzle represents a recurring phenomenon observed in several newly discovered hadronic states. When these states are interpreted within the conventional hadron spectrum, a significant challenge arises: their masses cannot be adequately reproduced by quenched quark models. This discrepancy appears to be systematic, affecting multiple hadronic systems.

In response to this novel phenomenological pattern, new theoretical approaches have been developed. Broadly, two main interpretive directions have been pursued:

1. **Exotic state explanations**—such as compact multi-quark configurations or hadronic molecular structures. This interpretation is particularly motivated by the proximity of states like  $D_{s0}^*(2317)$ ,  $D_{s1}'(2460)$ ,  $X(3872)$ , and  $\Lambda_c(2940)$  to the respective thresholds of  $DK$ ,  $D^*K$ ,  $D\bar{D}^*$ , and  $D^*N$ , which aligns with expectations for molecular systems (see reviews [241, 16, 242, 19, 17, 18, 21, 22, 23, 24, 243, 26, 27, 244, 245, 28, 29, 246, 247, 248]).
2. **Corrections within the conventional quark model**—especially through coupled-channel effects. Studies on  $\Lambda(1405)$ ,  $a_0(980)$ , and  $f_0(980)$  have demonstrated that incorporating channel coupling via self-energy loops can lower theoretical masses to match experimental values [36, 302, 303]. Notably, when a state lies near an  $S$ -wave threshold, such loop corrections become substantial and cannot be simply absorbed into potential model parameters.

While earlier work suggested that such loop effects are generally negligible in most systems [144, 148, 138, 11, 12], they become crucial for states close to relevant thresholds. In the past, limited experimental data restricted such

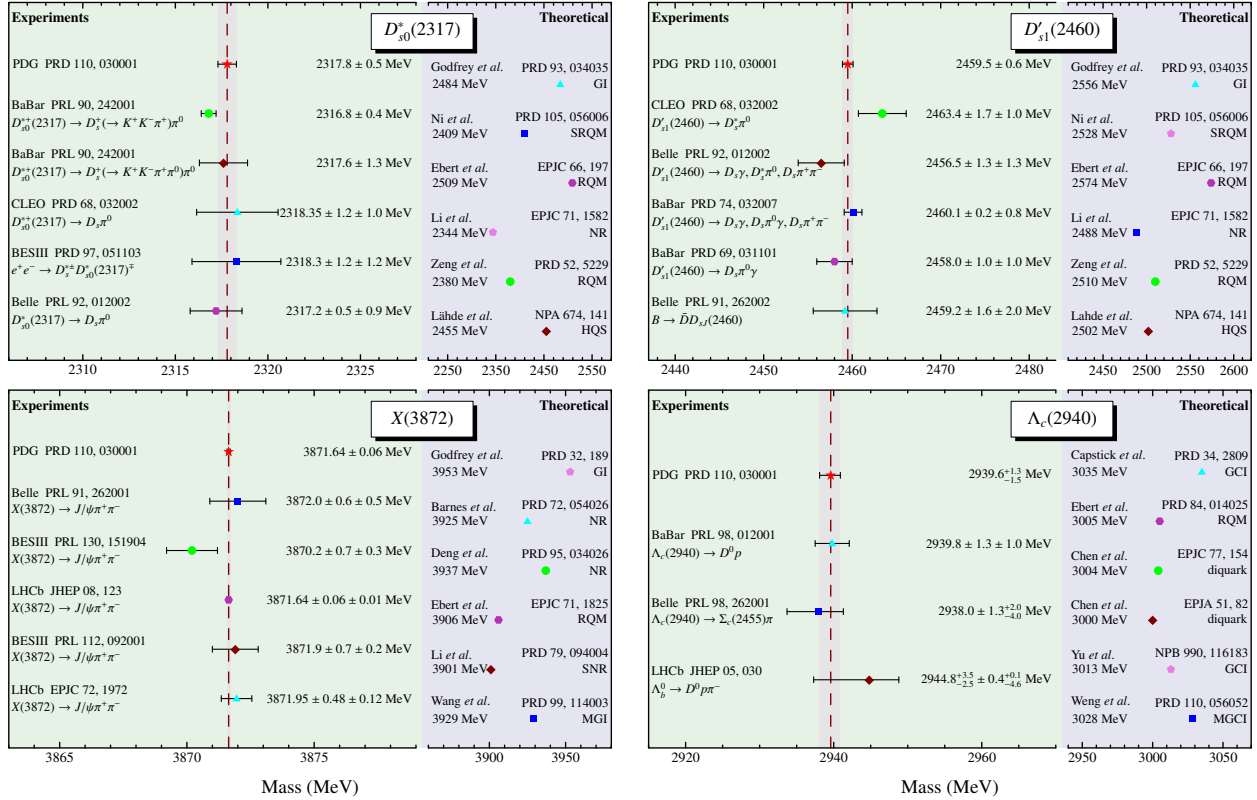


Figure 15: The comparison between experimental and theoretical masses is shown in each subfigure. The experimental values are positioned on the left, and the theoretical values on the right. The experimental data are taken from Refs. [94, 33, 34, 252, 251, 34, 251, 250, 286, 249, 32, 287, 288, 289, 290, 35, 277, 278], while the theoretical results are from Refs. [291, 292, 293, 294, 295, 296, 13, 132, 297, 298, 299, 300, 279, 281, 283, 282, 285, 301]. The GI, SRQM, RQM, NR, GCI, HQS, SNR, MGI, MGCI, and 'diquark' imply the theoretical methods of Godfrey-Isgur model, semi-relativistic quark model, relativistic quark model, non-relativistic quark model, Godfrey-Capstick-Isgur model, heavy quark symmetry, screened non-relativistic quark model, modified (screened) Godfrey-Isgur model, modified (screened) Godfrey-Capstick-Isgur model, and diquark model, respectively.

analyses to only a few candidates. However, the discovery of  $X(3872)$  and numerous other new hadronic states in recent years has provided renewed impetus to systematically study these unquenched dynamics, offering a clearer window into how open-channel effects reshape hadron spectroscopy.

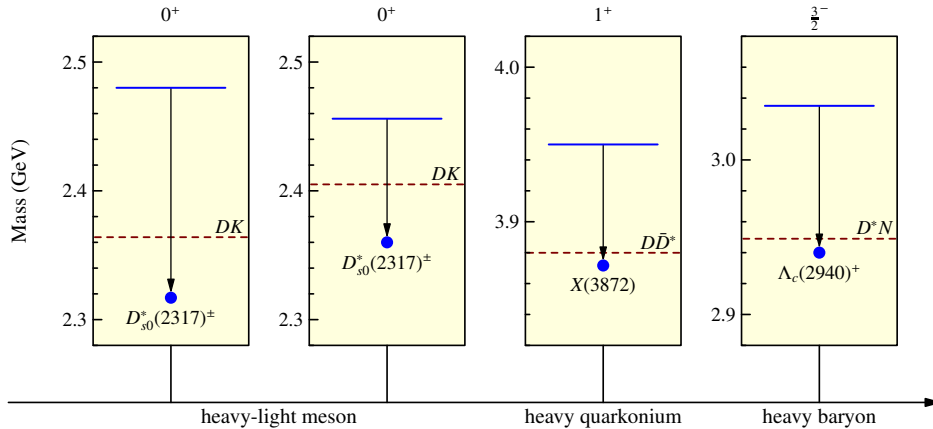


Figure 16: The low-mass puzzle for selected hadrons. This figure is updated from Ref. [45]. The theoretical masses (shown as solid blue lines) are taken from Refs. [291, 13, 279]. The blue points represent experimental results from Ref. [94]. The dashed lines indicate the thresholds of the relevant decay channels.

### 3.2. The role of coupled-channel effects in alleviating the $X(3872)$ low-mass puzzle

In the study of  $D_{s0}^*(2317)$ , van Beveren and Rupp found that the  $c\bar{s}$  configuration can strongly couple to the OZI-allowed  $S$ -wave  $DK$  channel [37]. Simonov and Tjon proposed that the mass of a  $P$ -wave  $c\bar{s}$  state could be lowered via coupling to the  $DK$  channel [304]. Ortega *et al.* used a coupled-channel framework to analyze the mixing between the  $c\bar{s}(0^+)$  core and a  $DK$  channel for  $D_{s0}^*(2317)$ , as well as  $c\bar{s}(1^+)$ - $D^*K$  for  $D'_{s1}(2460)$ , showing that such core-meson-meson mixing can significantly alter the properties of these states [305]. Cheng and Yu calculated the self-energy modifications for charm-strange and bottom-strange systems within heavy meson chiral perturbation theory (HMChPT) [306, 307]. In Ref. [308], Dai *et al.* interpreted  $D_{s0}^*(2317)$  and  $D'_{s1}(2460)$  with sum rules in heavy quark effective theory. The results implied that  $D_{s0}^*(2317)$  and  $D'_{s1}(2460)$  could be included in  $j_\ell = \frac{1}{2}$  doublets with  $0^+$  and  $1^+$ , respectively.

Alongside the  $D_{s0}^*(2317)$  and  $D'_{s1}(2460)$  states,  $X(3872)$  provides another prominent example of the critical role played by coupled-channel effects. In 2005, Kalashnikova applied the coupled-channel approach to charmonium and identified a mechanism that generates a structure at the  $D\bar{D}^*$  threshold, crucial for interpreting  $X(3872)$  [39]. Barnes and Swanson established general theorems for the unquenched quark model in charmonium [309]. They found that for low-lying  $c\bar{c}$  states, the mass shifts induced by hadron loops are identical within a given  $NL$  multiplet. Although these shifts are sizable, they can be absorbed into the parameters of potential models. A similar conclusion was reached in  $b\bar{b}$  systems [310]. The method has since been extended to bottomonium with more refined potential models, wave functions, and inclusion of higher excited states [311, 312, 313, 314, 315, 316]. Ortega *et al.* performed a coupled-channel calculation for the  $1^{++}$   $c\bar{c}$ - $D\bar{D}^*$  system, successfully explaining the mass of  $X(3872)$  and indicating a large  $D\bar{D}^*$  component in its wave function [42, 317]. This interpretation was supported by Ferretti, who also emphasized the important role of the  $D\bar{D}^*$  continuum [318].

Pennington and Wilson developed subtracted dispersion relations to handle meson loops [159], a technique later adopted in several works [319, 320, 321, 322, 323, 324]. Danilkin and Simonov demonstrated within a coupled-channel framework that  $X(3872)$  emerges from the charmonium  $2^3P_1$  state, whose pole is shifted to the  $D\bar{D}^*$  threshold by strong coupling to open-charm channels, thereby accounting for its narrow width and precise threshold location [325, 43]. Li *et al.* compared coupled-channel and screening effects, finding that while both give consistent results for some excited states, the coupled-channel effect is significantly stronger for  $X(3872)$  [40]. This conclusion was later confirmed for higher excited  $P$ -wave charmonium states [322]. Wang *et al.* analyzed  $X(3872)$  with coupled-channel dynamics, the results concluded that  $X(3872)$  originates from the  $D\bar{D}^*$  pole with over 99.7% confidence [326].

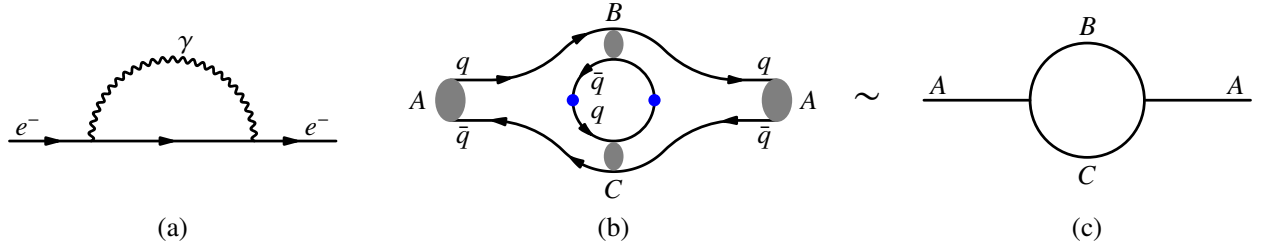


Figure 17: Loop diagrams: (a) electron-photon, (b) quark-level hadron, (c) hadron-level hadron.

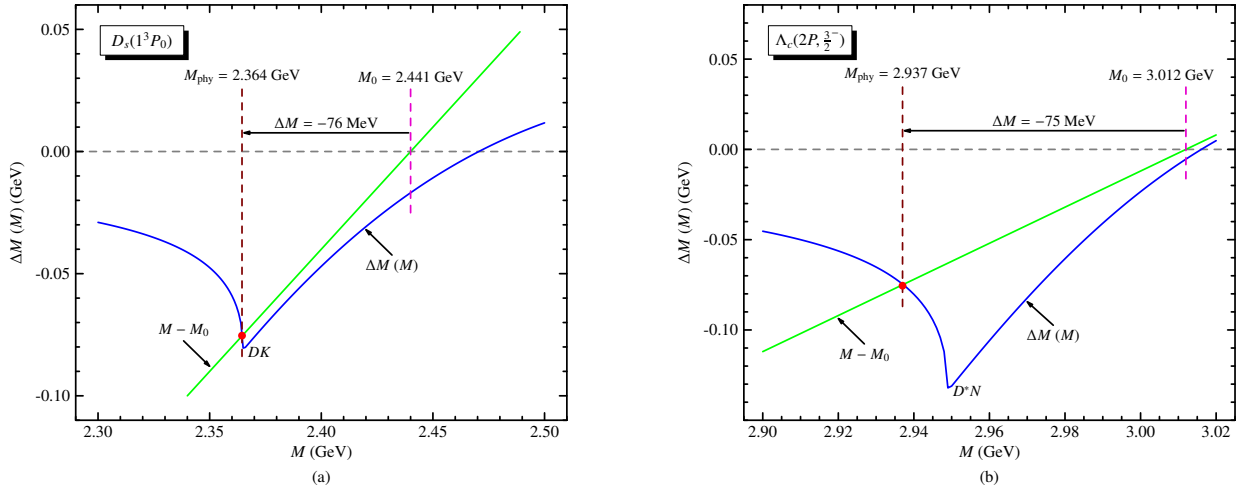


Figure 18: Solutions of the coupled-channel equation for  $D_{s0}^*(2317)$  (a) and  $\Lambda_c(2940)$  (b). Subfigures (a) and (b) are adapted from Ref. [46] and Ref. [45], respectively.

Given the limitations of the conventional quark model, the unquenched quark model has been developed as an effective extension. Among the popular approaches to incorporate unquenched effects are screened potentials and coupled-channel mechanisms. The screened potential, which suppresses the interaction at long distances, describes higher radial excitations well [327, 300, 328, 40, 322]. However, it struggles to explain states near thresholds such as  $D_{s0}^*(2317)$ ,  $D'_{s1}(2460)$ ,  $\Lambda_c(2940)$ , and  $X(3872)$ . For these states, coupled-channel effects are expected to play a decisive role. Within the coupled-channel framework itself, several schemes exist. This review will focus on introducing two primary approaches to the coupled-channel equations.

In quantum field theory, the mass of electron could be modified by the loop of electron-photon (see Fig. 17 (a)). One could promote this scenario to hadron, i.e., the mass of a hadron also could be modified by hadron loop (as shown in Fig. 17 (b-c)). Based on this, theorists developed coupled-channel equations to calculate the masses of hadrons with hadron loops. Here, we introduce two popular formalisms of the coupled-channel equations.

The first method is based on a quantum mechanical framework. The coupled-channel equation is given by

$$M_0 + \Delta M(M) = M, \quad (17)$$

where  $M_0$  is the bare mass obtained from the conventional (quenched) quark model, and  $\Delta M(M)$  represents the mass shift arising from hadron loops. The mass shift is defined as

$$\Delta M(M) = \int \frac{|H_{A \rightarrow BC}(\mathbf{p})|^2}{M - E_B(p) - E_C(p)} d^3 \mathbf{p}, \quad (18)$$

where  $H_{A \rightarrow BC}(\mathbf{p})$  is the transition Hamiltonian for the process  $A \rightarrow BC$ , and  $E_B(p) = \sqrt{M_B^2 + p^2}$  and  $E_C(p) =$

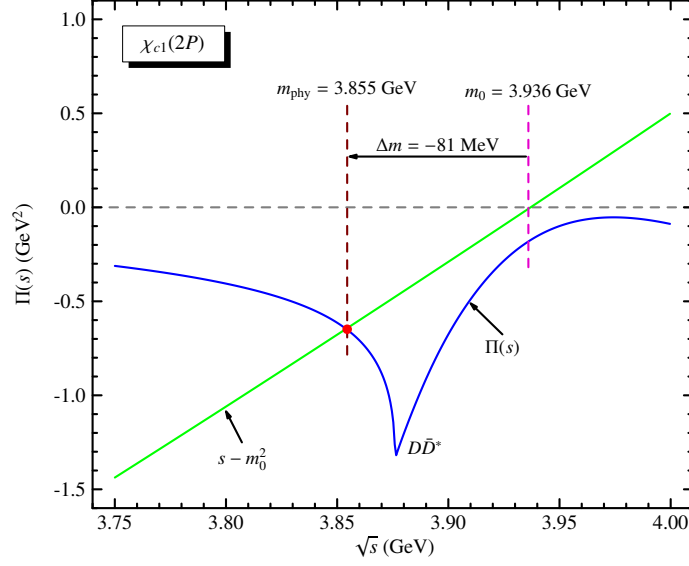


Figure 19: Solution of the coupled-channel equation for  $\chi_{c1}(2P)$ . The data are taken from Ref. [321].

$\sqrt{M_C^2 + p^2}$  are the energies of particles  $B$  and  $C$ , respectively. Here,  $M$  denotes the physical mass, i.e., the solution of Eq. (17).

A key element in this approach is the transition Hamiltonian  $H_{A \rightarrow BC}(\mathbf{p})$ . It is common to relate it to the decay amplitude  $\mathcal{M}_{A \rightarrow BC}(p)$ . In this case, Eq. (18) can be rewritten as

$$\Delta M(M) = \int \frac{|\mathcal{M}_{A \rightarrow BC}(p)|^2}{M - E_{BC}(p)} p^2 dp. \quad (19)$$

To illustrate the application of this method, we consider the states  $D_s(1^3P_0)$  and  $\Lambda_c(2P, 3/2^-)$ . As shown in Fig. 18, the bare masses of  $D_s(1^3P_0)$  and  $\Lambda_c(2P, 3/2^-)$  from conventional quenched models [46, 45] are 2.441 GeV and 3.012 GeV, respectively. Using the quark-pair-creation (QPC) model, one can compute the transition amplitudes  $\mathcal{M}_{D_s(1^3P_0) \rightarrow DK}(p)$  and  $\mathcal{M}_{\Lambda_c(2P, 3/2^-) \rightarrow D^*N}(p)$ , from which the mass shifts  $\Delta M(M)$  are obtained (blue curves in Fig. 18). The intersection points of the lines  $M - M_0$  and the curves  $\Delta M(M)$  give the solutions of the coupled-channel equations. The resulting physical masses are 2.364 GeV for  $D_s(1^3P_0)$  and 2.937 GeV for  $\Lambda_c(2P, 3/2^-)$ , corresponding to mass shifts of  $-76$  MeV and  $-75$  MeV, respectively. These values agree well with the observed masses of  $D_{s0}^*(2317)$  and  $\Lambda_c(2940)$ . The coupled-channel effects for  $D_{s0}^*(2317)$  and  $D_{s1}'(2460)$  have been extensively discussed in the literature using various approaches [37, 308, 38, 304, 305, 307, 306, 46, 48].

The second method is formulated within quantum field theory. The normalized propagator of a particle could be written as

$$\text{---} \text{---} \text{---} = \text{---} + \text{---} \text{---} \text{---} + \text{---} \text{---} \text{---} \text{---} + \dots,$$

which could be expressed as the following formula

$$\frac{A\bar{A}}{X - \bar{A}YA} = \frac{A\bar{A}}{X} + \frac{A\bar{A}}{X} Y \frac{A\bar{A}}{X} + \frac{A\bar{A}}{X} Y \frac{A\bar{A}}{X} Y \frac{A\bar{A}}{X} + \dots. \quad (20)$$

If we set  $A$  as the field of the particle (may contain index with spin  $\geq 1$ ) and  $X = s - M_0^2$ , one could define the self-energy function with  $\Pi(s) = \bar{A}YA$ , which could describe the contribution from one loop. The pole position  $s$  of a particle satisfies

$$s - M_0^2 - \Pi(s) = 0. \quad (21)$$

Thus the crucial difference of the two scheme of coupled-channel equations is that for one channel, Eq. (17) contains one loop while Eq. (21) contains infinite loops. A direct evaluation of  $\Pi(s)$  in quantum field theory often leads to divergent integrals [307, 306]. To circumvent this, more effective methods are required for practical computation. For  $\sqrt{s} > M_B + M_C$ , an imaginary part emerges in  $\Pi(s)$ , related to the decay width by

$$\text{Im } \Pi(s) = -\sqrt{s} \Gamma_{A \rightarrow BC}. \quad (22)$$

Using the same decay amplitude as in Eq. (19), the imaginary part can be expressed as

$$\text{Im } \Pi(s) = -2\pi E_B(p) E_C(p) |\mathcal{M}_{A \rightarrow BC}(p)|^2, \quad (23)$$

with the momentum  $p$  given by

$$p = \frac{\sqrt{M_B^4 + (M_C^2 - s)^2 - 2M_B^2(M_C^2 + s)}}{2\sqrt{s}}. \quad (24)$$

The real part of  $\Pi(s)$  is then obtained via a dispersion relation,

$$\text{Re } \Pi(s) = \frac{1}{\pi} \mathcal{P} \int_{z_R}^{\infty} dz \frac{\text{Im } \Pi(z)}{z - s}, \quad (25)$$

where  $\mathcal{P}$  denotes the principal value. In practice, a hadron couples to infinitely many intermediate channels, making a complete calculation infeasible. A practical solution is provided by the once-subtracted dispersion relation [159],

$$\begin{aligned} \text{Re } \Pi(s) &= \frac{1}{\pi} \mathcal{P} \int_{z_R}^{\infty} dz \frac{\text{Im } \Pi(z)}{z - s} - \frac{1}{\pi} \mathcal{P} \int_{z_R}^{\infty} dz \frac{\text{Im } \Pi(z)}{z - s_0} \\ &= \frac{s - s_0}{\pi} \mathcal{P} \int_{z_R}^{\infty} dz \frac{\text{Im } \Pi(z)}{(z - s)(z - s_0)}, \end{aligned} \quad (26)$$

where  $s_0$  is a subtraction point, often chosen as the squared mass of the corresponding ground state.

We apply this second method to examine the coupled-channel effect on the  $\chi_{c1}(2P)$  state. As shown in Fig. 19, the bare mass of  $\chi_{c1}(2P)$  is calculated to be 3.936 GeV within the GI model with updated parameters [321]. Choosing the subtraction point  $s_0 = m_{J/\psi}^2$ , the contribution from the  $D\bar{D}^*$  channel induces a mass shift of  $-81$  MeV, yielding a final mass of 3.855 GeV, which matches the measured mass of  $X(3872)$ . The coupled-channel effects for  $X(3872)$  have also been widely studied [42, 39, 321, 40].

As illustrated in Figs. 18–19, both the mass shift  $\Delta M(M)$  and the self-energy  $\Pi(s)$  exhibit cusp-like structures at the relevant thresholds, where their magnitudes increase rapidly. These curves vividly demonstrate how coupled-channel effects lower the hadron masses. A closer examination reveals that such cusp structures arise specifically from  $S$ -wave couplings between the state and the intermediate channel. This can be understood from the form of the decay amplitude  $\mathcal{M}_{A \rightarrow BC}(p)$ . For a partial wave with relative orbital angular momentum  $L$ , the amplitude behaves as

$$\mathcal{M}_{A \rightarrow BC}(p) \sim p^L e^{-\alpha p^2}. \quad (27)$$

For  $S$ -wave ( $L = 0$ ), a mathematical analysis confirms the presence of a cusp at threshold. However, if the coupling is not  $S$ -wave, or even if it is  $S$ -wave but the bare mass lies far from the threshold, the pronounced effects shown in the figures do not occur. In Section 3.3.2, we will use  $\chi_{c0}(2P)$  and  $\chi_{c2}(2P)$  as examples to further elaborate on this point.

### 3.3. $X(3915)$ and $Z(3930)$ as $2P$ charmonium states

#### 3.3.1. Initial research

Following the discovery of  $X(3872)$ , the Belle Collaboration observed a new charmonium-like state around 3.93 GeV in the process  $\gamma\gamma \rightarrow D\bar{D}$  in 2005 [50]. This state, denoted  $Z(3930)$ , is shown in Fig. 20 (a) and was reported with a statistical significance of  $5.3\sigma$ . Its measured resonance parameters are

$$\begin{aligned} M &= 3929 \pm 5(\text{stat}) \pm 2(\text{syst}) \text{ MeV}, \\ \Gamma &= 29 \pm 10(\text{stat}) \pm 2(\text{syst}) \text{ MeV}. \end{aligned} \quad (28)$$

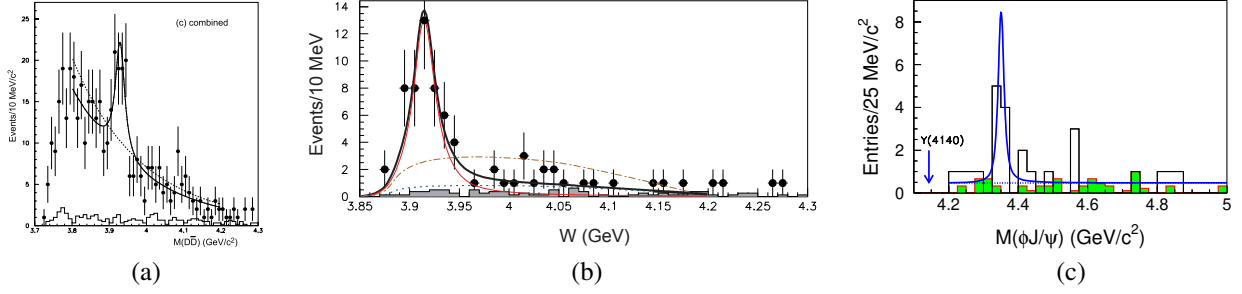


Figure 20: (a) The  $D\bar{D}$  invariant mass spectrum from  $\gamma\gamma \rightarrow D\bar{D}$  [50]. (b) The  $\omega J/\psi$  invariant mass ( $W$ ) distribution from  $\gamma\gamma \rightarrow \omega J/\psi$  candidate events [49]. (c) The  $\phi J/\psi$  invariant mass spectrum from  $\gamma\gamma \rightarrow \phi J/\psi$  [329]. All results are from the Belle Collaboration.

Furthermore, the product of its two-photon partial decay width and the branching fraction to  $D\bar{D}$  was measured as

$$\Gamma_{\gamma\gamma} \times \mathcal{B}(Z(3930) \rightarrow D\bar{D}) = 0.18 \pm 0.05(\text{stat}) \pm 0.03(\text{syst}) \text{ keV (assuming } J = 2). \quad (29)$$

The angular distribution was found to be consistent with spin  $J = 2$ . Since  $Z(3930)$  is produced in  $\gamma\gamma$  fusion, its  $C$ -parity is positive ( $C = +1$ ). Based on these quantum numbers,  $Z(3930)$  was identified as a good candidate for the  $\chi_{c2}(2P)$  charmonium state with  $J^{PC} = 2^{++}$ , an assignment that gained wide acceptance.

In 2009, the Belle Collaboration reported another charmonium-like state,  $X(3915)$ , observed in  $\gamma\gamma \rightarrow \omega J/\psi$  as shown in Fig. 20 (b) [49]. The signal had a statistical significance of  $7.7\sigma$ , with mass and width

$$\begin{aligned} M &= 3915 \pm 3 \pm 2 \text{ MeV}, \\ \Gamma &= 17 \pm 10 \pm 3 \text{ MeV}. \end{aligned} \quad (30)$$

The product of the two-photon decay width and the branching fraction to  $\omega J/\psi$  was measured for two possible spin-parity assignments:

$$\Gamma_{\gamma\gamma} \times \mathcal{B}(X(3915) \rightarrow \omega J/\psi) = \begin{cases} (61 \pm 17 \pm 8) \text{ eV} & \text{for } J^P = 0^+ \\ (18 \pm 5 \pm 2) \text{ eV} & \text{for } J^P = 2^+ \end{cases}. \quad (31)$$

Motivated by the earlier CDF observation of the  $Y(4140)$  in  $B^+ \rightarrow J/\psi \phi K^+$  decays [330], the Belle Collaboration also searched for structures in  $\gamma\gamma \rightarrow \phi J/\psi$  in 2009 [329]. While no significant  $Y(4140)$  signal was found, a new narrow structure,  $X(4350)$ , was identified (Fig. 20 (c)) with  $8.8_{-3.2}^{+4.2}$  signal events and a significance of  $3.2\sigma$ . Its parameters are

$$\begin{aligned} M &= 4350.6_{-5.1}^{+4.6}(\text{stat}) \pm 0.7(\text{syst}) \text{ MeV}, \\ \Gamma &= 13_{-9}^{+18}(\text{stat}) \pm 4(\text{syst}) \text{ MeV}. \end{aligned} \quad (32)$$

The corresponding product of the two-photon decay width and the branching fraction to  $\phi J/\psi$  is

$$\Gamma_{\gamma\gamma} \times \mathcal{B}(X(4350) \rightarrow \phi J/\psi) = \begin{cases} 6.7_{-2.4}^{+3.2}(\text{stat}) \pm 1.1(\text{syst}) \text{ eV} & \text{for } J^P = 0^+ \\ 1.5_{-0.6}^{+0.7}(\text{stat}) \pm 0.3(\text{syst}) \text{ eV} & \text{for } J^P = 2^+ \end{cases}. \quad (33)$$

The  $\gamma\gamma$  fusion process is particularly suited for producing mesonic states with positive  $C$ -parity. According to the Landau–Yang theorem [332, 333], two photons in an  $S$ -wave can only couple to final states with quantum numbers  $J^{PC} = 0^{++}$  or  $2^{++}$ . Consequently,  $\gamma\gamma$  collisions have long been an important way for studying  $P$ -wave quarkonia, as exemplified by the early observations of the ground-state charmonia  $\chi_{c0}(1P)$  and  $\chi_{c2}(1P)$  [334, 335]. It is therefore natural to interpret the charmonium-like states observed in  $\gamma\gamma$  fusion at  $B$ -factories as potential conventional  $P$ -wave charmonia.

A prime candidate is  $X(3915)$ , observed in  $\gamma\gamma \rightarrow \omega J/\psi$  with a mass of  $3915 \pm 3 \pm 2$  MeV and a narrow width. This state appeared to fill a specific gap in the known spectrum. The first radial excitation multiplet ( $n = 2$ ) already

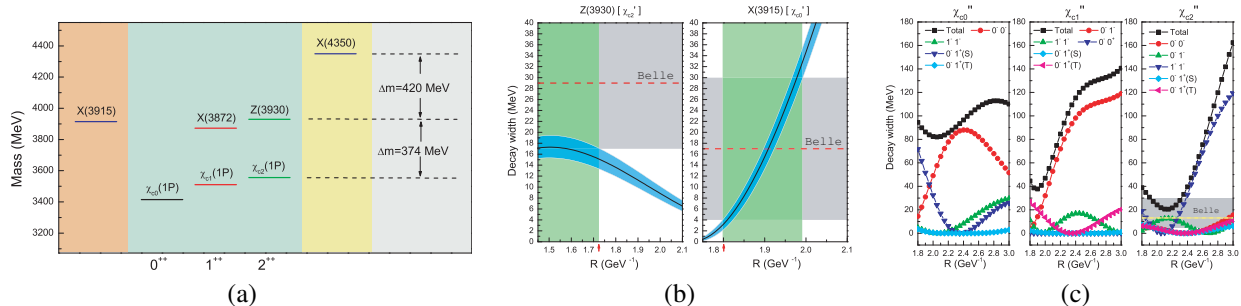


Figure 21: The observed  $P$ -wave charmonium states and candidates (a), the comparisons of theoretical and experimental decay widths of  $Z(3930)$  with assignment of  $\chi_{c2}(2P)$  and  $X(3915)$  with interpretation of  $\chi_{c0}(2P)$ , and the theoretical widths of  $\chi_{cJ}(3P)$  and the comparisons of theoretical and experimental decay widths of  $X(4350)$  with interpretation of  $\chi_{c2}(3P)$ . The figures are taken from Ref. [331]. Here,  $\chi'_{cJ}$  and  $\chi''_{cJ}$  are  $\chi_{cJ}(2P)$  and  $\chi_{cJ}(3P)$ , respectively.

contained the  $1^{++}$  candidate  $X(3872)$  and the well-established  $2^{++}$  state  $Z(3930)$ , but the corresponding scalar partner  $\chi_{c0}(2P)$  ( $0^{++}$ ) was missing. The mass of  $X(3915)$  aligns well with model predictions for  $\chi_{c0}(2P)$ . Furthermore, the pattern of mass differences among these  $n = 2$  states can be understood through coupled-channel effects, which are typically weaker for  $0^{++}$  and  $2^{++}$  states than for the  $1^{++}$  case (see Fig. 21 (a)).

Additional support comes from calculations of open-charm decays using the quark pair creation (QPC) model [331]. These calculations reproduce the measured width of  $X(3915)$  using parameter values consistent with those needed to describe  $Z(3930)$ , as shown in Fig. 21 (b). Collectively, this evidence strongly suggested that  $X(3915)$  is the conventional  $\chi_{c0}(2P)$  charmonium, completing the first radially excited  $P$ -wave triplet. Its assignment as a  $0^{++}$  state, testable via angular distribution analyses, underscores the continuing value of  $\gamma\gamma$  fusion in mapping out the conventional quarkonium spectrum.

While states like  $X(4350)$  were also observed in similar  $\gamma\gamma$  processes and are discussed as higher excitations, the case of  $X(3915)$  illustrates how combining systematic spectroscopy with decay calculations can successfully determine the nature of new resonances within the conventional quark model.

In 2012, the BaBar Collaboration performed an angular analysis of  $X(3915)$  and confirmed that its quantum numbers are consistent with  $J^{PC} = 0^{++}$  [336]. This experimental finding agreed with earlier theoretical predictions in Ref. [331], leading to the subsequent listing of  $X(3915)$  as  $\chi_{c0}(2P)$  in the 2013 edition of the PDG review [337].

Despite the overall consistency among its measured mass, width, and established quantum numbers—which collectively support the  $\chi_{c0}(2P)$  interpretation—several intriguing puzzles remained unresolved:

1. Quenched quark model calculations typically predict a significantly larger mass splitting between  $\chi_{c2}(2P)$  and  $\chi_{c0}(2P)$  than the observed  $\sim 12$  MeV between  $Z(3930)$  and  $X(3915)$  [338, 215, 339]. In addition, the  $\chi_{c0}(2P)$  could decay into  $D\bar{D}$  via  $S$ -wave, but the width of  $X(3915)$  is too narrow. What mechanisms are responsible for this anomalously small splitting of  $\chi_{c2}(2P) - \chi_{c0}(2P)$  and small width of  $X(3915)$ ?
2. The decay  $X(3915) \rightarrow J/\psi, \omega$  is an OZI-suppressed process, yet its measured branching fraction is relatively large [338, 15, 339]. Why is this hidden-charm mode strongly enhanced?
3. If  $X(3915)$  is indeed the conventional  $\chi_{c0}(2P)$ , its dominant decay channel should be  $D\bar{D}$ . However, a clear signal of  $X(3915)$  was not observed in the  $D\bar{D}$  invariant mass spectrum [338, 339]. What suppresses or masks its expected open-charm decay?

These persistent issues rendered the final identification of  $X(3915)$  both subtle and challenging. In the following sections, we address each of these problems systematically.

### 3.3.2. Anomalous small mass gap between $X(3915)$ and $Z(3930)$

The assignment of  $X(3915)$  as the conventional  $\chi_{c0}(2P)$  charmonium state faced significant theoretical scrutiny, primarily centered on two seemingly contradictory properties: its anomalously small mass splitting with the established  $\chi_{c2}(2P)$  candidate  $Z(3930)$  (see Fig. 22 (a)), and its remarkably narrow width despite lying above the  $S$ -wave  $D\bar{D}$  decay threshold. A consistent resolution to both puzzles has emerged from advanced *unquenched* theoretical

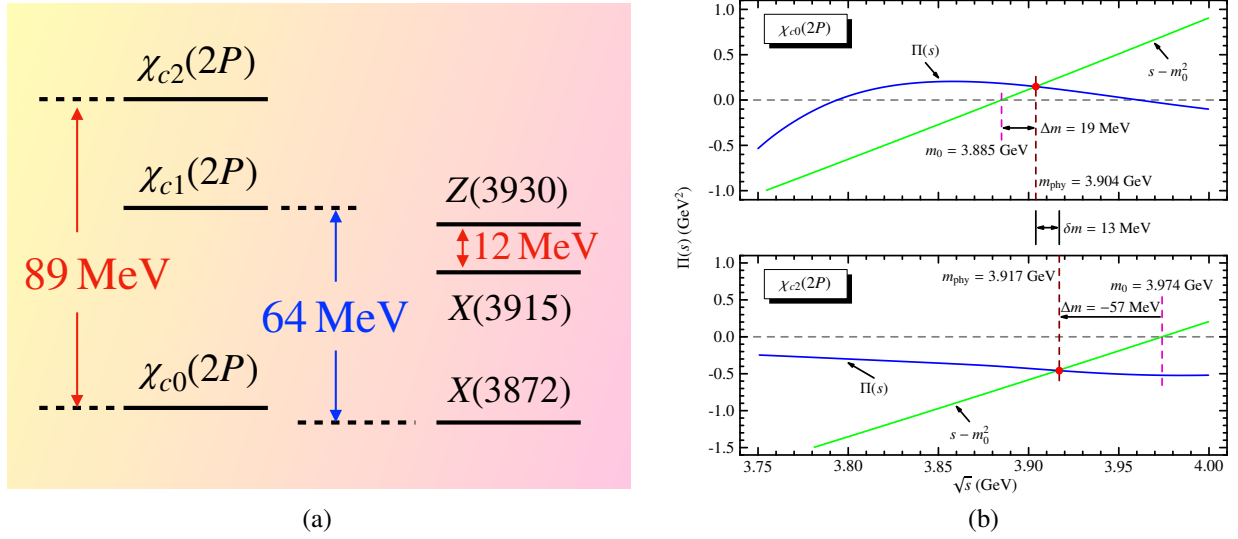


Figure 22: Comparison of masses between  $\chi_{cJ}(2P)$  states from the GI model and the observed  $X(3872)$ ,  $X(3915)$ , and  $Z(3930)$ . The figures are taken from Ref. [321].

frameworks that move beyond the static quark model by dynamically incorporating the dressing of the bare  $c\bar{c}$  core with virtual hadron loops [321]. These frameworks treat the physical state as a superposition of the bare quark-model configuration and coupled hadronic channels—primarily  $D\bar{D}$  and  $D\bar{D}^*$ —with contributions computed using effective models such as the QPC model.

The mass puzzle is addressed by considering significant and differential mass shifts induced by the coupling to open-charm channels. The numerical results of Ref. [321] are presented in Fig. 22 (b). In a quenched GI model with updated parameters, the bare  $\chi_{c0}(2P)$  and  $\chi_{c2}(2P)$  states are separated by nearly 89 MeV. However, unquenched calculations reveal a more complex physical picture. The  $\chi_{c1}(2P)$  state (associated with  $X(3872)$ ) couples strongly to  $D\bar{D}^*$  in an  $S$ -wave, resulting in a large attractive mass shift of approximately  $-80$  MeV, which explains its unusually low mass (discussed previously; see Fig. 19). In contrast, the  $\chi_{c0}(2P)$  couples to  $D\bar{D}$  in an  $S$ -wave but experiences a modest *positive* shift of about  $+20$  MeV<sup>1</sup>. The  $\chi_{c2}(2P)$  state, coupling to  $D\bar{D}$  and  $D\bar{D}^*$  in a  $D$ -wave, undergoes a moderate negative shift of about  $-60$  MeV due to centrifugal suppression. Crucially, the large bare splitting is dramatically compensated: the opposing shifts for the scalar (+) and tensor (−) states pull their physical masses closer together (see Fig. 22 (b)). The net physical mass difference reduces to approximately 13 MeV, in striking agreement with the observed  $\sim 14$  MeV gap between  $X(3915)$  and  $Z(3930)$ . This result demonstrates that the small splitting is a direct signature of coupled-channel effects rather than an anomaly.

The width puzzle is resolved through a subtle quantum mechanical phenomenon known as the node effect. As shown in Fig. 23(a), the radial wave function of a  $2P$  state, being the first radial excitation, possesses a single node. The partial width for the dominant open-charm decay  $\chi_{c0}(2P) \rightarrow D\bar{D}$  is proportional to the square of the decay amplitude  $\mathcal{M}$ , which is governed by a spatial overlap integral,  $I$ , between the initial charmonium wave function and the final-state  $D$ -meson wave functions. This integral can be decomposed as  $I = I_+ + I_-$ , where  $I_+$  ( $I_-$ ) arises from integrating over the region where the radial wave function is positive (negative). As illustrated in Fig. 23(b), these two contributions are opposite in sign, leading to significant destructive interference. This near-cancellation drastically suppresses the decay amplitude, resulting in a much narrower total width than naive phase-space estimates would suggest. Detailed calculations yield a total width of 20–30 MeV for  $\chi_{c0}(2P)$ , aligning perfectly with the experimental width of  $X(3915)$ . This mechanism not only explains the narrowness of  $X(3915)$  but also provides a critical discriminant against alternative interpretations. For instance, a broad state like  $X(3860)$ <sup>2</sup> ( $\Gamma \approx 200$  MeV) cannot be the  $\chi_{c0}(2P)$

<sup>1</sup>This positive shift arises when the physical mass lies above the  $D\bar{D}$  threshold ( $m_{\text{phy}} > M_B + M_C$ ). In this case, principal-value integration is required in the mass shift formulas [Eqs. (18) and (25)], which can yield positive contributions.

<sup>2</sup>In 2017, the Belle Collaboration observed a broad state  $X(3860)$  [340] in the  $D\bar{D}$  invariant mass spectrum from  $e^+e^- \rightarrow J/\psi D\bar{D}$ , with mass

because its large width is incompatible with the node-effect suppression inherent to a conventional radially excited  $P$ -wave charmonium.

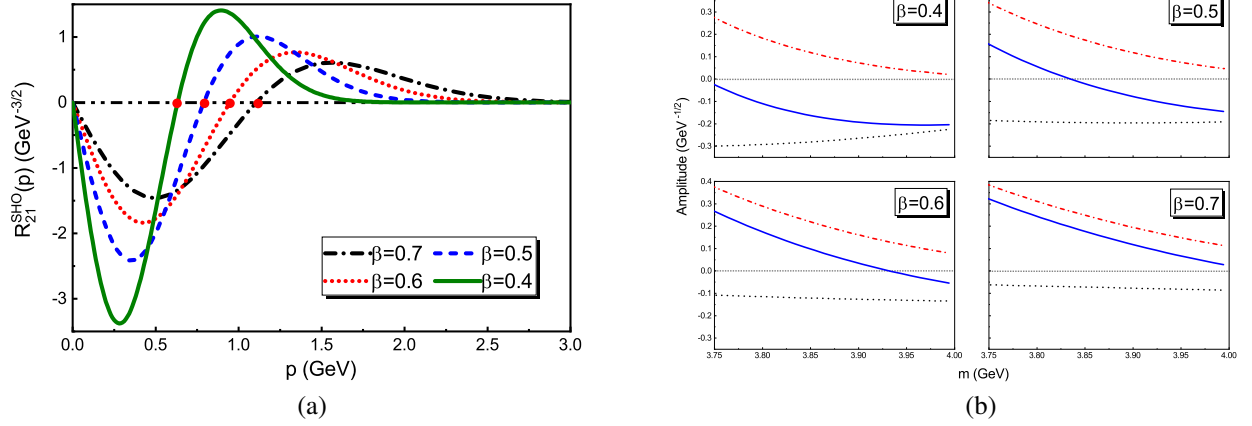


Figure 23: (a) Radial wave functions of  $\chi_{cJ}(2P)$  states for different values of the oscillator parameter  $\beta$ . (b) Decay amplitude for  $\chi_{c0}(2P) \rightarrow D\bar{D}$  as a function of  $\beta$ , showing contributions from positive ( $R_{nL}(p) > 0$ , dashed-dotted) and negative ( $R_{nL}(p) < 0$ , dotted) wave function regions, and the total amplitude (solid). Figures from Ref. [321].

In summary, the initially puzzling spectroscopic features of  $X(3915)$ —its small mass gap with  $Z(3930)$  and its narrow width—find a natural and unified explanation within the unquenched quark model. The mass splitting is determined by state-specific coupled-channel shifts, while the width is suppressed by the nodal structure of the radial wavefunction. Together, these insights provide a robust theoretical foundation for identifying  $X(3915)$  as the long-sought  $\chi_{c0}(2P)$  state, thereby completing the first radially excited  $P$ -wave charmonium triplet.

### 3.3.3. Anomalous large the branching ratio for the $X(3915) \rightarrow J/\psi\omega$ decay

$X(3915)$  and  $Z(3930)$  were both observed in  $\gamma\gamma$  collisions.  $X(3915)$  was first discovered in the decay  $X(3915) \rightarrow J/\psi\omega$  by Belle [49], with quantum numbers later measured as  $J^{PC} = 0^{++}$  by BaBar [336].  $Z(3930)$  was observed in  $\gamma\gamma \rightarrow D\bar{D}$  by Belle [50] and BaBar [344] and is a strong candidate for  $\chi_{c2}(2P)$ . If both states are indeed the first radial excitations of the  $P$ -wave charmonia  $\chi_{c0}$  and  $\chi_{c2}$ , they should both decay into  $J/\psi\omega$ . However, experimentally only  $X(3915)$  is seen in this channel. This raises the question: why is  $Z(3930)$  not observed in  $J/\psi\omega$ ? The answer likely lies in a mechanism that strongly suppresses  $\chi_{c2}(2P) \rightarrow J/\psi\omega$  relative to  $\chi_{c0}(2P) \rightarrow J/\psi\omega$ , despite the latter being an OZI-suppressed process.

To address this puzzle, the decay widths for  $\chi_{c0}(2P) \rightarrow J/\psi\omega$  and  $\chi_{c2}(2P) \rightarrow J/\psi\omega$  can be computed using a hadronic loop approach. Since both states lie above the  $D\bar{D}$  and  $D\bar{D}$  thresholds but below  $D\bar{D}^*$ , their dominant decays are to open-charm meson pairs:  $X(3915) \rightarrow D\bar{D}$  and  $Z(3930) \rightarrow D\bar{D}, D\bar{D}^* + \text{c.c.}$  The hidden-charm decays  $J/\psi\omega$  are assumed to proceed via rescattering of these dominant modes through intermediate charmed meson loops, as illustrated in Fig. 24. The loop integrals are evaluated using the Cutkosky cutting rules, with form factors to account for off-shell effects and vertex structure:  $\mathcal{F}(q^2) = \left(\frac{m_E^2 - \Lambda^2}{q^2 - \Lambda^2}\right)^N$ , where  $\Lambda = m_E + \alpha\Lambda_{\text{QCD}}$ ,  $\Lambda_{\text{QCD}} = 220 \text{ MeV}$ ,  $\alpha \sim \mathcal{O}(1)$ , and  $N = 1$  (monopole) or  $N = 2$  (dipole).

The partial decay widths are calculated as functions of  $\alpha$ . For  $\chi_{c0}(2P) \rightarrow J/\psi\omega$ , the width ranges from  $3.5 \times 10^{-3}$  MeV to 0.15 MeV for  $\alpha \in [1, 4]$  with a monopole form factor. For  $\chi_{c2}(2P) \rightarrow J/\psi\omega$ , the width is much smaller:  $4.1 \times 10^{-6}$  MeV to  $1.1 \times 10^{-4}$  MeV (case  $++$ ) or  $4.0 \times 10^{-5}$  MeV to  $1.1 \times 10^{-3}$  MeV (case  $+-$ ). The dipole form factor yields widths about an order of magnitude smaller.

More importantly, the ratio  $R = \Gamma[\chi_{c0}(2P) \rightarrow J/\psi\omega] / \Gamma[\chi_{c2}(2P) \rightarrow J/\psi\omega]$  is large and robust:

$$R_{++}^{\text{Monopole}} \simeq 850\text{--}1400, \quad R_{++}^{\text{Dipole}} \simeq 239\text{--}558, \quad R_{+-}^{\text{Monopole}} \simeq 87\text{--}130, \quad R_{+-}^{\text{Dipole}} \simeq 27\text{--}59.$$

$3862^{+26+40}_{-32-13}$  MeV and width  $201^{+154+88}_{-67-82}$  MeV. The  $J^{PC} = 0^{++}$  hypothesis was favored over  $2^{++}$  at the  $2.5\sigma$  level. Some theoretical works interpreted  $X(3860)$  as  $\chi_{c0}(2P)$  [341, 342, 343], but it is omitted from the PDG summary table [94].

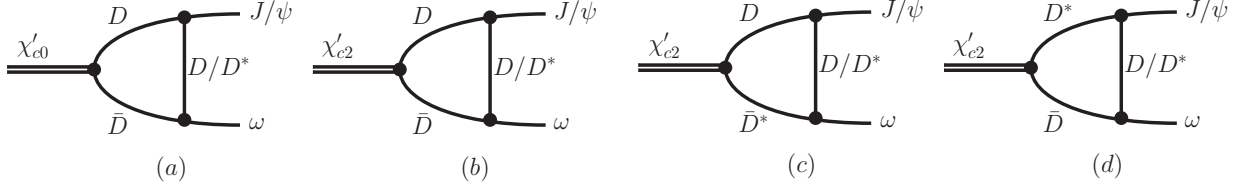


Figure 24: Diagrams for the decays  $\chi'_{c0} \rightarrow J/\psi\omega$  (a) and  $\chi'_{c2} \rightarrow J/\psi\omega$  (b-d), taken from Ref. [224]. Here  $\chi'_{c0}$  and  $\chi'_{c2}$  are  $\chi_{c0}(2P)$  and  $\chi_{c2}(2P)$ , respectively.

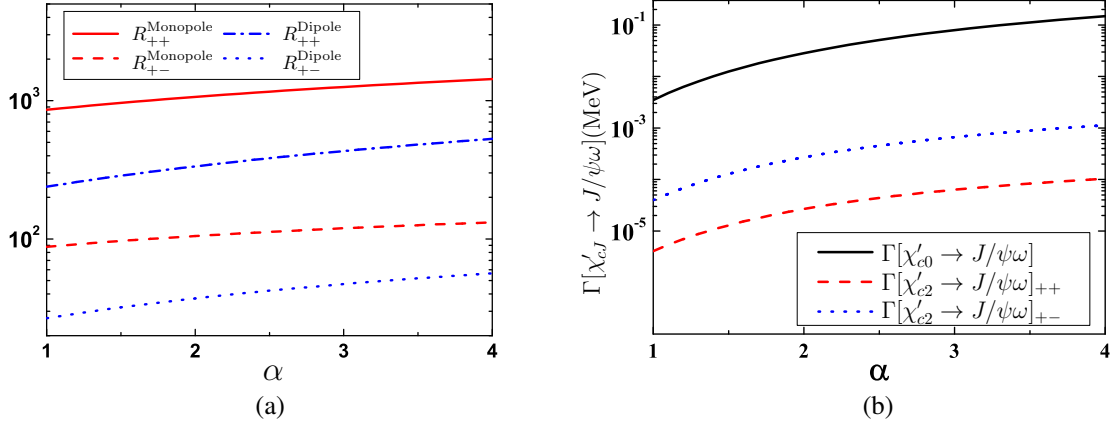


Figure 25: Dependence on the parameter  $\alpha$  of (a) the ratio of decay widths  $\Gamma(\chi'_{c0} \rightarrow J/\psi\omega)/\Gamma(\chi'_{c2} \rightarrow J/\psi\omega)$ , and (b) the partial widths for  $\chi'_{c0,c2} \rightarrow J/\psi\omega$  (shown for the monopole form factor as an example). Figure adapted from Ref. [224]. Here  $\chi'_{c0}$  and  $\chi'_{c2}$  are  $\chi_{c0}(2P)$  and  $\chi_{c2}(2P)$ , respectively.

Thus,  $\chi_{c0}(2P) \rightarrow J/\psi\omega$  is at least one order of magnitude larger than  $\chi_{c2}(2P) \rightarrow J/\psi\omega$ , regardless of the form factor or coupling sign.

This suppression explains why  $Z(3930)$  is not observed in  $J/\psi\omega$ . Using theoretical estimates for the two-photon widths of  $\chi_{c0}(2P)$  (1–5 keV) [13, 345, 346, 347, 348] and the measured  $\Gamma_{\gamma\gamma} \times \mathcal{B}(\chi_{c0}(2P) \rightarrow J/\psi\omega)$  [49, 336], the partial width for  $\chi_{c0}(2P) \rightarrow J/\psi\omega$  is estimated to be between 200 eV and 1 MeV, consistent with the calculated result (up to 150 keV for  $\alpha = 4$ ) [49].

The hadronic loop mechanism provides a natural explanation for the observed pattern: the decay  $Z(3930) \rightarrow J/\psi\omega$  is strongly suppressed compared to  $X(3915) \rightarrow J/\psi\omega$ . This supports the identification of  $X(3915)$  as  $\chi_{c0}(2P)$  and  $Z(3930)$  as  $\chi_{c2}(2P)$ . The study also underscores the importance of coupled-channel effects in charmonium decays, particularly for states above open-charm thresholds.

### 3.3.4. Unexpected disappear of $X(3915)$ in $\gamma\gamma \rightarrow D\bar{D}$

As discussed above, the decay  $X(3915) \rightarrow J/\psi\omega$  is an OZI-suppressed process, where hadron loop mechanisms are crucial. In contrast, the assignment of  $Z(3930)$  as  $\chi_{c2}(2P)$  appears more straightforward since both Belle [50] and BaBar [344] observed it directly in the OZI-allowed channel  $\gamma\gamma \rightarrow D\bar{D}$ . According to the OZI rule and spin-parity conservation, both  $\chi_{c0}(2P)$  ( $0^{++}$ ) and  $\chi_{c2}(2P)$  ( $2^{++}$ ) should decay into  $D\bar{D}$ . In particular,  $D\bar{D}$  is expected to be the dominant decay mode for  $\chi_{c0}(2P)$  [349]. However, the experimental data from Belle and BaBar in  $\gamma\gamma \rightarrow D\bar{D}$  reported only the  $Z(3930)$  enhancement without a clear signal for  $X(3915)$ , raising a puzzle regarding the  $\chi_{c0}(2P)$  identification.

To resolve this puzzle, Chen *et al.* proposed that the observed  $Z(3930)$  enhancement might contain contributions from both  $\chi_{c0}(2P)$  and  $\chi_{c2}(2P)$  [349]. Since both states can be produced via  $\gamma\gamma$  fusion and decay into  $D\bar{D}$ , they may appear as a single overlapping structure in the invariant mass spectrum due to their close masses.

Their analysis considered two mechanisms for  $\gamma\gamma \rightarrow D\bar{D}$ , illustrated in Fig. 26: (a) a non-resonant (NOR) direct process providing a smooth background, and (b) resonant contributions via intermediate states  $R = \chi_{c0}(2P), \chi_{c2}(2P)$ .

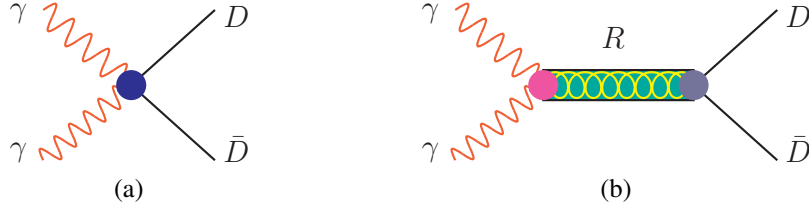


Figure 26: Feynman diagrams for (a) the direct non-resonant process and (b) the resonant contributions via  $\chi_{cJ}(2P)$  in  $\gamma\gamma \rightarrow D\bar{D}$ , adapted from Ref. [349].

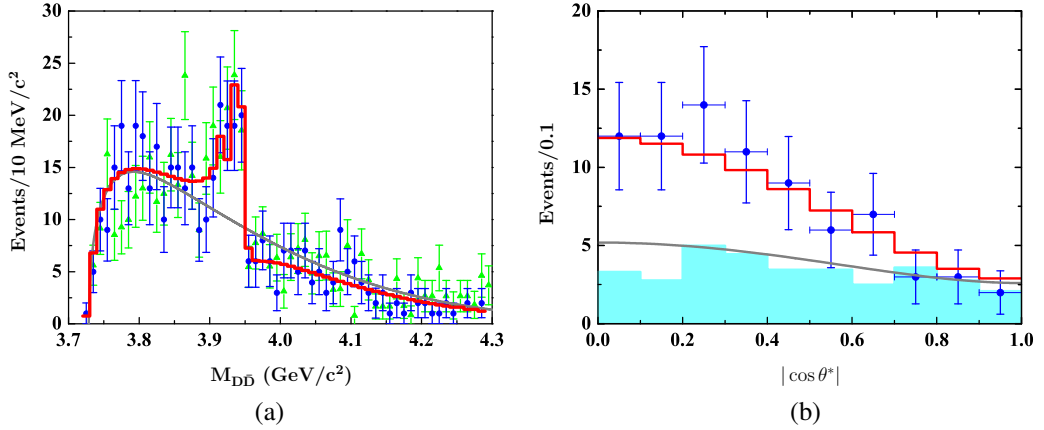


Figure 27: (a) Fitted  $D\bar{D}$  invariant mass spectrum (red histogram) compared with Belle (blue dots) and BaBar (green triangles) data. (b) Fitted  $\cos \theta^*$  distribution (red histogram) compared with Belle data (blue dots) and background (cyan histogram). Figures from Ref. [349].

The total amplitude was constructed as

$$\mathcal{M}_{\text{Total}} = \mathcal{A}_{\text{NOR}} + e^{i\phi_0} \mathcal{A}_{\chi_{c0}(2P)} + e^{i\phi_2} \mathcal{A}_{\chi_{c2}(2P)}, \quad (34)$$

where  $\phi_0$  and  $\phi_2$  account for possible interference phases.

By performing a combined fit to the  $D\bar{D}$  invariant mass spectrum and the  $\cos \theta^*$  angular distribution from Belle data, Chen *et al.* extracted the resonance parameters for both states. The best-fit results yield:

$$\begin{aligned} m_{\chi_{c0}(2P)} &= 3.920 \pm 0.007 \text{ GeV}, & \Gamma_{\chi_{c0}(2P)} &= 8.1 \pm 9.7 \text{ MeV}, \\ m_{\chi_{c2}(2P)} &= 3.942 \pm 0.003 \text{ GeV}, & \Gamma_{\chi_{c2}(2P)} &= 12.0 \pm 7.0 \text{ MeV}. \end{aligned} \quad (35)$$

These masses are remarkably close, separated by only about 20 MeV, and both widths are narrow, consistent with expectations for  $2P$  charmonia.

The fitting results, shown in Fig. 27, demonstrate that including both  $\chi_{c0}(2P)$  and  $\chi_{c2}(2P)$  provides a good description of the experimental data, including the steep drop near 3.95 GeV in the invariant mass spectrum and the  $\cos \theta^*$  angular distribution. Although the fitted coupling strength for  $\chi_{c0}(2P)$  is numerically smaller than that for  $\chi_{c2}(2P)$ , its contribution remains significant due to differing dimensional factors. The calculated cross-section ratio  $\sigma(\chi_{c2})/\sigma(\chi_{c0}) \approx 1.45$  further supports the necessity of including both resonances.

Thus, the observed  $Z(3930)$  enhancement is likely not a single resonance but an overlapping structure of  $\chi_{c0}(2P)$  and  $\chi_{c2}(2P)$ . Their near-degenerate masses make them difficult to resolve in existing data, explaining why only one broad structure was reported. This interpretation resolves the puzzle of the missing  $\chi_{c0}(2P)$  signal and provides a coherent picture of the  $P$ -wave charmonium spectrum. Future high-statistics experiments at Belle II and other facilities will be crucial to test this hypothesis through more precise angular analyses and possibly direct observation of the two separated states as indicated in Ref. [349] explicitly.

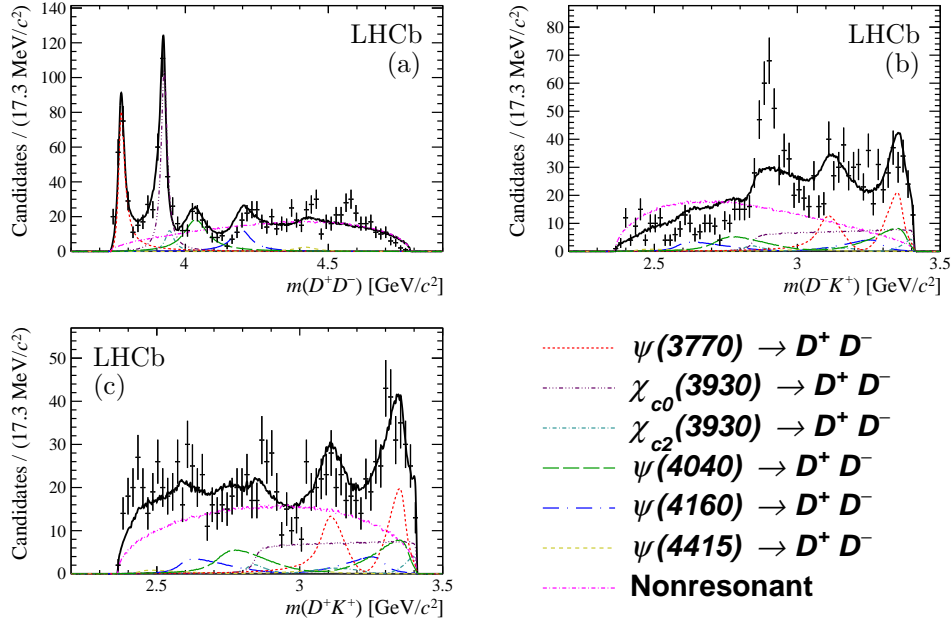


Figure 28: The invariant mass spectra of  $D^+D^-$  (a),  $D^-K^+$  (b), and  $D^+K^+$  (c) in  $B^+ \rightarrow D^+D^-K^+$  process from LHCb [350].

### 3.3.5. The experimental measurement of $B \rightarrow K D \bar{D}$ from the LHCb Collaboration

The decay  $B^+ \rightarrow D^+D^-K^+$  proceeds via a  $\bar{b} \rightarrow c\bar{c}s$  transition and offers a clean environment to study charmonium spectroscopy due to low background levels. Resonances in the  $D^-K^+$  system would be manifestly exotic, possessing minimal quark content  $\bar{c}d\bar{u}s$  (or  $\bar{c}d\bar{u}s$  for  $D^+K^+$ ), i.e., open charm and strangeness. While many exotic hadrons containing hidden charm ( $c\bar{c}$ ) have been observed, no significant evidence for exotic states with open flavour existed prior to LHCb's studies.

The LHCb Collaboration reported an analysis of the  $B^+ \rightarrow K^+D^+D^-$  process, with invariant mass spectra shown in Fig. 28 [350, 351]. The key results are:

1. The amplitude analysis confirms several established charmonium resonances in the  $D^+D^-$  channel, including  $\psi(3770)$ ,  $\psi(4040)$ ,  $\psi(4160)$ , and  $\psi(4415)$ . Notably, both spin-0 and spin-2 components are required in the  $\chi_{cJ}(3930)$  region:

$$\chi_{c0}(3930) : M = 3.9238 \pm 0.0015 \pm 0.0004 \text{ GeV}, \quad \Gamma = 17.4 \pm 5.1 \pm 0.8 \text{ MeV},$$

$$\chi_{c2}(3930) : M = 3.9268 \pm 0.0024 \pm 0.0008 \text{ GeV}, \quad \Gamma = 34.2 \pm 6.6 \pm 1.1 \text{ MeV}.$$

2. The analysis requires two new resonances in the  $D^-K^+$  system to describe the structure near 2.9, GeV:

$$X_0(2900) : M = 2866.3 \pm 6.5 \pm 2.0 \text{ MeV}/c^2, \quad \Gamma = 57.2 \pm 12.2 \pm 4.1 \text{ MeV},$$

$$X_1(2900) : M = 2904.1 \pm 4.8 \pm 1.3 \text{ MeV}/c^2, \quad \Gamma = 110.3 \pm 10.7 \pm 4.3 \text{ MeV}.$$

Based on their decay patterns,  $X_0(2900)$  and  $X_1(2900)$  were identified as singly charmed tetraquark candidates [352, 353, 354, 355, 356, 357, 358, 359, 360, 361, 362, 363, 364, 365, 366, 367, 368, 369, 370, 371, 372, 373, 374, 375, 376, 377], offering new insights into exotic hadrons.

3. No obvious resonant structures are seen in the  $D^+K^+$  spectrum.

As reported by LHCb [350, 351], the measured properties of  $\chi_{c0}(3930)$  and  $\chi_{c2}(3930)$  are very close to those of the previously observed  $X(3915)$  and  $Z(3930)$ , respectively. This is consistent with theoretical predictions that the  $\chi_{c0}(2P)$  and  $\chi_{c2}(2P)$  states should have close masses and narrow widths [321, 331]. Prior to the LHCb experiment,  $X(3915)$  had not been observed in the  $D\bar{D}$  decay channel. LHCb's work filled this gap, providing key evidence that

ultimately supported identifying  $X(3915)$  as the  $\chi_{c0}(2P)$  state. Consequently, in the 2022 edition of the PDG [378],  $X(3915)$  was listed once again as the  $\chi_{c0}(2P)$  charmonium state.

#### 4. Y Problem and its solution

Since the discovery of  $X(3872)$  by the Belle collaboration in 2003 [32], an increasing number of  $Y$  states have been observed in experiments. Among them, the  $Y$  states produced directly via  $e^+e^-$  annihilation form a particularly important subgroup. Their current status is summarized in Fig. 29. These observations not only enrich the family of charmonium-like  $XYZ$  states [14, 15, 16, 17, 18, 19, 20, 21, 22, 23, 24, 25, 26, 27, 28, 29, 30, 31], but also offer an opportunity to re-examine the  $J/\psi$  family, especially the construction of its high-lying states. This, in turn, helps deepen our understanding of the non-perturbative behavior of the strong interaction.

The  $Y(4260)$  stands out prominently in the  $XYZ$  family, as it was the first  $Y$  state discovered in this context [51]. Various resonant interpretations have been proposed, including assignments as a conventional charmonium, a multiquark state, or a hybrid meson [19]. However, these explanations face a significant challenge: the  $Y(4260)$  is not observed in the measured  $R$  values or in open-charm decay channels [19]. Consequently, a non-resonant interpretation was suggested, in which the  $Y(4260)$  structure can be reproduced through the interference between the charmonia  $\psi(4160)$  and  $\psi(4415)$  [213]. This picture has also been applied to describe the  $Y(4360)$  structure observed in  $e^+e^- \rightarrow \psi(3686)\pi^+\pi^-$  [216].

The year 2017 marked an important watershed with the accumulation of more precise experimental data. The BESIII collaboration performed high-precision measurements of the cross section for  $e^+e^- \rightarrow J/\psi\pi^+\pi^-$  [55]. Their results revealed that the previously identified  $Y(4260)$  actually consists of two substructures, now denoted as  $Y(4220)$ <sup>3</sup> and  $Y(4320)$  [55]. At the same time, the  $Y(4008)$  state previously reported by Belle in the same process was not confirmed by the more precise BESIII data [379, 55]. As a result, the designation  $Y(4260)$  is no longer used in the PDG listings [94], with  $Y(4220)$  being considered the relevant state. To date, ten  $Y$  states have been reported experimentally:  $Y(4220)$ ,  $Y(4320)$ ,  $Y(4360)$ ,  $Y(4380)$ ,  $Y(4390)$ ,  $Y(4500)$ ,  $Y(4630)$ ,  $Y(4660)$ ,  $Y(4710)$ , and  $Y(4790)$  (see Fig. 29) [55, 56, 380, 381, 382, 383, 384, 385, 386, 387, 388, 389, 390, 391, 392, 393, 394, 395].

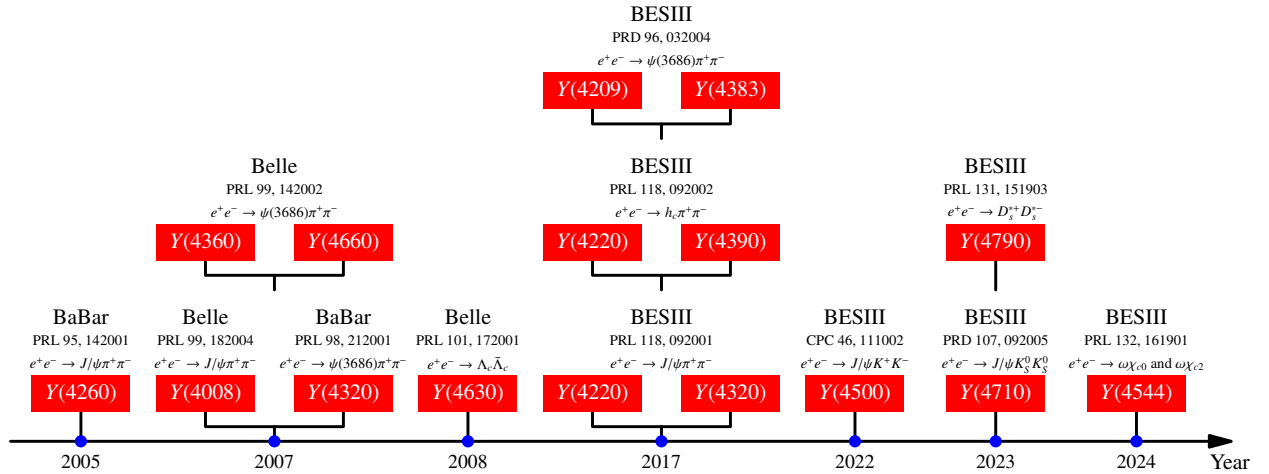


Figure 29: The observations of charmonium-like  $Y$  states. The data are obtained from Refs. [51, 379, 52, 53, 54, 56, 55, 380, 388, 392, 396, 397].

The abundance of phenomena associated with these  $Y$  states presents a challenging yet promising issue: how to understand their nature. This has become known as the "Y problem", as highlighted in *White Paper on the Future Physics Programme of BESIII* [57]. Addressing this problem requires not only high-precision measurements and comprehensive experimental input to uncover the properties of these states but also theoretical breakthroughs.

<sup>3</sup>This state is also referred to as  $Y(4230)$  in some experimental and theoretical analyses, reflecting the slightly different central values obtained from various measurements and fitting schemes. In this review, we adopt the notation  $Y(4220)$ .

In the present review, we examine how the unquenched picture provides a unified framework for addressing the  $Y$  problem.

#### 4.1. $Y(4260)$ and its evolving interpretations

##### 4.1.1. Experimental timeline and key results

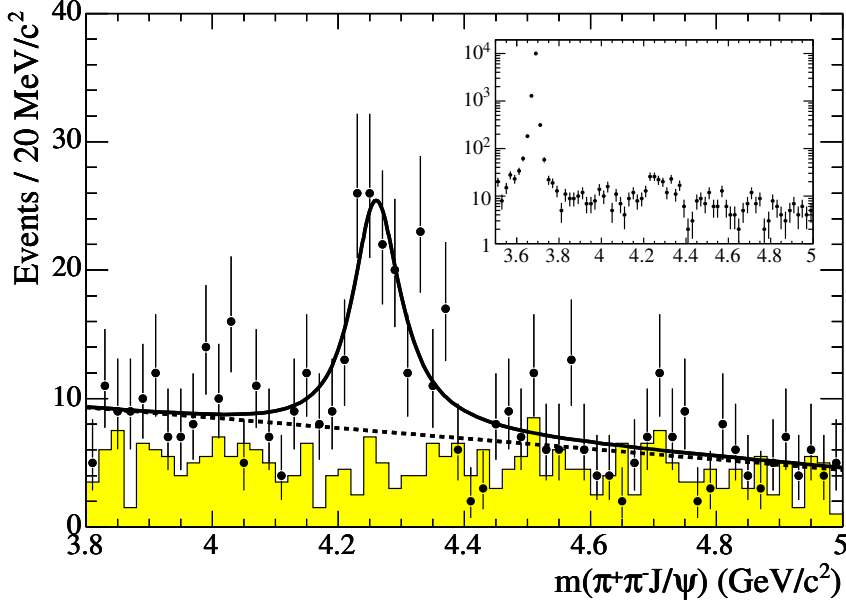


Figure 30: The observed  $Y(4260)$  in the  $e^+e^- \rightarrow J/\psi\pi^+\pi^-$  process from the BaBar Collaboration [51].

The experimental journey of  $Y(4260)$  resonance commenced in 2005 with the BaBar collaboration's analysis of initial-state radiation (ISR) events using  $233 \text{ fb}^{-1}$  of data collected at the  $\Upsilon(4S)$  resonance. Studying the process  $e^+e^- \rightarrow \gamma_{\text{ISR}}\pi^+\pi^-J/\psi$ , they observed a clear accumulation of events near 4.26 GeV (see Fig. 30) in the  $\pi^+\pi^-J/\psi$  invariant mass spectrum [51]. A fit with a single Breit-Wigner function described this structure, yielding  $125 \pm 23$  signal events, a mass of  $M = 4259 \pm 8_{-3}^{+2} \text{ MeV}$ , and a width of  $\Gamma = 88 \pm 23_{-5}^{+6} \text{ MeV}$  [51]. The product  $\Gamma_{e^+e^-} \times \mathcal{B}(Y(4260) \rightarrow \pi^+\pi^-J/\psi)$  was measured to be  $5.5 \pm 1.0_{-0.7}^{+0.8} \text{ eV}$ . Checks of the  $m_{\text{Rec}}^2$  distribution and the fraction of events with a detected ISR photon confirmed the ISR production mechanism, firmly establishing the quantum numbers as  $J^{PC} = 1^{--}$ . BaBar designated this new structure  $Y(4260)$ . While the data were adequately described by a single resonance, the BaBar Collaboration also explored a two-resonance hypothesis with interference, finding suggestive but statistically inconclusive solutions involving a second state near 4.33 GeV.

The need for independent confirmation was met promptly by the CLEO collaboration in 2006 [398]. Using a different data set of  $13.3 \text{ fb}^{-1}$  collected at the  $\Upsilon(1S - 4S)$  resonances with the CLEO III detector at CESR, they performed a similar ISR search [398]. A clear signal around 4.26 GeV was observed with low background. A single-resonance fit gave a mass of  $M = 4284_{-16}^{+17} \pm 4 \text{ MeV}$ , a width of  $\Gamma = 73_{-25}^{+39} \pm 5 \text{ MeV}$ , and  $\Gamma_{e^+e^-} \times \mathcal{B}(Y(4260) \rightarrow \pi^+\pi^-J/\psi) = 8.9_{-3.1}^{+3.9} \pm 1.8 \text{ eV}$  [398], consistent with BaBar's results [51] and providing a solid  $5.4\sigma$  confirmation. In a complementary study using data from direct  $e^+e^-$  annihilation at  $\sqrt{s} = 4.26 \text{ GeV}$ , CLEO extended the understanding of the  $Y(4260)$ 's decay properties [399]. They not only confirmed the  $\pi^+\pi^-J/\psi$  mode at  $11\sigma$  but also reported the first observation of  $Y(4260) \rightarrow \pi^0\pi^0J/\psi$  ( $5.1\sigma$ ) and evidence for  $Y(4260) \rightarrow K^+K^-J/\psi$  ( $3.7\sigma$ ). The measured Born cross sections were  $\sigma(\pi^+\pi^-J/\psi) = 58_{-10}^{+12} \pm 4 \text{ pb}$ ,  $\sigma(\pi^0\pi^0J/\psi) = 23_{-8}^{+12} \pm 1 \text{ pb}$ , and  $\sigma(K^+K^-J/\psi) = 9_{-5}^{+9} \pm 1 \text{ pb}$  [399]. These findings demonstrated the resonance's significant coupling to hidden-charm final states with light hadrons, with a dipion mass spectrum consistent with an S-wave phase space model.

The narrative took a more complex turn with the high-precision measurement from the Belle Collaboration in 2007. Utilizing a much larger data sample of  $548 \text{ fb}^{-1}$  collected at the  $\Upsilon(4S)$ , Belle measured the  $e^+e^- \rightarrow \pi^+\pi^-J/\psi$  cross section via ISR from  $\sqrt{s} = 3.8$  to  $5.5 \text{ GeV}$  [379]. Their results overwhelmingly confirmed the  $Y(4260)$  peak

near 4.25 GeV (significance  $> 15\sigma$ ) but also revealed a significant, previously unresolved cluster of events near 4.05 GeV (significance  $> 8\sigma$ ). An unbinned maximum likelihood fit to the mass spectrum showed that a model with two coherent Breit-Wigner resonances provided a significantly better description of the data than a single resonance, particularly for the lower-mass side of the 4.25 GeV enhancement. The fit yielded two solutions with interference. The parameters for the lower resonance ( $R1$ ) were  $M = 4008 \pm 40^{+14}_{-28}$  MeV,  $\Gamma = 226 \pm 44 \pm 87$  MeV; and for the higher resonance ( $R2$ , associated with  $Y(4260)$ )  $M = 4247 \pm 12^{+17}_{-32}$  Me,  $\Gamma = 108 \pm 19 \pm 10$  MeV [379]. Belle noted that  $R1$ 's parameters did not match those of the known  $\psi(4040)$ , hinting at a more intricate underlying structure. A single-resonance fit, for comparison, yielded parameters consistent with the earlier BaBar [51] and CLEO [398, 399] results.

In summary, experimental studies from 2005 to 2007 firmly established  $Y(4260)$  resonance with  $J^{PC} = 1^{--}$ . Its defining feature was a surprisingly strong coupling to hidden-charm final states such as  $\pi\pi J/\psi$  and  $K\bar{K}J/\psi$ , while it remained difficult to observe in open-charm and inclusive hadronic channels. Although interpretations within the conventional (quenched) charmonium picture were explored, this distinctive decay pattern ultimately challenged such descriptions. This motivated the introduction of exotic state explanations, a topic reviewed in the following section.

#### 4.1.2. Resonant explanations and confronted difficulties

Several theoretical explanations have been proposed in response to the reported  $Y(4260)$  signal; the main interpretations are summarised below (further details can be found in review articles, e.g., [15, 16, 17, 18, 19, 20, 21, 22, 23, 24, 25, 26, 27, 28, 29, 400]).

- Charmonium explanations: early phenomenological attempts to place  $Y(4260)$  within the conventional charmonium spectrum. For example, Zhang suggested the  $3^3D_1$  state assignment using Regge trajectory combined with hyperfine splitting relations [401]. In Ref. [402], Llanes-Estrada interpreted  $Y(4260)$  as a  $4S$  charmonium state, although their calculated mass of 4347 MeV for the  $4S$  state is obviously larger than that of  $Y(4260)$ , and argued that  $S$ - $D$ -wave interference could explain the absence of the  $Y(4260)$  signal in the  $R$ -value scan. Subsequently, several refined analyses of the mass spectrum and decay properties reach different conclusions [403, 404]. Studies based on the Cornell coupled channel model concluded that the  $2^3D_1$  assignment is incompatible with the properties of  $Y(4260)$  [403]. In a constituent quark model study, Segovia *et al.* [404] identified  $Y(4360)$  as the  $4S$  charmonium and the  $\psi(4415)$  as the  $3D$  state, while finding no natural place for  $Y(4260)$  within the conventional charmonium spectrum. Further analysis incorporating  $\pi\pi/K\bar{K}$  final state interactions revealed a two-pole structure with strong coupling to  $\omega\chi_{c0}$  [405], suggesting  $Y(4260)$  as a confining state with either a hybrid meson or a  $3D$  charmonium component. Recent constituent quark model calculations with a Cornell-like potential likewise conclude that  $Y(4260)$  does not fit the conventional meson picture [406]. In fact, the spectroscopic overpopulation problem associated with  $Y(4260)$  can be partially alleviated by the inclusion of unquenching effects. Comparisons between coupled channel approach and screened potential models confirm that both incorporate vacuum polarization from light quark pairs and yield similar global spectral features [40]. Within the screened potential framework [299], Li and Chao predicted the mass of  $\psi(4S)$  to be around 4.27 GeV, close to  $Y(4260)$ , a result also supported by calculations using a Martin-like potential [407]. Furthermore, the experimental observation that  $Y(4260)$  splits into two substructures,  $Y(4220)$  and  $Y(4320)$  [55], adds another layer of complexity to its assignment within the conventional charmonium spectrum.
- The molecular state explanations: a prominent exotic interpretation for  $Y(4260)$  is the hadronic molecular picture, motivated by the general expectation that near-threshold dynamics can generate bound states. Early proposals considered a variety of constituent combinations, such as  $\rho\chi_{c1}$  [408, 409],  $\omega\chi_{c1}$  [410], and  $D_1\bar{D}$  [411]. A distinctive scenario regarded the state as a  $\Lambda_c\bar{\Lambda}_c$  baryonium [412], where the binding does not require color-singlet constituents and could reach several hundred MeV, representing a non-typical near-threshold molecule. With accumulating data, attention focused on the  $S$ -wave  $D_1\bar{D}$  threshold, which naturally admits  $J^{PC} = 1^{--}$ . In this picture,  $Y(4260)$  is viewed as an isospin-singlet  $D_1\bar{D} + \text{c.c.}$  molecule [411, 413, 414, 415, 416, 417, 418, 419], where the narrow  $D_1(2420)$  belonging to the heavy-quark spin-symmetry multiplet with light angular momentum  $j_l = 3/2$  plays a central role. Quantitative coupled channel studies have examined the  $D_1\bar{D}$  interaction and its coupling to related channels such as  $D_0\bar{D}^*$  [413]. Analyses of the line shapes in  $e^+e^- \rightarrow J/\psi\pi^+\pi^-$ ,  $h_c\pi^+\pi^-$ , and  $D\bar{D}$ , which incorporate  $D_1\bar{D}$  scattering dynamics, extract a pole position

around  $4217 \pm 2 \text{ MeV}$  [417, 418], consistent with  $Y(4260)$ . Further combined analyses based on this assignment assumption have been presented in Refs. [420, 421].

- **Hidden-charm compact tetraquark:** the compact tetraquark picture, often formulated in terms of constituent diquark-antidiquark degrees of freedom, was proposed early as a popular exotic explanation for  $Y(4260)$ . In such models, the mass spectrum is organized by spin-spin and spin-orbit interactions within and between the (anti)diquarks, giving rise to multiplets of states with various quantum numbers [422, 423, 424, 425].  $Y(4260)$  has been frequently identified as a vector member of a  $[cs][\bar{c}\bar{s}]$  tetraquark multiplet [422, 423, 424]. Based on the mass relation of Eq. (3.1) without tensor-force in Ref. [422], the spectroscopy of  $P$ -wave  $[cs][\bar{c}\bar{s}]$  tetraquark has been updated by two different assignment scenarios [426], which assumed that  $Y(4008)/Y(4260)$  and  $Y(4260)/Y(4360)$  are two lowest vector tetraquark states, respectively. It should be emphasized that compact  $[cs][\bar{c}\bar{s}]$  tetraquark interpretation of  $Y(4260)$  was not supported in other theoretical frameworks. Relativistic quark model calculations based on a quasipotential formalism [427, 428], which systematically treats the diquark-antidiquark interaction via a one-gluon-exchange plus confining kernel, predict vector  $[cs][\bar{c}\bar{s}]$  states substantially heavier (by about 200 MeV) than  $Y(4260)$ . These works instead suggest that a  $[cq][\bar{c}\bar{q}]$  configuration could be a more natural candidate [427, 428], although such models tend to predict a much richer spectrum of  $1^{--}$  tetraquarks than currently observed. Similarly, QCD sum rule analyses using interpolating currents for  $1^{--}$  hidden-charm tetraquarks consistently yield mass estimates around 4.6-4.7 GeV for a wide range of continuum-threshold and Borel-window choices, disfavoring the identification of  $Y(4260)$  with a lowest-lying compact tetraquark state [429].
- **$c\bar{c}g$  hybrid:** the charmonium hybrid interpretation, in which a  $c\bar{c}$  pair is coupled to an explicit gluonic excitation, provides a distinctive framework for exotic vector states. A characteristic theoretical feature is the selection rule for heavy hybrids [430, 431, 432, 433, 434]: decays of a vector hybrid meson into two  $S$ -wave charmed mesons (e.g.,  $D^{(*)}\bar{D}^{(*)}$ ,  $D_s^{(*)}\bar{D}_s^{(*)}$ ) are strongly suppressed, while channels involving at least one orbitally excited charmed meson (such as  $D_1\bar{D}^{(*)}$ ) are favoured. Early phenomenological and lattice studies anticipated the lightest vector charmonium hybrid near 4.0-4.2 GeV [435, 436, 437, 438, 439, 440, 441, 442, 443]. The Hadron Spectrum Collaboration, using a large basis of interpolators, identified a hybrid supermultiplet containing a  $1^{--}$  state within  $m_\pi \approx 400$  MeV [444], in which the mass difference  $M_{1^{--}} - M_{\eta_c} \approx 1.3$  GeV agreed with  $Y(4260)$ , but subsequent studies with lighter pion masses ( $m_\pi \approx 240$  MeV) shift the mass upward to  $\sim 4.4$  GeV [445]. Independent quenched lattice studies (e.g., TWQCD [408]) also place the lightest vector hybrid about 250 MeV above  $Y(4260)$ . Additional insight was obtained from a lattice calculation employing nonlocal hybrid-like operators in which the  $c\bar{c}$  pair and the chromomagnetic gluonic field are spatially separated [446], which found a vector state at 4.33(2) GeV with a strongly suppressed leptonic width  $\Gamma_{e^+e^-} < O(40 \text{ eV})$ . Predictions from Born-Oppenheimer effective field theory place the lightest vector hybrid multiplet in the 4.0-4.3 GeV range [447]. Thus, although the hybrid picture offers an interesting explanation for  $Y(4260)$ , definitive support from lattice QCD remains ambiguous due to significant variations in the predicted mass across different methodologies and pion masses.

Whether interpreting the observed  $Y(4260)$  as a conventional charmonium state or as an exotic hadronic state (such as a  $D_1\bar{D}$  molecule, a hidden-charm compact tetraquark, or a  $c\bar{c}g$  hybrid), we face a serious problem: its hidden-charm decays cannot account for the total width of  $Y(4260)$ . As a resonance, its main decay channels should be open-charm modes. However,  $Y(4260)$  is not observed in the measured cross sections for  $e^+e^-$  annihilation into open-charm channels, such as  $D\bar{D}$ ,  $D\bar{D}^* + \text{c.c.}$ ,  $D^*\bar{D}^*$ ,  $D_s^+D_s^-$ ,  $D_s^-D_s^{*+}$ ,  $D_s^{*+}D_s^{*-}$ ,  $D^0D^{*-}\pi^+$ , and  $D^*\bar{D}^*\pi$  [448, 449, 450, 451, 452, 453, 454] (see Fig. 31). More importantly,  $Y(4260)$  does not produce a noticeable enhancement in the measured  $R$  value, as shown in Fig. 32. Typically, vector states such as the  $\rho$ ,  $\phi$ , and  $J/\psi$  exhibit clear peaks in the  $R$  value. In Fig. 32, we present the details of  $R$  value around 4.2 GeV.

How to explain this puzzling phenomenon remains a major challenge when considering  $Y(4260)$  as a resonance.

#### 4.1.3. Non-resonant picture: concept and applications

The study of charmonium-like  $XYZ$  states has been significantly enriched with the discovery of  $Y(4260)$  by the BaBar Collaboration in 2005 [51] and  $Y(4360)$  shortly thereafter [52, 53]. These states, produced in initial-state-radiation  $e^+e^-$  collisions and decaying to  $J/\psi\pi^+\pi^-$  and  $\psi(3686)\pi^+\pi^-$  respectively, possess the quantum numbers

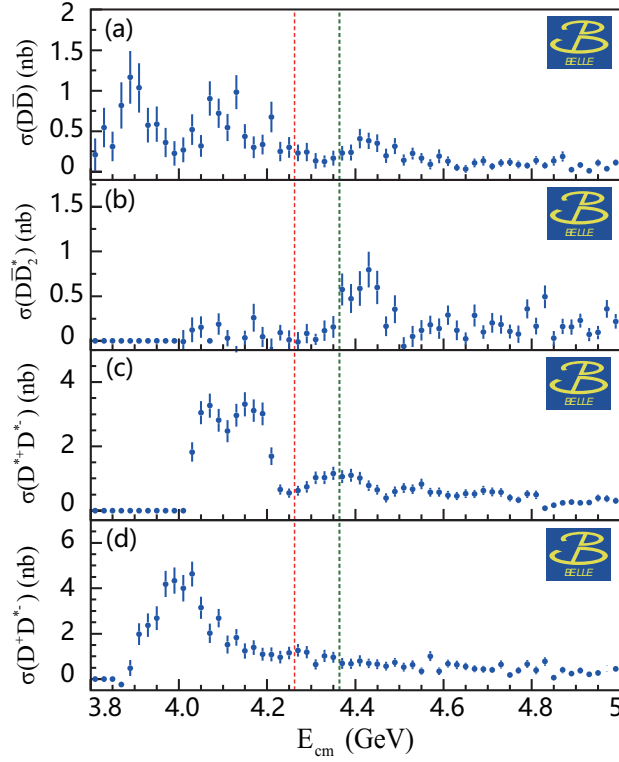


Figure 31: The experimental cross sections of  $e^+e^-$  annihilation from Belle Collaboration in  $e^+e^- \rightarrow D\bar{D}$  (a) [455],  $e^+e^- \rightarrow D^0D^-\pi^+$  (b) [450],  $e^+e^- \rightarrow D^{*+}D^{*-}$  (c) [449], and  $e^+e^- \rightarrow D^+D^{*-}$  (d) [449] channels. The vertical red and green dashed lines represent the central masses of  $Y(4260)$  and  $Y(4360)$ , respectively. The figure is taken from Ref. [19].

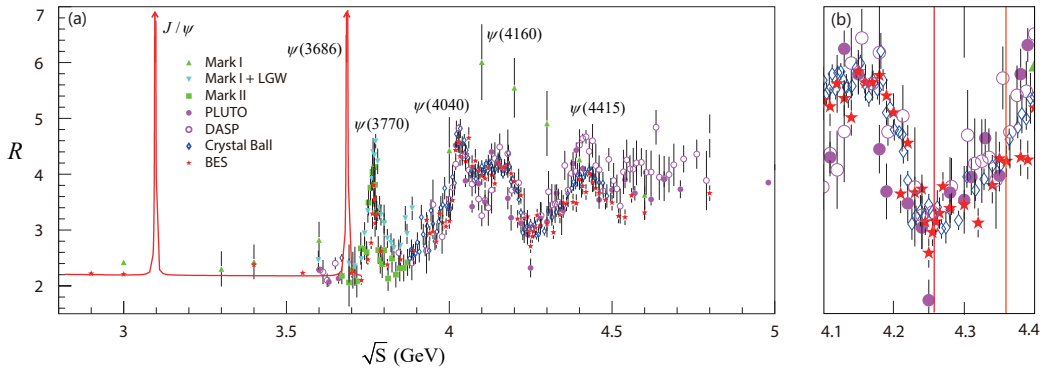


Figure 32: The experimental  $R$  value taken from the PDG [456] (a) and the detailed data in the range of  $\sqrt{s} = 4.1\sim 4.4$  GeV (b). The vertical red lines in figure (b) represent the central masses of  $Y(4260)$  and  $Y(4360)$ . The figure is taken from Ref. [19].

$J^{PC} = 1^{--}$  but exhibit peculiar decay patterns. Contrary to expectations for conventional charmonium states above open-charm threshold, neither  $Y(4260)$  nor the  $Y(4360)$  has been observed in exclusive open-charm decays (e.g., to  $D\bar{D}$ ,  $D^*\bar{D}^*$ ) [448, 449, 450, 451, 452, 453, 454] or in the hadronic  $R$ -value scan [452, 457, 458, 459, 460, 461]. This discrepancy has fueled extensive theoretical debate, with interpretations spanning hybrid mesons, tetraquarks, hadronic molecules, and conventional  $c\bar{c}$  excitations. However, the absence in key channels poses a serious challenge to many of these resonant models. In response, a conceptually distinct explanation has been developed—the non-resonant picture—which attributes the observed peaks not to new particles but to the interference of known production amplitudes.

The core concept of the non-resonant picture is elegantly straightforward. For processes such as  $e^+e^- \rightarrow J/\psi\pi^+\pi^-$  [51] and  $e^+e^- \rightarrow \psi(3686)\pi^+\pi^-$  [52], the total production amplitude can receive contributions from distinct mechanisms. The first is a direct, non-resonant production where the virtual photon from  $e^+e^-$  annihilation directly couples to the final state. The second proceeds through the formation of known intermediate resonances, such as the established charmonia  $\psi(4160)$  and  $\psi(4415)$ , which subsequently decay into the same final state via hadronic loops. The key insight is that the coherent sum of these amplitudes, particularly when they possess a relative phase, can constructively and destructively interfere in the invariant mass ( $\sqrt{s}$ ) spectrum. This interference can produce distinct peaks or enhancements that mimic resonant signals, even in the absence of poles in the scattering matrix. This mechanism provides a natural explanation for structures that appear prominently in specific final states (governed by the interfering pathways) but leave no imprint in other channels where the interfering terms are absent or negligible.

The work by Chen, He, and Liu provides concrete and quantitative realizations of this idea for both  $Y(4260)$  [213] and the  $Y(4360)$  [216]. Their model constructs the total amplitude  $\mathcal{M}_{\text{tot}} = \mathcal{M}_{\text{NoR}} + e^{i\phi_1}\mathcal{A}_{\psi_1} + e^{i\phi_2}\mathcal{A}_{\psi_2}$ , where  $\mathcal{M}_{\text{NoR}}$  describes the direct  $e^+e^- \rightarrow$  hidden-charm +  $\pi\pi$  production with an empirically parameterized form factor, and  $\mathcal{A}_{\psi_i}$  represent the amplitudes for production via the intermediate states  $\psi_1 = \psi(4160)$  and  $\psi_2 = \psi(4415)$ , as illustrated in Fig. 33. The decay of these charmonia into the final state is calculated using a hadronic loop mechanism, which serves as a crucial non-perturbative bridge. In this framework, the charmonia couple to pairs of charmed mesons ( $D^{(*)}\bar{D}^{(*)}$ ), which then rescatter via the exchange of charmed mesons to form the final  $J/\psi$  or  $\psi(3686)$  and a scalar meson ( $\sigma$  or  $f_0(980)$ ), which subsequently decays to  $\pi^+\pi^-$ . This approach incorporates effective Lagrangians, form factors to account for off-shell effects and finite hadron size, and experimentally constrained couplings.

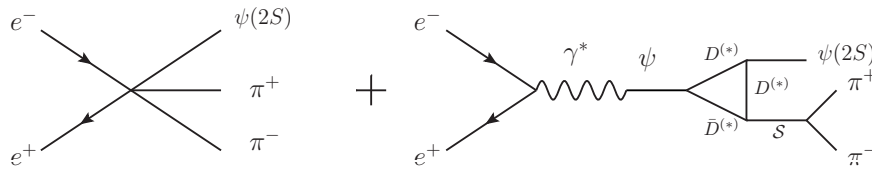


Figure 33: The diagram depicting the direct production (left panel) and the production via intermediate charmonium (right panel). The figure is adapted from Ref. [216].

For the  $Y(4260)$ , the numerical analysis demonstrates that with a small set of free parameters (primarily coupling strengths and relative phases), the theoretical line shape yields an excellent fit to the  $e^+e^- \rightarrow J/\psi\pi^+\pi^-$  cross-section data from BaBar, successfully reproducing the prominent peak located between the masses of  $\psi(4160)$  and  $\psi(4415)$ . The step-by-step decomposition of the cross-section into its components—the direct term  $|\mathcal{M}_{\text{NoR}}|^2$ , the individual resonant terms  $|\mathcal{A}_{\psi_i}|^2$ , and, most importantly, their interference terms  $2\text{Re}(\mathcal{A}_{\psi_i}\mathcal{M}_{\text{NoR}}^*)$ —visually illustrates how the interference between the direct and  $\psi(4160)$ -mediated amplitudes is primarily responsible for generating the observed enhancement, as illustrated in Fig. 34. This result provides strong quantitative support for the non-resonant hypothesis.

Encouraged by this success, the same group extended the non-resonant picture to  $Y(4360)$  observed in  $e^+e^- \rightarrow \psi(3686)\pi^+\pi^-$ . Employing a similar framework but with adjusted parameters to account for the different final state ( $\psi(3686)$  instead of  $J/\psi$ ), they again achieved a remarkable fit to the experimental data from both BaBar and Belle. The  $Y(4360)$  structure is similarly reproduced through the interference of direct production and intermediate charmonia contributions, with the interference playing a crucial role in shaping the peak, as shown in Fig. 35. This successful application to a second, independent channel significantly strengthens the credibility of the non-resonant explanation. It demonstrates that the mechanism is not a curiosity tailored to a single dataset but a potentially general phenomenon that can account for multiple puzzling structures in the charmonium-like spectrum.

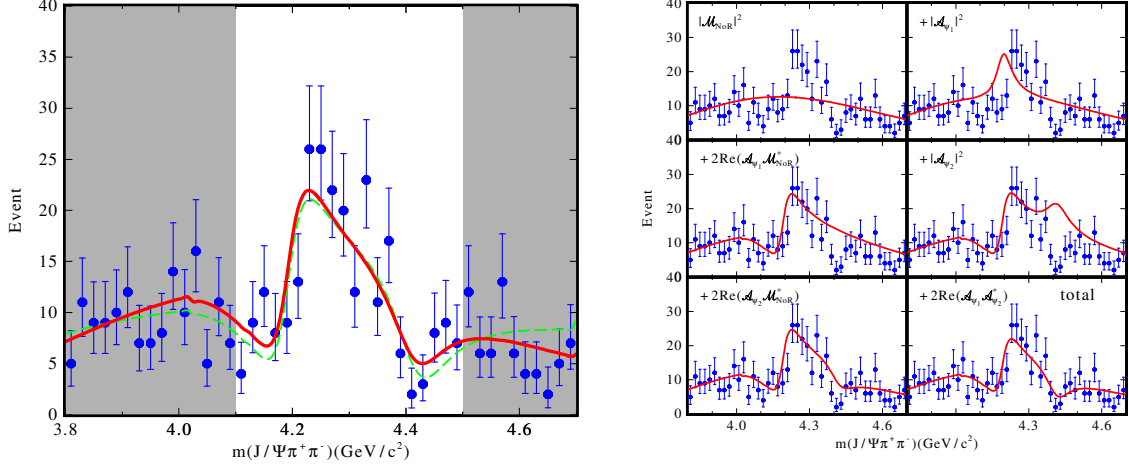


Figure 34: The fitted results of the  $e^+e^- \rightarrow J/\psi\pi^+\pi^-$  events distribution (left panel), and the change of the line shape of the cross section by adding the contributions from the terms  $|\mathcal{M}_{NoR}|^2$ ,  $|\mathcal{A}_{\psi_1}|^2$ ,  $2\text{Re}(\mathcal{A}_{\psi_1}\mathcal{M}_{NoR}^*)$ ,  $|\mathcal{A}_{\psi_2}|^2$ ,  $2\text{Re}(\mathcal{A}_{\psi_2}\mathcal{M}_{NoR}^*)$ , and  $2\text{Re}(\mathcal{A}_{\psi_1}\mathcal{A}_{\psi_2}^*)$ , step by step. The figure is adapted from Ref. [216].

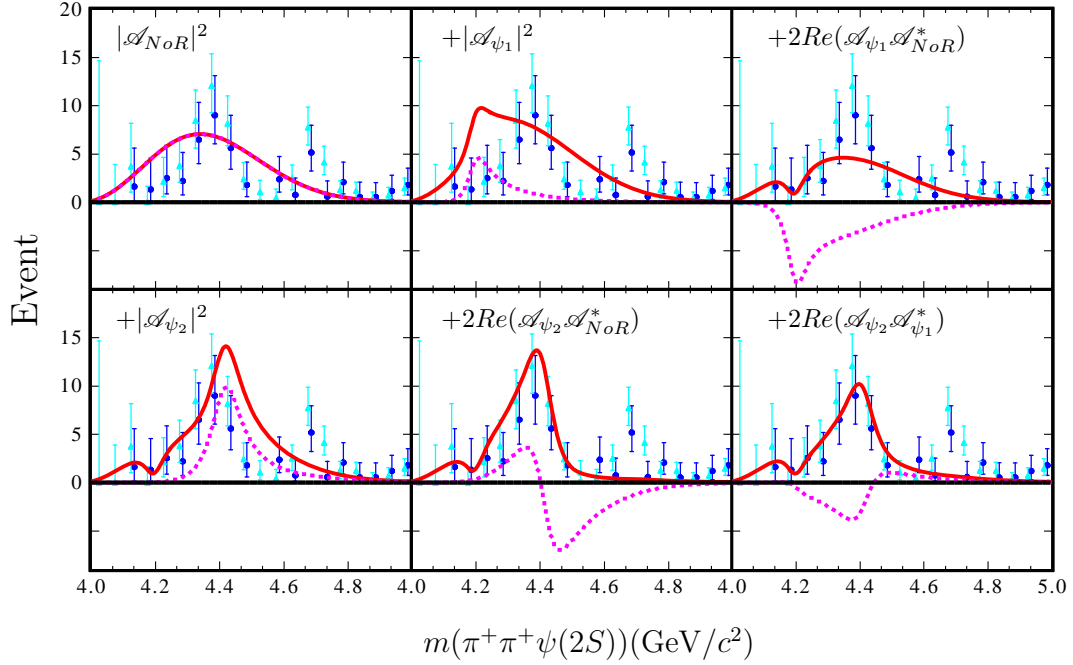


Figure 35: The fitted results of the  $e^+e^- \rightarrow \psi(3686)\pi^+\pi^-$  events distribution. The figure is adapted from Ref. [213].

Furthermore, the model inherently explains the non-observation of  $Y(4260)$  and  $Y(4360)$  in other channels: since no new resonant degrees of freedom are introduced, there is no mechanism to enhance open-charm decay rates or the inclusive  $R$  value near their masses. The structures are specific fingerprints of the interference patterns in their respective hidden-charm  $\pi^+\pi^-$  channels alone.

The non-resonant picture offers distinct advantages and opens new avenues for investigation. It provides a parsimonious explanation that operates within the realm of known particles and established non-perturbative mechanisms (hadronic loops), avoiding the need for exotic constituents or finely tuned dynamics. Its success with both  $Y(4260)$  and  $Y(4360)$  suggests it should be considered a viable alternative, especially for other charmonium-like states that are observed prominently in specific hidden-charm hadronic decays from  $e^+e^-$  annihilation but are elusive elsewhere.

In conclusion, the non-resonant picture represents a valuable and conceptually distinct approach in the theorist's toolkit, reminding us that not every peak in a cross-section necessitates a new particle, and that the rich interference of quantum mechanical amplitudes can itself be the source of striking structures in the spectrum of hadronic states.

## 4.2. From quenched to unquenched: the evolution of charmonium potential models

### 4.2.1. 1978: The Cornell potential—establishing the quenched framework

The discovery of the  $J/\psi$  in 1974 [3, 4] opened the era of charmonium spectroscopy. It was followed by the observation of  $\psi(3686)$  later that same year [462]. Subsequently,  $\chi_{c1}(1P)$  state was reported in 1975 [463], with  $\chi_{c2}(1P)$  [464] and the higher-mass  $\psi(4415)$  [465] identified in 1976. The year 1977 proved particularly productive, witnessing the discoveries of  $\psi(3770)$  [466],  $\chi_{c0}(1P)$  [467], and  $\psi(4040)$  [468]. Moreover, the first bottomonium state,  $\Upsilon(1S)$ , was also observed in 1977 [469], marking the parallel inception of bottomonium spectroscopy. The  $\psi(4160)$  was discovered in 1978 [458]. Later discoveries included the  $\eta_c(1S)$  in 1980 [470], the  $\eta_c(2S)$  in 1982 [471], and finally the  $h_c(1P)$  in 1986 [472] (with its confirmation coming in 1992 [473]). This series of discoveries, summarized chronologically in Fig. 1, provided the foundational experimental data that stimulated the development of the quenched potential model, most notably the Cornell potential.

This systematic experimental progress established the charmonium spectrum in the late twentieth century as a central testing ground for the nonperturbative behavior of strong interaction and for phenomenological models. Consequently, a pivotal theoretical advance was the formulation of the Cornell potential [10, 11, 12]. This model, proposed shortly after the initial charmonium discoveries, provided the first quantitative framework for hadron spectroscopy. It achieved this by capturing the essential features of QCD—asymptotic freedom at short distances and confinement at long distances—in a simple phenomenological form:

$$\mathcal{V}(r) = -\frac{\kappa}{r} + \frac{r}{a^2}, \quad (36)$$

where the first term represents a Coulomb-type potential originating from one-gluon exchange at short distances, and the second term is a linear confining potential that dominates at large distances, reflecting the phenomenon of quark confinement.

The Cornell group initially applied this model to determine the quantum numbers of  $J/\psi$  and  $\psi(3686)$  from their dielectron widths, and to predict properties of other low-lying  $S$ -,  $P$ -, and some  $D$ -wave states [10] (Fig. 36). The framework was later extended to incorporate a coupled-channel formalism [11]. A subsequent 1980 study [12] further refined the model, accurately reproducing masses and leptonic width ratios, extending it to the  $\Upsilon$  and heavy-light sectors, and providing a charmonium spectrum (Table 5).

Building upon the Cornell potential, subsequent phenomenological quark models sought to address its limitations. A key development was the 1985 Godfrey–Isgur (GI) model [13], which introduced relativistic corrections to the kinetic term and potential, achieving a unified description of mesons from light to heavy quarkonia and successfully predicting numerous unobserved states. Despite the advancement to more sophisticated frameworks like the GI model, the original Cornell potential remains a foundational, quenched benchmark. Its successful spectrum explained the charmonia observed in the late twentieth century, and its intuitive form continues to serve as a conceptual and computational cornerstone in hadron physics.

### 4.2.2. 1995: From lattice QCD to the screened potential—a step toward unquenching

The non-relativistic quark potential model has long served as an indispensable tool for understanding the spectrum of heavy quarkonia, systems where the relative motion of the heavy quark and antiquark is slow enough to warrant a

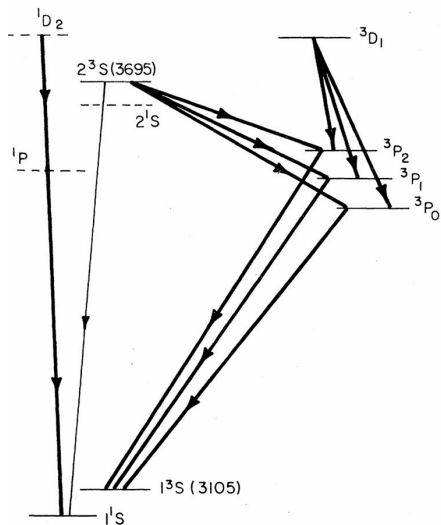


Figure 36: The charmonium spectrum obtained by Cornell group [10]. The vertical scale is schematic.

State	Mass (GeV)	Exp	Exp Mass (GeV)
1S	3.095	$J/\psi$	3.096
1P	3.522	$\chi_{c1}(1P)$	3.510
2S	3.684	$\psi(3686)$	3.686
1D	3.810	$\psi(3770)$	3.773
3S	4.110	$\psi(4040)$	4.040
2D	4.190	$\psi(4160)$	4.160
4S	4.460	$\psi(4415)$	4.415
5S	4.790	×	×

Table 5: The charmonium spectrum obtained by Cornell model [12] and is compared with the experimental data. For the state have not been observed in experiment at a period of Ref. [12] publication, a symbol "×" is presented.

Schrödinger equation treatment. The cornerstone of this approach is the Cornell potential, which combines a short-range Coulomb interaction from one-gluon exchange with a long-range linearly rising confining term<sup>4</sup>,  $V(r) = -\frac{4\alpha_s}{3r} + \sigma r$ . This model successfully described the masses and splittings of the low-lying  $c\bar{c}$  and  $b\bar{b}$  states. However, as experimental data on higher excitations accumulated in the 1980s and early 1990s, significant challenges arose.

A central puzzle involved the charmonium states  $\psi(4160)$  and  $\psi(4415)$ . In the standard linear potential model, the calculated mass of the  $2D$  state fell near 4160 MeV, while the  $4S$  state was predicted around 4415 MeV. This led to the natural assignments  $\psi(4160) = \psi(2D)$  and  $\psi(4415) = \psi(4S)$ . While the mass agreement was acceptable, the predicted leptonic widths were in severe conflict with data. The leptonic width of a  $^3S_1$  state is proportional to  $|\psi(0)|^2$ , the square of the wave function at the origin. For a  $D$ -wave state,  $\psi(0) = 0$  in the non-relativistic limit, leading to a vanishing leptonic width. Even with  $S$ - $D$  mixing or coupled-channel effects, the theoretical width for a  $2D$ -dominated state remained far too small to match the measured value of  $\Gamma_{e^+e^-}(\psi(4160)) \approx 0.77$  keV, which was comparable to that of the  $\psi(4040)$  ( $3S$ ) state [140]. Conversely, for  $\psi(4415)$  assigned as the  $4S$  state, the linear potential model typically predicted  $\Gamma_{e^+e^-} \sim 1.1$  keV, over a factor of two larger than the observed  $0.47 \pm 0.10$  keV. These difficulties suggested that the linear confining potential might be too rigid for highly excited states, overestimating both level spacings and wave function concentrations at the origin [140].

The key to resolving this impasse came from considering the dynamic nature of the QCD vacuum. In the quenched approximation, which neglects virtual quark-antiquark pair creation, the color electric flux between a static  $Q\bar{Q}$  pair forms a string-like tube with constant energy density, leading to a linearly rising potential. However, when dynamical light quarks are present, as in full QCD, the string can break via the creation of a light  $q\bar{q}$  pair when the stored energy is sufficient. This phenomenon, known as color screening, softens the potential at large distances, causing it to saturate. Lattice QCD simulations with dynamical fermions by Laermann *et al.* in 1986 provided early evidence for this effect [474, 475], showing a clear deviation from linearity at separations beyond roughly 1 fm.

Building on this physical insight, phenomenological studies introduced modified confining potentials that incorporated screening. A particularly instructive form, adopted by Ding, Chao, and Qin [140], was:

$$V_{\text{conf}}(r) = \sigma r \left( \frac{1 - e^{-\mu r}}{\mu r} \right),$$

<sup>4</sup>The Cornell potential used here differs slightly from the standard form given in Refs. [10, 11, 12]. For practical purposes, we retain this modified version throughout the present subsection.

which reduces to  $\sigma r$  for  $r \ll 1/\mu$  and approaches the constant  $\sigma/\mu$  for  $r \gg 1/\mu$ . The parameter  $\mu$  represents the inverse screening length. Combined with the Coulomb term, the total potential becomes  $V(r) = -\frac{4\alpha_s}{3r} + V_{\text{conf}}(r)$ . Independently, Dong *et al.* employed an error-function form,  $V_{\text{conf}}(r) = V_\mu \text{erf}(\mu_0 r)$ , which exhibits similar asymptotic behavior [476].

The work of Ding, Chao, and Qin performed a comprehensive analysis of both  $c\bar{c}$  and  $b\bar{b}$  spectra using the screened potential [139, 140]. They found that a good simultaneous fit to masses and leptonic widths (including QCD radiative corrections) required a relatively large string tension,  $\sigma = (0.26 - 0.32) \text{ GeV}^2$ , and a screening parameter  $\mu \approx 0.14 - 0.16 \text{ GeV}$  [140]. With these parameters, the calculated spectrum underwent a significant rearrangement for higher states. The  $\psi(4160)$  was naturally identified as the  $4S$ -dominated state, while  $\psi(4415)$  became the  $5S$  state. This reassignment immediately solved the leptonic width puzzle: the  $4S$  state, being an  $S$ -wave, naturally had a sizable  $\Gamma_{e^+e^-}$ , and the screened potential reduced  $|\psi(0)|^2$  for higher  $S$ -waves, bringing  $\Gamma_{e^+e^-}(\psi(4415))$  down into agreement with experiment. Their calculations also successfully reproduced the masses and leptonic widths of the  $\Upsilon$  family, including the higher  $6S$  state.

The study by Dong *et al.* reached very similar conclusions using the error-function potential [476]. They obtained five  $S$ -wave charmonium solutions below 4.41 GeV, with the fourth and fifth matching  $\psi(4160)$  and  $\psi(4415)$  in both mass and leptonic width. They emphasized that the screening effect not only lowered the energies of high-lying states but also modified their wave functions, reducing their amplitude at the origin and hence the leptonic widths.

These works marked a paradigm shift. By moving from a strictly linear, quenched potential to one that incorporates the screening effect expected from dynamical quarks, they took a crucial step toward an "unquenched" phenomenological description. This approach naturally explained the anomalous mass gap between what was then considered the  $3S$  and  $4S$  states (now  $4S$  and  $5S$ ) and resolved long-standing discrepancies in leptonic widths. The need for a larger string tension than the canonical Regge slope value of  $0.18 \text{ GeV}^2$  was an interesting outcome, potentially reflecting the difference between the static quark-antiquark tension and the effective tension in the presence of screening.

The introduction of the screened potential also had important implications for the interpretation of other states and opened new avenues. It suggested that the  $\psi(4415)$  might not be the highest  $S$ -wave state in that mass region and hinted at the possibility of missing states, a theme later explored in the prediction of a narrow  $\psi(4S)$  around 4.26 GeV.

Furthermore, Refs. [40, 322] demonstrated the consistency between the screening potential model and the coupled-channel quark model, emphasizing the role of coupled-channel and threshold effects. In this picture, the flattening of the confining potential is intrinsically linked to the opening of heavy–light meson decay channels.

In summary, research on screened potentials in the mid-1990s, driven largely by lattice QCD results, resolved key difficulties in heavy quarkonium spectroscopy. By including color screening effects from the light quark sea, it advanced beyond the quenched approximation and provided a more realistic approach for describing highly excited states. This framework enabled a systematic treatment of high-lying charmonium and can be naturally extended to bottomonium [328], heavy–light mesons [44, 477], and light-flavor mesons [478].

#### 4.2.3. 2014: Mass gaps and a prediction—evidence for a narrow charmonium state near 4.2 GeV

The comparison between the charmonium ( $c\bar{c}$ ) and bottomonium ( $b\bar{b}$ ) systems has long revealed intriguing spectroscopic regularities. A particularly clear pattern emerges when examining the mass gaps between successive radial excitations of the  $S$ -wave vector states ( $J^{PC} = 1^{--}$ ). For the well-established bottomonium family, the states  $\Upsilon(1S)$ ,  $\Upsilon(2S)$ ,  $\Upsilon(3S)$ , and  $\Upsilon(4S)$  exhibit smoothly progressing mass differences  $\Delta M_{n,n-1} = M(nS) - M((n-1)S)$ . In the charmonium sector, the analogous states  $J/\psi(1S)$ ,  $\psi(2S)$  ( $\psi(3686)$ ), and  $\psi(3S)$  ( $\psi(4040)$ ) show a strikingly similar pattern: the mass gap  $\Delta M_{21}$  is nearly identical for both families ( $\sim 589 \text{ MeV}$  for charmonium vs.  $\sim 563 \text{ MeV}$  for bottomonium), and  $\Delta M_{32}$  is also comparable (383 MeV vs. 333 MeV). However, this harmonious pattern appears to break for the next excitation. If the established  $\psi(4415)$  is assigned as  $\psi(4S)$ , the resulting mass gap  $\Delta M_{43}$  is about 375 MeV, which is significantly larger than the corresponding  $\Upsilon(4S)$ - $\Upsilon(3S)$  gap of approximately 224 MeV. This discrepancy suggests a possible misassignment or a missing state in the charmonium spectrum around 4.2 GeV, as shown in Fig. 38.

The 2014 work by He, Chen, Liu, and Matsuki directly confronted this puzzle by hypothesizing a missing  $\psi(4S)$  state [479]. The guiding principle was the assumed persistence of the mass-gap similarity between the two families. By adding the well-measured  $\Upsilon(4S)$ - $\Upsilon(3S)$  mass difference (224 MeV) to the mass of the charmonium  $\psi(3S)$  (4040 MeV), they predicted the mass of the missing  $\psi(4S)$  to be around 4263 MeV. This estimate is also consistent with

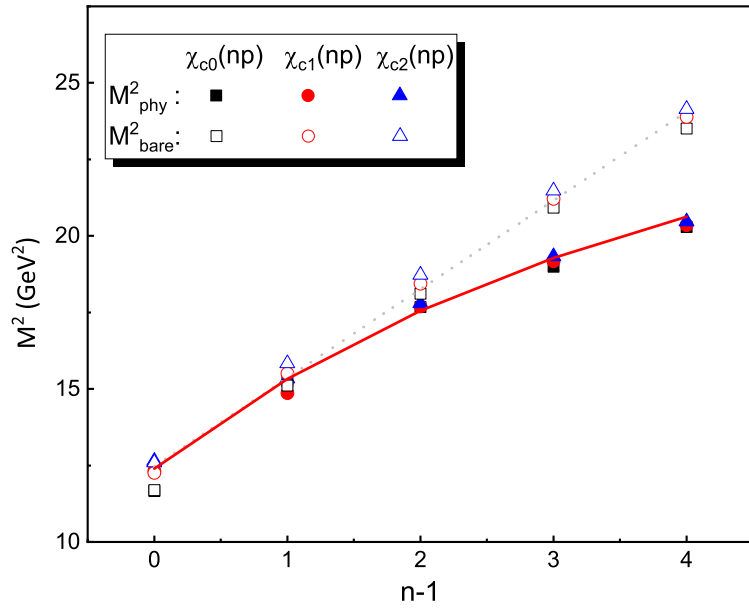


Figure 37: Comparison of the physical masses of the  $\chi_{cJ}(nP)$  ( $J = 0, 1, 2$ ) states in the coupled-channel quark model and the screening potential model (red solid curves), illustrating their equivalence. The grey dotted lines represent the predictions of the quenched GI model. Figure adapted from Ref. [322].

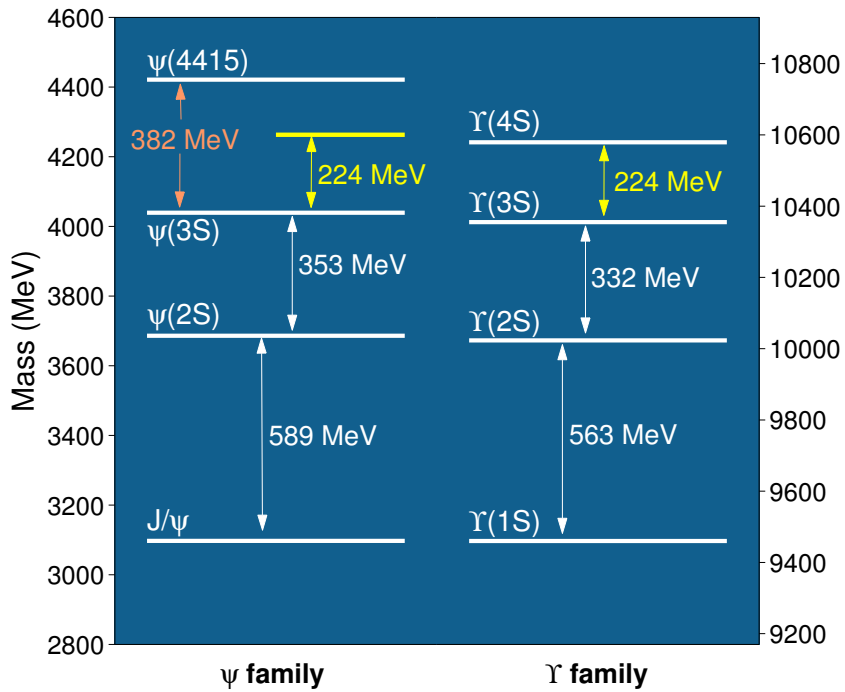


Figure 38: A comparison between the  $J/\psi$  and  $\Upsilon$  families [479].

the predictions for  $\psi(4S)$  obtained in the unquenched picture [139, 140, 299, 476]. This simple, symmetry-based prediction gained immediate theoretical credence from independent calculations. Notably, studies employing a screened potential, which incorporates the color-screening effects of dynamic light quark pairs, had already predicted the mass of the  $\psi(4S)$  to be around 4273 MeV [299], in excellent agreement with the mass-gap estimate. Another potential model calculation yielded a similar value of 4247 MeV [476]. This convergence of different approaches underscored the plausibility of a missing state in this mass region.

The central and most surprising result of the investigation lay in the decay properties of this predicted  $\psi(4S)$ . Using the QPC model to calculate its OZI-allowed open-charm decays ( $D\bar{D}$ ,  $D\bar{D}^* + c.c.$ ,  $D^*\bar{D}^*$ ,  $D_s\bar{D}_s$ , etc.), the authors found that the predicted total width was remarkably narrow, approximately 6 MeV, and stable across a reasonable range of model parameters. This narrow width persisted even when varying the input mass of the  $\psi(4S)$  within a range of 4241–4285 MeV, as illustrated in Fig. 39. The physical origin of this narrowness was attributed to strong node effects in the wavefunctions of higher radial excitations, which lead to significant cancellations in the decay amplitudes. This result was exceptional, as all other known charmonium states above the  $D\bar{D}$  threshold— $\psi(3770)$ ,  $\psi(4040)$ ,  $\psi(4160)$ , and  $\psi(4415)$ —possess widths on the order of tens to over a hundred MeV. The predicted narrow width provided a natural and compelling explanation for why such a state had escaped detection in previous experiments focused on open-charm final states and inclusive  $R$ -value scans, which are less sensitive to very narrow resonances.

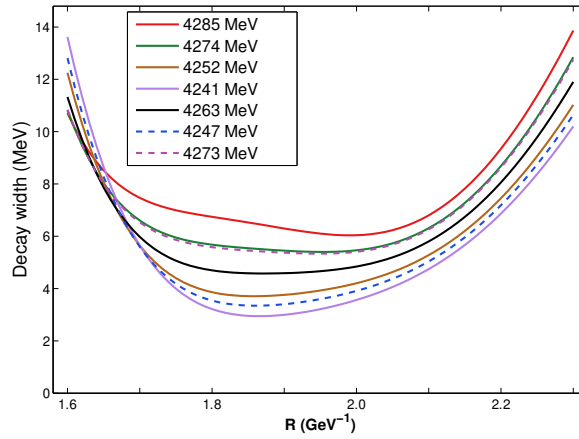


Figure 39: The dependence of the total decay width of  $\psi(4S)$  on the mass of  $\psi(4S)$  [479].

The study naturally addressed the relationship between the predicted narrow  $\psi(4S)$  and the broader charmonium-like states  $Y(4260)$  and  $Y(4360)$  observed in hidden-charm dipion transitions. Given the large disparity in widths (the predicted  $\sim 6$  MeV versus the experimental  $\sim 95$  MeV and  $\sim 74$  MeV for  $Y(4260)$  and  $Y(4360)$ , respectively), the authors concluded that neither of these observed structures could be identified with the conventional  $\psi(4S)$ . This conclusion was consistent with earlier non-resonant explanations proposed for  $Y(4260)$  and  $Y(4360)$ , which attributed their enhancements to interference effects in the production process rather than to genuine resonances.

A crucial experimental connection emerged from the analysis by Yuan in [480]. Yuan examined the BESIII data on  $e^+e^- \rightarrow h_c(1P)\pi^+\pi^-$  and identified two structures: a narrow one with mass  $4216 \pm 18$  MeV and width  $39 \pm 22$  MeV, and a broad one around 4293 MeV. The narrow structure, denoted  $Y(4216)$ , bears a striking resemblance to the predicted  $\psi(4S)$  in both mass and width. Although its central mass is about 47 MeV lower than the predicted 4263 MeV, this difference is within the combined theoretical and experimental uncertainties. More importantly, its narrow width aligns qualitatively with the theoretical expectation. This observation provides a tangible experimental hint that the missing  $\psi(4S)$  might indeed be present in the data, awaiting further confirmation through more precise measurements and analyses.

The work also examined the properties of other states. It strongly supported the identification of  $X(3940)$  with  $\eta_c(3S)$ , as its calculated width and dominant decay to  $D\bar{D}^*$  matched the experimental data. Conversely, it decisively excluded the  $\eta_c(4S)$  assignment for  $X(4160)$ , as the predicted  $\eta_c(4S)$  was also found to be very narrow, incompatible with the broad width of  $X(4160)$ . Finally, the analysis explored the possibility of  $\psi(4415)$  being  $\psi(5S)$ , finding general

consistency with several measured branching ratios, though some tensions remained.

In summary, the 2014 study proposed a semi-quantitative and predictive framework from a phenomenological perspective, which resolved a spectroscopic irregularity by positing a missing, narrow  $\psi(4S)$  state near 4.26 GeV. The prediction was rooted in the comparative analysis of heavy quarkonia, bolstered by potential model calculations, and received tentative support from emerging experimental data. The analysis by Yuan in [480] offered a promising experimental counterpart in the form of  $Y(4216)$ , reinforcing the relevance of this prediction. By highlighting the profound impact of wavefunction nodes on the decays of high radial excitations, it offered a deeper understanding of charmonium dynamics above open-charm thresholds. This work stands as a testament to the enduring value of spectroscopic systematics and continues to motivate precise experimental investigations at facilities like BESIII, Belle, and Belle II.

#### 4.3. 2017: Precise data reveal more charmonium-like $Y$ structures—the $Y$ problem

In 2017, the BESIII Collaboration performed a high precise measurement of the  $e^+e^- \rightarrow J/\psi\pi^+\pi^-$  process [55], which was a representative channel through which  $Y(4260)$  was originally discovered. The new results brought important surprises: the line shape of  $Y(4260)$  enhancement in total cross section was found to be highly asymmetric, and detailed analyses revealed that it actually contains two substructures: one is a newly observed state, now called  $Y(4320)$ , while the other corresponds to the main enhancement previously attributed to  $Y(4260)$ . Compared with the resonance parameters of  $Y(4260)$ , it shifts downward by about 40 MeV in mass and becomes narrower in width, from over 70 MeV to roughly 40 MeV. This state has therefore been renamed as  $Y(4220)$ . It is worth mentioning that the updated  $Y(4220)$  closely resembles a narrow peak around 4.23 GeV reported by BESIII as early as in 2016 in the  $\chi_{c0}\omega$  channel [481]. Additionally,  $Y(4220)$  also was soon discovered in several other independent processes, including  $e^+e^- \rightarrow h_c\pi^+\pi^-$  [56],  $e^+e^- \rightarrow \psi(3686)\pi^+\pi^-$  [380] and  $e^+e^- \rightarrow h_c\eta$  [381].

The updated measurements of  $Y(4260)$  have significantly reshaped our understanding of this state, particularly the long-standing puzzle of why no clear signal of  $Y(4260)$  was observed in open-charm cross sections or in  $R$ -value scans. In fact, in recent years, new experimental measurements have revealed the existence of peaks or dip-like structures around  $\sqrt{s} \approx 4.22$  GeV not only in several open-charm channels [382, 389] but also in the  $e^+e^- \rightarrow \mu^+\mu^-$  process [386], which is closely tied to the  $R$ -value measurement. The extracted resonance parameters in these channels are highly consistent with those of  $Y(4220)$  [55, 56, 380, 381], indicating that earlier knowledge of  $Y(4260)$  indeed require substantial revision. These experimental developments suggest that many of the previous theoretical discussions regarding  $Y(4260)$  may need to be reconsidered.

The study of  $Y(4220)$  has in fact become one of the central physics topics for the BESIII experiment over the past decade. Now, the existence of this state is firmly established, as it has been observed in more than ten different processes, including both hidden-charm and open-charm decay channels [55, 56, 380, 381, 382, 383, 384, 385, 386, 387, 388, 389, 390, 391, 392, 393, 394, 395]. A summary of the measured total cross sections of the relevant processes and corresponding  $Y(4220)$  resonance signals are presented in Fig. 40. Remarkably, the fitted masses across these processes consistently point to a value around 4.22 GeV, as compiled in Table 6, which also lists the resonance parameters of  $Y(4220)$  and its combined product of di-lepton width and decay branching fractions in different channels. It can be seen that the decays of  $Y(4220)$  are characterized by a relatively higher contribution from open-charm final states, while hidden-charm modes remain important, representing a considerable departure from some of the earlier conclusions drawn for  $Y(4260)$ .

Additionally, the BESIII Collaboration also measured the cross sections of the processes  $e^+e^- \rightarrow \pi^+\pi^-\psi(3770)$  [482],  $e^+e^- \rightarrow \eta_c\pi^+\pi^-$  [387],  $e^+e^- \rightarrow \eta_c\pi^0\gamma$  [387],  $e^+e^- \rightarrow \chi_{cJ}\pi^+\pi^-$  [483],  $e^+e^- \rightarrow \eta\psi(3686)$  [484, 485] and  $e^+e^- \rightarrow \pi^+\pi^-D^+D^-$  [486], but in which they cannot find any significant signal of  $Y(4220)$ . Beyond hidden- and open-charm processes, channels involving purely light mesons or even baryon–antibaryon pairs are also of great interest. This is because different underlying structures of  $Y(4220)$  are expected to lead to very different decay behaviors. For instance, if the state contains a sizable compact component such as a charmonium or glueball, one might expect decay patterns analogous to those of  $J/\psi$  or  $\psi(3686)$ , where three-gluon annihilation decay leads to abundant light-hadron final states. By contrast, such mechanisms are not naturally anticipated if  $Y(4220)$  is instead a hadronic molecular state. In recent years, BESIII has carried out extensive searches in these channels [487, 488, 489, 490, 491, 492, 493, 494, 495, 496, 497, 498, 499, 500, 501, 502, 503, 504, 505, 506, 507, 508, 509, 510]. Although no definite evidence of  $Y(4220)$  decays into purely light hadrons has been observed so far, largely due to limited statistics, these measurements nevertheless provide important implications for understanding its nature. The relevant cross section

measurement results with possible hint of a structure around 4.2 GeV exhibiting in the line shape are summarized and presented in Fig. 41.

Since 2017, high-statistics energy scans performed by the BESIII experiment have revealed more vector charmonium-like  $Y$  states above 4.3 GeV. In the measurement of the process  $e^+e^- \rightarrow \pi^+\pi^-J/\psi$  [55], based on an integrated luminosity of about  $9 \text{ fb}^{-1}$  collected at center-of-mass energies from 3.77 GeV to 4.60 GeV, the observed cross section exhibits a line shape that requires more than one resonant contribution. A fit with two coherent Breit–Wigner amplitudes indicates a structure near 4.23 GeV, referred to as  $Y(4220)$ , together with a higher-mass enhancement around 4.32 GeV, denoted as  $Y(4320)$ . The resonance parameters of  $Y(4320)$  are determined to be  $M = (4320.0 \pm 10.4 \pm 7.0) \text{ MeV}/c^2$  and  $\Gamma = (101.4^{+25.3}_{-19.7} \pm 10.2) \text{ MeV}$ , with a statistical significance exceeding  $7.6\sigma$ . Its measured mass is noticeably lower than that of  $Y(4360)$  previously observed in the  $\pi^+\pi^-\psi(3686)$  channel [52, 53], although the two structures have comparable widths within uncertainties. No evidence for  $Y(4008)$  is found in the  $\pi^+\pi^-J/\psi$  final state with highly precise data [55]. The information of another higher  $Y$  state is obtained from the study of  $e^+e^- \rightarrow \pi^+\pi^-h_c$  [56], where BESIII measured the cross section at 79 center-of-mass energy points between 3.896 GeV and 4.600 GeV. The data clearly favor a two-resonance description, with significant structures observed at  $\sqrt{s} \approx 4.23 \text{ GeV}$  and 4.39 GeV. For the higher-mass structure, referred to as  $Y(4390)$ , the fit yields a mass of  $M = (4391.5^{+6.3}_{-6.8} \pm 1.0) \text{ MeV}$  and a width of  $\Gamma = (139.5^{+16.2}_{-20.6} \pm 0.6) \text{ MeV}$ , and the two-resonance hypothesis is favored over a single-resonance description with a significance exceeding  $10\sigma$  [56].

Further information of vector charmonium-like states in the 4.3–4.4 GeV region was provided from precise BESIII measurements of the process  $e^+e^- \rightarrow \pi^+\pi^-\psi(3686)$  [380]. Over the measured energy range between 4.008 GeV and 4.600 GeV, the measured cross section exhibits pronounced energy dependence and shows, in addition to  $Y(4220)$ , a higher-mass enhancement associated with the state historically referred to as  $Y(4360)$ . A line-shape analysis yields resonance parameters of  $M = (4383.8 \pm 4.2 \pm 0.8) \text{ MeV}$  and  $\Gamma = (84.2 \pm 12.5 \pm 2.1) \text{ MeV}$  [380]. This state was originally observed as the  $Y(4360)$  in the  $\pi^+\pi^-\psi(3686)$  channel in initial-state radiation measurements [52, 53], however, within the current experimental uncertainties with higher precision, the resonance parameters determined by BESIII are consistent with those of  $Y(4390)$  observed in  $e^+e^- \rightarrow \pi^+\pi^-h_c$ . Evidence for a vector state with compatible mass and width was also reported in an independent study of the process  $e^+e^- \rightarrow \eta J/\psi$  [384], where a resonance with mass  $M = (4382.0 \pm 13.3 \pm 1.7) \text{ MeV}$  and width  $\Gamma = (135.8 \pm 60.8 \pm 22.5) \text{ MeV}$  is observed. Together with the BESIII observations of  $Y(4320)$  and  $Y(4390)$  in other hidden-charm decay channels, these results demonstrate that multiple structures appear in the 4.3–4.4 GeV energy region across different final states, while whether these structures arise from a common resonance or differ significantly among decay channels remains an open question.

The BESIII Collaboration has extended the study of vector charmonium-like states to the strange meson channel  $e^+e^- \rightarrow K^+K^-J/\psi$  using data collected at center-of-mass energies between 4.127 GeV and 4.600 GeV [388]. The measured cross sections exhibit two resonant contributions, one consistent with the established  $Y(4220)$  and a second structure observed for the first time with a statistical significance exceeding  $8\sigma$ . This higher-mass state is denoted as  $Y(4500)$ , with a measured mass of  $(4484.7 \pm 13.3 \pm 24.1) \text{ MeV}$  and a width of  $(111.1 \pm 30.1 \pm 15.2) \text{ MeV}$ . The observation of  $Y(4500)$  in the  $K^+K^-J/\psi$  final state establishes a new vector charmonium-like  $Y$  state in this mass region and provides a qualitatively new experimental input beyond non-strange hidden-charm processes.

Prior to 2017, two vector charmonium-like  $Y$  states,  $Y(4630)$  and  $Y(4660)$ , had been established in the vicinity of 4.6 GeV through  $e^+e^-$  annihilation.  $Y(4630)$  was first observed by Belle in the baryonic channel  $e^+e^- \rightarrow \Lambda_c^+\Lambda_c^-$ , with a mass of  $4634^{+8+5}_{-7-8} \text{ MeV}/c^2$  and a width of  $92^{+40+10}_{-24-21} \text{ MeV}$  [54].  $Y(4660)$  was discovered in the hidden-charm process  $e^+e^- \rightarrow \psi(3686)\pi^+\pi^-$  by Belle, with a mass of  $4664 \pm 11 \pm 5 \text{ MeV}$  and a width of about  $48 \pm 15 \pm 3 \text{ MeV}$  [53]. Since 2017, the experimental landscape of  $Y$  states above 4.6 GeV has also become increasingly rich. In 2019, Belle reported a vector charmonium-like state in  $e^+e^- \rightarrow D_s^+D_{s1}(2536)^-$ , with a mass of  $4625.9^{+6.2}_{-6.0} \pm 0.4 \text{ MeV}$  and a width of  $49.8^{+13.9}_{-11.5} \pm 4.0 \text{ MeV}$  [511], whose resonant parameters are consistent with those of  $Y(4630)$  within the uncertainties.

Recent high-precision measurements by the BESIII Collaboration in the open-charm channel  $e^+e^- \rightarrow D^{*0}D^{*-}\pi^+$  have revealed three vector charmonium-like states [389]. The third state has a mass of  $4675.3 \pm 29.5 \pm 3.5 \text{ MeV}/c^2$  and a width of  $218.3 \pm 72.9 \pm 9.3 \text{ MeV}$ . While its mass is consistent with that of the earlier  $Y(4660)$ , its width is significantly larger, likely reflecting different interference effects or different theoretical origins. This marks the first clear observation of a  $Y(4660)$ -like state in an open-charm decay. Additionally, a second resonance, with mass  $4469.1 \pm 26.2 \pm 3.6 \text{ MeV}/c^2$  and width  $246.3 \pm 36.7 \pm 9.4 \text{ MeV}$ , is compatible with those of the  $Y(4500)$  previously observed in  $e^+e^- \rightarrow K^+K^-J/\psi$  [388]. If assuming them to be the same state, the substantial branching fraction of  $Y(4500)$  to  $D^*\bar{D}^*\pi$  compared to  $K\bar{K}J/\psi$  [389], would challenge a hidden-strangeness tetraquark interpretation for

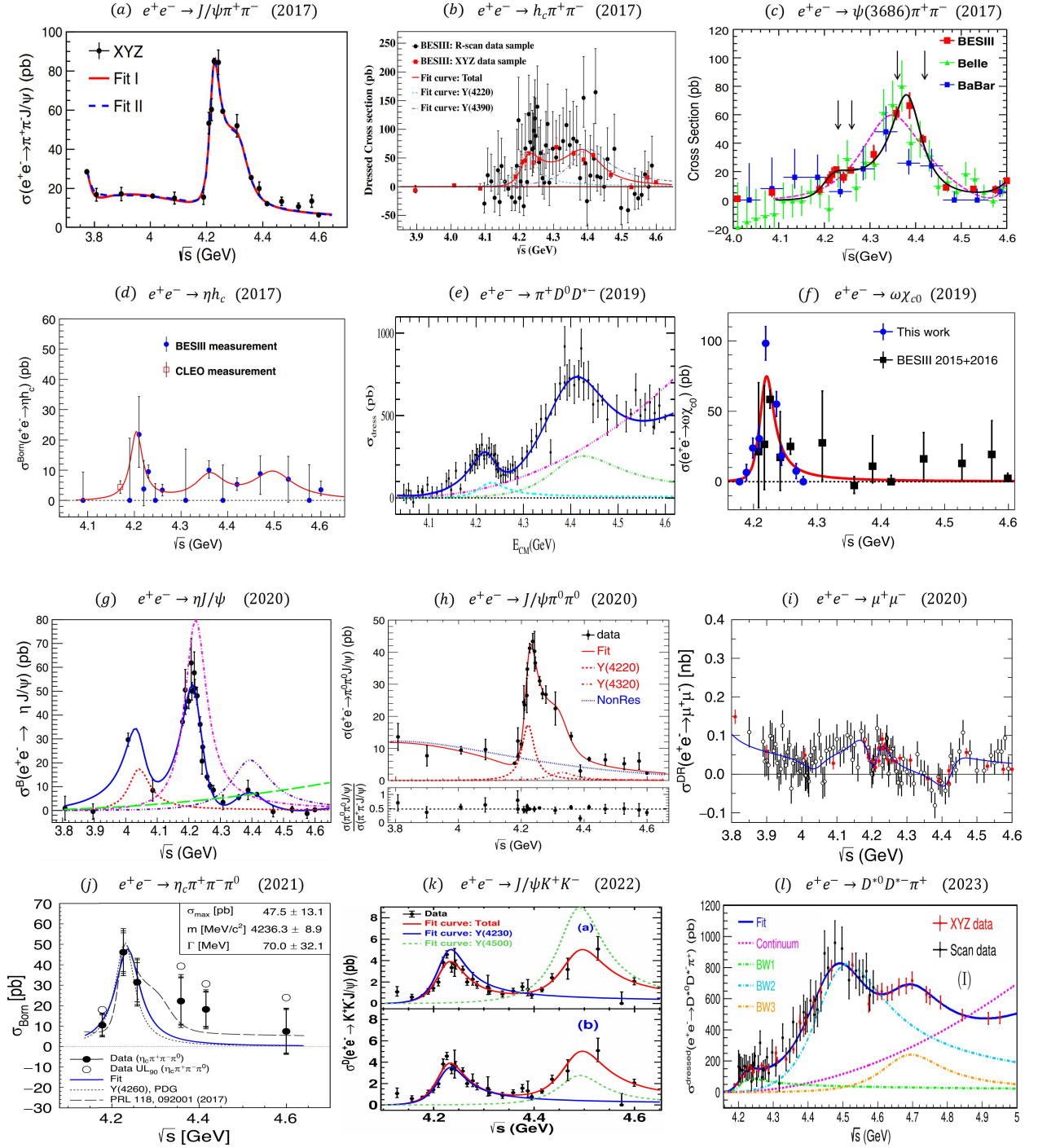


Figure 40: The measured cross sections of  $e^+e^- \rightarrow J/\psi\pi^+\pi^-$  [55],  $e^+e^- \rightarrow h_c\pi^+\pi^-$  [56],  $e^+e^- \rightarrow \psi(3686)\pi^+\pi^-$  [380],  $e^+e^- \rightarrow h_c\eta$  [381],  $e^+e^- \rightarrow D^0D^{*-}\pi^+$  [382],  $e^+e^- \rightarrow \chi_{c0}\omega$  [383],  $e^+e^- \rightarrow J/\psi\eta$  [384],  $e^+e^- \rightarrow J/\psi\pi^0\pi^0$  [385],  $e^+e^- \rightarrow \mu^+\mu^-$  [386],  $e^+e^- \rightarrow \eta_c\pi^+\pi^-\pi^0$  [387],  $e^+e^- \rightarrow J/\psi K^+K^-$  [388] and  $e^+e^- \rightarrow D^{*0}D^{*+}\pi^+$  [389], in which the Y(4220) state had been observed.

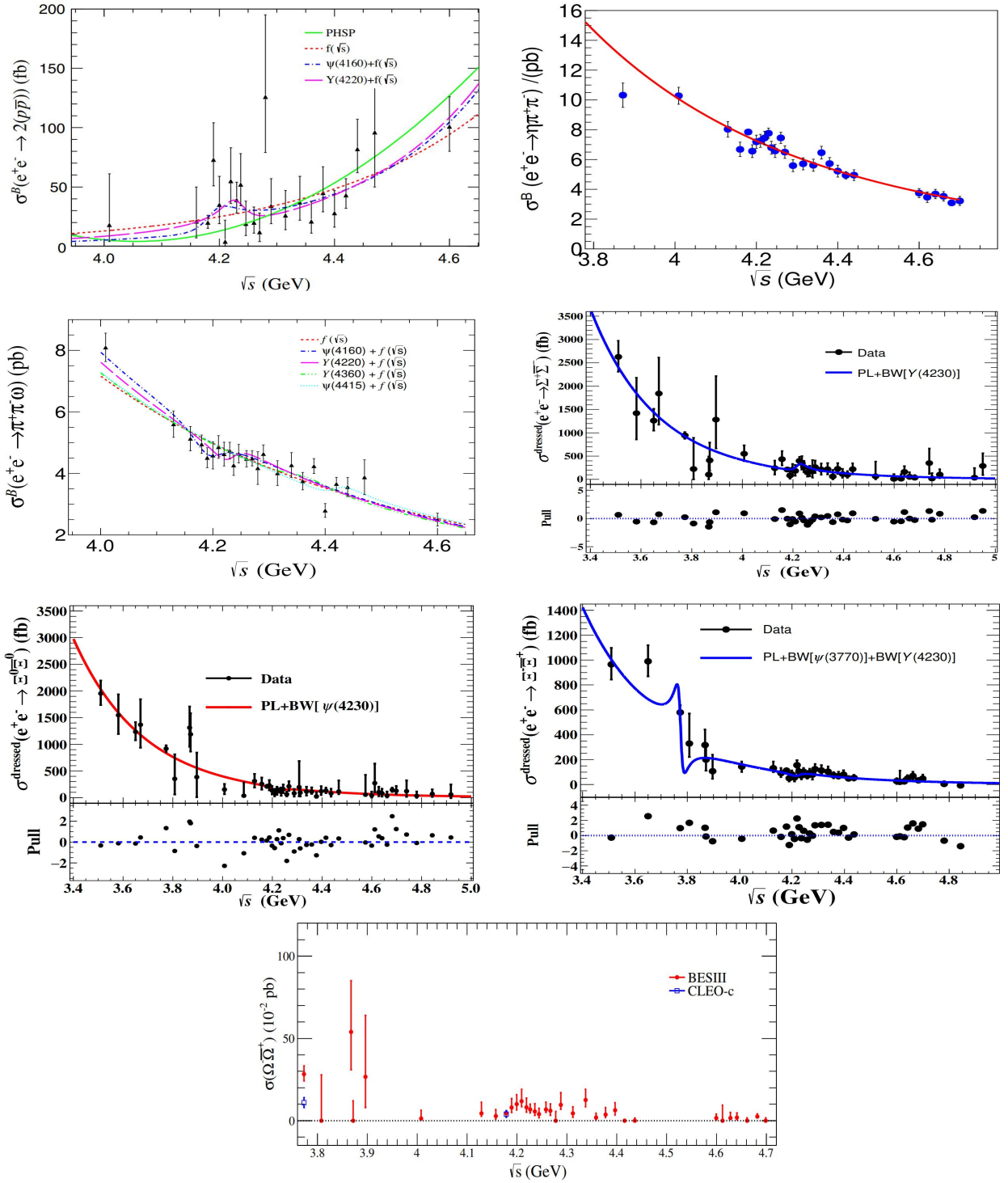


Figure 41: Measured cross sections of  $e^+e^-$  annihilation into light hadronic final states, in which although no obvious  $Y(4220)$  signal is observed, their line shapes exhibit possible structures around 4.2 GeV that warrant confirmation with higher-statistics data in the future. These processes include  $e^+e^- \rightarrow 2(p\bar{p})$  [487],  $e^+e^- \rightarrow \eta\pi^+\pi^-$  [488],  $e^+e^- \rightarrow \omega\pi^+\pi^-$  [489],  $e^+e^- \rightarrow \Sigma^+\Sigma^-$  [490],  $e^+e^- \rightarrow \Xi^0\bar{\Xi}^0$  [491],  $e^+e^- \rightarrow \Xi^-\bar{\Xi}^+$  [492] and  $e^+e^- \rightarrow \Omega^-\bar{\Omega}^+$  [493].

Table 6: The summary of the experimental resonance parameters of  $Y(4220)$  and its combined product of di-lepton width and decay branching fractions in different channels, which are obtained by a Breit-Wigner fit to total cross section.

Resonance parameters	Mass (MeV)	Width (MeV)	$\Gamma_{e^+e^-} \mathcal{B}_{\text{Final states}}$ (eV)
$e^+e^- \rightarrow Y(4220) \rightarrow J/\psi\pi^+\pi^-$ [55]	$4222.0 \pm 3.1(4220.9 \pm 2.9)$	$44.1 \pm 4.3(44.1 \pm 3.8)$	$13.3 \pm 1.4(12.0 \pm 1.0)$
			$9.2 \pm 0.7(8.9 \pm 0.6)$
			$2.3 \pm 0.6(2.1 \pm 0.4)$
			$1.6 \pm 0.4(1.5 \pm 0.3)$
$e^+e^- \rightarrow Y(4220) \rightarrow h_c\pi^+\pi^-$ [56]	$4218.4^{+5.5}_{-4.5} \pm 0.9$	$66.0^{+12.3}_{-8.3} \pm 0.4$	$4.6^{+2.9}_{-1.4}$
$e^+e^- \rightarrow Y(4220) \rightarrow \psi(3686)\pi^+\pi^-$ [380]	$4209.5 \pm 7.4$	$80.1 \pm 24.6$	$0.8 \pm 0.7$ $0.4 \pm 0.3$
$e^+e^- \rightarrow Y(4220) \rightarrow h_c\eta$ [381]	$4204 \pm 6$	$32 \pm 22$	...
$e^+e^- \rightarrow Y(4220) \rightarrow D^0D^{*-}\pi^+$ [382]	$4228.6 \pm 4.1$	$77.0 \pm 6.8$	$77.4 \pm 10.1$
			$8.6 \pm 1.6$
			$99.5 \pm 14.6$
			$11.1 \pm 2.3$
$e^+e^- \rightarrow Y(4220) \rightarrow \chi_{c0}\omega$ [383]	$4218.5 \pm 1.6$	$28.2 \pm 3.9$	$2.5 \pm 0.2$
$e^+e^- \rightarrow Y(4220) \rightarrow J/\psi\eta$ [384]	$4218.6 \pm 3.8$	$82.0 \pm 5.7$	$8.0 \pm 1.7$
			$4.8 \pm 1.0$
			$7.0 \pm 1.5$
$e^+e^- \rightarrow Y(4220) \rightarrow J/\psi\pi^0\pi^0$ [385]	$4220.4 \pm 2.4$	$46.2 \pm 4.7$	$0.99 \pm 0.17$
			$4.13 \pm 0.28$
			$1.38 \pm 0.30$
			$5.72 \pm 0.57$
$e^+e^- \rightarrow Y(4220) \rightarrow \mu^+\mu^-$ [386]	$4216.7 \pm 8.9 \pm 4.1$	$47.2 \pm 22.8 \pm 10.5$	$1.53 \pm 1.26 \pm 0.54$
	$4213.6 \pm 7.5 \pm 4.1$	$39.9 \pm 19.5 \pm 8.9$	$1.28 \pm 1.09 \pm 0.46$
	$4213.7 \pm 6.0 \pm 4.1$	$38.5 \pm 12.8 \pm 8.5$	$1.20 \pm 0.67 \pm 0.42$
	$4216.2 \pm 5.7 \pm 4.1$	$45.5 \pm 13.3 \pm 10.1$	$1.46 \pm 0.89 \pm 0.52$
	$4219.4 \pm 11.2 \pm 4.1$	$49.6 \pm 22.6 \pm 11.0$	$1.50 \pm 1.03 \pm 0.53$
	$4212.8 \pm 7.2 \pm 4.0$	$36.4 \pm 16.8 \pm 8.1$	$1.12 \pm 0.89 \pm 0.40$
	$4216.1 \pm 7.5 \pm 4.1$	$37.8 \pm 18.5 \pm 8.4$	$1.09 \pm 0.84 \pm 0.39$
$4217.3 \pm 9.1 \pm 4.1$	$45.5 \pm 21.2 \pm 10.1$	$1.40 \pm 1.08 \pm 0.50$	
$e^+e^- \rightarrow Y(4220) \rightarrow \eta_c\pi^+\pi^-\pi^0$ [387]	$4236.3 \pm 8.9$	$70.0 \pm 32.1$	...
$e^+e^- \rightarrow Y(4220) \rightarrow J/\psi K^+K^-$ [388]	$4225.3 \pm 2.3 \pm 21.5$	$72.9 \pm 6.1 \pm 30.8$	$0.42 \pm 0.04 \pm 0.15$
			$0.29 \pm 0.02 \pm 0.10$

These values denote the partial width of  $Y(4220) \rightarrow e^+e^-$  in units of keV by assuming  $\Gamma_{e^+e^-} = \Gamma_{\mu^+\mu^-}$  as in the BESIII analysis [386].

Table 6: Table 6 (continued).

Resonance parameters	Mass (MeV)	Width (MeV)	$\Gamma_{e^+e^-} \mathcal{B}_{\text{Final states}}$ (eV)
$e^+e^- \rightarrow Y(4220) \rightarrow D^{*0}D^{*-}\pi^+$ [389]	$4209.6 \pm 4.7$	$81.6 \pm 17.8$	$5.4 \pm 1.1$
			$6.0 \pm 1.3$
			$4.8 \pm 0.9$
			$5.3 \pm 1.1$
			$17.9 \pm 7.2$
			$19.8 \pm 6.6$
			$20.2 \pm 7.4$
			$22.4 \pm 9.0$
$e^+e^- \rightarrow Y(4220) \rightarrow \psi(3686)\pi^+\pi^-$ [390]	$4234.4 \pm 3.2$	$17.6 \pm 8.1$	$1.59 \pm 0.75$
			$1.63 \pm 0.78$
			$0.02 \pm 0.01$
			$0.02 \pm 0.01$
$e^+e^- \rightarrow Y(4220) \rightarrow J/\psi\pi^+\pi^-$ [391]	$4221.4 \pm 1.5(4220.1 \pm 1.2)$	$41.8 \pm 2.9(43.6 \pm 2.6)$	$1.7 \pm 0.2(1.7 \pm 0.2)$
			$8.2 \pm 0.9(8.6 \pm 0.5)$
			$3.0 \pm 0.5(2.5 \pm 0.3)$
			$14.6 \pm 1.2(12.7 \pm 0.8)$
$e^+e^- \rightarrow Y(4220) \rightarrow J/\psi K_S^0 K_S^0$ [392]	$4226.9 \pm 6.6 \pm 22.0$	$71.7 \pm 16.2 \pm 32.8$	$0.13 \pm 0.02 \pm 0.05$
			$0.14 \pm 0.03 \pm 0.06$
			$0.18 \pm 0.05 \pm 0.07$
			$0.20 \pm 0.04 \pm 0.07$
$e^+e^- \rightarrow Y(4220) \rightarrow J/\psi\eta$ [393]	$4219.7 \pm 2.5$	$80.7 \pm 4.4$	$4.0 \pm 0.5$
			$5.5 \pm 0.7$
			$8.7 \pm 1.0$
			$11.9 \pm 1.1$
$e^+e^- \rightarrow Y(4220) \rightarrow h_c\eta$ [394]	$4188.8 \pm 4.7 \pm 8.0$	$49 \pm 16 \pm 19$	$0.80 \pm 0.19 \pm 0.45$
$e^+e^- \rightarrow Y(4220) \rightarrow h_c\pi^+\pi^-$ [395]	$4223.6^{+3.6+2.6}_{-3.7-2.9}$	$58.5^{+10.8+6.7}_{-11.4-6.5}$	$10.2^{+1.2+1.4}_{-1.5-1.4}$ $0.9^{+0.4+0.3}_{-0.4-0.2}$

$Y(4500)$ .

Very recently, the BESIII measurements of the  $e^+e^- \rightarrow K_S^0 K_S^0 J/\psi$  cross section reported evidence for a new vector charmonium-like state,  $Y(4710)$ , with a statistical significance of  $4.2\sigma$  [392]. Its mass and width are determined to be  $M = 4704.0 \pm 52.3 \pm 69.5$  MeV and  $\Gamma = 183.2 \pm 114.0 \pm 96.1$  MeV, respectively. Notably, no significant signal is observed for  $Y(4500)$  in this decay mode [392], in contrast to its clear appearance in  $K^+K^-J/\psi$ . Independently, a high-precision study of  $e^+e^- \rightarrow D_s^{*+}D_s^{*-}$  reveals another distinct structure near 4.79 GeV, denoted  $Y(4790)$ , with a significance exceeding  $6.1\sigma$  [396]. Its mass and width are found to be  $4786 \sim 4793$  MeV and  $27.1 \sim 60$  MeV, respectively, depending on the concrete fit scenario. These accumulating observations above 4.6 GeV further underscore the complexity of understanding the sector of vector  $Y$  states in the XYZ family.

As summarized in Fig. 29, a growing number of charmonium-like  $Y$  states have been observed with improving experimental precision. Explaining these states—particularly within a unified framework that can systematically assign them—poses a major theoretical challenge. The so-called "Y problem" was formally articulated in the *White Paper on the Future Physics Program of BESIII* [57]. A central issue is the overabundance of  $Y$  states, which presents a significant challenge regardless of whether they are interpreted as exotic hadrons or conventional charmonia.

We need novel approaches to address the  $Y$  problem. In fact, several key advances have been made over the past decade since 2011: the introduction of a Fano-like interference mechanism as a "resonance killer" [213, 216, 512, 513], the identification of  $Y(4220)$ —a narrow structure near 4.2 GeV—as a scaling point for constructing the higher charmonium family within an unquenched framework, and the emergence of a distinctive mass spectrum for vector charmonia in the 4-4.5 GeV region, which aligns with all available experimental data and has garnered experimental support. Indeed, this resulting mass spectrum helps clarify why the mass of  $\psi(4160)$  appears shifted to about 4190 MeV. In the following section, we review this progress. We note that this review article does not aim to comprehensively survey the current theoretical status of these newly observed  $Y$  states, especially from the viewpoint of exotic hadronic states. Interested readers are referred to the reviews in Refs. [14, 15, 16, 17, 18, 19, 20, 21, 22, 23, 24, 25, 26, 27, 28, 29, 30] for further details.

#### 4.4. Toward a unified theoretical framework for the $Y$ problem

##### 4.4.1. Non-resonant interference revisited: killing $Y(4320)$ and $Y(4390)$ and confirming $Y(4220)$ as a genuine resonance

The non-resonant Fano-like interference mechanism has proven to be a powerful tool for understanding charmonium-like  $Y$  states [213, 216, 512, 513]. Initially, it was used to explain the broad  $Y(4260)$  as an interference effect rather than a true resonance [213]. Following that work, as early as in 2015, Chen, *et al.* pointed to the existence of a distinct narrow resonance signal near 4.22 GeV by analyzing cross section data from channels like  $\pi^+\pi^- \psi(3686)$  and  $\omega\chi_{c0}$  independently in the electron-positron annihilation [225, 228]. Theoretical study of OZI-allowed two-body strong decays of higher charmonia further supported its interpretation as a missing conventional  $\psi(4S)$  charmonium [479]. Therefore, the high-precision measurements of the cross sections of  $e^+e^- \rightarrow \pi^+\pi^- J/\psi$  [55] and  $e^+e^- \rightarrow \pi^+\pi^- h_c$  [56] as well as open-charm process  $e^+e^- \rightarrow D^0 D^{*-} \pi^+$  [382] by BESIII allow us to re-examine the role of this non-resonant framework in understanding the observed enhancement structures. In Ref. [513], Chen, Liu and Matsuki analyzed these data with a coherent sum of amplitudes from a smooth background (parameterized phenomenologically) and the intermediate resonant contributions:

$$\mathcal{M}_{\text{Total}} = gu^2 e^{-au^2} + e^{i\phi_k} \sum_k \frac{\sqrt{12\pi R_k \Gamma_k}}{s - m_k^2 + im_k \Gamma_k} \cdot \sqrt{\frac{\Phi(s)}{\Phi(m_k^2)}},$$

where  $k$  corresponds to two established charmonium states  $\psi(4160)$  and  $\psi(4415)$  or other new resonance state, and  $R_k \equiv \Gamma_k^{e^+e^-} \mathcal{B}(k \rightarrow \text{final states})$ . This model, with only two resonances  $\psi(4160)$  and  $\psi(4415)$  (2R fit), fails to describe the data near 4.2 GeV for the  $e^+e^- \rightarrow \pi^+\pi^- J/\psi$  and  $e^+e^- \rightarrow D^0 D^{*-} \pi^+$ . The fit quality dramatically improves upon introducing an additional resonance,  $Y(4220)$  (3R fit), yielding  $\chi^2/\text{n.d.f.} = 118/153$  and  $226/78$  compared to  $\chi^2/\text{n.d.f.} = 205/157$  and  $69/74$  of the 2R fit scheme for  $e^+e^- \rightarrow \pi^+\pi^- J/\psi$  and  $e^+e^- \rightarrow D^0 D^{*-} \pi^+$ , respectively. The interference between  $\psi(4160)$ ,  $\psi(4415)$ , and the background successfully reproduces the broad enhancements reported as  $Y(4320)$  and  $Y(4390)$  [55, 56], effectively removing them as necessary independent states. Simultaneously, it explains the lack of clear  $\psi(4160)$  and  $\psi(4415)$  peaks in these data. The key quantitative result is the consistent extraction of the  $Y(4220)$  parameters:  $m = 4207 \pm 12$  MeV and  $\Gamma = 58 \pm 38$  MeV from  $e^+e^- \rightarrow \pi^+\pi^- J/\psi$ , and

$m = 4211 \pm 6$  MeV and  $\Gamma = 47 \pm 13$  MeV from  $e^+e^- \rightarrow \pi^+\pi^-h_c$ . Crucially, the same  $Y(4220)$  is essential to describe the open-charm process  $e^+e^- \rightarrow D^0D^{*-}\pi^+$ , where it shows a large production rate consistent with dominant open-charm decays. The survival of  $Y(4220)$  against this interference-based filter, which confirms its intrinsic resonant nature. The relevant fitted line shapes of cross sections for these three processes are presented in Fig. 42. This work highlights that a comprehensive evaluation of non-resonant explanations is crucial, as it decisively distinguishes persistent spectroscopic signals from interference artifacts. Indeed, the non-resonant interpretation adheres to Occam’s Razor principle, which holds that “*Numquam ponenda est pluralitas sine necessitate*”—plurality should not be posited without necessity.

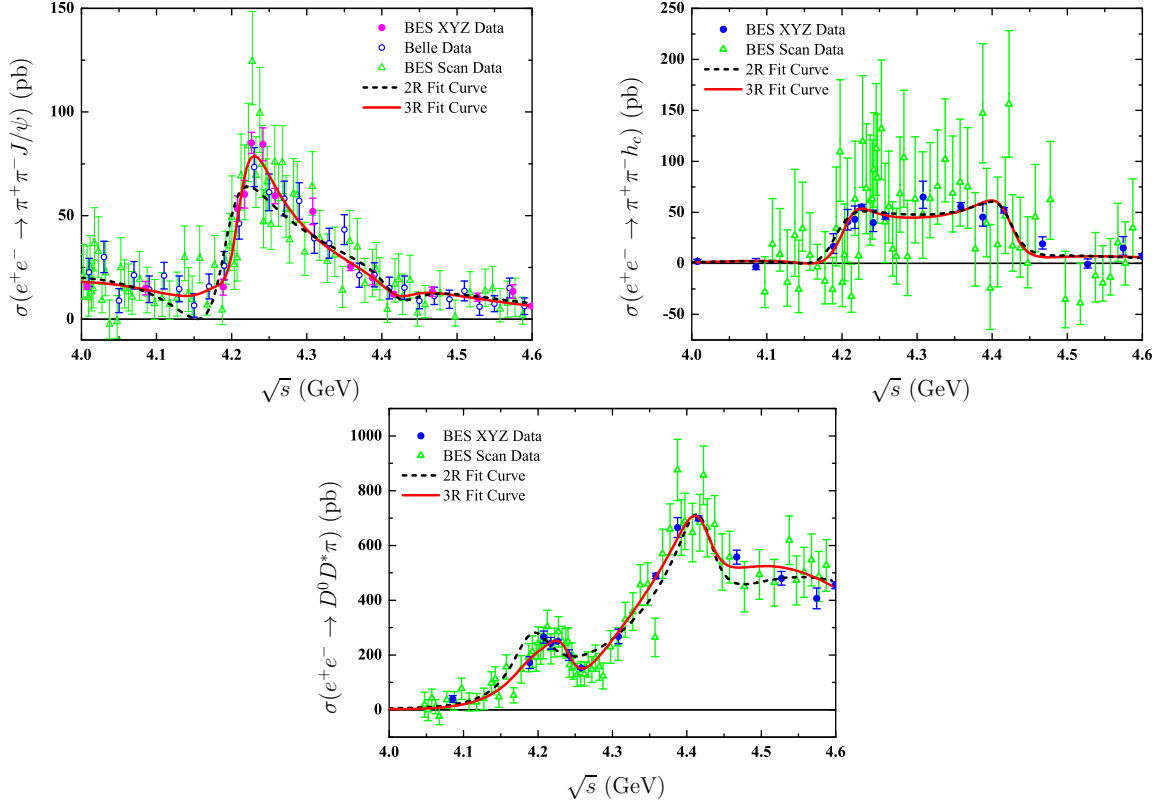


Figure 42: The Fano-like interference fit to the cross sections for the  $e^+e^- \rightarrow \pi^+\pi^-J/\psi$ ,  $e^+e^- \rightarrow \pi^+\pi^-h_c$  and  $e^+e^- \rightarrow D^0D^{*-}\pi^+$  under the 2R and 3R fit schemes. Figures are from Refs. [513].

#### 4.4.2. $Y(4220)$ as a scaling point to reconstruct $J/\psi$ family within the unquenched picture

As discussed in the previous subsections, once the non-resonant interference mechanism is properly incorporated, several wide structures previously assigned as members of the  $Y$  family, such as  $Y(4320)$ ,  $Y(4360)$ , and  $Y(4390)$ , can be consistently understood as the non-resonant enhancements from the interference between the background and two established charmonium states  $\psi(4160)$  and  $\psi(4415)$  [213, 216, 512, 513]. This reasoning follows Occam’s razor by favoring a simpler physical picture with fewer assumed resonant states, among competing descriptions that reproduce the same phenomenology. From this perspective, as of the experimental status around 2019, the energy region between 4.0 and 4.5 GeV accommodates only the single well-established and unambiguous  $Y$  particle, namely  $Y(4220)$ , as summarized in Fig. 43. It is worth emphasizing that the remaining higher  $Y$  states,  $Y(4630)$  and  $Y(4660)$ , can also be accommodated in a unified manner within the same theoretical framework, as will be discussed at the end of this subsection. Consequently,  $Y(4220)$  is the key to understanding the entire  $Y$  state family.

In fact, well before  $Y(4220)$  was conclusively established by experiment in 2017 [55, 56], the existence of a narrow vector state around 4.22 GeV had been pointed out as introduced in subsection 4.2.3. In brief, early experimental hints

for such a narrow structure already appeared in the BESIII measurement of the cross section  $e^+e^- \rightarrow h_c\pi^+\pi^-$  in 2013 [514], which suggested a possible enhancement near 4.2 GeV [480]. Subsequent measurements of  $e^+e^- \rightarrow \omega\chi_{cJ}$  by BESIII revealed a narrow structure with a mass of  $m = 4230 \pm 8 \pm 6$  MeV and a width of  $\Gamma = 38 \pm 12 \pm 2$  MeV [481], which was interpreted as the long-missing  $\psi(4S)$  charmonium state in Ref. [225]. In 2014, based on a naive comparison of the mass spectra between the charmonium  $J/\psi$  and bottomonium  $\Upsilon$  families, He, *et al.* argued that the  $\psi(4S)$  mass should lie around 4.263 GeV and that this state is expected to be relatively narrow [479], whose property is highly consistent with this narrow state around 4.2 GeV [514, 481]. Further support came from the analysis of the  $e^+e^- \rightarrow \pi^+\pi^-\psi(3686)$  process. In 2015, Chen and Liu *et al.* pointed out that the missing  $\psi(4S)$  should manifest itself in this channel [228], which was finally confirmed by the precise measurement of BESIII [380]. A combined analysis of three hidden-charm channels  $e^+e^- \rightarrow \psi(3686)\pi^+\pi^-$ ,  $h_c\pi^+\pi^-$ , and  $\chi_{c0}\omega$  demonstrated that the narrow structures observed around 4.2 GeV can be consistently attributed to a single underlying state [228].

Building upon these theoretical and experimental developments, in Ref. [300], Wang, Chen, Liu, and Matsuki proposed that  $Y(4220)$  can serve as a benchmark state for calibrating unquenched corrections to the linear confining potential of the charmonium system above 4 GeV, which provides a direct and quantitative manifestation of unquenched effects in the vector charmonium family. Based on this idea, it was found that  $Y(4220)$  can be successfully described as a mixed  $4S$ - $3D$  unquenched charmonium state within a relativistic quark model [300], with the  $4S$  component being dominant. In the following, we present a detailed discussion of this work and its implications for the spectroscopy of higher charmonium states.

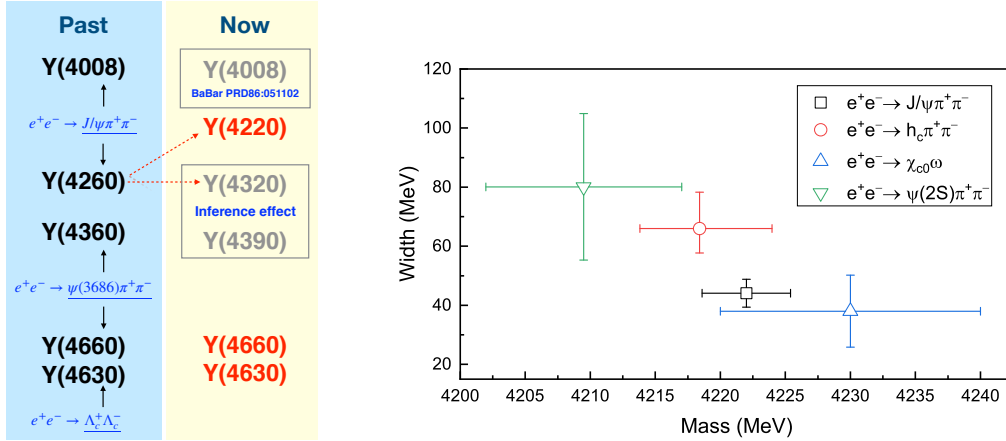


Figure 43: Status of the charmonium-like  $Y$  states before 2017 and their updated situation after 2017 (left panel), and the measured resonance parameters of the  $Y(4220)$  state in several hidden-charm processes (right panel). Figure adapted from Refs. [327, 300].

In Ref. [300], interpreting  $Y(4220)$  as a higher vector charmonium state shaped by unquenched effects leads to several nontrivial consistency requirements. First, the assignment of the well-established charmonium spectrum below 4.2 GeV must remain compatible within the unquenched theoretical framework. Second, the scenario implies the existence of an partner state of  $Y(4220)$  with correlated mass and decay properties, whose presence or absence in current data provides a decisive test. Third, the well-known  $\psi(4415)$  must be accommodated consistently within the same unquenched dynamics, rather than as an isolated exception. Addressing these interrelated constraints is essential to evaluate the role of  $Y(4220)$  as a scaling point for the unquenched charmonium spectrum above 4 GeV.

To quantitatively illustrate these three key points, an unquenched potential model is adopted to describe the charmonium spectrum [300]. In this approach, the interaction between the quark and anti-quark can be expressed by the Hamiltonian

$$H = E_q + E_{\bar{q}} + V_{\text{eff}}(r), \quad (37)$$

where  $E_q = (p^2 + m_q^2)^{1/2}$  and  $E_{\bar{q}} = (p^2 + m_{\bar{q}}^2)^{1/2}$  represent the relativistic kinetic energies of the quark and antiquark, respectively, and  $V_{\text{eff}}(r)$  denotes the effective quark–antiquark interaction. The effective potential consists of

$$V_{\text{eff}}(r) = H_{q\bar{q}}^{\text{conf}} + H_{q\bar{q}}^{\text{SO}} + H_{q\bar{q}}^{\text{hyp}}, \quad (38)$$

where  $H_{q\bar{q}}^{\text{conf}}$  contains the short-range one-gluon-exchange interaction,  $G(r) = -\frac{4\alpha_s(r)}{3r}$ , and the long-range confinement potential  $S(r)$ . To incorporate unquenched effects associated with virtual quark–antiquark pair creation from the vacuum fluctuation, the linear confinement potential adopted in Ref. [13]

$$S(r) = br + c, \quad (39)$$

is modified by a screened form,

$$S^{\text{scr}}(r) = \frac{b(1 - e^{-\mu r})}{\mu} + c, \quad (40)$$

which effectively accounts for the coupled channel effect at large distances and is proved to partly equivalent to the coupled-channel effect [40]. The remaining terms,  $H_{q\bar{q}}^{\text{SO}}$  and  $H_{q\bar{q}}^{\text{hyp}}$  represent the spin–orbit interaction and the color–hyperfine interaction, respectively [13]. Relativistic corrections in the unquenched potential model are implemented in two aspects: the smearing transformation of the interaction and the introduction of momentum-dependent factors [13]. By introducing the smearing function

$$\rho(\mathbf{r} - \mathbf{r}') = \frac{\sigma^3}{\pi^{3/2}} \exp[-\sigma^2(\mathbf{r} - \mathbf{r}')^2], \quad (41)$$

the screened confinement potential  $S^{\text{scr}}(r)$  and the one-gluon exchange potential  $G(r)$  are smeared out according to

$$\tilde{S}^{\text{scr}}(r)/\tilde{G}(r) = \int d^3\mathbf{r}' \rho(\mathbf{r} - \mathbf{r}') S^{\text{scr}}(r')/G(r'). \quad (42)$$

This smearing procedure effectively incorporates the nonlocality property of the quark–antiquark interaction. Besides, in a relativistic framework the effective interaction generally depends on the momenta of the interacting quarks in the center-of-mass frame. As a result, the smeared potential  $\tilde{V}_i(r)$  is modified as

$$\tilde{V}_i(r) \rightarrow \left(\frac{m_q m_{\bar{q}}}{E_q E_{\bar{q}}}\right)^{1/2+\varepsilon_i} \tilde{V}_i(r) \left(\frac{m_q m_{\bar{q}}}{E_q E_{\bar{q}}}\right)^{1/2-\varepsilon_i}, \quad (43)$$

where the parameter  $\varepsilon_i$  depends on the specific type of interaction, such as contact, vector spin–orbit, and tensor terms [13]. By fitting the masses of fourteen experimentally established charmonium states, including  $J/\psi$ ,  $\psi(3686)$ ,  $\psi(3770)$ ,  $\psi(4040)$ ,  $\psi(4160)$ ,  $\psi_2(3823)$ ,  $\eta_c(1S)$ ,  $\eta_c(2S)$ ,  $h_c(1P)$ ,  $\chi_{cJ}(1P)$  ( $J = 0, 1, 2$ ),  $\chi_{c0}(2P)$ , and  $\chi_{c2}(2P)$ , together with  $Y(4220)$  assigned as the  $\psi(4S)$  state, all model parameters can be constrained, which induced the mass of  $\psi(4S)$  as 4274 MeV. Additionally, the charmonium mass spectrum below 4.2 GeV can be well described, especially for the  $S$ -wave ground states (see Table II of Ref. [300] for details). Thus, the first key point of constructing the unquenched charmonium spectrum by the updated  $Y(4220)$  as scaling point can be achieved.

After fixing  $Y(4220)$  as the  $\psi(4S)$  charmonium state, the authors in Ref. [300] further examine whether its decay properties are compatible with existing experimental information and investigate the expected features of its  $D$ -wave partner state. The analysis is performed within the quark pair creation model combined with the input of exact wave function directly solved from the unquenched potential model, with particular emphasis on open-charm decay channels. The total width of  $\psi(4S)$  is calculated to be  $\Gamma_{\psi(4S)} = 27.2$  MeV, which is consistent with the experimentally observed narrow width of  $Y(4220)$ . The predicted decay pattern is highly selective. The  $D^*\bar{D}^*$  channel dominates, contributing about 88% of the total width  $\Gamma_{\psi(4S)}$ , while the  $D\bar{D}$  mode is relatively suppressed with branching ratio of 9.39% and decays into strange open-charm channels and  $D\bar{D}^*$  are found to be almost negligible, which are not contradict the collected Belle data of open-charm channels as shown in Fig. 44. Although the decay  $\psi(4S) \rightarrow D_1(2420)\bar{D}$  is not kinematically allowed, the strong  $S$ -wave coupling to the  $D_1(2420)\bar{D}$  channel is emphasized as an important source of coupled-channel effects, which may influence production processes such as  $e^+e^- \rightarrow D^0 D^{*-} \pi^+$  by the virtual  $D_1(2420)^0 \bar{D}^0$  channel as revealed by BESIII [382].

The existence of a  $\psi(4S)$  state naturally implies the presence of a partner vector charmonium  $\psi(3D)$ . Within the same framework, this  $\psi(3D)$  state is predicted to have a mass of  $M_{\psi(3D)} \simeq 4.33$  GeV and a total width of  $\Gamma_{\psi(3D)} = 28.8$  MeV. Its decay pattern differs qualitatively from that of  $\psi(4S)$ . The dominant decay mode is expected to be  $D\bar{D}$ ,

accounting for about 37% of the total width, with sizable contributions also arising from the  $D\bar{D}^*$  and  $D^*\bar{D}^*$  channels. Experimentally, however, no clear enhancement corresponding to a resonance around 4.33 GeV is observed in these open-charm channels as shown in Fig. 44.

Additional experimental hints arise from the open-charm process  $e^+e^- \rightarrow D\bar{D}_2^*(2460)$ . A possible enhancement around 4.37 GeV is visible in early Belle data for the  $D^0D^-\pi^+$  final state as shown in the right panel of Fig. 44. However, the calculated partial width for the decay  $\psi(3D) \rightarrow D\bar{D}_2^*(2460)$  is only 67.6 keV, corresponding to an extremely small branching fraction. Consequently, this potential structure in this channel cannot be attributed to a pure  $\psi(3D)$  resonance. In addition, the electronic width of a vector  $D$ -wave charmonium is expected to be one to two orders of magnitude smaller than that of an  $S$ -wave state, implying that a pure  $\psi(3D)$  resonance would be strongly suppressed in  $e^+e^-$  annihilation and therefore difficult to observe through hidden-charm channels. Taken together, these observations indicate that while the decay properties of  $\psi(4S)$  are broadly compatible with existing experimental information, there is no experimental evidence supporting the existence of its partner  $\psi(3D)$  state. To understand this puzzling phenomenon, a new idea of the  $S$ - $D$  mixing was further proposed [300].

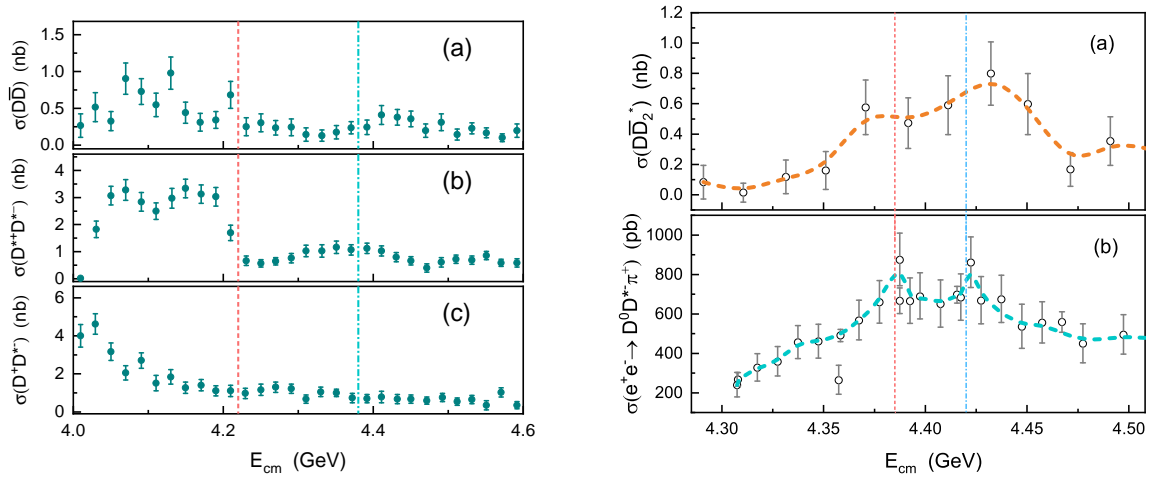


Figure 44: Experimental cross sections of selected open-charm production channels in  $e^+e^-$  annihilation. The left panel shows two-body open-charm channels, including  $e^+e^- \rightarrow D\bar{D}$ ,  $D^{*+}D^{*-}$ , and  $D^+\bar{D}^{*-}$ , where the vertical dashed lines indicate the center-of-mass energies at 4.22 GeV and 4.38 GeV, respectively. The right panel presents open-charm channels  $e^+e^- \rightarrow D^0\bar{D}_2^*$  and  $e^+e^- \rightarrow D^0D^{*+}\pi^+$ , with dashed lines marking the energies around 4.385 GeV and 4.420 GeV. Figures are from Refs. [300].

#### 4.4.3. The $4S$ - $3D$ mixing scheme in charmonium

To address this difficulty mentioned above, the authors of Ref. [300] further develop and explore a concrete  $4S$ - $3D$  mixing framework. In this scheme, the physical states are linear combinations of the pure  $\psi(4S)$  and  $\psi(3D)$  basis states, parameterized by a mixing angle  $\theta$ , i.e.,

$$\begin{pmatrix} |\psi'_{4S-3D}\rangle \\ |\psi''_{4S-3D}\rangle \end{pmatrix} = \begin{pmatrix} \cos \theta & \sin \theta \\ -\sin \theta & \cos \theta \end{pmatrix} \begin{pmatrix} |4^3S_1\rangle \\ |3^3D_1\rangle \end{pmatrix}. \quad (44)$$

Using the unquenched potential model masses  $m_{4S} = 4274$  MeV and  $m_{3D} = 4334$  MeV as input, the eigenstate masses of  $\psi'_{4S-3D}$  and  $\psi''_{4S-3D}$  are obtained through diagonalization of the mass matrix, i.e.,

$$m_{\psi'_{4S-3D}}^2 = \frac{1}{2} \left( m_{4S}^2 + m_{3D}^2 - \sqrt{(m_{3D}^2 - m_{4S}^2)^2 \sec^2 2\theta} \right), \quad (45)$$

$$m_{\psi''_{4S-3D}}^2 = \frac{1}{2} \left( m_{4S}^2 + m_{3D}^2 + \sqrt{(m_{3D}^2 - m_{4S}^2)^2 \sec^2 2\theta} \right). \quad (46)$$

Constraining the mixing scenario by the lower-mass eigenstate  $\psi'_{4S-3D}$  as experimentally observed  $Y(4220)$  with mass interval of 4204~4243 MeV. This condition implies a relatively large mixing angle of  $\theta \simeq \pm(30^\circ-36^\circ)$ . In Sec. 4.5.1,

a coupled-channel dynamics mechanism explains the origin of such a large mixing angle. Consequently, the higher-mass partner state  $\psi'_{4S-3D}$  is predicted to lie in the range of 4364~4400 MeV and is tentatively labeled as  $\psi(4380)$ . These results are presented in the left panel of Fig. 45.

The decay properties of the mixed  $\psi'_{4S-3D}$  are systematically analyzed. For the positive mixing angle, the total width of  $\psi'_{4S-3D}$  is calculated to be around 26.0 MeV, consistent with the observed narrow width of  $Y(4220)$ . Its open-charm decay pattern remains dominated by the  $D^*\bar{D}^*$  channel, closely resembling the predictions for a pure  $\psi(4S)$  assignment. In contrast, a negative mixing angle leads to a significantly narrower width and an altered branching ratio structure, which seems to be disfavored by data.

Crucially, the mixing framework dramatically alters the predicted observables for the partner state  $\psi(4380)$ . Its total width is enhanced by approximately a factor of three compared to that of a pure  $\psi(3D)$  state. The decay pattern undergoes a qualitative transformation: the dominant channels shift to  $DD_1(2430)$ ,  $D^*\bar{D}^*$ , and, most notably, a significantly enhanced  $DD_2^*(2460)$  mode, which can be seen in the right panel of Fig. 45. This pronounced increased decay ratio in the  $DD_2^*(2460)$  channel provides a natural explanation for the potential structure around 4.37 GeV observed in the  $e^+e^- \rightarrow DD_2^*(2460)$  process in early Belle data as shown in Fig. 44.

Furthermore, the dielectron widths of the mixed states were obtained. For the positive mixing angle solution, both  $Y(4220)$  and  $\psi(4380)$  are predicted to have  $\Gamma_{e^+e^-}$  of 0.25–0.30 keV. This value is substantially larger than the expected order-of-magnitude suppression for a pure  $D$ -wave charmonium, thereby significantly improving the prospects for observing the  $\psi(4380)$  companion in  $e^+e^-$  annihilation experiments. Overall, the  $S$ - $D$  mixing mechanism offers a unified and quantitative explanation for the key spectroscopic and decay puzzles associated with  $Y(4220)$  and its partner state  $\psi(4380)$ .

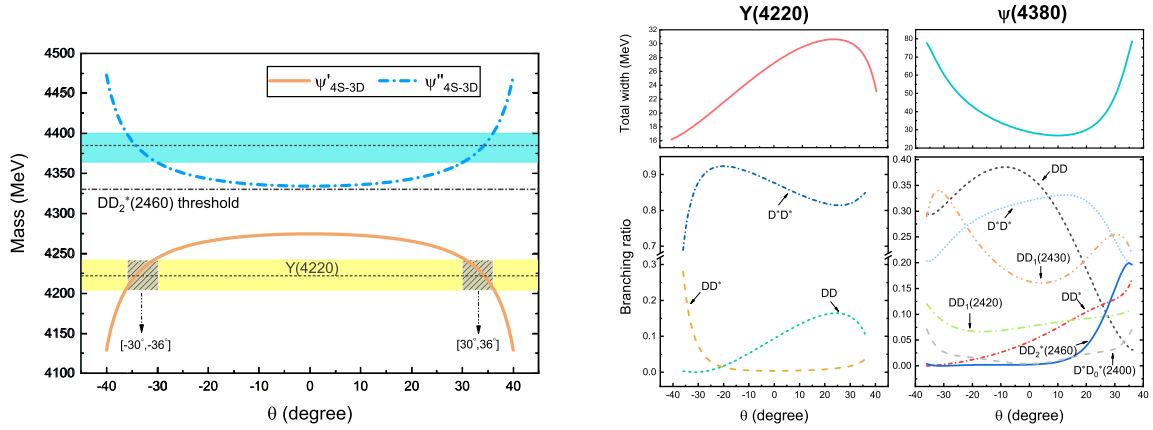


Figure 45: The masses and the open-charm decay behaviors of  $\psi'_{4S-3D}$  and  $\psi''_{4S-3D}$  with dependence on the  $4S$ - $3D$  mixing angle  $\theta$ . For the left panel, the yellow and cyan bands denote the measured mass range of  $Y(4220)$  and the predicted mass range of  $\psi(4380)$ , respectively, and the two shaded regions represent the mixing angle interval, in which the theoretical results of  $\psi'_{4S-3D}$  meet the measurements of  $Y(4220)$ .

In the proposed  $4S$ - $3D$  mixing framework,  $\psi(4380)$  as the partner of  $Y(4220)$  is expected to have a non-negligible dilepton width, similar to  $Y(4220)$  itself, suggesting that it could be observable in hidden-charm production channels. The high-precision cross section measurements of  $e^+e^- \rightarrow \psi(3686)\pi^+\pi^-$  released by BESIII [380] provided an ideal opportunity to test this prediction. In Ref. [300], the Fano-like interference mechanism again was applied to analyze whether evidence for the predicted  $\psi(4380)$  could be identified in this process. The analysis firstly combines a non-resonant continuum amplitude with resonant contributions from established charmonium states  $\psi(4160)$  and  $\psi(4415)$  together with  $Y(4220)$ , allowing for interference effects. A  $3R$  fit including only these three resonances contributions describes much of the data, it fails to fully capture a distinct enhancement structure observed around 4.36 GeV in the cross-section distribution. Introducing a fourth resonance with free mass and width significantly improves the fit quality, yielding parameters  $m = 4374 \pm 13$  MeV and  $\Gamma = 106 \pm 29$  MeV. These values are consistent with the predicted mass and enhanced width of the  $\psi(4380)$  state within the  $4S$ - $3D$  mixing scheme, thereby providing direct evidence for its existence in the hidden-charm decay channel and further validating the mixing interpretation of  $Y(4220)$ .

#### 4.4.4. The vector charmonium mass spectrum in the unquenched picture for the 4–4.5 GeV region

There remains one final problem in the construction of the  $J/\psi$  family within the unquenched framework, i.e., the placement of the experimentally established charmonium  $\psi(4415)$ . In the calculated higher mass spectrum, the mass of the pure  $\psi(5S)$  state is 4443 MeV, which lies closer to  $\psi(4415)$  than the pure  $\psi(4S)$  state. Given the compelling evidence that  $Y(4220)$  structure is well described by a  $4S$ - $3D$  mixing scheme, it is natural to explore whether a similar mixing mechanism operates in the description of  $\psi(4415)$ . The  $5S$ - $4D$  mixing scheme is therefore proposed to interpret  $\psi(4415)$ , whose formula is very similar to those in Eqs. (44)-(46).

Using the experimental mass range (4397~4438) MeV of  $\psi(4415)$  as input, the  $5S$ - $4D$  mixing model yields a mixing angle of  $\phi = \pm(18^\circ-36^\circ)$  and predicts a new partner state  $\psi''_{5S-4D}$ , denoted  $\psi(4500)$ , with a mass between 4489 and 4529 MeV. The calculated total width (12.6~19.9) MeV of  $\psi(4415)$  is notably smaller than the PDG average of  $62 \pm 20$  MeV. This apparent discrepancy is interpreted in the context of substantial inconsistencies in historical experimental determinations of the resonant parameters of  $\psi(4415)$ , as summarized in the PDG [94].

The analysis identifies  $D^*\bar{D}^*$ ,  $DD_1(2420)$ , and  $DD_1(2430)$  as the dominant open-charm decay channels of  $\psi(4415)$ . This prediction finds support in several experimental observations:

- The BaBar Collaboration reported ratios  $\Gamma(\psi(4415) \rightarrow D\bar{D})/\Gamma(\psi(4415) \rightarrow D\bar{D}) = 0.14 \pm 0.12 \pm 0.03$  and  $\Gamma(\psi(4415) \rightarrow D^*\bar{D} + \text{c.c.})/\Gamma(\psi(4415) \rightarrow D^*\bar{D}^*) = 0.17 \pm 0.25 \pm 0.03$ , indicating a significantly larger  $D^*\bar{D}^*$  partial width compared to other two-body open-charm modes.
- The BESIII measurement of  $e^+e^- \rightarrow D^0D^{*-}\pi^+$  shows a structure around 4.42 GeV consistent with  $\psi(4415)$  production via decay chains such as  $D\bar{D}_1 \rightarrow D\bar{D}^*\pi$ .
- The Belle collaboration's observation of  $\psi(4415) \rightarrow D\bar{D}_2(2460)$  with a peak cross section of  $0.74 \pm 0.17 \pm 0.08$  nb is compatible with the predicted branching fraction range of (0.12 – 10.6)% for this channel, given the considerable uncertainties in experimental resonance parameters.

The pattern of  $\psi(4415)$  decays to final states involving charmed-strange mesons also aligns with experimental findings. While  $\psi(4415) \rightarrow D_s^{*+}D_s^{*-}$  has been observed, the  $D_s^{*+}D_s^-$  mode has not been seen, consistent with calculations showing substantially smaller partial widths for  $D_s\bar{D}_s^*$  compared to  $D_s^*\bar{D}_s^*$ . Regarding the dilepton width, the predicted range of (0.147~0.344) keV depending on the mixing angle sign encompasses the values reported by MARK I (0.44 ± 0.14) keV [465] and BESII (0.35 ± 0.12) keV [515] within experimental uncertainties.

For the predicted partner state  $\psi(4500)$ , the total width is 30~45 MeV with dominant decays into  $D\bar{D}_1(2430)$ ,  $D^*\bar{D}^*$ ,  $D\bar{D}$ ,  $D\bar{D}(2550)$ , and  $D\bar{D}_1(2420)$ . The dilepton width of  $\psi(4500)$  is predicted to be  $(2.25 \times 10^{-3} \sim 0.189)$  keV, suggesting that its discovery in  $e^+e^-$  collisions will be challenging. In conclusion, the  $5S$ - $4D$  mixing scheme provides a self-consistency framework for interpreting  $\psi(4415)$  within the unquenched charmonium spectrum. While current experimental data exhibit large uncertainties that preclude definitive tests, the theoretical predictions show no contradiction with available observations and naturally lead to the prediction of a missing partner state,  $\psi(4500)$ . Interestingly, a prediction for this  $\psi(4500)$  state exists prior to the relevant experimental discovery. Merely two years after, the BESIII experiment reported the first observation of a new vector state  $Y(4500)$  around 4.5 GeV in the process  $e^+e^- \rightarrow K^+K^-J/\psi$  [388]. The connection between this observed  $Y(4500)$  and the predicted  $\psi(4500)$  has been studied in Ref. [233] and will be discussed later.

In conclusion, the unquenched framework leads to a characterized energy level of charmonium spectrum. In the energy region between 4.0 and 4.5 GeV, this spectrum accommodates the sequence  $\psi(4040)$ ,  $\psi(4160)$ ,  $Y(4220)$ ,  $\psi(4380)$ ,  $\psi(4415)$ , and the predicted  $\psi(4500)$ , as shown in Fig. 46, which goes beyond the level structures anticipated in the quenched picture such as typical Cornell potential model, as summarized in Fig. 36 and Table 5. The emergence of such a reorganized characterized level structure indicates that the high excited charmonium spectrum encodes dynamical information beyond that of a static confining potential. From a broader perspective, these characterized energy levels provide a valuable probe of how confinement manifests itself in the presence of unquenched effects, offering insights into the nature of confinement in realistic physical systems.

#### 4.4.5. Are these $Y$ states around 4.6 GeV from $e^+e^-$ annihilation higher charmonia?

As illustrated in Fig. 43, two prominent states,  $Y(4630)$  and  $Y(4660)$ , remained unclassified. The  $Y(4660)$  was first observed by Belle in the hidden-charm process  $e^+e^- \rightarrow \psi(3686)\pi^+\pi^-$  [53], while the  $Y(4630)$  was reported in

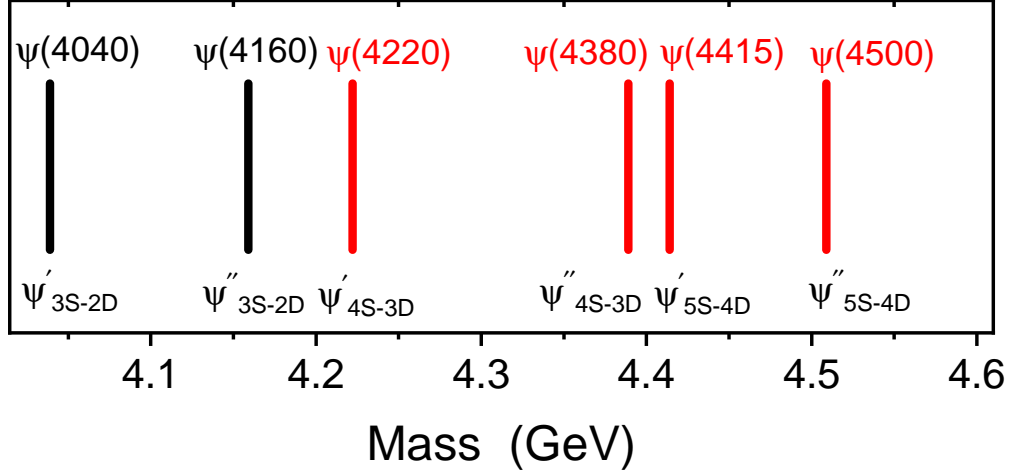


Figure 46: Characteristic energy levels of the vector charmonium states in the unquenched charmonium spectrum. Figure is from Ref. [516].

the open-charm channel  $e^+e^- \rightarrow \Lambda_c^+\bar{\Lambda}_c^-$  [54]. A persistent theoretical debate centered on whether these were distinct particles or different manifestations of a single structure [517, 518, 519]. Building upon that all  $Y$  states between 4.0 and 4.5 GeV and the associated puzzles could be understood within a concise and unified manner as introduced above, in Ref. [327], Wang, Qian, Liu and Matsuki further extend to study the higher energy region, seeking to determine if a unified unquenched charmonium spectrum could provide a complete explanation for all observed  $Y$  states.

A critical insight found in Ref. [327] is the inherent limitation of the model when extrapolated beyond its calibration region. It has been demonstrated that while a range of screening parameter  $\mu$  values (e.g., 0.11–0.15 GeV limited by only single  $Y(4220)$  state) can equally well describe the established charmonium spectrum below 4.5 GeV, they lead to drastically different predictions for states near and above 4.6 GeV. Specifically, the predicted mass of a pure  $\psi(6S)$  state varies by about 100 MeV across this  $\mu$  range [327]. This large uncertainty indicates that the properties of the lower states do not uniquely constrain the relatively long-distance behavior of the confinement potential, and a new scaling point around the 4.6 GeV region itself is essential for a reliable description of higher mass spectrum.

With this theoretical ambiguity, the analysis first studied the possibility of interpreting  $Y(4660)$  as a pure  $\psi(6S)$  charmonium to play the role of this new scaling point [327]. However, they noted that such an assignment faces immediate difficulties. First, quark model calculations, including the results within a large range of  $\mu$  value, typically predict a  $\psi(6S)$  mass below 4.65 GeV, which is somewhat lower than the measured mass of  $Y(4660)$ . More importantly, the experimental mass difference  $M_{Y(4660)} - M_{\psi(4415)} \approx 231$  MeV is found to be obviously larger than  $M_{\psi(4415)} - M_{Y(4220)} \approx 191$  MeV. This trend contradicts the expected decreasing mass gap between consecutive radial excitations in a standard potential model, casting doubt on a simple  $\psi(6S)$  assignment for  $Y(4660)$ . When moving the focus on another state  $Y(4630)$ , a puzzling experimental feature on the high-precision cross section of  $e^+e^- \rightarrow \Lambda_c^+\bar{\Lambda}_c^-$  from BESIII was noted, which revealed a distinct "platform" enhancement near the threshold in the 4.57–4.60 GeV region [520], starkly differing from the single peak structure  $Y(4630)$  previously reported by Belle [54]. This new experimental hint motivates the proposal that this novel structure near threshold may imply the existence of an additional resonance, which can be treated as candidate of the  $\psi(6S)$  state and would naturally resolve the above tension.

To test this idea, a combined analysis of the processes  $e^+e^- \rightarrow \psi(3686)\pi^+\pi^-$  and  $e^+e^- \rightarrow \Lambda_c^+\bar{\Lambda}_c^-$  is performed [327], incorporating high-precision BESIII data collected near the  $\Lambda_c^+\bar{\Lambda}_c^-$  threshold [520], as shown in Fig 47. The analysis conclusively favored the existence of two vector resonances and described experimental data well with  $\chi^2/\text{d.o.f.}=1.49$ . The fitted resonance parameters of two vector states denoted as  $Y_1$  and  $Y_2$  have the following masses and widths:

$$\begin{aligned}
 m_{Y_1} &= 4585 \pm 2 \text{ MeV}, & \Gamma_{Y_1} &= 29.8 \pm 8.0 \text{ MeV}, \\
 m_{Y_2} &= 4676 \pm 7 \text{ MeV}, & \Gamma_{Y_2} &= 85.7 \pm 15.0 \text{ MeV}.
 \end{aligned}$$

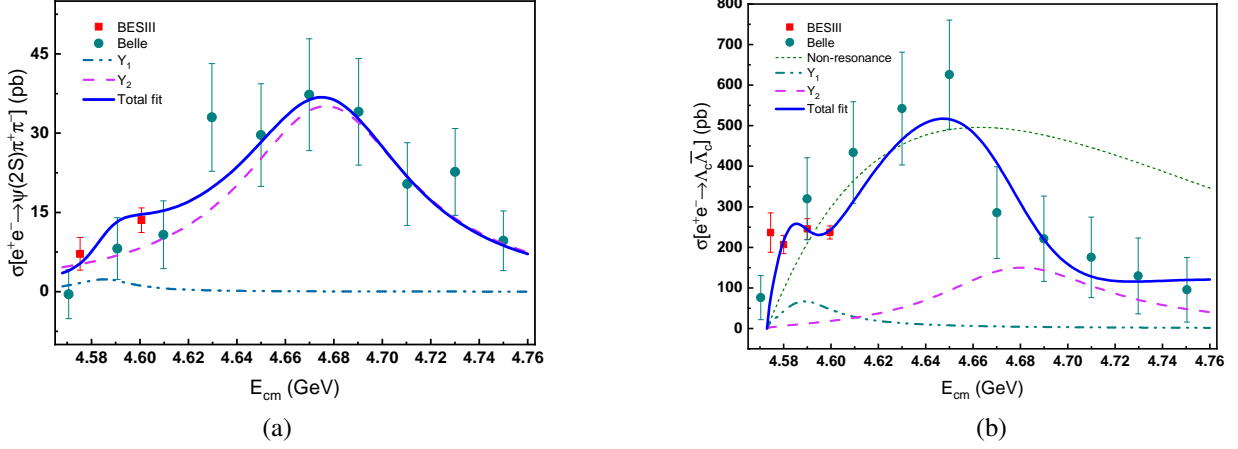


Figure 47: (a) The fitted results of the  $e^+e^- \rightarrow \psi(3686)\pi^+\pi^-$  from Belle and BESIII [380, 521]. (b) The fitted results of the  $e^+e^- \rightarrow \Lambda_c\bar{\Lambda}_c$  from Belle and BESIII [54, 520]. The figures are adopted from Ref. [327].

From Fig. 47, it can be seen that the "platform" behavior near the  $\Lambda_c\bar{\Lambda}_c$  threshold naturally emerge from the interplay of  $Y_1$ ,  $Y_2$  and non-resonant contributions. The  $Y_1$  and  $Y_2$  can be identified as the physical mixtures of the pure  $\psi(6S)$  and  $\psi(5D)$  with  $\mu = 0.12$ . For a mixing angle of  $|\theta| \approx 34^\circ$ , the predicted mass of  $\psi'_{6S-5D}$  (4587 MeV) and mass of  $\psi''_{6S-5D}$  (4675 MeV) align strikingly with the fitted  $Y_1$  and  $Y_2$ , respectively. Fig 48 (a) illustrates the dependence of the masses and total widths of  $\psi'_{6S-5D}$  and  $\psi''_{6S-5D}$  on the mixing angle  $\theta$ . In this scheme, it is argued that the reported  $Y(4630)$  and  $Y(4660)$  likely correspond to the same broader  $Y_2$  resonance observed in different final states.

This interpretation received independent validation from the discovery of a new vector state,  $Y(4626)$ , in the open-charm process  $e^+e^- \rightarrow D_s^+D_{s1}(2536)^- + \text{c.c.}$  by the Belle collaboration [511]. Its mass of  $4625.9^{+6.2}_{-6.0} \pm 0.4$  MeV and width of  $49.8^{+13.9}_{-11.5} \pm 4.0$  MeV placed it within the energy range of interest. To understand this new structure, the branching fractions  $\mathcal{B}(\psi'_{6S-5D} \rightarrow D_s D_{s1}(2536))$  and  $\mathcal{B}(\psi''_{6S-5D} \rightarrow D_s D_{s1}(2536))$  were calculated within the  $6S-5D$  mixing scheme using the QPC model [327]. The results exhibited an obvious dependence on the sign of the mixing angle  $\theta$ . For  $\theta = -34^\circ$ , the predicted branching ratios were 0.09% for the lower state  $\psi'$  and 0.80% for the higher state  $\psi''$ . Conversely, for  $\theta = +34^\circ$ , the pattern reversed with  $\psi'$  and  $\psi''$  having branching ratios of 0.64% and 0.17%, respectively. Crucially, both scenarios yielded branching fractions of the expected order of  $10^{-3} \sim 10^{-2}$  for a conventional charmonium decaying into an open charm-strange pair. A subsequent fit to the measured  $e^+e^- \rightarrow D_s^+D_{s1}(2536)^-$  cross section, incorporating contributions from both  $\psi'$  and  $\psi''$  resonances along with a non-resonant background term, successfully reproduced the experimental line shape within both positive and negative mixing angle scenario as shown in Fig. 48 (b). Therefore, this interpretation not only resolves the apparent mass gap problem but provides a unified description of the relevant experimental observations.

Because the  $Y_1$  state provides a new scaling point for the higher unquenched charmonium spectrum, the study proceeded to predict the properties of even higher-lying vector charmonia above 4.6 GeV [327]. The mass spectrum and open-charm decay widths were calculated for the next six states:  $\psi(7S)$ ,  $\psi(8S)$ ,  $\psi(9S)$ ,  $\psi(6D)$ ,  $\psi(7D)$ , and  $\psi(8D)$ . Their predicted masses lie in the range of approximately 4.7 to 4.9 GeV, indicating a dense spectrum in this region. A key and somewhat counterintuitive prediction is that these highly excited states remain relatively narrow, with total widths of only 10 to 30 MeV. This is attributed to strong node suppression effects in their decay amplitudes, i.e., the wave functions of high radial excitations possess multiple nodes, leading to significant cancellations in the overlap integrals with final-state meson wave functions during the decay process. The analysis also provided detailed predictions for their dominant open-charm decay channels. For the higher  $S$ -wave states, modes such as  $DD_1(2430)$ ,  $D^*D_0^*(2400)$ , and  $D^*D_1(2430)$  are prominent. For the higher  $D$ -wave states, decays into  $D^*D^*$ ,  $DD$ , and  $D^*D_1(2420)$  are among the most important. These concrete predictions serve as a valuable guide for future experimental searches at facilities like BESIII, Belle II, and a possible Super Tau-Charm Factory, highlighting a rich and unexplored spectroscopy awaiting discovery in the 4.6–5.0 GeV energy range.

Collectively, this series of works presents a complete and unified solution to the long-standing "Y problem" across

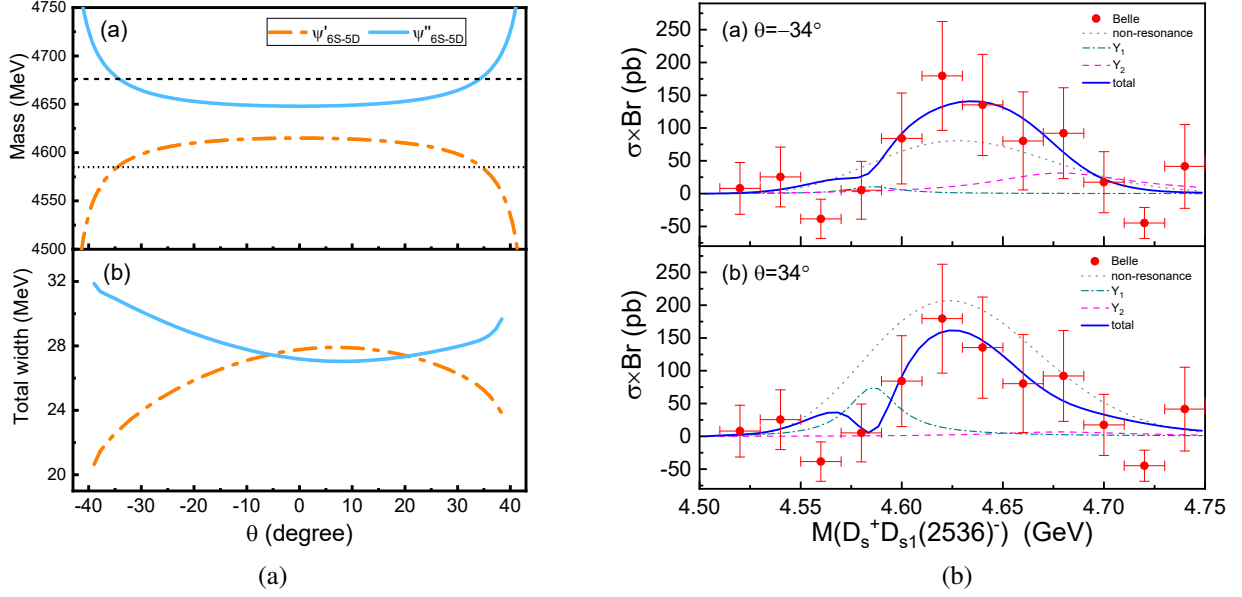


Figure 48: (a) The dependence of masses and widths of  $\psi'_{6S-5D}$  and  $\psi''_{6S-5D}$  on mixing angle  $\theta$  in the  $6S-5D$ . (b) The reproduction of the experimental line shape of the  $e^+e^- \rightarrow D_s^+ D_{s1}^-(2536)^-$  from Belle [511]. The figures are adopted from Ref. [327].

the relevant energy region. Its success critically highlights the inclusion of unquenched effects, which are essential for correctly describing the spectrum and properties of higher excitations, and a concrete embodiment of the Occam's razor principle by the non-resonant mechanism in the research of hadron spectroscopy, achieving a comprehensive description of multiple anomalous structures without introducing exotic states. It therefore stands as a notable example of how the sustained interplay between theoretical modeling and experimental data yields a systematic resolution in spectroscopy.

#### 4.4.6. Accumulating experimental evidence

The spectroscopy of higher vector charmonium states above 4 GeV has long been a challenging problem in hadron physics. Quenched potential models predict only three states in this region:  $\psi(4040)$ ,  $\psi(4160)$ , and  $\psi(4415)$ . However, high-precision experiments in recent years have revealed complex resonance structures that cannot be accommodated within this conventional picture. A series of studies by the Lanzhou group has proposed a characterized energy level structure consisting of six vector charmonium states in the 4–4.5 GeV range:  $\psi(4040)$ ,  $\psi(4160)$ ,  $\psi(4220)$ ,  $\psi(4380)$ ,  $\psi(4415)$ , and  $\psi(4500)$ . This framework, based on an unquenched potential model, has been systematically tested against data from multiple decay channels measured by BESIII [382, 393, 388], Belle [522], CLEO [452] and LHCb [523], providing a consistent and unified description of the observed structures.

1. The emergence of the characterized energy level structures of higher charmonium in the  $e^+e^- \rightarrow D^0 D^{*-} \pi^+$ . In the process  $e^+e^- \rightarrow \pi^+ D^0 D^{*-}$  [382], BESIII observed two broad enhancements around 4.2 and 4.4 GeV. Earlier analyses attempted to describe these with single resonances but encountered inconsistencies in extracted widths. A combined fit incorporating the predicted states  $\psi(4160)$ ,  $\psi(4220)$ ,  $\psi(4380)$ ,  $\psi(4415)$ , and  $\psi(4500)$  yields an excellent description of the data with  $\chi^2/\text{d.o.f.} = 0.74$ . The enhancement near 4.4 GeV is explained not by a single wide resonance but by the interference between  $\psi(4380)$  and  $\psi(4415)$ . Similarly, the structure around 4.2 GeV involves both  $\psi(4160)$  and  $\psi(4220)$ . This multi-resonance interference naturally accounts for the observed line shapes and resolves the earlier discrepancy in the width of the  $Y(4220)$ -like structure, which is now understood as a composite signal rather than a single particle.
2. Explaining the puzzling data of the  $e^+e^- \rightarrow \eta J/\psi$  by the unquenched charmonium spectroscopy. The channel  $e^+e^- \rightarrow \eta J/\psi$  [393] presents another puzzle: BESIII reported a  $Y(4220)$  with a width of about 80 MeV, significantly larger than the narrow width observed in other hidden-charm channels. By including the contributions of

$\psi(4040)$ ,  $\psi(4160)$ ,  $\psi(4220)$ ,  $\psi(4380)$ , and  $\psi(4415)$ , and calculating their decay branching ratios to  $\eta J/\psi$  via the hadronic loop mechanism, the data can be well described. The apparent large width and asymmetric line shape around 4.2 GeV arise from the overlap and interference of  $\psi(4160)$  and  $\psi(4220)$ . Two fitting schemes were explored, one with a common cutoff parameter and another with individual parameters, both yielding good fits and demonstrating the importance of including multiple nearby resonances in the analysis.

3. Confirming the existence of a new higher charmonium  $\psi(4500)$  by the newly released data of  $e^+e^- \rightarrow K^+K^-J/\psi$ . In  $e^+e^- \rightarrow K^+K^-J/\psi$  [388], BESIII observed a new structure around 4.5 GeV, denoted  $Y(4500)$ , with a mass consistent with the predicted  $\psi(4500)$ . A fit with  $\psi(4220)$  and  $\psi(4500)$  alone already captures the main features, but including  $\psi(4160)$  and  $\psi(4415)$  improves the description significantly. The extracted mass of  $\psi(4500)$  is  $4504 \pm 4$  MeV, and its narrower intrinsic width resolves the apparent discrepancy with the initially reported broader experimental width. Theoretical calculations of  $\mathcal{B}(\psi \rightarrow K^+K^-J/\psi)$  via charmed meson loops support this assignment. The analysis also indicates that  $\psi(4380)$  should contribute noticeably in this channel, with a predicted branching ratio of  $(4.0 - 6.0) \times 10^{-3}$ , suggesting that future more precise data may reveal its presence.
4. Reevaluating the  $\psi(4160)$  resonance parameter by the unquenched charmonium spectroscopy. The decay  $B^+ \rightarrow K^+\mu^+\mu^-$  [523] provides an independent probe of charmonium states through dimuon invariant mass spectra. LHCb data showed a peak around 4190 MeV, originally interpreted as  $\psi(4160)$  but with a mass higher than earlier measurements. Reanalyzing the spectrum with the full set of predicted charmonium states reveals that the 4190 MeV structure is actually the result of interference between  $\psi(4160)$  and  $\psi(4220)$ . When the contributions of both are properly accounted for, the true mass of  $\psi(4160)$  is found to be around 4146 MeV, consistent with earlier experimental determinations. This clarifies a long-standing puzzle regarding the apparent mass shift of  $\psi(4160)$  and underscores the importance of considering nearby resonances in line-shape analyses.

In summary, the characterized energy level structure of vector charmonium in the 4–4.5 GeV region, comprising six states within an unquenched potential model, successfully unifies a wide range of experimental observations. It resolves previous puzzles such as the  $\psi(4160)$  mass shift and the broad widths of structures in  $\eta J/\psi$  and  $\pi^+D^0D^{*-}$ , and predicts new states like  $\psi(4500)$  that have since been observed.

#### 4.5. Coupled-channel analysis for key charmonium(-like) states

##### 4.5.1. $S$ - $D$ mixing scheme induced by the coupled-channel mechanism

The vector charmonium spectrum above open-charm thresholds is known to be strongly influenced by unquenched effects induced by intermediate charmed meson loops. In this energy region, the conventional quark model picture becomes increasingly inadequate, as nearby open-charm thresholds can induce sizable mass shifts. In particular, the nature of  $\psi(4220)$  and  $\psi(4380)$  states has remained an open issue, since their observed properties cannot be simultaneously accommodated within quenched potential models [12, 13].

Ref. [300] shows that a  $4S$ - $3D$  mixing scheme can naturally accommodate  $Y(4220)$ , reproducing its mass for a mixing angle in the range  $\pm(30^\circ \sim 36^\circ)$ . Nevertheless, the large mixing angle required in this phenomenological framework lacks a clear dynamical origin. Such a sizable mixing cannot be generated by the tensor interaction in conventional potential models [13]. This motivates an investigation of the underlying dynamical mechanism responsible for the large  $4S$ - $3D$  mixing and a further clarification of the internal structure of  $\psi(4220)$ .

A systematic investigation of the  $4S$ - $3D$  mixing mechanism was carried out in Ref. [323] within a coupled-channel framework, as illustrated schematically in Fig. 50 (a). Starting from the bare charmonium spectrum obtained using the GI model, the authors first examined the contribution from the tensor force. It was shown that the tensor interaction alone generates only a very small mixing between the  $\psi(4S)$  and  $\psi(3D)$  states, with a mixing angle well below  $1^\circ$ . This result confirms earlier expectations that the tensor force is insufficient to account for the large mixing angles [525, 313, 311].

The dominant source of the  $S$ - $D$  mixing was identified as open-charm meson loop effects. Within this framework, the mixing angles of the relevant vector states can be determined accordingly [142, 313, 526, 527, 311]. The mixing angle can be determined by solving the following equation:

$$\det \begin{vmatrix} M_S^0 + \Delta M_S(M) - M & \langle \psi_S | H_T | \psi_D \rangle + \Delta M_{SD}(M) \\ \langle \psi_D | H_T | \psi_S \rangle + \Delta M_{SD}(M) & M_D^0 + \Delta M_D(M) - M \end{vmatrix} = 0. \quad (47)$$

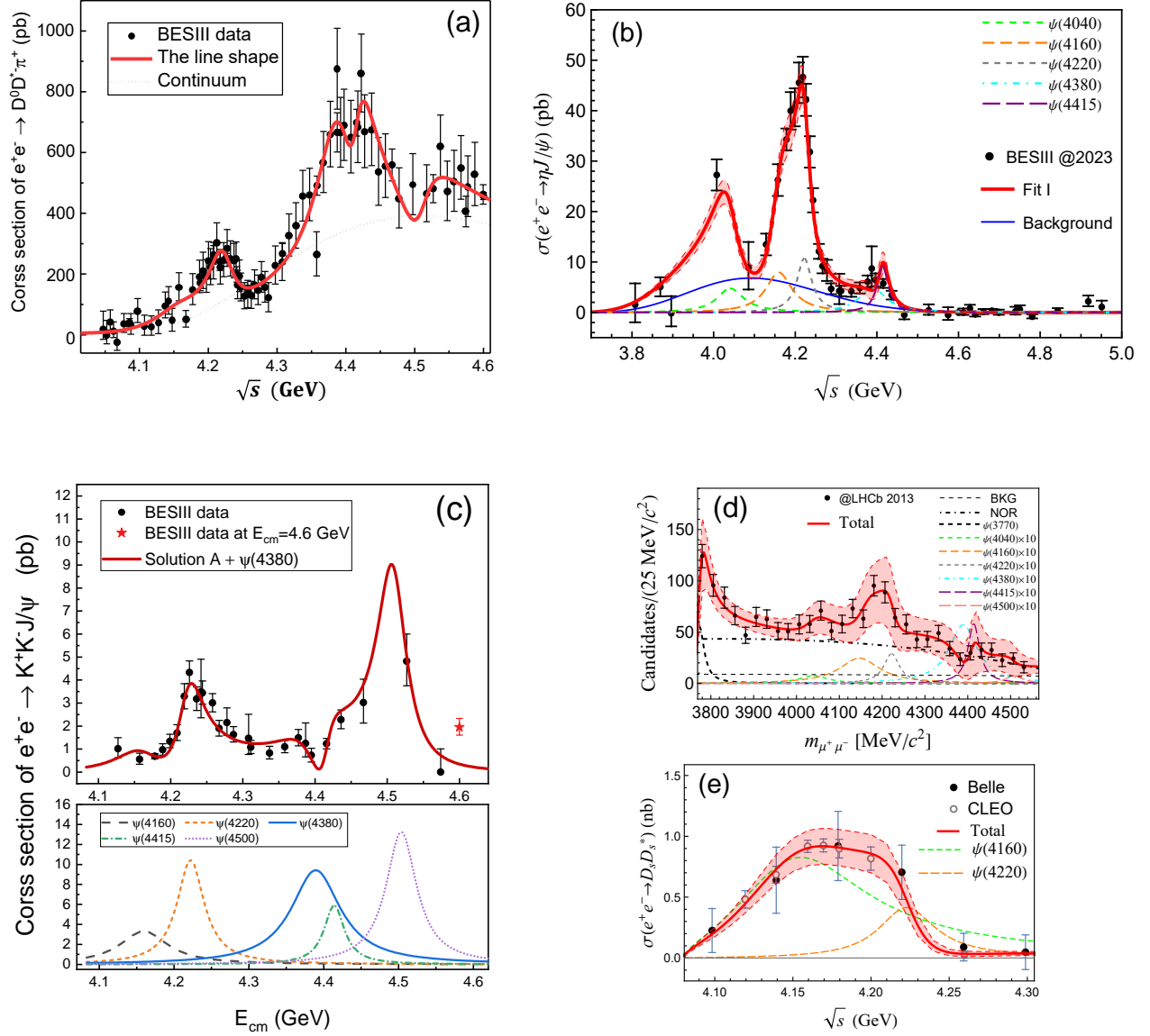


Figure 49: The fitted results of the  $e^+e^- \rightarrow \pi^+ D^0 D^{*-}$  (a) [516],  $e^+e^- \rightarrow \eta J/\psi$  (b) [236],  $e^+e^- \rightarrow K^+ K^- J/\psi$  (c) [233], dimuon invariant mass spectra in  $B^+ \rightarrow K^+ \mu^+ \mu^-$  (d) [524] and  $e^+e^- \rightarrow D_s D_s^*$  (e) [524] processes by the unquenched charmonium spectroscopy.

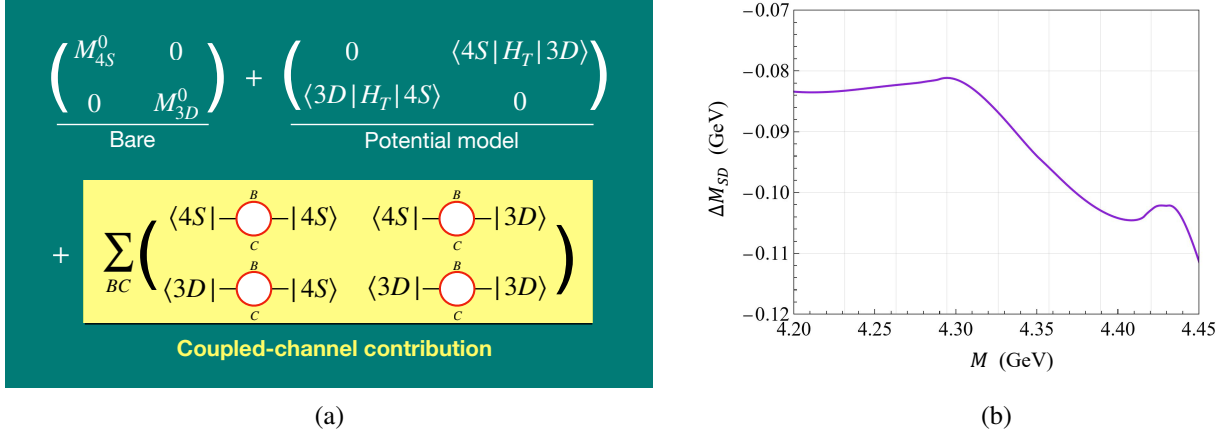


Figure 50: (a) Schematic diagram illustrating the  $4S$ - $3D$  mixing in the potential model and the coupled-channel mechanism. For the coupled-channel contribution, hadronic loops involving  $B$  and  $C$  mesons are considered in the calculation. (b) The dependence of  $\Delta M_{SD}$  on  $M$ . The figures are adopted from Ref. [323].

Here,  $M_{S(D)}^0$  denotes the bare masses of the  $\psi(3^3S_1)$  and  $\psi(2^3D_1)$  states as predicted by the GI model [13]. The quantities  $\Delta M_{S(D)}(M)$  correspond to the self-energy corrections arising from meson-loop effects, while the off-diagonal term  $\Delta M_{SD}(M)$  governs the mixing between the  $\psi(3^3S_1)$  and  $\psi(2^3D_1)$  configurations. In addition, the matrix element  $\langle \psi_S | H_T | \psi_D \rangle$ , originating from the tensor interaction in the GI model.

Using the Quark Pair Creation model to evaluate both diagonal  $\Delta M_{S(D)}(M)$  and off-diagonal  $\Delta M_{SD}(M)$ , several relevant coupled channels were analyzed in detail. Fig 50 (b) shows the dependence of  $\Delta M_{SD}$  on  $M$ . It is found that the magnitude of  $\Delta M_{SD}$  is comparable to those of  $\Delta M_S$  and  $\Delta M_D$ , indicating that the mixing effects provide a non-negligible contribution. The combined effect of relevant channels results in a large dynamical mixing angle,

$$\theta \simeq 35^\circ.$$

This value supports the large  $4S$ - $3D$  mixing in  $\psi(4220)$  previously obtained from fits to experimental data [300].

After diagonalization of the coupled-channel mass matrix, two physical mixed states were obtained. The lower state, dominated by the  $\psi(4S)$  component, has a mass around 4.23 GeV and can be naturally identified with the  $\psi(4220)$ . The higher state, with a dominant  $\psi(3D)$  component, appears near 4.39 GeV and was associated with the  $\psi(4380)$ . Furthermore, it is found that the proximity of the  $DD_1$  threshold leads to a substantial mass shift of the lower mixed state, while the  $D^*D_1$  channel primarily affects the higher state. The predicted total widths and open-charm decay patterns of these states were shown to be compatible with available experimental data, providing further support for this assignment.

The study of  $\psi(4220)$  further strengthens the view that unquenched dynamics are essential for a unified and self-consistent description of the charmonium spectrum above open-charm thresholds.

Parallel to  $\psi(4220)$  and  $\psi(4380)$  system,  $\psi(4040)$  (also denoted  $\psi(3^3S_1)$  in quenched quark model classifications) represents another cornerstone in understanding unquenched effects in the vector charmonium spectrum above open-charm thresholds. First observed by the DASP Collaboration in  $e^+e^-$  annihilation in 1978 [458],  $\psi(4040)$  is a well-established resonance listed in the Particle Data Group (PDG) reviews [94], yet its intrinsic structure and mixing dynamics remain incompletely resolved. A key open question revolves around the strength of the  $3S$ - $2D$  mixing between  $\psi(4040)$  and its higher-mass counterpart  $\psi(4160)$  ( $\psi(2^3D_1)$ ), as well as the extent to which coupled-channel effects drive this mixing.

Early phenomenological studies inferred significant  $3S$ - $2D$  mixing for  $\psi(4040)$  and  $\psi(4160)$  by fitting experimental dielectronic decay widths ( $\Gamma_{e^+e^-}$ ) or their ratios [529, 299, 530, 532, 533, 233, 531, 406]. In Table 7, we summarize the current understanding of  $3S$ - $2D$  mixing, including the inferred mixing angles and the corresponding approaches employed to extract them.

Using the ratio of  $\Gamma_{e^+e^-}(\psi(4040)) \sim 0.86$  keV to  $\Gamma_{e^+e^-}(\psi(4160)) \sim 0.83$  keV, a mixing angle of about  $35^\circ$  was extracted in Refs. [529, 530, 299]. Later analyses incorporating updated BESIII Collaboration data, which reported a

Table 7: The obtained  $3S$ - $2D$  mixing angle for  $\psi(4040)$  and  $\psi(4160)$ .

$\Gamma_{e^+e^-}^{\psi(4040)}$ (keV)	$\Gamma_{e^+e^-}^{\psi(4160)}$ (keV)	Mixing angle
$0.86 \pm 0.07$ [94]	$0.83 \pm 0.08$ [528]	$\phi = -35^\circ, +55^\circ$ [529] <sup>1</sup>
		$\phi = -37^\circ$ [299] <sup>1</sup>
	$0.48 \pm 0.22$ [515]	$\theta = 34.8^\circ, -55.7^\circ$ [530] <sup>1</sup>
		$\theta = 20^\circ$ [233] <sup>2</sup>
		$\phi = 45^\circ$ [531] <sup>3</sup>
		$\phi = -21.1^\circ, 62.6^\circ$ [406] <sup>4</sup>

smaller value of  $\Gamma_{e^+e^-}(\psi(4160)) \sim 0.48$  keV [515], revised the mixing angle to approximately  $\sim 20^\circ$  [233, 406]. These relatively large mixing angles, comparable to those inferred for the  $\psi(4220)$ - $\psi(4380)$  system, initially suggested the presence of a universal strong  $S$ - $D$  mixing mechanism in higher charmonium states.

However, the dielectronic width of the  $\psi(4160)$  suffers from substantial experimental uncertainties. In 2010, Mo, Yuan, and Wang reanalyzed the BES data and pointed out that the dielectronic width of the  $\psi(4160)$  reported in Ref. [515] represents only one of four possible solutions, with values ranging from 0.4 to 1.1 keV [534]. It is important to emphasize that the presence of multiple possible solutions for the dielectronic width introduces significant uncertainties in extracting the  $3S$ - $2D$  mixing angle. Furthermore, early measurements of  $\psi(4040)$  and  $\psi(4160)$  were mainly based on inclusive  $e^+e^- \rightarrow$  hadrons processes, with only limited information from exclusive decay channels. In particular, the dielectronic width of the  $\psi(4160)$  extracted from inclusive data suffers from large uncertainties. This is primarily due to the presence of multiple open-charm thresholds in this energy region, which generate complicated structures in the measured cross sections. As a result, inclusive measurements alone are insufficient for a detailed characterization of high-mass charmonium states. Although several exclusive processes involving  $\psi(4160)$  have been reported [523, 396], its dielectronic width has not yet been precisely determined. Consequently, approaches that rely on experimentally extracted dielectronic widths to infer the  $3S$ - $2D$  mixing angle may be subject to significant uncertainties and should be treated with caution.

Therefore, a more comprehensive understanding of the internal structure and mixing dynamics of  $\psi(4040)$  and  $\psi(4160)$  is highly desirable.

Recent work by Man, Luo, and Liu [324] extended the coupled-channel framework to the  $\psi(4040)$ - $\psi(4160)$  system. Starting from the bare masses of the  $\psi(3^3S_1)$  and  $\psi(2^3D_1)$  states, taken as 4089 MeV and 4172 MeV from the GI model [13], unquenched effects were incorporated through intermediate open-charm meson loops. By solving Eq. (76) within this coupled-channel formalism, the physical masses of the mixed states  $\psi'_{3S-2D}$  and  $\psi''_{3S-2D}$  were obtained as  $4006.4^{+7.4}_{-8.3}$  MeV and  $4089.5^{+8.8}_{-8.6}$  MeV, respectively. The corresponding eigenvectors were simultaneously determined. The eigenvector components ( $C_{S1(2)}, C_{D1(2)}$ ) quantify the admixtures of the  $3^3S_1$  and  $2^3D_1$  configurations in each physical state. Based on these coefficients, the mixing angles were extracted using the relations  $\theta_1 = \arctan(-C_{D1}/C_{S1})$  and  $\theta_2 = \arctan(C_{S2}/C_{D2})$  for  $\psi'_{3S-2D}$  and  $\psi''_{3S-2D}$ , respectively.

As a result, the mixing angles were determined to be

$$\theta_1 = (7.3^{+0.1}_{-0.4})^\circ \quad \text{for } \psi'_{3S-2D}, \quad (48)$$

and

$$\theta_2 = (10.4^{+2.0}_{-3.5})^\circ \quad \text{for } \psi''_{3S-2D}. \quad (49)$$

Unlike  $\psi(4220)$  and  $\psi(4380)$ , which exhibit relatively large mixing angle, the mixing between the  $\psi(3^3S_1)$  and  $\psi(2^3D_1)$  states is found to be weaker [324].

The calculated dielectronic width of  $\psi(4040)$  (0.92 keV) agrees with the PDG value ( $0.86 \pm 0.07$  keV) [94], while the predicted width of  $\psi(4160)$  (0.22 keV) lies at the lower bound of experimental measurements [534]. As illustrated in Fig. 51, the calculation yields a ratio of approximately 4.1, which is larger than the experimental determinations of  $1.04 \pm 0.12$  and  $1.79 \pm 0.83$  [94]. This tension between theory and experiment provides a clear and testable prediction that can be examined in future high-precision measurements.

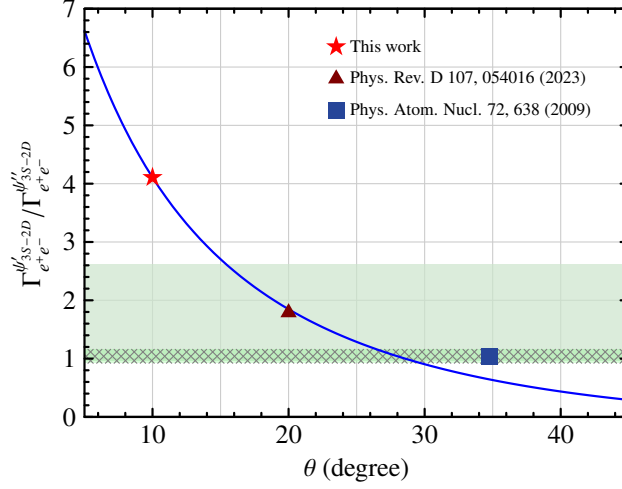


Figure 51: The ratio of dielectronic widths  $\Gamma_{e^+e^-}^{\psi'_{3S-2D}} / \Gamma_{e^+e^-}^{\psi''_{3S-2D}}$  as a function of the  $3S-2D$  mixing angles. The red pentagram represents the prediction of this work ( $\theta \approx 10^\circ$  and ratio  $\Gamma_{e^+e^-}^{\psi'_{3S-2D}} / \Gamma_{e^+e^-}^{\psi''_{3S-2D}} \approx 4.1$ ). The light green and dark green shaded bands indicate the experimental values  $1.79 \pm 0.83$  and  $1.04 \pm 0.12$ , respectively, from the PDG [94]. The triangle and square indicate the mixing angles  $20^\circ$  and  $34.8^\circ$ , as obtained in Refs. [233] and [530], respectively.

Future experiments, particularly the upgraded BESIII facility with an expected threefold increased in luminosity [535], is anticipated to play a crucial role in resolving the remaining ambiguities. Precision measurements of exclusive decay channels and dielectronic widths will constrain the  $3S-2D$  mixing angle further, while searches for the predicted  $\psi(4380)$  (via  $DD_2^*$  decays), will offer a critical test of the universality of coupled-channel induced  $S-D$  mixing. Collectively, these efforts will advance a unified framework for describing charmonium states above open-charm thresholds, where unquenched effects are the primary driver of mass shifts, mixing angles, and decay dynamics.

#### 4.5.2. Coherent coupled-channel description of near-threshold structures: $\psi(3770)$ , $G(3900)$ , $R(3760)$ , $R(3780)$ , and $R(3810)$

As the first charmonium state above the open-charm threshold,  $\psi(3770)$  displays several anomalous properties. It exhibits a significant non-open-charm hadron (nOCH) decay fraction of approximately 15% [70, 71], in contrast to the nearly negligible nOCH partial widths of  $\psi(3686)$  and  $J/\psi$ . Moreover, its line shape deviates from a standard Breit-Wigner distribution—a discrepancy that has led to proposal that two distinct structures might be present [536]. Recent measurements by the BESIII collaboration have further enriched this picture. Both the hadronic cross section [537] and the nOCH cross section [538] unveil intricate structures in the  $3.7 - 3.82$  GeV region, which are well described by the interference among three resonances:  $R(3760)$ ,  $R(3780)$ , and  $R(3810)$ . Clearly, only one of these can correspond to the  $\psi(1D)$  state, as no additional conventional charmonia are predicted in this mass range.

In addition to the structures near the  $\psi(3770)$ , a resonance-like feature denoted as  $G(3900)$  has been observed just above the  $\psi(3770)$  peak in the  $e^+e^- \rightarrow D\bar{D}$  cross section [539, 448, 540, 455, 31]. Theoretical attempts have been made from different perspectives to understand the  $G(3900)$  structure, such as  $P$ -wave  $D\bar{D}^*$  resonance states [541] and coupled-channel frameworks [542, 543, 544, 545, 546, 547]. However, these studies have yielded conflicting results; while some [543, 546, 547] found a pole near 3.9 GeV, others did not [544, 545]. To resolve these debates, a critical question is whether the  $G(3900)$  structure can be generated from the coupled-channel dynamics of nearby  $c\bar{c}$  states such as  $\psi(3770)$  and  $\psi(4040)$ .

Interestingly, the structures near the  $D\bar{D}$  threshold can be explained within a unified coupled-channel framework. In Ref. [548], Qian and Liu propose a unified coupled-channel description to these structures. The coupled-channel framework incorporates the bare  $c\bar{c}$  core, hadron-hadron kinematics, and transition interactions between bare  $c\bar{c}$  states and various hadronic channels:

$$H = H_{c\bar{c}} + H_{c\bar{c} \leftrightarrow \text{hadrons}} + H_{\text{hadrons}}. \quad (50)$$

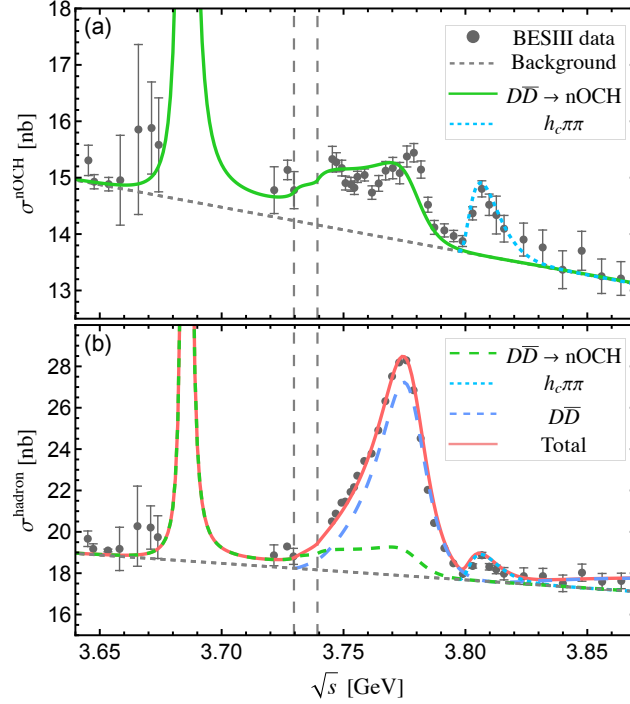


Figure 52: Coupled-channel description of (a) the  $e^+e^- \rightarrow$  nonopen-charm hadron and (b) the inclusive hadronic cross sections. Vertical dashed lines indicate the  $D^0\bar{D}^0$  and  $D^+\bar{D}^-$  thresholds. nonopen-charm hadron data are from Ref. [538], inclusive hadronic data are from Ref. [537]. Source: Taken from Ref. [548].

Here, the  $H_{c\bar{c}}$  is modeled using a quenched model [13]. The hadronic Hamiltonian  $H_{hadrons}$  include kinematics and possibly interaction of hadronic channels. By including the  $\psi(1D)$ ,  $\psi(2S)$  and  $\psi(3S)$   $c\bar{c}$  bare states, and modeling the transition from  $c\bar{c}$  to  $D^{(*)}\bar{D}^{(*)}$  via the QPC model, this coupled-channel model reproduce the  $\psi(3770)$  and  $G(3900)$  structure in  $e^+e^- \rightarrow D\bar{D}$  process. Removing either  $\psi(3686)$  or  $\psi(3S)$  eliminates this structure, indicating a nontrivial interference pattern. The authors found three poles near the real axis, corresponding to the  $\psi(3686)$ ,  $\psi(3770)$ , and  $\psi(4040)$ , but but no additional pole near 3.9 GeV close to the physical axis.

Beyond structures in open-charm channels, the authors of Ref. [548] find that the  $R(3760)$  and  $R(3780)$  resonances in non-open-charm channels can be explained by including a  $D\bar{D} \rightarrow$  nOCH transition, while the  $R(3810)$  can be attributed to the  $\psi(1D)$ - $h_c\pi\pi$  coupling. The  $D\bar{D} \rightarrow$  nOCH process corresponds to rescattering from  $D\bar{D}$  to non-open-charm hadrons, modeled by

$$V_{\text{nOCH},D\bar{D}}(\mathbf{q}) = g_{\text{nOCH}} q e^{-q/\Lambda_{\text{nOCH}}} Y_1^{1*}(\Omega_{\mathbf{q}}), \quad (51)$$

where  $q$  is the momentum of the  $D\bar{D}$  system and  $Y_1^1$  is the spherical harmonic function. The authors find a characteristic momentum scale  $\Lambda_{\text{nOCH}} \approx 100$  MeV for this rescattering process, meaning the process is only significant when the  $D\bar{D}$  relative momentum is small. This naturally explains the significant nOCH decay width of the  $\psi(3770)$ : its large nOCH branching fraction arises from its proximity to the  $D\bar{D}$  threshold, enabling decay via the rescattering process  $D\bar{D} \rightarrow$  nOCH. Assuming the two pions are in relative  $P$ -wave ( $L_{\pi\pi} = 1$ ), the  $\psi(1D)$ - $h_c\pi\pi$  coupling is modeled as

$$f_{\psi(1D),h_c\pi\pi}(\mathbf{q}, \mathbf{p}) = \frac{g_{h_c\pi\pi}}{\sqrt{4\pi}} p e^{-(q^2+p^2)/\Lambda_{h_c}^2} \frac{1}{\sqrt{2}} (Y_1^{0*}(\Omega_p) - Y_1^{1*}(\Omega_p)),$$

where  $\mathbf{q}$  is the  $h_c$  momentum in the c.m. frame, and  $\mathbf{p}$  is the relative momentum between the pions. The authors find a characteristic momentum scale  $\Lambda_{h_c} \approx 40$  MeV, which is easily understood because the bare mass of the  $\psi(1D)$  (3.82 GeV) is only about 100 MeV above the  $h_c\pi\pi$  threshold, leaving only tens of MeV for the momentum of the  $h_c\pi\pi$  system.

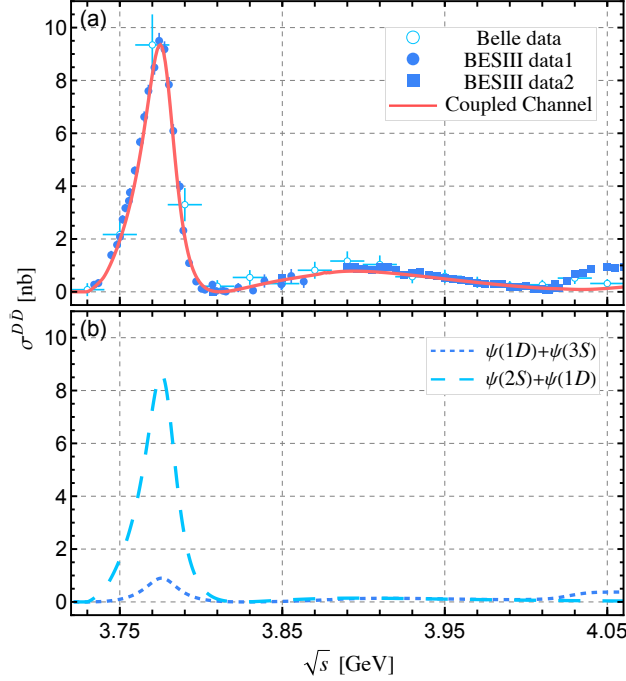


Figure 53: (a) Coupled-channel description of the  $e^+e^- \rightarrow D\bar{D}$  cross section. The red solid line represents the full model including  $\psi(2S)$ ,  $\psi(1D)$ , and  $\psi(3S)$ . Experimental data are from Belle [455] and BESIII [545, 539]. (b) Cross section when either  $\psi(2S)$  or  $\psi(3S)$  is removed. Source: Taken from Ref. [548]

## 5. The initial single pion emission mechanism: explaining charged $Z_b$ and predicting charmonium-like charged $Z_c/Z_{cs}$

Of the many charmonium-like  $XYZ$  states discovered over the past two decades, those that carry electric charge are collectively referred to as  $Z$  states. A prominent example is provided by the bottomonium-like charged states  $Z_b(10610)$  and  $Z_b(10650)$ , reported by the Belle Collaboration [80]. These  $Z_b$  states have attracted extensive attention from the entire community, as their identification as hadrons necessarily implies an exotic nature beyond conventional quark models. An alternative theoretical framework for understanding their properties is the *Initial Single Pion Emission* (ISPE), proposed in Ref. [81]. As reviewed in this section, the ISPE mechanism embodies an unquenched picture of hadron dynamics.

This section outlines the motivation behind the ISPE mechanism, which was originally developed to explain the hidden-bottom dipion decay anomaly observed in  $\Upsilon(10860)$  [549]. The mechanism is not restricted to bottomonium systems but can also be applied to hidden-charm dipion decays of higher charmonium(-like) states. It successfully predicted the existence of charged charmonium-like  $Z_c$  structures near the  $D\bar{D}^*$  and  $D^*\bar{D}$  thresholds, which should appear in the invariant mass spectra of  $J/\psi\pi^\pm$ ,  $\psi(3686)\pi^\pm$ , and  $h_c(1P)\pi^\pm$  [82]. In 2013, the BESIII and Belle collaborations observed  $Z_c(3900)$  in the  $J/\psi\pi^\pm$  invariant mass spectrum of the process  $e^+e^- \rightarrow J/\psi\pi^+\pi^-$  at  $\sqrt{s} = 4.26$  GeV [550, 551]. Since then, additional charged  $Z_c$  structures have been reported in other channels [552, 553, 380, 554, 482, 555, 556, 557, 558, 385, 559, 514, 560]. Furthermore, the ISPE framework has been extended to a more general initial single chiral particle emission mechanism. This extension suggests that  $Z_{cs}$  structures could exist in the  $J/\psi K^\pm$  invariant mass spectrum of  $e^+e^- \rightarrow J/\psi K^+ K^-$  at several energy points [561], presenting a clear task for future experimental searches.

In the following, we review the formulation of the ISPE mechanism and its application across different quarkonium systems.

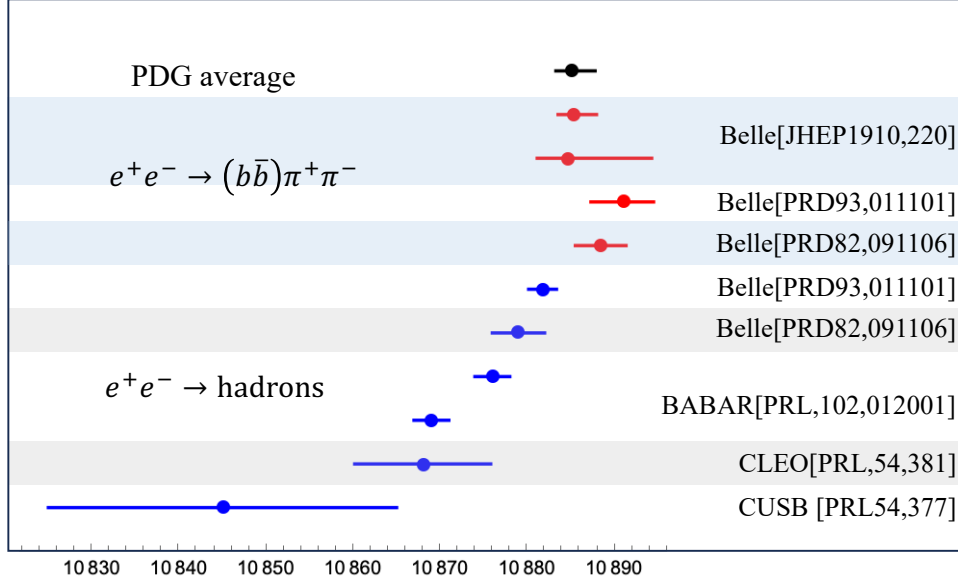


Figure 54: The mass of  $\Upsilon(10860)$  in the inclusive process  $e^+e^- \rightarrow \text{hadrons}$  (blue dots with error bars) and in the hidden bottom processes  $e^+e^- \rightarrow (b\bar{b})\pi^+\pi^-$  with  $\{(b\bar{b}) = \Upsilon(1S, 2S, 3S), h_b(1P, 2P)\}$  (red dots with error bars). The PDG average (black dot with error bar) is also present for comparison.

## 5.1. Anomalous phenomena related to $\Upsilon(10860)$

### 5.1.1. Experimental observation of $\Upsilon(10860)$

The bottomonia  $\Upsilon(5S)$  was first reported in the  $e^+e^-$  annihilation cross section into hadrons by the CUSB Collaboration, the observed mass and width of  $\Upsilon(5S)$  were measured to be  $(10845 \pm 20)$  and  $(110 \pm 15)$  MeV, respectively [562]. The signal of  $\Upsilon(5S)$  had been successively reported by the CLEO [563], BaBar [564], and Belle [565] Collaborations in the same inclusive process but with higher observed mass. The most precise mass of  $\Upsilon(5S)$  from the inclusive process is  $(10881.8^{+1.0}_{-1.1} \pm 1.2)$  MeV reported by the Belle Collaboration [565].

The first exclusive production cross sections for  $e^+e^- \rightarrow \Upsilon(mS)\pi^+\pi^-$  (with  $m = 1, 2, 3$ ) as a function of the center-of-mass energy  $\sqrt{s}$  were reported by the Belle Collaboration [549], where the process  $\Upsilon(5S) \rightarrow \Upsilon(mS)\pi^+\pi^-$  (with  $m = 1, 2, 3$ ) was observed. The fitted mass and width of the resonance were determined to be  $(10888.4^{+2.7}_{-2.6} \pm 1.2)$  MeV and  $(30.7^{+8.3}_{-7.0} \pm 3.1)$  MeV, respectively, where the first uncertainties are statistical and the second are systematic. These values are not fully consistent with the conventional  $\Upsilon(5S)$  lineshape observed in the inclusive  $e^+e^-$  annihilation cross sections [549]. Subsequently, using more precise data samples, the Belle Collaboration reported further measurements of  $\Upsilon(5S)$  in the processes  $e^+e^- \rightarrow \Upsilon(nS)\pi^+\pi^-$  (with  $n = 1, 2, 3$ ) and  $e^+e^- \rightarrow h_b(mP)\pi^+\pi^-$  (with  $m = 1, 2$ ) [566]. The observed masses of  $\Upsilon(5S)$  from the inclusive processes (blue dots with error bars) and from the exclusive hidden-bottom decay processes (red dots with error bars) are presented in Fig. 54. From the figure, one can clearly see that the masses observed in the exclusive hidden-bottom decay processes are systematically higher than those observed in the inclusive processes. Whether the states observed in the inclusive and exclusive processes correspond to the same resonance has become an intriguing question and has stimulated considerable theoretical interest. Given that the community has not reached a definitive agreement on the nature of this state, we refer to this resonance as  $\Upsilon(10860)$  in the following discussion.

Besides the discrepancy in the resonance parameters observed in the inclusive  $e^+e^-$  annihilation cross sections and exclusive hidden bottom decay processes, the Belle Collaboration also reported the partial widths of  $\Upsilon(1S)\pi^+\pi^-$  and  $\Upsilon(2S)\pi^+\pi^-$ , which are  $(0.59 \pm 0.04(\text{stat.}) \pm 0.09(\text{syst.}))$  MeV and  $(0.85 \pm 0.07(\text{stat.}) \pm 0.16(\text{syst.}))$  MeV, respectively [79]. The dipion transitions between the bottomonia should be suppressed by the OZI suppression rule. As shown in Table 8, the partial widths of dipion decay of  $\Upsilon(2S/3S/4S)$  are of order 1 keV, which are consistent with the expectations of OZI suppression rule. However, for  $\Upsilon(10860)$ , the partial widths of the dipion decays exceed by more than two orders of magnitude of the dipion transitions between lower  $\Upsilon$  resonances as shown in Table 8. How to understand the

Table 8: The partial widths of dipion transitions between  $\Upsilon$  states [94, 567, 79, 130]. The partial width of  $\Upsilon(3S)$  dipion decays are estimated by the PDG average of  $\Upsilon(3S)$  width and the branching fractions of the corresponding processes.

Processes	Width	Processes	Width
$\Upsilon(2S) \rightarrow \Upsilon(1S)\pi^+\pi^-$	$(105.4 \pm 1.0 \pm 4.2)$ eV [567]	$\Upsilon(10860) \rightarrow \Upsilon(2S)\pi^+\pi^-$	$(590 \pm 40 \pm 90)$ keV [79]
$\Upsilon(3S) \rightarrow \Upsilon(2S)\pi^+\pi^-$	$(0.57 \pm 0.06)$ keV [94]	$\Upsilon(10860) \rightarrow \Upsilon(1S)\pi^+\pi^-$	$(850 \pm 70 \pm 16)$ keV [79]
$\Upsilon(3S) \rightarrow \Upsilon(1S)\pi^+\pi^-$	$(0.89 \pm 0.08)$ keV [94]		
$\Upsilon(4S) \rightarrow \Upsilon(2S)\pi^+\pi^-$	$(2.7 \pm 0.8 \pm 4.2)$ keV [130]		
$\Upsilon(4S) \rightarrow \Upsilon(1S)\pi^+\pi^-$	$(1.8 \pm 0.4)$ keV [130]		

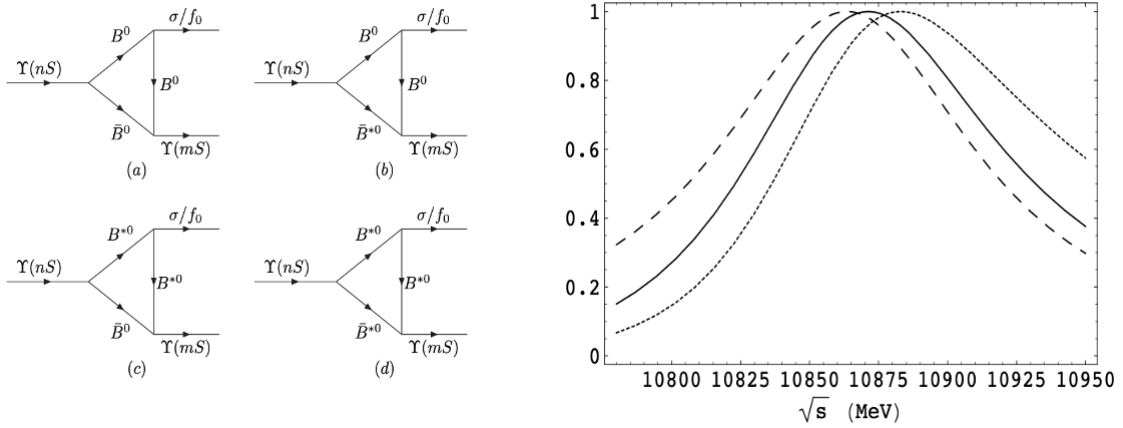


Figure 55: The diagram contributing to  $\Upsilon(nS) \rightarrow \Upsilon(mS)\pi^+\pi^-$  (left panel) and the peak shifts caused by the triangle diagrams (right panel). Source: Taken from [568].

anomalous large partial widths of  $\Upsilon(10860)$  hidden-bottom dipion decays are also a challenge to our understanding of the properties of higher bottomonia.

### 5.1.2. Theoretical interpretations of $\Upsilon(10860)$ : bottomonium vs tetraquark

To explain the mass difference between the inclusive  $e^+e^-$  annihilation cross section and the dipion decay process and the anomalous large hidden-bottom dipion decay width of  $\Upsilon(10860)$ , one should carefully check the mass spectrum of bottomonia family. For  $\Upsilon(10860)$ , its mass is above the thresholds of  $B_{(s)}^*\bar{B}_{(s)}^*$ , which indicate that  $\Upsilon(5S)$  should dominantly decay into a pair of bottom mesons. Considering this fact, Meng and Chao investigated dipion transitions between  $\Upsilon(5S)$  and  $\Upsilon(mS)$  ( $m = 1, 2, 3$ ) in the final state interaction mechanism induced by unquench effect [153, 568, 154], where the hidden-bottom dipion transitions mainly proceed through the real process  $\Upsilon(5S) \rightarrow B^{(*)}\bar{B}^{(*)}$  and  $B^{(*)}\bar{B}^{(*)} \rightarrow \Upsilon(mS)\sigma/f_0$  and the scalar meson  $\sigma/f_0$  couples to  $\pi^+\pi^-$  as shown in the left panel of Fig. 55. In the final state interaction mechanism, the large branching fractions of the hidden-bottom dipion transition processes could be well interpreted. Similar conclusion can be drawn from the study in Ref. [569].

In addition, Meng and Chao introduced a form factor in each  $\Upsilon(5S)B^{(*)}\bar{B}^{(*)}$  coupling to naturally balance the otherwise over-increased decay width with increased phase space in the rescattering model [568]. They found that the energy distributions of  $\Upsilon(mS)\pi^+\pi^-$  markedly differ from that of  $\Upsilon(5S) \rightarrow B^{(*)}\bar{B}^{(*)}$ , and as shown in the right panel of Fig. 55, the resonance peak is pushed up by about 7 – 20 MeV for the hidden-bottom dipion transitions relative to the open-bottom decay modes [568], which naturally explain the discrepancy of the observed mass in the inclusive process and exclusive hidden-bottom dipion decay processes.

Besides the conventional  $\Upsilon(5S)$  interpretations, the particular properties of  $\Upsilon(10860)$ , observed in the cross sections for  $e^+e^- \rightarrow \Upsilon(mS)\pi^+\pi^-$ , also stimulated the exotic interpretation. For example, the estimations within the

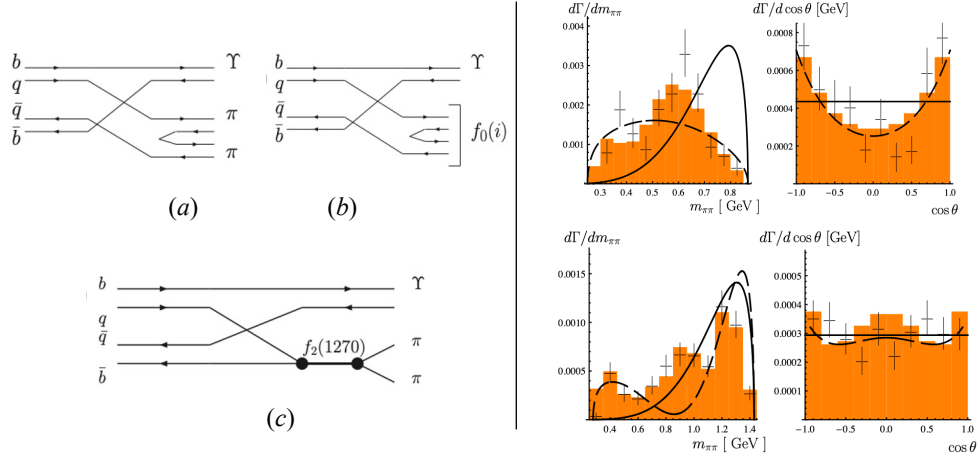


Figure 56: The diagram contributing to  $Y_b(10890) \rightarrow \Upsilon\pi^+\pi^-$  in tetraquark scenario (left panel) and dipion invariant mass ( $m_{\pi\pi}$ ) distribution and the  $\cos\theta$  distributions measured by Belle [79] for the final state  $\Upsilon(1S)\pi^+\pi^-$  (upper row of right panel) and  $\Upsilon(2S)\pi^+\pi^-$  (lower row of right panel), and the theoretical distributions based on the tetraquark estimations (histograms) [571]. The solid and dashed lines show purely continuum contributions for different  $\beta$ .

Source: Taken from [571].

constituent quark model [570, 571, 572, 573, 574], QCD sum rules [575] suggested that the mass of  $P$ -wave  $[bq][\bar{b}\bar{q}]$  tetraquark state agrees with the experimental measurements of  $\Upsilon(10860)$  in the exclusive hidden-bottom dipion decay processes. In addition to the resonance parameters, the Belle Collaboration also reported the dipion invariant mass spectra and the helicity angle distributions of the  $\Upsilon(10890) \rightarrow \Upsilon(1S/2S)\pi^+\pi^-$  processes. In the tetraquark framework, Ali *et. al.*, considered the non-resonance contribution (Fig. 56(a)), the resonance contributions from scalar meson  $f_0(600)$  and  $f_0(980)$  (Fig. 56(b)), and tensor meson  $f_2(1270)$  (Fig. 56(c)) in  $\Upsilon(10860) \rightarrow \Upsilon(1S/2S)\pi^+\pi^-$ . With these contributions, the authors in Ref. [571] claimed that the experimental data could be well reproduced in the tetraquark scenario as shown in the right panel of Fig. 56<sup>5</sup>.

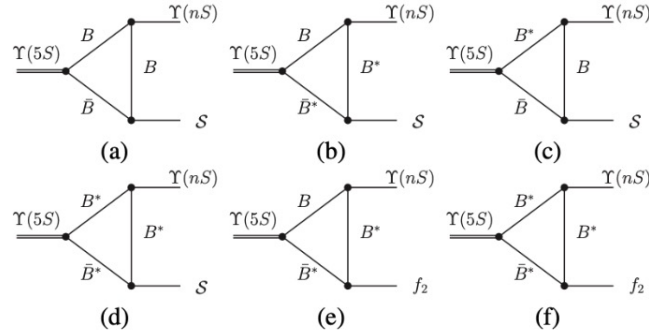


Figure 57: The schematic diagrams for  $\Upsilon(5S)$  decays into  $\Upsilon(nS)S$  (diagrams (a)-(d)) and  $\Upsilon(nS)f_2(1270)$  (diagrams (e)-(f)) ( $n = 1, 2$ ) via bottom meson loops.

Source: Taken from [576].

### 5.1.3. Puzzles in the dipion invariant mass distributions and $\cos\theta$ distributions.

In their study of  $\Upsilon(5S)$  decays, Chen *et al.* extended the final-state interaction mechanism developed in Refs. [153, 568, 154] to investigate the dipion invariant mass spectra and helicity angle distributions of the processes  $\Upsilon(5S) \rightarrow$

<sup>5</sup>However, in the erratum to this work, the authors indicated that the dipion invariant mass distributions and the  $\cos\theta$  distributions of  $\Upsilon(10860) \rightarrow \Upsilon(2S)\pi^+\pi^-$  cannot be reproduced simultaneously, as will be discussed in the following section.



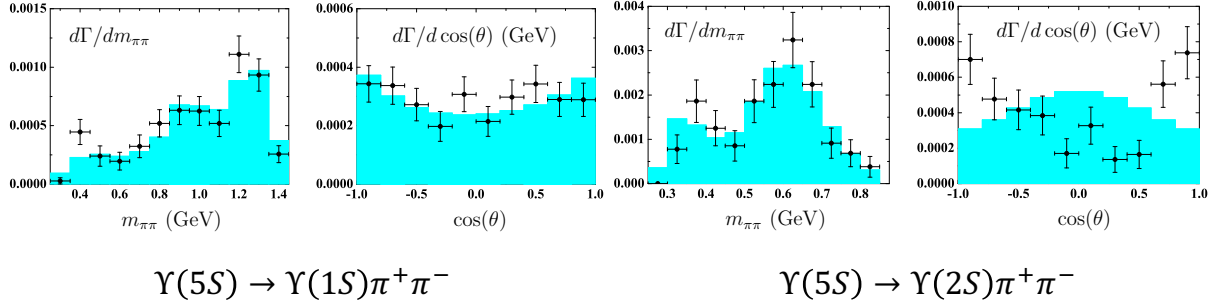


Figure 58: Dipion invariant mass ( $m_{\pi\pi}$ ) distributions (1st and 3rd frames) and the  $\cos\theta$  distributions (2nd and 4th frames) measured by Belle for the final state  $\Upsilon(1S)\pi^+\pi^-$  (1st and 2nd frames, crosses) and  $\Upsilon(2S)\pi^+\pi^-$  (3rd and 4th frames, crosses) and the theoretical distributions in the conventional  $\Upsilon(5S)$  frame (histograms).  
Source: Taken from [576].

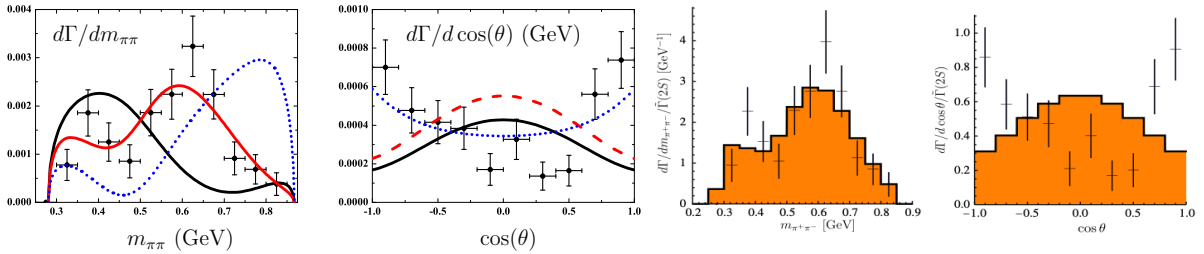


Figure 59: Dipion invariant mass ( $m_{\pi\pi}$ ) distributions (1st and 3rd frames) and the  $\cos\theta$  distributions (2nd and 4th frames) of  $\Upsilon(5S) \rightarrow \Upsilon(2S)\pi^+\pi^-$  reproduced by Chen *et al* in Ref. [576] (left panel) and in the in the erratum of Ref. [571].  
Source: Taken from [576, 571].

In Ref. [576], Chen and Liu also examined the dipion invariant mass spectra and  $\cos\theta$  distributions of  $\Upsilon(10860) \rightarrow \Upsilon(2S)\pi^+\pi^-$  using the same formalism as in Ref. [571]. They found that the fitted results reported in Ref. [571] could not be reproduced (see left panel of Fig. 59). They concluded that the dipion invariant mass spectrum and  $\cos\theta$  distributions of  $\Upsilon(10860) \rightarrow \Upsilon(2S)\pi^+\pi^-$  cannot be simultaneously reproduced within either the conventional bottomonium or tetraquark frameworks, presenting a new and intriguing puzzle in the hidden-bottom dipion decays of  $\Upsilon(10860)$ . Subsequently, Ali *et al.* acknowledged this issue in the erratum associated with Ref. [571], noting that one cannot simultaneously reproduce the dipion invariant mass spectrum and  $\cos\theta$  distribution of  $\Upsilon(5S) \rightarrow \Upsilon(2S)\pi^+\pi^-$  using only non-resonance and dipion resonance contributions within the tetraquark framework (see right panel of Fig. 59).

#### 5.1.4. Charged bottomoniumlike structures $Z_b(10610)$ and $Z_b(10650)$

In addition to the anomalously large branching fractions of the dipion decays of  $\Upsilon(10860)$  and the puzzles in the dipion invariant mass spectrum and  $\cos\theta$  distribution of  $\Upsilon(10860) \rightarrow \Upsilon(2S)\pi^+\pi^-$  discussed in the previous subsection, another interesting phenomenon associated with  $\Upsilon(10860)$  is the observation of charged bottomonium-like states, namely  $Z_b(10610)$  and  $Z_b(10650)$ . In 2011, the Belle Collaboration reported these two new bottomonium-like states [80], which were identified through the invariant mass distributions of  $\pi^\pm\Upsilon(nS)$  (with  $n = 1, 2, 3$ ) and  $\pi^\pm h_b(mP)$  (with  $m = 1, 2$ ) in the decay processes  $\Upsilon(5S) \rightarrow \Upsilon(nS)\pi^+\pi^-$  (as shown in Fig. 60) and  $\Upsilon(5S) \rightarrow h_b(mP)\pi^+\pi^-$  (as shown in Fig. 61). The weighted averages over all five channels yield the masses and widths of these two bottomonium-like states to be [80],

$$\begin{aligned}
m_{Z_b} &= (10607.2 \pm 2.0) \text{ MeV}, & \Gamma_{Z_b} &= (18.4 \pm 2.5) \text{ MeV}, \\
m_{Z'_b} &= (10652.2 \pm 1.5) \text{ MeV}, & \Gamma_{Z'_b} &= (11.5 \pm 2.2) \text{ MeV},
\end{aligned} \tag{55}$$

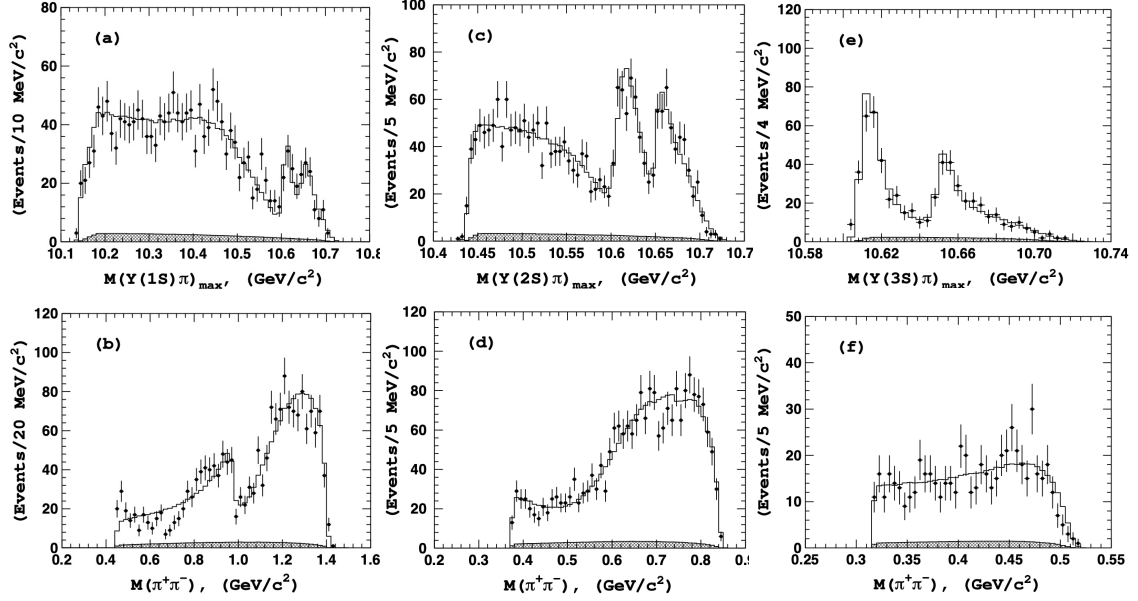


Figure 60: Comparison of fit results (open histogram) with experiment data (points with error bars) for event in the  $\Upsilon(1S)$  (a,b),  $\Upsilon(2S)$  (c,d), and  $\Upsilon(3S)$  (e,f) signal regions. The hatched histogram shows the background component.

Source: Taken from [80].

respectively.

The analysis of the charged pion angular distribution indicates that the quantum numbers of the two states are consistent with  $I^G(J^P) = 1^+(1^+)$  [581]. Furthermore, an amplitude analysis of the process  $e^+e^- \rightarrow \Upsilon(nS)\pi^+\pi^-$  confirms  $I^G(J^P) = 1^+(1^+)$  for both  $Z_b(10610)$  and  $Z_b(10650)$  [582]. The observation of their neutral partners,  $Z_b(10610)^0$  and  $Z_b(10650)^0$ , was achieved through a Dalitz analysis of the decay  $\Upsilon(5S) \rightarrow \pi^0\pi^0\Upsilon(nS)$ , as reported by the Belle Collaboration [583, 584], providing evidence that these two bottomonium-like states exhibit isovector characteristics. In addition to hidden-bottom decay processes, the Belle Collaboration has also observed  $Z_b(10610)$  in the  $B^*\bar{B}$  invariant mass spectra and  $Z_b(10650)$  in the  $B^*\bar{B}^*$  invariant mass distributions of the open-bottom pion decays of  $\Upsilon(5S)$  [585, 580]. The branching fractions of  $Z_b(10610)$  and  $Z_b(10650)$  decaying into bottomonia  $\Upsilon(nS)\pi$ ,  $h_b(mP)\pi$ , and  $B^*\bar{B}^{(*)}$  are compiled in Table 9. From these data, it can be seen that  $Z_b(10610)$  and  $Z_b(10650)$  decay predominantly into open-bottom channels, while the hidden-bottom channels are relatively suppressed.

### 5.1.5. Role of $Z_b(10610)$ and $Z_b(10650)$ in solving the puzzles of the process $\Upsilon(5S) \rightarrow \Upsilon(2S)\pi^+\pi^-$

As indicated in Ref. [576], the contributions from non-resonance and dipion resonance processes alone could not simultaneously reproduce the dipion invariant mass spectra and  $\cos\theta$  distributions of the decay  $\Upsilon(5S) \rightarrow \Upsilon(2S)\pi^+\pi^-$ . Following the observations of  $Z_b(10610)$  and  $Z_b(10650)$ , Chen *et al.* incorporated the contributions of these two bottomonium-like states into the analysis of  $\Upsilon(5S) \rightarrow \Upsilon(2S)\pi^+\pi^-$ . The contributing diagrams for this process are shown in Fig. 62. In this framework, the contributions from  $Z_b(10610)$  and  $Z_b(10650)$  are parameterized as

$$\begin{aligned} \mathcal{M}[\Upsilon(5S) \rightarrow Z_b^+\pi^- \rightarrow \Upsilon(2S)\pi^+\pi^-]_{Z_b^+} &= F_{Z_b^+} \epsilon_{\Upsilon(5S)}^\mu \epsilon_{\Upsilon(2S)}^{*\nu} \frac{-g_{\mu\nu} + (p_1^\mu + p_2^\mu)(p_1^\nu + p_2^\nu)/m_{Z_b}^2}{(p_1 + p_2)^2 - m_{Z_b}^2 + im_{Z_b}\Gamma_{Z_b}} \\ \mathcal{M}[\Upsilon(5S) \rightarrow Z_b^-\pi^+ \rightarrow \Upsilon(2S)\pi^-\pi^+]_{Z_b^-} &= F_{Z_b^-} \epsilon_{\Upsilon(5S)}^\mu \epsilon_{\Upsilon(2S)}^{*\nu} \frac{-g_{\mu\nu} + (p_1^\mu + p_3^\mu)(p_1^\nu + p_3^\nu)/m_{Z_b}^2}{(p_1 + p_3)^2 - m_{Z_b}^2 + im_{Z_b}\Gamma_{Z_b}}, \end{aligned} \quad (56)$$

respectively, with  $F_{Z_b^+} = g_{\Upsilon(5S)Z_b^+\pi} g_{Z_b^+\Upsilon(2S)\pi^+}$  and  $F_{Z_b^-} = g_{\Upsilon(5S)Z_b^-\pi} g_{Z_b^-\Upsilon(2S)\pi^-}$ . Since Fig. 62 (c) and (d) are related to each other by charge-conjugation, thus  $F_{Z_b^-} = F_{Z_b^+} = F_{Z_b}$ .

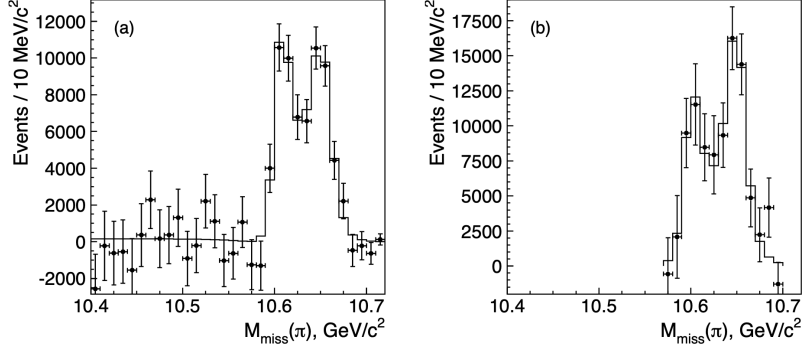


Figure 61: The  $h_b(1P)$  (a) and  $h_b(2P)$  (b) yields as a function of  $M_{\text{miss}}(\pi)$  (points with error bars) and results of the fit (histogram).  
Source: Taken from [80]

Table 9: The branching fractions for  $Z_b(10610)^+$  and  $Z_b(10650)^+$  measured by the Belle Collaboration [580]. The first and second uncertainties are statistical and systematic, respectively.  
Source: Taken from [580].

Channel	Branching Fraction (%)	
	$Z_b(10610)^+$	$Z_b(10650)^+$
$\Upsilon(1S)\pi^+$	$0.54^{+0.16+0.11}_{-0.13-0.08}$	$0.17^{+0.07+0.03}_{-0.06-0.02}$
$\Upsilon(2S)\pi^+$	$3.62^{+0.76+0.79}_{-0.59-0.53}$	$1.39^{+0.48+0.34}_{-0.38-0.23}$
$\Upsilon(3S)\pi^+$	$2.15^{+0.55+0.60}_{-0.42-0.43}$	$1.63^{+0.53+0.39}_{-0.42-0.28}$
$h_b(1P)\pi^+$	$3.45^{+0.87+0.86}_{-0.71-0.63}$	$8.41^{+2.43+1.49}_{-2.12-1.06}$
$h_b(2P)\pi^+$	$4.67^{+1.24+1.18}_{-1.00-0.89}$	$14.7^{+3.2+2.8}_{-2.8-2.3}$
$B^+\bar{B}^{*0} + B^{*+}\bar{B}^0$	$85.6^{+1.5+1.5}_{-2.0-2.1}$	—
$B^{*+}\bar{B}^{*0}$	—	$73.7^{+3.4+2.7}_{-4.4-3.5}$

The total decay amplitude of the  $\Upsilon(5S) \rightarrow \Upsilon(2S)\pi^+\pi^-$  decay is

$$\begin{aligned}
\mathcal{M}_{\text{total}} = & \mathcal{M}[\Upsilon(5S) \rightarrow \Upsilon(2S)\pi^+\pi^-]_{\text{Direct}} \\
& + e^{i\phi_\sigma} \mathcal{M}[\Upsilon(5S) \rightarrow \Upsilon(2S)\sigma(600) \rightarrow \Upsilon(2S)\pi^+\pi^-] + e^{i\phi_{f_0}} \mathcal{M}[\Upsilon(5S) \rightarrow \Upsilon(2S)f_0(980) \rightarrow \Upsilon(2S)\pi^+\pi^-] \\
& + \sum_{Z_b} e^{i\varphi_{Z_b}} \left\{ \mathcal{M}[\Upsilon(5S) \rightarrow Z_b^+\pi^- \rightarrow \Upsilon(2S)\pi^+\pi^-]_{Z_b^+} + \mathcal{M}[\Upsilon(5S) \rightarrow Z_b^-\pi^+ \rightarrow \Upsilon(2S)\pi^+\pi^-]_{Z_b^-} \right\}, \quad (57)
\end{aligned}$$

with these introduced phase angles  $\phi_\sigma$ ,  $\phi_{f_0}$ ,  $\varphi_{Z_b(10610)}$  and  $\varphi_{Z_b(10650)}$ .

In Ref. [586], following the inclusion of contributions from  $Z_b(10610)$  and  $Z_b(10650)$ , it was found that the dipion invariant mass spectrum, the  $\cos\theta$  distributions, and the  $\Upsilon(2S)\pi$  spectrum could all be well reproduced simultaneously, as shown in Fig. 63. The  $Z_b(10610)$  and  $Z_b(10650)$  states were found to be related to the anomalous features observed in  $\Upsilon(2S)\pi^+\pi^-$  production near the  $\Upsilon(5S)$  resonance, previously reported by Belle [79]. By comparing the fitting results obtained with and without the contributions from these newly observed bottomonium-like states, the analysis in Ref. [586] demonstrated that the intermediate  $Z_b(10610)$  and  $Z_b(10650)$  play a crucial role in shaping the behavior of  $d\Gamma(\Upsilon(5S) \rightarrow \Upsilon(2S)\pi^+\pi^-)/d\cos\theta$ . The inclusion of  $Z_b(10610)$  and  $Z_b(10650)$  contributions to  $\Upsilon(5S) \rightarrow \Upsilon(2S)\pi^+\pi^-$  thus provides a unique mechanism for understanding the puzzling  $\cos\theta$  distribution observed in  $\Upsilon(2S)\pi^+\pi^-$  production near the  $\Upsilon(5S)$  resonance [79].

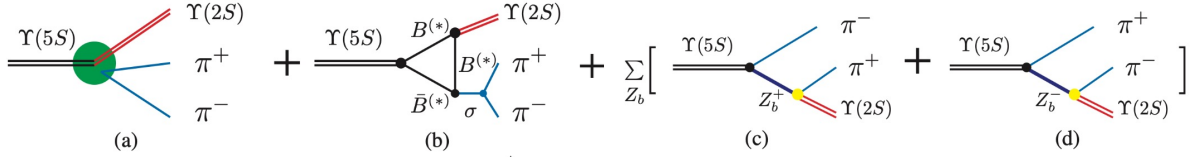


Figure 62: Diagrams contributing to  $\Upsilon(5S) \rightarrow \Upsilon(2S)\pi^+\pi^-$ . Here, diagram (a) represents the  $\Upsilon(5S)$  direct decay into  $\Upsilon(2S)\pi^+\pi^-$ , while diagram (b) denotes the intermediate hadronic loop contribution to  $\Upsilon(5S) \rightarrow \Upsilon(2S)\pi^+\pi^-$ . (c) and (d) describe the intermediate  $Z_b^\pm$  contribution to  $\Upsilon(5S) \rightarrow \Upsilon(2S)\pi^+\pi^-$ , where  $Z_b^\pm = \{Z_b(10610)^\pm, Z_b(10650)^\pm\}$ .  
Source: Taken from [586]

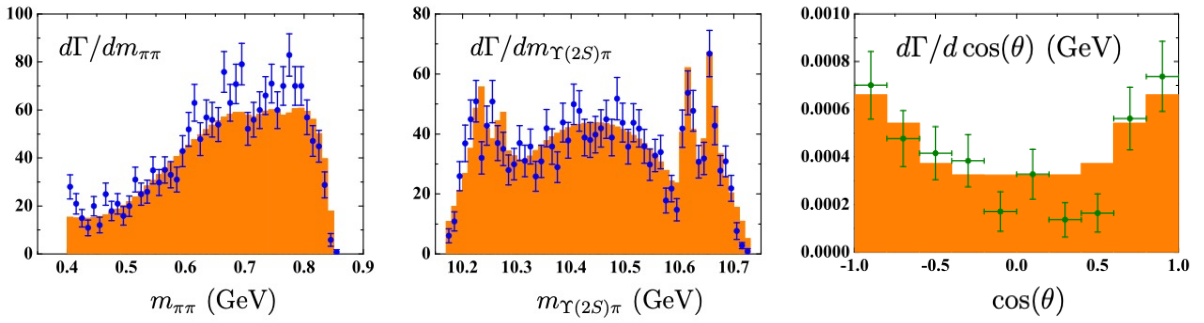


Figure 63: The  $m_{\pi\pi}$  (left frame),  $m_{\Upsilon(2S)\pi}$  (middle frame) invariant mass spectra, and  $\cos\theta$  distribution (right frame) for  $\Upsilon(5S) \rightarrow \Upsilon(2S)\pi^+\pi^-$  process. The histograms are the fitting results with the contributions from  $Z_b(10610)$  and  $Z_b(10650)$ , and the dots with errors correspond to the Belle data [79, 80].  
Source: Taken from [586].

## 5.2. Initial single pion emission mechanism

### 5.2.1. Charged $Z_b$ states and the proposal of the initial single pion emission mechanism

The proximity of their masses to the thresholds and their nonzero electric charges have stimulated considerable theoretical interest in understanding the nature of the  $Z_b(10610)$  and  $Z_b(10650)$  states. Motivated by their distinctive properties, various interpretations have been proposed, including descriptions as  $B^*\bar{B}^*$  molecular states [587, 588, 589, 590, 591, 592, 593, 594, 595, 596, 597, 598, 599, 600, 601, 602, 603, 604, 605, 606],  $[bq][\bar{b}\bar{q}]$  tetraquark states [607, 608, 609, 610, 611, 612], and kinematic effects [613, 614].

In addition to these QCD-exotic and kinematic interpretations, the authors of Ref. [81] extended the description of the  $Z_b(10610)/Z_b(10650)$  contributions in  $\Upsilon(5S)$  dipion decays (as shown in Figs. 62(c) and (d)) to the diagrams in Fig. 64. In this extended picture, the initial  $\Upsilon(5S)$  transitions into a pair of  $B^{(*)}$  and  $\bar{B}^{(*)}$  mesons accompanied by the emission of a single pion. Owing to the continuous energy distribution of the emitted pion, the  $B^{(*)}$  and  $\bar{B}^{(*)}$  mesons, when produced with low relative momentum, can interact with each other and subsequently transition into  $\Upsilon(nS)\pi$  via the exchange of an appropriate  $B^{(*)}$  meson. This specific mechanism in  $\Upsilon(5S)$  dipion decays was termed the ISPE mechanism by the authors of Ref. [81]. To some extent, the role of the pion in the ISPE mechanism within  $\Upsilon$  decays is analogous to that of the photon in the well-known Initial State Radiation (ISR) mechanism in  $e^+e^-$  collisions, which has enabled a series of observations of charmonium-like  $XYZ$  states in recent years.

Using the effective Lagrangian approach [578, 579, 187], the general expressions for the hadron-level amplitudes

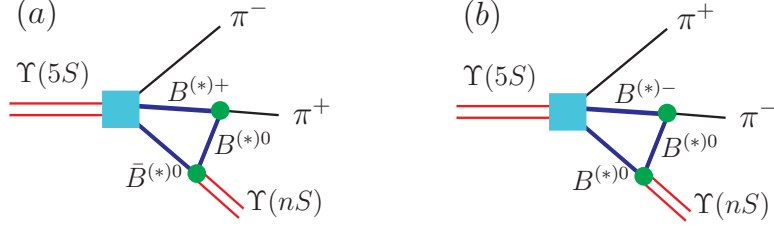


Figure 64: The schematic diagrams for  $\Upsilon(5S) \rightarrow \Upsilon(nS)\pi^+\pi^-$  by the ISPE mechanism. Here, diagrams (a) and (b) are related to each other by particle antiparticle conjugation, i.e.,  $B^{(*)} \rightleftharpoons \bar{B}^{(*)}$  and  $\pi^+ \rightleftharpoons \pi^-$ . After performing the transformations  $B^{(*)+} \rightleftharpoons B^{(*)0}$ ,  $B^{(*)-} \rightleftharpoons \bar{B}^{(*)0}$  and  $\pi^+ \rightleftharpoons \pi^-$ , we obtain the remaining diagrams. By replacing  $\Upsilon(nS)$  with  $h_b(mP)$ , one obtains the diagrams for  $\Upsilon(5S) \rightarrow h_b(mP)\pi^+\pi^-$ .  
*Source:* Taken from [81].

corresponding to Figs. 64(a) and (b) are given by

$$\begin{aligned}
& \mathcal{M}\{\Upsilon(5S) \rightarrow \pi^- + [B^{(*)+}\bar{B}^{(*)0} \rightarrow \Upsilon(nS)\pi^+]_{B^{(*)0}}\} \\
&= \prod_i g_i \int \frac{d^4q}{(2\pi)^4} \frac{[p_1, p_2, p_3, q]_{\mu\nu} \epsilon_{\Upsilon(5S)}^\mu \epsilon_{\Upsilon(nS)}^\nu}{[(p_2 + q)^2 - m_{B^{(*)}}^2][(p_1 - q)^2 - m_{B^{(*)}}^2]} \frac{1}{q^2 - m_{B^{(*)}}^2} \mathcal{F}^2(q^2, m_{B^{(*)}}^2), \\
& \mathcal{M}\{\Upsilon(5S) \rightarrow \pi^+ + [B^{(*)-}B^{(*)0} \rightarrow \Upsilon(nS)\pi^-]_{B^{(*)0}}\} \\
&= \prod_i g_i \int \frac{d^4q}{(2\pi)^4} \frac{[p_1, p_2, p_3, q]_{\mu\nu} \epsilon_{\Upsilon(5S)}^\mu \epsilon_{\Upsilon(nS)}^\nu}{[(p_3 + q)^2 - m_{B^{(*)}}^2][(p_1 - q)^2 - m_{B^{(*)}}^2]} \frac{1}{q^2 - m_{B^{(*)}}^2} \mathcal{F}^2(q^2, m_{B^{(*)}}^2), \quad (58)
\end{aligned}$$

where  $[p_1, p_2, p_3, q]_{\mu\nu}$  denotes the Lorentz structures constructed by four-momenta  $p_1$ ,  $p_2$ ,  $p_3$  and  $q$ . In the above amplitude, a form factor is introduced to depict the internal structure of the involved bottom mesons and make the loop integral finite in the ultraviolet region, the concrete form of the form factor is,

$$\mathcal{F}(q^2, m_{B^{(*)}}^2) = \frac{\Lambda^2 - m_{B^{(*)}}^2}{\Lambda^2 - q^2}, \quad (59)$$

where  $\Lambda = m_{B^{(*)}} + \alpha\Lambda_{\text{QCD}}$  with  $\Lambda_{\text{QCD}} = 220$  MeV.  $\alpha$  is a model parameter, which should be of order unity [188].

The estimations in Ref. [81] found that lineshapes of  $d\Gamma(\Upsilon(5S) \rightarrow \Upsilon(nS)\pi^+\pi^-)/dm_{\Upsilon(nS)\pi^+}$  generated by the ISPE mechanism are almost independent on the model parameter  $\alpha$  introduced by the form factor in the amplitudes. From the estimated lineshapes with different intermediate states, one can obtain,

- For the  $\Upsilon(5S) \rightarrow \Upsilon(nS)\pi^+\pi^-$  ( $n = 1, 2, 3$ ) processes, just shown in the first and the second columns of Fig. 65, combined with the corresponding reflections, the sharp peaks around  $B\bar{B}^*$  and  $B^*\bar{B}$  thresholds appear in the  $m_{\Upsilon(1S)\pi^+}$  and  $m_{\Upsilon(2S)\pi^+}$  distributions of  $d\Gamma(\Upsilon(5S) \rightarrow \Upsilon(1S)\pi^+\pi^-)/dm_{\Upsilon(1S)\pi^+}$  and  $d\Gamma(\Upsilon(5S) \rightarrow \Upsilon(2S)\pi^+\pi^-)/dm_{\Upsilon(2S)\pi^+}$ . The comparison of these results with the Belle data [80] indicates that we indeed can mimic the peak structures similar to the  $Z_b(10610)$  and  $Z_b(10650)$  reported by Belle if introducing the ISPE mechanism. The theoretical result of the  $\Upsilon(5S) \rightarrow \Upsilon(3S)\pi^+\pi^-$  decay further indicates that there also exists a peak around 10610 MeV, which combines with its reflection in the  $m_{\Upsilon(3S)\pi^+}$  distribution to form a broad structure. In addition, a structure at  $\sim 10650$  MeV and its reflection are reproduced. These results qualitatively and naturally explain why there are three structures appearing in the  $\Upsilon(3S)\pi^+$  invariant mass spectrum just announced by Belle [80].
- For the  $\Upsilon(5S) \rightarrow h_b(mP)\pi^+\pi^-$  ( $m = 1, 2$ ) processes, the ISPE mechanism has also extend to study the  $\Upsilon(5S) \rightarrow h_b(mP)\pi^+\pi^-$  ( $m = 1, 2$ ) decays. Similar to the situation of  $\Upsilon(5S) \rightarrow \Upsilon(1S, 2S)\pi^+\pi^-$ , one can find two structures around 10610 MeV and 10650 MeV and their reflections in the theoretical line shape of  $d\Upsilon(5S) \rightarrow h_b(mP)\pi^+\pi^-/dm_{h_b(mP)\pi^+}$  as shown in Fig. 66. These structures are well consistent with the centers of peaks reported by the Belle Collaboration [80].
- In addition, the Belle data also give a very intriguing phenomenon, i.e., there does not exist the structure near the  $B\bar{B}$  threshold. The ISPE mechanism can provide a direct explanation to it. If only considering the  $B\bar{B}$

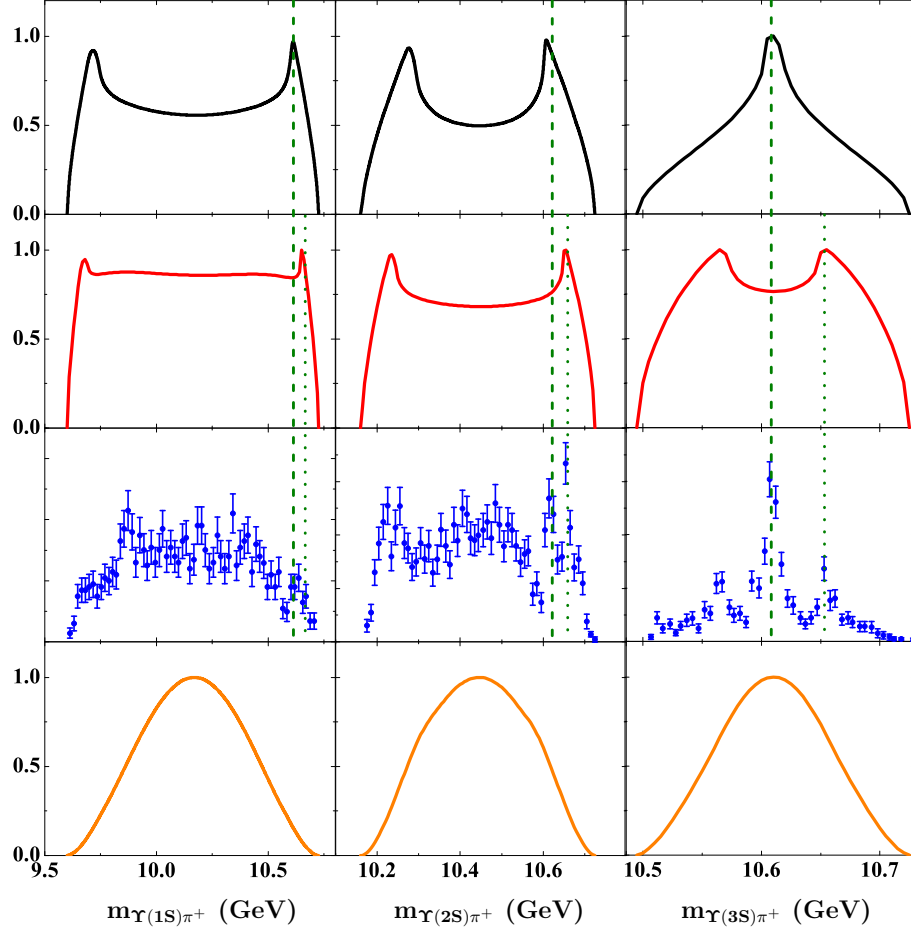


Figure 65: The obtained theoretical line shapes of  $d\Gamma(\Upsilon(5S) \rightarrow \Upsilon(nS)\pi^+\pi^-)/dm_{\Upsilon(nS)\pi^+}$ , and the comparison of our result with the Belle data (the third column) [80]. The first, the second and the fourth columns correspond to the numerical result considering  $B\bar{B}^* + h.c.$ ,  $B^*\bar{B}^*$  and  $B\bar{B}$  intermediate state contributions respectively, while the first, the second and the third rows are the results corresponding to the distributions of the  $\Upsilon(1S)\pi^+$ ,  $\Upsilon(2S)\pi^+$  and  $\Upsilon(3S)\pi^+$  invariant mass spectra. We use the vertical dashed and dotted lines to mark the masses of  $Z_b(10610)$  and  $Z_b(10650)$ , respectively. Here, the maximum of the theoretical line shape is normalized to 1.

Source: Taken from [81]

contribution in Fig. 64, the calculation shows that there are no peak structure close to the  $B\bar{B}$  threshold in the  $\Upsilon(nS)\pi^+$  and  $h_b(mP)\pi^+$  invariant mass spectra. Alternately, the smooth line shapes similar to phase space of corresponding decay processes appear in the invariant mass spectra of  $\Upsilon(nS)\pi^+$  and  $h_b(mP)\pi^+$ .

Besides the  $\Upsilon(5S)$  hidden-bottom dipion decays, the ISPE mechanism has also applied to investigate the hidden-bottom dipion decays of  $\Upsilon(11020)$  [615], where clear peak structures near  $B^*\bar{B}$  and  $B^*\bar{B}^*$  thresholds are predicted in the  $\Upsilon(nS)\pi^+$  ( $n = 1, 2, 3$ ) and  $h_b(mP)\pi^+$  ( $m = 1, 2$ ) invariant mass distributions. In addition to the hidden-bottom decay process, in the open bottom pion decays of  $\Upsilon(5S)$ , the lineshapes of  $B^*\bar{B}$  and  $B^*\bar{B}^*$  invariant mass distributions estimated by ISPE mechanism also emerge peak structures in the vicinity of  $B^*\bar{B}$  and  $B^*\bar{B}^*$  thresholds, which well correspond to  $Z_b(10610)$  and  $Z_b(10610)$  observed by the Belle Collaboration [616].

### 5.2.2. Prediction of charmonium-like charged $Z_c$ structure

Considering the ISPE mechanism is a universal mechanism existing in heavy quarkonium decay, one can naturally extend such physical picture to study hidden-charm decays of higher vector charmonia due to the similarity between charmonium and bottomonium families, and predict some novel phenomena similar to the  $Z_b$  structures. In Ref. [82], the dipion decays of the charmonia  $\psi(4040)$ ,  $\psi(4160)$  and  $\psi(4415)$  and the charmonium-like state  $Y(4260)$  have been

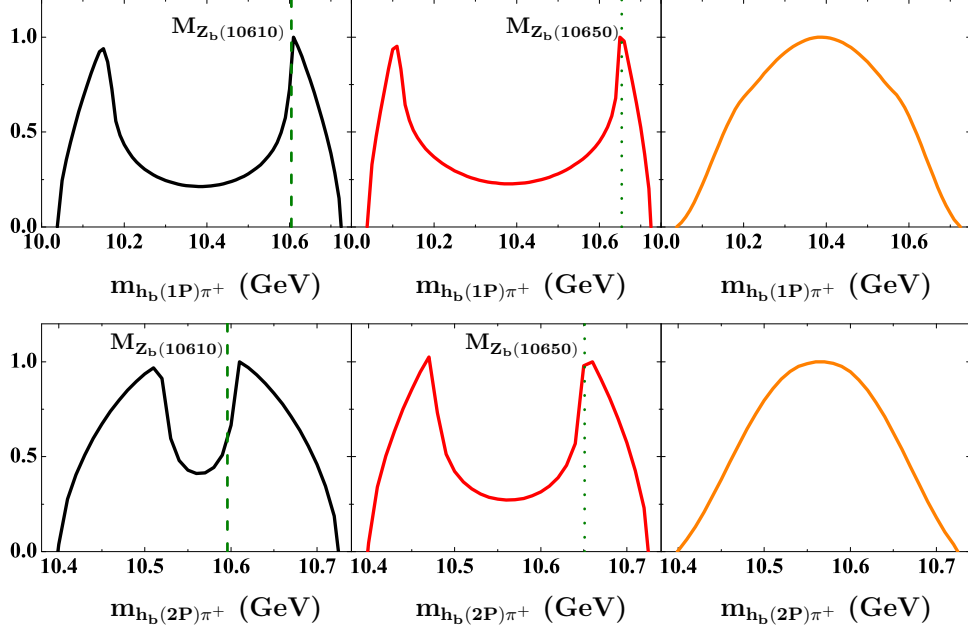


Figure 66: The theoretical curves of  $d\Gamma(Y(5S) \rightarrow h_b(1P)\pi^+\pi^-)/dm_{h_b(1P)\pi^+}$  (the first column) and  $d\Gamma(Y(5S) \rightarrow h_b(2P)\pi^+\pi^-)/dm_{h_b(2P)\pi^+}$  (the second column). For easily comparing our result with the experimental data, one adopts the vertical dashed and dotted lines to denote the masses of  $Z_b(10610)$  and  $Z_b(10650)$  respectively. The first, the second and the third rows correspond to the numerical result respectively considering  $B\bar{B}^* + h.c.$ ,  $B^*\bar{B}^*$  and  $B\bar{B}$  intermediate state contributions in Fig. 64. Here, the maximum of the theoretical line shape is normalized to 1.   
Source: Taken from [81]

investigated by ISPE mechanism. In Fig. 67, the results of  $d\Gamma/dm_{J/\psi\pi^+}$ ,  $d\Gamma/dm_{\psi(3686)\pi^+}$  and  $d\Gamma/dm_{h_c(1P)\pi^+}$  of  $\psi(4040)$ ,  $\psi(4160)$ ,  $\psi(4415)$ ,  $Y(4260)$  decays into  $J/\psi\pi^+\pi^-$ ,  $\psi(3686)\pi^+\pi^-$ ,  $h_c(1P)\pi^+\pi^-$  are presented, from the lineshapes, one can find the following intriguing properties.

- For the dipion decays of  $\psi(4040)$ , there exist sharp peak structures close to the  $D^*\bar{D}$  threshold and the corresponding reflections in the distributions of  $d\Gamma/dm_{J/\psi\pi^+}$ ,  $d\Gamma/dm_{\psi(3686)\pi^+}$  and  $d\Gamma/dm_{h_c(1P)\pi^+}$  of  $\psi(4040) \rightarrow J/\psi\pi^+\pi^-$ ,  $\psi(4040) \rightarrow \psi(3686)\pi^+\pi^-$  and  $\psi(4040) \rightarrow h_c(1P)\pi^+\pi^-$  decays. While this structure appearing in  $d\Gamma(\psi(4040) \rightarrow J/\psi\pi^+\pi^-)/dm_{J/\psi\pi^+}$  is not obvious comparing with the structure in the  $\psi(3686)\pi^+$  and  $h_c(1P)\pi^+$  invariant mass spectra in the processes  $\psi(4040) \rightarrow \psi(3686)\pi^+\pi^-$  and  $\psi(4040) \rightarrow h_c(1P)\pi^+\pi^-$ , respectively.
- For the dipion decay of  $\psi(4160)$ , two sharp peaks appear in the distributions of  $d\Gamma(\psi(4160) \rightarrow J/\psi\pi^+\pi^-)/dm_{J/\psi\pi^+}$  and  $d\Gamma(\psi(4160) \rightarrow h_c(1P)\pi^+\pi^-)/dm_{h_c(1P)\pi^+}$ , which are close to the  $D^*\bar{D}$  threshold. The structure in the  $J/\psi\pi^+$  invariant mass spectrum is more narrow than that in the  $h_c(1P)\pi^+$  invariant mass spectrum.
- In the hidden-charm dipion decays of  $\psi(4415)$ , we find two sharp peak structures around the  $D^*\bar{D}$  and  $D^*\bar{D}^*$  thresholds appearing in the  $J/\psi\pi^+$  invariant mass spectra. In addition, a sharp peak close to the  $D^*\bar{D}^*$  threshold is observed in the  $h_c(1P)\pi^+$  invariant mass spectrum distribution. In the  $d\Gamma(\psi(4415) \rightarrow \psi(3686)\pi^+\pi^-)/dm_{\psi(3686)\pi^+}$  distribution, a peak near  $D^*\bar{D}^*$  with its reflection forms a broad structure. Under the ISPE mechanism, the intermediate  $D^*\bar{D}$  can result in a very broad structure in the  $h_c(1P)\pi^+$  invariant mass spectrum distribution.
- In the hidden-charm dipion decays of  $Y(4260)$ , there exist the sharp peaks close to the  $D^*\bar{D}$  threshold in the  $d\Gamma(\psi(4260) \rightarrow J/\psi\pi^+\pi^-)/dm_{J/\psi\pi^+}$  and  $d\Gamma(\psi(4260) \rightarrow h_c(1P)\pi^+\pi^-)/dm_{h_c(1P)\pi^+}$  distributions. In the distributions of  $d\Gamma(\psi(4260) \rightarrow \psi(3686)\pi^+\pi^-)/dm_{\psi(3686)\pi^+}$  and  $d\Gamma(\psi(4260) \rightarrow h_c(1P)\pi^+\pi^-)/dm_{h_c(1P)\pi^+}$ , the ISPE mechanism also leads to the structures around the  $D^*\bar{D}^*$  threshold. As for  $Y(4260) \rightarrow h_c(1P)\pi^+\pi^-$  process, the peak close to the  $D^*\bar{D}$  threshold and its reflection overlap with each other to form a broad structure in the  $h_c(1P)\pi^+$  invariant mass spectrum.

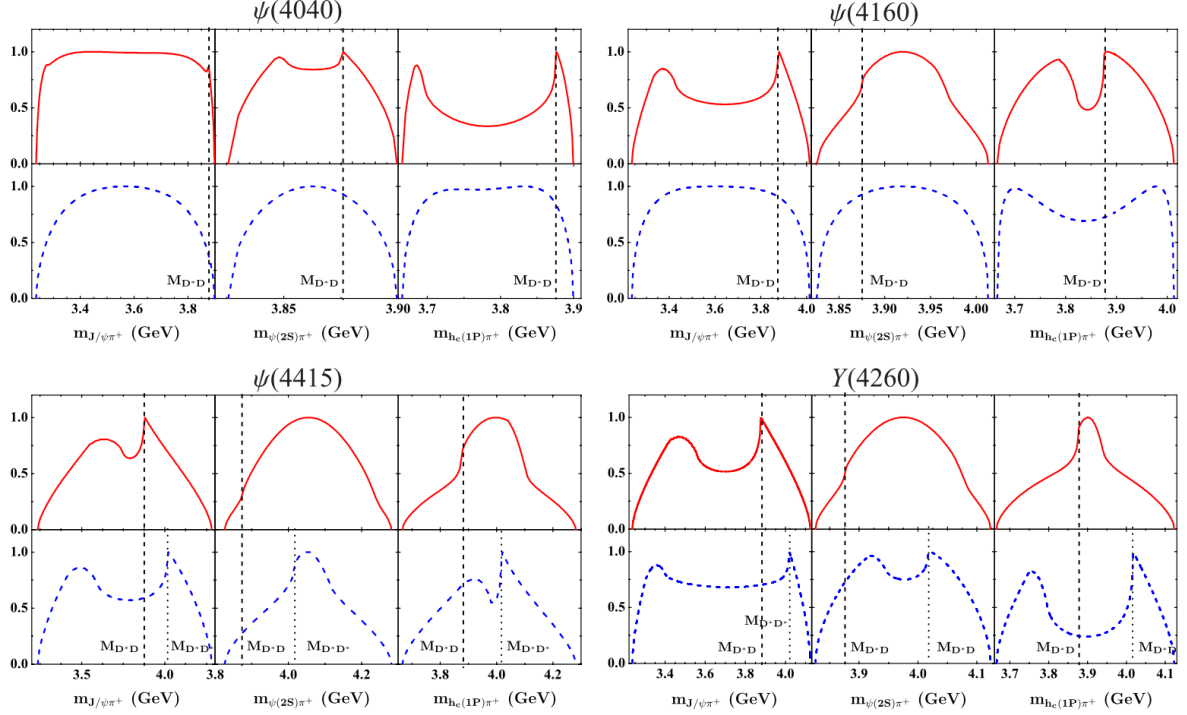


Figure 67: (Color online.) The invariant mass spectra of  $J/\psi\pi^+$ ,  $\psi(3686)\pi^+$  and  $h_c(1P)\pi^+$  for the  $\psi(4040)$ ,  $\psi(4160)$ ,  $\psi(4415)$  and  $Y(4260)$  decays into  $J/\psi\pi^+\pi^-$ ,  $\psi(3686)\pi^+\pi^-$  and  $h_c(1P)\pi^+\pi^-$ . Here, the solid, dashed correspond to the results considering intermediate  $D\bar{D}^* + h.c.$  and  $D^*\bar{D}^*$  respectively. The vertical dashed lines and the dotted lines denote the threshold of  $D^*\bar{D}$  and  $D^*\bar{D}^*$  respectively. Here, the maximum of the line shape is normalized to 1.

Source: Taken from [82]

In 2011, the CLEO-c Collaboration announced the preliminary measurements of the  $h_c(1P)\pi^\pm$  mass distribution from  $e^+e^- \rightarrow h_c(1P)\pi^+\pi^-$  at  $E_{CM} = 4170$  MeV (the points with errors in Fig. 4 (b) of Ref. [617]). In Ref. [82], Chen and Liu compared the predicted  $h_c\pi^\pm$  mass distribution of  $\psi(4160) \rightarrow h_c(1P)\pi^+\pi^-$  (see Fig. 67) with the CLEO-c data. They noticed that the predicted theoretical line shape of the  $h_c(1P)\pi^\pm$  mass distribution of  $\psi(4160) \rightarrow h_c(1P)\pi^+\pi^-$  is consistent with the data measured by CLEO-c, which is listed in Fig. 68, where there indeed exist a broad structure around  $D\bar{D}^*$  threshold and its reflection. To some extent, this fact provides a direct test to ISPE prediction in Ref. [82].

In Ref. [379], the Belle Collaboration measured the cross sections for  $e^+e^- \rightarrow \pi^+\pi^-J/\psi$  via initial state radiation, the  $\pi^+\pi^-$  invariant mass distributions were reported. At the conference "Hadron Structure and Interactions in 2011", Yuan reported peak structures at  $12 \text{ GeV}^2$  and  $15 \text{ GeV}^2$  in the  $\pi^\pm J/\psi$  invariant mass squared ( $M_{\pi^\pm J/\psi}^2$ ) distribution from Belle data [618]; these could be evidence of the enhancement predicted by the ISPE mechanism [82].

In addition to the dipion decays of  $Y(4260)$ , Chen *et al.* also investigated the hidden-charm dipion decays of the charmonium-like state  $Y(4360)$  by the ISPE mechanism in Ref. [619]. The estimations shows that there also exist charge charmonium-like structure near  $D\bar{D}^*$  and  $D^*\bar{D}^*$  threshold in the  $J/\psi\pi^+$ ,  $\psi(3686)\pi^+$  and  $h_c(1P)\pi^+$  invariant mass spectra of the corresponding hidden-charm dipion decays processes. Using the ISPE mechanism, the authors in Refs. [82, 619] not only predicted existences of the charmonium-like structures near the  $D^*\bar{D}^*$  thresholds but also provided specific schemes for observing these structures experimentally, such as the hidden-charm dipion decays processes,  $Y(4260) \rightarrow J/\psi\pi^+\pi^-$ ,  $Y(4260) \rightarrow \psi(3686)\pi^+\pi^-$ , and  $Y(4260) \rightarrow h_c\pi^+\pi^-$ .

### 5.2.3. Experimental observations of the $Z_c$ structures

In 2013, the BESIII Collaboration studied the process  $e^+e^- \rightarrow \pi^+\pi^-J/\psi$  at a center-of-mass energy of 4.260 GeV using a data sample of  $525 \text{ pb}^{-1}$  collected with the BESIII detector. The cross section was measured to be  $62.9 \pm 1.9 \pm 3.7 \text{ pb}$ , which is in good agreement with previous measurements from the BaBar [620], Belle [379], and

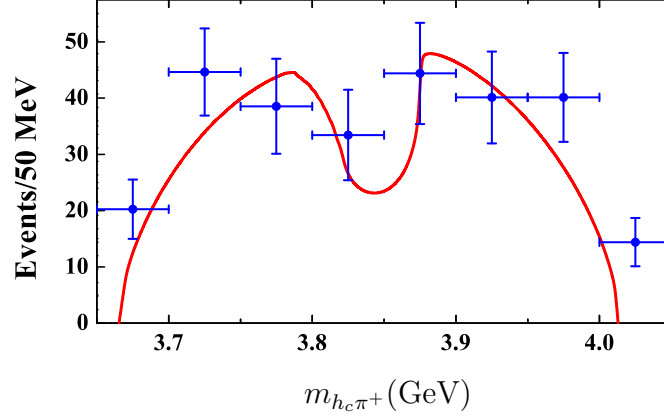


Figure 68: (Color online.) A comparison of the  $h_c \pi^\pm$  mass distribution of  $\psi(4160) \rightarrow h_c(1P)\pi^+\pi^-$  (solid line) predicted in this work and measurement by CLEO-c (points with errors) [617]. Here, CLEO-c measured the  $h_c(1P)\pi^\pm$  mass distribution from  $e^+e^- \rightarrow h_c(1P)\pi^+\pi^-$  at  $E_{CM} = 4170$  MeV [617]. We normalize our numbers for a real comparison with the available CLEO-c data.  
Source: Taken from [82]

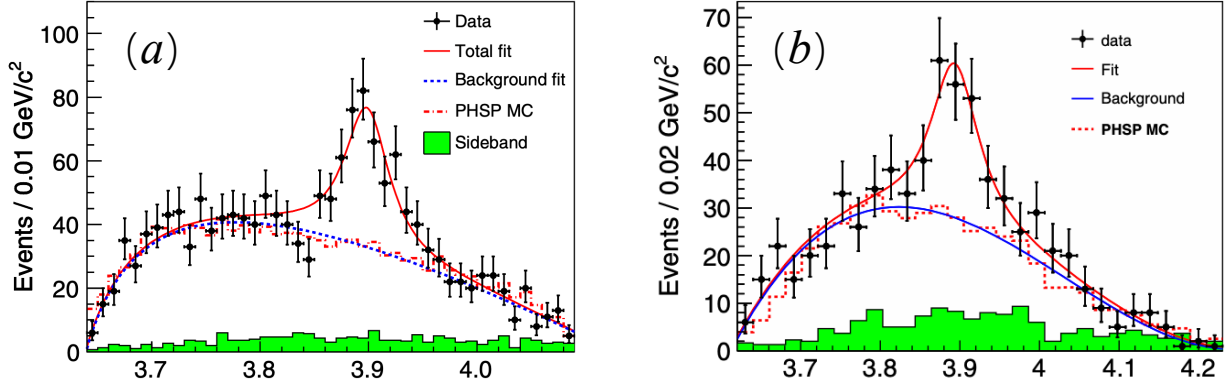


Figure 69: Fit to the  $M_{\max}(\pi^\pm J/\psi)$  distributions of  $e^+e^- \rightarrow \pi^+\pi^- J/\psi$  at  $\sqrt{s} = 4.26$  GeV from the BESIII (diagram (a)) [550] and Belle (diagram (b)) [551] Collaborations. Dots with error bars are experimental data from BESIII and Belle Collaborations [550, 551], the red solid curves show the total fit, and the blue dotted curves show the results of a phase space Mento Carlo simulation and the green shaded histogram shows the normalized  $J/\psi$  sideband events.  
Source: Taken from [550, 551].

CLEO [399] collaborations. In addition, a new structure at around 3.9 GeV in the  $\pi^\pm J/\psi$  mass spectrum, subsequently named  $Z_c(3900)$ , was observed, as shown in Fig. 69 (a). The signal shape was parameterized using an  $S$ -wave Breit-Wigner function. Neglecting interference between the Breit-Wigner signal and the background, the mass and width were reported to be [550]

$$M = (3899.0 \pm 3.6 \pm 4.9) \text{ MeV}, \quad \Gamma = 46 \pm 10 \pm 20 \text{ MeV}.$$

At nearly the same time, the Belle Collaboration reported cross section measurements for  $e^+e^- \rightarrow \pi^+\pi^- J/\psi$  between 3.8 GeV and 5.5 GeV, using a  $967 \text{ fb}^{-1}$  data sample collected by the Belle detector at or near the  $\Upsilon(nS)$  (with  $n = 1$  to 5) resonances via the ISR technique [551]. A structure in the  $\pi^\pm J/\psi$  mass spectrum was observed with a significance of  $5.2\sigma$ , as shown in Fig. 69(b). The resonance parameters were determined to be [551]

$$M = (3894.5 \pm 6.6 \pm 4.5) \text{ MeV}, \quad \Gamma = (63 \pm 24 \pm 26) \text{ MeV}.$$

Subsequently, former members of the CLEO-c collaboration, Xiao *et al.*, reanalyzed data collected by the CLEO-c detector at the  $\psi(4160)$  resonance and observed the charged  $Z_c(3900)$  structure [555], consistent with the findings of

the BESIII [550] and Belle [551] collaborations. In addition, evidence for the neutral  $Z_c(3900)$  was first reported at a significance of  $3\sigma$  [555], and was later firmly established by the BESIII Collaboration in the process  $e^+e^- \rightarrow \pi^0\pi^0 J/\psi$  with a significance of  $10.4\sigma$  [557]. A partial wave analysis of the processes  $e^+e^- \rightarrow \pi^+\pi^- J/\psi$  and  $\pi^0\pi^0 J/\psi$  determined the spin and parity of the  $Z_c(3900)$  to be  $J^P = 1^+$  [558, 385]. In addition to hidden-charm decays, the BESIII Collaboration also reported a near-threshold structure in the  $D\bar{D}^*$  system, denoted  $Z_c(3885)$ , observed in the processes  $e^+e^- \rightarrow (D\bar{D}^*)^\pm\pi^\mp$  [556] and  $e^+e^- \rightarrow (D\bar{D}^*)^0\pi^0$  [559].

Furthermore, in the  $\pi^\pm h_c$  invariant mass distributions of the processes  $e^+e^- \rightarrow \pi^\pm h_c$ , the BESIII Collaboration reported another charged charmonium-like structure,  $Z_c(4020)$ , with masses of  $4022.9 \pm 0.8 \pm 2.7$  MeV and  $4023.0 \pm 2.2 \pm 3.8$  MeV for the charged and neutral states, respectively [514, 560]. In the open-charm sector, a near-threshold structure in the  $D^*\bar{D}^*$  system, referred to as  $Z_c(4025)$ , was observed in the  $(D^*\bar{D}^*)^\pm$  and  $(D^*\bar{D}^*)^0$  invariant mass spectra of the processes  $e^+e^- \rightarrow (D^*\bar{D}^*)^\pm\pi^\mp$  [552] and  $e^+e^- \rightarrow (D^*\bar{D}^*)^0\pi^0$  [553]. Beyond these channels, the BESIII Collaboration has also searched for charmonium-like structures in the processes  $e^+e^- \rightarrow \pi^+\pi^-\psi(3686)$  [380],  $e^+e^- \rightarrow \pi^0\pi^0\psi(3686)$  [554], and  $e^+e^- \rightarrow \pi^+\pi^-\psi(3770)$  [482].

In addition to studies in  $e^+e^-$  annihilation, the charmonium-like structures  $Z_c(3900)$  and  $Z_c(4020)$  have also been searched for in  $B$  meson decays. For example, the Belle Collaboration searched for  $Z_c(3900)$  in the decay  $\bar{B}^0 \rightarrow J/\psi K^-\pi^+$  and found no significant signal [621]. Using  $p\bar{p}$  collision data collected by the DØ experiment at the Fermilab Tevatron collider, the DØ Collaboration reported evidence for  $Z_c(3900)^\pm$  decaying to  $J/\psi\pi^\pm$  in semi-inclusive weak decays of  $b$ -flavored hadrons [622].

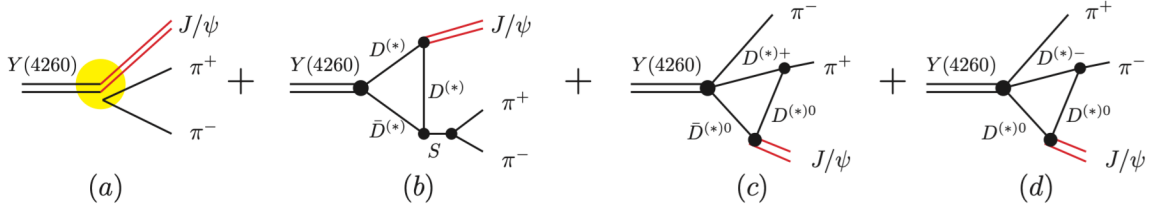


Figure 70: The typical diagrams depicting  $Y(4260) \rightarrow J/\psi\pi^+\pi^-$  decay. Here, diagram (a) denotes  $Y(4260)$  direct decay into  $J/\psi\pi^+\pi^-$ , diagram (b) describes the intermediate hadronic loop contribution to  $Y(4260) \rightarrow J/\psi\pi^+\pi^-$ , and diagrams (c) and (d) are from the ISPE mechanism.

Source: Taken from [623]

#### 5.2.4. Reproduce $Z_c(3900)$ in the $\pi^\pm J/\psi$ invariant mass spectra of $e^+e^- \rightarrow \pi^+\pi^- J/\psi$ at $\sqrt{s} = 4.260$ GeV

The observations of  $Z_c$  structures in the hidden-charm decay processes suggested by the ISPE mechanism provide important evidence in support of the ISPE mechanism. With abundant experimental information on the distributions of the  $J/\psi\pi^\pm$  and  $\pi^+\pi^-$  invariant mass spectra in  $Y(4260) \rightarrow \pi^+\pi^- J/\psi$  [550, 551, 555], the authors of Refs. [82, 619] conducted further in-depth studies of these processes using the ISPE mechanism to gain a deeper understanding of these charmonium-like structures.

Following the observations of  $Z_c(3900)$  in the  $\pi^+ J/\psi$  invariant mass distributions of the process  $e^+e^- \rightarrow \pi^+\pi^- J/\psi$  at  $\sqrt{s} = 4.260$  GeV by the BESIII and Belle collaborations [550, 551], Chen, Liu, and Matsuki considered contributions from the direct decay of  $Y(4260)$ , the dipion scalar resonance contributions, and the ISPE contributions, as illustrated in Fig. 70 of Ref. [623]. The corresponding amplitudes are expressed as,

$$\begin{aligned}
\mathcal{M}_{\text{Direct}} &= \frac{F}{f_\pi^2} \epsilon_{Y(4260)} \cdot \epsilon_{J/\psi} \left\{ \left[ q^2 - \kappa(\Delta M)^2 \left( 1 + \frac{2m_\pi^2}{q^2} \right) \right]_{\text{S-wave}} + \left[ \frac{3}{2} \kappa((\Delta M)^2 - q^2) \left( 1 - \frac{4m_\pi^2}{q^2} \right) \left( \cos^2 \theta - \frac{1}{3} \right) \right]_{\text{D-wave}} \right\} \\
\mathcal{M}_{\text{S}} &= \epsilon_{Y(4260)}^\mu \epsilon_{J/\psi}^\nu g_{\mu\nu} \frac{F_S}{(p_1 + p_2)^2 - m_S^2 + im_S \Gamma_S}, \\
\mathcal{M}_{\text{ISPE}}^{D\bar{D}} &= g_{Y(4260)D\bar{D}} \epsilon_{Y(4260)}^\mu \epsilon_{J/\psi}^\nu [A_0 g_{\mu\nu} + (A_1 p_{1\mu} p_{1\nu} + A_2 p_{1\mu} p_{2\nu} + A_3 p_{2\mu} p_{1\nu} + A_4 p_{2\mu} p_{2\nu})], \\
\mathcal{M}_{\text{ISPE}}^{D\bar{D}^*} &= g_{Y(4260)D^*\bar{D}^*} \epsilon_{Y(4260)}^\mu \epsilon_{J/\psi}^\nu [B_0 g_{\mu\nu} + (B_1 p_{1\mu} p_{1\nu} + B_2 p_{1\mu} p_{2\nu} + B_3 p_{2\mu} p_{1\nu} + B_4 p_{2\mu} p_{2\nu})], \\
\mathcal{M}_{\text{ISPE}}^{D^*\bar{D}^*} &= g_{Y(4260)D^*\bar{D}^*} \epsilon_{Y(4260)}^\mu \epsilon_{J/\psi}^\nu [C_0 g_{\mu\nu} + (C_1 p_{1\mu} p_{1\nu} + C_2 p_{1\mu} p_{2\nu} + C_3 p_{2\mu} p_{1\nu} + C_4 p_{2\mu} p_{2\nu})], \tag{60}
\end{aligned}$$

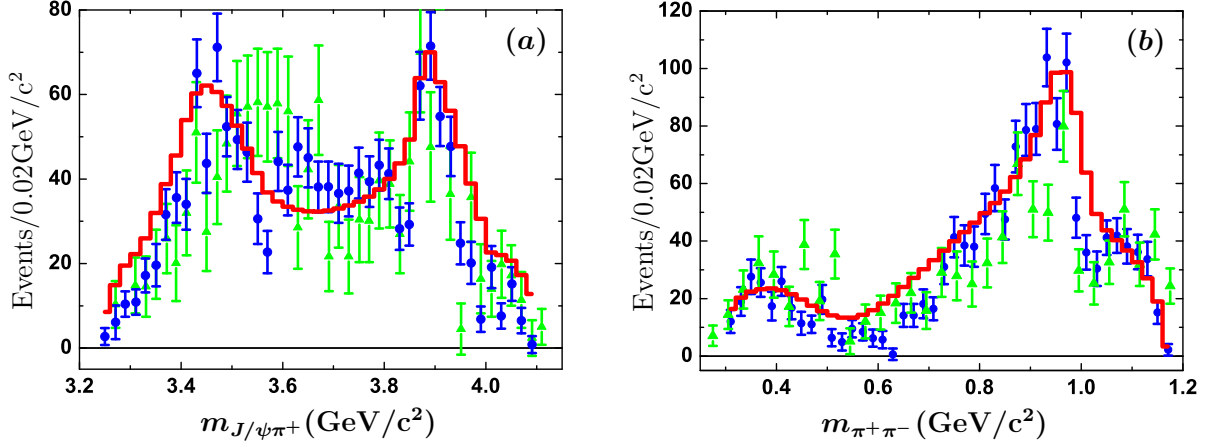


Figure 71: (color online). The distributions of the  $J/\psi\pi^+$  and  $\pi^+\pi^-$  invariant mass spectra of  $Y(4260) \rightarrow \pi^+\pi^- J/\psi$ . The blue and green dots with error bars are the experimental data given by BESIII [550] and Belle [551], respectively. The red histograms are our results considering contributions of the ISPE mechanism to the  $Y(4260) \rightarrow \pi^+\pi^- J/\psi$  decay. *Source*: Taken from [623]

where the coefficients  $A_i$ ,  $B_i$ , and  $C_i$  (with  $i = 0$  to 4) associated with the various Lorentz structures are evaluated from the loop integrals in the ISPE mechanism (see Ref. [82] for further details). In this framework, the total decay amplitude for  $Y(4260) \rightarrow \pi^+\pi^- J/\psi$  is given by the sum of these sub-amplitudes, i.e.,

$$\mathcal{M}^{\text{Total}}[Y(4260) \rightarrow \pi^+\pi^- J/\psi] = \mathcal{M}_{\text{Direct}} + e^{i\phi_\sigma} \mathcal{M}_\sigma + e^{i\phi_{f_0(980)}} \mathcal{M}_{f_0(980)} + e^{i\phi_{\text{ISPE}}} \left( \mathcal{M}_{\text{ISPE}}^{D\bar{D}} + \mathcal{M}_{\text{ISPE}}^{D\bar{D}^*} + \mathcal{M}_{\text{ISPE}}^{D^*\bar{D}^*} \right), \quad (61)$$

where three phase angles  $\phi_\sigma$ ,  $\phi_{f_0(980)}$ , and  $\phi_{\text{ISPE}}$  are introduced. With the amplitude given above, the differential decay width for  $Y(4260) \rightarrow \pi^+\pi^- J/\psi$  is expressed as

$$d\Gamma(Y(4260) \rightarrow \pi^+\pi^- J/\psi) = \frac{1}{3} \frac{1}{(2\pi)^3} \frac{1}{32m_{Y(4260)}^3} |\mathcal{M}^{\text{Total}}|^2 dm_{J/\psi\pi^\pm}^2 dm_{\pi^+\pi^-}^2, \quad (62)$$

where  $m_{J/\psi\pi^\pm}^2 = (p_2 + p_3)^2$  and  $m_{\pi^+\pi^-}^2 = (p_1 + p_2)^2$ . Using the above differential decay width, the theoretical distributions for the  $J/\psi\pi^\pm$  and  $\pi^+\pi^-$  invariant mass spectra can be obtained and subsequently applied in fitting to the BESIII and Belle data [550, 551].

In Fig. 71, the  $J/\psi\pi^+$  (left panel) and  $\pi^+\pi^-$  (right panel) invariant mass spectra for  $Y(4260) \rightarrow \pi^+\pi^- J/\psi$  are shown. The two red histograms represent the fit results to the BESIII data using the ISPE mechanism. For comparison, the data from the Belle Collaboration [551] are also included. From the figure, one can see that the present fit agrees well with the experimental data reported by both the BESIII and Belle Collaborations [550, 551]. In particular, two peaks—the  $Z_c(3900)$  structure and its reflection—are nicely reproduced, with the fitting results clearly reflecting that  $Z_c(3900)$  is much sharper than its reflection. In addition, the double-peak structures in the dipion invariant mass distributions are also well described.

As shown in Fig. 71, the  $Z_c(3900)$  structure is remarkably reproduced within the ISPE framework, which incorporates interference effects among different intermediate processes. This result affirmatively confirms that  $Z_c(3900)$  corresponds to the charged charmonium-like structure near the  $D\bar{D}^*$  threshold predicted via the ISPE mechanism in Ref. [82].

### 5.2.5. Reproduce the enhancement structures in the $\pi^\pm\psi(3686)$ invariant mass spectra of $e^+e^- \rightarrow \pi^+\pi^-\psi(3686)$

In Ref. [380], the BESIII Collaboration investigated the process  $e^+e^- \rightarrow \pi^+\pi^-\psi(3686)$  using a  $5.1 \text{ fb}^{-1}$  data sample collected with the BESIII detector at 16 center-of-mass energy points ranging from 4.008 to 4.600 GeV. The cross sections were measured with improved precision and found to be consistent with previous measurements from the Belle and BaBar collaborations. In addition, a charged charmonium-like structure was observed in the  $\pi^\pm\psi(3686)$

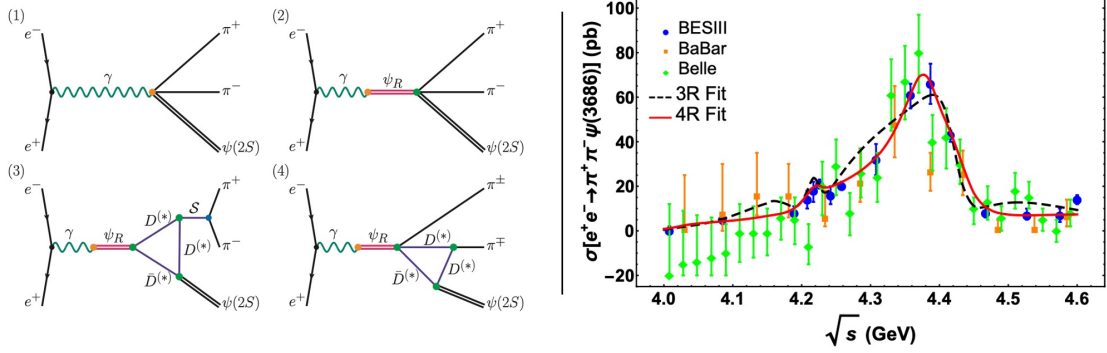


Figure 72: (color online). Feynman diagrams contributing to the process  $e^+e^- \rightarrow \pi^+\pi^-\psi(3686)$  (left panel) and the fitted cross sections for  $e^+e^- \rightarrow \pi^+\pi^-\psi(3686)$  given by the BESIII Collaboration in Ref. [380]. The data from the BaBar [52, 624] and Belle [53, 521] collaborations are also presented for comparison.

Source: Taken from [625]

invariant mass spectrum for the data at  $\sqrt{s} = 4.416$  GeV, with a significance of  $9.2\sigma$ . The resonance parameters of this structure were fitted to be [380],

$$M = (4032.1 \pm 2.4) \text{ MeV}, \quad \Gamma = (26.1 \pm 5.3) \text{ MeV}, \quad (63)$$

respectively. It should be mentioned that this process is also one of the processes suggested by the ISPE mechanism for searching charged charmonium-like structures, as proposed in Ref. [82].

Moreover, unlike the  $Z_c(3900)$  observed in  $e^+e^- \rightarrow \pi^+\pi^-J/\psi$  at  $\sqrt{s} = 4.260$  GeV, the BESIII Collaboration has reported on the dipion and  $\pi^+\psi(3686)$  invariant mass spectra in the process  $e^+e^- \rightarrow \pi^+\pi^-\psi(3686)$  at six different center-of-mass energies:  $\sqrt{s} = 4.226, 4.258, 4.358, 4.387, 4.416, 4.600$  GeV. The lineshapes of the  $\pi^+\psi(3686)$  distributions vary significantly across these energy points. Therefore, reproducing these invariant mass distributions within a unified ISPE mechanism would provide even stronger evidence in support of the ISPE mechanism.

In the left panel of Fig. 72, the Feynman diagrams contributing to the process  $e^+e^- \rightarrow \pi^+\pi^-\psi(3686)$  are presented. Fig. 72-(1) shows the non-resonance production process, where the virtual photon directly couples to  $\pi^+\pi^-\psi(3686)$ . Fig. 72-(2) depicts the direct production process, in which the dipion is produced directly via gluon emission. Fig. 72-(3) illustrates the dipion resonance production process, where the dipion is produced through a scalar meson, and Fig. 72-(4) represents the production process involving the ISPE mechanism. In the three-charmonium scenario,  $\psi(4160)$ ,  $\psi(4220)$ , and  $\psi(4415)$  were included in the fit. As shown in the right panel of Fig. 72, this three-charmonium fit accurately reproduces the structure in the vicinity of 4.2 GeV and the broad enhancement near 4.4 GeV. However, the fitted curve lies above the experimental data around 4.3 GeV, which indicates the need for an additional resonance contribution. In the 4R fit scenario, an additional resonance,  $\psi(4380)$ , was taken into consideration, and one finds that the cross sections can be better described than in the three-charmonium scenario.

In addition to the cross sections, the dipion and  $\pi^+\psi(3686)$  invariant mass distributions are also fitted simultaneously. As shown in Fig. 73, the clear peak structures in the  $\psi(3686)\pi^+$  invariant mass spectra at  $\sqrt{s} = 4.226, 4.258, 4.416$  GeV, as reported by the BESIII Collaboration [380], are well described by the ISPE mechanism. For the data at 4.600 GeV, however, the fitted curves obtained from both fit scenarios lie below the experimental data for the  $\pi^+\psi(3686)$  invariant mass distributions, suggesting possible contributions from a charmonium state around 4.6 GeV.

The predictions of charmonium-like structures near the  $D^*\bar{D}$  and  $D^*\bar{D}^*$  thresholds, along with subsequent successful descriptions of various processes related to  $Z_c(3900)$  and  $Z_c(4020)$  using the ISPE mechanism after their experimental observation, demonstrate that the ISPE mechanism is universal in heavy quarkonium decay processes. The ISPE mechanism is crucial for understanding the observed near-threshold structures.

Besides the ISPE mechanism, other theoretical interpretations of these charmonium-like structures have been proposed based on their proximity to the  $D^*\bar{D}^{(*)}$  thresholds and their isovector nature. These include compact tetraquark states composed of  $[cq][\bar{c}\bar{q}]$  [626, 627, 628, 629, 630, 631], bound states or resonance states resulting from  $D^*\bar{D}/D^*\bar{D}^*$  interactions [610, 632, 633, 634, 635, 636, 637, 638, 222, 639, 640, 641, 416, 642, 643, 644, 645, 646, 647, 648, 649,

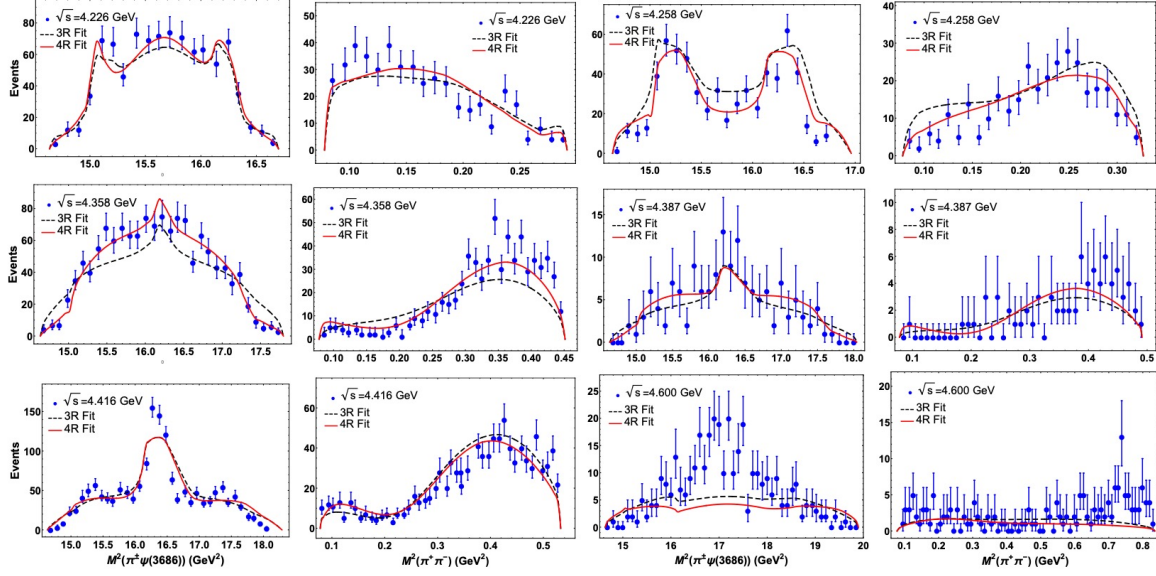


Figure 73: (color online). Combined fit for the  $\psi(3686)\pi^\pm$  and  $\pi^+\pi^-$  invariant mass spectra at different center-of-mass energies reported by the BESIII Collaboration in Ref. [380]. The black dashed and red solid curves are the fitted results under three-charmonium and four-charmonium scenarios, respectively.

Source: Taken from [625]

650, 651, 652], and kinematic effects [653, 654, 642, 655].

It is worth mentioning again that in the  $e^+e^- \rightarrow \pi^+\pi^-\psi(3686)$  process, the BESIII Collaboration reported the  $\psi(3686)\pi^\pm$  and  $\pi^+\pi^-$  invariant mass spectra at different center-of-mass energies. From Fig. 73, one can notice that the lineshapes at different center-of-mass energies are rather different. This distinct property of the lineshape poses a great challenge for the aforementioned tetraquark and molecular interpretations, which are generally expected to behave similarly across different channels and center-of-mass energies. Unlike a "genuine state," and as indicated in Fig. 67, the predicted lineshapes of the  $J/\psi\pi$  invariant mass distributions vary with the initial state energy, which is consistent with the experimental measurements from the BESIII Collaboration. The reproduction of experimental data at different center-of-mass energy points within a unified framework in Ref. [625] further proves the validity of the ISPE mechanism.

In addition, the nature of these charged charmonium-like structures has been comprehensively investigated using lattice QCD. In Refs. [656, 657], the authors searched for charged charmonium-like structure  $J$  with masses below 4.2 GeV in the channel  $I^G(J^{PC}) = 1^+(1^{+-})$  using lattice QCD, where the two-meson channels  $J/\psi\pi$ ,  $\psi(3686)\pi$ ,  $\psi(1D)\pi$ ,  $D\bar{D}^*$ ,  $D^*\bar{D}$ , and  $\eta_c\rho$  were included. The spectrum of eigenstates was extracted using a number of meson-meson and diquark-antidiquark interpolating fields, but no additional candidate for  $Z_c(3900)$  below 4.2 GeV was found with a pion mass of 266 MeV. The HAL QCD Collaboration studied  $Z_c(3900)$  using the method of coupled-channel scattering in lattice QCD, where the interactions among  $\pi J/\psi$ ,  $\rho\eta_c$ , and  $D\bar{D}^*$  channels were derived from (2+1)-flavor QCD simulations at  $m_\pi = 410 - 700$  MeV [658, 659]. Their analysis found that the interactions were dominated by the off-diagonal  $\pi J/\psi - \bar{D}D^*$  and  $\rho\eta_c - \bar{D}D^*$  couplings, suggesting that  $Z_c(3900)$  is not a genuine resonance but rather a threshold cusp. Similarly, using the coupled-channel Lüscher finite-size formalism, the CLQCD Collaboration investigated the charmonium-like structure  $Z_c(3900)$  within a two-channel scattering model [660]. Combined with the two-channel Ross-Shaw theory, the scattering parameters were extracted from the energy levels by solving a generalized eigenvalue problem. However, the scattering length parameters suggested that the best-fit parameters for the particular lattice setup do not correspond to a peak in the elastic scattering cross-section near the threshold.

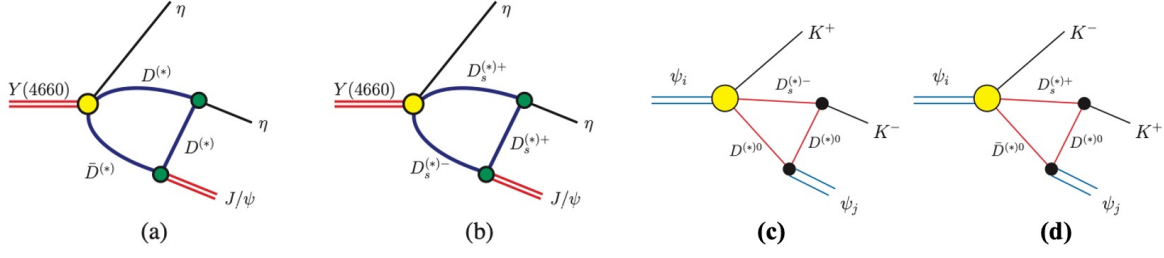


Figure 74: The di- $\eta$  (diagrams (a) and (b)) and di-kaon (diagrams (c) and (d)) decays in the ISChE mechanism. It's worth mentioning that in the di- $\eta$  decay process, the initial and final states could be connected by both the charmed meson loops (diagram (a)) and charmed-strange meson loops (diagram (b)).

Source: Taken from [661, 561].

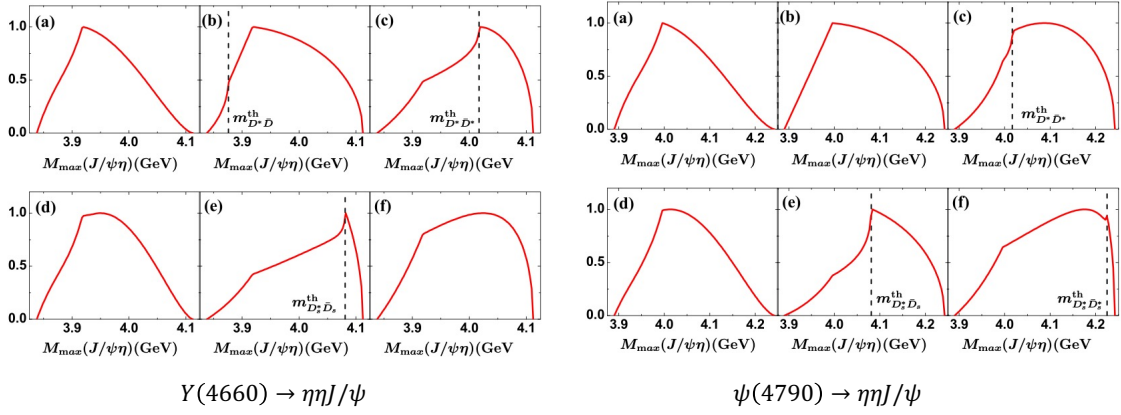


Figure 75: The  $M_{\max}(J/\psi\eta)$  distributions of  $Y(4660) \rightarrow \eta\eta J/\psi$  (left panel) and  $\psi(4790) \rightarrow \eta\eta J/\psi$  (right panel). Here, the diagrams (a), (b) and (c) are the lineshapes resulted from the intermediate  $DD^*$ ,  $D^*\bar{D} + H.c.$  and  $D^*\bar{D}^*$ , respectively, while the diagrams (d), (e) and (f) are the results considering the intermediate  $D_s\bar{D}_s$ ,  $D_s^*\bar{D}_s + H.c.$  and  $D_s^*\bar{D}_s^*$  contributions, respectively. The thresholds of  $DD^*$ ,  $D^*\bar{D}^*$  and  $D_s^*\bar{D}_s$  are marked by the vertical dashed lines. The maxima of these lineshapes are normalized to 1.

Source: Taken from [661].

### 5.3. Initial single chiral particle emission mechanism and the predicted $Z_{c_s}$ structures

The ISPE mechanism was originally proposed to explain the observation of  $Z_b(10610)$  and  $Z_b(10650)$  in the hidden-bottom dipion decays of  $\Upsilon(5S)$ , where the structures near the  $B^*\bar{B}$  and  $B^*\bar{B}^*$  thresholds were well reproduced [81]. Motivated by the similarity between the charmonium and bottomonium systems, Chen, Liu, and Matsuki extended the ISPE mechanism in 2011 to investigate the hidden-charm decays of higher charmonium(-like) states. Peak structures near the  $D^*\bar{D}$  and  $D^*\bar{D}^*$  thresholds were predicted [82], and the authors suggested searching for these structures in specific processes such as  $Y(4260)/\psi(4040)/\psi(4160)/\psi(4415)$  decays into  $\pi^+\pi^- J/\psi$ ,  $\pi^+\pi^-\psi(3686)$ , and  $\pi^+\pi^- h_c$  [82]. In 2013, the near-threshold structure at the  $D^*\bar{D}$  threshold, named  $Z_c(3900)$ , was reported in the process  $e^+e^- \rightarrow \pi^+\pi^- J/\psi$  at  $\sqrt{s} = 4.260$  GeV by the BESIII [550] and Belle Collaborations [551]. Subsequently, the structure near the  $D^*\bar{D}^*$  threshold, named  $Z_c(4020)$ , was observed in  $e^+e^- \rightarrow \pi^+\pi^- h_c$  at the same center-of-mass energy [514]. These experimental confirmations in the suggested channels further motivated the authors to explore the broader applicability of the ISPE mechanism, including its extension to other decay processes and the formulation of additional theoretical predictions.

Recognizing that the pion is a chiral particle, the authors in Ref. [561] generalized the ISPE mechanism to the Initial Single Chiral particle Emission (ISChE) mechanism, wherein the pion in the ISPE framework can be replaced by any other chiral particle, such as a kaon or an  $\eta$  meson. Within the ISChE mechanism, the di- $\eta$  decay [661] and dikaon decay processes of higher charmonia have been investigated [561]. These studies predicted the existence of isoscalar partners of the  $Z_c$  states near the  $D^*\bar{D}^*/D_s^*\bar{D}_s^*$  thresholds, as well as charmonium-like states with

strangeness, i.e.,  $Z_{c_s}$  structures. Moreover, analogous to the predictions made for the  $Z_c$  structures, the authors in Refs. [661, 561] not only anticipated the presence of these charmonium-like structures but also clearly identified the specific channels in which they could be experimentally observed.

### 5.3.1. Prediction of isoscalar partner of $Z_c$

In Ref. [661], the hidden-charm di- $\eta$  decay processes of  $Y(4660)$  and  $\psi(4790)$  were investigated using the ISChE mechanism, where the decays  $Y(4660)/\psi(4790) \rightarrow J/\psi\eta\eta$  proceed through intermediate states involving  $\eta$  coupled to  $D^*\bar{D}^{(*)}$  and/or  $\eta$  coupled to  $D_s^{(*)+}D_s^{(*)-}$ . Through this process, one can address the important question of whether isoscalar charmonium-like structures exist near the  $D\bar{D}^*$ ,  $D^*\bar{D}^*$ ,  $D_s^+D_s^{*-}$ , and  $D_s^{*+}D_s^{*-}$  thresholds. From the ISChE-based analysis of the  $Y(4660)/\psi(4790) \rightarrow J/\psi\eta\eta$  processes, the following key insights were obtained:

- For the  $Y(4660) \rightarrow \eta\eta J/\psi$  process, a clear structure around 3.92 GeV appears in the  $M_{\max}(\eta J/\psi)$  distributions across all diagrams shown in the left panel of Fig. 75. This structure arises from the phase space integral of  $M_{\max}(J/\psi\eta)$ . In addition, peak structures are visible near the  $D^*\bar{D}$ ,  $D^*\bar{D}^*$ , and  $D_s^+D_s^{*-}$  thresholds. However, these structures are relatively broad, and the enhancement near the  $D^*\bar{D}$  threshold is less pronounced compared to those observed in the  $\pi^\pm J/\psi$  invariant mass distributions.
- For the  $\psi(4790) \rightarrow \eta\eta J/\psi$  process, clear peak structures near the  $D^*\bar{D}^*$  and  $D_s^+D_s^{*-}$  thresholds were predicted in the  $M_{\max}(\eta J/\psi)$  distributions. In contrast, the structures near the  $D\bar{D}^*$  and  $D_s^{*+}D_s^{*-}$  thresholds are less prominent, as illustrated in the right panel of Fig. 75. The peak resulting from the phase space integral for  $\psi(4790) \rightarrow \eta\eta J/\psi$  is centered around 4.0 GeV.

In 2026, the BESIII Collaboration searched for the isospin partner of  $Z_c(3900)$  in the  $J/\psi\eta$  invariant mass distributions of  $e^+e^- \rightarrow \eta\eta J/\psi$  at center-of-mass energies ranging from  $\sqrt{s} = 4.226$  to 4.690 GeV [662]. Due to the low statistical significance observed at nearly all energy points, no evidence of an isospin partner of  $Z_c(3900)$  decaying to  $\eta J/\psi$  was found.

### 5.3.2. Predictions of charged $Z_{c_s}$ structures

Similar to the hidden-charm dipion decay processes, the hidden-charm di-kaon decay processes of  $\psi(4415)$ ,  $Y(4660)$ , and  $\psi(4790)$  were investigated in Ref. [561], where structures with hidden charm and open strangeness were predicted. Within the ISChE mechanism, the following results were obtained:

- The vector charmonium  $\psi(4415)$  lies below the thresholds of  $D_s^*\bar{D}\bar{K}/D_s\bar{D}^*\bar{K}$  and  $D_s^*\bar{D}^*\bar{K}$ . Consequently, under the ISChE mechanism,  $\psi(4415) \rightarrow J/\psi K^+ K^-$  proceeds only via the intermediate  $D\bar{D}_s + \text{H.C.}$ . The lineshape of  $d\Gamma/dm_{J/\psi K^+}$  is smooth and does not exhibit a sharp peak near the  $D\bar{D}_s + \text{H.C.}$  threshold. This behavior also holds for the decays  $Y(4660) \rightarrow J/\psi K^+ K^-$  and  $\psi(4790) \rightarrow J/\psi K^+ K^-$ , as shown in Fig. 76 (a) and (d).
- When considering the intermediate  $D^*\bar{D}_s + D\bar{D}_s^* + \text{H.C.}$  contribution to  $Y(4660) \rightarrow J/\psi K^+ K^-$ , two structures are observed in the lineshape presented in Fig. 76 (b). The higher one is a sharp peak near the  $D_s\bar{D}^*/\bar{D}_s^*D$  thresholds, while the lower one is a broad structure that appears as its reflection. If only the intermediate  $D^*\bar{D}_s + \text{H.C.}$  is included, the resulting  $d\Gamma/dm_{J/\psi K^+}$  distribution for  $Y(4660) \rightarrow J/\psi K^+ K^-$  exhibits a small, sharp peak around the  $D^*\bar{D}_s/\bar{D}_s^*D_s^*$  threshold. In addition, its reflection, appearing around 3.7 GeV, is less pronounced (see Fig. 76 (c) for further details).
- For the  $\psi(4790) \rightarrow J/\psi K^+ K^-$  decay, the corresponding  $d\Gamma/dm_{J/\psi K^+}$  lineshapes are presented, considering the intermediate  $D^*\bar{D}_s + D\bar{D}_s^* + \text{H.C.}$  and  $D^*\bar{D}_s^* + \text{H.C.}$  contributions in diagrams (e) and (f) of Fig. 76. Figure 76 (e) shows an enhancement structure in the  $d\Gamma/dm_{J/\psi K^+}$  distribution, composed of a sharp peak near the  $D_s\bar{D}^*/\bar{D}_s^*D$  threshold and its reflection. This situation differs from that of  $Y(4660) \rightarrow J/\psi K^+ K^-$  discussed above. Figure 76 (f) reveals a sharp peak close to the  $D^*\bar{D}_s^*/\bar{D}_s^*D_s^*$  threshold and a corresponding broad structure from its reflection, both of which are more distinct compared to the features shown in Fig. 76 (c).

It should be mentioned that, besides the ISChE mechanism, the existence of hidden-charm and open-strange states has also been predicted within the relativistic diquark-antidiquark framework [428]. Estimates from QCD sum rules

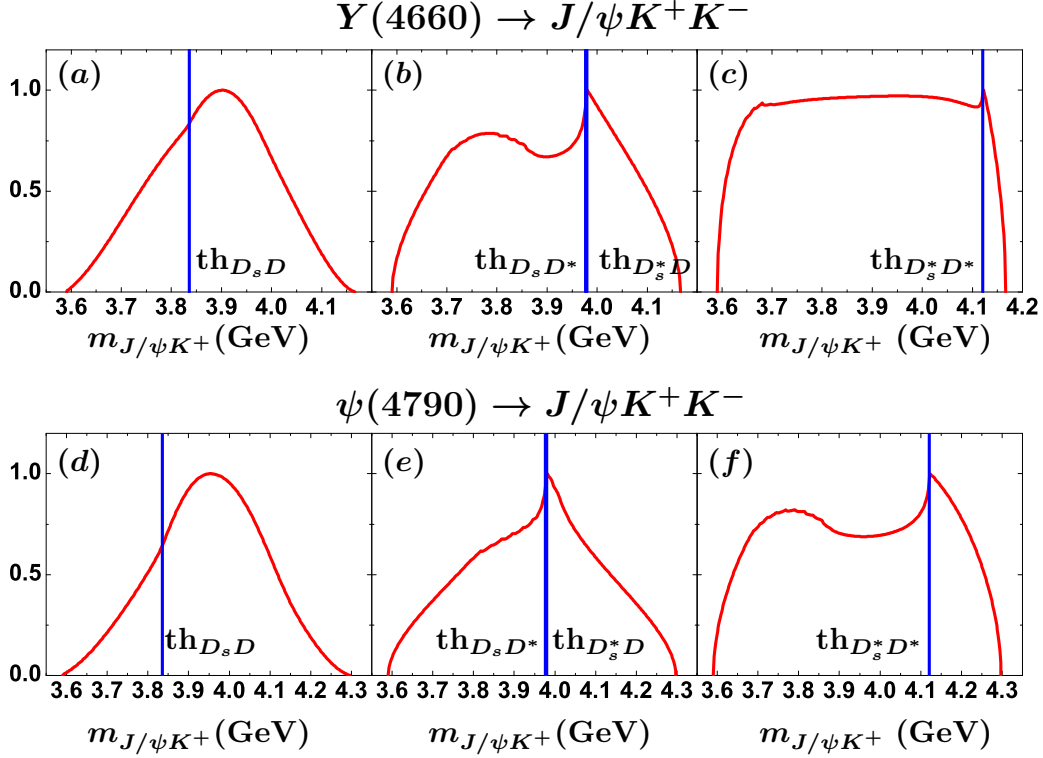


Figure 76: Dependence of the distribution of  $d\Gamma/dm_{J/\psi K^+}$  on the  $J/\psi K^+$  invariant mass spectrum (red solid curves). The diagrams (a) and (d), diagrams (b) and (e), and diagrams (c) and (f), are the results considering the intermediate  $D\bar{D}_s + H.C.$ ,  $D^*\bar{D}_s + D\bar{D}_s^* + H.C.$ , and  $D^*\bar{D}_s^* + H.C.$  contributions, respectively. Here, the line shape of distribution of  $d\Gamma/dm_{J/\psi K^+}$  is normalized to 1.  
Source: Taken from [561].

have also indicated the possible existence of a  $D_s^- D^* + D_s^{*-} D$  molecular state [663]<sup>6</sup>. In Ref. [664], the decay properties of charged states near the  $D_s \bar{D}^*/D_s^* \bar{D}$  threshold were investigated using QCD sum rules.

### 5.3.3. Experimental searches for $Z_{cs}$ structures

As discussed above, charged hidden-charm four quark matters with strangeness near the  $D_s^- D^{*0}/D_s^{*-} D^0$  thresholds have been theoretically predicted by various models, including the compact tetraquark scenario [428], the hadronic molecular model [663], and the ISChE mechanism [561]. Experimental searches for these charged charmonium-like structures provide a crucial test of the above predictions. In the following, we present a brief review of the experimental progress on charmonium-like structures with strangeness.

- Search for  $Z_{cs}$  structures in  $e^+ e^- \rightarrow K^+ K^- J/\psi$  by the Belle Collaboration. In 2014, the Belle Collaboration accumulated a sample of  $e^+ e^- \rightarrow K^+ K^- J/\psi$  events via initial-state radiation at center-of-mass energies between the threshold and 6.0 GeV, using a data sample of  $673 \text{ fb}^{-1}$  collected at or near  $\sqrt{s} = 10.58 \text{ GeV}$  [665]. The cross sections for  $e^+ e^- \rightarrow K^+ K^- J/\psi$  and  $K_S^0 K_L^0 J/\psi$  were measured, and possible intermediate states in the selected  $K^+ K^- J/\psi$  events were investigated by examining the Dalitz plot. As shown in Fig. 77, no clear structure was observed in the  $K^\pm J/\psi$  system at that level of statistical precision. A larger data sample is required to obtain more detailed information about possible structures in the  $K^\pm J/\psi$  system.
- Observation of  $Z_{cs}$  by the BESIII Collaboration. Based on  $e^+ e^-$  annihilation data samples collected by the BESIII detector at five center-of-mass energies ranging from 4.628 to 4.698 GeV, with a total integrated luminosity

<sup>6</sup>It is worth noting that these studies primarily focus on the calculation of mass spectra.

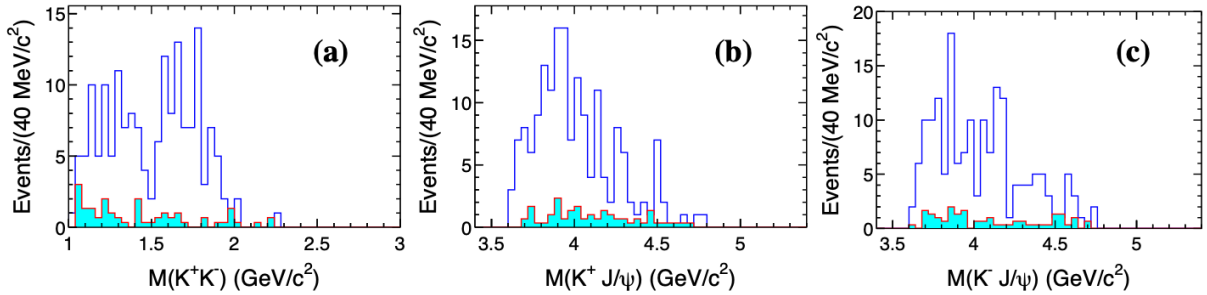


Figure 77: Invariant mass distributions of (a)  $K^+K^-$ , (b)  $K^+J/\psi$ , and (c)  $K^-J/\psi$  for  $K^+K^-J/\psi$  events with  $4.4 < M(K^+K^-J/\psi) < 5.5$   $\text{GeV}/c^2$ . Solid histograms are for events in the  $J/\psi$  signal region, and the shaded histograms are normalized background from the  $J/\psi$  mass sidebands. *Source:* Taken from [665]

of  $3.7 \text{ fb}^{-1}$ , the BESIII Collaboration analyzed the processes  $e^+e^- \rightarrow K^+D_s^-D^{*0}$  and  $K^+D_s^{*-}D^0$  [666]. As shown in the left panel of Fig. 78, the  $K^+$  recoil-mass distributions for events collected at  $\sqrt{s} = 4.681$   $\text{GeV}$  exhibit an excess of events over the known contributions from conventional charmed mesons, near the  $D_s^-D^*$  and  $D_s^{*-}D^0$  thresholds. Fitting this near-threshold structure with a mass-dependent-width Breit-Wigner function yields a pole mass and width of [666]

$$m = (3982.5_{-2.6}^{+1.8} \pm 2.1) \text{ MeV}, \quad \Gamma = (12.8_{-4.4}^{+5.3} \pm 3.0) \text{ MeV},$$

where the first uncertainties are statistical and the second are systematic. The significance of the resonance hypothesis over contributions from conventional charmed mesons alone is about  $5.3\sigma$ . This marks the first observation of a candidate charged hidden-charm structure with strangeness, consistent with predictions from the ISChE mechanism [561] and other QCD exotic estimates [428, 663, 664].

Subsequently, the BESIII Collaboration studied the neutral component of charmonium-like structures with strangeness, i.e.,  $Z_{cs}^0$ , in the process  $e^+e^- \rightarrow K_S^0(D_s^+D^{*-} + D_s^{*+}D^-)$  and its charge conjugate, at five center-of-mass energies between 4.628 and 4.699  $\text{GeV}$ . In the  $K_S^0$  recoil-mass spectrum, evidence for a structure near the  $D_s^+D^{*-}$  and  $D_s^{*+}D^-$  thresholds was reported (see right panel of Fig. 78). Fitting with a Breit-Wigner lineshape, the BESIII Collaboration obtained the mass and width of this structure as

$$m = (3992.2 \pm 1.7 \pm 1.6) \text{ MeV}, \quad \Gamma = (7.7_{-3.8}^{+4.1} \pm 4.3) \text{ MeV},$$

where the first uncertainties are statistical and the second are systematic. The significance of the signal, including both statistical and systematic uncertainties, is  $4.6\sigma$ . The measured mass of  $Z_{cs}(3985)^0$  is close to that of  $Z_{cs}(3985)^+$ , suggesting that  $Z_{cs}(3985)^0$  is the neutral isospin partner of  $Z_{cs}(3985)^+$ .

In the hidden-charm decay channel, the BESIII Collaboration searched for charged charmonium-like structures  $Z_{cs}$  in the  $M_{\text{max}}(K^\pm J/\psi)$  distributions of the process  $e^+e^- \rightarrow K^+K^-J/\psi$ , using data samples with an integrated luminosity of  $5.85 \text{ fb}^{-1}$  collected at center-of-mass energies from 4.61 to 4.95  $\text{GeV}$ . As shown in Fig. 79, a small excess corresponding to a  $Z_{cs}$  signal is observed above other components. The mass and width are fitted to be  $4044 \pm 6$   $\text{MeV}$  and  $36 \pm 16$   $\text{MeV}$ , respectively. The uncertainties are statistical only, and the significance is  $2.3\sigma$ .

In addition, the BESIII Collaboration searched for  $Z_{cs}$  structures in the processes  $e^+e^- \rightarrow K^+K^-\psi(3686)$  [669] and  $e^+e^- \rightarrow K_S^0K_S^0\psi(3686)$  [670]. In Ref. [669], the BESIII Collaboration fitted the  $M_{K^\pm}^2$  distributions using two different schemes. The mass of  $Z_{cs}$  was assumed to be around 4.205  $\text{GeV}$  in Fit I (as shown in Fig. 80 (a)) and around 4.315  $\text{GeV}$  in Fit II (as shown in Fig. 80 (b)). In Fit I, the mass and width for  $Z_{cs}^\pm$  were fitted to be  $(4208 \pm 3.1)$   $\text{MeV}$  and  $6.1 \pm 5.7$   $\text{MeV}$ , respectively, with a global significance of  $1.2\sigma$ . In Fit II, the resonance parameters of  $Z_{cs}^\pm$  were determined to be  $M = (4316 \pm 2.7)$   $\text{MeV}$  and  $\Gamma = (9.0 \pm 8.6)$   $\text{MeV}$ , with a global significance of  $1.1\sigma$ . The BESIII Collaboration also searched for the  $Z_{cs}^0$  in the  $K_S^0\psi(3686)$  invariant mass distributions of the process  $e^+e^- \rightarrow K_S^0K_S^0\psi(3686)$  [670]. As shown in Fig. 80 (c), the  $K_S^0\psi(3686)$  invariant mass distribution is consistent with three-body phase space, and no obvious structure is observed.

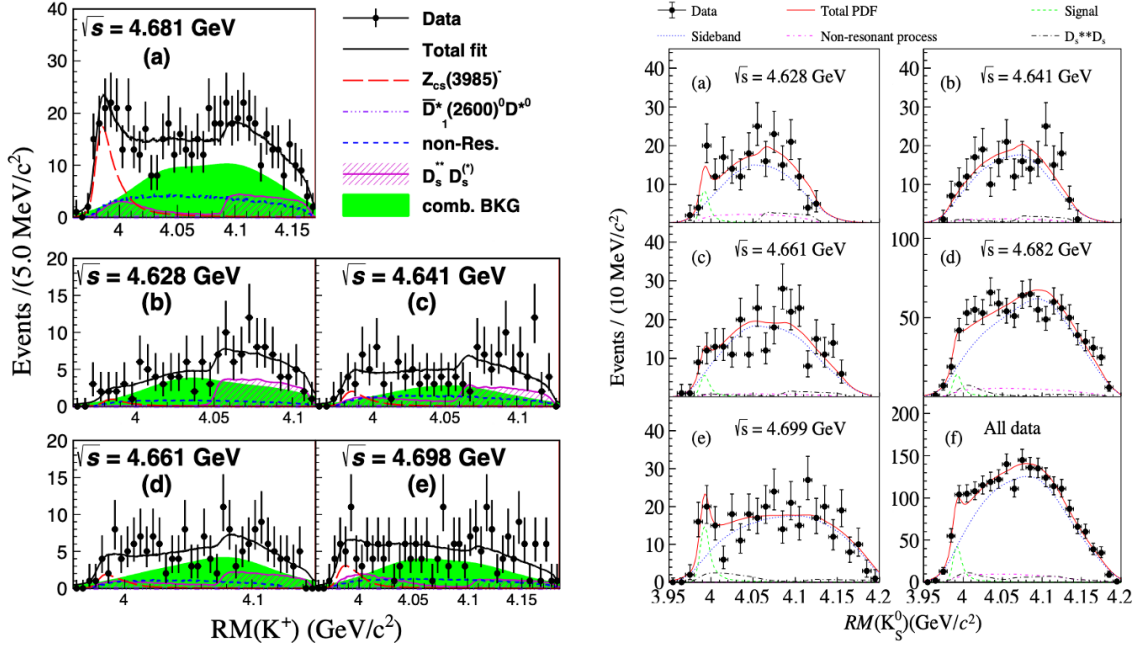


Figure 78: The experimental observation of  $Z_{cs}^-$  (left panel) in the  $K^+$  recoil mass spectra of  $e^+e^- \rightarrow K^+(D_s^- D^{*0} + D_s^- D^0)$  [666] and  $Z_{cs}^0$  (right panel) in the  $K_S^0$  recoil mass spectra of  $e^+e^- \rightarrow K_S^0(D_s^+ D^{*0} + D_s^+ D^0)$  [667] by the BESIII Collaboration.

Source: Taken from [666, 667]

As indicated in Ref. [561], the lineshapes of the  $Z_{cs}$  structures depend on the initial state. For example, the structure near the  $D_s D^*/D_s^* D$  threshold is prominent in the di-kaon decay of  $Y(4660)$ , whereas the structure near the  $D_s^* D^*$  threshold is expected to be more evident in the  $\psi(4790)$  decay. To further investigate the  $Z_{cs}$  structures in the hidden-charm di-kaon decays of higher charmonia, larger data samples are required, which should be accessible to the BESIII and Belle II Collaborations.

It should also be noted that the LHCb Collaboration has reported two charmonium-like structures with strangeness in  $B$  meson decays [671, 672]. Specifically, in the decay  $B^+ \rightarrow J/\psi \phi K^+$ , two  $Z_{cs}$  structures were observed in the  $J/\psi K^+$  invariant mass spectrum [671]. The resonance parameters of the lower-mass state, denoted  $Z_{cs}(4000)$ , were measured to be  $m = (4003 \pm 6_{-14}^{+4})$  MeV and  $\Gamma = (131 \pm 15 \pm 26)$  MeV [671]. While its mass is consistent with the structure observed by the BESIII Collaboration, there is a significant discrepancy in the width. For the higher-mass structure, referred to as  $Z_{cs}(4200)$ , the mass and width were reported as  $(4216 \pm 24_{-30}^{+43})$  MeV and  $(233 \pm 52_{-73}^{+97})$  MeV, respectively [671]. In addition, a neutral partner of the  $Z_{cs}(4000)^+$  was observed in the  $J/\psi K_S^0$  invariant mass distribution of the decay  $B^0 \rightarrow J/\psi \phi K_S^0$ , with a mass of  $(3991_{-10-17}^{+12+9})$  MeV and a width of  $(105_{-25-23}^{+29+17})$  MeV [672]. Given the substantial difference in width between the  $Z_{cs}(3985)$  and  $Z_{cs}(4000)$ , it remains an open question whether these two structures share the same origin.

Following the observation of the  $Z_{cs}$  structures, their distinctive properties have stimulated considerable theoretical interest. Their mass spectra, decay behaviors, and production mechanisms have been extensively investigated within various frameworks, including the compact tetraquark picture [673, 674, 675, 676, 677, 678, 679, 680, 681], the  $(D_s^{*+} \bar{D}^0 + D_s^+ \bar{D}^{*0})$  molecular or resonance scenario [682, 683, 684, 685, 686, 687, 676, 688, 689, 690, 691, 692, 693, 694, 695, 696, 697, 698], and kinematic effects [699, 700, 701].

## 6. Interaction between hadrons involved in charmonia

### 6.1. Experimental observation of di- $J/\psi$ invariant mass spectrum from $pp$ collisions

In 2020, the LHCb Collaboration reported the observation of a narrow structure near 6.9 GeV and a broad enhancement just above the di- $J/\psi$  threshold, using  $pp$  collision data at  $\sqrt{s} = 7, 8, 13$  TeV ( $9 \text{ fb}^{-1}$ ) [84]. A fit with only

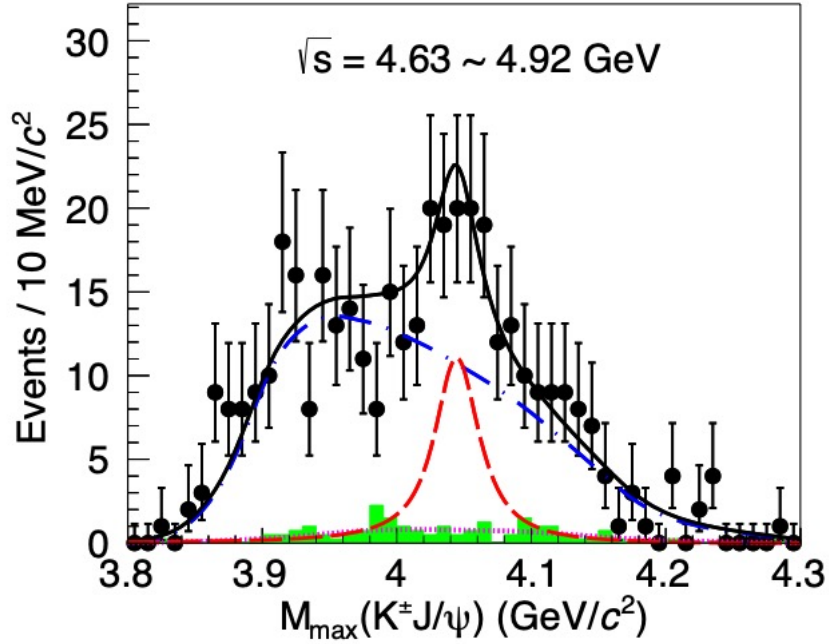


Figure 79: Distributions of  $M_{\max}(K^\pm J/\psi)$  of  $e^+e^- \rightarrow K^+K^-J/\psi$  reported by BESIII Collaboration [668]. The red dashed, blue dash-dotted, and pink dotted lines are the signal component of  $Z_{cs}$ , the phase space and the combinatorial background, respectively.  
Source: Taken from [668]

non-resonant single-parton scattering (NRSPS) and double-parton scattering (DPS) failed to describe the spectrum (Fig. 81(a)). Including two threshold Breit-Wigner functions and one resonance near 6.9 GeV (model I) gave a good description, with the resonance parameters  $M = 6905 \pm 11 \pm 7$  MeV,  $\Gamma = 80 \pm 19$  MeV (Fig. 81(b)). An alternative model II introducing interference between the NRSPS and a threshold resonance improved the description of a dip near 6.75 GeV, yielding  $M = 6886 \pm 11$  MeV,  $\Gamma = 168 \pm 33$  MeV (Fig. 81(c)). Both models confirmed a new structure, denoted  $X(6900)$ .

Subsequently, CMS and ATLAS confirmed the existence of  $X(6900)$ . In 2022, CMS analyzed  $135 \text{ fb}^{-1}$  of 13 TeV data and reported three structures:  $X(6600)$ ,  $X(6900)$  and  $X(7100)$  [86]. Two fit scenarios were used: one with three incoherent Breit-Wigners plus background, and another including interference among them (Fig. 82). The resonant parameters are listed in Table 10. Interference significantly improved the description of dips near 6.75 and 7.15 GeV,

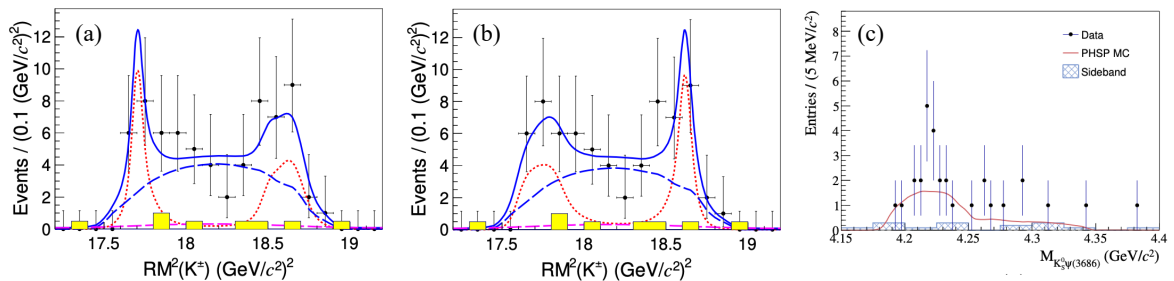


Figure 80: Distributions of  $RM^2(K^\pm)$  of  $e^+e^- \rightarrow K^+K^-\psi(3686)$  (diagram (a) and (b)) and  $m_{K_S^0 \psi(3686)}$  of  $e^+e^- \rightarrow K_S^0 K_S^0 \psi(3686)$  reported by BESIII Collaboration [669, 670].  
Source: Taken from [669, 670]

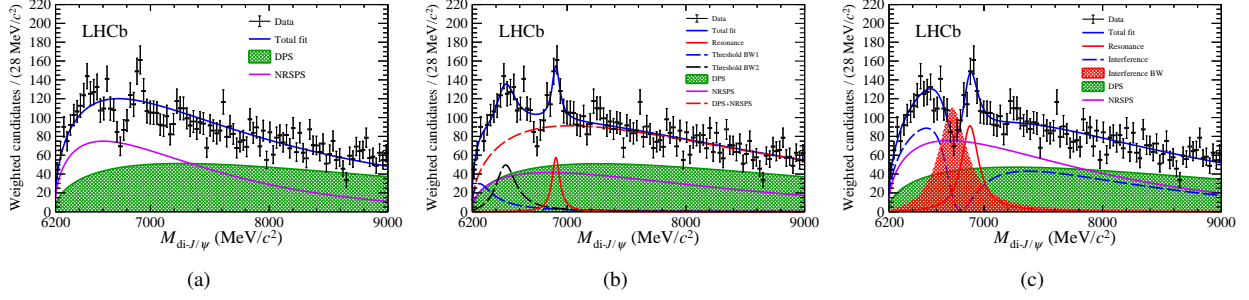


Figure 81: Di- $J/\psi$  invariant mass spectra with  $p_T^{di-J/\psi} > 5.2$  GeV from LHCb, showing fits with (a) NRSPS+DPS, (b) model I, and (c) model II [84].

though it altered the extracted masses and widths.

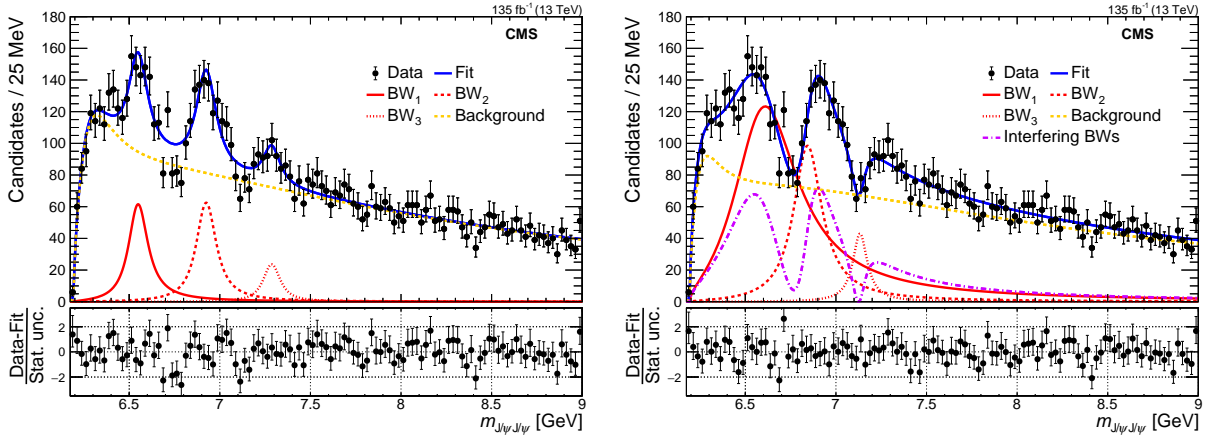


Figure 82: CMS di- $J/\psi$  mass spectrum fitted with three Breit-Wigners without (left) and with (right) interference [86].

ATLAS also analyzed di- $J/\psi$  and  $J/\psi + \psi(2S)$  channels using  $140 \text{ fb}^{-1}$  at 13 TeV [85]. For di- $J/\psi$ , two models were employed: model A included three interfering resonances; model B considered interference between one resonance and the SPS background, requiring only two resonances. Both models confirmed  $X(6600)$  and  $X(6900)$ , but  $X(7100)$  was not clearly seen. In the  $J/\psi + \psi(2S)$  channel, two similar fit models  $\alpha$  and  $\beta$  yielded modest significances ( $\sim 4\sigma$ ) for structures near 6.9–7.2 GeV (Table 11, Fig. 83).

In 2024, CMS updated the di- $J/\psi$  analysis with  $315 \text{ fb}^{-1}$  (Run 2+Run 3) [88]. Using an interference model similar to the earlier one, they obtained consistent but more precise parameters (Table 12), with all three structures now exceeding  $5\sigma$  significance. The dips near 6.75 and 7.15 GeV were confirmed with high significance ( $9.7\sigma$  and  $6.5\sigma$ ), and the interference pattern suggests the three states likely share the same  $J^{PC}$ .

In 2025, CMS also reported the  $J/\psi + \psi(2S)$  channel using  $314 \text{ fb}^{-1}$  [89]. An interference fit with two resonances gave  $m_{X(6900)} = 6876^{+46+110}_{-29-110}$  MeV,  $\Gamma_{X(6900)} = 253^{+290+120}_{-100-120}$  MeV and  $m_{X(7100)} = 7169^{+26+74}_{-52-70}$  MeV,  $\Gamma_{X(7100)} = 154^{+110+140}_{-82-160}$  MeV, consistent with the di- $J/\psi$  results within uncertainties. The significances were  $7.9\sigma$  for  $X(6900)$  and  $4.0\sigma$  for  $X(7100)$ . Furthermore, a CMS analysis of angular distributions using a matrix-element likelihood approach favored the quantum numbers  $2^{++}$  for  $X(6600)$ ,  $X(6900)$  and  $X(7100)$  over other  $J^{PC}$  hypotheses [90].

Through analyses conducted by different experiments, the extracted resonance parameters for structures observed in the di- $J/\psi$  invariant mass spectrum differ, as presented in Tables 10, 11, and 12<sup>7</sup>. This leads to ambiguity to make conclusion when only comparing theoretical results with the experimental resonance parameters.

<sup>7</sup>We need to clarify that they represent typical data analysis, which is distinct from physics analysis. As noted in Ref. [702], as theorists, we

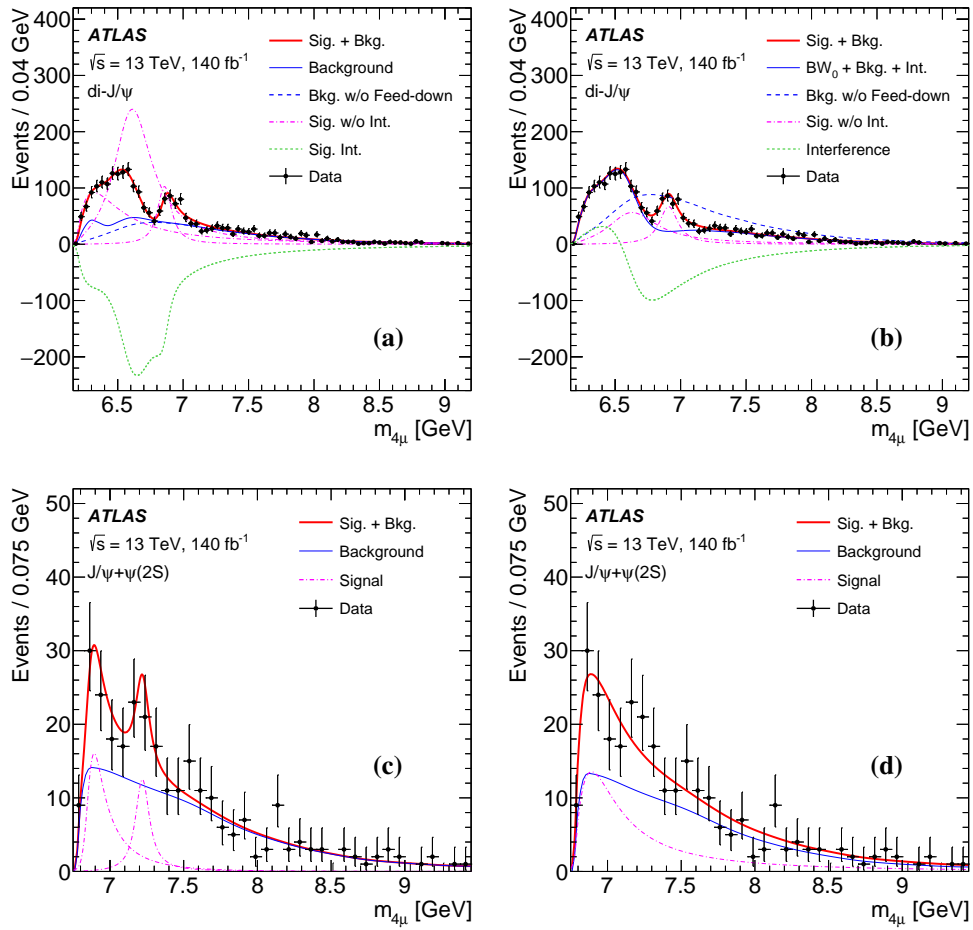


Figure 83: Fitted spectra in di- $J/\psi$  channel with models A (a), B (b), and in  $J/\psi + \psi(2S)$  channel with models  $\alpha$  (c) and  $\beta$  (d), by ATLAS [85].

Table 10: Fitted masses and widths (MeV) of the three structures from CMS [86].

		BW <sub>1</sub>	BW <sub>2</sub>	BW <sub>3</sub>
No interference	$m$ (MeV)	$6552 \pm 10 \pm 12$	$6927 \pm 9 \pm 4$	$7287^{+20}_{-18} \pm 5$
	$\Gamma$ (MeV)	$124^{+32}_{-26} \pm 33$	$122^{+24}_{-21} \pm 18$	$95^{+59}_{-40} \pm 19$
	Significance	$6.5\sigma$	$9.4\sigma$	$4.1\sigma$
Interference	$m$ (MeV)	$6638^{+43+16}_{-38-31}$	$6847^{+44+48}_{-28-20}$	$7134^{+48+41}_{-25-15}$
	$\Gamma$ (MeV)	$440^{+230+110}_{-200-240}$	$191^{+66+25}_{-49-17}$	$97^{+40+29}_{-29-26}$
	Significance	$7.9\sigma$	$9.8\sigma$	$4.7\sigma$

Table 11: ATLAS fit results on di- $J/\psi$  and  $J/\psi\psi(2S)$  spectra in GeV [85].

di- $J/\psi$	model A	model B
$m_0$	$6.41 \pm 0.08^{+0.08}_{-0.03}$	$6.65 \pm 0.02^{+0.03}_{-0.02}$
$\Gamma_0$	$0.59 \pm 0.35^{+0.12}_{-0.20}$	$0.44 \pm 0.05^{+0.06}_{-0.05}$
$m_1$	$6.63 \pm 0.05^{+0.08}_{-0.01}$	—
$\Gamma_1$	$0.35 \pm 0.11^{+0.11}_{-0.04}$	—
$m_2$	$6.86 \pm 0.03^{+0.01}_{-0.02}$	$6.91 \pm 0.01 \pm 0.01$
$\Gamma_2$	$0.11 \pm 0.05^{+0.02}_{-0.01}$	$0.15 \pm 0.03 \pm 0.01$
$J/\psi+\psi(2S)$	model $\alpha$	model $\beta$
$m_3$	$7.22 \pm 0.03^{+0.01}_{-0.04}$	$6.96 \pm 0.05 \pm 0.03$
$\Gamma_3$	$0.09 \pm 0.06^{+0.06}_{-0.05}$	$0.51 \pm 0.17^{+0.11}_{-0.10}$

Table 12: Updated fit results of the  $J/\psi J/\psi$  mass spectrum with interference (Run 2+Run 3) in MeV (uncertainties are statistical followed by systematic), from CMS [88].

		BW <sub>1</sub>	BW <sub>2</sub>	BW <sub>3</sub>
Interference (Run 2 + Run 3)	$m$ (MeV)	$6593^{+15}_{-14} \pm 25$	$6847^{+10}_{-10} \pm 15$	$7173^{+9}_{-10} \pm 13$
	$\Gamma$ (MeV)	$446^{+66}_{-54} \pm 87$	$135^{+16}_{-14} \pm 14$	$73^{+18}_{-15} \pm 10$
	Significance	$15.2\sigma$	$16.7\sigma$	$7.7\sigma$

## 6.2. Theoretical status and challenges in identifying genuine multi-quark states

The theoretical exploration of heavy flavor tetraquarks, particularly the fully heavy systems with the  $QQ\bar{Q}\bar{Q}$  configuration, has a history spanning nearly five decades. Initial speculations emerged soon after the "November Revolution" of particle physics [3, 4], with early works attempting to address the possible existence of such states, albeit with primitive numerical results due to the lack of experimental guidance [703, 704, 705, 706, 707, 708]. The landscape transformed with the rapid advancement of charm physics, where precise measurements of charmonium spectra across various  $J^{PC}$  quantum numbers enabled the refinement of theoretical models. This progress ignited a renewed wave of interest in fully heavy exotic states [709, 710, 711, 712, 713, 714, 715, 716, 717, 718, 719, 720, 721, 722, 723], as models and their parameters could now be more reliably constrained.

A significant early contribution came from Chao *et al.*, who proposed that peculiar structures in  $R(e^+e^- \rightarrow \text{hadrons})$  around  $\sqrt{s} = 6 - 7$  GeV might be attributed to predicted  $P$ -wave  $(cc)$ - $(\bar{c}\bar{c})$  states produced between 6.4 and 6.8 GeV, predominantly decaying into charmed mesons [705]. Subsequent foundational studies employed the

only trust the experimental data provided by experimentalists. To a certain extent, exploring the underlying mechanism behind the experimental data should be left to theorists.

potential model [706, 707] and the MIT bag model within the Born-Oppenheimer approximation [724]. While a non-relativistic potential analysis initially found no  $QQ\bar{Q}\bar{Q}$  bound state [725], Lloyd *et al.* later reported several closely-lying states using a parameterized Hamiltonian with a large oscillator basis [709].

Starting around 2003, systematic calculations of the fully heavy tetraquark spectrum proliferated. These employed diverse frameworks including constituent quark models [709, 710, 711, 712], diquark models [713, 714], analyses of hyperfine splitting and color-magnetic interactions [715, 716, 717, 718], and QCD sum rules [719, 720]. Mass predictions for the fully charmed tetraquark varied widely from about 5.8 to 7.4 GeV. A common feature emerged from quark model approaches: the lowest-lying state was typically an  $S$ -wave configuration, and due to the Pauli principle, it was almost invariably assigned the quantum numbers  $J^{PC} = 0^{++}$ . Representative mass predictions from this era include those by Karliner *et al.* ( $M(X_{cc\bar{c}\bar{c}}) = 6192 \pm 25$  MeV,  $M(X_{bb\bar{b}\bar{b}}) = 18826 \pm 25$  MeV for  $0^{++}$ ) [718], Anwar *et al.* ( $(18.72 \pm 0.02)$  GeV for  $bb\bar{b}\bar{b}$ ) [721], and Bai *et al.* (using diffusion Monte Carlo for  $bb\bar{b}\bar{b}$ ) [722]. Further insights came from an updated Cornell model applied to a diquark-antidiquark configuration [723] and moment QCD sum rules supporting compact states, suggesting searches in the  $J/\psi J/\psi$  and  $\eta_c(1S)\eta_c(1S)$  channels [719].

The experimental quest for these states intensified with accumulating data. Early hints came from CMS, which reported a structure near 18.4 GeV in the four-lepton channel (global significance  $3.6\sigma$ ), proposed as a fully-bottom tetraquark candidate [726], though it was not confirmed later [727]. LHCb also found no significant  $bb\bar{b}\bar{b}$  signal in the  $\Upsilon(1S)\mu^+\mu^-$  spectrum between 17.5 and 20.0 GeV [728]. A major breakthrough arrived in 2020 with the LHCb discovery of the narrow  $X(6900)$  resonance in the di- $J/\psi$  spectrum, alongside a broad structure (6.2–6.8 GeV) and a potential peak near 7.3 GeV [84]. Subsequent measurements by ATLAS and CMS confirmed  $X(6900)$  and revealed additional structures [86, 729, 730], sparking extensive theoretical discussion on their nature [714, 731, 732, 733, 734, 735, 736, 737, 738, 739, 740, 741, 742, 743, 744, 745, 746, 747, 732, 748, 749, 737, 750, 751, 752, 738, 753, 754, 755, 756, 735, 744, 757, 758, 759, 760, 761, 762, 763, 764, 765, 766, 746, 747, 732, 748, 749, 737, 750, 751, 752, 738, 753, 754, 755, 756, 735, 744, 757, 758, 759, 760, 761, 762, 763, 764, 765, 766, 767, 756, 768, 769, 770, 771, 772, 767, 773, 774, 775, 776, 777, 778, 779, 780, 781, 782, 783, 784, 785, 786, 787, 788, 789, 745, 790, 791, 792, 793, 794, 795, 796, 797, 798, 799, 800, 801, 802, 803].

Post-discovery, a significant volume of theoretical work aimed to interpret the observed di- $J/\psi$  structures. Since these states lie above the di- $J/\psi$  threshold, many studies started to focus on their internal dynamics and resonant production mechanisms. A prominent interpretation, supported by numerous works [746, 747, 732, 748, 749, 737, 750, 751, 752, 738, 753, 754, 755, 756, 735, 744, 757, 758, 759, 760, 761, 762, 763, 764, 765, 766, 803], posits them as excited (radial or orbital) compact tetraquark states. Alternative ideas include the interpretation of  $X(6900)$  as a tetracharm hybrid [739, 804, 802]. Crucially, to reproduce resonant masses in the experimental range, studies highlight the essential role of coupled-channel effects and the mixing between different color configurations (e.g.,  $\mathbf{3}_c \otimes \bar{\mathbf{3}}_c$  and  $\mathbf{6}_c \otimes \bar{\mathbf{6}}_c$  within the diquark-antidiquark picture) [756, 768, 769, 770, 771, 772, 767, 773, 774, 775, 776]. This underscores that the formation of these states, mostly interpreted as compact tetraquark states, likely involves complex interactions among components with different spin and color structures.

However, the fundamental question of stability for the ground-state fully heavy tetraquark remains contentious. Some studies, such as those using an updated Cornell model [713], an extended chromomagnetic model [805], or the quark delocalization color screening model [768], suggest bound states can exist. Conversely, other comprehensive analyses conclude the opposite. For instance, Wang *et al.* found ground states approximately 300–450 MeV above the lowest meson-meson thresholds in nonrelativistic quark models [711]. Lattice nonrelativistic QCD calculations found no  $bb\bar{b}\bar{b}$  state below the bottomonium-pair threshold [806], and Richard *et al.* argued that a properly treated four-body problem in a standard quark model does not yield a stable  $QQ\bar{Q}\bar{Q}$  configuration [807]. Wu *et al.* performed a benchmark calculations of fully heavy compact tetraquark states using three different quark potential models, which does not find the existence of any bound states for both  $cc\bar{c}\bar{c}$  and  $bb\bar{b}\bar{b}$  systems [773]. In light of the current lack of a theoretical consensus on stability, it would be valuable to engage in more discussion [758, 759, 762, 764, 775, 808, 809, 810, 803, 745, 791].

This situation highlights the profound challenges in identifying genuine multiquark states. The plethora of theoretical investigations within quark models faces a critical problem: most interpretations heavily rely on matching predicted masses to experimentally extracted resonance parameters, which themselves vary significantly across different experimental analyses. Furthermore, theoretical predictions are sensitive to model details and parameter fitting schemes, leading to substantial discrepancies. Also, the eigenvalue problem approach in quark-level calculations often yields a dense spectrum of excited states with similar masses but different configurations, complicating unambiguous

state assignment. Therefore, confirming the nature of these states demands more than just mass comparisons. Future progress will require richer experimental input—such as detailed decay properties and production rates—coupled with a deeper theoretical understanding of the interactions between heavy quarkonia and the non-perturbative dynamics governing multi-quark systems.

### 6.3. Employing scattering between charmonia to understand these observed enhancements in the di- $J/\psi$ invariant mass spectrum

Experimental analyses on the enhancement structures observed in the di- $J/\psi$  invariant mass spectrum typically extract masses and widths of possible resonances by fitting these peaks with phenomenological functions. However, the resulting resonance parameters vary noticeably across different experiments and depend sensitively on the specific fitting assumptions, as illustrated in the above subsection. Quark-model interpretations then rely on these extracted parameters to test whether compact  $cc\bar{c}\bar{c}$  tetraquark configurations can accommodate the observed states, rendering their conclusions contingent upon the reliability of the resonance parameter extraction procedure. An alternative and more direct approach is to interpret the experimental line shape through dynamical scattering mechanisms. Rather than invoking pre-extracted resonance parameters, this perspective considers the rescattering of intermediate charmonium pairs directly produced in  $pp$  collisions, which subsequently transform into the final  $J/\psi J/\psi$  state. By connecting the observed invariant mass distribution directly to the underlying scattering amplitudes, this approach circumvents the intermediate step of resonance parameter extraction from experiments and its associated model dependence, thereby offering a more immediate way to explore the nature and structure of these fully-charm enhancements.

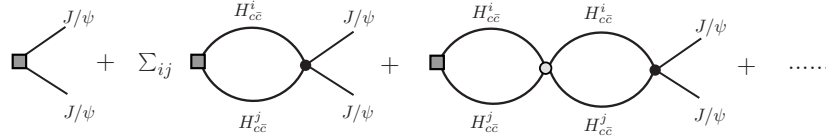


Figure 84: The schematic diagrams for the production mechanism of a double charmonium  $J/\psi J/\psi$ , where  $H_{c\bar{c}}$  stands for allowed intermediate charmonium states, such as  $\eta_c$ ,  $J/\psi$ ,  $\chi_{cJ}$  with  $J = 0, 1, 2$ , etc. Here, the gray rectangle corresponds to direct production of a double charmonium in hadron collisions, fit I or II means the cutoff parameters are set as the same or independent [743].

A preliminary study was carried out by Refs. [742, 743] through the rescattering mechanism, where the final  $J/\psi J/\psi$  invariant mass spectrum were produced by the rescattering of the intermediate charmonia  $H_{c\bar{c}}$  as given in Fig. 84. The key dynamical quantity is the scalar two-point loop integral describing the rescattering of an intermediate charmonium pair  $H_{c\bar{c}}^i H_{c\bar{c}}^j$  into the same pair. In the nonrelativistic limit, this loop function takes the form

$$L_{ij}(m_{J/\psi J/\psi}) = \frac{-1}{4m_i m_j} \left( -\frac{2\mu\alpha}{(2\pi)^{3/2}} + \frac{2\mu\sqrt{2\mu m_0} \left( \text{erf} \left[ \frac{\sqrt{8\mu m_0}}{\alpha} \right] - i \right)}{2\pi e^{\frac{8\mu m_0}{\alpha^2}}} \right),$$

where  $\mu = m_i m_j / (m_i + m_j)$ ,  $m_0 = m_{J/\psi J/\psi} - m_i - m_j$ , and  $\alpha$  is a cutoff parameter of regulating the ultraviolet behavior. By summing the infinite series of loop diagrams (see Fig. 84), the full production amplitude for a given intermediate channel  $ij$  is obtained as

$$\mathcal{A}_{ij}^2(m_{J/\psi J/\psi}) = \frac{g_{ij}^2 L_{ij}(m_{J/\psi J/\psi})^2}{(1 + C_{ij} L_{ij}(m_{J/\psi J/\psi}))^2} \frac{e^{c_0 m_{J/\psi J/\psi}} p_{J/\psi}^{2L+1}}{m_{J/\psi J/\psi}},$$

where  $p_{J/\psi}$  is the momentum of the final  $J/\psi$ ,  $L = 0$  for parity-even systems and  $L = 1$  for parity-odd ones, and  $C_{ij}$  represents the coupling strength of the rescattering interaction. The total scattering amplitude is then constructed by summing coherently over the continuum term and all relevant channels with appropriate phase factors.

After considering the intermediate states as  $\eta_c \chi_{c1}$ ,  $h_c J/\psi$ ,  $\chi_{c0} \chi_{c1}$ , and  $J/\psi J/\psi$  itself, Ref. [742] successfully reproduced the LHCb data as in Fig. 85 (I), and then, a improved work in Ref. [743] also reproduced the CMS data by considering the  $\eta_c \chi_{c1}$ ,  $J/\psi \psi(3686)$ ,  $\chi_{c0} \chi_{c1}$ ,  $\chi_{c2} \chi_{c2}$ , and  $J/\psi J/\psi$  channels as in Fig. 85 (II). Especially, during the fit on the CMS data, Ref. [743] found three resonant poles that mainly related to the  $\chi_{c1} \eta_c$ ,  $\chi_{c0} \chi_{c1}$ , and  $\chi_{c2} \chi_{c2}$  channels,

respectively, which can be assigned to the experimental enhancements around 6.6 and 7.1 GeV. In addition, several virtual poles below the  $J/\psi J/\psi$ ,  $J/\psi\psi(3686)$ ,  $\eta_c\chi_{c1}$ , and  $\chi_{c2}\chi_{c2}$  thresholds were also found, which indicates that the interaction between these charmonia should be attractive, but not strong enough to form bound states. Meanwhile, the extracted positive scattering lengths in Ref. [743] with the following scattering amplitude  $A_0$ , i.e.,  $A_0^{-1} = \frac{1}{a_0} - i\sqrt{2\mu E}$ , where  $E$  is the binding energy, and  $\mu$  is the reduced mass of the intermediate two body channel, also proves that the attractive property of the interaction between these charmonia.

Furthermore, Ref. [743] provides predictions for the  $J/\psi\psi(3686)$  invariant mass spectrum, which are compared with preliminary ATLAS data, showing good agreement and lending additional support to the proposed dynamical mechanism. The authors in Ref. [743] emphasize that future lattice QCD calculations will be essential to quantitatively determine the coupling strengths of double charmonium scattering and to clarify the nature of these structures.

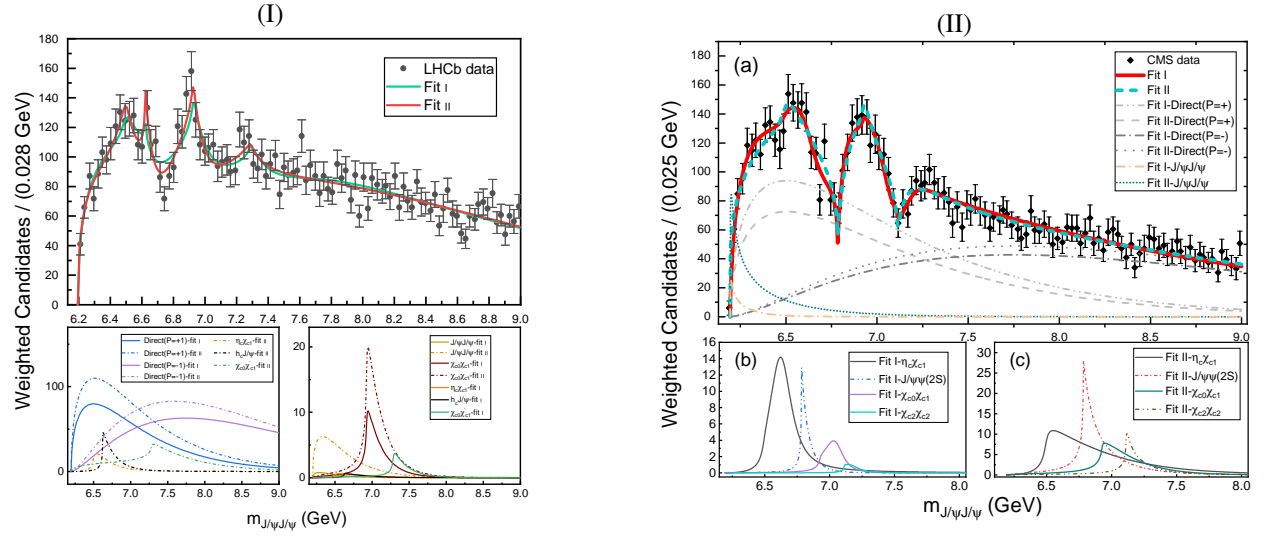


Figure 85: Fit results to the experimental results, where (I) for LHCb data fit [742] and (II) for CMS data fit [743].

Concurrently, Ref. [779] also performed an analysis of the di- $J/\psi$  spectrum measured by LHCb. Different from Refs. [742, 743], where the scattering amplitude is directly parameterized, Ref. [779] obtained the transition matrix through the Bethe-Salpeter equation, where the interactions between charmonia were described by contact terms, and only  $\{J/\psi J/\psi, J/\psi\psi(3686)\}$  channels were considered. Two fit schemes were considered, one is a two channel model employing  $\{J/\psi J/\psi, J/\psi\psi(3686)\}$  as parameterized potential as

$$V_{2\text{ch}}(E) = \begin{pmatrix} a_1 + b_1 k_1^2 & c \\ c & a_2 + b_2 k_2^2 \end{pmatrix}, \quad (64)$$

where  $a_i$ ,  $b_i$ , and  $c$  are free parameters, and the introduction of the momentum dependence in the potential is to produce nontrivial structures above the higher threshold [779]. The other is a  $\{J/\psi J/\psi, J/\psi\psi(3686), J/\psi\psi(3770)\}$  three channel model, and the potential contains only energy independent contact terms as

$$V_{3\text{ch}}(E) = \begin{pmatrix} a_{11} & a_{12} & a_{13} \\ a_{12} & a_{22} & a_{23} \\ a_{13} & a_{23} & a_{33} \end{pmatrix}. \quad (65)$$

It turns out that although much less channels are considered, the fit results on the LHCb data are also quiet well. In addition, the extracted pole positions are also given as in Fig. 86 with the two upper panels. Obviously, in these two fit schemes, the extracted pole positions are quite different, which is reflected by the existence of a pole with wide width around 6.6 GeV, along with the description on the structures around 6.8 GeV, since either the positions and

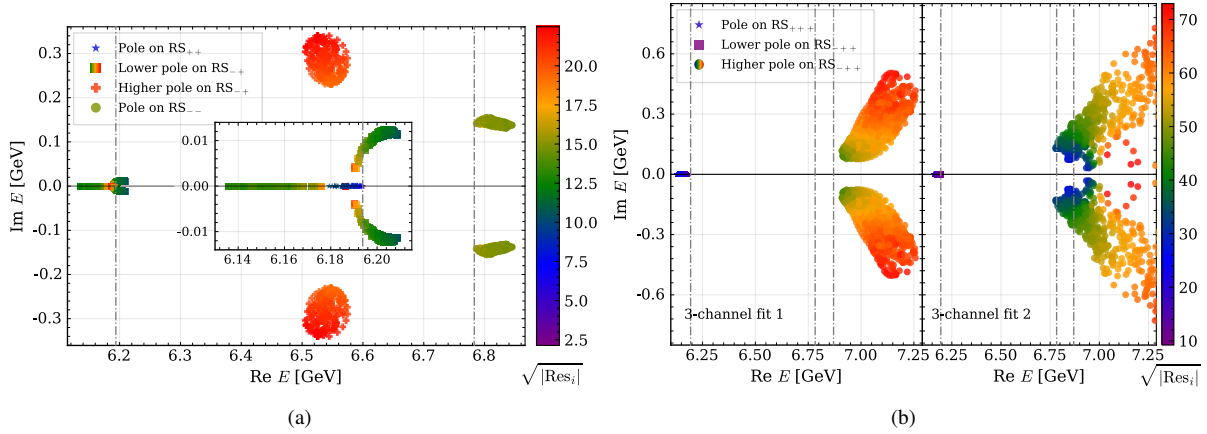


Figure 86: Extracted pole positions from Refs. [779], where left is for the two channel model, right is for the three channel model [779].

the stabilities of the poles there are different. This means, if there actually exists  $X(6600)$ , and the description on the dip and  $X(6900)$  in the experimental data, is model dependent here. However, in both models, a pole below  $J/\psi J/\psi$  threshold is also found, and the extracted scattering parameters also indicate that the interaction between  $J/\psi J/\psi$  is attractive, which is consistent with the results given by Ref. [743], although the compositeness analysis through  $\bar{X}_A$  that defined as  $\bar{X}_A = (1 + 2|r_0/a_0|)^{-1/2}$  are a little different, where the two channel model indicates that the pole around 6.2 GeV is a compact state, while the three channel model supports it as a molecule. Such a phenomena indicates that the current experimental data is still insufficient to determine the properties of the experimental enhancements, i.e., fitting the experimental data only is far from enough to understand these states. After the release of CMS and ATLAS data, Ref. [784] fit the experimental data again with the same procedure, and the results of poles are quite similar to those given by Ref. [779]. However, as presented in Fig. 87, the descriptions on the  $J/\psi\psi(3686)$  invariant mass spectrum are too different, even in the same work with different models.

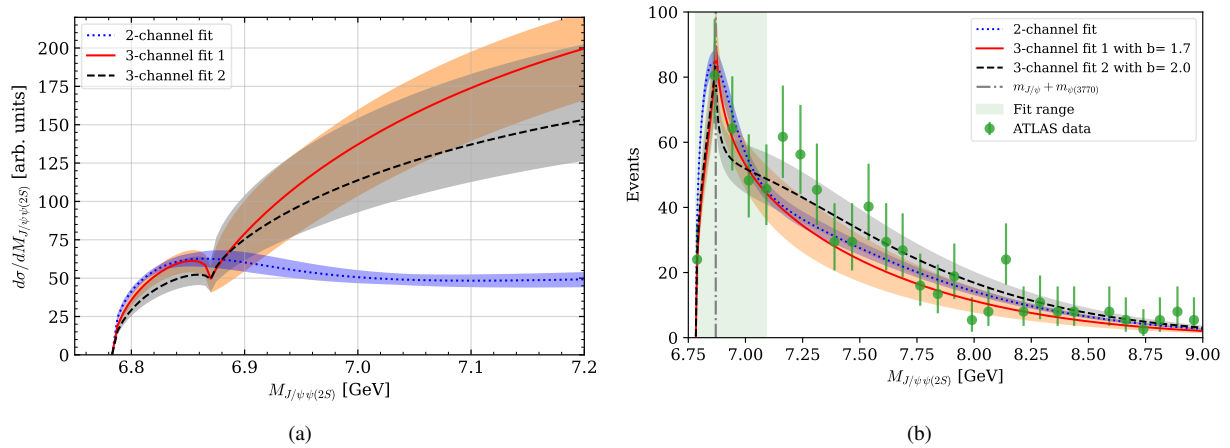


Figure 87: The  $J/\psi\psi(2S)$  invariant mass spectrum, where (a) is the predictions given by Ref. [779], (b) is a comparison with ATLAS data presented in Ref. [784].

Then, to further study the quantum numbers of the experimental observed structures in di- $J/\psi$  spectrum, Ref. [780] performed a partial wave analysis on the LHCb data, where the analysis scheme is similar to Ref. [779] as presented in Fig. 88, but replacing the potential from just free parameters to the following form, where for a  $V_1(p_1, \epsilon_1)V_2(p_2, \epsilon_2) \rightarrow$

$V_3(p_3, \epsilon_3)V_4(p_4, \epsilon_4)$  process, as  $V_{ij} = C_1\epsilon_1 \cdot \epsilon_2\epsilon_3^\dagger \cdot \epsilon_4^\dagger + C_2\epsilon_1 \cdot \epsilon_3^\dagger\epsilon_2 \cdot \epsilon_4^\dagger + C_3\epsilon_1 \cdot \epsilon_4^\dagger\epsilon_2 \cdot \epsilon_3^\dagger$ , with  $C_i$  being constants that related to the undetermined coupling constants of the 4-vector contact interactions. After doing a partial wave projection on the potential to the  $0^{++}$  and  $2^{++}$  quantum numbers, Ref. [780] performed a series of fits on the LHCb data, and the corresponding pole positions were extracted, as presented in Fig. 88. Similarly, the LHCb data can also be well

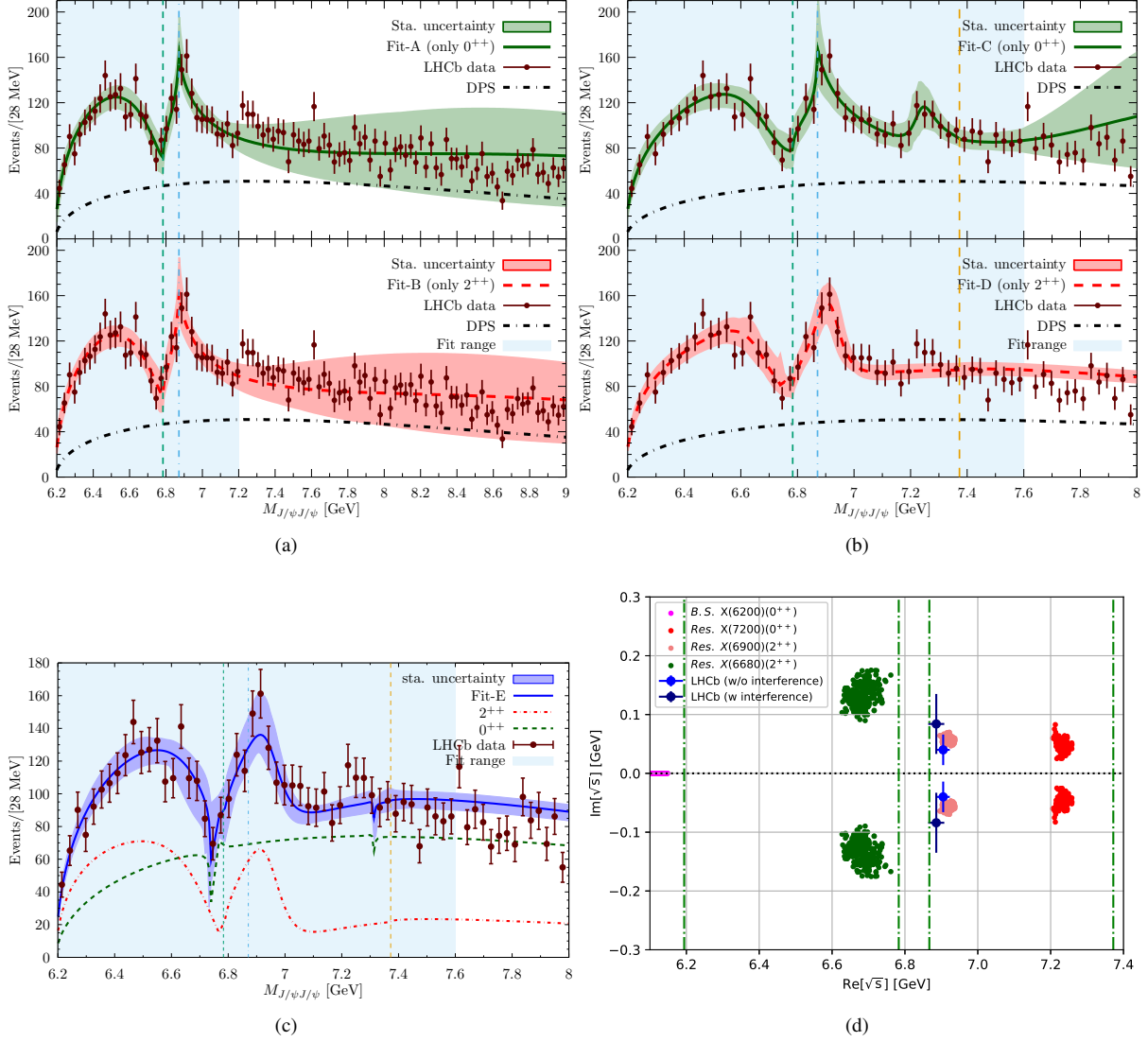


Figure 88: Fit results to the LHCb data. Here, the top left figure considers  $\{J/\psi J/\psi, J/\psi\psi(3686), J/\psi\psi(3770)\}$ , the top right one is for  $\{J/\psi J/\psi, J/\psi\psi(3686), J/\psi\psi(3770), \psi(3686)\psi(3686)\}$  channels, the bottom left result is a combined fit with both  $0^{++}$  and  $2^{++}$  potentials in  $\{J/\psi J/\psi, J/\psi\psi(3686), \psi(3686)\psi(3686)\}$  channels, and the one located at bottom right is the poles for the four channel model [780].

described in both  $0^{++}$  and  $2^{++}$  quantum numbers. In addition, a state below the  $J/\psi J/\psi$  threshold is also found, whose quantum number is  $0^{++}$ , i.e., the  $J = 0$  partial wave potential between  $J/\psi J/\psi$  should be attractive. However, it immediately arises the same question as in Ref. [779, 784] that what is exactly the interpretation of X(6600), since it appears as a pole in  $2^{++}$  fit but disappears in  $0^{++}$  configuration, but whether it is a pole or not, the experimental data can be nicely fit. Another one is from the comprehensive comparisons between the figures in Fig. 88, which indicates that the  $J/\psi\psi(3770)$  channel, about 330 MeV away from the location of X(7200), will have a significant influence on the formation of X(7200), since it is so clear in the four channel fit under  $0^{++}$ , but disappears in the combined fit

that without  $J/\psi\psi(3770)$  channel. Whatsmore, the  $X(6900)$  here is found dominantly contributed by a  $2^{++}$  resonance. However, Refs. [781, 783] found that, after considering the scattering amplitudes up to next-to-leading order as shown in Fig. 89, under pole counting rule,  $X(6900)$  changes to a  $0^{++}$  compact state.

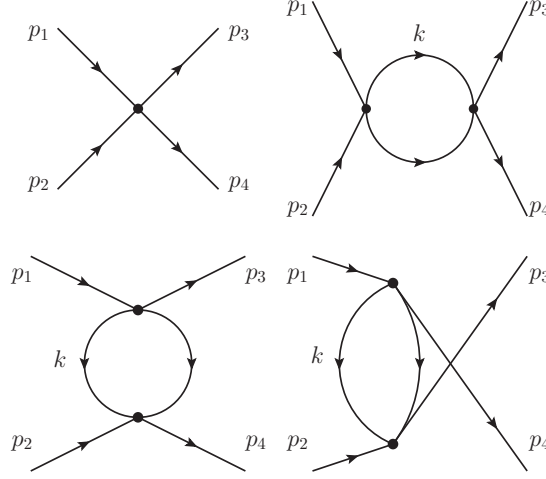


Figure 89: Feynman diagrams of the scattering amplitudes of charmonia given in Ref. [781].

To decode the nature of  $X(7200)$ , Ref. [782] carried out an analysis on the experimental data, and pointed out that the controversy around 7.2 GeV among the three collaborations might be the key to further understand the fully charmed tetraquarks. Thus, considering  $X(6600)$  is near the  $\eta_c\eta'_c$  threshold and  $X(7200)$  is close to the  $\eta'_c\eta'_c$  threshold, Ref. [782] carried out a more complex coupled channel analysis on the experimental data, where six channels as  $\{\eta_c\eta_c, J/\psi J/\psi, \eta_c\eta'_c, J/\psi\psi(3686), \eta'_c\eta'_c, \psi(3686)\psi(3686)\}$  were considered. By adopting different fit schemes with  $0^{++}$  and  $2^{++}$  quantum numbers, although Ref. [782] could obtain good fit quality on the experimental data in all the cases, the extracted pole positions changed a lot, where for  $X(6600)$ , it appears as a pole only in one kind of  $2^{++}$  fit scheme so that its existence is still questionable. For  $X(6900)$ , its pole appears in all situations, i.e., it can be either a  $0^{++}$  or  $2^{++}$  state, but the pole positions are a little different in these two quantum numbers. As for  $X(7200)$ , it appears only in the  $0^{++}$  fit scheme, that is because to form a  $2^{++}$  state in  $\eta'_c\eta'_c$  channel, the partial wave must be  $D$ -wave, which is not easy to form a resonance. Furthermore, it turns out that after considering so many channels, the binding energy of the  $0^{++}$  state mentioned above that below  $J/\psi J/\psi$  threshold will become much deeper. additionally, its  $2^{++}$  partner also shows up.

Obviously, for  $X(6600)$  and  $X(7200)$ , not only their quantum numbers are not determined, but also their existences are still questionable. Actually, even for the firstly observed  $X(6900)$ , by just using the fit approach, similar disagreements also existed. For example, apart from the controversy on its quantum number, Ref. [742, 745] proposed that  $X(6900)$  might be only a cusp effect. In addition, for the pole property, except the compact state interpretation [781, 786, 791, 785], molecular state interpretation might also be permitted [787]. Such a mess situation, which can spark to an entire inspection on the whole experimental spectra, indicates that, the current experimental data is still far from enough to allow us to just integrate all the possible degrees of freedom out to pinch the interactions between charmonia as contact terms, i.e., to truly understand the nature of these fully charmed states, we must try our best to make deeper exploration on the interaction mechanisms between charmonia under a more microscopical and detailed level. At least, we should find some reliable constraints on the fitted parameters from the first principle, if we use contact interactions.

#### 6.4. Exploration on microscopic mechanism of the interaction between charmonia

Unlike hadronic systems containing light quarks, where long-range interactions can be mediated by exchanges of light mesons such as pions, the fully heavy charmonium pairs lack such light degrees of freedom. This feature suggests

that the interaction between charmonia may naturally arise from short-distance dynamics, although the full interaction picture could be more complex. A common effective field theory treatment in this context is to integrate out all possible degrees of freedom and parametrize the interaction via contact terms as introduced in the above subsection. However, integrating out all possible degrees of freedom to capture the interactions between charmonia as contact terms may not be sufficient to reveal the interaction mechanisms responsible for producing the fully charmed tetraquark structures, since this treatment reflects nearly no clear dynamics at this stage. Thus, further explorations are still needed, and this subsection is devoted to exploring various theoretical attempts in this direction. For this purpose, Ref. [740] proposed a microscopic model, where charmonia scatter in short distance through Pomeron exchange as in Fig. 90. After using the same scattering equation as Ref. [779], but replacing the contact terms with the partial wave potentials derived from Fig. 90, it is found that this model can provide very strong contributions to the interactions between vector charmonia, since there all exists poles near thresholds, including  $J/\psi J/\psi$ ,  $J/\psi\psi(2S)$ , and  $\psi(2S)\psi(2S)$  channels. Furthermore, a comparison of the scattering cross section to the experimental data of LHCb is performed, in which the peak around 6.9 GeV is nicely reproduced, demonstrating the effectiveness of this model. In addition, it indicates that there may exist a state around 6.3 GeV, although it maybe covered by the very wide structure. Furthermore, the  $J/\psi\psi(3686)$  spectrum is also predicted, which shows a significant enhancement caused by the pole around  $J/\psi\psi(3686)$  threshold.

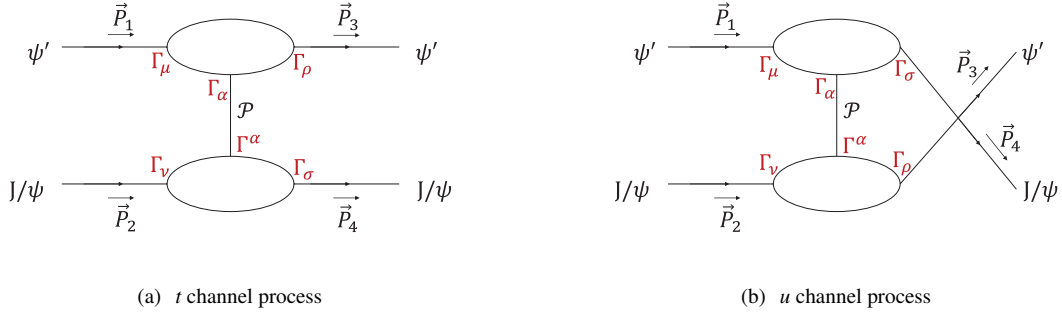


Figure 90: Illustrative diagrams for (a)  $t$  channel and (b)  $u$  channel Pomeron exchanges in  $J/\psi \psi' \rightarrow J/\psi \psi'$  [740]. Here,  $\psi'$  denotes  $\psi(3686)$

Notably, in this model, the parameters, such as cutoffs, that relate to the interaction between charmonia and Pomeron are previously fixed by the typical size of charmonia, i.e.,  $\sim \hbar c/\Lambda \approx 0.3$  fm, what are changed just the relative ratios that channels contribute to the scattering. Absolutely, such an approach obtain a new insight into the dynamical interaction between charmonia. However, the Pomeron itself is a phenomenological object, in addition, such a model is still a short-distance interaction, which may compete with, even be absorbed by the model parameters, gluon exchange, makes it hard to examine.

To reveal the possible midrange or long-distance interaction between charmonia and explore the plausibility of the predicted  $X(6200)$  in Ref. [779], Ref. [788] proposed that two pion or two kaon exchange can also give considerable contributions in the scattering of charmonia, which can be seen as a hadronic level reflection of soft gluon exchange between charmonia as in Fig. 91. After the determinations on the coupling constants, such as  $\alpha_{\psi(3686)J/\psi}$  and  $\alpha_{J/\psi J/\psi}$ , Ref. [788] gives the potential for  $J/\psi J/\psi$  scattering and such potentials indicate that both two pion and two kaon exchanges can provide considerably attractive contributions.

Especially, the result finds that the contribution from  $f_0(500)$ , i.e.,  $\sigma$  particle, dominates in the mid-range, which is consistent with the usual experiences in one boson exchange model. Then, combining the adopted potential with contact term, Ref. [788] further investigate the ratio of the light meson exchange contribution to the total potential, and it shows that this ratio can indeed reach above 50%, makes such a mechanism plausible in explaining the existence of the state below  $J/\psi J/\psi$  threshold, although there also exists some uncertainties, i.e., (1) there still exists uncertainties in the determination on the  $\alpha_{J/\psi J/\psi}$  due to the lack of the experimental information on the  $J/\psi J/\psi$  system, thus it can only start from an educated guess that the meson-exchange picture may be important; (2) although the ratio implies that the meson-exchange contribution may be important, the value of it varies a lot with different model parameters and assumptions. Thus, Ref. [788] calls for a lattice QCD calculation, which will help in more robust predictions.

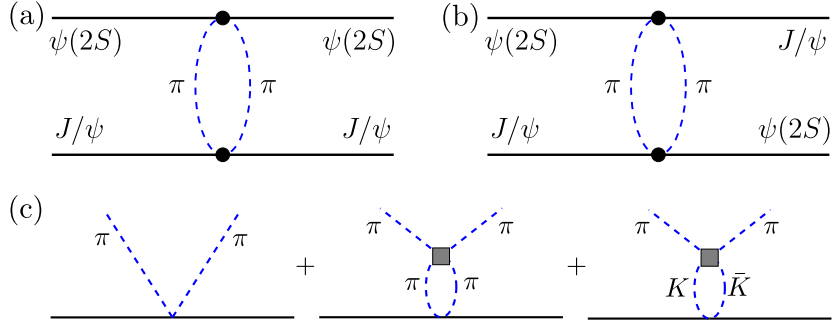


Figure 91: Two-pion exchanges between the  $\psi(2S)$  and  $J/\psi$ , where (a) is for  $t$ -channel and (b) is for  $u$ -channel. (c) The contributions to the amplitude for the transition  $\psi_\alpha \rightarrow \psi_\beta \pi \pi$  including the coupled-channel ( $\pi\pi$  and  $K\bar{K}$ ) FSI. In (c), the solid and dashed lines label charmonia and light mesons, respectively, the filled squares denote the  $\pi\pi$  and  $K\bar{K}$  interactions and the black dots mean that the interactions between the light mesons, as depicted in (c), have been taken into account [788].

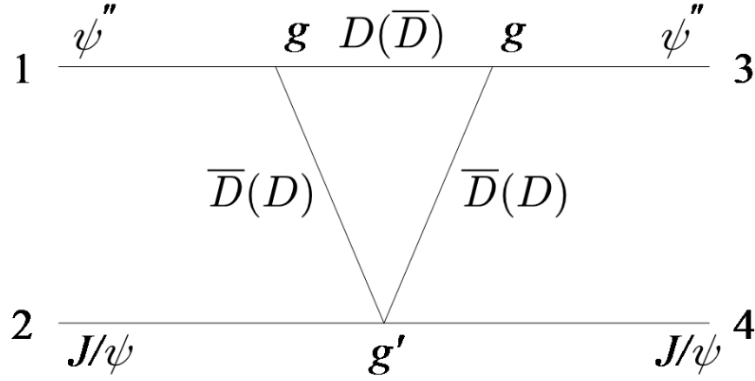


Figure 92: The  $D\bar{D}$  triangle diagram in  $J/\psi\psi(3770)$  scattering process, where  $\psi''$  denotes the  $\psi(3770)$  meson [790].

Another mechanism to explore the nature of  $X(6900)$  is proposed by Ref. [790]. Since this peak is closed to the  $J/\psi\psi(3770)$  threshold, considering that  $\psi(3770)$  can strongly couple to a pair of charmed mesons  $D\bar{D}$ , Ref. [790] proposed a possible mechanism for the  $J/\psi\psi(3770) \rightarrow J/\psi\psi(3770)$  scattering process as Fig. 92. After transiting such a diagram into the scattering amplitude, Ref. [790] pointed out that the loop integral will contain the effect of anomalous triangle singularity, whose position is located at

$$s_A = 4m^2 - \frac{(M^2 - 2m^2)^2}{m^2}, \quad (66)$$

with  $M$  and  $m$  as the masses of  $\psi(3770)$  and  $D$  meson, respectively. As a result, since the mass of  $\psi(3770)$  is above the  $D\bar{D}$  threshold, these two charmed mesons in the loop can be real particles as long as the scattering energy is above the  $J/\psi\psi(3770)$  threshold. At this time, apart from the normal threshold effect caused by  $D\bar{D}$ , anomalous threshold may also give a considerable contribution as in Fig. 93 (a), which will lead to an enhancement around 6.98 GeV as in Fig. 93 (b). However, when substituting this mechanism into the fit, Ref. [790] found that the triangle diagram contributions are small, and the reason might be that the peak position through anomalous threshold contribution is roughly 60 – 80 MeV above the  $X(6900)$  peak, and hence the fit does not like it. In addition, from Yukawa's theorem [811], the direct exchanges of charmed mesons between charmonia is still a short-distance interaction with effective range about  $\hbar c/m_D \approx 0.1$  fm, which, in our view, is a little unnatural to be used under the hadronic level. A similar discussion can be also used for Ref. [791], where exchanged bosons there are charmonia. While if not, the contact four particle interaction, i.e.,  $J/\psi J/\psi DD$  in Fig. 92 will still have detailed information loss on the interaction mechanism.

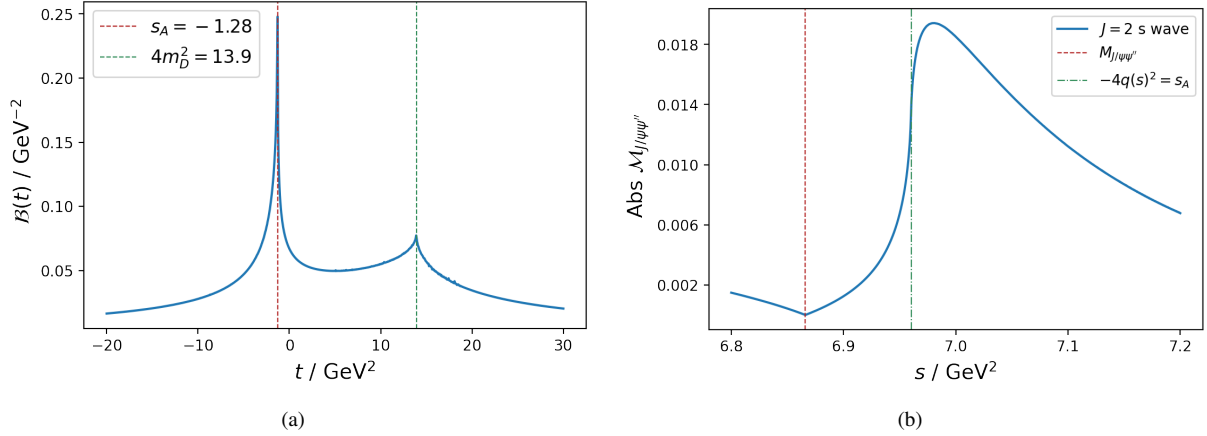


Figure 93: (a): Triangle diagram contribution, with  $t$  as the Mandelstam variable. Here, the left sharp peak is caused by the anomalous threshold, while the small one on the right is due to normal threshold effect. (b): The enhancement of the  $J/\psi\psi(3770)$  scattering amplitude from the triangle diagram. [790].

Nevertheless, in our view, such  $D$  loop mechanism can absolutely be viewed as an important application of the unquenched effect. Since the fully charmed tetraquark states are observed in the di- $J/\psi$  spectrum, it is natural to image that in the experimental detector, the amount of charmonia is extremely abundant. These charmonia, especially the ones above the open-charm threshold, may have large probabilities to oscillate between itself and a pair of charmed mesons in the unquenched picture. Thus, there indeed exists environment for the happening of such a mechanism, and the contribution of it may be not negligible. Guided by this motivation, Ref. [812] proposed a new mechanism for the interactions between charmonia, where both the charmonia can oscillate into a pair of charmed mesons, and light mesons can exchange between these intermediate charmed mesons, as in Fig. 94. At this time, due to conservation of  $C$ -parity, the exchanged light mesons can only be  $\eta$  and  $\sigma$ . In addition, due to the heavy quark symmetry, all the coupling constants can be previously determined.

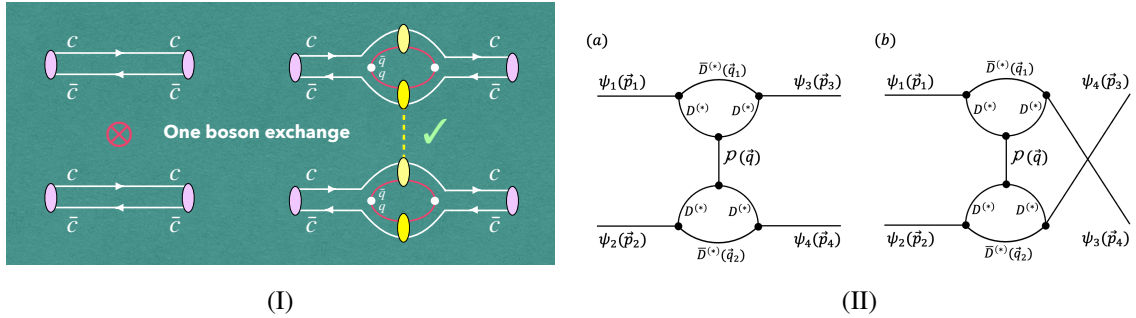


Figure 94: (I) A novel approach enabling one-boson exchange for effective charmonium scattering. The cross symbol on the left indicates that direct light flavor one-boson exchange ( $\pi, \rho, \sigma, \dots$ ) cannot occur. (II) The scattering mechanisms of the  $\psi_1\psi_2 \rightarrow \psi_3\psi_4$  process involve  $D$  meson loop-s, with diagram (a) representing the  $t$ -channel contribution and diagram (b) representing the  $u$ -channel contribution. Here,  $\psi_i$  can be  $J/\psi$ ,  $\psi(3686)$ , or  $\psi(3770)$ , and  $\mathcal{P}$  can be  $\eta$  or  $\sigma$ . Furthermore, when  $\psi_1 = \psi_2$  and  $\psi_3 = \psi_4$ , there is no  $u$ -channel contribution [812].

To illustrate the effectiveness of this mechanism, Ref. [812] applies this mechanism on the experimental data from CMS with both  $0^{++}$  and  $2^{++}$  configurations, and the result is presented in Fig. 95. Obviously, for either  $0^{++}$  or  $2^{++}$  configuration, the fit results are good, while the  $\chi^2/\text{d.o.f.}$  suggests a slight preference for the  $0^{++}$  configuration. In addition, for the peak around 6.9 GeV, an explicit twist can be found, and the reason is easy to see from the sharp but narrow peak around 6.865 GeV in the  $J/\psi\psi(3770)$  channel. Such an effect generates because when the scattering energy reach up to the  $J/\psi\psi(3770)$  threshold, rescattering between coupled channels exceed the branch point located at the  $J/\psi\psi(3770)$  threshold, which can cause a cusp at this threshold [742]. In addition, since  $\psi(3770)$  can be a real

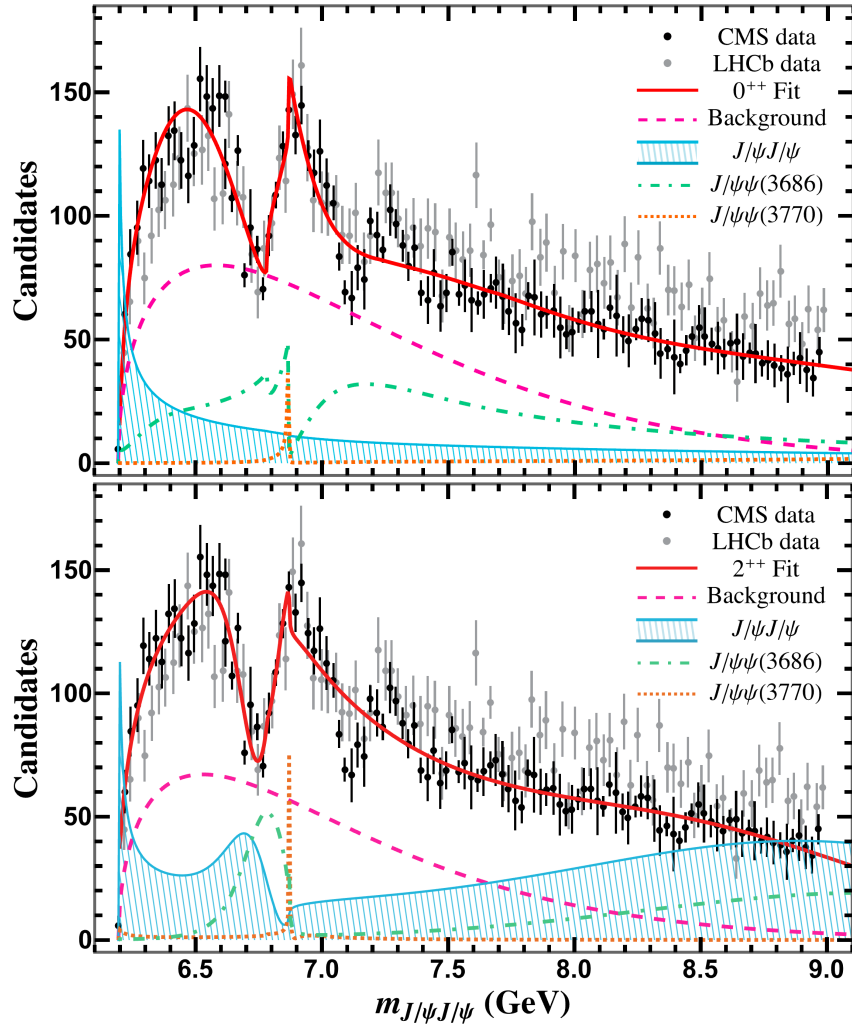


Figure 95: The fit results on experimental data are presented, with the top panel for  $0^{++}$  configuration and the bottom panel for  $2^{++}$  configuration. In each panel, the dark and light grey error bars represent the CMS data and LHCb data respectively, and the red solid line indicates the fit result. The magenta dashed line, light blue line filled with shadows, light green dot-dashed line, and orange dotted line show the contributions of background,  $J/\psi J/\psi$  channel,  $J/\psi(3686)$  channel, and  $J/\psi(3770)$  channel, respectively [812].

particle at this time, when the two charmed mesons linked with it are  $D\bar{D}$ , the branch point located at  $D\bar{D}$  threshold is simultaneously triggered, which may result into further enhancements, and consequently modifies the shape of the peak near 6.9 GeV and becomes a crucial feature of this mechanism. Furthermore, from the extracted pole positions, it is found that for either  $0^{++}$  or  $2^{++}$  configurations, there always exists a states below the  $J/\psi J/\psi$  threshold. In addition,  $X(6600)$  is not a real physical state but an effect of interference, while the dip around 6.8 GeV correspond to a pole mainly generated by the  $J/\psi\psi(3686)$  channel. Also, the peak around 6.9 GeV is dominantly generated by a physical state emerging from the  $J/\psi\psi(3770)$  channel. Last but not least, after analyzing the contributions from different light meson exchanges, it is found that the  $\sigma$  exchange dominants, which is consistent with the usual experience on one boson exchange model.

Absolutely, the mechanism proposed by Ref. [812] answers a critical issue that how traditional one boson exchange model is introduced in understanding the charmonia scattering. Also, it gives a more refined description on the interaction vertex between charmonia and light mesons, which can make all the coupling constants previously determined. Furthermore, due to the heavy quark symmetry, such a mechanism should also exist in  $\Upsilon\Upsilon$ ,  $J/\psi\Upsilon$ ,  $\chi_{bJ}\chi_{bJ}$ ,  $\chi_{cJ}\chi_{bJ}$  channels, which can result into the generations of near threshold states. However, such a mechanism still have some problems to be solved, one is for the suppression on the loop, especially in Fig. 94 the diagrams contain two loops, which may be further suppressed and make the practical contribution not considerable, another is that, there still exists many undetermined parameters in this model, especially the cutoff parameters from the form factors in both loops and exchanged light mesons, which may also lead to large uncertainties on the contributions. Nevertheless, such a mechanism also make a step to a deeper understanding on the scattering mechanisms in fully heavy hadron systems, although further investigations are eager to be carried on to clarify the importance of this mechanism.

### 6.5. Lattice QCD result of interactions involved in fully heavy hadrons

After observing these enhancement structures in the di- $J/\psi$  invariant mass spectrum [84, 86, 85, 88], some lattice QCD research groups joined the effort. For the scattering between  $S$ -wave charmonia, Ref. [813] performed a lattice QCD calculation of the single-channel  $S$ -wave scattering length in the  $0^{++}$  sector of  $\eta_c\eta_c$  and the  $2^{++}$  sector of  $J/\psi J/\psi$ . However, the result indicates that the interactions between the two charmonium pairs are repulsive in both cases, making  $2^{++}$  states below the  $J/\psi J/\psi$  threshold disfavored in lattice QCD. This finding was subsequently confirmed by another lattice QCD study in Refs. [814, 815], where an additional investigation on the  $0^{++}$  sector of  $J/\psi J/\psi$  scattering reveals an attractive interaction, suggesting a  $0^{++}$  virtual state located 20-40 MeV below the threshold. In addition, although the  $2^{++}$  sector of  $J/\psi J/\psi$  scattering is repulsive, a  $2^{++}$  resonance compatible with the  $X(6600)$  is found [814, 815]. Although there is still a long way to go before drawing a conclusion on charmonium scattering from lattice QCD results, this information can provide useful hints for understanding charmonium scattering.

The interactions involving fully heavy hadrons have recently become a topic of interest for lattice QCD research groups [91, 92, 813, 814, 815, 816, 817, 818]. As two primary approaches in lattice QCD for studying hadron-hadron interactions, the HAL QCD method is applied to obtain an energy-independent, non-local potential by analyzing the spatiotemporal correlations between two hadrons [91, 92, 816]. For example, the  $S$ -wave  $c\bar{c}-N$  potentials were extracted at  $t/a = 13, 14,$  and  $15$  for  $J/\psi-N$  with  $^4S_{3/2}$  and  $^4S_{1/2}$  and  $\eta_c-N$  with  $^3S_{1/2}$  (see Fig. 96 for the details of these potentials) [91]. The HAL QCD method has also been employed to extract the potential of  $\Omega_{ccc}-\Omega_{ccc}$  in the  $^1S_0$  channel [92] as illustrated in Fig. 97. These findings provide a window into understanding how fully heavy hadrons interact with each other or with other hadrons.

Returning to the theme of this review—unquenched charmonium—may offer a unique perspective for understanding the underlying mechanisms. Based on the experience from nuclear force studies, the one-boson exchange model [811, 819, 820] has been regarded as an effective approach for investigating hadronic interactions, with numerous applications over the past years in the study of new hadronic states (see review papers [16, 19, 21, 17, 23, 26, 244, 28, 29, 247] for more details). However, when applying this model to interactions involving fully heavy hadrons, the one-boson exchange model encounters a difficulty: no light bosons can be exchanged to mediate the interaction between hadrons. In such cases, one often attempts to introduce extremely short-range exchange contributions [742, 743, 779, 784, 780, 781, 783, 782]. However, this picture is inconsistent with our understanding of low-energy strong interactions. In studying the interactions of charmonia, as introduced in the previous section, an interaction mechanism based on the unquenched picture [812] offers a promising alternative. More importantly, such an unquenched mechanism may serve as a universal framework for studying interactions involving all types of fully heavy hadrons.

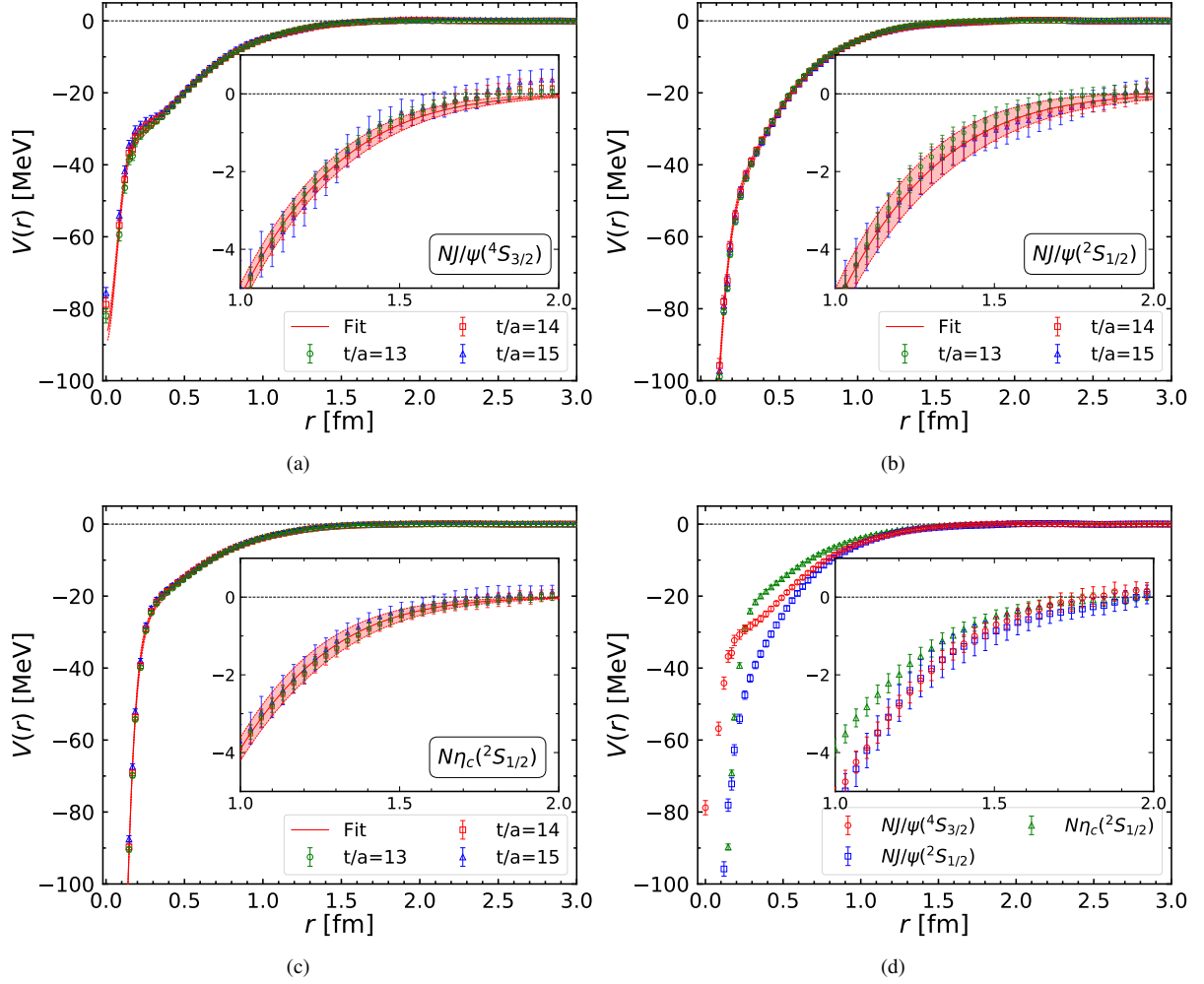


Figure 96: The S-wave  $N$ - $c\bar{c}$  potential extracted at  $t/a = 13, 14$ , and  $15$  for  $N$ - $J/\psi$  with  $^4S_{3/2}$  (a), with  $^2S_{1/2}$  (b), and  $N$ - $\eta_c$  with  $^2S_{1/2}$  (c). The red bands show the fit results with phenomenological three-range Gaussians at  $t/a = 14$ . The three potentials at  $t/a = 14$  are also shown in (d) for a direct comparison. A magnification is shown in the inset for each panel [91].

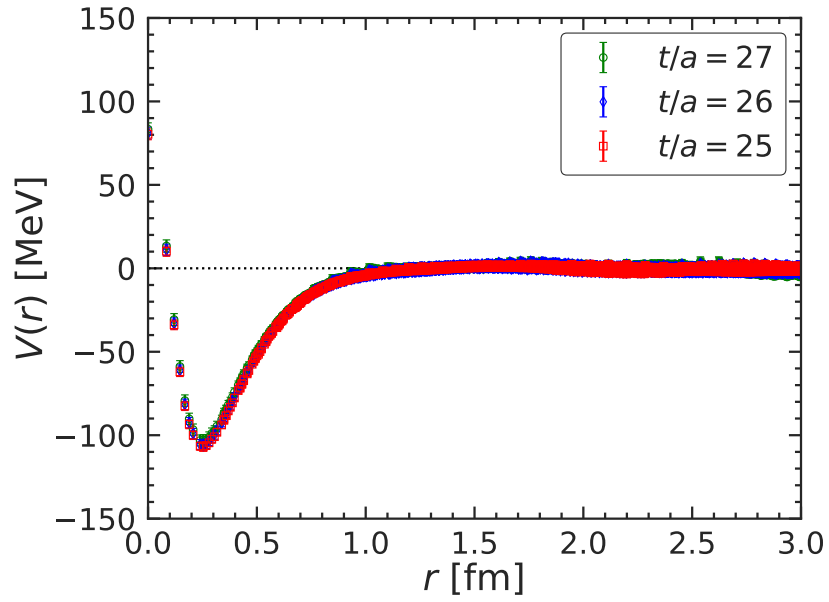


Figure 97: (Color online). The  $\Omega_{ccc}-\Omega_{ccc}$  potential  $V(r)$  in the  $^1S_0$  channel as a function of separation  $r$  at Euclidean time  $t/a = 25$  (red square), 26 (blue diamond) and 27 (green circle).

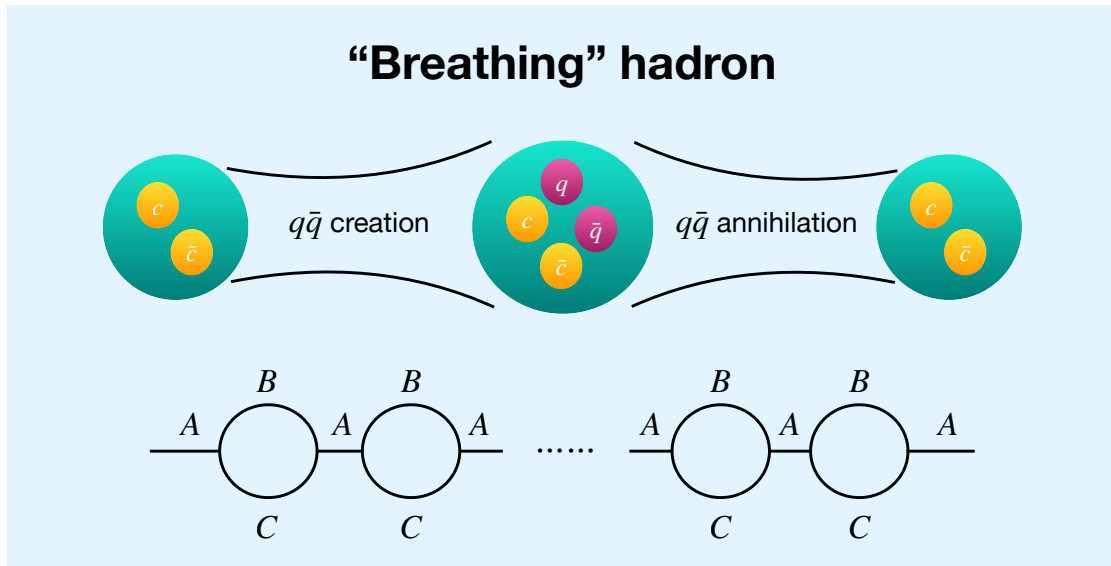


Figure 98: Breathing hadron inspired by unquenched picture.

Thus, for fully heavy hadrons, we cannot treat them as static objects. According to the unquenched picture, fully heavy hadrons can couple to corresponding hadron channels via the heavy quarks capturing the sea quarks created from the vacuum. Of course, the light quarks in these hadron channels can also annihilate, transitioning back to a fully heavy hadron state. Such a process can occur repeatedly, much like a "breathing" object, as illustrated in Fig. 98. This picture provides a clear and universally applicable microscopic mechanism for the hadronic interactions involving fully heavy hadrons. Since the intermediate hadron channels contain light quarks, the one-boson exchange mechanism can still play a role in understanding these interactions involving fully heavy hadrons (see Fig. 94 for the application of this mechanism to charmonium interactions). With more experimental data, lattice QCD results, and corresponding phenomenological studies, we believe this research issue is valuable and merits sustained attention.

## 7. Extension to $\Upsilon$ family and light flavor vector mesonic states

### 7.1. Universality of vector mesonic structures in $e^+e^-$ annihilation

In particle physics, the  $R$  value is a fundamental observable that has played a pivotal historical role. It is defined as the ratio of the total cross section for electron-positron annihilation into hadrons to the cross section for annihilation into a muon pair at the same center-of-mass energy, i.e.,

$$R \equiv \frac{\sigma(e^+e^- \rightarrow \text{hadrons})}{\sigma(e^+e^- \rightarrow \mu^+\mu^-)}. \quad (67)$$

Fig. 99 displays the measured  $R$  values as a function of the center-of-mass energy  $\sqrt{s}$ , ranging from low energies (around 1 GeV) to high energies (up to several hundred GeV). The data exhibit the characteristic step-like structure predicted by the quark-parton model, with distinct steps at the charm and bottom quark thresholds. Narrow resonances such as the  $J/\psi$  and  $\Upsilon$  families appear as sharp peaks. Above the  $Z$  boson resonance, the ratio is dominated by  $Z$  boson exchange and by the interference between photon and  $Z$  exchange.

Section 4 reviews how unquenched effects play a crucial role in the charmonium sector for resolving the so-called  $Y$  problem [132]. A unified framework can be established to understand the puzzling phenomena associated with charmonium-like  $Y$  structures produced directly in  $e^+e^-$  collisions. Indeed, a remarkable universality emerges across different flavor sectors when examining vector mesonic structures in  $e^+e^-$  annihilation.

Prominent examples include the anomalous  $Y(4260)$  observed in  $e^+e^- \rightarrow J/\psi\pi^+\pi^-$  [51] (later resolved into two substructures by BESIII [55]), the  $Y(2175)$  seen in  $e^+e^- \rightarrow \phi\pi^+\pi^-$  [822] as a typical light-flavor strangeonium-like state, and the  $\Upsilon(10860)$  produced in  $e^+e^-$  annihilation into  $\Upsilon(nS)\pi^+\pi^-$  ( $n = 1, 2, 3$ ) [79, 565, 566]. These states have been the subject of extensive theoretical investigations [823, 824, 825, 153, 568, 300].

Their similar phenomenological behaviors and analogous decay patterns suggest a possible universal dynamical mechanism related to unquenched effects. Building on insights gained from addressing the  $Y$  problem in the charmonium sector, it is plausible that a unified approach based on unquenched effects can be extended to explain these vector mesonic structures across light-flavor, charmonium, and bottomonium sectors. The following sections extend this unquenched analysis systematically to the bottomonium family and light-flavor vector mesonic states.

### 7.2. Higher bottomonia in the unquenched picture

#### 7.2.1. Higher bottomonium

As a prominent member of the heavy quarkonium family, bottomonium holds a unique position in hadron spectroscopy, offering crucial insights into the strong-interaction dynamics governed by QCD. Over the past decades, concerted experimental and theoretical efforts have been dedicated to studying bottomonium, resulting in a series of discoveries that have greatly enriched our knowledge of its spectral properties. The discovery of the  $\Upsilon(1S)$  state in 1977 [469], which first established the existence of the bottom quark, was followed by the gradual mapping of a rich spectrum of bottomonium resonances. Subsequent experiments identified a sequence of radially excited  $\Upsilon(nS)$  states ( $n = 2-6$ ) [826, 563, 562], as well as the  $P$ -wave spin-triplet states  $\chi_{bJ}(1P)$  and  $\chi_{bJ}(2P)$  ( $J = 0, 1, 2$ ) almost four decades ago [827, 828, 829, 830].

The experimental landscape of bottomonium physics has advanced considerably in recent years, thanks to improved capabilities at the  $B$ -factories BaBar and Belle, the upgraded Belle II experiment, and the high-energy collisions at the LHC. A number of new states have been firmly established, including the pseudoscalar ground state

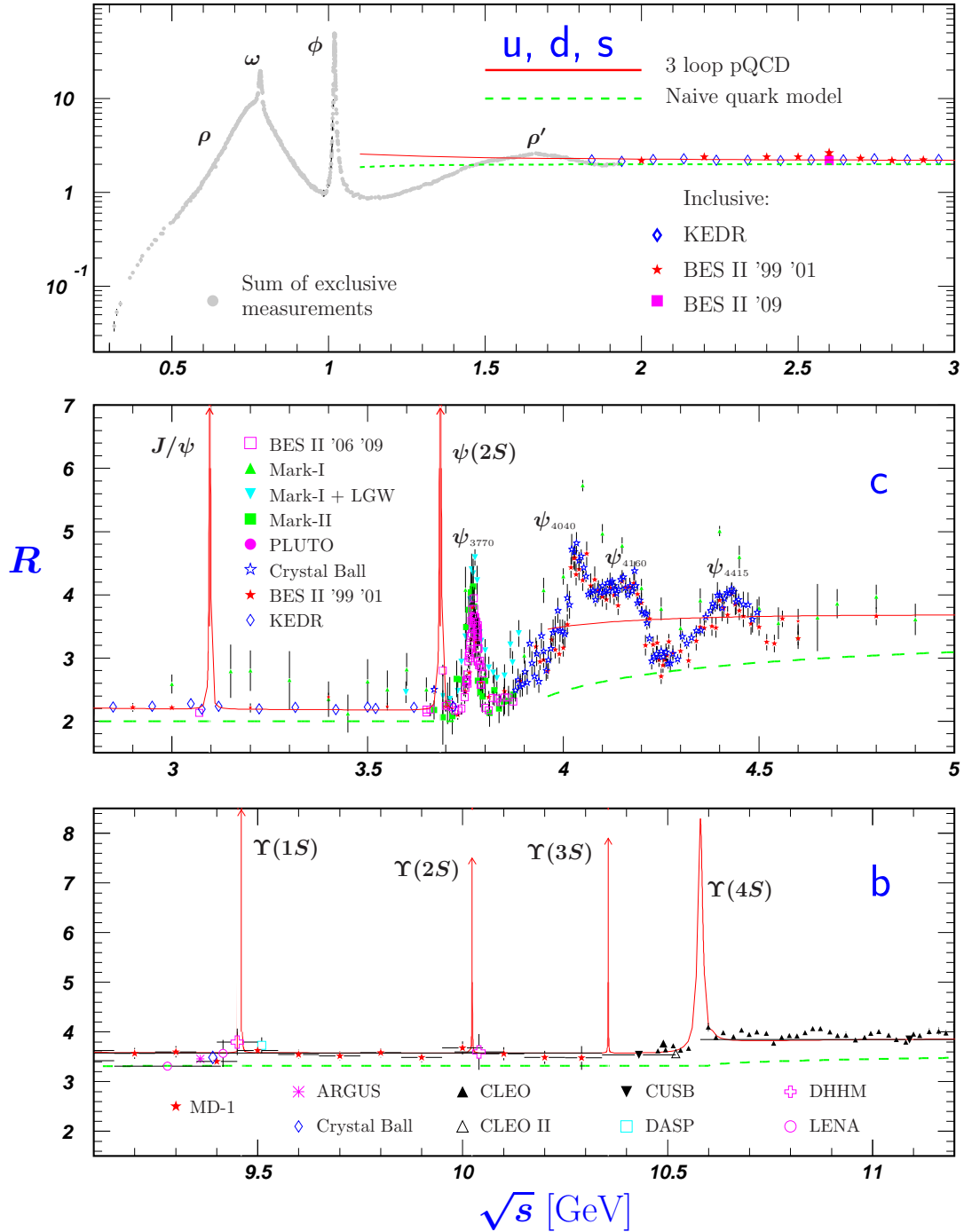


Figure 99: The  $R$  value as a function of center-of-mass energy  $\sqrt{s}$  from various experiments. The step-like structure corresponds to the opening of new quark flavor thresholds, while sharp peaks indicate vector meson resonances. Notable structures include the  $\phi(1020)$ ,  $J/\psi$ ,  $\psi(2S)$ ,  $\Upsilon$  family, and the  $Z$  boson. The regions containing the anomalous  $Y$  structures discussed in this work are highlighted. Figure adapted from [821].

$\eta_b(1S)$  [831, 832, 833, 134], its first radial excitation  $\eta_b(2S)$  [834, 833, 134], the  $P$ -wave excitations  $\chi_{b1}(3P)$  [835, 836],  $h_b(1P)$  [836, 837],  $h_b(2P)$  [837], the  $D$ -wave state  $\Upsilon(1^3D_2)$  [838, 839], and the puzzling  $\Upsilon(10753)$  [566]. This wealth of experimental data offers an excellent testing ground for phenomenological models of bottomonium spectroscopy [840, 841, 842, 13, 843, 844, 139, 140, 845, 846, 847, 848, 849, 850, 316, 851, 852, 853, 854, 855, 856, 328, 311, 857, 858].

As in the charmonium sector, quenched potential models—notably the GI model [13, 854]—provide a satisfactory description of the low-lying bottomonium spectrum. However, they systematically overpredict the masses of higher-lying states when compared with experimental measurements. A clear example is the  $\Upsilon(6S)$  state, whose predicted mass in the GI model exceeds the measured mass of the  $\Upsilon(11020)$  by about 100 MeV, as illustrated in Table 13. Such discrepancies highlight the increasing relevance of unquenched effects, which become more pronounced for excited states with larger spatial extensions.

Table 13: A comparison of the mass of the  $\Upsilon(11020)$  state among the modified GI (MGI) model, the original GI model, and experimental measurements.

Theory vs. Experiment	MGI [328]	GI [13, 854]	Experiment [94]
Mass (MeV)	11001	11102	$11000 \pm 4$

In Sec. 4, it has been demonstrated that a series of  $Y$  structures in the 4.0–4.7 GeV region can be successfully described within the charmonium spectrum once unquenched effects are incorporated into the GI model. Specifically, the linear confining term is modified as  $br \rightarrow b(1 - e^{-\mu r})/\mu$ , which softens the potential at large distances due to vacuum polarization induced by light-quark pair creation [474, 475]. Although meson–meson channels are not explicitly included, this phenomenological treatment effectively mimics coupled-channel dynamics and thus represents an unquenched correction to the conventional quenched potential.

Inspired by the success of this screened potential in resolving the long-standing “ $Y$  problem” in charmonium(-like) sector, it is natural to expect analogous unquenched effects to be important for high-lying bottomonium spectroscopy. Following this motivation, in Ref. [328], Wang, Sun, Liu, and Matsuki introduced the same screening mechanism into a modified GI model to reanalyze the bottomonium spectrum. The screening parameter  $\mu = 0.075$  GeV and other parameters are determined by a  $\chi^2$  fit to well-established experimental bottomonium states.

Using the fitted parameters of the modified GI model, the bottomonium spectrum can be calculated systematically. The resulting masses, together with the original GI predictions and available experimental data, are displayed in Fig. 100. For low-lying states, the GI model typically yields masses of 10 ~ 20 MeV below the experimental values, whereas the modified GI model shows noticeably better agreement. In contrast, for higher-lying states, the quenched GI model systematically overestimates the masses, in which a representative case is  $\Upsilon(11020)$  and its measured mass is nearly 100 MeV lower than the GI prediction. This discrepancy is largely resolved once screening effect is included. Notably, the recently observed  $\Upsilon(10753)$  [566] can be naturally interpreted within this framework as a  $4S$ - $3D$  mixed state with dominant  $3D$  character, consistent with expectations from the unquenched potential model. A detailed discussion of this assignment will be given in subsequent sections. Overall, these results indicate that the unquenched potential model effectively remedies the shortcomings of the quenched approach and provides a more accurate and unified description of the bottomonium spectrum. Moreover, as shown in Sec. 4, the results from the screening potential model and the coupled-channel model are compatible in the charmonium sector. This compatibility also holds in the bottomonium sector, as illustrated in Fig. 101, further underscoring the equivalence of these two unquenched formulations.

An exception is  $\Upsilon(10860)$ , for which the predicted mass of  $\Upsilon(5S)$  in the present work lies about 60 MeV below the experimental value. It is noteworthy that measurements reported by BaBar and Belle after 2010 tend to be roughly 30 MeV higher than earlier determinations [94], as illustrated in Fig. 54. In addition, the total width of  $\Upsilon(10860)$  measured by Belle differs from earlier results that suggested a rather broad state. Furthermore, the cross section data for  $e^+e^- \rightarrow \Upsilon(nS)\pi^+\pi^-$  ( $n = 1, 2, 3$ ) around 10.88 GeV from Belle do not appear to be fully described by a single  $\Upsilon(10860)$  resonance [566]. Similar difficulties in reproducing the  $\Upsilon(5S)$  mass are encountered in other non-relativistic potential models that incorporate screening effects [139, 850, 856], indicating that a complete understanding of this state remains an open issue.

By taking the obtained mass spectra and the corresponding spatial wave function as input, Ref. [328] further

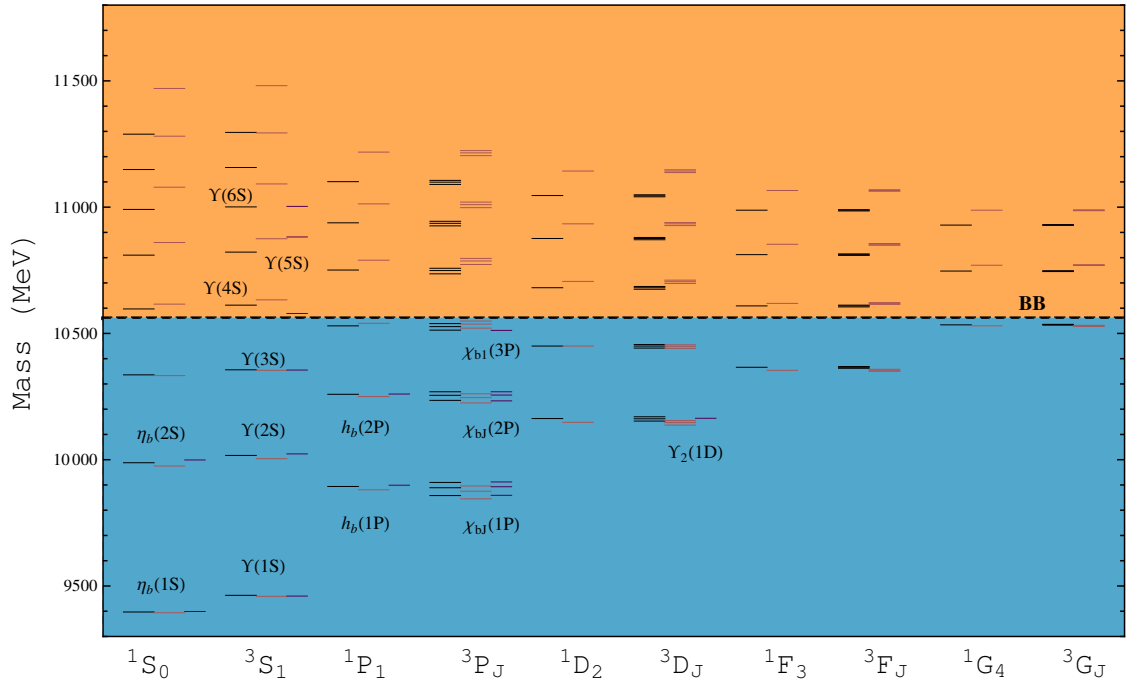


Figure 100: Bottomonium mass spectrum. From left to right: predictions of the modified GI model [328] (black lines), original GI model [13, 854] (pink lines), and experimental values from the PDG [859] (purple lines). The open-bottom threshold is indicated by the dashed line. Figure adapted from Ref. [328].

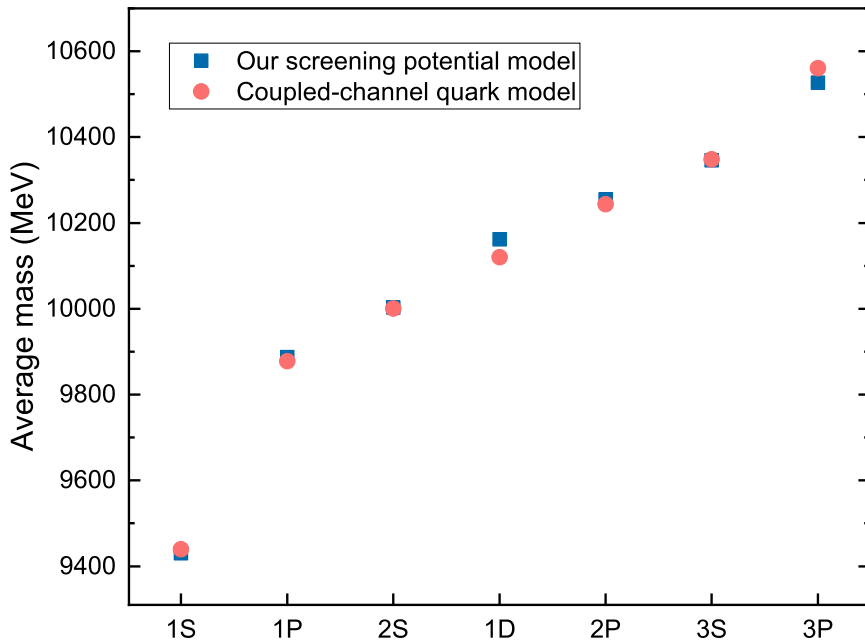


Figure 101: A comparison of the results of screening potential model and those obtained by a coupled-channel quark model [316] for bottomonium spectra. The figure is adapted from Ref. [328].

systematically calculated partial widths for allowed radiative transitions, annihilation decays, hidden-bottom hadronic transitions, and open-bottom two-body strong decays for each bottomonium state, providing useful benchmarks for future experimental searches.

### 7.2.2. Anomalous hidden-bottom decay phenomena of several high-lying bottomonia

While the rich spectrum of higher bottomonium states reflects the importance of unquenched effects in spectroscopy, their decay properties provide an equally complementary window into the underlying dynamics. In particular, several anomalous exclusive hidden-bottom transitions of high-lying bottomonium states have been observed, highlighting the role of unquenched effects in their decay dynamics.

Prior to the high-precision measurements from the  $B$ -factories, the QCD multipole expansion (QCDME) approach had been established as a reliable theoretical framework for studying hadronic transitions among low-lying heavy quarkonia [860, 861, 862, 863, 864, 865, 131, 866, 77, 867]. This method relies on the clear separation of energy scales in heavy-quark systems: the spatial size of the quarkonium is small compared with the wavelength of the emitted soft gluons, allowing the heavy quarkonium system to be regarded as a compact color source emitting soft gluons, and thereby permitting a multipole expansion of the gluon field analogous to that in classical electrodynamics. As depicted in Fig. 102, the transition amplitude factorizes into a multipole gluon emission (MGE) part—which depends on the quarkonium wave function—and a subsequent hadronization ( $H$ ) part, where the emitted gluons form light hadron(s) at the scale of light-flavor dynamics.

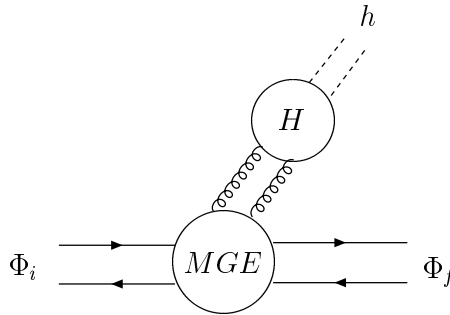


Figure 102: Schematic diagram for a typical hadronic transition in the QCDME approach. Here, MGE denotes multipole gluon emission from the heavy quark–antiquark pair, and  $H$  represents the hadronization of the emitted gluons into light hadron(s). Figure adapted from Ref. [867].

However, with the accumulation of high-precision data from Belle and BaBar, several unexpected features have emerged in the hadronic transitions of heavy quarkonia, especially above the open-flavor thresholds. These observations pose serious challenges to the conventional QCDME picture.

Anomalous decay features have been observed in several transitions of the  $\Upsilon(10580)$  state. One representative manifestation is found in the dipion invariant mass spectrum measured by the BaBar Collaboration [130]. As shown in Fig. 103, the measured  $m_{\pi^+\pi^-}$  distribution for  $\Upsilon(10580) \rightarrow \Upsilon(1S)\pi^+\pi^-$  is broadly consistent with the line shape predicted by the QCDME approach [131]. However, the corresponding distribution for  $\Upsilon(10580) \rightarrow \Upsilon(2S)\pi^+\pi^-$  exhibits a pronounced deviation from the QCDME predictions.

Another class of anomalies arises in the transitions  $\Upsilon(nS) \rightarrow \Upsilon(1S)\eta$  ( $n \geq 2$ ). Within the QCDME framework, such processes are expected to be highly suppressed due to the spin-flip effects of the heavy quarks [131]. The ratio

$$R(n) = \frac{BR[\Upsilon(nS) \rightarrow \Upsilon(1S)\eta]}{BR[\Upsilon(nS) \rightarrow \Upsilon(1S)\pi^+\pi^-]}, \quad (68)$$

is typically of the order  $\mathcal{O}(10^{-3})$ , in good agreement with the QCDME expectations for  $n = 2, 3$ . However, the Belle Collaboration reported a significantly enhanced decay rate for  $\Upsilon(4S) \rightarrow \Upsilon(1S)\eta$  [567], with the corresponding ratio determined to be  $R(4) = 2.41 \pm 0.40 \pm 0.12$ , which is about two orders of magnitude larger than the QCDME prediction.

In addition, the OZI-suppressed spin-flip transition  $\Upsilon(4S) \rightarrow h_b(1P)\eta$  has been found to have the largest non- $B\bar{B}$  branching fraction among known  $\Upsilon(4S)$  hadronic transitions [868], even though spin-flipping processes are generally expected to be power suppressed [867, 869].

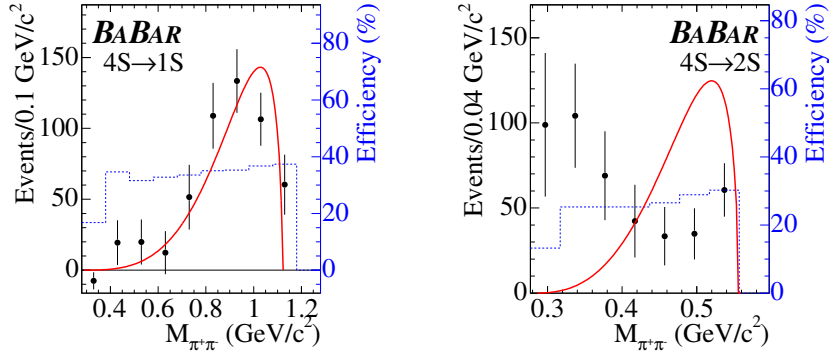


Figure 103: Measured dipion invariant mass distributions for the processes  $\Upsilon(10580) \rightarrow \Upsilon(nS)\pi^+\pi^-$  ( $n = 1, 2$ ), compared with the predictions of the QCDF approach. The figure is adapted from Ref. [130].

Anomalous decay behaviors have also been reported in the transitions of the  $\Upsilon(10860)$  state, as discussed in Sec. 5. In particular, the hidden-bottom dipion transitions  $\Upsilon(10860) \rightarrow \Upsilon(nS)\pi^+\pi^-$  ( $n = 1, 2, 3$ ) exhibit anomalously large partial widths. As summarized in Table 8, the decay rates for  $\Upsilon(10860) \rightarrow \Upsilon(1S, 2S)\pi^+\pi^-$  are approximately two orders of magnitude larger than those of conventional dipion transitions  $\Upsilon(mS) \rightarrow \Upsilon(nS)\pi^+\pi^-$  with  $n < m \leq 4$ . For lower-lying bottomonium states, both the magnitudes of the dipion transition rates and the associated invariant mass distributions are well described within the QCDF framework. By contrast, the exceptionally large widths of  $\Upsilon(10860) \rightarrow \Upsilon(nS)\pi^+\pi^-$  ( $n = 1, 2, 3$ ) clearly exceed the expectations of QCDF. Moreover, similar to the situation encountered in the  $\Upsilon(10580)$  transitions, the experimentally measured dipion invariant mass spectra in the  $\Upsilon(10860)$  decays exhibit pronounced deviations from the typical QCDF patterns. Anomalous behaviors are also observed in spin-flipping transitions. The Belle Collaboration reported the processes  $\Upsilon(10860) \rightarrow h_b(nP)\pi^+\pi^-$  ( $n = 1, 2$ ) with branching fractions at the level of  $\mathcal{O}(10^{-3})$  [837], which are significantly larger than the corresponding upper limits for  $\Upsilon(3S) \rightarrow h_b(nP)\pi^+\pi^-$  ( $n = 1, 2$ ) measured by the BaBar Collaboration [870]. As discussed in Sec. 5, these enhanced transition rates are closely correlated with the experimentally observed  $Z_b$  structures, which can be naturally understood within the ISPE mechanism. In addition, the Belle Collaboration observed the OZI-suppressed transitions  $\Upsilon(10860) \rightarrow \chi_{bJ}\omega$  ( $J = 0, 1, 2$ ) [871], whose measured branching fractions are also at the level of  $\mathcal{O}(10^{-3})$ , far exceeding naive expectations.

### 7.2.3. A global description of the anomalous bottomonium decays via the hadronic loop mechanism

In light of these anomalous transitions observed in experiments, numerous efforts have been devoted to elucidating their underlying mechanisms, including improvements to the QCDF approach [867] and exotic interpretations of the  $\Upsilon(5S)$ , such as tetraquark scenarios [570, 571, 572]. In particular, Ref. [872] successfully reproduced the anomalous dipion invariant-mass spectra in the processes  $\Upsilon(10580) \rightarrow \Upsilon(1S/2S)\pi^+\pi^-$  by introducing an additional sequential decay mechanism,  $\Upsilon(10580) \rightarrow \pi X \rightarrow \Upsilon(1S/2S)\pi^+\pi^-$ , together with the  $\pi\pi$  final-state interaction, where  $X$  denotes an intermediate  $b\bar{b}q\bar{q}$  state.

Beyond such extensions, the hadronic loop mechanism, as outlined in Sec. 2, offers a global framework to account for all the anomalous transitions discussed above. An important reason why the QCDF works well for low-lying states but fails for high-lying ones may be attributed to the increasing importance of long-distance final state interactions associated with unquenched effects. For low-lying bottomonium, such contributions are not obvious because their masses lie far below the open-flavor  $B\bar{B}$  threshold [143]. In contrast, for high-lying bottomonium states close to or above the open-flavor threshold, long-distance effects will become dominant, and some of the power counting rules underlying the QCDF approach may break down. In the following, a concise review within this mechanism will be presented.

**7.2.3.1. Dipion transitions of  $\Upsilon(10580)$  and  $\Upsilon(10860)$ .** Analyses of the transitions  $\Upsilon(10580/10860) \rightarrow \Upsilon(1S/2S)\pi^+\pi^-$  within the hadronic loop mechanism have been carried out in Ref. [153, 568, 78, 576]. As illustrated in Fig. 55, the initial states  $\Upsilon(10580)$  and  $\Upsilon(10860)$  first decay into a  $B^{(*)}\bar{B}^{(*)}$  pair, which subsequently undergoes a rescattering process. Through the exchange of a  $B^{(*)}$  meson, the intermediate  $B^{(*)}\bar{B}^{(*)}$  converts into a lower  $\Upsilon$  state accompanied by

Table 14: Transition widths, in units of keV, for the processes  $\Upsilon(4S, 5S) \rightarrow \Upsilon(nS)\pi^+\pi^-$  and  $K^+K^-$ . The table is adapted from Ref. [153].

	from $\sigma$	from $f_0(980)$	total	Experimental data
$\Upsilon(4S) \rightarrow \Upsilon(1S)\pi^+\pi^-$	$0.54^{+0.00}_{-0.00}$	$0.93^{+0.03}_{-0.03}$	$1.47 \pm 0.03$	$1.8 \pm 0.4$
$\Upsilon(4S) \rightarrow \Upsilon(2S)\pi^+\pi^-$	$1.09^{+0.23}_{-0.21}$	$0.05^{+0.00}_{-0.01}$	$1.14^{+0.23}_{-0.21}$	$2.7 \pm 0.8$
$\Upsilon(5S) \rightarrow \Upsilon(1S)\pi^+\pi^-$	$102^{+1+42+21}_{-0-35-9}$	$225^{+1+93+47}_{-1-77-43}$	$327^{+114}_{-97}$	$590 \pm 40 \pm 90$
$\Upsilon(5S) \rightarrow \Upsilon(2S)\pi^+\pi^-$	$385^{+10+164+87}_{-11-135-78}$	$37^{+4+16+9}_{-3-13-7}$	$422^{+187}_{-157}$	$850 \pm 70 \pm 160$
$\Upsilon(5S) \rightarrow \Upsilon(3S)\pi^+\pi^-$	$306^{+78+133+73}_{-64-108-64}$	$13^{+1+6+4}_{-1-4-2}$	$319^{+171}_{-141}$	$520^{+200}_{-170} \pm 100$
$\Upsilon(5S) \rightarrow \Upsilon(1S)K^+K^-$		$32^{+5+13+5}_{-5-11-6}$	$32^{+15}_{-13}$	$67^{+17}_{-13} \pm 13$

a scalar meson,  $\sigma/f_0$ , which then decays into a  $\pi^+\pi^-$  pair. In this picture, the initial and final states are dynamically connected by a hadronic loop composed of  $B^{(*)}$  mesons.

As shown in Table 14, the obtained branching ratios for  $\Upsilon(10580, 10860) \rightarrow \Upsilon(1S, 2S)\pi^+\pi^-$  are in good agreement with the available experimental measurements. A consistent description is also obtained by incorporating the coupled-channel effects [873, 874]. Moreover, the much larger transition rates of  $\Upsilon(10860)$  relative to those of  $\Upsilon(10580)$  can be mainly attributed to the difference in the available phase space for the open-bottom processes  $\Upsilon(10580, 10860) \rightarrow B^{(*)}\bar{B}^{(*)}$ , which is characterized by the three-momentum  $\vec{p}_1$  of the  $B^{(*)}$  mesons in the initial-state rest frame. With reasonable choices of the model parameters, the ratios of the transition rates are estimated to lie in the range of 200–600 (see Refs. [153, 568] for details).

In particular, Ref. [568] studied the energy distributions of the dipion transitions  $\Upsilon(10860) \rightarrow \Upsilon(1S, 2S, 3S)\pi^+\pi^-$  within the hadronic loop framework. It was found that this mechanism can shift the resonance peak of the  $\Upsilon(10860)$  upward by about 7–20 MeV in the processes  $e^+e^- \rightarrow \Upsilon(1S, 2S, 3S)\pi^+\pi^-$  relative to that observed in the dominant open-bottom channels  $e^+e^- \rightarrow B^{(*)}\bar{B}^{(*)}$ , as shown in Fig. 55. Such an effect provide a possible clue to why the masses of  $\Upsilon(10860)$  extracted from exclusive hidden-bottom decay modes by the BaBar and Belle Collaborations are systematically higher than those obtained from earlier inclusive measurements, and may also be relevant for understanding the difficulties in assigning  $\Upsilon(10860)$  to the previously discussed unquenched spectra.

Besides the magnitudes of the branching ratios, the dipion invariant mass spectra provide crucial information on the underlying decay mechanisms. The  $\pi^+\pi^-$  mass distributions for the processes  $\Upsilon(10580) \rightarrow \Upsilon(1S, 2S)\pi^+\pi^-$  and  $\Upsilon(10860) \rightarrow \Upsilon(1S, 2S)\pi^+\pi^-$  have been analyzed in Refs. [78, 576]. In these studies, both the dominant hadronic loop contributions and the direct decay mechanisms were taken into account, as exemplified by Eq. (52) for the case of  $\Upsilon(10860)$ . By incorporating the interference between the corresponding decay amplitudes, the experimental dipion invariant mass spectra were well reproduced, as shown in Figs. 104 and 57. In addition, the resulting angular distributions for the  $\Upsilon(10860) \rightarrow \Upsilon(1S)\pi^+\pi^-$  transitions are consistent with the available experimental data (the disagreement for  $\Upsilon(10860) \rightarrow \Upsilon(2S)\pi^+\pi^-$  process is related to the  $Z_b$  problem, see Sec. 5 for details), while those for the  $\Upsilon(10580)$  transitions constitute clear theoretical predictions awaiting future experimental tests.

**7.2.3.2.  $\Upsilon(10860)$  and  $\Upsilon(10580)$  transitions with  $\eta$  and  $\omega$  emission.** The transitions  $\Upsilon(10580), \Upsilon(10860) \rightarrow \Upsilon(1S, 2S)\eta$  were studied within the hadronic loop mechanism in Ref. [154]. The corresponding diagram is illustrated in Fig. 105. The resulting partial width for  $\Upsilon(10580) \rightarrow \Upsilon(1S)\eta$  is found to be 2.94 keV. Combined with the partial width of  $\Upsilon(10580) \rightarrow \Upsilon(1S)\pi^+\pi^-$  obtained in the same framework and listed in Table 14, the ratio

$$R(4) = \frac{BR[\Upsilon(10580) \rightarrow \Upsilon(1S)\eta]}{BR[\Upsilon(10580) \rightarrow \Upsilon(1S)\pi^+\pi^-]} \simeq 2.0, \quad (69)$$

is consistent with the experimental measurement.

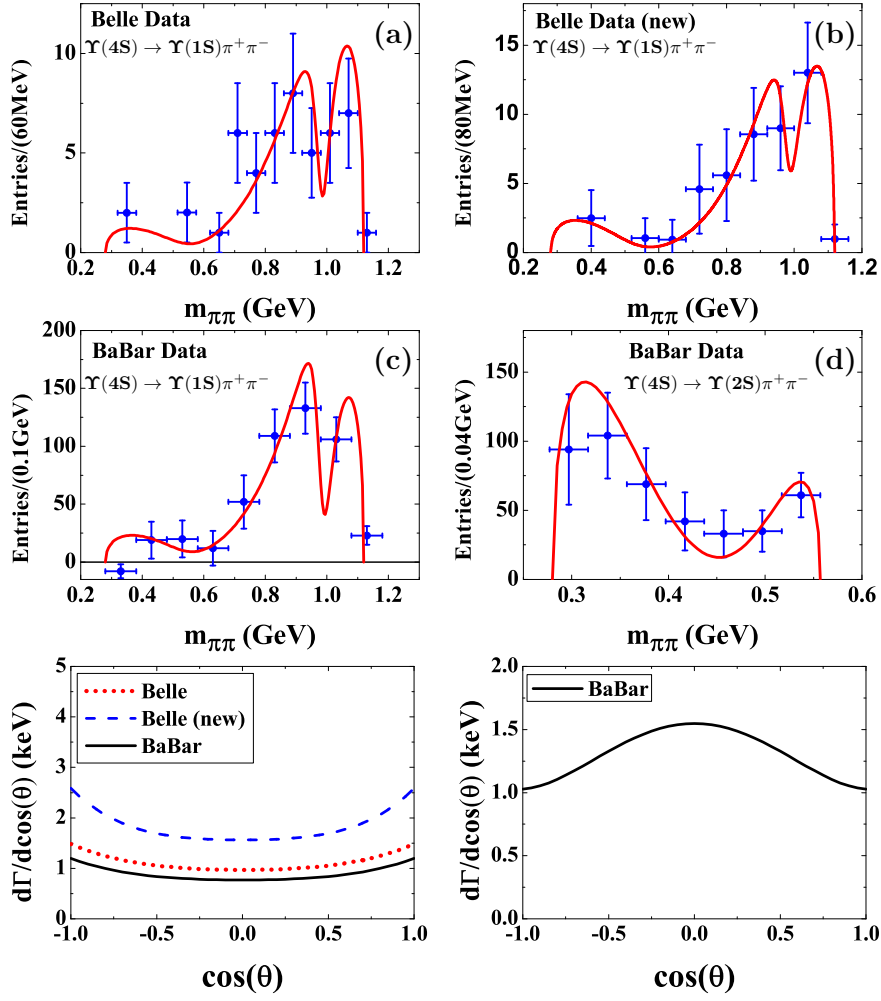


Figure 104: The fitted dipion invariant mass distributions and the corresponding predictions for the angular distributions  $d\Gamma/d\cos\theta$  for  $\Upsilon(10580) \rightarrow \Upsilon(1S)\pi^+\pi^-$  (left panel) and  $\Upsilon(4S) \rightarrow \Upsilon(2S)\pi^+\pi^-$  (right panel). Figure adapted from Ref. [78].

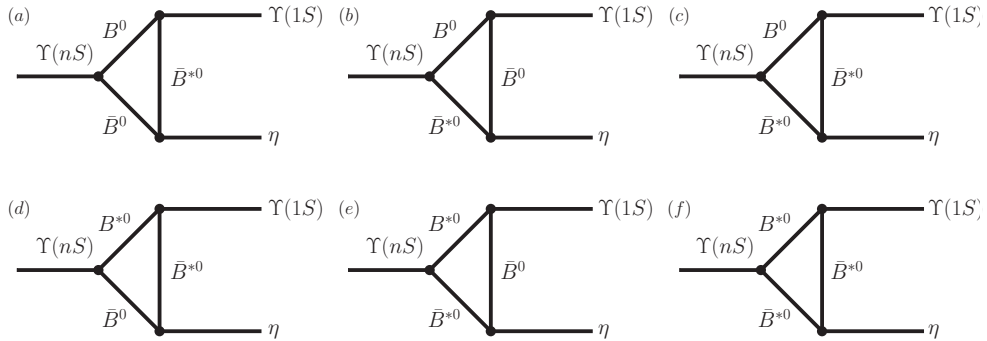


Figure 105: Feynman diagram illustrating the hadronic loop contributions to the transitions  $\Upsilon(10580)$ ,  $\Upsilon(10860) \rightarrow \Upsilon(1S)\eta$ . Figure adapted from Ref. [154].

For the  $\eta$  transitions of the  $\Upsilon(10860)$ , the widths are highly sensitive to the coupling constants  $g_{\Upsilon(5S)B^{(*)}B^{(*)}}$ , due to a substantial cancellation among the contributions from the  $B\bar{B}$ ,  $B\bar{B}^* + \text{c.c.}$ , and  $B^* \bar{B}^*$  channels. Consequently, only a rough estimate can be provided, yielding  $\Gamma(\Upsilon(10860) \rightarrow \Upsilon(1S, 2S)\eta) = 10 - 200 \text{ keV}$ , which correspond to branching fractions in the range  $(0.3-5.4) \times 10^{-3}$  by take  $\Gamma(\Upsilon(10860)) = 37 \text{ MeV}$  as a reference [94]. While recent Belle measurements reported  $BR(\Upsilon(10860) \rightarrow \Upsilon(1S)\eta) = (0.85 \pm 0.15 \pm 0.08) \times 10^{-3}$ , and  $BR(\Upsilon(10860) \rightarrow \Upsilon(2S)\eta) = (4.13 \pm 0.41 \pm 0.37) \times 10^{-3}$  [875], which are in good agreement with the above estimates. One may further consider the ratio

$$R(5) = \frac{BR[\Upsilon(10860) \rightarrow \Upsilon(1S)\eta]}{BR[\Upsilon(10860) \rightarrow \Upsilon(1S)\pi^+\pi^-]} \simeq 0.03 - 0.30, \quad (70)$$

which also encompasses the value measured by the Belle Collaboration,  $R(5) = 0.19 \pm 0.04 \pm 0.01$  [875].

The estimated contributions from virtual hadronic loops to the transitions  $\Upsilon(2S, 3S) \rightarrow \Upsilon(1S)\eta$  are small, with the contribution for  $n = 3$  roughly consistent with the experimental upper limit and that for  $n = 2$  an order of magnitude below the measured value [876]. This indicates that the QCDME mechanism remains dominant for the  $\Upsilon(2S) \rightarrow \Upsilon(1S)\eta$  transition, as expected for a state lying far below the  $B\bar{B}$  threshold.

Ref. [877] investigated the processes  $\Upsilon(10580)$ ,  $\Upsilon(10860)$ ,  $\Upsilon(11020) \rightarrow h_b(1P)\eta$  within the hadronic loop mechanism. The corresponding loop diagrams are shown in Fig. 106. The calculated branching ratios for  $\Upsilon(10580)$  were found to be consistent with the experimental measurements, indicating that hadronic loop effects can substantially enhance spin-flipping hidden-bottom transitions. It was further shown that the predicted branching ratios for  $\Upsilon(10860)$  and  $\Upsilon(11020)$  are approximately one and two orders of magnitude smaller, respectively, than that for  $\Upsilon(10580)$ . This suppression may partially account for the absence of experimental signals for these two processes so far.

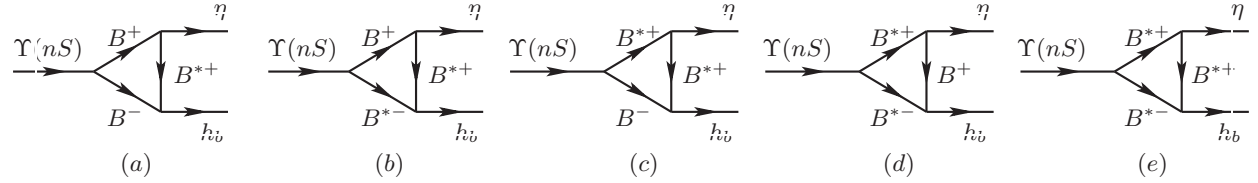


Figure 106: Feynman diagram illustrating the hadronic loop contributions to the transitions  $\Upsilon(10580)$ ,  $\Upsilon(10860)$ ,  $\Upsilon(11020) \rightarrow h_b(1P)\eta$ . Figure adapted from Ref. [877].

Furthermore, the  $\eta$  transitions of  $\Upsilon(10860)$  into the  $D$ -wave bottomonium states  $\Upsilon(1^3D_J)$  with  $J = 1, 2, 3$  were systematically investigated in Ref. [878]. Experimentally, only the  $\Upsilon(1^3D_2)$  state has been firmly established so far [838, 839], while the  $\Upsilon(1^3D_1)$  and  $\Upsilon(1^3D_3)$  states remain unobserved. The corresponding hadronic loop diagrams are illustrated in Fig. 107. The predicted branching ratios, together with their characteristic ratios, are presented in Fig. 108.

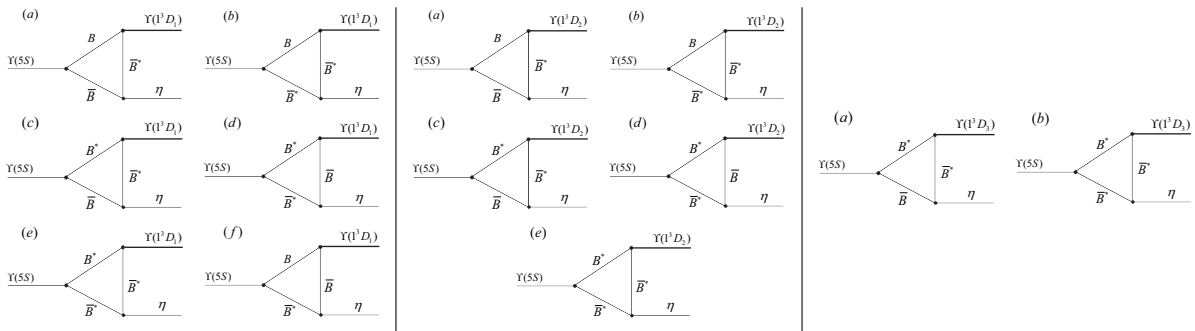


Figure 107: Feynman diagrams illustrating the  $\eta$  transitions of  $\Upsilon(10860) \rightarrow \Upsilon(1^3D_J)\eta$  with  $J = 1, 2, 3$ . Adapted from Ref. [878].

It is found that the branching ratios for  $\Upsilon(10860) \rightarrow \Upsilon(1^3D_J)\eta$  are of the order of  $\mathcal{O}(10^{-3})$ , which are comparable to those of the experimentally observed dipion transitions  $\Upsilon(10860) \rightarrow \Upsilon(nS)\pi^+\pi^-$  ( $n = 1, 2, 3$ ). This indicates that

these  $\eta$  transitions possess considerable discovery potential in future experiments. Moreover, the characteristic ratios reveal that the  $\eta$  transitions into  $\Upsilon(1^3D_1)$  and  $\Upsilon(1^3D_2)$  occur at a similar magnitude, whereas the decay  $\Upsilon(10860) \rightarrow \Upsilon(1^3D_3)\eta$  is suppressed by approximately one order of magnitude relative to the former two channels.

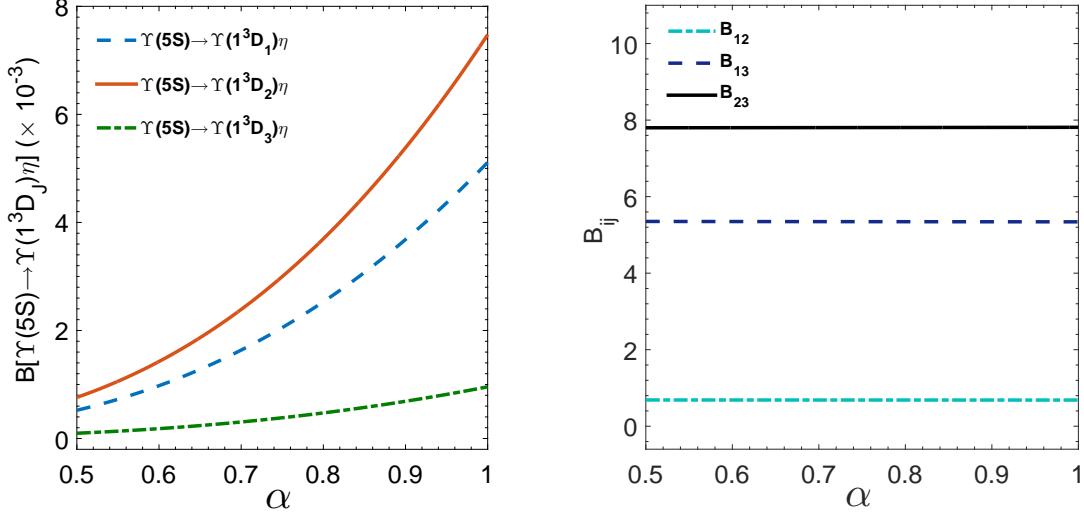


Figure 108: The predicted branching ratios of  $\Upsilon(10860) \rightarrow \Upsilon(1^3D_J)\eta$  (left panel), as well as the ratios between them (right panel). Figure adapted from Ref. [878].

Following the publication of the theoretical work, the Belle Collaboration reported the first observation of the process  $\Upsilon(10860) \rightarrow \Upsilon_J(1D)$  [879]. The measured branching fraction,  $(4.82 \pm 0.92 \pm 0.67) \times 10^{-3}$ , agrees well with the expectation from the hadronic loop mechanism [878]. However, no direct experimental evidence has been established for the simultaneous presence of all three members of the  $\Upsilon_J(1D)$  triplet. Consequently, only 90% confidence-level upper limits are set on the production fractions of the  $J = 1$  and  $J = 3$  states relative to the  $J = 2$  state.

These overall agreements provide further support for the hadronic loop mechanism in describing the anomalous  $\eta$  transitions of  $\Upsilon(10580)$  and  $\Upsilon(10860)$ .

The hadronic loop mechanism also provides a natural explanation for the large branching ratios of  $\Upsilon(10860) \rightarrow \chi_{bJ}\omega$  ( $J = 0, 1, 2$ ) [880]. The corresponding Feynman diagrams are presented in Fig. 109. The resulting branching ratios are shown in Fig. 110, where the experimentally measured values are well reproduced with reasonable choices of parameters, indicating that hadronic loop effects give dominant contributions to these decay processes.

In short, within the unquenched picture, the bottomonium spectrum can be described more accurately, and the observed anomalous hidden-bottom decays of high-lying bottomonium states can be naturally understood by incorporating hadronic loop effects. Moreover, several corresponding predictions have been confirmed by subsequent experiments. These results suggest that the observed anomalous phenomena can be accommodated within the unquenched quarkonium framework, and that exotic interpretations may not be necessary.

**7.2.3.3. Investigation of hidden-bottom decays of  $\Upsilon(11020)$ .** In the above discussions, we have shown that a series of anomalous hidden-bottom decay behaviors observed in  $\Upsilon(10580)$  and  $\Upsilon(10860)$  can be well understood within a global hadronic loop mechanism. These studies indicate that unquenched hadronic loop effects play a dominant role in the hidden-bottom decays of high-lying bottomonium states.

As the highest established vector bottomonium state,  $\Upsilon(11020)$  is also located above the open-flavor  $B^*\bar{B}^*$  thresholds, where similar hadronic loop effects are expected to be significant. Given that our current knowledge of  $\Upsilon(11020)$  remains rather limited due to the scarcity of relevant experimental information [94], it is therefore worthwhile to extend the hadronic loop framework to  $\Upsilon(11020)$  and to explore its possible hidden-bottom decay behaviors. Since the corresponding loop diagrams are analogous to those involved in the  $\Upsilon(10860)$  transitions, we do not repeat the detailed diagrams here, but instead summarize the main results from the related studies in Table 15. These results may provide useful guidance for future experimental investigations of this state.

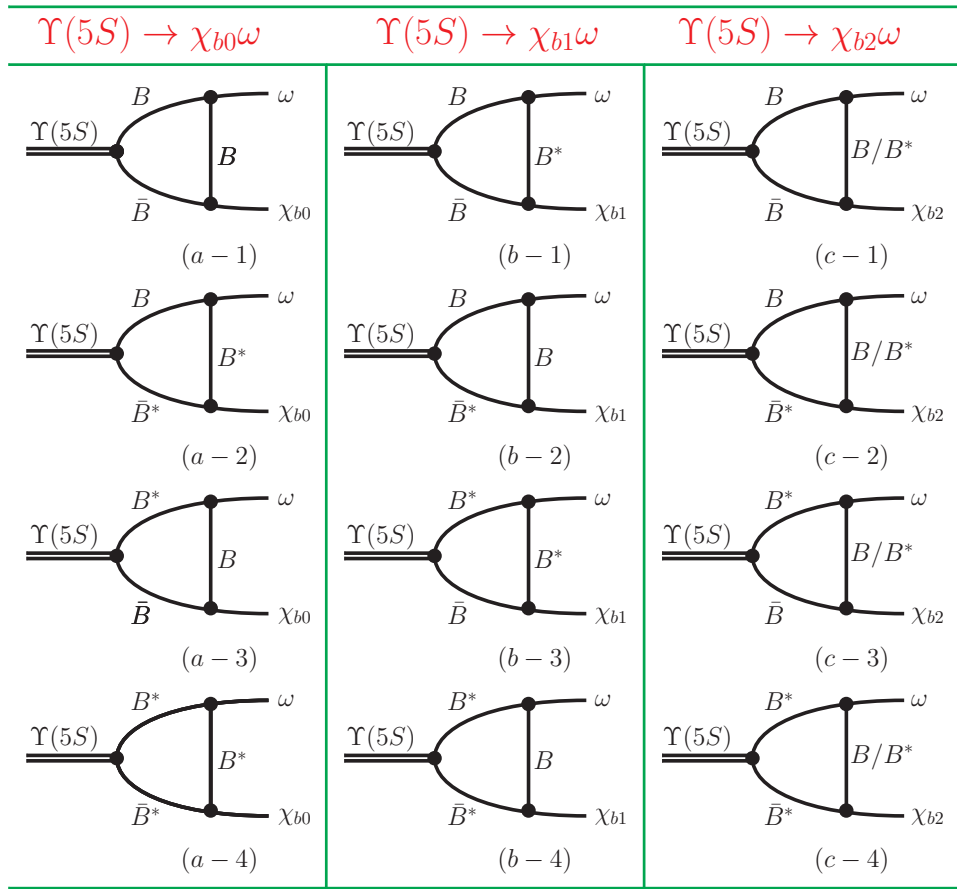


Figure 109: Feynman diagram depicting  $\Upsilon(10860) \rightarrow \chi_{bj}\omega$  decay within the hadronic loop mechanism. Figure adapted from Ref. [880].

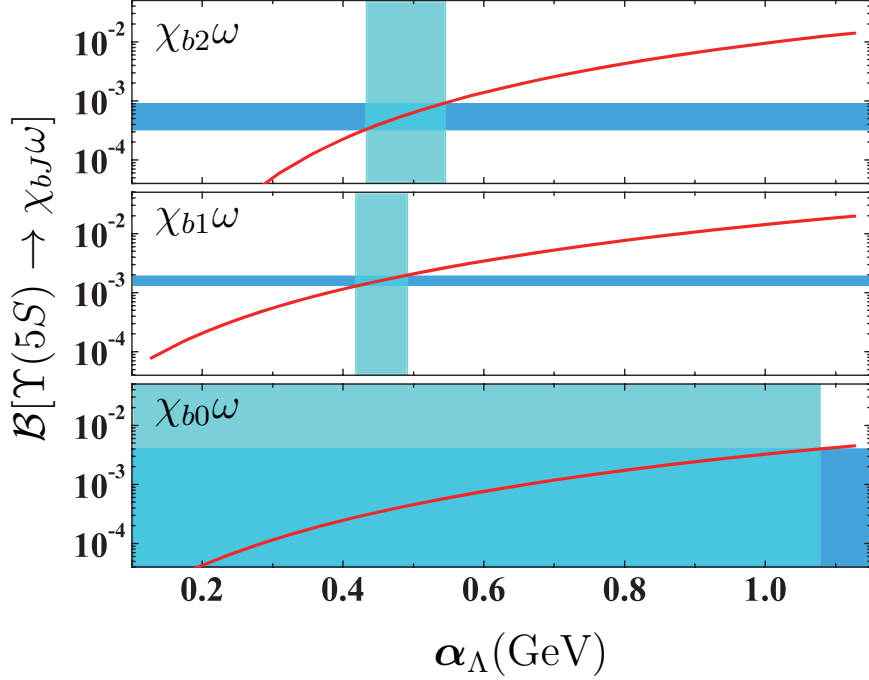


Figure 110: The branching ratios of  $\Upsilon(10860) \rightarrow \chi_{bJ}\omega$  as functions of the parameter  $\alpha_\Lambda$ . The horizontal bands represent the experimental measurements reported by the Belle Collaboration [871], while the vertical bands indicate the reasonable ranges of  $\alpha_\Lambda$  where the theoretical results overlap with the Belle data. The figure is adapted from Ref. [880].

Table 15: Predicted branching ratios for the hidden-bottom decays of  $\Upsilon(11020)$ , together with several characteristic ratios among them. The results are summarized from Refs. [881, 882, 883, 877].

Final states	$BR(\times 10^{-3})$	characteristic ratios		
$\Upsilon(nS)\eta$ [881]	$\Upsilon(1S)\eta$	3.238	$BR[(\Upsilon(2S)\eta)]/BR[(\Upsilon(1S)\eta)]$	0.579–0.626
	$\Upsilon(2S)\eta$	1.947	$BR[(\Upsilon(3S)\eta)]/BR[(\Upsilon(1S)\eta)]$	0.039–0.045
	$\Upsilon(3S)\eta$	0.135	$BR[(\Upsilon(3S)\eta)]/BR[(\Upsilon(2S)\eta)]$	0.067–0.072
$\Upsilon(nS)\eta'$ [881]	$\Upsilon(1S)\eta'$	1.448	$BR[(\Upsilon(1S)\eta)]/BR[(\Upsilon(1S)\eta)']$	2.231–2.241
	$\Upsilon(2S)\eta'$	$1.305 \times 10^{-3}$	$BR[(\Upsilon(2S)\eta)]/BR[(\Upsilon(2S)\eta)']$	$(1.478-1.508) \times 10^3$
$\Upsilon(1^3D_J)\eta$ [882]	$\Upsilon(1^3D_1)\eta$	0.174–1.720	$BR[(\Upsilon(1^3D_2)\eta)]/BR[(\Upsilon(1^3D_1)\eta)]$	0.841–0.853
	$\Upsilon(1^3D_2)\eta$	0.149–1.440	$BR[(\Upsilon(1^3D_3)\eta)]/BR[(\Upsilon(1^3D_1)\eta)]$	1.289–1.306
	$\Upsilon(1^3D_3)\eta$	0.228–2.210	$BR[(\Upsilon(1^3D_3)\eta)]/BR[(\Upsilon(1^3D_2)\eta)]$	1.531–1.533
$\chi_{bJ}\phi$ [883]	$\chi_{b0}\phi$	$(0.68-4.62) \times 10^{-3}$	$BR[(\chi_{b1}\phi)]/BR[(\chi_{b0}\phi)]$	0.74
	$\chi_{b1}\phi$	$(0.50-3.43) \times 10^{-3}$	$BR[(\chi_{b2}\phi)]/BR[(\chi_{b0}\phi)]$	3.28
	$\chi_{b2}\phi$	$(2.22-15.18) \times 10^{-3}$	$BR[(\chi_{b2}\phi)]/BR[(\chi_{b1}\phi)]$	4.43
$\chi_{bJ}\omega$ [883]	$\chi_{b0}\omega$	0.15–2.81	$BR[(\chi_{b1}\omega)]/BR[(\chi_{b0}\omega)]$	4.11
	$\chi_{b1}\omega$	0.63–11.68	$BR[(\chi_{b2}\omega)]/BR[(\chi_{b0}\omega)]$	7.06
	$\chi_{b2}\omega$	1.08–20.02	$BR[(\chi_{b2}\omega)]/BR[(\chi_{b1}\omega)]$	1.72
$h_b(1P)\eta$ [877]	0.1–10.0	...		

As summarized in Table 15, several decay channels, including  $\Upsilon(nS)\eta$ ,  $\Upsilon(1S)\eta'$ ,  $\Upsilon(1^3D_J)\eta$ , and  $\chi_{bJ}\omega$ , are predicted to possess relatively large branching ratios and thus represent promising modes for experimental investigation. Subsequently, experimental analyses have reported evidence for the decay  $\Upsilon(11020) \rightarrow \chi_{bJ}\omega$ , although the spin assignment ( $J = 1$  or  $2$ ) could not be unambiguously determined. This signal was observed via the process  $\Upsilon(11020) \rightarrow \chi_{bJ}\pi^+\pi^-\pi^0$ , with a measured branching ratio of  $(8.7 \pm 4.3 \pm 6.1_{-2.5}^{+4.5}) \times 10^{-3}$ , which is compatible with the theoretical expectations obtained in Ref. [883].

#### 7.2.4. A consistent assignment of $\Upsilon(10753)$ into the bottomonium family

7.2.4.1. *Observation of  $\Upsilon(10753)$  and subsequent theoretical interpretations.* In 2019, the Belle Collaboration updated its analysis of the processes  $e^+e^- \rightarrow \Upsilon(nS)\pi^+\pi^-$  ( $n = 1, 2, 3$ ) [566], superseding earlier measurements [565]. Besides the known resonances  $\Upsilon(10860)$  and  $\Upsilon(11020)$ , a new structure with a statistical significance of  $5.2\sigma$  was observed near 10.75 GeV, as shown in Fig. 111. This state is now listed by the PDG as  $\Upsilon(10753)$  [94]. The measured resonance parameters are

$$M = 10752.7 \pm 5.9_{-1.1}^{+0.7} \text{ MeV} \quad \Gamma = 35.5_{-11.3-3.3}^{+17.6+3.9} \text{ MeV} \quad (71)$$

Following its experimental observation, this bottomonium-like structure has stimulated extensive theoretical investigations into its nature. A variety of interpretations have been proposed, including its assignment as a conventional bottomonium state [884, 885, 886, 887, 857, 858, 888], as well as several exotic scenarios, such as a tetraquark configuration [889, 890, 891] and a hybrid state [892, 893]. In Ref. [894],  $\Upsilon(10753)$  is interpreted as a dressed hadronic resonance, whose structure consists of an approximately equal admixture of a conventional  $b\bar{b}$  bottomonium component and a  $B^*\bar{B}^*$  molecular component. In addition, Refs. [895, 896] described  $\Upsilon(10753)$  as a dynamical meson–meson resonance with about 76% meson–meson content, while Ref. [311] proposed that the observed structure may instead arise from a threshold effect associated with the coupling of the  $B^*\bar{B}^*$  channel to  $\Upsilon(4S)$ , rather than corresponding to a genuine resonance.

The production of  $\Upsilon(10753)$  in  $e^+e^-$  annihilation identifies it as a vector state, with quantum numbers  $J^{PC} = 1^{--}$ . Its mass lies between the experimentally observed  $\Upsilon(10580)$  and  $\Upsilon(10860)$ , commonly identified as the  $\Upsilon(4S)$  and  $\Upsilon(5S)$  states, respectively. A natural preliminary interpretation is therefore to assign  $\Upsilon(10753)$  as a  $\Upsilon(3D)$  bottomonium state [884]. However, such an assignment encounters serious difficulties.

First, the measured mass of  $\Upsilon(10753)$  is significantly higher than theoretical expectations for the  $\Upsilon(3D)$  state [884]. Specifically, it exceeds the prediction of the unquenched model discussed above by about 80 MeV [328], is roughly 100 MeV higher than the nonrelativistic constituent quark model result [855], and is about 55 MeV and 35–55 MeV above the predictions of the quenched GI model [13, 854] and the relativistic string Hamiltonian approach [897, 525], respectively. Second, the dielectron width expected for a conventional  $\Upsilon(3D)$  state is extremely small. Various theoretical studies estimate  $\Gamma_{ee}[\Upsilon(3D)]$  to be only 1–3 eV [13, 854, 328, 897, 525]. Compared with the dielectron widths of the  $\Upsilon(4S)$  and  $\Upsilon(5S)$ , this represents a suppression of nearly two orders of magnitude, making the  $\Upsilon(3D)$  state difficult to observe directly in the  $e^+e^-$  annihilation process. This expectation is clearly at odds with the prominent signal of  $\Upsilon(10753)$  observed in the  $e^+e^- \rightarrow \Upsilon(nS)\pi^+\pi^-$  processes [566].

7.2.4.2. *4S–3D mixing scheme.* To address these difficulties, it is instructive to recall some established experience in constructing the charmonium family. In Ref. [104], Rosner introduced a mixing scheme between the  $2S$  and  $1D$  charmonium states to account for puzzling phenomena such as the “ $\rho\pi$  puzzle” associated with the  $\psi(3686)$  and  $\psi(3770)$  states. When extending to higher charmonia, the  $4S$ – $3D$  and  $5S$ – $4D$  mixing schemes were further introduced to construct a coherent vector charmonium mass spectrum in the 4.0–4.5 GeV region within the unquenched picture, as illustrated in Sec. 4. This framework successfully accommodates a wide range of experimental observations. From these previous experiences in constructing the charmonium family, it can be concluded that the  $S$ – $D$  mixing effect is rather universal and should not be neglected in a realistic description of heavy quarkonium spectroscopy.

Motivated by the studies on charmonium spectroscopy [104, 300], it has been suggested that an analogous  $S$ – $D$  wave mixing mechanism may also play an important role in resolving the mass puzzle associated with the  $\Upsilon(10753)$  [887]. According to the PDG compilation [94], the experimentally measured mass of  $\Upsilon(10580)$ , 10579.4 MeV, is noticeably lower than the mass range predicted for the  $\Upsilon(4S)$  state, 10607–10640 MeV, in various potential model

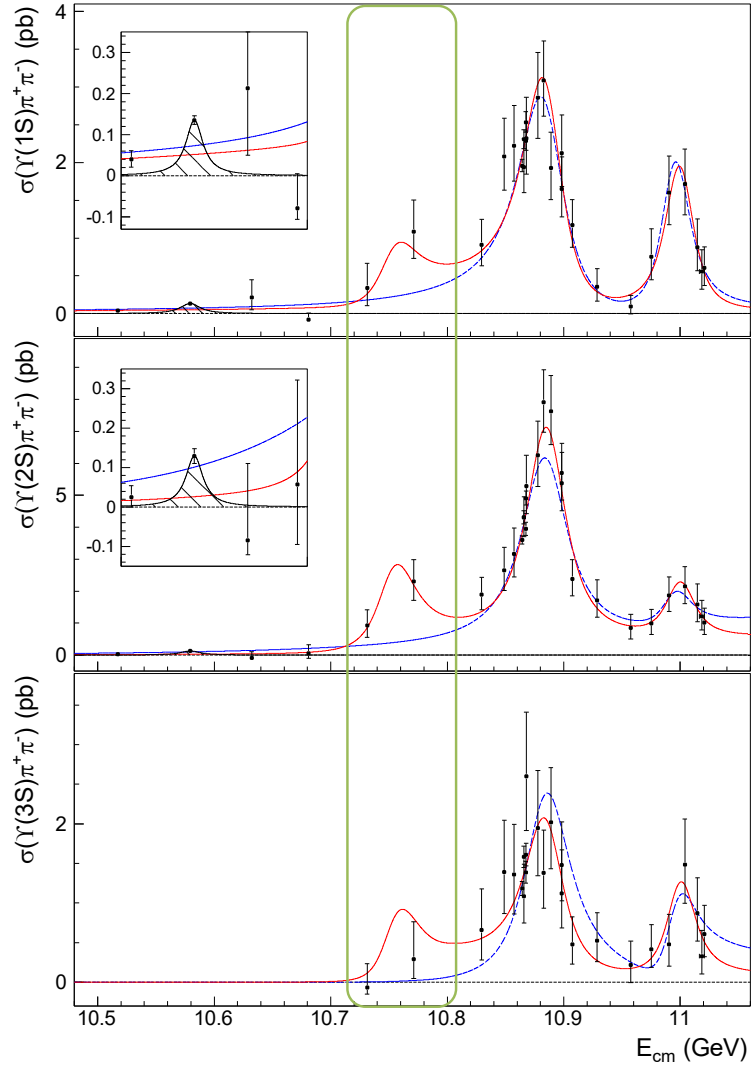


Figure 111: Cross sections for  $e^+e^- \rightarrow \Upsilon(nS)\pi^+\pi^-$  measured by the Belle Collaboration [566], showing the structure of  $\Upsilon(10753)$ . The figure is adapted from Ref. [566].

calculations [855, 328, 854, 897, 525]. Meanwhile, the observed mass of  $\Upsilon(10753)$  is located above the predicted mass region of the  $\Upsilon(3D)$  state, 10653–10717 MeV. Such a mass ordering provides a typical environment for level repulsion induced by  $S$ – $D$  mixing and thus naturally motivates the introduction of a  $4S$ – $3D$  mixing scheme, within which the mass discrepancy associated with  $\Upsilon(10753)$  can be effectively accommodated. In particular, the physical vector bottomonium states  $\Upsilon(10580)$  and  $\Upsilon(10753)$ , resulting from the  $4S$ – $3D$  mixing can be written as

$$\begin{pmatrix} |\Upsilon'_{4S-3D}\rangle \\ |\Upsilon''_{4S-3D}\rangle \end{pmatrix} = \begin{pmatrix} \cos \theta & \sin \theta \\ -\sin \theta & \cos \theta \end{pmatrix} \begin{pmatrix} |\Upsilon(4S)\rangle \\ |\Upsilon(3D)\rangle \end{pmatrix}, \quad (72)$$

where  $\theta$  denotes the mixing angle.

After introducing the  $4S$ – $3D$  mixing scheme, the predicted masses and dielectron widths of the mixed states as functions of the mixing angle  $\theta$  are shown in Fig. 112. The mixing angle can be determined by matching the calculated dielectron width  $\Gamma_{e^+e^-}(\Upsilon'_{4S-3D})$  to the experimentally measured value of  $\Upsilon(10580)$ , yielding [887]

$$\theta = (33 \pm 4)^\circ. \quad (73)$$

This result is consistent with the estimation in Refs. [897, 525, 888]. With the above mixing angle, the masses of  $\Upsilon(10580)$  and the  $\Upsilon(10753)$  are simultaneously reproduced. Meanwhile, the dielectron width of  $\Upsilon(10753)$  is enhanced by nearly two orders of magnitude relative to the pure  $3D$  assignment, becoming comparable to that of an  $S$ -wave state, which makes its observation in  $e^+e^-$  annihilation feasible, as shown in Fig. 112.

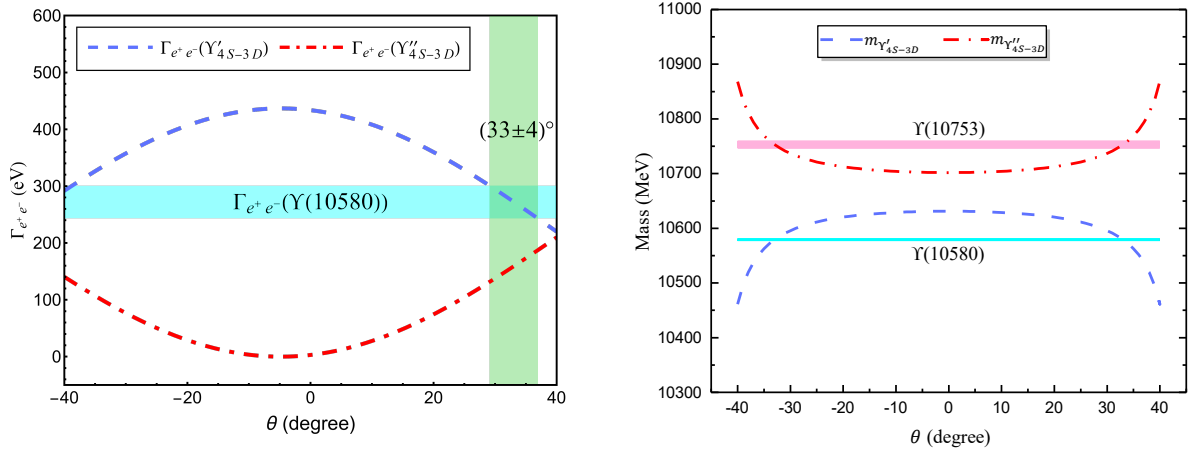


Figure 112: The predicted masses (left panel) and dielectron widths (right panel) of the mixed bottomonium states  $\Upsilon'_{4S-3D}$  and  $\Upsilon''_{4S-3D}$  as functions of the mixing angle  $\theta$  [887]. The blue horizontal bands denote the experimental values, while the green vertical band indicates the favored mixing angle.

**7.2.4.3. Hidden-bottom decay properties.** To further assess the plausibility of assigning the newly observed  $\Upsilon(10753)$  to the mixed  $\Upsilon''_{4S-3D}$  state, its hidden-bottom decay channel  $\Upsilon(10753) \rightarrow \Upsilon(nS)\pi^+\pi^-$  ( $n = 1, 2, 3$ )—which serves as the discovery mode of this state—was examined in Ref. [898]. Since  $\Upsilon(10753)$  lies above the open-flavor thresholds of  $B^{(*)}\bar{B}^{(*)}$ , hadronic loop effects are expected to play a dominate role in its hidden decay dynamics, as already illustrated in the cases of  $\Upsilon(10580)$  and  $\Upsilon(10860)$  discussed above. Within this framework, Ref. [898] employed the hadronic loop mechanism to investigate the transitions  $\Upsilon(10753) \rightarrow \Upsilon(nS)\pi^+\pi^-$ , in which the dipion system is generated through intermediate scalar meson contributions, as shown in Fig. 113. It is worth noting that, when  $\Upsilon(10753)$  is treated as the mixed  $4S$ – $3D$  state  $\Upsilon''_{4S-3D}$ , the decay amplitudes receive contributions from both the  $4S$ -wave and  $3D$ -wave components; further technical details can be found in Ref. [898].

The calculated branching ratios of the processes  $\Upsilon(10753) \rightarrow \Upsilon(nS)\pi^+\pi^-$  ( $n = 1, 2, 3$ ) are presented in Fig. 114. On the experimental side, the Belle Collaboration has extracted the physical quantities

$$\mathcal{R}_n = \Gamma_{e^+e^-}(\Upsilon(10753)) \times BR[\Upsilon(10753) \rightarrow \Upsilon(nS)\pi^+\pi^-] \quad (n = 1, 2, 3), \quad (74)$$

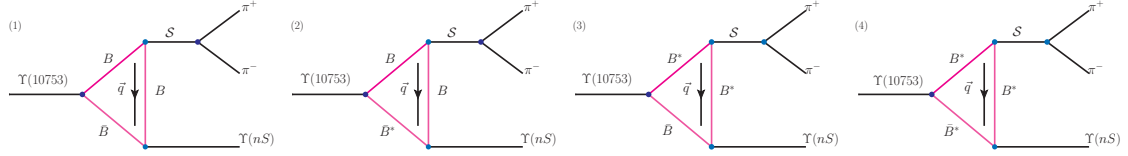


Figure 113: Schematic diagrams for the  $\Upsilon(10753) \rightarrow \Upsilon(nS)\pi^+\pi^-$  ( $n = 1, 2, 3$ ) processes within the hadronic-loop mechanism. Here,  $S$  represents the scalar mesons  $\sigma$  and  $f_0(980)$ . The figure is adapted from Ref. [898].

from the measured cross sections [566]. These quantities are directly proportional to the transition amplitudes of the processes  $e^+e^- \rightarrow \Upsilon(nS)\pi^+\pi^-$  mediated by the  $\Upsilon(10753)$  resonance.

Treating  $\Upsilon(10753)$  as the mixed  $\Upsilon''_{4S-3D}$  state with the mixing angle  $\theta = (33 \pm 4)^\circ$ , the corresponding dielectron width  $\Gamma_{e^+e^-}(\Upsilon(10753))$  can be estimated, as illustrated in the left panel of Fig. 112. Combining this result with the experimentally extracted  $\mathcal{R}_n$  values, the branching ratios  $BR[\Upsilon(10753) \rightarrow \Upsilon(nS)\pi^+\pi^-]$  can be deduced. The resulting experimental ranges are shown as the grey bands in Fig. 114.

As illustrated in Fig. 114, for reasonable choices of the model parameters, the calculated branching ratios are in good agreement with the available experimental constraints, providing further support for assigning the  $\Upsilon(10753)$  as a  $4S-3D$  mixed state. In addition, the dipion invariant mass distributions for the decays  $\Upsilon(10753) \rightarrow \Upsilon(nS)\pi^+\pi^-$  ( $n = 1, 2, 3$ ) are predicted, as shown in Fig. 115.

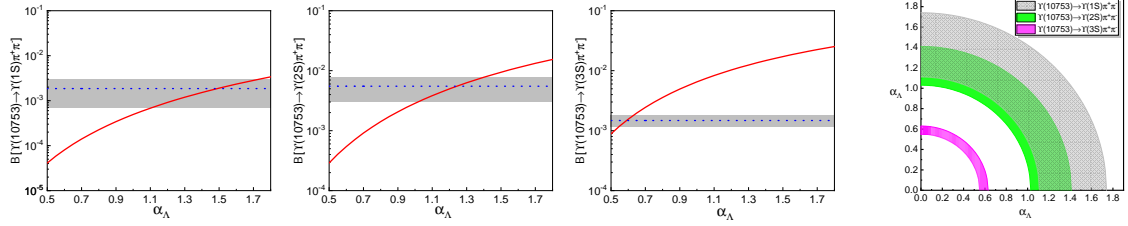


Figure 114: Dependence of the branching ratios  $BR[\Upsilon(10753) \rightarrow \Upsilon(nS)\pi^+\pi^-]$  ( $n = 1, 2, 3$ ) on the parameter  $\alpha_\Lambda$ . The red solid lines represent the predictions from the hadronic loop mechanism [898], while the gray bands with blue dotted lines indicate the experimental values extracted by the Belle Collaboration [566]. The rightmost panel shows the ranges of  $\alpha_\Lambda$  for which the theoretical predictions are consistent with the experiment, showing that these values are of order unity and thus lie within a phenomenologically reasonable range, as suggested in Ref. [188]. Figure Adapted from Ref. [898].

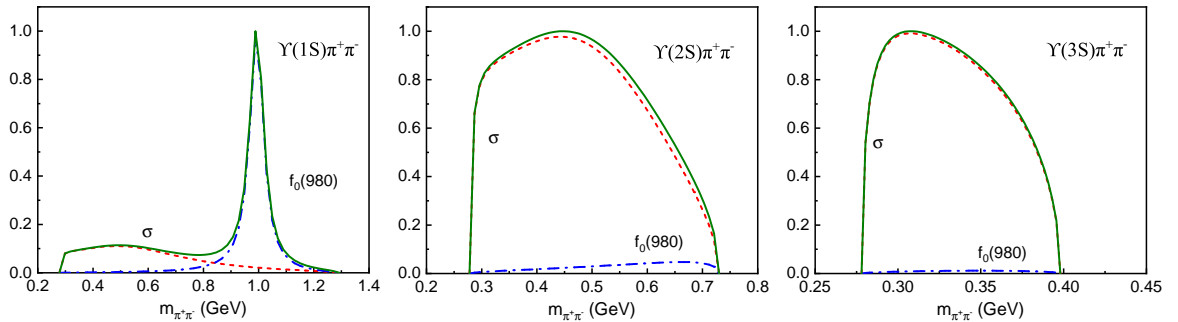


Figure 115: Predicted dipion invariant-mass spectra for the decays  $\Upsilon(10753) \rightarrow \Upsilon(nS)\pi^+\pi^-$  ( $n = 1, 2, 3$ ), normalized to unity at their respective maxima. Adapted from Ref. [898].

The forthcoming Belle II experiments have confirmed the  $\Upsilon(10753)$  signals in the  $e^+e^- \rightarrow \Upsilon(1S, 2S)\pi^+\pi^-$  processes, while no evidence is observed in the  $\Upsilon(3S)\pi^+\pi^-$  channel [899]. The measured dipion invariant mass distribu-

tions are shown in Fig. 116.

At the current level of experimental precision, the measured distributions do not appear to be fully consistent with the theoretical expectations based on the hadronic-loop mechanism shown in Fig. 115. On the theoretical side, although the hadronic-loop contributions are expected to be dominant, additional effects—such as direct decay contributions and interference among different amplitudes—may slightly modify the line shapes, as discussed above in the  $\Upsilon(10580)$  and  $\Upsilon(10860)$  analyses. On the experimental side, the present measurements still suffer from relatively large uncertainties. As a result, no definite conclusion can be drawn at this stage. More precise measurements with improved statistics from future Belle II Collaboration are expected.

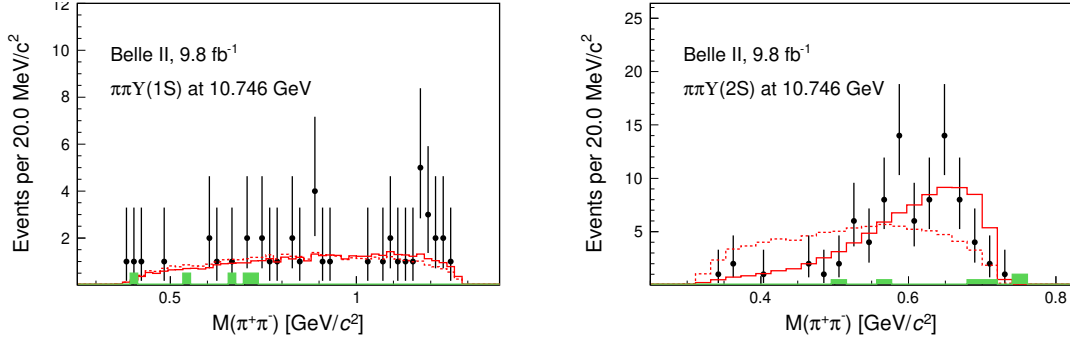


Figure 116: Distributions of dipion mass at  $\sqrt{s} = 10.746$  GeV for  $\Upsilon(1S)\pi^+\pi^-$  (left panel) and  $\Upsilon(2S)\pi^+\pi^-$  (right panel). Adapted from Ref. [899].

The other two-body hidden-bottom decay channels of  $\Upsilon(10753)$  have also been systematically studied within the hadronic loop mechanism, where  $\Upsilon(10753)$  is interpreted as the  $4S-3D$  mixed state  $\Upsilon''_{4S-3D}$  [887, 900, 901]. The corresponding results are summarized in Figs. 117 and 118, and the main features can be outlined as follows:

- The branching ratios of the transitions  $\Upsilon(10753) \rightarrow \Upsilon(1S)\eta^{(\prime)}$ ,  $\Upsilon(1^3D_J)\eta$  ( $J = 1, 2$ ),  $h_b(1P)\eta$ , and  $\chi_{bJ}(1P)\omega$  ( $J = 0, 1, 2$ ) are found to be of order  $\mathcal{O}(10^{-4}-10^{-3})$ , indicating that these modes should be accessible at the Belle II experiment.
- The  $\Upsilon(1^3D_1)$  and  $\Upsilon(1^3D_2)$  states may be accessible via the  $\eta$  transitions of  $\Upsilon(10753)$ . In contrast, the observation of the  $\Upsilon(1^3D_3)$  state is not expected to be favorable in this process due to its small decay rate [900]. At present, neither the  $\Upsilon(1^3D_1)$  nor the  $\Upsilon(1^3D_3)$  state has been experimentally observed, rendering this channel a potentially viable avenue for searching for the as-yet unestablished  $\Upsilon(1^3D_1)$  state.
- The theoretical ratios  $BR[\Upsilon(10753) \rightarrow \eta_b(1S)\eta]/BR[\Upsilon(10753) \rightarrow \Upsilon(1S, 2S)\pi^+\pi^-]$  are compatible with the experimental upper limits, as shown in the rightmost panel of Fig. 118. This consistency, to some extent, supports the interpretation of the  $\Upsilon(10753)$  as the  $4S-3D$  mixed state  $\Upsilon''_{4S-3D}$  [901].
- Within the  $4S-3D$  mixing scenario, the partial decay width of  $\Upsilon(10753) \rightarrow \eta_b(1S)\omega$  is predicted to be in the range (5.6–38.8) keV, which is significantly smaller than the value expected from the tetraquark assignment,  $2.46^{+4.70}_{-1.60}$  MeV [889]. This marked difference provides an important discriminator for probing the internal structure of the  $\Upsilon(10753)$  [901].

Following the theoretical study in Ref. [887], the Belle II Collaboration reported the first observation of signals for  $e^+e^- \rightarrow \chi_{b1}\omega$  and evidence for  $e^+e^- \rightarrow \chi_{b2}\omega$  at  $\sqrt{s} = 10.745$  GeV [903]. The measured energy dependences of the Born cross sections are consistent with the shape of the  $\Upsilon(10753)$  state. In a more recent update, Belle II reported measurements of the products of the dielectron width and the corresponding branching ratios, yielding  $(1.46 \pm 0.25 \pm 0.20)$  eV and  $(1.29 \pm 0.38 \pm 0.31)$  eV for  $e^+e^- \rightarrow \Upsilon(10753) \rightarrow \chi_{b1}\omega$  and  $e^+e^- \rightarrow \Upsilon(10753) \rightarrow \chi_{b2}\omega$ , respectively [904]. Using the estimated dielectron width  $\Gamma_{e^+e^-} = 159 \pm 30$  eV [887, 898], the corresponding branching ratios are inferred to be  $(9.2 \pm 2.7) \times 10^{-3}$  and  $(8.1 \pm 3.4) \times 10^{-3}$  for the  $\Upsilon(10753) \rightarrow \chi_{b1}\omega$  and  $\Upsilon(10753) \rightarrow \chi_{b2}\omega$  decays, respectively. The former slightly exceeds the theoretical expectation of  $(0.25-2.16) \times 10^{-3}$ , whereas the latter is compatible with

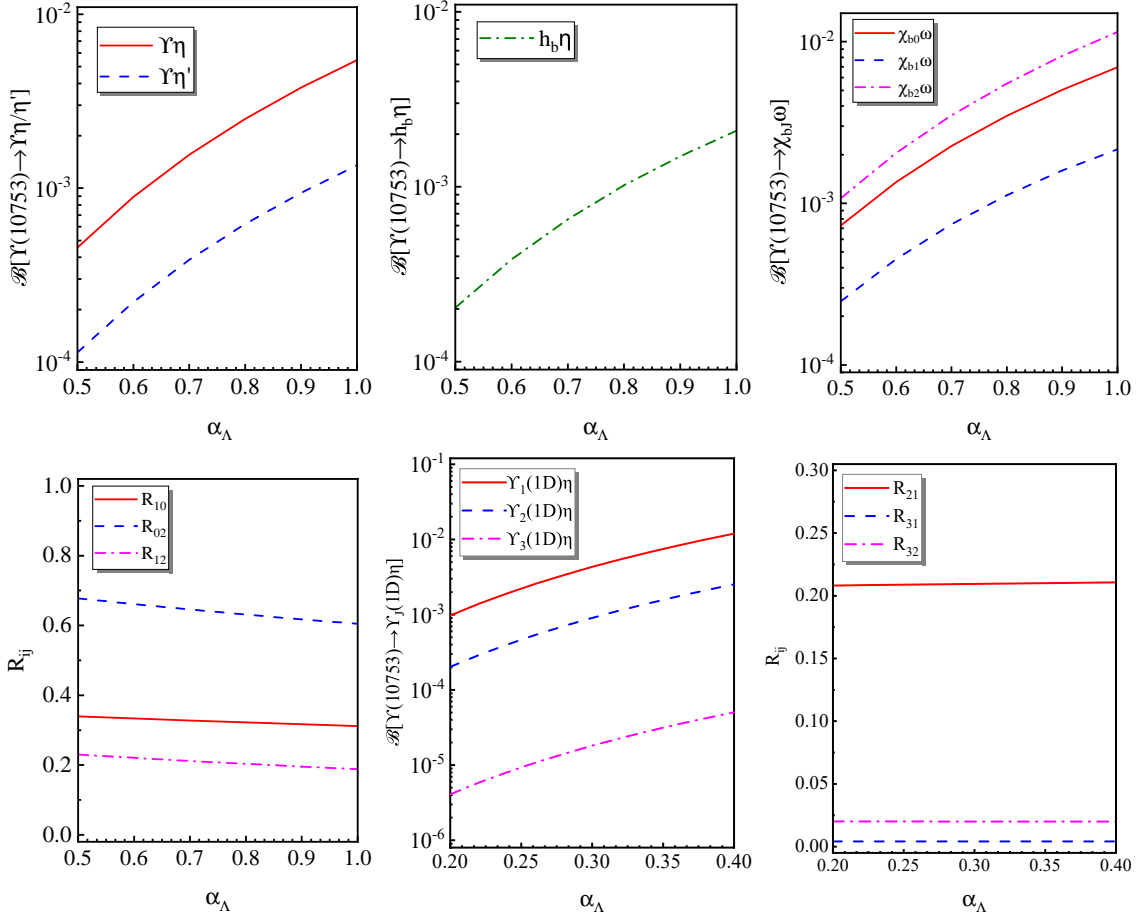


Figure 117: The predicted branching ratios and characteristic ratios for the two-body hidden-bottom decay channels of  $Y(10753)$ , interpreted as the  $4S$ - $3D$  mixed state  $Y''_{4S-3D}$ , within the hadronic loop mechanism. The quantities shown include: (1)  $BR[Y(10753) \rightarrow Y(1S)\eta^{(\prime)}]$ ; (2)  $BR[Y(10753) \rightarrow h_b\eta]$ ; (3)  $BR[Y(10753) \rightarrow \chi_{bJ}\omega]$  with  $J = 0, 1, 2$ ; (4) the ratios  $R_{ij}^{cb} \equiv BR[Y(10753) \rightarrow \chi_{bi}\omega]/BR[Y(10753) \rightarrow \chi_{bj}\omega]$ ; (5)  $BR[Y(10753) \rightarrow Y(1^3D_J)\eta]$  with  $J = 1, 2, 3$ ; and (6) the ratios  $R_{ij}^D \equiv BR[Y(10753) \rightarrow Y(1^3D_i)\eta]/BR[Y(10753) \rightarrow Y(1^3D_j)\eta]$ . These figures are adapted from Ref. [887, 900].

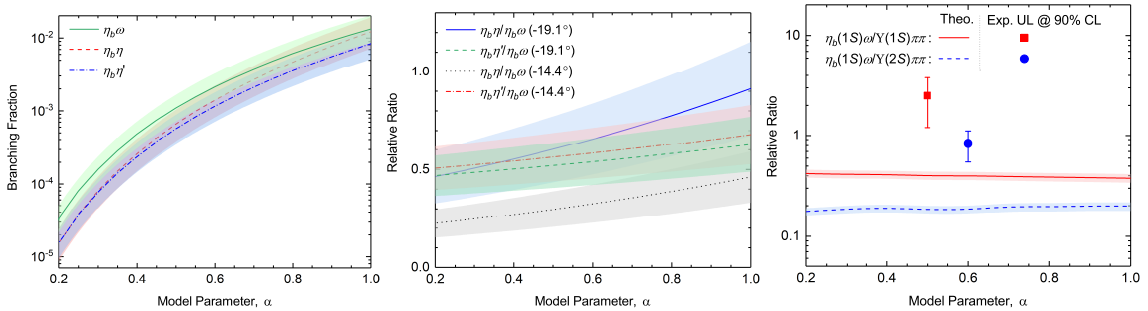


Figure 118: (1) The predicted branching ratios for  $Y(10753) \rightarrow \eta_b\eta^{(\prime)}$  and  $Y(10753) \rightarrow \eta_b(1S)\omega$  within the hadronic loop mechanism; (2) the characteristic ratios between  $BR[Y(10753) \rightarrow \eta_b\eta^{(\prime)}]$  and  $BR[Y(10753) \rightarrow \eta_b\omega]$ , evaluated with the  $\eta$ - $\eta'$  mixing angle taken as  $-19.1^\circ$  or  $-14.4^\circ$ ; (3) the characteristic ratio  $BR[Y(10753) \rightarrow \eta_b\eta]/BR[Y(10753) \rightarrow Y(1S, 2S)\pi^+\pi^-]$ , where the points denote the upper limits extracted from experimental measurements [566, 902]. In the calculations,  $Y(10753)$  is interpreted as the  $4S$ - $3D$  mixed state  $Y''_{4S-3D}$ , with the favored  $\alpha$  parameter in the range 0.3–0.5. The figures are adapted from Ref. [901].

the predicted range  $(1.08\text{--}11.5) \times 10^{-3}$  [887]. Furthermore, the experimentally determined ratio

$$\frac{BR[\Upsilon(10753) \rightarrow \chi_{b1}\omega]}{BR[\Upsilon(10753) \rightarrow \chi_{b2}\omega]} = 1.13 \pm 0.38 \pm 0.34$$

is consistent with the theoretical prediction of 0.2 [887] at the  $1.8\sigma$  level.

Ref. [905] also investigated the radiative transitions  $\Upsilon(10753) \rightarrow \gamma X_b$ , where  $X_b$  denotes the heavy quark flavor symmetry counterpart of  $X(3872)$  in the bottomonium sector. It was found that the corresponding partial decay width is of the order of 10 keV. Based on this result, the authors suggested that the Belle II experiment search for the  $X_b$  state via the process  $e^+e^- \rightarrow \gamma X_b$ , mediated by  $\Upsilon(10753)$ , with the subsequent decay  $X_b \rightarrow \chi_{b1}\pi\pi$ .

In summary, a consistent assignment of  $\Upsilon(10753)$  into the bottomonium family can be achieved by interpreting it as the  $4S\text{--}3D$  mixed state  $\Upsilon''_{4S\text{--}3D}$  in the unquenched picture. This scenario provides a coherent description of its mass spectrum, production properties, and several observed decay behaviors. The predicted decay patterns and the mixing-induced features offer clear experimental signatures, which can be stringently tested by future high-luminosity  $e^+e^-$  facilities, such as Belle II.

### 7.3. Construction of light-flavor vector mesons around the 2 GeV mass region

#### 7.3.1. Status of light-flavor meson spectroscopy

Light hadron spectroscopy occupies an important position in hadron physics owing to both its historical significance and the richness of the observed spectrum. The systematic study of light-flavor hadrons played a central role in the establishment of SU(3) flavor symmetry and ultimately led to the formulation of the quark model [8, 9]. Since then, the light-flavor sector has continued to dominate the experimental landscape, exhibiting a dense spectrum and a wide variety of production and decay channels.

Over the past decade, the construction of the light-flavor meson spectrum has primarily relied on systematic comparisons between theoretically estimated masses and total decay widths, and the corresponding experimental measurements, following an initial classification based on fundamental quantum numbers. Among them, Regge trajectory analyses [906] have provided a simple and widely used framework for organizing experimentally observed states, particularly in the low-lying region where the spectrum appears relatively sparse. Following this methodology, the Lanzhou research group has systematically constructed the spectroscopy of light-flavor meson families [907, 908, 909, 910, 911, 912, 913, 914, 915, 916].

This conventional construction strategy has proven to be relatively effective for the identification of low-lying light meson states. This effectiveness can be traced to a generic feature of hadron spectra governed by color confinement: with increasing excitation energy, the level spacing between successive states gradually decreases. As a consequence, states in the low-energy region remain relatively well separated, allowing experimentally observed resonances to be matched to theoretical expectations with limited ambiguity. In the highly excited region, the energy level of spectrum is usually compressed beyond the expectations of simple Regge systematics, enhancing correlations among neighboring excited states. As a result, different production and decay processes often exhibit markedly different line-shape structures in the same mass region. If these structures are naively interpreted as originating from a single excited state, the extracted resonance parameters such as masses and widths can differ substantially from one reaction to another. This problem is most clearly illustrated in the spectroscopy of light-flavor vector mesons around 2.0 GeV, where the identification and classification of excited states remain highly controversial. As illustrated in Fig. 120, the low-lying vector states show good correspondence with the experimental data, whereas the high-exciting states above 2.0 GeV remain far from being established.

A typical example is the strangeonium-like state  $Y(2175)$  (referred to as  $\phi(2170)$  in the PDG [94]), which was first reported by the BABAR Collaboration in the process  $e^+e^- \rightarrow Y(2175) \rightarrow \phi f_0(980)$  via the initial-state radiation technique [917]. This observation was subsequently confirmed by the Belle [822], BABAR [918, 919], and BESIII [920] collaborations in the same channel, as well as in the processes  $e^+e^- \rightarrow \eta Y(2175) \rightarrow \eta \phi f_0(980)$  [921, 922, 923],  $e^+e^- \rightarrow Y(2175) \rightarrow \phi \eta^{(\prime)}$  [924, 925] reported by the BES and BESIII Collaborations. The  $Y(2175)$  has been suggested as the strange-sector partner of the  $Y(4260)$ , since both states are observed prominently in hidden-flavor final states. Various theoretical interpretations have been proposed for the  $Y(2175)$ , including a vector strangeonium state in the  $2D$  [926, 927, 928, 908, 927] or  $3S$  [929, 930, 927] assignment, an  $s\bar{s}g$  hybrid [931, 932], a tetraquark state [933, 934, 935, 936, 937, 938], a  $\Lambda\bar{\Lambda}$  bound state [939, 940, 941], a threshold effect [942], and a  $\phi K\bar{K}$  resonance state

[943, 944, 945]. As shown in Fig. 119, the resonance parameters reported by different experimental groups exhibit substantial discrepancies, a situation similar to that observed for the  $\rho(2150)$ .

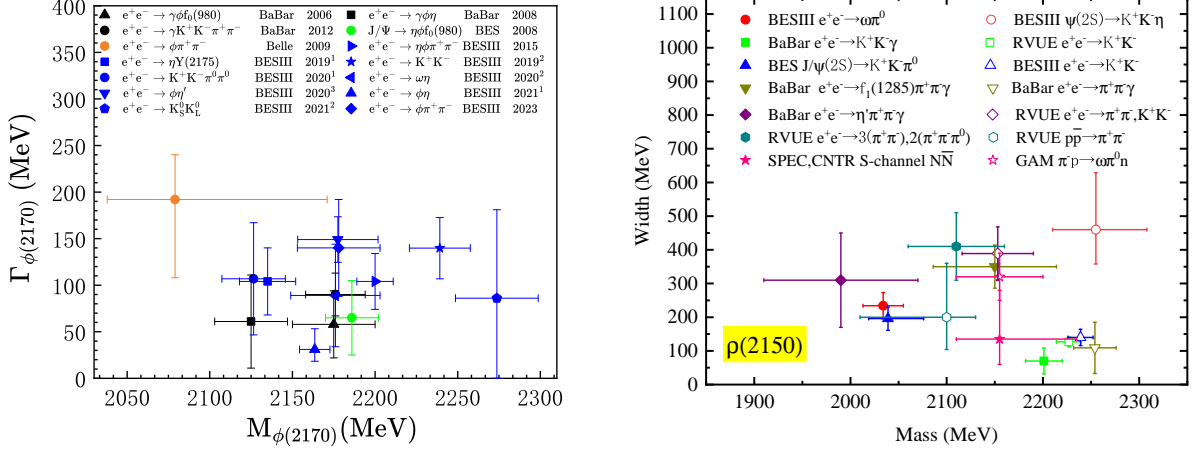


Figure 119: Measured resonance parameters of the  $Y(2175)$  (left panel) and the  $\rho(2150)$  (right panel) from different experimental processes. The figures are adapted from Refs. [946, 916].

The current difficulties encountered in the construction of high-exciting light-flavor mesons are closely related to the analysis way of experimental cross-section data, in which different production or decay processes are studied independently, and the observed structures are interpreted through fits to individual data sets without the theoretical support of spectroscopy. As a result, the extracted resonance parameters tend to be highly process dependent, obscuring the underlying structure of the high-exciting spectrum. Thus, it is not a simple task to solve this messy situation associated with the vector meson spectrum around 2.0 GeV.

Here, a new perspective of constructing high-exciting light-flavor meson spectroscopy was provided in Refs. [478, 947]. A guiding principle comes from the well-established success of unquenched approaches in the spectroscopy of charmonium and bottomonium, as introduced in Sec. 4 and Sec. 7, respectively. Motivated by these achievements, it is natural to extend the same unquenched spectroscopy description to the light-flavor meson sector, where such effects are expected to be even more pronounced. Compared with traditional spectroscopic analysis based on Regge trajectory, this approach can offer a more precise description of the high-exciting spectrum and provide exact spatial wave functions for the physical states. These wave functions enable more reliable calculations of decay amplitudes and production strengths, which are indispensable for connecting spectroscopy with experimental observables. With such spectroscopic support, the cross sections measured in different processes can be analyzed in a unified and consistent manner, rather than through isolated fits. The strategy outlined above actually provides a systematic and generally applicable framework for the construction of high-exciting spectra. In the following, we illustrate the application of this strategy by decoding the nature of the well-known  $Y(2175)$  through a combined analysis of scattering cross sections in open-strange channels from electron-positron collision.

### 7.3.2. The unquenched spectrum of light vector meson and their contribution in the cross sections of the $e^+e^-$ annihilations into open-strange channels

Recent measurements of open-strange processes in  $e^+e^-$  annihilation have provided a series of intriguing cross-section data in the  $\sqrt{s} \sim 2.2$  GeV region [948, 949]. The BESIII collaboration reported a clear enhancement in the cross section for  $e^+e^- \rightarrow K^+K^-$  with a mass of  $2239.2 \pm 7.1 \pm 11.3$  MeV and width of  $139.8 \pm 12.3 \pm 20.6$  MeV [948]. Subsequently, a combined analysis of the process  $e^+e^- \rightarrow K^+K^-\pi^0\pi^0$  through its sub-processes  $e^+e^- \rightarrow K^+(1460)K^-$ ,  $K_1^+(1400)K^-$ ,  $K_1^+(1270)K^-$ , and  $K^{*+}K^-$  extracted a structure with a significantly lower mass of  $2126.5 \pm 16.8 \pm 12.4$  MeV and width of  $106.9 \pm 32.1 \pm 28.1$  MeV [949]. It is worth mentioning that open-strange decay channels are usually dominant for exciting light vector meson states, so these reaction processes actually provide very key information to construct high-exciting  $\phi$ ,  $\rho$  and  $\omega$ -meson spectra. Although both observed structures lie near the mass region of  $Y(2175)$ , the mass difference of about 110 MeV poses a challenge to a simple single-resonance

interpretation. The observed discrepancies of resonance parameters in different open-strange processes suggest that a more comprehensive analysis, incorporating the possible contributions from multiple light vector mesons, is necessary. In addition, the BESIII measurement shows the absence of a clear signal in the typical open-strange mode  $K^{*+}K^{*-}$  channel [949], which also should be appropriately understood.

To clarify this situation, in Ref. [478], Wang, Wang, Liu and Matsuki first systematically study the spectrum and decay properties of light vector mesons above 2 GeV using an unquenched relativized potential model, whose formula have been introduced in Sec. 4. The model parameters, particularly the color screening constant  $\mu$ , are constrained by fitting to the experimental masses of established higher excitations in other light meson families (such as  $\pi(2360)$  [950],  $\pi_2(2285)$  [951],  $\rho_2(2285)$  [952], and  $\rho_3(2250)$  [953]) up to about 2.3 GeV. This calibration yields  $\mu = 0.081$  GeV, indicating significant unquenched effects. The mass spectra of light-flavor mesons are systematically predicted and it is found that the global features of the  $S$ -wave and  $D$ -wave light-flavor meson spectra are in good overall agreement with the available experimental data [478]. The predicted spectrum for the vector mesons is presented in Fig. 120. Using the resulting wave functions, the open-strange strong decay branching ratios are calculated via the quark pair creation model, and the dilepton widths  $\Gamma_{e^+e^-}$  are derived from wave-function overlaps. As shown in Table 16, di-lepton width predictions for well-known low-lying vector mesons agree reasonably with experimental averages, supporting the theoretical extrapolation to that of higher states.

Table 16: Comparison of theoretical predictions with experimental data for selected decays of established light vector mesons. The di-lepton width  $\Gamma_{e^+e^-}$  is in keV. Table data is adapted from Ref. [478].

Observable quantity	Theory	Experiment (PDG) [94]
$\Gamma_{e^+e^-}(\rho(770))$	6.98	$7.04 \pm 0.06$
$\mathcal{B}_{e^+e^-}(\rho(1450)) \cdot \mathcal{B}_{\omega\pi}(\rho(1450)) (10^{-6})$	4.4	$3.7 \pm 0.4$
$\Gamma_{e^+e^-}(\omega(782))$	0.78	$0.60 \pm 0.02$
$\mathcal{B}_{e^+e^-}(\omega(1420)) \cdot \mathcal{B}_{\omega\pi}(\omega(1420)) (10^{-7})$	2.74	$6.58 \pm 1.49$
$\Gamma_{e^+e^-}(\phi(1020))$	3.19	$1.27 \pm 0.04$
$\mathcal{B}_{e^+e^-}(\phi(1680)) \cdot \mathcal{B}_{K\bar{K}}(\phi(1680)) (10^{-7})$	20.4	$22.2 \pm 8.7$

Crucially, this unquenched spectroscopic study reveals that the electron-positron annihilation into the open-strange channels are dominated by strangeonium states  $\phi(3S)$ ,  $\phi(2D)$ , and  $\phi(4S)$ . The calculated dilepton widths for excited  $\omega$  states are about an order of magnitude smaller than those for  $\rho$  states, and both have branching ratios into open-strange final states typically below a few percent. In contrast, the  $\phi$ -meson resonances have comparable or larger  $\Gamma_{e^+e^-}$  and significantly larger branching ratios into open-strange channels, often exceeding 10%. This systematic difference justifies neglecting the numerous possible  $\rho$  and  $\omega$  contributions, which would otherwise make a combined analysis intractable due to the large number of free parameters.

With this strong support from the theoretical spectroscopy, a combined analysis of the seven measured open-strange cross sections ( $e^+e^- \rightarrow K^+K^-, K\bar{K}^* + \text{c.c.}, K^{*+}K^{*-}, K_1(1270)^+K^-, K_1(1400)^+K^-, K_2^*(1430)\bar{K} + \text{c.c.},$  and  $K(1460)^+K^-$ ) is performed in Ref. [478]. The theoretical description for each process  $e^+e^- \rightarrow K_{(J)}^{(*)}\bar{K}_{(J)}^{(*)}$  includes a direct production amplitude and resonant contributions from selected light vector mesons:

$$\mathcal{M}_{\text{Total}} = \mathcal{M}_{\text{Direct}} + e^{i\theta_n} \sum_{V_n} \mathcal{M}_{V_n},$$

where the sum runs over well-known  $\phi(1020)$ ,  $\phi(1680)$ , and predicted  $\phi(1D)$ ,  $\phi(3S)$ ,  $\phi(2D)$ , and  $\phi(4S)$ . The corresponding cross section is given by

$$\sigma = \int \frac{1}{64\pi s} \frac{1}{|\mathbf{p}_{3\text{cm}}|^2} |\mathcal{M}_{\text{Total}}|^2 dt.$$

It is worth emphasizing that all relevant coupling constants in resonance contributions of  $\phi(1D)$ ,  $\phi(3S)$ ,  $\phi(2D)$ , and  $\phi(4S)$  have been fixed by the theoretical calculations. The simultaneous fit to all seven channels achieves a good

description with  $\chi^2/\text{d.o.f.} = 2.29$ . The combined fitted cross section for open-strange channels are shown in Fig. 121. The fitted resonance parameters for the higher strangeonia are:

$$\begin{aligned} m_{\phi(3S)} &= 2183 \pm 1 \text{ MeV}, & \Gamma_{\phi(3S)} &= 185 \pm 4 \text{ MeV}, \\ m_{\phi(2D)} &= 2290 \pm 3 \text{ MeV}, & \Gamma_{\phi(2D)} &= 312 \pm 6 \text{ MeV}, \\ m_{\phi(4S)} &= 2485 \pm 5 \text{ MeV}, & \Gamma_{\phi(4S)} &= 165 \pm 3 \text{ MeV}. \end{aligned}$$

These masses are consistent with expectations for higher radial and orbital excitations in an unquenched potential model. The widths, particularly of  $\phi(3S)$  and  $\phi(2D)$ , are broad, in line with theoretical estimates but notably larger than the 100 MeV width extracted from simple Breit-Wigner fits to individual channels [948, 949]. This discrepancy is precisely resolved by the interference mechanism: the  $\phi(3S)$  and  $\phi(2D)$  states, with their substantial intrinsic widths, interfere constructively and destructively with each other and with the non-resonant background across different final states. This interference pattern naturally produces the apparent peak near 2.2 GeV, but with a lineshape that is narrower than either individual resonance, mimicking a single narrower state. It also provides a direct explanation for the mass difference of about 110 MeV observed between the  $K^+K^-$  and the  $K^+K^-\pi^0\pi^0$  sub-processes, which means that the interference result, and hence the peak position, is sensitive to the relative phases and amplitudes specific to each final state.

A particularly instructive outcome concerns the  $e^+e^- \rightarrow K^{*+}K^{*-}$  channel, where no significant resonant enhancement was observed. The analysis traces this absence to a specific dynamical suppression: the branching ratio  $\mathcal{B}(\phi(3S) \rightarrow K^*\bar{K}^*)$  is predicted to be only  $\sim 0.7\%$ , an order of magnitude smaller than its decays to other open-strange modes like  $K_1(1270)K$  or  $K(1460)K$ . This suppression originates from a nodal structure in the overlap integral of the  $\phi(3S)$  wave function with the  $K^*\bar{K}^*$  final state, a direct consequence of the radial excitation. Thus, what might have seemed like a puzzling null result becomes a successful postdiction and a non-trivial test of the unquenched model.

Finally, this analysis predicted the existence of a new resonance,  $\phi(4S)$ , with a mass around 2.485 GeV. Its contribution, though less prominent than the lower  $\phi$  states in the current data, is discernible in several channels, most notably  $e^+e^- \rightarrow K\bar{K}(1460)$ , offering a clear target for future high-statistics experiments at BESIII and Belle II. In conclusion, this analysis demonstrates that a global analysis of production cross sections, guided by spectroscopic calculations, can coherently resolve experimental puzzles and constrain the high-exciting light vector meson spectrum. It thereby provides a new interpretation of  $Y(2175)$ : rather than an isolated particle, it manifests as a pronounced interference structure between the broad, overlapping  $\phi(3S)$  and  $\phi(2D)$  resonances.

### 7.3.3. Unified description of the cross sections for more relevant reaction processes within the support of the unquenched spectroscopy

**7.3.3.1. High-lying  $\phi$ -related process.** In 2023, the BESIII Collaboration measured the cross section of the process  $e^+e^- \rightarrow \Lambda\bar{\Lambda}$  at center-of-mass energies from the production threshold up to 3.0 GeV [955], as shown in Fig. 122. It is observed that the cross section data in the vicinity of 2.4 GeV are not well accommodated by the experimental fit. Notably, this energy region overlaps with the masses of several predicted high-lying strangeonium states. This feature naturally motivates the investigation of the decays of high-lying strangeonia into  $\Lambda\bar{\Lambda}$ .

In Ref. [960], Bai, Zhou, and Liu investigated the decays of  $\phi(4S)$  and  $\phi(3D)$  into  $\Lambda\bar{\Lambda}$  via the hadronic loop mechanism, as illustrated in the left panel of Fig. 123. In the unquenched spectroscopy, the masses of these states are predicted to be around 2.4 GeV. A refit to the measured cross section of  $e^+e^- \rightarrow \Lambda\bar{\Lambda}$  was performed by including the contributions from  $\phi(4S)$ ,  $\phi(3D)$ , and a continuum background, together with their mutual interference. The fit result, shown in the right panel of Fig. 123, demonstrates that the cross section data are well reproduced. In particular, the deviation around 2.4 GeV can be mainly attributed to the contribution from the  $\phi(4S)$  state. The extracted branching ratios of  $\phi(4S)/\phi(3D) \rightarrow \Lambda\bar{\Lambda}$  are in good agreement with the theoretical predictions based on the hadronic loop mechanism.

Motivated by these results, the decays of higher strangeonia ( $\phi(nS)$  with  $n = 4, 5, 6$  and  $\phi(mD)$  with  $m = 3, 4, 5$ ) into light-flavor baryon–antibaryon pairs, such as  $\Lambda\bar{\Lambda}$ ,  $\Sigma\bar{\Sigma}$ , and  $\Xi\bar{\Xi}$ , were further investigated within the same framework. The corresponding branching ratios are found to lie in the range of  $10^{-5}$ – $10^{-2}$ , indicating that these processes may be accessible in future experimental measurements.

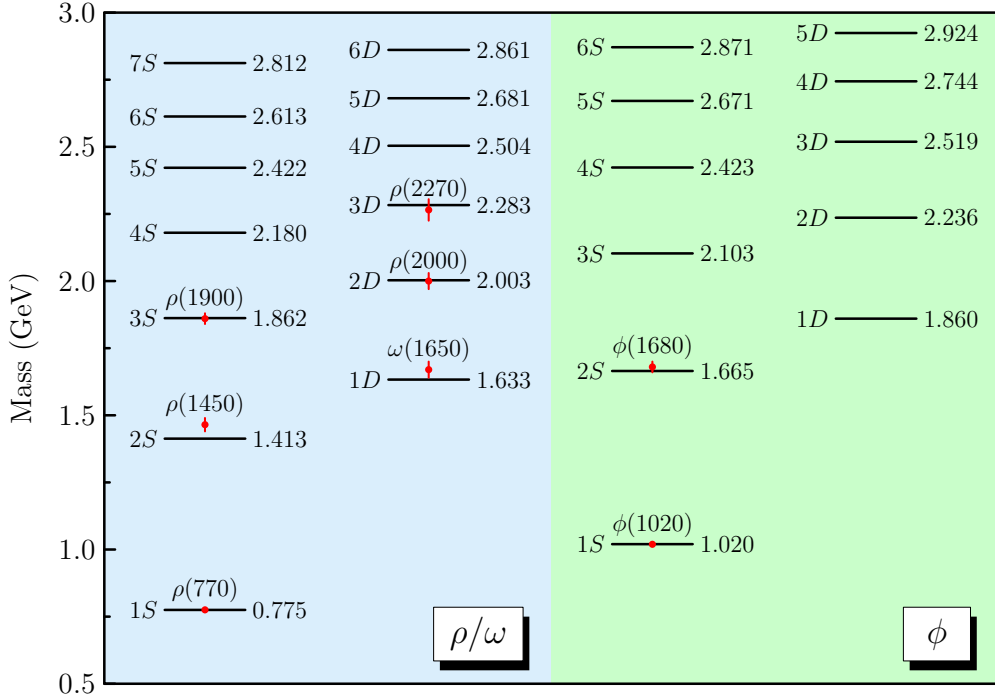


Figure 120: Comparison between the theoretical predictions and experimental measurements for the masses of light-flavor vector mesons. Adapted from Ref. [954].

7.3.3.2. *High-lying  $\omega$ -related processes.* Recently, the BESIII Collaboration reported measurements of the cross sections for the processes  $e^+e^- \rightarrow \omega\eta$  [961] and  $e^+e^- \rightarrow \omega\pi^0\pi^0$  [962] at center-of-mass energies ranging from 2.00 to 3.08 GeV. These channels are related to high-lying  $\omega$  meson states due to isospin conservation. Two structures were observed and interpreted in terms of resonances with the following parameters:  $m_1 = 2222 \pm 7 \pm 2$  MeV,  $\Gamma_1 = 59 \pm 30 \pm 6$  MeV, and  $m_2 = 2179 \pm 21 \pm 3$  MeV,  $\Gamma_2 = 89 \pm 28 \pm 5$  MeV. Notably, the resonance parameters  $(m_1, \Gamma_1)$  and  $(m_2, \Gamma_2)$  extracted from the two processes show noticeable differences. When comparing the two reported  $\omega$ -like states with  $\omega(2205)$ ,  $\omega(2290)$ , and  $\omega(2330)$  listed as "further states" in the PDG [94], as illustrated in Fig. 124, their resonance parameters are found to differ significantly. It is evident that the accumulation of the five  $\omega$  states within the same energy region is puzzling from a spectroscopic point of view.

To clarify this puzzling situation, in Ref. [963], Zhou, Wang, and Liu introduced the contributions from the intermediate  $\omega(4S)$  and  $\omega(3D)$  states, whose masses are around 2.2 GeV according to the unquenched spectrum of light vector mesons, to reproduce the cross section data of  $e^+e^- \rightarrow \omega\eta$  and  $e^+e^- \rightarrow \omega\pi^0\pi^0$ . Specifically, two reaction mechanisms are considered here. One corresponds to the direct annihilation of the initial  $e^+e^-$  pair into the final state via a virtual photon, which provides a nonresonant background contribution. The other proceeds via the intermediate  $\omega(4S)$  and  $\omega(3D)$  states, as illustrated in Fig. 125.

The coupling constants entering the resonance amplitudes are fixed by the decay properties of the  $\omega(4S)$  and  $\omega(3D)$  states as provided by the unquenched spectroscopy. By taking into account the interference between the direct amplitude and the corresponding resonance amplitudes, the measured cross section data of  $e^+e^- \rightarrow \omega\eta$  and  $e^+e^- \rightarrow \omega\pi^0\pi^0$  can be well reproduced, as shown in Fig. 126. Notably,  $\omega(4S)$  dominates in  $e^+e^- \rightarrow \omega\eta$ , whereas in  $e^+e^- \rightarrow \omega\pi^0\pi^0$ , both  $\omega(4S)$  and  $\omega(3D)$  contribute with comparable significance.

Subsequently, in 2024, the BESIII Collaboration measured the cross sections for the processes  $e^+e^- \rightarrow \rho\pi$  and  $e^+e^- \rightarrow \rho(1450)\pi$  through a partial wave analysis of  $e^+e^- \rightarrow \pi^+\pi^-\pi^0$  process, and reported a resonance structure with a mass of  $M = 2119 \pm 11 \pm 15$  MeV and a width of  $\Gamma = 69 \pm 30 \pm 5$  MeV [964], as shown in Fig. 127. This resonance, with a significance of  $5.9\sigma$ , is hereafter referred to as the  $Y(2119)$ . The observed decay channels of the  $Y(2119)$  indicate that it is a typical  $\omega$ -like mesonic state with isospin  $I = 0$ .

However, a comparison of the observed  $Y(2119)$  with the predicted mass spectrum of the  $\omega$ -meson family reveals

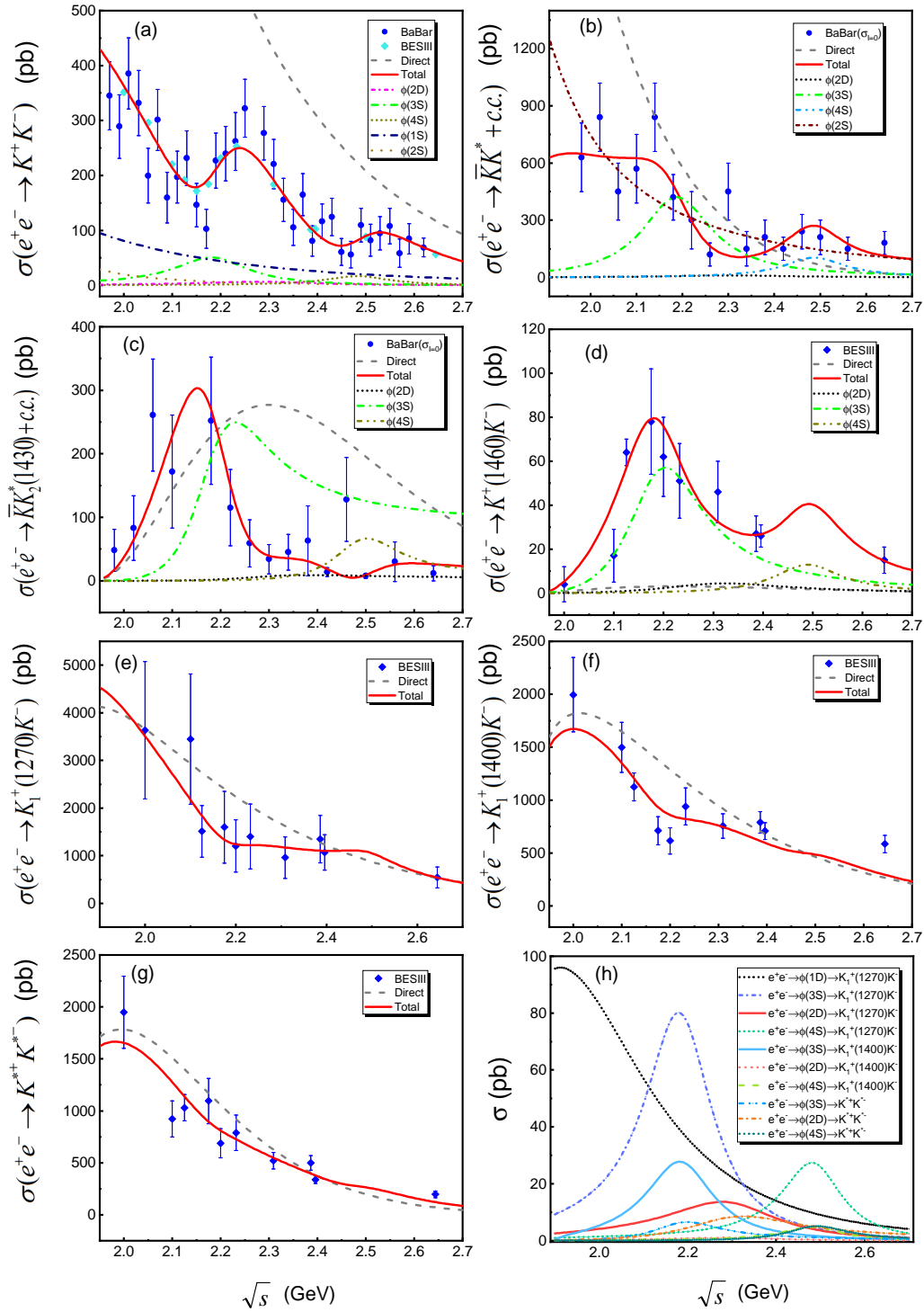


Figure 121: Simultaneous description of the cross sections for the seven open-strange processes  $e^+e^- \rightarrow K^+K^-$ ,  $K\bar{K}^* + c.c.$ ,  $K^{*+}K^{*-}$ ,  $K_1(1270)^+K^-$ ,  $K_1(1400)^+K^-$ ,  $K_2^*(1430)\bar{K} + c.c.$ , and  $K(1460)^+K^-$ . Figure adapted from Ref. [478].

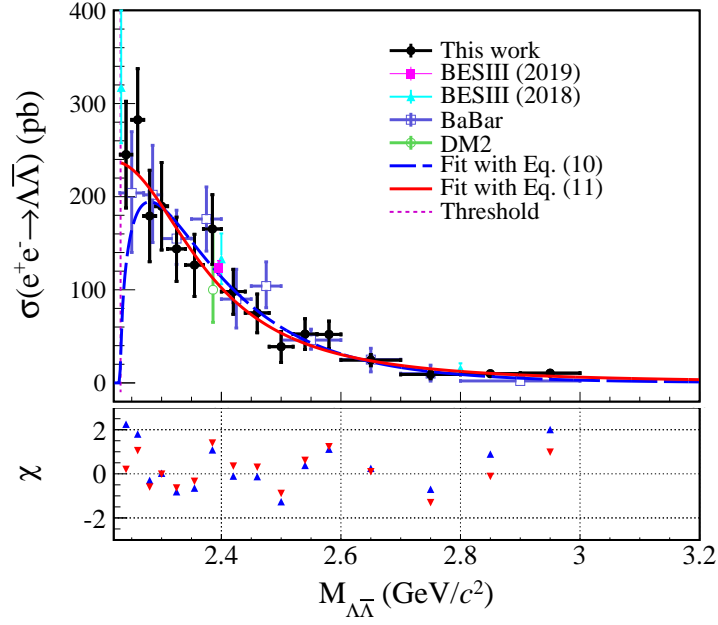


Figure 122: Measured cross section for the process  $e^+e^- \rightarrow \Lambda\bar{\Lambda}$  reported by the BESIII Collaboration in 2023 [955], together with previous measurements [956, 957, 958, 959]. Adapted from Ref. [955].

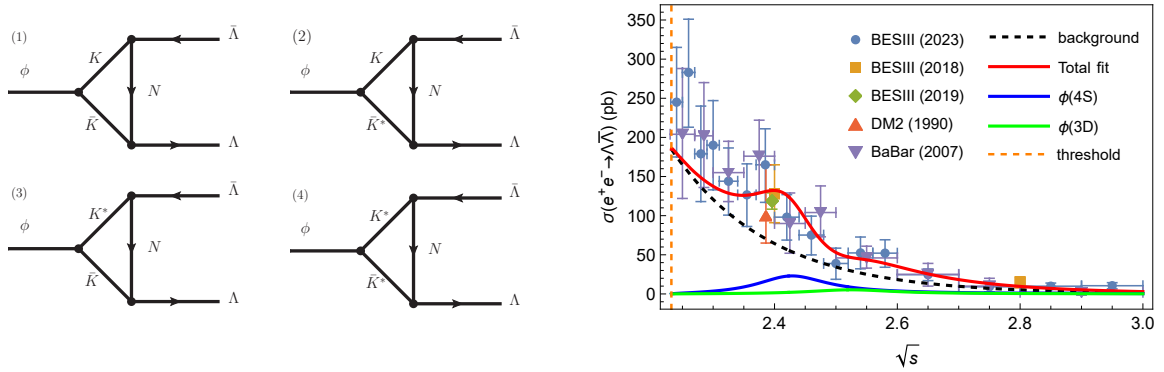


Figure 123: Left panel: Feynman diagrams for the processes  $\phi(4S)/\phi(3D) \rightarrow \Lambda\bar{\Lambda}$  within the hadronic loop mechanism. Right panel: Fit to the cross section of  $e^+e^- \rightarrow \Lambda\bar{\Lambda}$  incorporating the contributions from  $\phi(4S)$  and  $\phi(3D)$ . Figures adapted from Ref. [960].

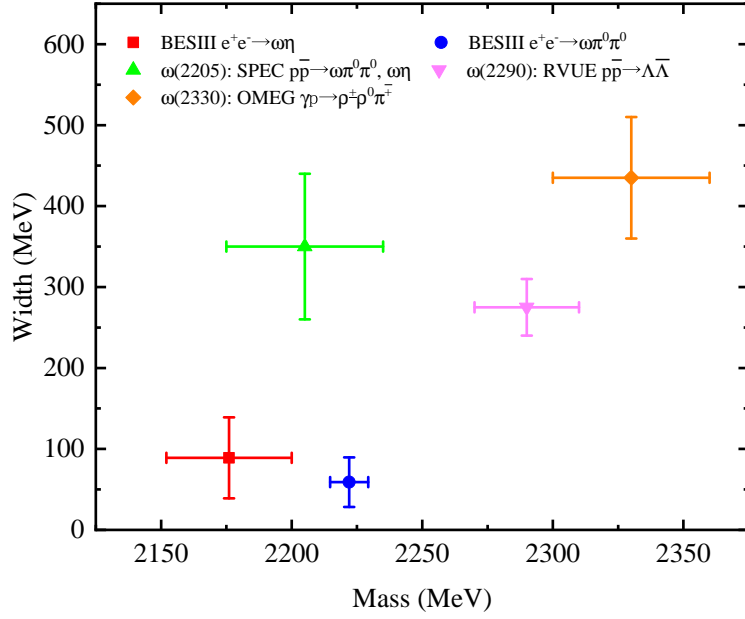


Figure 124: A comparison of resonance parameters of the reported  $\omega$  states with masses around 2.2 GeV [94, 961, 962]. Adapted from Ref. [963].

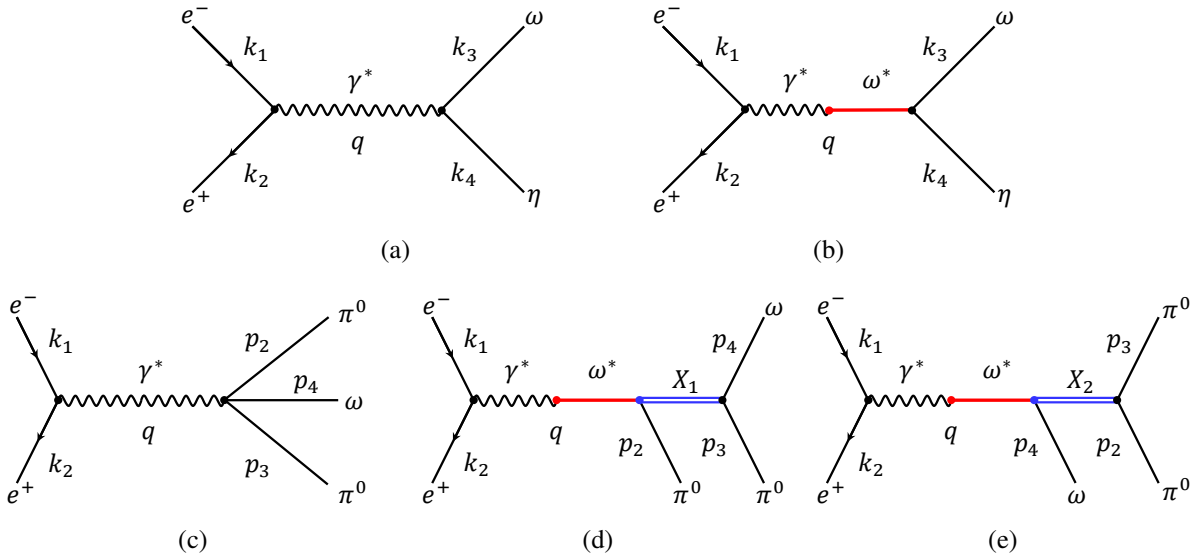


Figure 125: Feynman diagrams for the reactions  $e^+e^- \rightarrow \omega\eta$  and  $e^+e^- \rightarrow \omega\pi^0\pi^0$ . Panels (a) and (b) correspond to  $e^+e^- \rightarrow \omega\eta$ . Panels (c)–(e) depict the mechanisms of  $e^+e^- \rightarrow \omega\pi^0\pi^0$ . Here,  $\omega^*$  denotes the  $\omega(4S)$  and  $\omega(3D)$  intermediate states, while  $X_1$  denotes  $\rho$ ,  $\rho(1450)$ , and  $b_1(1235)$ , and  $X_2$  represents  $f_2(1270)$ . Adapted from Ref. [963].

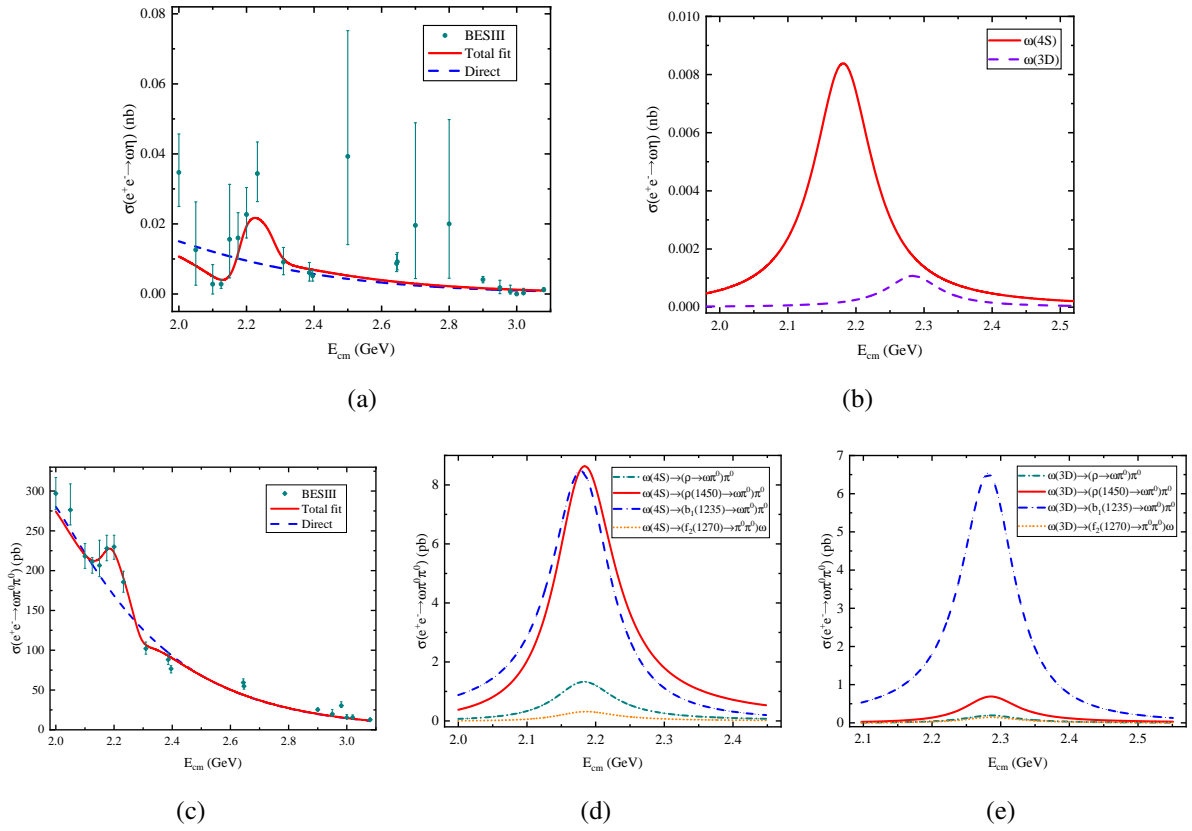


Figure 126: Fitted results to the experimental cross section data and the corresponding resonance contributions for  $e^+e^- \rightarrow \omega\eta$  (Panels (a) and (b)) and  $e^+e^- \rightarrow \omega\pi^0\pi^0$  (Panels (c)–(e)). Figures adapted from Ref. [963].

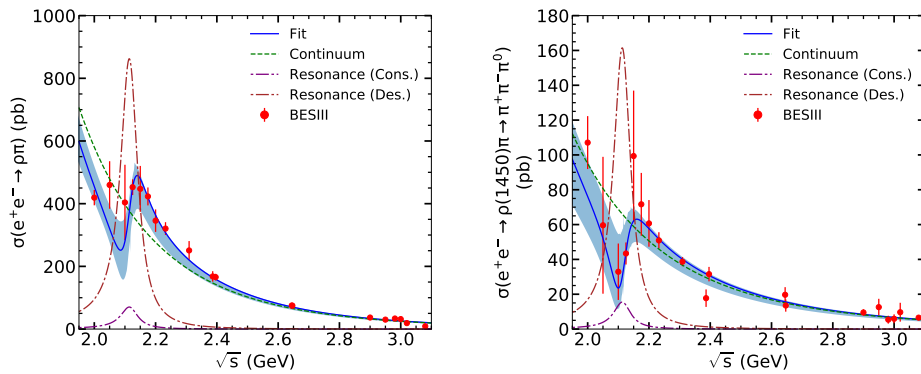


Figure 127: The measured cross sections for (a)  $e^+e^- \rightarrow \rho\pi$  and (b)  $e^+e^- \rightarrow \rho(1450)\pi \rightarrow \pi^+\pi^-\pi^0$ . The red points with error bars denote the experimental data. The blue solid curve with the shaded band represents the total fit, while the green dashed curve shows the continuum contribution. The purple dot-dashed and brown dot-dashed curves correspond to the resonance amplitudes for the constructive and destructive interference solutions, respectively. Adapted from Ref. [964].

a significant discrepancy, as illustrated in Table 17. Furthermore, the structure cannot be attributed to interference effects, since its measured mass lies far from the dominant  $S$ -wave states, while the contributions from nearby  $D$ -wave states are expected to be negligible due to the suppression of their dielectron widths. These considerations suggest that the  $Y(2119)$  cannot be readily accommodated within the conventional  $\omega$ -meson family.

Table 17: The predicted mass spectrum of the selected high-lying  $\omega$  meson states from Ref. [478], together with a comparison to the observed  $Y(2119)$  [964]. Table adapted from Ref. [965]

$\omega$ states	$\omega(2D)$	$\omega(4S)$	$\omega(3D)$	$Y(2119)$
Mass (MeV)	2003	2180	2283	$2119 \pm 11 \pm 15$
Width (MeV)	181	104	94	$69 \pm 30 \pm 5$
$\Gamma_{e^+e^-}$ (eV)	2.2	7.0	1.8	...

Upon examining the details of the above comparison, we observe that the mass of the  $\omega(4S)$  is higher than that of the  $Y(2119)$ . To address this discrepancy, it is essential to identify a mechanism capable of lowering the mass of the  $\omega(4S)$  to align with that of the  $Y(2119)$ . A natural solution is to introduce a  $4S$ - $3D$  state mixing scheme. The  $4S$ - $3D$  mixing scheme has been employed in the analyses of the charmoniumlike state  $Y(4220)$  and the bottomoniumlike state  $Y(10753)$ , as reviewed in the previous sections. In view of these applications, it is natural to consider extending this framework to the  $\omega$ -meson family. Specifically, in Ref. [965], Bai, Zhou, and Liu proposed the following mixing scheme:

$$\begin{pmatrix} |\omega'_{4S-3D}\rangle \\ |\omega''_{4S-3D}\rangle \end{pmatrix} = \begin{pmatrix} \cos \theta & \sin \theta \\ -\sin \theta & \cos \theta \end{pmatrix} \begin{pmatrix} |\omega(4S)\rangle \\ |\omega(3D)\rangle \end{pmatrix}, \quad (75)$$

and extracted a mixing angle of  $\theta = \pm(31.1^{+2.1}_{-3.1})^\circ$  by associating the observed  $Y(2119)$  with the  $\omega'_{4S-3D}$  state, as shown in Fig. 128.

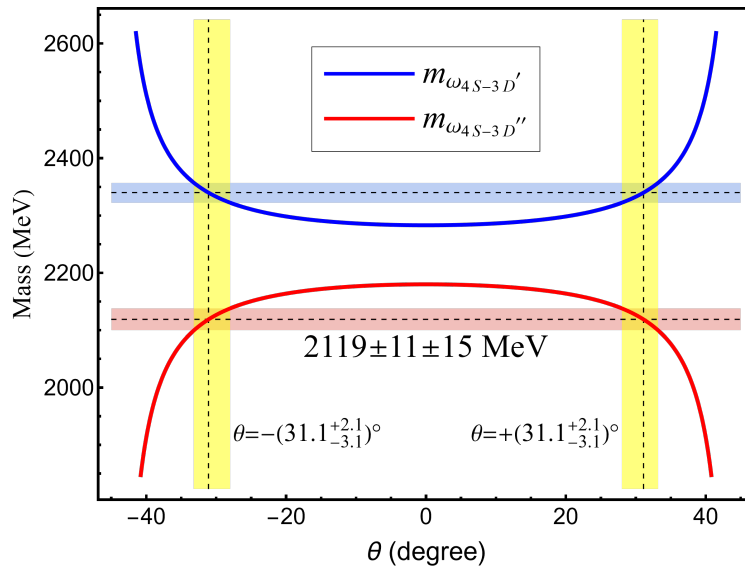


Figure 128: The masses of the mixed state  $\omega'_{4S-3D}$  and  $\omega''_{4S-3D}$  as function of the  $4S$ - $3D$  mixing angle  $\theta$ . The light red horizontal band represents the measured mass of the  $Y(2119)$ , while the yellow vertical bands indicate the mixing angles at which the theoretical mass of  $\omega'_{4S-3D}$  coincides with the  $Y(2119)$ . Additionally, the light blue horizontal band represents the predicted mass of  $\omega''_{4S-3D}$  at these mixing angles. Adapted from Ref. [965].

Then, the decay properties of  $Y(2119)$  were studied by assuming  $Y(2119)$  as the mixed state  $\omega'_{4S-3D}$ , and a comparison between the theoretical calculations and the corresponding experimental measurements for the relevant decay

channels is presented in Table 18.

Table 18: Theoretical predictions for the mixed  $\omega'_{4S-3D}$  state's mass, width ( $\Gamma$ ), dielectron width ( $\Gamma_{e^+e^-}^{\mathcal{R}}$ ), partial widths of  $\rho\pi$  and  $\rho(1450)\pi$  channels, and products  $\Gamma_{e^+e^-}^{\mathcal{R}} \times BR_{\mathcal{R}\rightarrow\rho\pi}$  and  $\Gamma_{e^+e^-}^{\mathcal{R}} \times BR_{\mathcal{R}\rightarrow\rho(1450)\pi\rightarrow\pi^+\pi^-\pi^0}$ , calculated for both negative and positive angles. Comparison with BESIII Collaboration measurements of the observed  $Y(2119)$  for constructive and destructive interference scenarios [964] is included. Adapted from Ref. [965].

Intermediate state $\mathcal{R}$	$\omega'_{4S-3D}$		$Y(2119)$ [964]	
	$\theta = -(31.1^{+2.1}_{-3.1})^\circ$	$\theta = +(31.1^{+2.1}_{-3.1})^\circ$	Constructive interference scenario	Destructive interference scenario
Mass (MeV)	$2119 \pm 11 \pm 15$	$2119 \pm 11 \pm 15$	$2119 \pm 11 \pm 15$	$2119 \pm 11 \pm 15$
$\Gamma$ (MeV)	$66.9^{+11.4}_{-9.9}$	$52.9^{+11.5}_{-9.5}$	$69 \pm 30 \pm 5$	$69 \pm 30 \pm 5$
$\Gamma_{e^+e^-}^{\mathcal{R}}$ (eV)	$10.0 \pm 0.2$	$2.6^{+0.4}_{-0.2}$	...	...
$\Gamma_{\mathcal{R}\rightarrow\rho\pi}$ (MeV)	$12.8^{+2.2}_{-1.9}$	$4.6^{+1.4}_{-1.0}$	...	...
$\Gamma_{\mathcal{R}\rightarrow\rho(1450)\pi}$ (MeV)	$24.8^{+4.4}_{-4.1}$	$8.5^{+3.0}_{-2.0}$	...	...
$\Gamma_{e^+e^-}^{\mathcal{R}} \times BR_{\mathcal{R}\rightarrow\rho\pi}$ (eV)	$1.9 \pm 0.5$	$0.2 \pm 0.1$	$1.5 \pm 0.7$	$17 \pm 12$
$\Gamma_{e^+e^-}^{\mathcal{R}} \times BR_{\mathcal{R}\rightarrow\rho(1450)\pi\rightarrow\pi^+\pi^-\pi^0}$ (eV)	$0.4 \pm 0.1$	$0.04 \pm 0.02$	$0.3 \pm 0.2$	$3 \pm 2$

As shown in Table 18, the calculated masses and total widths are consistent with the measured parameters of the  $Y(2119)$  for both positive and negative mixing angles. A further comparison between the experimental measurements and the theoretical calculations of the products of the dielectron width and branching ratios for the  $\rho\pi$  and  $\rho(1450)\pi$  channels is performed. These quantities are directly proportional to the amplitudes for  $e^+e^-$  annihilation into the corresponding final states via the  $Y(2119)$  resonance. It is found that the  $\omega'_{4S-3D}$  state with a negative mixing angle yields  $\Gamma_{e^+e^-}^{\mathcal{R}} \times BR_{\mathcal{R}\rightarrow\rho\pi}$  and  $\Gamma_{e^+e^-}^{\mathcal{R}} \times BR_{\mathcal{R}\rightarrow\rho(1450)\pi\rightarrow\pi^+\pi^-\pi^0}$ , that are in excellent agreement with those of the measured  $Y(2119)$  in the constructive interference scenario. This supports the assignment of the  $Y(2119)$  to the mixed state  $\omega'_{4S-3D}$  with a negative mixing angle  $\theta = -(31.1^{+2.1}_{-3.1})^\circ$ . Moreover, the experimental analysis provides two interference solutions, corresponding to constructive and destructive interference between the resonance amplitude and the continuum background for the  $Y(2119)$ , as shown in Fig. 127. The present analysis indicates that only the constructive interference solution is physically viable, whereas the destructive interference solution does not correspond to a viable physical scenario.

Furthermore, the dominant decay channels of the  $Y(2119)$  are investigated within the mixed state scenario with the negative mixing angle. In addition to the  $\rho\pi$  and  $\rho(1450)\pi$  modes, the  $\rho a_0(980)$  and  $b_1(1235)\pi$  channels are identified as promising for future experimental searches for the  $Y(2119)$ . In this framework, a  $D$ -wave dominated partner of the  $Y(2119)$  is also expected, with a mass around 2340 MeV. However, there are significant experimental challenges in observing this state in  $e^+e^-$  collisions, since its dielectron width is predicted to be extremely small. Such a state may instead be accessible at other experimental facilities, such as meson beam experiments.

**7.3.3.3. High-lying  $\rho$ -related processes.** Theoretically, the dielectron widths of the  $\rho$ -mesonic states are generally about one order of magnitude larger than those of the  $\omega$ -mesonic states [478], implying that  $\rho$  mesons are produced more copiously at  $e^+e^-$  collision facilities. In recent years, several structures associated with high-lying  $\rho$  states have been reported in experimental measurements of exclusive cross sections around 2 GeV, including  $e^+e^- \rightarrow \pi^+\pi^-$  [966, 967],  $e^+e^- \rightarrow f_1(1285)\pi^+\pi^-$  [968, 969],  $e^+e^- \rightarrow \omega\pi^0$  [961, 970],  $e^+e^- \rightarrow \eta'\pi^+\pi^-$  [971], and  $e^+e^- \rightarrow \eta\pi^+\pi^-$  [972].

In the mass region around 2 GeV, three  $\rho$ -mesonic states, namely  $\rho(1900)$ ,  $\rho(2000)$ , and  $\rho(2150)$ , have been collected by the PDG [94]. In Refs. [947, 973, 916], the Lanzhou group pointed out that interference effects play an essential role in understanding these reported structures and the corresponding measured cross-section data. In particular, the measured cross sections for  $e^+e^- \rightarrow \pi^+\pi^-$ ,  $e^+e^- \rightarrow f_1(1285)\pi^+\pi^-$ , and  $e^+e^- \rightarrow \omega\pi^0$  can be well

reproduced by the intermediate  $\rho(1900)$  and  $\rho(2150)$  contributions, together with the interference effect between them. Meanwhile, the cross section for the  $e^+e^- \rightarrow \eta'\pi^+\pi^-$  process can be well described by the coherent contributions of  $\rho(2000)$  and  $\rho(2150)$ . Within these interpretations,  $\rho(1900)$ ,  $\rho(2000)$ , and  $\rho(2150)$  are assigned as the  $\rho(3S)$ ,  $\rho(2D)$ , and  $\rho(4S)$  states, respectively.

More recently, the BESIII Collaboration reported precise measurements of the cross sections for the process  $e^+e^- \rightarrow \eta\pi^+\pi^-$  at center-of-mass energies ranging from 2.00 to 3.08 GeV [972]. Through a partial wave analysis, a  $\rho$ -like structure, denoted as  $Y(2044)$ , was observed in the cross section distribution of the subprocess  $e^+e^- \rightarrow a_2(1320)\pi$ , with a fitted mass  $M = 2044 \pm 21 \pm 4$  MeV and a fitted width  $\Gamma = 163 \pm 69 \pm 24$  MeV. Furthermore, the product of the dielectron width and the branching ratio,  $\Gamma_{e^+e^-} BR_{a_2(1320)\pi}$ , was determined to be  $(34.6 \pm 17.1 \pm 6.0)$  eV or  $(137.1 \pm 73.3 \pm 2.1)$  eV, depending on whether constructive or destructive interference was assumed in the cross section analysis.

The extracted resonance parameters of  $Y(2044)$  are broadly consistent with the theoretical expectations for the  $\rho(2D)$  state. Nevertheless, assigning  $Y(2044)$  as the  $\rho(2D)$  state is challenged by a notable discrepancy. In the unquenched spectroscopy framework, the theoretical predictions for the dielectron width  $\Gamma_{e^+e^-}$  and the branching ratio  $BR_{a_2(1320)\pi}$  of the pure  $\rho(2D)$  state are about 20 eV and 3.6%, respectively. Consequently, the resulting product  $\Gamma_{e^+e^-} BR_{a_2(1320)\pi}$  is nearly two orders of magnitude smaller than the corresponding experimental values reported for  $Y(2044)$ . This inconsistency disfavors an interpretation of  $Y(2044)$  as a pure  $\rho(2D)$  state.

To understand the  $Y(2044)$  structure observed in the measured cross section of  $e^+e^- \rightarrow a_2(1320)\pi$ , a first attempt was made in Ref. [974] by considering the interference effects among the four high-lying  $\rho$  meson states around 2 GeV. However, the fitting results for the  $e^+e^- \rightarrow a_2(1320)\pi$  cross section indicate that the peak structure around 2044 MeV cannot be reproduced by taking into account only the interference among these states, as shown in Fig. 129. This result suggests that the unsuccessful fit may be attributed to the limited contribution of the  $\rho(2D)$  state to the  $e^+e^- \rightarrow a_2(1320)\pi$  cross section.

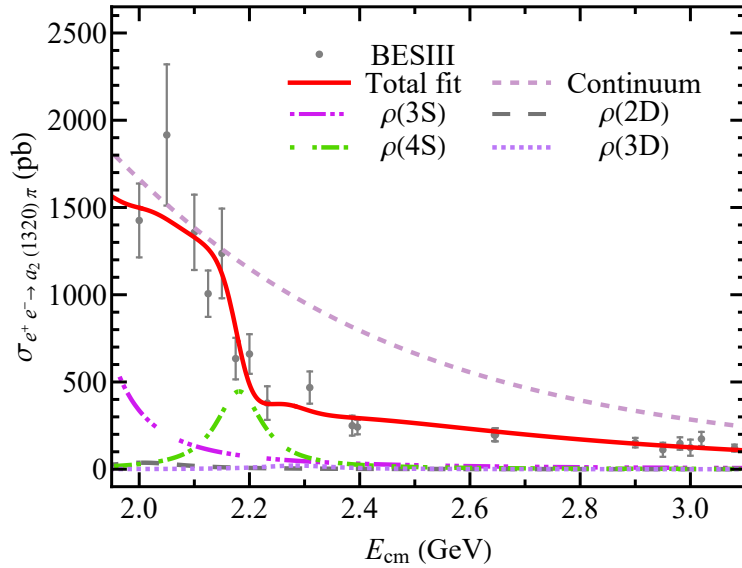


Figure 129: Fit to the measured cross section of the process  $e^+e^- \rightarrow a_2(1320)\pi$  including only the interference among the  $\rho(3S)$ ,  $\rho(2D)$ ,  $\rho(4S)$ , and  $\rho(3D)$  states [972], where the resonance contributions are fixed by the unquenched spectroscopy framework. The figure is adapted from Ref. [974].

It has been shown that the  $S$ - $D$  mixing effect plays a crucial role in understanding the spectroscopy of meson families in both the heavy- and light-flavor sectors, as discussed above. In Ref. [974], Zhou, Bai, Wang, Xu, and Liu proposed the  $3S$ - $2D$  and  $4S$ - $3D$  mixing schemes to reanalyze the cross sections of  $e^+e^- \rightarrow a_2(1320)\pi$ , as well as several additional high-lying  $\rho$ -related processes, including  $e^+e^- \rightarrow \omega\pi^0$ ,  $e^+e^- \rightarrow f_1(1285)\pi^+\pi^-$ ,  $e^+e^- \rightarrow \pi^+\pi^-$ ,  $e^+e^- \rightarrow \rho\eta$ , and  $e^+e^- \rightarrow \eta'\pi^+\pi^-$ .

Within the  $S$ - $D$  mixing framework, the  $\rho(nS)$ - $\rho((n-1)D)$  mixing can be expressed as [974]

$$\begin{pmatrix} |\rho'_{nS-(n-1)D}\rangle \\ |\rho''_{nS-(n-1)D}\rangle \end{pmatrix} = \begin{pmatrix} \cos \theta & \sin \theta \\ -\sin \theta & \cos \theta \end{pmatrix} \begin{pmatrix} |\rho(nS)\rangle \\ |\rho((n-1)D)\rangle \end{pmatrix}, \quad (76)$$

where  $\theta$  denotes the mixing angle between  $\rho(nS)$  and  $\rho((n-1)D)$ . The masses and decay properties of the mixed states  $\rho'_{3S-2D}$ ,  $\rho''_{3S-2D}$ ,  $\rho'_{4S-3D}$ , and  $\rho''_{4S-3D}$  as functions of the mixing angle  $\theta$  are shown in Figs. 130 and 131, respectively.

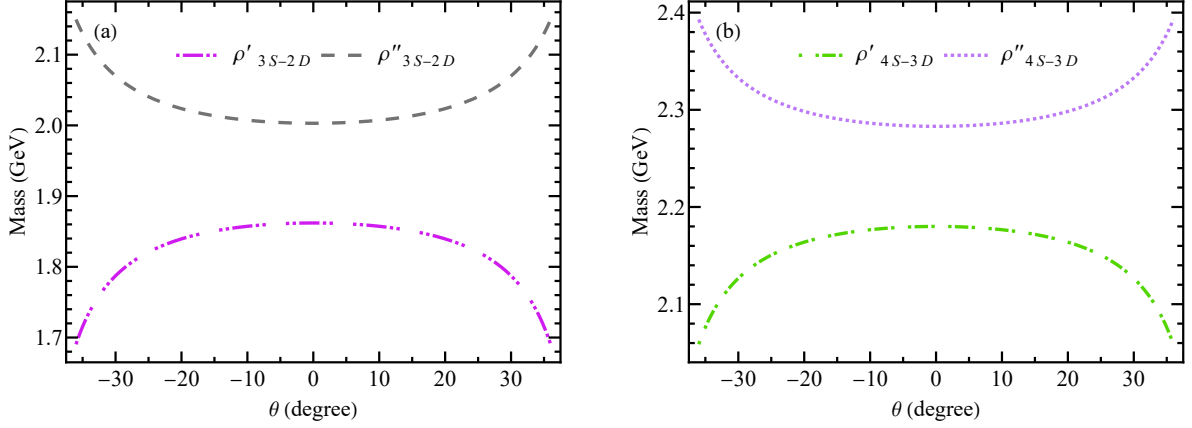


Figure 130: Masses of the mixed states as functions of the mixing angle  $\theta$ . Panel (a) shows the masses of the mixed states  $\rho'_{3S-2D}$  and  $\rho''_{3S-2D}$ , while panel (b) shows those of  $\rho'_{4S-3D}$  and  $\rho''_{4S-3D}$ . Adapted from Ref. [974].

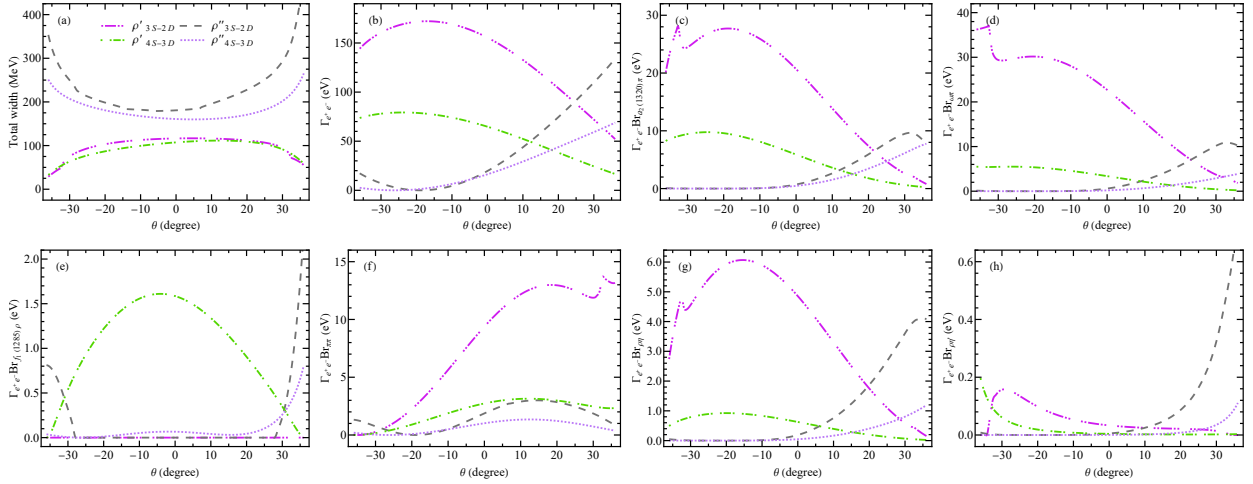


Figure 131: Decay behaviors of the mixed states  $\rho'_{3S-2D}$ ,  $\rho''_{3S-2D}$ ,  $\rho'_{4S-3D}$ , and  $\rho''_{4S-3D}$  as functions of the mixing angle  $\theta$ . Panel (a) shows the total widths, panel (b) shows the dielectron widths, and panels (c)–(h) show the products of the dielectron width and branching ratios for  $a_2(1320)\pi$  (panel (c)),  $\omega\pi$  (panel (d)),  $f_1(1285)\rho$  (panel (e)),  $\pi\pi$  (panel (f)),  $\rho\eta$  (panel (g)), and  $\rho\eta'$  (panel (h)). Figures adapted from Ref. [974].

From Fig. 131, it is evident that the  $S$ - $D$  mixing effects have a significant impact on the decay behaviors of these high-lying  $\rho$  states. The central idea for determining the mixing angles is to identify the ideal processes in which a specific intermediate  $\rho$  state dominates over other  $\rho$  states in the 2 GeV energy region, such that the corresponding interference effects can be neglected.

Following this strategy, the  $3S$ - $2D$  mixing angle  $\theta_{3S-2D}$  is first constrained to be positive in order to enhance the contribution of  $\rho''_{3S-2D}$  to the cross section of  $e^+e^- \rightarrow a_2(1320)\pi$ , as shown in Fig. 131(c). In this positive  $\theta_{3S-2D}$

scenario, the contribution of  $\rho''_{3S-2D}$  dominates the  $Y(2034)$  structure observed in the  $e^+e^- \rightarrow \omega\pi^0$  process [961], while the contribution from the adjacent  $\rho'_{4S-3D}$  state is relatively small, as shown in Fig. 131(d). Moreover, the masses of the other two mixed states are considerably distant from 2034 MeV, so their interference effects are expected to be negligible. Therefore, the  $Y(2034)$  structure can be regarded as a good candidate for  $\rho''_{3S-2D}$ , leading to a determination of the mixing angle  $\theta_{3S-2D} = 23.4^\circ$ . The theoretical width of  $\rho''_{3S-2D}$  at this mixing angle is also consistent with the measured width of  $Y(2034)$ .

The process  $e^+e^- \rightarrow f_1(1285)\rho$  then provides an ideal channel to determine the  $4S-3D$  mixing angle. The study by the BaBar Collaboration on  $e^+e^- \rightarrow f_1(1285)\pi^+\pi^-$  [969] shows that the  $\pi^+\pi^-$  system is dominantly produced via  $\rho(770)$ . Consequently, when  $\rho'_{3S-2D}$  and  $\rho''_{3S-2D}$  serve as intermediate states, their contributions are suppressed because the  $\rho(770)$  is off shell. In addition, the BABAR data reveal an enhancement only around 2150 MeV, with no evidence of additional structures at higher energies, and the mixing angle  $\theta_{4S-3D}$  is unlikely to be very large. This further indicates that the contribution of  $\rho''_{4S-3D}$  should be not significant in this channel. Hence, the  $\rho(2150)$  structure can be safely assigned to  $\rho'_{4S-3D}$ , yielding  $\theta_{4S-3D} = \pm 25.1^\circ$ .

Based on the proposed mixing scheme, a combined fit to the cross section data of the processes  $e^+e^- \rightarrow a_2(1320)\pi$ ,  $e^+e^- \rightarrow \omega\pi^0$ ,  $e^+e^- \rightarrow f_1(1285)\pi^+\pi^-$ ,  $e^+e^- \rightarrow \pi^+\pi^-$ ,  $e^+e^- \rightarrow \rho\eta$ , and  $e^+e^- \rightarrow \eta'\pi^+\pi^-$  is performed, where four mixed states around 2 GeV,  $\rho'_{3S-2D}$ ,  $\rho''_{3S-2D}$ ,  $\rho'_{4S-3D}$ , and  $\rho''_{4S-3D}$ , are taken as intermediate resonances. The contributions of these resonances to the corresponding cross sections are fixed by the unquenched spectroscopy framework. Two initial schemes,  $\theta_{4S-3D} = -25.1^\circ$  and  $\theta_{4S-3D} = 25.1^\circ$ , are adopted in the fit. It is found that the negative- $\theta_{4S-3D}$  scheme fails to reproduce the measured cross section data, whereas the positive- $\theta_{4S-3D}$  scheme provides a good description of all six processes, as shown in Fig. 132. These results indicate that the  $\rho(4S)-\rho(3D)$  mixing angle favors a positive value,  $\theta_{4S-3D} = 25.1^\circ$ . In this framework, the  $Y(2044)$  structure observed in  $e^+e^- \rightarrow a_2(1320)\pi$  [972] is reproduced by the four  $S-D$  mixed  $\rho$  states, with the dominant contribution arising from  $\rho''_{3S-2D}$  and a non-negligible interference effect among the resonances.

Table 19: Masses, total widths, and dielectron widths of the mixed states  $\rho'_{3S-2D}$ ,  $\rho''_{3S-2D}$ ,  $\rho'_{4S-3D}$ , and  $\rho''_{4S-3D}$  in Ref. [974], evaluated with the mixing angles  $\theta_{3S-2D} = 23.4^\circ$  and  $\theta_{4S-3D} = 25.1^\circ$ .

$\rho$ states	$\rho'_{3S-2D}$	$\rho''_{3S-2D}$	$\rho'_{4S-3D}$	$\rho''_{4S-3D}$
Mass (MeV)	1828	2034	2150	2311
Width (MeV)	109	243	103	182
$\Gamma_{e^+e^-}$ (eV)	93.4	85.9	31.0	51.8

Overall, by introducing four theoretically constructed mixed states,  $\rho'_{3S-2D}$ ,  $\rho''_{3S-2D}$ ,  $\rho'_{4S-3D}$ , and  $\rho''_{4S-3D}$  (listed in Table 19), the measured cross section data for the high-lying  $\rho$ -related processes can be well described within a unified theoretical framework.

Collectively, the puzzles of the apparent inconsistencies among the reported resonance parameters in various final states—spanning the  $\rho$ ,  $\omega$ , and  $\phi$  sectors around 2 GeV—are coherently solved within a unified framework that combines the same unquenched spectroscopy with the interference effects. This series of concrete applications validates the proposed strategy for constructing the high-lying spectra via spectroscopy-guided cross section analysis, demonstrating its viability for studying the light-flavor vector meson family and its promising potential for extension to other light hadron sectors with different quantum numbers.

## 8. Summary

Driven by sustained advances in experimental techniques and the continual accumulation of data, hadron spectroscopy has undergone rapid development over the past two decades. This progress is evident from the multitude of high-quality reviews and related literature. It has not only fueled the extensive search for exotic hadrons—a cornerstone in building the "Particle Zoo 2.0"—but also established itself as a major direction in contemporary hadron spectroscopy research.

Confronted with a wealth of recent experimental discoveries, it is instructive to recall pivotal moments in the history of particle physics. In the 1950s and 1960s, the discovery of light hadrons spurred the study of hadron

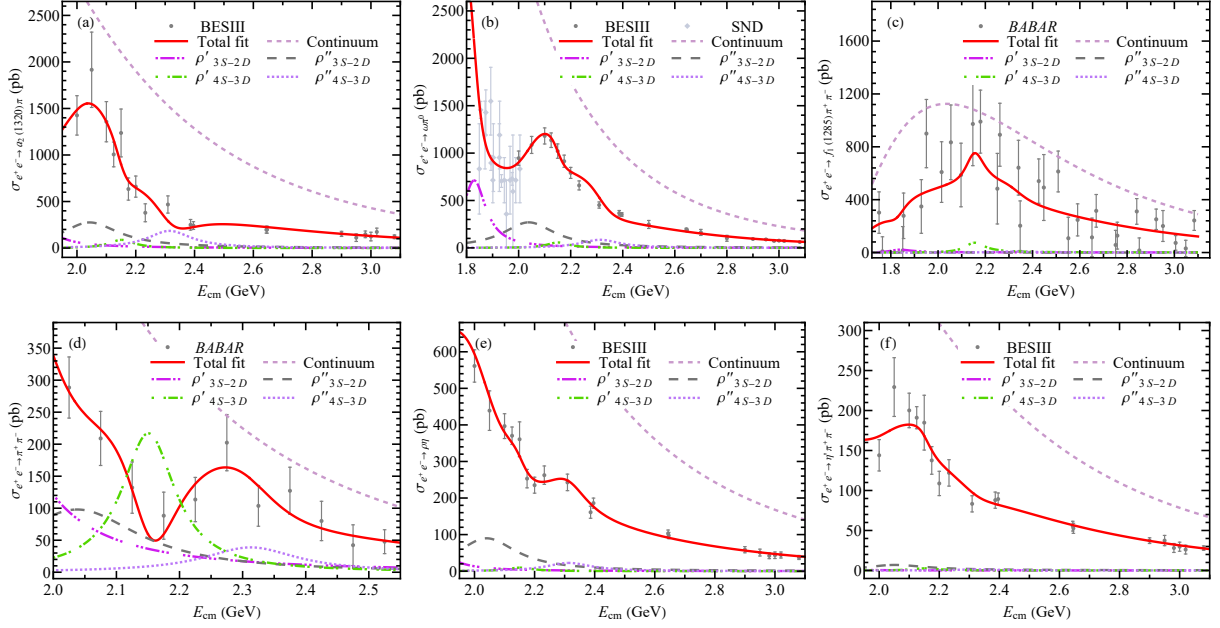


Figure 132: Combined fit to the measured cross sections for the processes  $e^+e^- \rightarrow a_2(1320)\pi$  [972] (panel (a)),  $e^+e^- \rightarrow \omega\pi^0$  [961, 970] (panel (b)),  $e^+e^- \rightarrow f_1(1285)\pi^+\pi^-$  [968, 969] (panel (c)),  $e^+e^- \rightarrow \pi^+\pi^-$  [968, 969] (panel (d)),  $e^+e^- \rightarrow \rho\eta$  [972] (panel (e)), and  $e^+e^- \rightarrow \eta'\pi^+\pi^-$  [971] (panel (f)). The figures are adapted from Ref. [974].

classification, leading to the establishment of SU(3) flavor symmetry. In the 1970s and 1980s, the subsequent discoveries of charmonia gave rise to the Cornell potential, a model describing quark interactions. This model not only successfully explained the charmonium spectrum at the time but also laid the quantitative foundation for hadron spectroscopy, becoming the progenitor of many subsequent spectroscopic models. Following this historical logic, the continuous emergence of high-statistics data over the last twenty years—primarily represented by charmonium-like XYZ states—gives us strong reason to anticipate new theoretical breakthroughs, just as history has repeatedly demonstrated. We find ourselves both witnesses and participants in this ongoing process.

While the search for exotic hadrons commands significant attention, an equally important parallel aspect must be emphasized: these high-precision data provide stringent tests for the reliability and applicability of various phenomenological models. This presents a rare opportunity. Due to the non-perturbative nature of the strong interaction, phenomenological models remain indispensable tools, on par with experiment and lattice QCD, for understanding non-perturbative strong dynamics. These three pillars can be likened to the three interlocked rings of a Borromean ring: intimately connected and mutually supportive, together they form a robust framework for hadron physics research.

The solution to the low-mass puzzles associated with new hadrons such as  $X(3872)$ ,  $D_{s0}^*(2317)$ ,  $D'_{s1}(2460)$ , and  $\Lambda_c(2940)$  has highlighted the critical importance of "unquenched effects" in hadron spectroscopy. Before the year 2000, the construction of the hadron spectrum focused predominantly on low-lying states. The quenched model achieved remarkable success in describing the spectroscopy of these states, primarily because most low-lying states lie below the thresholds of their allowed hadronic channels, thus experiencing negligible coupled-channel effects. Consequently, the physical states largely coincide with the bare states.

However, since 2003, a large number of newly discovered hadrons are closely related to high-lying states. Within the framework of coupled-channel dynamics, these states often exhibit strong couplings to open hadronic channels. This leads to significant modifications of the physical states, resulting in various novel phenomena. These phenomena appear "anomalous" precisely because they deviate from the predictions and calculations of the quenched model. This context makes the two statements quoted in Fig. 1 self-evident:

“The discovered charmonia prompted the development of the quenched potential model.”

“The quenched potential model has become outdated in light of the discovery of new hadronic states.”

Therefore, we are experiencing a "*paradigm shift from the quenched to the unquenched picture*".

This review adopts this very perspective to examine hadron spectroscopy. Through a series of concrete examples, it systematically demonstrates how unquenched effects manifest in spectroscopic studies. These effects are not only prominently displayed in (charmonium-like) charmonium spectroscopy but are also universally relevant to bottomonium and light hadron spectroscopy. This universality underscores that unquenched effects are not isolated curiosities but a general rule. Such pervasiveness typically indicates that we are touching upon the essence of the phenomena—an insight that cannot be overlooked.

The research trajectory outlined here spans the past two decades. We take satisfaction in using this review to illustrate the enduring vitality of the unquenched picture in hadron spectroscopy. Our sentiment at this juncture is aptly captured by the ancient Chinese poetic line: “**The falling leaf reveals the coming of autumn** (一叶落而知天下秋)” —perceiving the overarching shift from a subtle sign.

Standing at the vantage point of 2026, this review has looked back on the past, but we must also look forward. A natural question arises: **What is the future direction of hadron spectroscopy?**

Our answer is clear: hadron spectroscopy is entering a "high-precision era". This is reflected not only in the continually improving experimental precision at facilities like BESIII, LHCb, and Belle II but also inevitably in the enhanced precision of theoretical studies. Now that the crucial role of unquenched effects is recognized, we must take this as our starting point to usher in a new phase of high-precision hadron spectroscopy. This entails developing more sophisticated unquenched models to deepen our understanding of non-perturbative strong interaction dynamics. This is not only our responsibility but also the shared mission of the new generation of particle physicists.

## Acknowledgements

We would like to thank Ri-Qing Qian, Zi-Long Man, Qin-Song Zhou, and Li-Ming Wang, Tian-Cai Peng, Xue-Qian Li for their collaboration. This review is also dedicated to the memory of two esteemed mentors. One of the authors, X.L., wishes to honor Professor Eef van Beveren, under whose guidance X.L. conducted postdoctoral research at the University of Coimbra with funding from FCT. Professor van Beveren was among the first internationally to recognize the importance of unquenched effects in hadron spectroscopy, as exemplified by his pioneering explanation for the low-mass puzzle of the  $D_{s0}^*(2317)$ . Beyond his scientific insight, he instilled in me a deep respect for experimental data and an enduring optimism in facing challenges. X.L. also dedicates this work to Professor Takayuki Matsuki. Many of the results presented here are the fruit of our collaboration that spanned over a decade. This work is also supported by the National Natural Science Foundation of China under Grant Nos. 12335001 and 12247101, the ‘111 Center’ under Grant No. B20063, the Natural Science Foundation of Gansu Province (No. 22JR5RA389, No. 25JRRA799), the fundamental Research Funds for the Central Universities, the project for top-notch innovative talents of Gansu province, and Lanzhou City High-Level Talent Funding.

## References

- [1] SLAC National Accelerator Laboratory, [SLAC celebrates 50 years of a nobel-winning discovery in particle physics](https://www6.slac.stanford.edu/news/2024-11-20-slac-celebrates-50-years-nobel-winning-discovery) (Nov. 20 2024).  
URL <https://www6.slac.stanford.edu/news/2024-11-20-slac-celebrates-50-years-nobel-winning-discovery>
- [2] IHEP–CERN Joint Symposium, [50 years of the  \$J/\psi\$  discovery: from the november revolution to the precision frontier](https://cds.cern.ch/record/2935663).  
URL <https://cds.cern.ch/record/2935663>
- [3] J. J. Aubert, et al., Experimental Observation of a Heavy Particle  $J$ , Phys. Rev. Lett. 33 (1974) 1404–1406. doi:10.1103/PhysRevLett.33.1404.
- [4] J. E. Augustin, et al., Discovery of a Narrow Resonance in  $e^+e^-$  Annihilation, Phys. Rev. Lett. 33 (1974) 1406–1408. doi:10.1103/PhysRevLett.33.1406.

- [5] S. L. Glashow, J. Iliopoulos, L. Maiani, Weak interactions with lepton-hadron symmetry, *Phys. Rev. D* 2 (1970) 1285–1292. doi:[10.1103/PhysRevD.2.1285](https://doi.org/10.1103/PhysRevD.2.1285).
- [6] M. Gell-Mann, The eightfold way: A theory of strong interaction symmetry (3 1961). doi:[10.2172/4008239](https://doi.org/10.2172/4008239).
- [7] Y. Ne’eman, Derivation of strong interactions from a gauge invariance, *Nucl. Phys.* 26 (1961) 222–229. doi:[10.1016/0029-5582\(61\)90134-1](https://doi.org/10.1016/0029-5582(61)90134-1).
- [8] M. Gell-Mann, A schematic model of baryons and mesons, *Phys. Lett.* 8 (1964) 214–215. doi:[10.1016/S0031-9163\(64\)92001-3](https://doi.org/10.1016/S0031-9163(64)92001-3).
- [9] G. Zweig, An SU(3) model for strong interaction symmetry and its breaking. Version 1 (1 1964). doi:[10.17181/CERN-TH-401](https://doi.org/10.17181/CERN-TH-401).
- [10] E. Eichten, K. Gottfried, T. Kinoshita, J. B. Kogut, K. D. Lane, T.-M. Yan, The spectrum of charmonium, *Phys. Rev. Lett.* 34 (1975) 369–372, [Erratum: *Phys.Rev.Lett.* 36, 1276 (1976)]. doi:[10.1103/PhysRevLett.34.369](https://doi.org/10.1103/PhysRevLett.34.369).
- [11] E. Eichten, K. Gottfried, T. Kinoshita, K. D. Lane, T.-M. Yan, Charmonium: The model, *Phys. Rev. D* 17 (1978) 3090, [Erratum: *Phys.Rev.D* 21, 313 (1980)]. doi:[10.1103/PhysRevD.17.3090](https://doi.org/10.1103/PhysRevD.17.3090).
- [12] E. Eichten, K. Gottfried, T. Kinoshita, K. D. Lane, T.-M. Yan, Charmonium: Comparison with experiment, *Phys. Rev. D* 21 (1980) 203. doi:[10.1103/PhysRevD.21.203](https://doi.org/10.1103/PhysRevD.21.203).
- [13] S. Godfrey, N. Isgur, Mesons in a relativized quark model with chromodynamics, *Phys. Rev. D* 32 (1985) 189–231. doi:[10.1103/PhysRevD.32.189](https://doi.org/10.1103/PhysRevD.32.189).
- [14] E. Klempt, A. Zaitsev, Glueballs, Hybrids, Multiquarks. Experimental facts versus QCD inspired concepts, *Phys. Rept.* 454 (2007) 1–202. [arXiv:0708.4016](https://arxiv.org/abs/0708.4016), doi:[10.1016/j.physrep.2007.07.006](https://doi.org/10.1016/j.physrep.2007.07.006).
- [15] N. Brambilla, et al., Heavy quarkonium: Progress, puzzles, and opportunities, *Eur. Phys. J. C* 71 (2011) 1534. [arXiv:1010.5827](https://arxiv.org/abs/1010.5827), doi:[10.1140/epjc/s10052-010-1534-9](https://doi.org/10.1140/epjc/s10052-010-1534-9).
- [16] X. Liu, An overview of XYZ new particles, *Chin. Sci. Bull.* 59 (2014) 3815–3830. [arXiv:1312.7408](https://arxiv.org/abs/1312.7408), doi:[10.1007/s11434-014-0407-2](https://doi.org/10.1007/s11434-014-0407-2).
- [17] A. Hosaka, T. Iijima, K. Miyabayashi, Y. Sakai, S. Yasui, Exotic hadrons with heavy flavors: X, Y, Z, and related states, *PTEP* 2016 (6) (2016) 062C01. [arXiv:1603.09229](https://arxiv.org/abs/1603.09229), doi:[10.1093/ptep/ptw045](https://doi.org/10.1093/ptep/ptw045).
- [18] J.-M. Richard, Exotic hadrons: review and perspectives, *Few Body Syst.* 57 (12) (2016) 1185–1212. [arXiv:1606.08593](https://arxiv.org/abs/1606.08593), doi:[10.1007/s00601-016-1159-0](https://doi.org/10.1007/s00601-016-1159-0).
- [19] H.-X. Chen, W. Chen, X. Liu, S.-L. Zhu, The hidden-charm pentaquark and tetraquark states, *Phys. Rept.* 639 (2016) 1–121. [arXiv:1601.02092](https://arxiv.org/abs/1601.02092), doi:[10.1016/j.physrep.2016.05.004](https://doi.org/10.1016/j.physrep.2016.05.004).
- [20] A. Esposito, A. Pilloni, A. D. Polosa, Multiquark resonances, *Phys. Rept.* 668 (2017) 1–97. [arXiv:1611.07920](https://arxiv.org/abs/1611.07920), doi:[10.1016/j.physrep.2016.11.002](https://doi.org/10.1016/j.physrep.2016.11.002).
- [21] H.-X. Chen, W. Chen, X. Liu, Y.-R. Liu, S.-L. Zhu, A review of the open charm and open bottom systems, *Rept. Prog. Phys.* 80 (7) (2017) 076201. [arXiv:1609.08928](https://arxiv.org/abs/1609.08928), doi:[10.1088/1361-6633/aa6420](https://doi.org/10.1088/1361-6633/aa6420).
- [22] R. F. Lebed, R. E. Mitchell, E. S. Swanson, Heavy-quark QCD exotica, *Prog. Part. Nucl. Phys.* 93 (2017) 143–194. [arXiv:1610.04528](https://arxiv.org/abs/1610.04528), doi:[10.1016/j.pnpnp.2016.11.003](https://doi.org/10.1016/j.pnpnp.2016.11.003).
- [23] F.-K. Guo, C. Hanhart, U.-G. Meißner, Q. Wang, Q. Zhao, B.-S. Zou, Hadronic molecules, *Rev. Mod. Phys.* 90 (1) (2018) 015004, [Erratum: *Rev.Mod.Phys.* 94, 029901 (2022)]. [arXiv:1705.00141](https://arxiv.org/abs/1705.00141), doi:[10.1103/RevModPhys.90.015004](https://doi.org/10.1103/RevModPhys.90.015004).

- [24] S. L. Olsen, T. Skwarnicki, D. Zieminska, Nonstandard heavy mesons and baryons: Experimental evidence, *Rev. Mod. Phys.* 90 (1) (2018) 015003. [arXiv:1708.04012](#), [doi:10.1103/RevModPhys.90.015003](#).
- [25] A. Ali, J. S. Lange, S. Stone, Exotics: Heavy pentaquarks and tetraquarks, *Prog. Part. Nucl. Phys.* 97 (2017) 123–198. [arXiv:1706.00610](#), [doi:10.1016/j.pnpnp.2017.08.003](#).
- [26] Y.-R. Liu, H.-X. Chen, W. Chen, X. Liu, S.-L. Zhu, Pentaquark and tetraquark states, *Prog. Part. Nucl. Phys.* 107 (2019) 237–320. [arXiv:1903.11976](#), [doi:10.1016/j.pnpnp.2019.04.003](#).
- [27] N. Brambilla, S. Eidelman, C. Hanhart, A. Nefediev, C.-P. Shen, C. E. Thomas, A. Vairo, C.-Z. Yuan, The XYZ states: Experimental and theoretical status and perspectives, *Phys. Rept.* 873 (2020) 1–154. [arXiv:1907.07583](#), [doi:10.1016/j.physrep.2020.05.001](#).
- [28] H.-X. Chen, W. Chen, X. Liu, Y.-R. Liu, S.-L. Zhu, An updated review of the new hadron states, *Rept. Prog. Phys.* 86 (2) (2023) 026201. [arXiv:2204.02649](#), [doi:10.1088/1361-6633/aca3b6](#).
- [29] L. Meng, B. Wang, G.-J. Wang, S.-L. Zhu, Chiral perturbation theory for heavy hadrons and chiral effective field theory for heavy hadronic molecules, *Phys. Rept.* 1019 (2023) 1–149. [arXiv:2204.08716](#), [doi:10.1016/j.physrep.2023.04.003](#).
- [30] F.-L. Wang, X.-D. Yang, R. Chen, X. Liu, Correlation of the hidden-charm molecular tetraquarks and the charmoniumlike structures existing in the  $B \rightarrow XYZ + K$  process, *Phys. Rev. D* 104 (9) (2021) 094010. [arXiv:2103.04698](#), [doi:10.1103/PhysRevD.104.094010](#).
- [31] X. Wang, X. Liu, Y. Gao, Colloquium: Hadron Production in Open-charm Meson Pair at  $e^+e^-$  Collider (2025). [arXiv:2502.15117](#).
- [32] S. K. Choi, et al., Observation of a narrow charmonium-like state in exclusive  $B^\pm \rightarrow K^\pm \pi^+ \pi^- J/\psi$  decays, *Phys. Rev. Lett.* 91 (2003) 262001. [arXiv:hep-ex/0309032](#), [doi:10.1103/PhysRevLett.91.262001](#).
- [33] B. Aubert, et al., Observation of a narrow meson decaying to  $D_s^+ \pi^0$  at a mass of 2.32 GeV/ $c^2$ , *Phys. Rev. Lett.* 90 (2003) 242001. [arXiv:hep-ex/0304021](#), [doi:10.1103/PhysRevLett.90.242001](#).
- [34] D. Besson, et al., Observation of a narrow resonance of mass 2.46 GeV/ $c^2$  decaying to  $D_s^{*+} \pi^0$  and confirmation of the  $D_{sJ}^*(2317)$  state, *Phys. Rev. D* 68 (2003) 032002, [Erratum: *Phys.Rev.D* 75, 119908 (2007)]. [arXiv:hep-ex/0305100](#), [doi:10.1103/PhysRevD.68.032002](#).
- [35] B. Aubert, et al., Observation of a charmed baryon decaying to  $D^0 p$  at a mass near 2.94 GeV/ $c^2$ , *Phys. Rev. Lett.* 98 (2007) 012001. [arXiv:hep-ex/0603052](#), [doi:10.1103/PhysRevLett.98.012001](#).
- [36] B. Silvestre-Brac, C. Gignoux, Unitary effects in spin orbit splitting of  $P$ -wave baryons, *Phys. Rev. D* 43 (1991) 3699–3708. [doi:10.1103/PhysRevD.43.3699](#).
- [37] E. van Beveren, G. Rupp, Observed  $D_s(2317)$  and tentative  $D(2100-2300)$  as the charmed cousins of the light scalar nonet, *Phys. Rev. Lett.* 91 (2003) 012003. [arXiv:hep-ph/0305035](#), [doi:10.1103/PhysRevLett.91.012003](#).
- [38] D. S. Hwang, D.-W. Kim, Mass of  $D_{sJ}^*(2317)$  and coupled channel effect, *Phys. Lett. B* 601 (2004) 137–143. [arXiv:hep-ph/0408154](#), [doi:10.1016/j.physletb.2004.09.040](#).
- [39] Y. S. Kalashnikova, Coupled-channel model for charmonium levels and an option for  $X(3872)$ , *Phys. Rev. D* 72 (2005) 034010. [arXiv:hep-ph/0506270](#), [doi:10.1103/PhysRevD.72.034010](#).
- [40] B.-Q. Li, C. Meng, K.-T. Chao, Coupled-channel and screening effects in charmonium spectrum, *Phys. Rev. D* 80 (2009) 014012. [arXiv:0904.4068](#), [doi:10.1103/PhysRevD.80.014012](#).
- [41] O. Zhang, C. Meng, H. Q. Zheng, Ambiversion of  $X(3872)$ , *Phys. Lett. B* 680 (2009) 453–458. [arXiv:0901.1553](#), [doi:10.1016/j.physletb.2009.09.033](#).

- [42] P. G. Ortega, J. Segovia, D. R. Entem, F. Fernandez, Coupled channel approach to the structure of the  $X(3872)$ , Phys. Rev. D 81 (2010) 054023. [arXiv:0907.3997](#), [doi:10.1103/PhysRevD.81.054023](#).
- [43] I. V. Danilkin, Y. A. Simonov, Dynamical origin and the pole structure of  $X(3872)$ , Phys. Rev. Lett. 105 (2010) 102002. [arXiv:1006.0211](#), [doi:10.1103/PhysRevLett.105.102002](#).
- [44] Q.-T. Song, D.-Y. Chen, X. Liu, T. Matsuki, Charmed-strange mesons revisited: mass spectra and strong decays, Phys. Rev. D 91 (2015) 054031. [arXiv:1501.03575](#), [doi:10.1103/PhysRevD.91.054031](#).
- [45] S.-Q. Luo, B. Chen, Z.-W. Liu, X. Liu, Resolving the low mass puzzle of  $\Lambda_c(2940)^+$ , Eur. Phys. J. C 80 (4) (2020) 301. [arXiv:1910.14545](#), [doi:10.1140/epjc/s10052-020-7874-1](#).
- [46] S.-Q. Luo, B. Chen, X. Liu, T. Matsuki, Predicting a new resonance as charmed-strange baryonic analog of  $D_{s0}^*(2317)$ , Phys. Rev. D 103 (7) (2021) 074027. [arXiv:2102.00679](#), [doi:10.1103/PhysRevD.103.074027](#).
- [47] Z.-L. Zhang, Z.-W. Liu, S.-Q. Luo, F.-L. Wang, B. Wang, H. Xu,  $\Lambda_c(2910)$  and  $\Lambda_c(2940)$  as conventional baryons dressed with the  $D^*N$  channel, Phys. Rev. D 107 (3) (2023) 034036. [arXiv:2210.17188](#), [doi:10.1103/PhysRevD.107.034036](#).
- [48] Z.-L. Zhang, Z.-W. Liu, S.-Q. Luo, P. Chen, Z.-H. Guo, Masses and radiative decay widths of  $D_{s0}^*(2317)$  and  $D_{s1}^*(2460)$  and their bottom analogs, Phys. Rev. D 110 (9) (2024) 094037. [arXiv:2409.05337](#), [doi:10.1103/PhysRevD.110.094037](#).
- [49] S. Uehara, et al., Observation of a charmonium-like enhancement in the  $\gamma\gamma \rightarrow \omega J/\psi$  process, Phys. Rev. Lett. 104 (2010) 092001. [arXiv:0912.4451](#), [doi:10.1103/PhysRevLett.104.092001](#).
- [50] S. Uehara, et al., Observation of a  $\chi'_{c2}$  candidate in  $\gamma\gamma \rightarrow D\bar{D}$  production at Belle, Phys. Rev. Lett. 96 (2006) 082003. [arXiv:hep-ex/0512035](#), [doi:10.1103/PhysRevLett.96.082003](#).
- [51] B. Aubert, et al., Observation of a broad structure in the  $\pi^+\pi^-J/\psi$  mass spectrum around 4.26 GeV/ $c^2$ , Phys. Rev. Lett. 95 (2005) 142001. [arXiv:hep-ex/0506081](#), [doi:10.1103/PhysRevLett.95.142001](#).
- [52] B. Aubert, et al., Evidence of a broad structure at an invariant mass of 4.32 GeV/ $c^2$  in the reaction  $e^+e^- \rightarrow \pi^+\pi^-\psi(2S)$  measured at BaBar, Phys. Rev. Lett. 98 (2007) 212001. [arXiv:hep-ex/0610057](#), [doi:10.1103/PhysRevLett.98.212001](#).
- [53] X. L. Wang, et al., Observation of two resonant structures in  $e^+e^- \rightarrow \pi^+\pi^-\psi(2S)$  via initial state radiation at Belle, Phys. Rev. Lett. 99 (2007) 142002. [arXiv:0707.3699](#), [doi:10.1103/PhysRevLett.99.142002](#).
- [54] G. Pakhlova, et al., Observation of a near-threshold enhancement in the  $e^+e^- \rightarrow \Lambda_c^+\Lambda_c^-$  cross section using initial-state radiation, Phys. Rev. Lett. 101 (2008) 172001. [arXiv:0807.4458](#), [doi:10.1103/PhysRevLett.101.172001](#).
- [55] M. Ablikim, et al., Precise measurement of the  $e^+e^- \rightarrow \pi^+\pi^-J/\psi$  cross section at center-of-mass energies from 3.77 to 4.60 GeV, Phys. Rev. Lett. 118 (9) (2017) 092001. [arXiv:1611.01317](#), [doi:10.1103/PhysRevLett.118.092001](#).
- [56] M. Ablikim, et al., Evidence of two resonant structures in  $e^+e^- \rightarrow \pi^+\pi^-h_c$ , Phys. Rev. Lett. 118 (9) (2017) 092002. [arXiv:1610.07044](#), [doi:10.1103/PhysRevLett.118.092002](#).
- [57] M. Ablikim, et al., Future physics programme of BESIII, Chin. Phys. C 44 (4) (2020) 040001. [arXiv:1912.05983](#), [doi:10.1088/1674-1137/44/4/040001](#).
- [58] F. A. Harris, Recent charmonium results from BES, in: American Physical Society (APS) Meeting of the Division of Particles and Fields (DPF 99), 1999. [arXiv:hep-ex/9903036](#).

- [59] X. Liu, X.-Q. Zeng, X.-Q. Li, Study on contributions of hadronic loops to decays of  $J/\psi \rightarrow$  vector + pseudoscalar mesons, Phys. Rev. D 74 (2006) 074003. [arXiv:hep-ph/0606191](#), [doi:10.1103/PhysRevD.74.074003](#).
- [60] X. Liu, B. Zhang, X.-Q. Li, The puzzle of excessive non- $D\bar{D}$  component of the inclusive  $\psi(3770)$  decay and the long-distant contribution, Phys. Lett. B 675 (2009) 441–445. [arXiv:0902.0480](#), [doi:10.1016/j.physletb.2009.04.047](#).
- [61] G. Li, X.-h. Liu, Q. Wang, Q. Zhao, Further understanding of the non- $D\bar{D}$  decays of  $\psi(3770)$ , Phys. Rev. D 88 (1) (2013) 014010. [arXiv:1302.1745](#), [doi:10.1103/PhysRevD.88.014010](#).
- [62] Y.-J. Zhang, G. Li, Q. Zhao, Towards a dynamical understanding of the non- $D\bar{D}$  decay of  $\psi(3770)$ , Phys. Rev. Lett. 102 (2009) 172001. [arXiv:0902.1300](#), [doi:10.1103/PhysRevLett.102.172001](#).
- [63] D.-Y. Chen, J. He, X.-Q. Li, X. Liu, Understanding the branching ratios of  $\chi_{c1} \rightarrow \phi\phi$ ,  $\omega\omega$ ,  $\omega\phi$  observed at BES-III, Phys. Rev. D 81 (2010) 074006. [arXiv:0912.4860](#), [doi:10.1103/PhysRevD.81.074006](#).
- [64] X.-H. Liu, Q. Zhao, The Evasion of helicity selection rule in  $\chi_{c1} \rightarrow VV$  and  $\chi_{c2} \rightarrow VP$  via intermediate charmed meson loops, Phys. Rev. D 81 (2010) 014017. [arXiv:0912.1508](#), [doi:10.1103/PhysRevD.81.014017](#).
- [65] D.-Y. Chen, Y.-B. Dong, X. Liu, Long-distant contribution and  $\chi_{c1}$  radiative decays to light vector meson, Eur. Phys. J. C 70 (2010) 177–182. [arXiv:1005.0066](#), [doi:10.1140/epjc/s10052-010-1449-5](#).
- [66] Q. Huang, J.-Z. Wang, R.-G. Ping, X. Liu, Detecting the polarization in  $\chi_{cJ} \rightarrow \phi\phi$  decays to probe hadronic loop effect, Phys. Rev. D 103 (9) (2021) 096006. [arXiv:2102.07104](#), [doi:10.1103/PhysRevD.103.096006](#).
- [67] D. Besson, et al., Measurement of  $\sigma(e^+e^- \rightarrow \psi(3770) \rightarrow$  hadrons) at  $E_{c.m.} = 3773$  MeV, Phys. Rev. Lett. 96 (2006) 092002, [Erratum: Phys.Rev.Lett. 104, 159901 (2010)]. [arXiv:1004.1358](#), [doi:10.1103/PhysRevLett.96.092002](#).
- [68] M. Ablikim, et al., Measurements of the branching fractions for  $\psi(3770) \rightarrow D^0\bar{D}^0, D^+D^-, D\bar{D}$  and the resonance parameters of  $\psi(3770)$  and  $\psi(2S)$ , Phys. Rev. Lett. 97 (2006) 121801. [arXiv:hep-ex/0605107](#), [doi:10.1103/PhysRevLett.97.121801](#).
- [69] M. Ablikim, et al., Measurements of the cross-sections for  $e^+e^- \rightarrow$  hadrons at 3.650 GeV, 3.6648 GeV, 3.773 GeV and the branching fraction for  $\psi(3770) \rightarrow$  non- $D\bar{D}$ , Phys. Lett. B 641 (2006) 145–155. [arXiv:hep-ex/0605105](#), [doi:10.1016/j.physletb.2006.08.049](#).
- [70] M. Ablikim, et al., Direct measurements of the non- $D\bar{D}$  cross section  $\sigma_{\psi(3770) \rightarrow \text{non-}D\bar{D}}$  at  $E_{cm} = 3.773$  GeV and the branching fraction for  $\psi(3770) \rightarrow$  non- $D\bar{D}$ , Phys. Rev. D 76 (2007) 122002. [doi:10.1103/PhysRevD.76.122002](#).
- [71] M. Ablikim, et al., Direct measurements of the cross sections for  $e^+e^- \rightarrow$  hadrons (non- $D\bar{D}$ ) in the range from 3.65 GeV to 3.87 GeV and the branching fraction for  $\psi(3770) \rightarrow$  non- $D\bar{D}$ , Phys. Lett. B 659 (2008) 74–79. [doi:10.1016/j.physletb.2007.11.078](#).
- [72] J. V. Bennett, et al., Observation of  $\chi_{cJ}$  radiative decays to light vector mesons, Phys. Rev. Lett. 101 (2008) 151801. [arXiv:0807.3718](#), [doi:10.1103/PhysRevLett.101.151801](#).
- [73] M. Ablikim, et al., Study of  $\chi_{cJ}$  radiative decays into a vector meson, Phys. Rev. D 83 (2011) 112005. [arXiv:1103.5564](#), [doi:10.1103/PhysRevD.83.112005](#).
- [74] M. Ablikim, et al., Observation of  $K^*(892)^0\bar{K}^*(892)^0$  in  $\chi_{cJ}$  decays, Phys. Rev. D 70 (2004) 092003. [arXiv:hep-ex/0408012](#), [doi:10.1103/PhysRevD.70.092003](#).
- [75] M. Ablikim, et al., Observation of  $\chi_{c1}$  decays into vector meson pairs  $\phi\phi$ ,  $\omega\omega$ , and  $\omega\phi$ , Phys. Rev. Lett. 107 (2011) 092001. [arXiv:1104.5068](#), [doi:10.1103/PhysRevLett.107.092001](#).

- [76] N. E. Adam, et al., Observation of  $\psi(3770) \rightarrow \pi\pi J/\psi$  and measurement of  $\Gamma_{ee}[\psi(2S)]$ , Phys. Rev. Lett. 96 (2006) 082004. [arXiv:hep-ex/0508023](https://arxiv.org/abs/hep-ex/0508023), [doi:10.1103/PhysRevLett.96.082004](https://doi.org/10.1103/PhysRevLett.96.082004).
- [77] Y.-P. Kuang, T.-M. Yan, Hadronic Transitions of  $D$  Wave Quarkonium and  $\psi(3770) \rightarrow J/\psi\pi\pi$ , Phys. Rev. D 41 (1990) 155. [doi:10.1103/PhysRevD.41.155](https://doi.org/10.1103/PhysRevD.41.155).
- [78] D.-Y. Chen, X. Liu, X.-Q. Li, Anomalous dipion invariant mass distribution of the  $\Upsilon(4S)$  decays into  $\Upsilon(1S)\pi^+\pi^-$  and  $\Upsilon(2S)\pi^+\pi^-$ , Eur. Phys. J. C 71 (2011) 1808. [arXiv:1109.1406](https://arxiv.org/abs/1109.1406), [doi:10.1140/epjc/s10052-011-1808-x](https://doi.org/10.1140/epjc/s10052-011-1808-x).
- [79] K. F. Chen, et al., Observation of anomalous  $\Upsilon(1S)\pi^+\pi^-$  and  $\Upsilon(2S)\pi^+\pi^-$  production near the  $\Upsilon(5S)$  resonance, Phys. Rev. Lett. 100 (2008) 112001. [arXiv:0710.2577](https://arxiv.org/abs/0710.2577), [doi:10.1103/PhysRevLett.100.112001](https://doi.org/10.1103/PhysRevLett.100.112001).
- [80] A. Bondar, et al., Observation of two charged bottomonium-like resonances in  $\Upsilon(5S)$  decays, Phys. Rev. Lett. 108 (2012) 122001. [arXiv:1110.2251](https://arxiv.org/abs/1110.2251), [doi:10.1103/PhysRevLett.108.122001](https://doi.org/10.1103/PhysRevLett.108.122001).
- [81] D.-Y. Chen, X. Liu,  $Z_b(10610)$  and  $Z_b(10650)$  structures produced by the initial single pion emission in the  $\Upsilon(5S)$  decays, Phys. Rev. D 84 (2011) 094003. [arXiv:1106.3798](https://arxiv.org/abs/1106.3798), [doi:10.1103/PhysRevD.84.094003](https://doi.org/10.1103/PhysRevD.84.094003).
- [82] D.-Y. Chen, X. Liu, Predicted charged charmonium-like structures in the hidden-charm dipion decay of higher charmonia, Phys. Rev. D 84 (2011) 034032. [arXiv:1106.5290](https://arxiv.org/abs/1106.5290), [doi:10.1103/PhysRevD.84.034032](https://doi.org/10.1103/PhysRevD.84.034032).
- [83] M. Ablikim, et al., Observation of a charged  $(D\bar{D}^*)^\pm$  mass peak in  $e^+e^- \rightarrow \pi D\bar{D}^*$  at  $\sqrt{s} = 4.26$  GeV, Phys. Rev. Lett. 112 (2) (2014) 022001. [arXiv:1310.1163](https://arxiv.org/abs/1310.1163), [doi:10.1103/PhysRevLett.112.022001](https://doi.org/10.1103/PhysRevLett.112.022001).
- [84] R. Aaij, et al., Observation of structure in the  $J/\psi$ -pair mass spectrum, Sci. Bull. 65 (23) (2020) 1983–1993. [arXiv:2006.16957](https://arxiv.org/abs/2006.16957), [doi:10.1016/j.scib.2020.08.032](https://doi.org/10.1016/j.scib.2020.08.032).
- [85] G. Aad, et al., Observation of an excess of dicharmonium events in the four-muon final state with the ATLAS detector, Phys. Rev. Lett. 131 (15) (2023) 151902. [arXiv:2304.08962](https://arxiv.org/abs/2304.08962), [doi:10.1103/PhysRevLett.131.151902](https://doi.org/10.1103/PhysRevLett.131.151902).
- [86] A. Hayrapetyan, et al., New structures in the  $J/\psi J/\psi$  mass spectrum in proton-proton collisions at  $\sqrt{s} = 13$  TeV, Phys. Rev. Lett. 132 (11) (2024) 111901. [arXiv:2306.07164](https://arxiv.org/abs/2306.07164), [doi:10.1103/PhysRevLett.132.111901](https://doi.org/10.1103/PhysRevLett.132.111901).
- [87] G. Aad, et al., Observation of structures in the  $J/\psi + \psi(2S)$  mass spectrum with the ATLAS detector (9 2025). [arXiv:2509.13101](https://arxiv.org/abs/2509.13101).
- [88] The CMS Collaboration, Observation of a family of all-charm tetraquark candidates at the LHC, CMS PAS BPH-24-003; <https://cds.cern.ch/record/2929472/files/BPH-24-003-pas.pdf>.
- [89] The CMS Collaboration, Observation of  $X(6900)$  and evidence of  $X(7100)$  in the  $J/\psi\psi(2S) \rightarrow \mu^+\mu^-\mu^+\mu^-$  mass spectrum in  $pp$  collisions at CMS, CMS PAS BPH-22-004; <https://cds.cern.ch/record/2929529/files/BPH-22-004-pas.pdf>.
- [90] A. Hayrapetyan, et al., Determination of the spin and parity of all-charm tetraquarks, Nature 648 (8092) (2025) 58–63. [arXiv:2506.07944](https://arxiv.org/abs/2506.07944), [doi:10.1038/s41586-025-09711-7](https://doi.org/10.1038/s41586-025-09711-7).
- [91] Y. Lyu, T. Doi, T. Hatsuda, T. Sugiura, Nucleon-charmonium interactions from lattice QCD, Phys. Lett. B 860 (2025) 139178. [arXiv:2410.22755](https://arxiv.org/abs/2410.22755), [doi:10.1016/j.physletb.2024.139178](https://doi.org/10.1016/j.physletb.2024.139178).
- [92] Y. Lyu, H. Tong, T. Sugiura, S. Aoki, T. Doi, T. Hatsuda, J. Meng, T. Miyamoto, Dibaryon with highest charm number near unitarity from lattice QCD, Phys. Rev. Lett. 127 (7) (2021) 072003. [arXiv:2102.00181](https://arxiv.org/abs/2102.00181), [doi:10.1103/PhysRevLett.127.072003](https://doi.org/10.1103/PhysRevLett.127.072003).
- [93] T. Appelquist, H. D. Politzer, Orthocharmonium and  $e^+e^-$  annihilation, Phys. Rev. Lett. 34 (1975) 43. [doi:10.1103/PhysRevLett.34.43](https://doi.org/10.1103/PhysRevLett.34.43).

- [94] S. Navas, et al., Review of particle physics, Phys. Rev. D 110 (3) (2024) 030001. [doi:10.1103/PhysRevD.110.030001](https://doi.org/10.1103/PhysRevD.110.030001).
- [95] W.-S. Hou, A. Soni, Vector gluonium as a possible explanation for anomalous  $\psi$  decays, Phys. Rev. Lett. 50 (1983) 569. [doi:10.1103/PhysRevLett.50.569](https://doi.org/10.1103/PhysRevLett.50.569).
- [96] S. J. Brodsky, G. P. Lepage, S. F. Tuan, Exclusive charmonium decays: The  $J/\psi(\psi') \rightarrow \rho\pi, K^*\bar{K}$  puzzle, Phys. Rev. Lett. 59 (1987) 621. [doi:10.1103/PhysRevLett.59.621](https://doi.org/10.1103/PhysRevLett.59.621).
- [97] S. J. Brodsky, M. Karliner, Intrinsic charm of vector mesons: A possible solution of the " $\rho\pi$  puzzle", Phys. Rev. Lett. 78 (1997) 4682–4685. [arXiv:hep-ph/9704379](https://arxiv.org/abs/hep-ph/9704379), [doi:10.1103/PhysRevLett.78.4682](https://doi.org/10.1103/PhysRevLett.78.4682).
- [98] T. Feldmann, P. Kroll, Implications of light quark admixtures on charmonium decays into meson pairs, Phys. Rev. D 62 (2000) 074006. [arXiv:hep-ph/0003096](https://arxiv.org/abs/hep-ph/0003096), [doi:10.1103/PhysRevD.62.074006](https://doi.org/10.1103/PhysRevD.62.074006).
- [99] X.-D. Guo, D.-Y. Chen, X.-Q. Li, Z.-Y. Yuan, S. Sang, Molecular components in  $J/\psi$  and  $\rho$ - $\pi$  puzzle, Chin. Phys. C 48 (5) (2024) 053110. [arXiv:2308.06121](https://arxiv.org/abs/2308.06121), [doi:10.1088/1674-1137/ad2a65](https://doi.org/10.1088/1674-1137/ad2a65).
- [100] L. J. Clavelli, G. W. Intemann, Vector meson mixing and hadronic decays of  $\psi$ , Phys. Rev. D 28 (1983) 2767. [doi:10.1103/PhysRevD.28.2767](https://doi.org/10.1103/PhysRevD.28.2767).
- [101] X.-Q. Li, D. V. Bugg, B.-S. Zou, A Possible explanation of the " $\rho\pi$  puzzle" in  $J/\psi, \psi'$  decays, Phys. Rev. D 55 (1997) 1421–1424. [doi:10.1103/PhysRevD.55.1421](https://doi.org/10.1103/PhysRevD.55.1421).
- [102] M. Suzuki, Long distance final state interactions and  $J/\psi$  decay, Phys. Rev. D 57 (1998) 5717–5722. [arXiv:hep-ph/9801284](https://arxiv.org/abs/hep-ph/9801284), [doi:10.1103/PhysRevD.57.5717](https://doi.org/10.1103/PhysRevD.57.5717).
- [103] M. Suzuki, Anomalies in  $\psi(2S)$  decay and the  $\rho - \pi$  puzzle, Phys. Rev. D 63 (2001) 054021. [arXiv:hep-ph/0006296](https://arxiv.org/abs/hep-ph/0006296), [doi:10.1103/PhysRevD.63.054021](https://doi.org/10.1103/PhysRevD.63.054021).
- [104] J. L. Rosner, Charmless final states and  $S$ - $D$  wave mixing in the  $\psi''$ , Phys. Rev. D 64 (2001) 094002. [arXiv:hep-ph/0105327](https://arxiv.org/abs/hep-ph/0105327), [doi:10.1103/PhysRevD.64.094002](https://doi.org/10.1103/PhysRevD.64.094002).
- [105] J. M. Gerard, J. Weyers, Phases and amplitudes in inclusive  $\psi$  and  $\psi'$  decays, Phys. Lett. B 462 (1999) 324–328. [arXiv:hep-ph/9906357](https://arxiv.org/abs/hep-ph/9906357), [doi:10.1016/S0370-2693\(99\)00849-7](https://doi.org/10.1016/S0370-2693(99)00849-7).
- [106] Y.-Q. Chen, E. Braaten, An explanation for the  $\rho\pi$  puzzle of  $J/\psi$  and  $\psi'$  decays, Phys. Rev. Lett. 80 (1998) 5060–5063. [arXiv:hep-ph/9801226](https://arxiv.org/abs/hep-ph/9801226), [doi:10.1103/PhysRevLett.80.5060](https://doi.org/10.1103/PhysRevLett.80.5060).
- [107] G. Karl, W. Roberts, Sequential fragmentation and rate oscillations in exclusive decays, Phys. Lett. B 144 (1984) 263–265. [doi:10.1016/0370-2693\(84\)91817-3](https://doi.org/10.1016/0370-2693(84)91817-3).
- [108] S. S. Pinsky, The  $\psi'$  to  $J/\psi$  hadronic decay puzzle, Phys. Lett. B 236 (1990) 479–482. [doi:10.1016/0370-2693\(90\)90387-L](https://doi.org/10.1016/0370-2693(90)90387-L).
- [109] M. Chaichian, N. A. Tornqvist, Preasymptotic versus asymptotic QCD relations for the hadronic form-factor and the anomalous  $J/\psi$  and  $\psi'$  decays, Nucl. Phys. B 323 (1989) 75–89. [doi:10.1016/0550-3213\(89\)90588-9](https://doi.org/10.1016/0550-3213(89)90588-9).
- [110] S. Okubo, Phi meson and unitary symmetry model, Phys. Lett. 5 (1963) 165–168. [doi:10.1016/S0375-9601\(63\)92548-9](https://doi.org/10.1016/S0375-9601(63)92548-9).
- [111] G. Zweig, An SU(3) model for strong interaction symmetry and its breaking. Version 2, 1964, pp. 22–101. [doi:10.17181/CERN-TH-412](https://doi.org/10.17181/CERN-TH-412).
- [112] J. Iizuka, Systematics and phenomenology of meson family, Prog. Theor. Phys. Suppl. 37 (1966) 21–34. [doi:10.1143/PTPS.37.21](https://doi.org/10.1143/PTPS.37.21).

- [113] H. J. Lipkin, The OZI rule and nucleons, *Int. J. Mod. Phys. E* 1 (1992) 603–628. doi:[10.1142/S0218301392000291](https://doi.org/10.1142/S0218301392000291).
- [114] V. P. Nomokonov, M. G. Sapozhnikov, Experimental tests of the Okubo-Zweig-Iizuka rule in hadron interactions, *Phys. Part. Nucl.* 34 (2003) 94–123. arXiv:[hep-ph/0204259](https://arxiv.org/abs/hep-ph/0204259).
- [115] G. Rong, D.-h. Zhang, J.-c. Chen, Determination of the branching fractions for  $\psi(3770) \rightarrow D^0 \bar{D}^0, D^+ D^-, D \bar{D}$  and  $\psi(3770) \rightarrow \text{non} - D \bar{D}$  (6 2005). arXiv:[hep-ex/0506051](https://arxiv.org/abs/hep-ex/0506051).
- [116] H. J. Lipkin, The OZI rule in charmonium decays above  $D \bar{D}$  threshold, *Phys. Lett. B* 179 (1986) 278. doi:[10.1016/0370-2693\(86\)90580-0](https://doi.org/10.1016/0370-2693(86)90580-0).
- [117] Y.-B. Ding, D.-H. Qin, K.-T. Chao, Electric dipole transitions of  $\psi(3770)$  and  $S$ - $D$  mixing between  $\psi(3686)$  and  $\psi(3770)$ , *Phys. Rev. D* 44 (1991) 3562–3566. doi:[10.1103/PhysRevD.44.3562](https://doi.org/10.1103/PhysRevD.44.3562).
- [118] N. N. Achasov, A. A. Kozhevnikov, Direct decays of heavy quarkonia, *Phys. Lett. B* 260 (1991) 425–428. doi:[10.1016/0370-2693\(91\)91637-B](https://doi.org/10.1016/0370-2693(91)91637-B).
- [119] N. N. Achasov, A. A. Kozhevnikov, Decays of heavy quarkonia which violate the OZI rule, *JETP Lett.* 54 (1991) 193–196.
- [120] N. N. Achasov, A. A. Kozhevnikov, Dynamical violation of the OZI rule and  $G$  parity in the decays of heavy quarkonia, *Phys. Rev. D* 49 (1994) 275–282. doi:[10.1103/PhysRevD.49.275](https://doi.org/10.1103/PhysRevD.49.275).
- [121] N. N. Achasov, A. A. Kozhevnikov, Branching ratios for the decays of  $\psi(3770)$  and  $\Upsilon(10580)$  mesons to a pair of light hadrons, *Phys. Atom. Nucl.* 69 (2006) 988–998. arXiv:[hep-ph/0505146](https://arxiv.org/abs/hep-ph/0505146), doi:[10.1134/S1063778806060093](https://doi.org/10.1134/S1063778806060093).
- [122] J. L. Rosner,  $\psi'$  decays to charmless final states, *Annals Phys.* 319 (2005) 1–12. arXiv:[hep-ph/0411003](https://arxiv.org/abs/hep-ph/0411003), doi:[10.1016/j.aop.2005.02.004](https://doi.org/10.1016/j.aop.2005.02.004).
- [123] M. B. Voloshin, The  $\bar{c}c$  purity of  $\psi(3770)$  and  $\psi'$  challenged, *Phys. Rev. D* 71 (2005) 114003. arXiv:[hep-ph/0504197](https://arxiv.org/abs/hep-ph/0504197), doi:[10.1103/PhysRevD.71.114003](https://doi.org/10.1103/PhysRevD.71.114003).
- [124] E. Eichten, S. Godfrey, H. Mahlke, J. L. Rosner, Quarkonia and their transitions, *Rev. Mod. Phys.* 80 (2008) 1161–1193. arXiv:[hep-ph/0701208](https://arxiv.org/abs/hep-ph/0701208), doi:[10.1103/RevModPhys.80.1161](https://doi.org/10.1103/RevModPhys.80.1161).
- [125] Z.-G. He, Y. Fan, K.-T. Chao, QCD prediction for the non- $D \bar{D}$  annihilation decay of  $\psi(3770)$ , *Phys. Rev. Lett.* 101 (2008) 112001. arXiv:[0802.1849](https://arxiv.org/abs/0802.1849), doi:[10.1103/PhysRevLett.101.112001](https://doi.org/10.1103/PhysRevLett.101.112001).
- [126] X.-Y. Qi, X.-D. Guo, D.-Y. Chen, Light meson decays of  $D$  wave charmonia, *Phys. Rev. D* 112 (5) (2025) 054003. arXiv:[2505.05960](https://arxiv.org/abs/2505.05960), doi:[10.1103/hdmz-b2xq](https://doi.org/10.1103/hdmz-b2xq).
- [127] V. L. Chernyak, A. R. Zhitnitsky, Exclusive decays of heavy mesons, *Nucl. Phys. B* 201 (1982) 492, [Erratum: *Nucl.Phys.B* 214, 547 (1983)]. doi:[10.1016/0550-3213\(83\)90251-1](https://doi.org/10.1016/0550-3213(83)90251-1).
- [128] V. L. Chernyak, A. R. Zhitnitsky, Asymptotic behavior of exclusive processes in QCD, *Phys. Rept.* 112 (1984) 173. doi:[10.1016/0370-1573\(84\)90126-1](https://doi.org/10.1016/0370-1573(84)90126-1).
- [129] A. Sokolov, et al., Observation of the decay  $\Upsilon(4S) \rightarrow \Upsilon(1S)\pi^+\pi^-$ , *Phys. Rev. D* 75 (2007) 071103. arXiv:[hep-ex/0611026](https://arxiv.org/abs/hep-ex/0611026), doi:[10.1103/PhysRevD.75.071103](https://doi.org/10.1103/PhysRevD.75.071103).
- [130] B. Aubert, et al., Observation of  $\Upsilon(4S)$  decays to  $\pi^+\pi^-\Upsilon(1S)$  and  $\pi^+\pi^-\Upsilon(2S)$ , *Phys. Rev. Lett.* 96 (2006) 232001. arXiv:[hep-ex/0604031](https://arxiv.org/abs/hep-ex/0604031), doi:[10.1103/PhysRevLett.96.232001](https://doi.org/10.1103/PhysRevLett.96.232001).
- [131] Y.-P. Kuang, T.-M. Yan, Predictions for hadronic transitions in the  $b\bar{b}$  system, *Phys. Rev. D* 24 (1981) 2874. doi:[10.1103/PhysRevD.24.2874](https://doi.org/10.1103/PhysRevD.24.2874).

- [132] T. Barnes, S. Godfrey, E. S. Swanson, Higher charmonia, Phys. Rev. D 72 (2005) 054026. [arXiv:hep-ph/0505002](#), [doi:10.1103/PhysRevD.72.054026](#).
- [133] Y.-J. Gao, Y.-J. Zhang, K.-T. Chao, Radiative decays of charmonium into light mesons, Chin. Phys. Lett. 23 (2006) 2376–2378. [arXiv:hep-ph/0607278](#), [doi:10.1088/0256-307X/23/9/008](#).
- [134] R. Mizuk, et al., Evidence for the  $\eta_b(2S)$  and observation of  $h_b(1P) \rightarrow \eta_b(1S)\gamma$  and  $h_b(2P) \rightarrow \eta_b(1S)\gamma$ , Phys. Rev. Lett. 109 (2012) 232002. [arXiv:1205.6351](#), [doi:10.1103/PhysRevLett.109.232002](#).
- [135] S. Godfrey, J. L. Rosner, Production of singlet  $P$ -wave  $c\bar{c}$  and  $b\bar{b}$  states, Phys. Rev. D 66 (2002) 014012. [arXiv:hep-ph/0205255](#), [doi:10.1103/PhysRevD.66.014012](#).
- [136] R. Kinnunen, N. A. Tornqvist, Prediction of the  $A_1$ - $B$ , the  $Q_1$ - $Q_2$  mass difference and the  $Q_1$ - $Q_2$  mixing, Lett. Nuovo Cim. 23 (1978) 517. [doi:10.1007/BF02770285](#).
- [137] N. A. Tornqvist, The meson mass spectrum and unitarity, Annals Phys. 123 (1979) 1. [doi:10.1016/0003-4916\(79\)90262-8](#).
- [138] S. Ono, N. A. Tornqvist, Continuum mixing and coupled channel effects in  $c\bar{c}$  and  $b\bar{b}$  quarkonium, Z. Phys. C 23 (1984) 59. [doi:10.1007/BF01558041](#).
- [139] Y.-B. Ding, K.-T. Chao, D.-H. Qin, Screened  $Q\bar{Q}$  potential and spectrum of heavy quarkonium, Chin. Phys. Lett. 10 (1993) 460–463. [doi:10.1088/0256-307X/10/8/004](#).
- [140] Y.-B. Ding, K.-T. Chao, D.-H. Qin, Possible effects of color screening and large string tension in heavy quarkonium spectra, Phys. Rev. D 51 (1995) 5064–5068. [arXiv:hep-ph/9502409](#), [doi:10.1103/PhysRevD.51.5064](#).
- [141] A. M. Badalian, L. P. Kok, M. I. Polikarpov, Y. A. Simonov, Resonances in coupled channels in nuclear and particle physics, Phys. Rept. 82 (1982) 31–177. [doi:10.1016/0370-1573\(82\)90014-X](#).
- [142] K. Heikkila, S. Ono, N. A. Tornqvist, Heavy  $c\bar{c}$  and  $b\bar{b}$  quarkonium states and unitarity effects, Phys. Rev. D 29 (1984) 110, [Erratum: Phys.Rev.D 29, 2136 (1984)]. [doi:10.1103/PhysRevD.29.2136](#).
- [143] H.-Y. Zhou, Y.-P. Kuang, Coupled channel effects in hadronic transitions in heavy quarkonium systems, Phys. Rev. D 44 (1991) 756–769. [doi:10.1103/PhysRevD.44.756](#).
- [144] P. Geiger, N. Isgur, The quenched approximation in the quark model, Phys. Rev. D 41 (1990) 1595. [doi:10.1103/PhysRevD.41.1595](#).
- [145] P. Geiger, N. Isgur, How the Okubo-Zweig-Iizuka rule evades large loop corrections, Phys. Rev. Lett. 67 (1991) 1066–1069. [doi:10.1103/PhysRevLett.67.1066](#).
- [146] P. Geiger, N. Isgur, Reconciling the OZI rule with strong pair creation, Phys. Rev. D 44 (1991) 799–808. [doi:10.1103/PhysRevD.44.799](#).
- [147] P. Geiger, N. Isgur, When can hadronic loops scuttle the OZI rule?, Phys. Rev. D 47 (1993) 5050–5059. [doi:10.1103/PhysRevD.47.5050](#).
- [148] N. Isgur, Spin orbit inversion of excited heavy quark mesons, Phys. Rev. D 57 (1998) 4041–4053. [doi:10.1103/PhysRevD.57.4041](#).
- [149] L. Maiani, F. Piccinini, A. D. Polosa, V. Riquer,  $J/\psi$  absorption in heavy ion collisions II, Nucl. Phys. A 748 (2005) 209–225. [arXiv:hep-ph/0408150](#), [doi:10.1016/j.nuclphysa.2004.10.023](#).
- [150] M. E. B. Franklin, et al., Measurement of  $\psi(3097)$  and  $\psi'(3686)$  decays into selected hadronic modes, Phys. Rev. Lett. 51 (1983) 963–966. [doi:10.1103/PhysRevLett.51.963](#).

- [151] Y.-S. Zhu, New results from  $\psi'$  decays and  $\psi'' \rightarrow \rho\pi$  decay, AIP Conf. Proc. 814 (1) (2006) 580–586. doi:[10.1063/1.2176546](https://doi.org/10.1063/1.2176546).
- [152] Q. Wang, G. Li, Q. Zhao, Open charm effects in the explanation of the long-standing ‘ $\rho\pi$  puzzle’, Phys. Rev. D 85 (2012) 074015. arXiv:[1201.1681](https://arxiv.org/abs/1201.1681), doi:[10.1103/PhysRevD.85.074015](https://doi.org/10.1103/PhysRevD.85.074015).
- [153] C. Meng, K.-T. Chao, Scalar resonance contributions to the dipion transition rates of  $\Upsilon(4S, 5S)$  in the rescattering model, Phys. Rev. D 77 (2008) 074003. arXiv:[0712.3595](https://arxiv.org/abs/0712.3595), doi:[10.1103/PhysRevD.77.074003](https://doi.org/10.1103/PhysRevD.77.074003).
- [154] C. Meng, K.-T. Chao,  $\Upsilon(4S, 5S) \rightarrow \Upsilon(1S)\eta$  transitions in the rescattering model and the new BaBar measurement, Phys. Rev. D 78 (2008) 074001. arXiv:[0806.3259](https://arxiv.org/abs/0806.3259), doi:[10.1103/PhysRevD.78.074001](https://doi.org/10.1103/PhysRevD.78.074001).
- [155] W. M. Yao, et al., Review of particle physics, J. Phys. G 33 (2006) 1–1232. doi:[10.1088/0954-3899/33/1/001](https://doi.org/10.1088/0954-3899/33/1/001).
- [156] C. Meng, K.-T. Chao, Decays of the  $X(3872)$  and  $\chi_{c1}(2P)$  charmonium, Phys. Rev. D 75 (2007) 114002. arXiv:[hep-ph/0703205](https://arxiv.org/abs/hep-ph/0703205), doi:[10.1103/PhysRevD.75.114002](https://doi.org/10.1103/PhysRevD.75.114002).
- [157] X. Liu, B. Zhang, L.-L. Shen, S.-L. Zhu,  $X(1576)$  and the final state interaction effect, Phys. Rev. D 75 (2007) 074017. arXiv:[hep-ph/0701022](https://arxiv.org/abs/hep-ph/0701022), doi:[10.1103/PhysRevD.75.074017](https://doi.org/10.1103/PhysRevD.75.074017).
- [158] B. Zhang, X. Liu, S.-L. Zhu, The Dispersive contribution of  $\rho(1450, 1700)$  decays and  $X(1576)$ , Chin. Phys. Lett. 24 (2007) 2537–2539. arXiv:[0705.3082](https://arxiv.org/abs/0705.3082), doi:[10.1088/0256-307X/24/9/020](https://doi.org/10.1088/0256-307X/24/9/020).
- [159] M. R. Pennington, D. J. Wilson, Decay channels and charmonium mass-shifts, Phys. Rev. D 76 (2007) 077502. arXiv:[0704.3384](https://arxiv.org/abs/0704.3384), doi:[10.1103/PhysRevD.76.077502](https://doi.org/10.1103/PhysRevD.76.077502).
- [160] E. van Beveren, G. Rupp, Relating multichannel scattering and production amplitudes in a microscopic OZI-based model, Annals Phys. 323 (2008) 1215–1229. arXiv:[0706.4119](https://arxiv.org/abs/0706.4119), doi:[10.1016/j.aop.2007.11.012](https://doi.org/10.1016/j.aop.2007.11.012).
- [161] M. Ablikim, et al., Search for  $\psi'' \rightarrow \rho\pi$  at BESII, Phys. Rev. D 72 (2005) 072007. arXiv:[hep-ex/0507092](https://arxiv.org/abs/hep-ex/0507092), doi:[10.1103/PhysRevD.72.072007](https://doi.org/10.1103/PhysRevD.72.072007).
- [162] G. S. Adams, et al., Decay of the  $\psi(3770)$  to light hadrons, Phys. Rev. D 73 (2006) 012002. arXiv:[hep-ex/0509011](https://arxiv.org/abs/hep-ex/0509011), doi:[10.1103/PhysRevD.73.012002](https://doi.org/10.1103/PhysRevD.73.012002).
- [163] F. E. Close, A. Kirk, The Mixing of the  $f_0(1370)$ ,  $f_0(1500)$  and  $f_0(1710)$  and the search for the scalar glueball, Phys. Lett. B 483 (2000) 345–352. arXiv:[hep-ph/0004241](https://arxiv.org/abs/hep-ph/0004241), doi:[10.1016/S0370-2693\(00\)00623-7](https://doi.org/10.1016/S0370-2693(00)00623-7).
- [164] G. Li, Q. Zhao, C.-H. Chang, Decays of  $J/\psi$  and  $\psi'$  into vector and pseudoscalar meson and the pseudoscalar glueball- $q\bar{q}$  mixing, J. Phys. G 35 (2008) 055002. arXiv:[hep-ph/0701020](https://arxiv.org/abs/hep-ph/0701020), doi:[10.1088/0954-3899/35/5/055002](https://doi.org/10.1088/0954-3899/35/5/055002).
- [165] C. Amsler, et al., Review of particle physics, Phys. Lett. B 667 (2008) 1–1340. doi:[10.1016/j.physletb.2008.07.018](https://doi.org/10.1016/j.physletb.2008.07.018).
- [166] S. I. Dolinsky, et al., Summary of experiments with the neutral detector at the  $e^+e^-$  storage ring VEPP-2M, Phys. Rept. 202 (1991) 99–170. doi:[10.1016/0370-1573\(91\)90127-8](https://doi.org/10.1016/0370-1573(91)90127-8).
- [167] M. Benayoun, L. DelBuono, S. Eidelman, V. N. Ivanchenko, H. B. O’Connell, Radiative decays, nonet symmetry and SU(3) breaking, Phys. Rev. D 59 (1999) 114027. arXiv:[hep-ph/9902326](https://arxiv.org/abs/hep-ph/9902326), doi:[10.1103/PhysRevD.59.114027](https://doi.org/10.1103/PhysRevD.59.114027).
- [168] A. Kucukarslan, U.-G. Meissner, Omega-phi mixing in chiral perturbation theory, Mod. Phys. Lett. A 21 (2006) 1423–1430. arXiv:[hep-ph/0603061](https://arxiv.org/abs/hep-ph/0603061), doi:[10.1142/S0217732306020743](https://doi.org/10.1142/S0217732306020743).

- [169] G. Li, Q. Zhao, Hadronic loop contributions to  $J/\psi$  and  $\psi'$  radiative decays into  $\gamma\eta_c$  or  $\gamma\eta'_c$ , Phys. Lett. B 670 (2008) 55–60. [arXiv:0709.4639](#), [doi:10.1016/j.physletb.2008.10.033](#).
- [170] G. Li, Q. Zhao, Revisit the radiative decays of  $J/\psi$  and  $\psi' \rightarrow \gamma\eta_c(\gamma\eta'_c)$ , Phys. Rev. D 84 (2011) 074005. [arXiv:1107.2037](#), [doi:10.1103/PhysRevD.84.074005](#).
- [171] K. Nakamura, et al., Review of particle physics, J. Phys. G 37 (2010) 075021. [doi:10.1088/0954-3899/37/7A/075021](#).
- [172] M. Ablikim, et al., First observation of the M1 transition  $\psi(3686) \rightarrow \gamma\eta_c(2S)$ , Phys. Rev. Lett. 109 (2012) 042003. [arXiv:1205.5103](#), [doi:10.1103/PhysRevLett.109.042003](#).
- [173] R. E. Mitchell, et al.,  $J/\psi$  and  $\psi(2S)$  radiative decays to  $\eta_c$ , Phys. Rev. Lett. 102 (2009) 011801, [Erratum: Phys.Rev.Lett. 106, 159903 (2011)]. [arXiv:0805.0252](#), [doi:10.1103/PhysRevLett.102.011801](#).
- [174] J. J. Dudek, R. Edwards, C. E. Thomas, Exotic and excited-state radiative transitions in charmonium from lattice QCD, Phys. Rev. D 79 (2009) 094504. [arXiv:0902.2241](#), [doi:10.1103/PhysRevD.79.094504](#).
- [175] D.-Y. Chen, X. Liu, T. Matsuki, Anomalous radiative transitions between  $h_b(nP)$  and  $\eta_b(mS)$  and hadronic loop effect, Phys. Rev. D 87 (9) (2013) 094010. [arXiv:1304.0372](#), [doi:10.1103/PhysRevD.87.094010](#).
- [176] P. Colangelo, G. Nardulli, N. Paver, Riazuddin, Long distance effects in  $b \rightarrow s$  exclusive decays, Z. Phys. C 45 (1990) 575. [doi:10.1007/BF01556270](#).
- [177] M. Beneke, G. Buchalla, M. Neubert, C. T. Sachrajda, QCD factorization for  $B \rightarrow \pi\pi$  decays: Strong phases and  $CP$  violation in the heavy quark limit, Phys. Rev. Lett. 83 (1999) 1914–1917. [arXiv:hep-ph/9905312](#), [doi:10.1103/PhysRevLett.83.1914](#).
- [178] M. Beneke, G. Buchalla, M. Neubert, C. T. Sachrajda, QCD factorization for exclusive, nonleptonic  $B$  meson decays: General arguments and the case of heavy light final states, Nucl. Phys. B 591 (2000) 313–418. [arXiv:hep-ph/0006124](#), [doi:10.1016/S0550-3213\(00\)00559-9](#).
- [179] H.-Y. Cheng, K.-C. Yang,  $B \rightarrow J/\psi K$  decays in QCD factorization, Phys. Rev. D 63 (2001) 074011. [arXiv:hep-ph/0011179](#), [doi:10.1103/PhysRevD.63.074011](#).
- [180] Y. Y. Keum, H.-N. Li, A. I. Sanda, Penguin enhancement and  $B \rightarrow K\pi$  decays in perturbative QCD, Phys. Rev. D 63 (2001) 054008. [arXiv:hep-ph/0004173](#), [doi:10.1103/PhysRevD.63.054008](#).
- [181] Y.-Y. Keum, H.-n. Li, A. I. Sanda, Fat penguins and imaginary penguins in perturbative QCD, Phys. Lett. B 504 (2001) 6–14. [arXiv:hep-ph/0004004](#), [doi:10.1016/S0370-2693\(01\)00247-7](#).
- [182] C.-D. Lu, K. Ukai, M.-Z. Yang, Branching ratio and  $CP$  violation of  $B \rightarrow \pi\pi$  decays in perturbative QCD approach, Phys. Rev. D 63 (2001) 074009. [arXiv:hep-ph/0004213](#), [doi:10.1103/PhysRevD.63.074009](#).
- [183] M. Beneke, G. Buchalla, M. Neubert, C. T. Sachrajda, QCD factorization in  $B \rightarrow \pi K, \pi\pi$  decays and extraction of Wolfenstein parameters, Nucl. Phys. B 606 (2001) 245–321. [arXiv:hep-ph/0104110](#), [doi:10.1016/S0550-3213\(01\)00251-6](#).
- [184] Z.-z. Song, K.-T. Chao, Problems of QCD factorization in exclusive decays of  $B$  meson to charmonium, Phys. Lett. B 568 (2003) 127–134. [arXiv:hep-ph/0206253](#), [doi:10.1016/j.physletb.2003.06.062](#).
- [185] M. Beneke, M. Neubert, QCD factorization for  $B \rightarrow PP$  and  $B \rightarrow PV$  decays, Nucl. Phys. B 675 (2003) 333–415. [arXiv:hep-ph/0308039](#), [doi:10.1016/j.nuclphysb.2003.09.026](#).
- [186] P. Colangelo, F. De Fazio, T. N. Pham,  $B^- \rightarrow K^- \chi_{c0}$  decay from charmed meson rescattering, Phys. Lett. B 542 (2002) 71–79. [arXiv:hep-ph/0207061](#), [doi:10.1016/S0370-2693\(02\)02306-7](#).

- [187] P. Colangelo, F. De Fazio, T. N. Pham, Nonfactorizable contributions in  $B$  decays to charmonium: The Case of  $B^- \rightarrow K^- h_c$ , Phys. Rev. D 69 (2004) 054023. [arXiv:hep-ph/0310084](#), [doi:10.1103/PhysRevD.69.054023](#).
- [188] H.-Y. Cheng, C.-K. Chua, A. Soni, Final state interactions in hadronic  $B$  decays, Phys. Rev. D 71 (2005) 014030. [arXiv:hep-ph/0409317](#), [doi:10.1103/PhysRevD.71.014030](#).
- [189] X. Liu, X.-Q. Li, Effects of hadronic loops on the direct  $CP$  violation of  $B_c$ , Phys. Rev. D 77 (2008) 096010. [arXiv:0707.0919](#), [doi:10.1103/PhysRevD.77.096010](#).
- [190] S. Fajfer, A. Prapotnik, P. Singer, J. Zupan, Final state interactions in the  $D_s^+ \rightarrow \omega\pi^+$  and  $D_s^+ \rightarrow \rho^0\pi^+$  decays, Phys. Rev. D 68 (2003) 094012. [arXiv:hep-ph/0308100](#), [doi:10.1103/PhysRevD.68.094012](#).
- [191] Y. Yu, Y.-K. Hsiao, B.-C. Ke, Study of the  $D_s^+ \rightarrow a_0(980)\rho$  and  $a_0(980)\omega$  decays, Eur. Phys. J. C 81 (12) (2021) 1093. [arXiv:2108.02936](#), [doi:10.1140/epjc/s10052-021-09895-y](#).
- [192] Y.-K. Hsiao, Y. Yu, B.-C. Ke, Resonant  $a_0(980)$  state in triangle rescattering  $D_s^+ \rightarrow \pi^+\pi^0\eta$  decays, Eur. Phys. J. C 80 (9) (2020) 895. [arXiv:1909.07327](#), [doi:10.1140/epjc/s10052-020-08468-9](#).
- [193] X.-Z. Ling, M.-Z. Liu, J.-X. Lu, L.-S. Geng, J.-J. Xie, Can the nature of  $a_0(980)$  be tested in the  $D_s^+ \rightarrow \pi^+\pi^0\eta$  decay?, Phys. Rev. D 103 (11) (2021) 116016. [arXiv:2102.05349](#), [doi:10.1103/PhysRevD.103.116016](#).
- [194] I. Bediaga, T. Frederico, P. C. Magalhães, Enhanced charm  $CP$  asymmetries from final state interactions, Phys. Rev. Lett. 131 (5) (2023) 051802. [arXiv:2203.04056](#), [doi:10.1103/PhysRevLett.131.051802](#).
- [195] A. Pich, E. Solomonidi, L. Vale Silva, Final-state interactions in the  $CP$  asymmetries of charm-meson two-body decays, Phys. Rev. D 108 (3) (2023) 036026. [arXiv:2305.11951](#), [doi:10.1103/PhysRevD.108.036026](#).
- [196] C.-Q. Geng, X.-N. Jin, C.-W. Liu, X. Yu, Hidden strangeness in meson weak decays to baryon pair, Phys. Rev. D 110 (11) (2024) 113008. [arXiv:2409.11374](#), [doi:10.1103/PhysRevD.110.113008](#).
- [197] Y.-L. Wang, S.-T. Cai, Y.-K. Hsiao, Rescattering-induced  $D \rightarrow SS$  weak decays (9 2025). [arXiv:2509.16879](#).
- [198] Y. Yu, Y.-K. Hsiao, Cabibbo-favored  $\Lambda_c^+ \rightarrow \Lambda a_0(980)^+$  decay in the final state interaction, Phys. Lett. B 820 (2021) 136586. [arXiv:2012.14575](#), [doi:10.1016/j.physletb.2021.136586](#).
- [199] C.-P. Jia, H.-Y. Jiang, J.-P. Wang, F.-S. Yu, Final-state rescattering mechanism of charmed baryon decays, JHEP 11 (2024) 072. [arXiv:2408.14959](#), [doi:10.1007/JHEP11\(2024\)072](#).
- [200] X.-G. He, C.-W. Liu, Large  $CP$  violation in charmed baryon decays, Sci. Bull. 70 (2025) 2598–2603. [arXiv:2404.19166](#), [doi:10.1016/j.scib.2025.05.045](#).
- [201] J.-P. Wang, F.-S. Yu,  $CP$  violation of baryon decays with  $N\pi$  rescatterings, Chin. Phys. C 48 (10) (2024) 101002. [arXiv:2407.04110](#), [doi:10.1088/1674-1137/ad75f4](#).
- [202] Z.-D. Duan, J.-P. Wang, R.-H. Li, C.-D. Lü, F.-S. Yu, Final-state rescattering mechanism in bottom-baryon decays, JHEP 09 (2025) 160. [arXiv:2412.20458](#), [doi:10.1007/JHEP09\(2025\)160](#).
- [203] Y.-K. Hsiao, S.-T. Cai, Y.-L. Wang, Hidden charm  $P_{cs}(4338)^0$  production in baryonic  $B^- \rightarrow J/\psi\Lambda\bar{p}$  decay, Phys. Rev. D 111 (7) (2025) 076020. [arXiv:2409.04951](#), [doi:10.1103/PhysRevD.111.076020](#).
- [204] F.-S. Yu, H.-Y. Jiang, R.-H. Li, C.-D. Lü, W. Wang, Z.-X. Zhao, Discovery potentials of doubly charmed baryons, Chin. Phys. C 42 (5) (2018) 051001. [arXiv:1703.09086](#), [doi:10.1088/1674-1137/42/5/051001](#).
- [205] R.-H. Li, J.-J. Hou, B. He, Y.-R. Wang, Weak decays of doubly heavy baryons:  $\mathcal{B}_{cc} \rightarrow \mathcal{B}D^{(*)}$ , Chin. Phys. C 45 (4) (2021) 043108. [arXiv:2010.09362](#), [doi:10.1088/1674-1137/abe0bc](#).

- [206] J.-J. Han, H.-Y. Jiang, W. Liu, Z.-J. Xiao, F.-S. Yu, Rescattering mechanism of weak decays of double-charm baryons, *Chin. Phys. C* 45 (5) (2021) 053105. [arXiv:2101.12019](#), [doi:10.1088/1674-1137/abec68](#).
- [207] X.-H. Hu, C.-P. Jia, Y. Xing, F.-S. Yu, Final-state rescattering mechanism of double-charm baryon decays:  $B_{cc} \rightarrow B_c P$ , *Phys. Rev. D* 111 (7) (2025) 076002. [arXiv:2403.09511](#), [doi:10.1103/PhysRevD.111.076002](#).
- [208] C.-Q. Geng, X.-N. Jin, C.-W. Liu, X.-Y. Liu, X. Yu, Potential of discovering  $\Xi_{cc}^+$  in  $\Lambda_b$  decays (10 2025). [arXiv:2510.22181](#).
- [209] H. Xu, X. Liu, T. Matsuki, Understanding  $B^- \rightarrow X(3823)K^-$  via rescattering mechanism and predicting  $B^- \rightarrow \eta_{c2}(^1D_2)/\psi_3(^3D_3)K^-$ , *Phys. Rev. D* 94 (3) (2016) 034005. [arXiv:1605.04776](#), [doi:10.1103/PhysRevD.94.034005](#).
- [210] M.-X. Duan, J.-Z. Wang, Y.-S. Li, X. Liu, Role of the newly measured  $B \rightarrow KD\bar{D}$  process to establish  $\chi_{c0}(2P)$  state, *Phys. Rev. D* 104 (3) (2021) 034035. [arXiv:2104.09132](#), [doi:10.1103/PhysRevD.104.034035](#).
- [211] Q.-W. Yuan, Q. Wu, M.-Z. Liu,  $B$ -meson decays to vector charmoniumlike states and a  $K$  meson: The role of final-state interactions, *Phys. Rev. D* 111 (11) (2025) 114035. [arXiv:2504.11121](#), [doi:10.1103/PhysRevD.111.114035](#).
- [212] X.-H. Liu, Q. Zhao, Further study of the helicity selection rule evading mechanism in  $\eta_c, \chi_{c0}$  and  $h_c$  decaying to baryon anti-baryon pairs, *J. Phys. G* 38 (2011) 035007. [arXiv:1004.0496](#), [doi:10.1088/0954-3899/38/3/035007](#).
- [213] D.-Y. Chen, J. He, X. Liu, Nonresonant explanation for the  $Y(4260)$  structure observed in the  $e^+e^- \rightarrow J/\psi\pi^+\pi^-$  process, *Phys. Rev. D* 83 (2011) 054021. [arXiv:1012.5362](#), [doi:10.1103/PhysRevD.83.054021](#).
- [214] F.-K. Guo, C. Hanhart, G. Li, U.-G. Meissner, Q. Zhao, Novel analysis of the decays  $\psi' \rightarrow h_c\pi^0$  and  $\eta'_c \rightarrow \chi_{c0}\pi^0$ , *Phys. Rev. D* 82 (2010) 034025. [arXiv:1002.2712](#), [doi:10.1103/PhysRevD.82.034025](#).
- [215] F.-K. Guo, C. Hanhart, G. Li, U.-G. Meissner, Q. Zhao, Effect of charmed meson loops on charmonium transitions, *Phys. Rev. D* 83 (2011) 034013. [arXiv:1008.3632](#), [doi:10.1103/PhysRevD.83.034013](#).
- [216] D.-Y. Chen, J. He, X. Liu, A Novel explanation of charmonium-like structure in  $e^+e^- \rightarrow \psi(2S)\pi^+\pi^-$ , *Phys. Rev. D* 83 (2011) 074012. [arXiv:1101.2474](#), [doi:10.1103/PhysRevD.83.074012](#).
- [217] Q. Wang, X.-H. Liu, Q. Zhao, Open charm effects in  $e^+e^- \rightarrow J/\psi\eta, J/\psi\pi^0$  and  $\phi\eta_c$ , *Phys. Rev. D* 84 (2011) 014007. [arXiv:1103.1095](#), [doi:10.1103/PhysRevD.84.014007](#).
- [218] Q. Wang, X.-H. Liu, Q. Zhao, Updated study of the  $\eta_c$  and  $\eta'_c$  decays into light vector mesons, *Phys. Lett. B* 711 (2012) 364–370. [arXiv:1202.3026](#), [doi:10.1016/j.physletb.2012.04.022](#).
- [219] D.-Y. Chen, X. Liu, T. Matsuki,  $\eta$  transitions between charmonia with meson loop contributions, *Phys. Rev. D* 87 (5) (2013) 054006. [arXiv:1209.0064](#), [doi:10.1103/PhysRevD.87.054006](#).
- [220] Z.-k. Guo, S. Narison, J.-M. Richard, Q. Zhao, Isospin violating decay of  $\psi(3770) \rightarrow J/\psi + \pi^0$ , *Phys. Rev. D* 85 (2012) 114007. [arXiv:1204.1448](#), [doi:10.1103/PhysRevD.85.114007](#).
- [221] G. Li, X.-H. Liu, Q. Zhao, Evasion of HSR in  $S$ -wave charmonium decaying to  $P$ -wave light hadrons, *Eur. Phys. J. C* 73 (2013) 2576. [doi:10.1140/epjc/s10052-013-2576-6](#).
- [222] G. Li, Hidden-charmonium decays of  $Z_c(3900)$  and  $Z_c(4025)$  in intermediate meson loops model, *Eur. Phys. J. C* 73 (11) (2013) 2621. [arXiv:1304.4458](#), [doi:10.1140/epjc/s10052-013-2621-5](#).
- [223] G. Li, X.-H. Liu, Investigating possible decay modes of  $Y(4260)$  under  $D_1(2420)\bar{D} + c.c.$  molecular state ansatz, *Phys. Rev. D* 88 (9) (2013) 094008. [arXiv:1307.2622](#), [doi:10.1103/PhysRevD.88.094008](#).

- [224] D.-Y. Chen, X. Liu, T. Matsuki, Hidden-charm decays of  $X(3915)$  and  $Z(3930)$  as the  $P$ -wave charmonia, PTEP 2015 (4) (2015) 043B05. [arXiv:1311.6274](#), [doi:10.1093/ptep/ptv038](#).
- [225] D.-Y. Chen, X. Liu, T. Matsuki, Observation of  $e^+e^- \rightarrow \chi_{c0}\omega$  and missing higher charmonium  $\psi(4S)$ , Phys. Rev. D 91 (9) (2015) 094023. [arXiv:1411.5136](#), [doi:10.1103/PhysRevD.91.094023](#).
- [226] Y. Dong, A. Faessler, T. Gutsche, V. E. Lyubovitskij, Selected strong decay modes of  $Y(4260)$ , Phys. Rev. D 89 (3) (2014) 034018. [arXiv:1310.4373](#), [doi:10.1103/PhysRevD.89.034018](#).
- [227] G. Li, C.-S. An, P.-Y. Li, D. Liu, X. Zhang, Z. Zhou, Investigations on the charmless decays of  $Y(4260)$ , Chin. Phys. C 39 (6) (2015) 063102. [arXiv:1412.3221](#), [doi:10.1088/1674-1137/39/6/063102](#).
- [228] D.-Y. Chen, X. Liu, T. Matsuki, Search for missing  $\psi(4S)$  in the  $e^+e^- \rightarrow \pi^+\pi^-\psi(2S)$  process, Phys. Rev. D 93 (3) (2016) 034028. [arXiv:1509.00736](#), [doi:10.1103/PhysRevD.93.034028](#).
- [229] B. Wang, H. Xu, X. Liu, D.-Y. Chen, S. Coito, E. Eichten, Using  $X(3823) \rightarrow J/\psi\pi^+\pi^-$  to identify coupled-channel effects, Front. Phys. (Beijing) 11 (2016) 111402. [arXiv:1507.07985](#), [doi:10.1007/s11467-016-0564-7](#).
- [230] X.-D. Guo, D.-Y. Chen, H.-W. Ke, X. Liu, X.-Q. Li, Study on the rare decays of  $Y(4630)$  induced by final state interactions, Phys. Rev. D 93 (5) (2016) 054009. [arXiv:1602.02222](#), [doi:10.1103/PhysRevD.93.054009](#).
- [231] R.-Q. Qian, Q. Huang, X. Liu, Predicted  $\Lambda\bar{\Lambda}$  and  $\Xi^-\Xi^+$  decay modes of the charmoniumlike  $Y(4230)$ , Phys. Lett. B 833 (2022) 137292. [arXiv:2111.13821](#), [doi:10.1016/j.physletb.2022.137292](#).
- [232] R.-Q. Qian, J.-Z. Wang, X. Liu, T. Matsuki, Charmonium decays into  $\Lambda_c\bar{\Lambda}_c$  pair governed by the hadronic loop mechanism, Phys. Rev. D 104 (9) (2021) 094001. [arXiv:2104.13270](#), [doi:10.1103/PhysRevD.104.094001](#).
- [233] J.-Z. Wang, X. Liu, Confirming the existence of a new higher charmonium  $\psi(4500)$  by the newly released data of  $e^+e^- \rightarrow K^+K^-J/\psi$ , Phys. Rev. D 107 (5) (2023) 054016. [arXiv:2212.13512](#), [doi:10.1103/PhysRevD.107.054016](#).
- [234] S. Liu, Z. Cai, Y. Zheng, G. Li, Hidden charmonium decays of  $\psi(nS)$  through charmed meson loops, Eur. Phys. J. C 83 (9) (2023) 820. [doi:10.1140/epjc/s10052-023-12012-w](#).
- [235] R.-Q. Qian, X. Liu, Production of charmonium  $\chi_{cJ}(2P)$  plus one  $\omega$  meson by  $e^+e^-$  annihilation, Phys. Rev. D 108 (9) (2023) 094046. [arXiv:2308.14072](#), [doi:10.1103/PhysRevD.108.094046](#).
- [236] T.-C. Peng, Z.-Y. Bai, J.-Z. Wang, X. Liu, How higher charmonia shape the puzzling data of the  $e^+e^- \rightarrow \eta J/\psi$  cross section, Phys. Rev. D 109 (9) (2024) 094048. [arXiv:2403.03705](#), [doi:10.1103/PhysRevD.109.094048](#).
- [237] T.-L. Gao, R.-Q. Qian, X. Liu, Discovery potential of charmonium  $2P$  states through the  $e^+e^- \rightarrow \gamma D\bar{D}$  processes, Phys. Rev. D 111 (5) (2025) 054021. [arXiv:2412.06400](#), [doi:10.1103/PhysRevD.111.054021](#).
- [238] Y. Zheng, Z. Cai, G. Li, S. Liu, J. Wu, Q. Wu, Hidden charmonium decays of spin-2 partner of  $X(3872)$ , Phys. Rev. D 109 (1) (2024) 014027. [arXiv:2401.03219](#), [doi:10.1103/PhysRevD.109.014027](#).
- [239] Z.-Y. Bai, B.-J. Lai, Q.-S. Zhou, X. Liu, Non- $D\bar{D}$  decays into light meson pairs of the  $D$ -wave charmonium  $\psi_3(3842)$ , Eur. Phys. J. C 85 (6) (2025) 649. [arXiv:2412.09408](#), [doi:10.1140/epjc/s10052-025-14376-7](#).
- [240] X.-Y. Qi, Q. Wu, X.-D. Guo, D.-Y. Chen, Two-body hidden charm decays of  $D$  wave charmonia, Eur. Phys. J. C 85 (1) (2025) 96. [arXiv:2501.16124](#), [doi:10.1140/epjc/s10052-025-13808-8](#).
- [241] E. Klempt, J.-M. Richard, Baryon spectroscopy, Rev. Mod. Phys. 82 (2010) 1095–1153. [arXiv:0901.2055](#), [doi:10.1103/RevModPhys.82.1095](#).

- [242] H.-Y. Cheng, Charmed baryons circa 2015, *Front. Phys. (Beijing)* 10 (6) (2015) 101406. doi:10.1007/s11467-015-0483-z.
- [243] C.-Z. Yuan, The XYZ states revisited, *Int. J. Mod. Phys. A* 33 (21) (2018) 1830018. arXiv:1808.01570, doi:10.1142/S0217751X18300181.
- [244] X.-K. Dong, F.-K. Guo, B.-S. Zou, A survey of heavy-antiheavy hadronic molecules, *Progr. Phys.* 41 (2021) 65–93. arXiv:2101.01021, doi:10.13725/j.cnki.pip.2021.02.001.
- [245] H.-Y. Cheng, Charmed baryon physics circa 2021, *Chin. J. Phys.* 78 (2022) 324–362. arXiv:2109.01216, doi:10.1016/j.cjph.2022.06.021.
- [246] F. Gross, et al., 50 Years of quantum chromodynamics, *Eur. Phys. J. C* 83 (2023) 1125. arXiv:2212.11107, doi:10.1140/epjc/s10052-023-11949-2.
- [247] M.-Z. Liu, Y.-W. Pan, Z.-W. Liu, T.-W. Wu, J.-X. Lu, L.-S. Geng, Three ways to decipher the nature of exotic hadrons: Multiplets, three-body hadronic molecules, and correlation functions, *Phys. Rept.* 1108 (2025) 1–108. arXiv:2404.06399, doi:10.1016/j.physrep.2024.12.001.
- [248] Z.-G. Wang, Review of the QCD sum rules for exotic states, *Front. Phys. (Beijing)* 21 (1) (2026) 016300. arXiv:2502.11351, doi:10.15302/frontphys.2026.016300.
- [249] P. Krokovny, et al., Observation of the  $D_{sJ}(2317)$  and  $D_{sJ}(2457)$  in  $B$  decays, *Phys. Rev. Lett.* 91 (2003) 262002. arXiv:hep-ex/0308019, doi:10.1103/PhysRevLett.91.262002.
- [250] B. Aubert, et al., A study of the  $D_{sJ}^*(2317)$  and  $D_{sJ}(2460)$  mesons in inclusive  $c\bar{c}$  production near  $\sqrt{s} = 10.6$  GeV, *Phys. Rev. D* 74 (2006) 032007. arXiv:hep-ex/0604030, doi:10.1103/PhysRevD.74.032007.
- [251] Y. Mikami, et al., Measurements of the  $D_{sJ}$  resonance properties, *Phys. Rev. Lett.* 92 (2004) 012002. arXiv:hep-ex/0307052, doi:10.1103/PhysRevLett.92.012002.
- [252] M. Ablikim, et al., Measurement of the absolute branching fraction of  $D_{s0}^{*\pm}(2317) \rightarrow \pi^0 D_s^\pm$ , *Phys. Rev. D* 97 (5) (2018) 051103. arXiv:1711.08293, doi:10.1103/PhysRevD.97.051103.
- [253] B. Aubert, et al., Study of  $B \rightarrow D_{sJ}^{(*)+} \bar{D}^{(*)}$  decays, *Phys. Rev. Lett.* 93 (2004) 181801. arXiv:hep-ex/0408041, doi:10.1103/PhysRevLett.93.181801.
- [254] T. Barnes, F. E. Close, H. J. Lipkin, Implications of a  $DK$  molecule at 2.32 GeV, *Phys. Rev. D* 68 (2003) 054006. arXiv:hep-ph/0305025, doi:10.1103/PhysRevD.68.054006.
- [255] H.-Y. Cheng, W.-S. Hou,  $B$  decays as spectroscopy for charmed four quark states, *Phys. Lett. B* 566 (2003) 193–200. arXiv:hep-ph/0305038, doi:10.1016/S0370-2693(03)00834-7.
- [256] A. Hayashigaki, K. Terasaki, Isospin quantum number of  $D_{s0}^+(2317)$ , *Prog. Theor. Phys.* 114 (2006) 1191–1200. arXiv:hep-ph/0410393, doi:10.1143/PTP.114.1191.
- [257] Y.-Q. Chen, X.-Q. Li, A Comprehensive four-quark interpretation of  $D_s(2317)$ ,  $D_s(2457)$  and  $D_s(2632)$ , *Phys. Rev. Lett.* 93 (2004) 232001. arXiv:hep-ph/0407062, doi:10.1103/PhysRevLett.93.232001.
- [258] V. Dmitrasinovic,  $D_{s0}^+(2317)^- D_0(2308)$  mass difference as evidence for tetraquarks, *Phys. Rev. Lett.* 94 (2005) 162002. doi:10.1103/PhysRevLett.94.162002.
- [259] H. Kim, Y. Oh,  $D_s(2317)$  as a four-quark state in QCD sum rules, *Phys. Rev. D* 72 (2005) 074012. arXiv:hep-ph/0508251, doi:10.1103/PhysRevD.72.074012.
- [260] K. Terasaki,  $D_{s0}^+(2317)$  as an iso-triplet four-quark meson, *Eur. Phys. J. A* 31 (2007) 676. arXiv:hep-ph/0609223, doi:10.1140/epja/i2006-10176-7.

- [261] A. Faessler, T. Gutsche, V. E. Lyubovitskij, Y.-L. Ma, Strong and radiative decays of the  $D_{s0}^*(2317)$  meson in the  $DK$ -molecule picture, Phys. Rev. D 76 (2007) 014005. [arXiv:0705.0254](#), [doi:10.1103/PhysRevD.76.014005](#).
- [262] Z.-X. Xie, G.-Q. Feng, X.-H. Guo, Analyzing  $D_{s0}^*(2317)^+$  in the  $DK$  molecule picture in the Beth-Salpeter approach, Phys. Rev. D 81 (2010) 036014. [doi:10.1103/PhysRevD.81.036014](#).
- [263] F. E. Close, P. R. Page, The  $D^{*0}\bar{D}^0$  threshold resonance, Phys. Lett. B 578 (2004) 119–123. [arXiv:hep-ph/0309253](#), [doi:10.1016/j.physletb.2003.10.032](#).
- [264] M. B. Voloshin, Interference and binding effects in decays of possible molecular component of  $X(3872)$ , Phys. Lett. B 579 (2004) 316–320. [arXiv:hep-ph/0309307](#), [doi:10.1016/j.physletb.2003.11.014](#).
- [265] C.-Y. Wong, Molecular states of heavy quark mesons, Phys. Rev. C 69 (2004) 055202. [arXiv:hep-ph/0311088](#), [doi:10.1103/PhysRevC.69.055202](#).
- [266] E. S. Swanson, Short range structure in the  $X(3872)$ , Phys. Lett. B 588 (2004) 189–195. [arXiv:hep-ph/0311229](#), [doi:10.1016/j.physletb.2004.03.033](#).
- [267] N. A. Tornqvist, Isospin breaking of the narrow charmonium state of Belle at 3872 MeV as a deuson, Phys. Lett. B 590 (2004) 209–215. [arXiv:hep-ph/0402237](#), [doi:10.1016/j.physletb.2004.03.077](#).
- [268] M. T. AlFiky, F. Gabbiani, A. A. Petrov,  $X(3872)$ : Hadronic molecules in effective field theory, Phys. Lett. B 640 (2006) 238–245. [arXiv:hep-ph/0506141](#), [doi:10.1016/j.physletb.2006.07.069](#).
- [269] Y.-R. Liu, X. Liu, W.-Z. Deng, S.-L. Zhu, Is  $X(3872)$  really a molecular state?, Eur. Phys. J. C 56 (2008) 63–73. [arXiv:0801.3540](#), [doi:10.1140/epjc/s10052-008-0640-4](#).
- [270] C. E. Thomas, F. E. Close, Is  $X(3872)$  a molecule?, Phys. Rev. D 78 (2008) 034007. [arXiv:0805.3653](#), [doi:10.1103/PhysRevD.78.034007](#).
- [271] X. Liu, Z.-G. Luo, Y.-R. Liu, S.-L. Zhu,  $X(3872)$  and other possible heavy molecular states, Eur. Phys. J. C 61 (2009) 411–428. [arXiv:0808.0073](#), [doi:10.1140/epjc/s10052-009-1020-4](#).
- [272] I. W. Lee, A. Faessler, T. Gutsche, V. E. Lyubovitskij,  $X(3872)$  as a molecular  $DD^*$  state in a potential model, Phys. Rev. D 80 (2009) 094005. [arXiv:0910.1009](#), [doi:10.1103/PhysRevD.80.094005](#).
- [273] D. Gamermann, J. Nieves, E. Oset, E. Ruiz Arriola, Couplings in coupled channels versus wave functions: application to the  $X(3872)$  resonance, Phys. Rev. D 81 (2010) 014029. [arXiv:0911.4407](#), [doi:10.1103/PhysRevD.81.014029](#).
- [274] E. Braaten, H. W. Hammer, T. Mehen, Scattering of an ultrasoft pion and the  $X(3872)$ , Phys. Rev. D 82 (2010) 034018. [arXiv:1005.1688](#), [doi:10.1103/PhysRevD.82.034018](#).
- [275] P. Wang, X. G. Wang, Study on  $X(3872)$  from effective field theory with pion exchange interaction, Phys. Rev. Lett. 111 (4) (2013) 042002. [arXiv:1304.0846](#), [doi:10.1103/PhysRevLett.111.042002](#).
- [276] V. Baru, E. Epelbaum, A. A. Filin, C. Hanhart, U. G. Meissner, A. V. Nefediev, Quark mass dependence of the  $X(3872)$  binding energy, Phys. Lett. B 726 (2013) 537–543. [arXiv:1306.4108](#), [doi:10.1016/j.physletb.2013.08.073](#).
- [277] K. Abe, et al., Experimental constraints on the possible  $J^P$  quantum numbers of the  $\Lambda_c(2880)^+$ , Phys. Rev. Lett. 98 (2007) 262001. [arXiv:hep-ex/0608043](#), [doi:10.1103/PhysRevLett.98.262001](#).
- [278] R. Aaij, et al., Study of the  $D^0 p$  amplitude in  $\Lambda_b^0 \rightarrow D^0 p \pi^-$  decays, JHEP 05 (2017) 030. [arXiv:1701.07873](#), [doi:10.1007/JHEP05\(2017\)030](#).

- [279] S. Capstick, N. Isgur, Baryons in a relativized quark model with chromodynamics, *Phys. Rev. D* 34 (9) (1986) 2809–2835. doi:[10.1103/physrevd.34.2809](https://doi.org/10.1103/physrevd.34.2809).
- [280] D. Ebert, R. N. Faustov, V. O. Galkin, Masses of excited heavy baryons in the relativistic quark model, *Phys. Lett. B* 659 (2008) 612–620. arXiv:[0705.2957](https://arxiv.org/abs/0705.2957), doi:[10.1016/j.physletb.2007.11.037](https://doi.org/10.1016/j.physletb.2007.11.037).
- [281] D. Ebert, R. N. Faustov, V. O. Galkin, Spectroscopy and Regge trajectories of heavy baryons in the relativistic quark-diquark picture, *Phys. Rev. D* 84 (2011) 014025. arXiv:[1105.0583](https://arxiv.org/abs/1105.0583), doi:[10.1103/PhysRevD.84.014025](https://doi.org/10.1103/PhysRevD.84.014025).
- [282] B. Chen, K.-W. Wei, A. Zhang, Assignments of  $\Lambda_Q$  and  $\Xi_Q$  baryons in the heavy quark-light diquark picture, *Eur. Phys. J. A* 51 (2015) 82. arXiv:[1406.6561](https://arxiv.org/abs/1406.6561), doi:[10.1140/epja/i2015-15082-3](https://doi.org/10.1140/epja/i2015-15082-3).
- [283] B. Chen, K.-W. Wei, X. Liu, T. Matsuki, Low-lying charmed and charmed-strange baryon states, *Eur. Phys. J. C* 77 (3) (2017) 154. arXiv:[1609.07967](https://arxiv.org/abs/1609.07967), doi:[10.1140/epjc/s10052-017-4708-x](https://doi.org/10.1140/epjc/s10052-017-4708-x).
- [284] H.-Y. Cheng, C.-W. Chiang, Quantum numbers of  $\Omega_c$  states and other charmed baryons, *Phys. Rev. D* 95 (9) (2017) 094018. arXiv:[1704.00396](https://arxiv.org/abs/1704.00396), doi:[10.1103/PhysRevD.95.094018](https://doi.org/10.1103/PhysRevD.95.094018).
- [285] G.-L. Yu, Z.-Y. Li, Z.-G. Wang, J. Lu, M. Yan, Systematic analysis of single heavy baryons  $\Lambda_Q$ ,  $\Sigma_Q$  and  $\Omega_Q$ , *Nucl. Phys. B* 990 (2023) 116183. arXiv:[2206.08128](https://arxiv.org/abs/2206.08128), doi:[10.1016/j.nuclphysb.2023.116183](https://doi.org/10.1016/j.nuclphysb.2023.116183).
- [286] B. Aubert, et al., Observation of a narrow meson decaying to  $D_s^+\pi^0\gamma$  at a mass of 2.458-GeV/ $c^2$ , *Phys. Rev. D* 69 (2004) 031101. arXiv:[hep-ex/0310050](https://arxiv.org/abs/hep-ex/0310050), doi:[10.1103/PhysRevD.69.031101](https://doi.org/10.1103/PhysRevD.69.031101).
- [287] M. Ablikim, et al., Observation of a new  $X(3872)$  production process  $e^+e^- \rightarrow \omega X(3872)$ , *Phys. Rev. Lett.* 130 (15) (2023) 151904. arXiv:[2212.07291](https://arxiv.org/abs/2212.07291), doi:[10.1103/PhysRevLett.130.151904](https://doi.org/10.1103/PhysRevLett.130.151904).
- [288] R. Aaij, et al., Study of the  $\psi_2(3823)$  and  $\chi_{c1}(3872)$  states in  $B^+ \rightarrow (J\psi\pi^+\pi^-)K^+$  decays, *JHEP* 08 (2020) 123. arXiv:[2005.13422](https://arxiv.org/abs/2005.13422), doi:[10.1007/JHEP08\(2020\)123](https://doi.org/10.1007/JHEP08(2020)123).
- [289] M. Ablikim, et al., Observation of  $e^+e^- \rightarrow \gamma X(3872)$  at BESIII, *Phys. Rev. Lett.* 112 (9) (2014) 092001. arXiv:[1310.4101](https://arxiv.org/abs/1310.4101), doi:[10.1103/PhysRevLett.112.092001](https://doi.org/10.1103/PhysRevLett.112.092001).
- [290] R. Aaij, et al., Observation of  $X(3872)$  production in  $pp$  collisions at  $\sqrt{s} = 7$  TeV, *Eur. Phys. J. C* 72 (2012) 1972. arXiv:[1112.5310](https://arxiv.org/abs/1112.5310), doi:[10.1140/epjc/s10052-012-1972-7](https://doi.org/10.1140/epjc/s10052-012-1972-7).
- [291] S. Godfrey, K. Moats, Properties of excited charm and charm-strange mesons, *Phys. Rev. D* 93 (3) (2016) 034035. arXiv:[1510.08305](https://arxiv.org/abs/1510.08305), doi:[10.1103/PhysRevD.93.034035](https://doi.org/10.1103/PhysRevD.93.034035).
- [292] R.-H. Ni, Q. Li, X.-H. Zhong, Mass spectra and strong decays of charmed and charmed-strange mesons, *Phys. Rev. D* 105 (5) (2022) 056006. arXiv:[2110.05024](https://arxiv.org/abs/2110.05024), doi:[10.1103/PhysRevD.105.056006](https://doi.org/10.1103/PhysRevD.105.056006).
- [293] D. Ebert, R. N. Faustov, V. O. Galkin, Heavy-light meson spectroscopy and Regge trajectories in the relativistic quark model, *Eur. Phys. J. C* 66 (2010) 197–206. arXiv:[0910.5612](https://arxiv.org/abs/0910.5612), doi:[10.1140/epjc/s10052-010-1233-6](https://doi.org/10.1140/epjc/s10052-010-1233-6).
- [294] D.-M. Li, P.-F. Ji, B. Ma, The newly observed open-charm states in quark model, *Eur. Phys. J. C* 71 (2011) 1582. arXiv:[1011.1548](https://arxiv.org/abs/1011.1548), doi:[10.1140/epjc/s10052-011-1582-9](https://doi.org/10.1140/epjc/s10052-011-1582-9).
- [295] J. Zeng, J. W. Van Orden, W. Roberts, Heavy mesons in a relativistic model, *Phys. Rev. D* 52 (1995) 5229–5241. arXiv:[hep-ph/9412269](https://arxiv.org/abs/hep-ph/9412269), doi:[10.1103/PhysRevD.52.5229](https://doi.org/10.1103/PhysRevD.52.5229).
- [296] T. A. Lahde, C. J. Nyfalt, D. O. Riska, Spectra and M1 decay widths of heavy light mesons, *Nucl. Phys. A* 674 (2000) 141–167. arXiv:[hep-ph/9908485](https://arxiv.org/abs/hep-ph/9908485), doi:[10.1016/S0375-9474\(00\)00154-8](https://doi.org/10.1016/S0375-9474(00)00154-8).
- [297] W.-J. Deng, H. Liu, L.-C. Gui, X.-H. Zhong, Charmonium spectrum and their electromagnetic transitions with higher multipole contributions, *Phys. Rev. D* 95 (3) (2017) 034026. arXiv:[1608.00287](https://arxiv.org/abs/1608.00287), doi:[10.1103/PhysRevD.95.034026](https://doi.org/10.1103/PhysRevD.95.034026).

- [298] D. Ebert, R. N. Faustov, V. O. Galkin, Spectroscopy and Regge trajectories of heavy quarkonia and  $B_c$  mesons, Eur. Phys. J. C 71 (2011) 1825. [arXiv:1111.0454](#), [doi:10.1140/epjc/s10052-011-1825-9](#).
- [299] B.-Q. Li, K.-T. Chao, Higher Charmonia and  $X$ ,  $Y$ ,  $Z$  states with Screened Potential, Phys. Rev. D 79 (2009) 094004. [arXiv:0903.5506](#), [doi:10.1103/PhysRevD.79.094004](#).
- [300] J.-Z. Wang, D.-Y. Chen, X. Liu, T. Matsuki, Constructing  $J/\psi$  family with updated data of charmoniumlike  $Y$  states, Phys. Rev. D 99 (11) (2019) 114003. [arXiv:1903.07115](#), [doi:10.1103/PhysRevD.99.114003](#).
- [301] X.-Z. Weng, W.-Z. Deng, S.-L. Zhu, Heavy baryons in the relativized quark model with chromodynamics, Phys. Rev. D 110 (5) (2024) 056052. [arXiv:2405.19039](#), [doi:10.1103/PhysRevD.110.056052](#).
- [302] N. A. Tornqvist, Understanding the scalar meson  $q\bar{q}$  nonet, Z. Phys. C 68 (1995) 647–660. [arXiv:hep-ph/9504372](#), [doi:10.1007/BF01565264](#).
- [303] N. A. Tornqvist, Scalar mesons in the unitarized quark model, Phys. Rev. Lett. 49 (1982) 624–627. [doi:10.1103/PhysRevLett.49.624](#).
- [304] Y. A. Simonov, J. A. Tjon, The Coupled-channel analysis of the  $D$  and  $D_s$  mesons, Phys. Rev. D 70 (2004) 114013. [arXiv:hep-ph/0409361](#), [doi:10.1103/PhysRevD.70.114013](#).
- [305] P. G. Ortega, J. Segovia, D. R. Entem, F. Fernandez, Molecular components in  $P$ -wave charmed-strange mesons, Phys. Rev. D 94 (7) (2016) 074037. [arXiv:1603.07000](#), [doi:10.1103/PhysRevD.94.074037](#).
- [306] H.-Y. Cheng, F.-S. Yu, Near mass degeneracy in the scalar meson sector: Implications for  $B_{(s)0}^*$  and  $B'_{(s)1}$  mesons, Phys. Rev. D 89 (11) (2014) 114017. [arXiv:1404.3771](#), [doi:10.1103/PhysRevD.89.114017](#).
- [307] H.-Y. Cheng, F.-S. Yu, Masses of scalar and axial-vector  $B$  Mesons revisited, Eur. Phys. J. C 77 (10) (2017) 668. [arXiv:1704.01208](#), [doi:10.1140/epjc/s10052-017-5252-4](#).
- [308] Y.-B. Dai, C.-S. Huang, C. Liu, S.-L. Zhu, Understanding the  $D_{sJ}^+(2317)$  and  $D_{sJ}^+(2460)$  with sum rules in HQET, Phys. Rev. D 68 (2003) 114011. [arXiv:hep-ph/0306274](#), [doi:10.1103/PhysRevD.68.114011](#).
- [309] T. Barnes, E. S. Swanson, Hadron loops: General theorems and application to charmonium, Phys. Rev. C 77 (2008) 055206. [arXiv:0711.2080](#), [doi:10.1103/PhysRevC.77.055206](#).
- [310] J.-F. Liu, G.-J. Ding, Bottomonium spectrum with coupled-channel effects, Eur. Phys. J. C 72 (2012) 1981. [arXiv:1105.0855](#), [doi:10.1140/epjc/s10052-012-1981-6](#).
- [311] R.-H. Ni, Q. Deng, J.-J. Wu, X.-H. Zhong, Bottomonia in an unquenched quark model, Phys. Rev. D 111 (11) (2025) 114027. [arXiv:2501.15110](#), [doi:10.1103/6x3t-x15s](#).
- [312] M. A. Sultan, W. Hao, E. S. Swanson, L. Chang, Bottomonium meson spectrum with quenched and unquenched quark models, Eur. Phys. J. A 61 (6) (2025) 137. [arXiv:2503.10178](#), [doi:10.1140/epja/s10050-025-01607-4](#).
- [313] Y. Lu, M. N. Anwar, B.-S. Zou, Coupled-Channel Effects for the Bottomonium with Realistic Wave Functions, Phys. Rev. D 94 (3) (2016) 034021. [arXiv:1606.06927](#), [doi:10.1103/PhysRevD.94.034021](#).
- [314] Y. Lu, M. N. Anwar, B.-S. Zou, How large is the contribution of excited mesons in coupled-channel effects?, Phys. Rev. D 95 (3) (2017) 034018. [arXiv:1701.00692](#), [doi:10.1103/PhysRevD.95.034018](#).
- [315] J. Ferretti, G. Galata, E. Santopinto, A. Vassallo, Bottomonium self-energies due to the coupling to the meson-meson continuum, Phys. Rev. C 86 (2012) 015204. [doi:10.1103/PhysRevC.86.015204](#).
- [316] J. Ferretti, E. Santopinto, Higher mass bottomonia, Phys. Rev. D 90 (9) (2014) 094022. [arXiv:1306.2874](#), [doi:10.1103/PhysRevD.90.094022](#).

- [317] P. G. Ortega, D. R. Entem, F. Fernandez, Molecular structures in charmonium spectrum: The XYZ puzzle, *J. Phys. G* 40 (2013) 065107. [arXiv:1205.1699](#), [doi:10.1088/0954-3899/40/6/065107](#).
- [318] J. Ferretti, G. Galatà, E. Santopinto, Interpretation of the  $X(3872)$  as a charmonium state plus an extra component due to the coupling to the meson-meson continuum, *Phys. Rev. C* 88 (1) (2013) 015207. [arXiv:1302.6857](#), [doi:10.1103/PhysRevC.88.015207](#).
- [319] Z.-Y. Zhou, Z. Xiao, Hadron loops effect on mass shifts of the charmed and charmed-strange spectra, *Phys. Rev. D* 84 (2011) 034023. [arXiv:1105.6025](#), [doi:10.1103/PhysRevD.84.034023](#).
- [320] Z.-Y. Zhou, Z. Xiao, Comprehending heavy charmonia and their decays by hadron loop effects, *Eur. Phys. J. A* 50 (10) (2014) 165. [arXiv:1309.1949](#), [doi:10.1140/epja/i2014-14165-y](#).
- [321] M.-X. Duan, S.-Q. Luo, X. Liu, T. Matsuki, Possibility of charmoniumlike state  $X(3915)$  as  $\chi_{c0}(2P)$  state, *Phys. Rev. D* 101 (5) (2020) 054029. [arXiv:2002.03311](#), [doi:10.1103/PhysRevD.101.054029](#).
- [322] M.-X. Duan, X. Liu, Where are  $3P$  and higher  $P$ -wave states in the charmonium family?, *Phys. Rev. D* 104 (7) (2021) 074010. [arXiv:2107.14438](#), [doi:10.1103/PhysRevD.104.074010](#).
- [323] Z.-L. Man, S.-Q. Luo, Z.-Y. Bai, X. Liu, Coupled-channel study of  $4S$ - $3D$  mixing dynamics in  $\psi(4220)$  and  $\psi(4380)$ , *Phys. Lett. B* 868 (2025) 139644. [arXiv:2502.08072](#), [doi:10.1016/j.physletb.2025.139644](#).
- [324] Z.-L. Man, S.-Q. Luo, X. Liu, Is the  $3S$ - $2D$  mixing strong for the charmonia  $\psi(4040)$  and  $\psi(4160)$ ?, *Phys. Rev. D* 112 (7) (2025) 074025. [arXiv:2507.18536](#), [doi:10.1103/76fd-njsy](#).
- [325] I. V. Danilkin, Y. A. Simonov, Channel coupling in heavy quarkonia: Energy levels, mixing, widths and new states, *Phys. Rev. D* 81 (2010) 074027. [arXiv:0907.1088](#), [doi:10.1103/PhysRevD.81.074027](#).
- [326] J.-Z. Wang, Z.-Y. Lin, Y.-K. Chen, L. Meng, S.-L. Zhu, Uncovering the mystery of  $X(3872)$  with the coupled-channel dynamics, *Phys. Rev. D* 111 (11) (2025) L111502. [arXiv:2404.16575](#), [doi:10.1103/929g-cv15](#).
- [327] J.-Z. Wang, R.-Q. Qian, X. Liu, T. Matsuki, Are the  $Y$  states around 4.6 GeV from  $e^+e^-$  annihilation higher charmonia?, *Phys. Rev. D* 101 (3) (2020) 034001. [arXiv:2001.00175](#), [doi:10.1103/PhysRevD.101.034001](#).
- [328] J.-Z. Wang, Z.-F. Sun, X. Liu, T. Matsuki, Higher bottomonium zoo, *Eur. Phys. J. C* 78 (11) (2018) 915. [arXiv:1802.04938](#), [doi:10.1140/epjc/s10052-018-6372-1](#).
- [329] C. P. Shen, et al., Evidence for a new resonance and search for the  $Y(4140)$  in the  $\gamma\gamma \rightarrow \phi J/\psi$  process, *Phys. Rev. Lett.* 104 (2010) 112004. [arXiv:0912.2383](#), [doi:10.1103/PhysRevLett.104.112004](#).
- [330] T. Aaltonen, et al., Evidence for a narrow near-threshold structure in the  $J/\psi\phi$  mass spectrum in  $B^+ \rightarrow J/\psi\phi K^+$  decays, *Phys. Rev. Lett.* 102 (2009) 242002. [arXiv:0903.2229](#), [doi:10.1103/PhysRevLett.102.242002](#).
- [331] X. Liu, Z.-G. Luo, Z.-F. Sun,  $X(3915)$  and  $X(4350)$  as new members in  $P$ -wave charmonium family, *Phys. Rev. Lett.* 104 (2010) 122001. [arXiv:0911.3694](#), [doi:10.1103/PhysRevLett.104.122001](#).
- [332] L. D. Landau, On the angular momentum of a system of two photons, *Dokl. Akad. Nauk SSSR* 60 (2) (1948) 207–209. [doi:10.1016/B978-0-08-010586-4.50070-5](#).
- [333] C.-N. Yang, Selection rules for the dematerialization of a particle into two photons, *Phys. Rev.* 77 (1950) 242–245. [doi:10.1103/PhysRev.77.242](#).
- [334] S. Uehara, et al., Study of charmonia in four-meson final states produced in two-photon collisions, *Eur. Phys. J. C* 53 (2008) 1–14. [arXiv:0706.3955](#), [doi:10.1140/epjc/s10052-007-0451-z](#).
- [335] S. Uehara, et al., High-statistics study of  $K_S^0$  pair production in two-photon collisions, *PTEP* 2013 (12) (2013) 123C01. [arXiv:1307.7457](#), [doi:10.1093/ptep/ptt097](#).

- [336] J. P. Lees, et al., Study of  $X(3915) \rightarrow J/\psi\omega$  in two-photon collisions, Phys. Rev. D 86 (2012) 072002. [arXiv:1207.2651](#), [doi:10.1103/PhysRevD.86.072002](#).
- [337] J. Beringer, et al., Review of particle physics (RPP), Phys. Rev. D 86 (2012) 010001. [doi:10.1103/PhysRevD.86.010001](#).
- [338] F.-K. Guo, U.-G. Meissner, Where is the  $\chi_{c0}(2P)$ ?, Phys. Rev. D 86 (2012) 091501. [arXiv:1208.1134](#), [doi:10.1103/PhysRevD.86.091501](#).
- [339] S. L. Olsen, Is the  $X(3915)$  the  $\chi_{c0}(2P)$ ?, Phys. Rev. D 91 (5) (2015) 057501. [arXiv:1410.6534](#), [doi:10.1103/PhysRevD.91.057501](#).
- [340] K. Chilikin, et al., Observation of an alternative  $\chi_{c0}(2P)$  candidate in  $e^+e^- \rightarrow J/\psi D\bar{D}$ , Phys. Rev. D 95 (2017) 112003. [arXiv:1704.01872](#), [doi:10.1103/PhysRevD.95.112003](#).
- [341] Z.-Y. Zhou, Z. Xiao, Understanding  $X(3862)$ ,  $X(3872)$ , and  $X(3930)$  in a Friedrichs-model-like scheme, Phys. Rev. D 96 (5) (2017) 054031, [Erratum: Phys.Rev.D 96, 099905 (2017)]. [arXiv:1704.04438](#), [doi:10.1103/PhysRevD.96.054031](#).
- [342] G. L. Yu, Z. G. Wang, Z. Y. Li, The analysis of the charmonium-like states  $X^*(3860)$ ,  $X(3872)$ ,  $X(3915)$ ,  $X(3930)$  and  $X(3940)$  according to its strong decay behaviors, Chin. Phys. C 42 (2018) 4. [arXiv:1704.06763](#), [doi:10.1088/1674-1137/42/4/043107](#).
- [343] P. G. Ortega, J. Segovia, D. R. Entem, F. Fernández, Charmonium resonances in the 3.9 GeV/ $c^2$  energy region and the  $X(3915)/X(3930)$  puzzle, Phys. Lett. B 778 (2018) 1–5. [arXiv:1706.02639](#), [doi:10.1016/j.physletb.2018.01.005](#).
- [344] B. Aubert, et al., Observation of the  $\chi_{c2}(2p)$  meson in the reaction  $\gamma\gamma \rightarrow D\bar{D}$  at BaBar, Phys. Rev. D 81 (2010) 092003. [arXiv:1002.0281](#), [doi:10.1103/PhysRevD.81.092003](#).
- [345] C. R. Munz, Two photon decays of mesons in a relativistic quark model, Nucl. Phys. A 609 (1996) 364–376. [arXiv:hep-ph/9601206](#), [doi:10.1016/S0375-9474\(96\)00265-5](#).
- [346] D. Ebert, R. N. Faustov, V. O. Galkin, Two photon decay rates of heavy quarkonia in the relativistic quark model, Mod. Phys. Lett. A 18 (2003) 601–608. [arXiv:hep-ph/0302044](#), [doi:10.1142/S021773230300971X](#).
- [347] C.-W. Hwang, R.-S. Guo, Two-photon and two-gluon decays of p-wave heavy quarkonium using a covariant light-front approach, Phys. Rev. D 82 (2010) 034021. [arXiv:1005.2811](#), [doi:10.1103/PhysRevD.82.034021](#).
- [348] G.-L. Wang, Annihilation rate of heavy  $0^{++}$  P-wave quarkonium in relativistic Salpeter method, Phys. Lett. B 653 (2007) 206–209. [arXiv:0708.3516](#), [doi:10.1016/j.physletb.2007.08.017](#).
- [349] D.-Y. Chen, J. He, X. Liu, T. Matsuki, T. Matsuki, Does the enhancement observed in  $\gamma\gamma \rightarrow D\bar{D}$  contain two P-wave higher charmonia?, Eur. Phys. J. C 72 (2012) 2226. [arXiv:1207.3561](#), [doi:10.1140/epjc/s10052-012-2226-4](#).
- [350] R. Aaij, et al., Amplitude analysis of the  $B^+ \rightarrow D^+D^-K^+$  decay, Phys. Rev. D 102 (2020) 112003. [arXiv:2009.00026](#), [doi:10.1103/PhysRevD.102.112003](#).
- [351] R. Aaij, et al., A model-independent study of resonant structure in  $B^+ \rightarrow D^+D^-K^+$  decays, Phys. Rev. Lett. 125 (2020) 242001. [arXiv:2009.00025](#), [doi:10.1103/PhysRevLett.125.242001](#).
- [352] F.-S. Yu, Weak-decay searches for  $Qs\bar{u}\bar{d}$  tetraquarks, Eur. Phys. J. C 82 (7) (2022) 641. [arXiv:1709.02571](#), [doi:10.1140/epjc/s10052-022-10567-8](#).

- [353] X.-H. Liu, M.-J. Yan, H.-W. Ke, G. Li, J.-J. Xie, Triangle singularity as the origin of  $X_0(2900)$  and  $X_1(2900)$  observed in  $B^+ \rightarrow D^+ D^- K^+$ , Eur. Phys. J. C 80 (12) (2020) 1178. [arXiv:2008.07190](#), [doi:10.1140/epjc/s10052-020-08762-6](#).
- [354] J.-R. Zhang, Open-charm tetraquark candidate: Note on  $X_0(2900)$ , Phys. Rev. D 103 (5) (2021) 054019. [arXiv:2008.07295](#), [doi:10.1103/PhysRevD.103.054019](#).
- [355] X.-G. He, W. Wang, R. Zhu, Open-charm tetraquark  $X_c$  and open-bottom tetraquark  $X_b$ , Eur. Phys. J. C 80 (11) (2020) 1026. [arXiv:2008.07145](#), [doi:10.1140/epjc/s10052-020-08597-1](#).
- [356] H.-X. Chen, W. Chen, R.-R. Dong, N. Su,  $X_0(2900)$  and  $X_1(2900)$ : hadronic molecules or compact tetraquarks, Chin. Phys. Lett. 37 (10) (2020) 101201. [arXiv:2008.07516](#), [doi:10.1088/0256-307X/37/10/101201](#).
- [357] Q.-F. Lü, D.-Y. Chen, Y.-B. Dong, Open charm and bottom tetraquarks in an extended relativized quark model, Phys. Rev. D 102 (7) (2020) 074021. [arXiv:2008.07340](#), [doi:10.1103/PhysRevD.102.074021](#).
- [358] Y. Huang, J.-X. Lu, J.-J. Xie, L.-S. Geng, Strong decays of  $\bar{D}^* K^*$  molecules and the newly observed  $X_{0,1}$  states, Eur. Phys. J. C 80 (10) (2020) 973. [arXiv:2008.07959](#), [doi:10.1140/epjc/s10052-020-08516-4](#).
- [359] Z.-G. Wang, Analysis of the  $X_0(2900)$  as the scalar tetraquark state via the QCD sum rules, Int. J. Mod. Phys. A 35 (30) (2020) 2050187. [arXiv:2008.07833](#), [doi:10.1142/S0217751X20501870](#).
- [360] M.-W. Hu, X.-Y. Lao, P. Ling, Q. Wang,  $X_0(2900)$  and its heavy quark spin partners in molecular picture, Chin. Phys. C 45 (2) (2021) 021003. [arXiv:2008.06894](#), [doi:10.1088/1674-1137/abcfaa](#).
- [361] M. Karliner, J. L. Rosner, First exotic hadron with open heavy flavor:  $cs\bar{u}\bar{d}$  tetraquark, Phys. Rev. D 102 (9) (2020) 094016. [arXiv:2008.05993](#), [doi:10.1103/PhysRevD.102.094016](#).
- [362] S. S. Agaev, K. Azizi, H. Sundu, New scalar resonance  $X_0(2900)$  as a molecule: mass and width, J. Phys. G 48 (8) (2021) 085012. [arXiv:2008.13027](#), [doi:10.1088/1361-6471/ac0b31](#).
- [363] G. Yang, J. Ping, J. Segovia, Tetra- and penta-quark structures in the constituent quark model, Symmetry 12 (11) (2020) 1869. [arXiv:2009.00238](#), [doi:10.3390/sym12111869](#).
- [364] Y.-K. Chen, J.-J. Han, Q.-F. Lü, J.-P. Wang, F.-S. Yu, Branching fractions of  $B^- \rightarrow D^- X_{0,1}(2900)$  and their implications, Eur. Phys. J. C 81 (1) (2021) 71. [arXiv:2009.01182](#), [doi:10.1140/epjc/s10052-021-08857-8](#).
- [365] H. Mutuk, Monte-Carlo based QCD sum rules analysis of  $X_0(2900)$  and  $X_1(2900)$ , J. Phys. G 48 (5) (2021) 055007. [arXiv:2009.02492](#), [doi:10.1088/1361-6471/abeb7f](#).
- [366] T. J. Burns, E. S. Swanson, Discriminating among interpretations for the  $X(2900)$  states, Phys. Rev. D 103 (1) (2021) 014004. [arXiv:2009.05352](#), [doi:10.1103/PhysRevD.103.014004](#).
- [367] X.-K. Dong, B.-S. Zou, Prediction of possible  $DK_1$  bound states, Eur. Phys. J. A 57 (4) (2021) 139. [arXiv:2009.11619](#), [doi:10.1140/epja/s10050-021-00442-7](#).
- [368] C.-J. Xiao, D.-Y. Chen, Y.-B. Dong, G.-W. Meng, Study of the decays of  $S$ -wave  $\bar{D}^* K^*$  hadronic molecules: The scalar  $X_0(2900)$  and its spin partners  $X_{J(J=1,2)}$ , Phys. Rev. D 103 (3) (2021) 034004. [arXiv:2009.14538](#), [doi:10.1103/PhysRevD.103.034004](#).
- [369] Y. Tan, J. Ping,  $X(2900)$  in a chiral quark model, Chin. Phys. C 45 (9) (2021) 093104. [arXiv:2010.04045](#), [doi:10.1088/1674-1137/ac0ba4](#).
- [370] H.-T. An, K. Chen, X. Liu, Manifestly exotic pentaquarks with a single heavy quark, Phys. Rev. D 105 (3) (2022) 034018. [arXiv:2010.05014](#), [doi:10.1103/PhysRevD.105.034018](#).

- [371] G.-J. Wang, L. Meng, L.-Y. Xiao, M. Oka, S.-L. Zhu, Mass spectrum and strong decays of tetraquark  $\bar{c}\bar{s}qq$  states, *Eur. Phys. J. C* 81 (2) (2021) 188. [arXiv:2010.09395](#), [doi:10.1140/epjc/s10052-021-08978-0](#).
- [372] L. M. Abreu,  $X_J(2900)$  states in a hot hadronic medium, *Phys. Rev. D* 103 (3) (2021) 036013. [arXiv:2010.14955](#), [doi:10.1103/PhysRevD.103.036013](#).
- [373] G. Yang, J. Ping, J. Segovia,  $sQ\bar{q}\bar{q}$  ( $q = u, d$ ;  $Q = c, b$ ) tetraquarks in the chiral quark model, *Phys. Rev. D* 103 (7) (2021) 074011. [arXiv:2101.04933](#), [doi:10.1103/PhysRevD.103.074011](#).
- [374] J.-J. Qi, Z.-Y. Wang, Z.-F. Zhang, X.-H. Guo, Studying the  $\bar{D}_1K$  molecule in the Bethe–Salpeter equation approach, *Eur. Phys. J. C* 81 (7) (2021) 639. [arXiv:2101.06688](#), [doi:10.1140/epjc/s10052-021-09422-z](#).
- [375] R. M. Albuquerque, S. Narison, D. Rabetiarivony, G. Randriamanatrika, The new charm-strange resonances in the  $D^-K^+$  channel, *Nucl. Part. Phys. Proc.* 312-317 (2021) 125–129. [arXiv:2102.04622](#), [doi:10.1016/j.nuclphysbps.2021.05.032](#).
- [376] B. Wang, S.-L. Zhu, How to understand the  $X(2900)$ ?, *Eur. Phys. J. C* 82 (5) (2022) 419. [arXiv:2107.09275](#), [doi:10.1140/epjc/s10052-022-10396-9](#).
- [377] H. Chen, H.-R. Qi, H.-Q. Zheng,  $X_1(2900)$  as a  $\bar{D}_1K$  molecule, *Eur. Phys. J. C* 81 (9) (2021) 812. [arXiv:2108.02387](#), [doi:10.1140/epjc/s10052-021-09603-w](#).
- [378] R. L. Workman, et al., Review of particle physics, *PTEP* 2022 (2022) 083C01. [doi:10.1093/ptep/ptac097](#).
- [379] C. Z. Yuan, et al., Measurement of  $e^+e^- \rightarrow \pi^+\pi^-J/\psi$  cross-section via initial state radiation at Belle, *Phys. Rev. Lett.* 99 (2007) 182004. [arXiv:0707.2541](#), [doi:10.1103/PhysRevLett.99.182004](#).
- [380] M. Ablikim, et al., Measurement of  $e^+e^- \rightarrow \pi^+\pi^-\psi(3686)$  from 4.008 to 4.600 GeV and observation of a charged structure in the  $\pi^\pm\psi(3686)$  mass spectrum, *Phys. Rev. D* 96 (3) (2017) 032004, [Erratum: *Phys. Rev. D* 99, 019903 (2019)]. [arXiv:1703.08787](#), [doi:10.1103/PhysRevD.96.032004](#).
- [381] M. Ablikim, et al., Observation of  $e^+e^- \rightarrow \eta h_c$  at center-of-mass energies from 4.085 to 4.600 GeV, *Phys. Rev. D* 96 (1) (2017) 012001. [arXiv:1704.08033](#), [doi:10.1103/PhysRevD.96.012001](#).
- [382] M. Ablikim, et al., Evidence of a resonant structure in the  $e^+e^- \rightarrow \pi^+D^0D^{*-}$  cross section between 4.05 and 4.60 GeV, *Phys. Rev. Lett.* 122 (10) (2019) 102002. [arXiv:1808.02847](#), [doi:10.1103/PhysRevLett.122.102002](#).
- [383] M. Ablikim, et al., Cross section measurements of  $e^+e^- \rightarrow \omega\chi_{c0}$  from  $\sqrt{s} = 4.178$  to 4.278 GeV, *Phys. Rev. D* 99 (9) (2019) 091103. [arXiv:1903.02359](#), [doi:10.1103/PhysRevD.99.091103](#).
- [384] M. Ablikim, et al., Observation of the  $Y(4220)$  and  $Y(4360)$  in the process  $e^+e^- \rightarrow \eta J/\psi$ , *Phys. Rev. D* 102 (3) (2020) 031101. [arXiv:2003.03705](#), [doi:10.1103/PhysRevD.102.031101](#).
- [385] M. Ablikim, et al., Study of the process  $e^+e^- \rightarrow \pi^0\pi^0J/\psi$  and neutral charmonium-like state  $Z_c(3900)^0$ , *Phys. Rev. D* 102 (1) (2020) 012009. [arXiv:2004.13788](#), [doi:10.1103/PhysRevD.102.012009](#).
- [386] M. Ablikim, Measurement of cross sections for  $e^+e^- \rightarrow \mu^+\mu^-$  at center-of-mass energies from 3.80 to 4.60 GeV, *Phys. Rev. D* 102 (2020) 112009. [arXiv:2007.12872](#), [doi:10.1103/PhysRevD.102.112009](#).
- [387] M. Ablikim, et al., Measurements of  $e^+e^- \rightarrow \eta_c\pi^+\pi^-\pi^0$ ,  $\eta_c\pi^+\pi^-$ , and  $\eta_c\pi^0\gamma$  at  $\sqrt{s}$  from 4.18 to 4.60 GeV, and search for a  $Z_c$  state close to the  $D\bar{D}$  threshold decaying to  $\eta_c\pi$  at  $\sqrt{s} = 4.23$  GeV, *Phys. Rev. D* 103 (3) (2021) 032006. [arXiv:2010.14415](#), [doi:10.1103/PhysRevD.103.032006](#).
- [388] M. Ablikim, et al., Observation of the  $Y(4230)$  and a new structure in  $e^+e^- \rightarrow K^+K^-J/\psi$ , *Chin. Phys. C* 46 (11) (2022) 111002. [arXiv:2204.07800](#), [doi:10.1088/1674-1137/ac945c](#).

- [389] M. Ablikim, et al., Observation of three charmoniumlike States with  $J^{PC} = 1^{--}$  in  $e^+e^- \rightarrow D^{*0}D^{*-}\pi^+$ , Phys. Rev. Lett. 130 (12) (2023) 121901. [arXiv:2301.07321](#), [doi:10.1103/PhysRevLett.130.121901](#).
- [390] M. Ablikim, et al., Cross section measurement of  $e^+e^- \rightarrow \pi^+\pi^-(3686)$  from  $\sqrt{s} = 4.0076$  to 4.6984 GeV, Phys. Rev. D 104 (5) (2021) 052012. [arXiv:2107.09210](#), [doi:10.1103/PhysRevD.104.052012](#).
- [391] M. Ablikim, et al., Study of the resonance structures in the process  $e^+e^- \rightarrow \pi^+\pi^-J/\psi$ , Phys. Rev. D 106 (7) (2022) 072001. [arXiv:2206.08554](#), [doi:10.1103/PhysRevD.106.072001](#).
- [392] M. Ablikim, et al., Observation of the  $Y(4230)$  and evidence for a new vector charmoniumlike state  $Y(4710)$  in  $e^+e^- \rightarrow K_S^0 K_S^0 J/\psi$ , Phys. Rev. D 107 (9) (2023) 092005. [arXiv:2211.08561](#), [doi:10.1103/PhysRevD.107.092005](#).
- [393] M. Ablikim, et al., Measurement of  $e^+e^- \rightarrow \eta J\psi$  cross section from  $\sqrt{s} = 3.808$  GeV to 4.951 GeV, Phys. Rev. D 109 (9) (2024) 092012. [arXiv:2310.03361](#), [doi:10.1103/PhysRevD.109.092012](#).
- [394] M. Ablikim, et al., Measurement of the born cross section for  $e^+e^- \rightarrow \eta h_c$  at center-of-mass energies between 4.1 and 4.6 GeV, Phys. Rev. D 111 (1) (2025) L011101. [arXiv:2404.06718](#), [doi:10.1103/PhysRevD.111.L011101](#).
- [395] M. Ablikim, et al., Observation of three resonance structure in the cross section of  $e^+e^- \rightarrow \pi^+\pi^-h_c$  (4 2025). [arXiv:2504.04096](#).
- [396] M. Ablikim, et al., Precise Measurement of the  $e^+e^- \rightarrow D_s^{*+}D_s^{*-}$  Cross Sections at Center-of-Mass Energies from Threshold to 4.95 GeV, Phys. Rev. Lett. 131 (15) (2023) 151903. [arXiv:2305.10789](#), [doi:10.1103/PhysRevLett.131.151903](#).
- [397] M. Ablikim, et al., Observation of Structures in the Processes  $e^+e^- \rightarrow \omega\chi_{c1}$  and  $\omega\chi_{c2}$ , Phys. Rev. Lett. 132 (16) (2024) 161901. [arXiv:2401.14720](#), [doi:10.1103/PhysRevLett.132.161901](#).
- [398] Q. He, et al., Confirmation of the  $Y(4260)$  resonance production in initial state radiation, Phys. Rev. D 74 (2006) 091104. [arXiv:hep-ex/0611021](#), [doi:10.1103/PhysRevD.74.091104](#).
- [399] T. E. Coan, et al., Charmonium decays of  $Y(4260)$ ,  $\psi(4160)$  and  $\psi(4040)$ , Phys. Rev. Lett. 96 (2006) 162003. [arXiv:hep-ex/0602034](#), [doi:10.1103/PhysRevLett.96.162003](#).
- [400] Q. Wang, Q. Zhao, A Short Review of the Vector Charmonium-Like State  $\psi(4230)$ , Chin. Phys. Lett. 42 (11) (2025) 110201. [arXiv:2508.05304](#), [doi:10.1088/0256-307X/42/11/110201](#).
- [401] A. Zhang, Charmonium spectrum and new observed states, Phys. Lett. B 647 (2007) 140–144. [arXiv:hep-ph/0603093](#), [doi:10.1016/j.physletb.2007.01.062](#).
- [402] F. J. Llanes-Estrada,  $Y(4260)$  and possible charmonium assignment, Phys. Rev. D 72 (2005) 031503. [arXiv:hep-ph/0507035](#), [doi:10.1103/PhysRevD.72.031503](#).
- [403] E. J. Eichten, K. Lane, C. Quigg, New states above charm threshold, Phys. Rev. D 73 (2006) 014014, [Erratum: Phys.Rev.D 73, 079903 (2006)]. [arXiv:hep-ph/0511179](#), [doi:10.1103/PhysRevD.73.014014](#).
- [404] J. Segovia, A. M. Yasser, D. R. Entem, F. Fernandez,  $J^{PC} = 1^{--}$  hidden charm resonances, Phys. Rev. D 78 (2008) 114033. [doi:10.1103/PhysRevD.78.114033](#).
- [405] L. Y. Dai, M. Shi, G.-Y. Tang, H. Q. Zheng, Nature of  $X(4260)$ , Phys. Rev. D 92 (1) (2015) 014020. [arXiv:1206.6911](#), [doi:10.1103/PhysRevD.92.014020](#).
- [406] Z. Zhao, K. Xu, A. Limphirat, W. Sreethawong, N. Tagsinsit, A. Kaewsnod, X. Liu, K. Khosonthongkee, S. Cheedket, Y. Yan, Mass spectrum of  $1^{--}$  heavy quarkonium, Phys. Rev. D 109 (1) (2024) 016012. [arXiv:2304.06243](#), [doi:10.1103/PhysRevD.109.016012](#).

- [407] M. Shah, A. Parmar, P. C. Vinodkumar, Leptonic and Digamma decay Properties of  $S$ -wave quarkonia states, Phys. Rev. D 86 (2012) 034015. [arXiv:1203.6184](#), [doi:10.1103/PhysRevD.86.034015](#).
- [408] T.-W. Chiu, T.-H. Hsieh,  $Y(4260)$  on the lattice, Phys. Rev. D 73 (2006) 094510. [arXiv:hep-lat/0512029](#), [doi:10.1103/PhysRevD.73.094510](#).
- [409] X. Liu, X.-Q. Zeng, X.-Q. Li, Possible molecular structure of the newly observed  $Y(4260)$ , Phys. Rev. D 72 (2005) 054023. [arXiv:hep-ph/0507177](#), [doi:10.1103/PhysRevD.72.054023](#).
- [410] C. Z. Yuan, P. Wang, X. H. Mo, The  $Y(4260)$  as an  $\omega\chi_{c1}$  molecular state, Phys. Lett. B 634 (2006) 399–402. [arXiv:hep-ph/0511107](#), [doi:10.1016/j.physletb.2006.01.031](#).
- [411] E. Swanson, Review of heavy hadron spectroscopy, Int. J. Mod. Phys. A 21 (2006) 733–738. [arXiv:hep-ph/0509327](#), [doi:10.1142/S0217751X0603196X](#).
- [412] C.-F. Qiao, One explanation for the exotic state  $Y(4260)$ , Phys. Lett. B 639 (2006) 263–265. [arXiv:hep-ph/0510228](#), [doi:10.1016/j.physletb.2006.06.038](#).
- [413] G.-J. Ding, Are  $Y(4260)$  and  $Z_2^+$  are  $D_1D$  or  $D_0D^*$  Hadronic Molecules?, Phys. Rev. D 79 (2009) 014001. [arXiv:0809.4818](#), [doi:10.1103/PhysRevD.79.014001](#).
- [414] F. Close, C. Downum, On the possibility of Deeply Bound Hadronic Molecules from single Pion Exchange, Phys. Rev. Lett. 102 (2009) 242003. [arXiv:0905.2687](#), [doi:10.1103/PhysRevLett.102.242003](#).
- [415] F. Close, C. Downum, C. E. Thomas, Novel Charmonium and Bottomonium Spectroscopies due to Deeply Bound Hadronic Molecules from Single Pion Exchange, Phys. Rev. D 81 (2010) 074033. [arXiv:1001.2553](#), [doi:10.1103/PhysRevD.81.074033](#).
- [416] Q. Wang, C. Hanhart, Q. Zhao, Decoding the riddle of  $Y(4260)$  and  $Z_c(3900)$ , Phys. Rev. Lett. 111 (13) (2013) 132003. [arXiv:1303.6355](#), [doi:10.1103/PhysRevLett.111.132003](#).
- [417] M. Cleven, Q. Wang, F.-K. Guo, C. Hanhart, U.-G. Meißner, Q. Zhao,  $Y(4260)$  as the first  $S$ -wave open charm vector molecular state?, Phys. Rev. D 90 (7) (2014) 074039. [arXiv:1310.2190](#), [doi:10.1103/PhysRevD.90.074039](#).
- [418] Q. Wang, M. Cleven, F.-K. Guo, C. Hanhart, U.-G. Meißner, X.-G. Wu, Q. Zhao,  $Y(4260)$ : hadronic molecule versus hadro-charmonium interpretation, Phys. Rev. D 89 (3) (2014) 034001. [arXiv:1309.4303](#), [doi:10.1103/PhysRevD.89.034001](#).
- [419] M.-T. Li, W.-L. Wang, Y.-B. Dong, Z.-Y. Zhang, A Study of  $P$ -wave Heavy Meson Interactions in A Chiral Quark Model (3 2013). [arXiv:1303.4140](#).
- [420] S.-R. Xue, H.-J. Jing, F.-K. Guo, Q. Zhao, Disentangling the role of the  $Y(4260)$  in  $e^+e^- \rightarrow D^*\bar{D}^*$  and  $D_s^*\bar{D}_s^*$  via line shape studies, Phys. Lett. B 779 (2018) 402–408. [arXiv:1708.06961](#), [doi:10.1016/j.physletb.2018.02.027](#).
- [421] W. Qin, S.-R. Xue, Q. Zhao, Production of  $Y(4260)$  as a hadronic molecule state of  $\bar{D}D_1 + c.c.$  in  $e^+e^-$  annihilations, Phys. Rev. D 94 (5) (2016) 054035. [arXiv:1605.02407](#), [doi:10.1103/PhysRevD.94.054035](#).
- [422] L. Maiani, V. Riquer, F. Piccinini, A. D. Polosa, Four quark interpretation of  $Y(4260)$ , Phys. Rev. D 72 (2005) 031502. [arXiv:hep-ph/0507062](#), [doi:10.1103/PhysRevD.72.031502](#).
- [423] N. V. Drenska, R. Faccini, A. D. Polosa, Exotic Hadrons with Hidden Charm and Strangeness, Phys. Rev. D 79 (2009) 077502. [arXiv:0902.2803](#), [doi:10.1103/PhysRevD.79.077502](#).
- [424] L. Maiani, F. Piccinini, A. D. Polosa, V. Riquer, The  $Z(4430)$  and a New Paradigm for Spin Interactions in Tetraquarks, Phys. Rev. D 89 (2014) 114010. [arXiv:1405.1551](#), [doi:10.1103/PhysRevD.89.114010](#).

- [425] A. Ali, L. Maiani, A. V. Borisov, I. Ahmed, M. Jamil Aslam, A. Y. Parkhomenko, A. D. Polosa, A. Rehman, A new look at the  $Y$  tetraquarks and  $\Omega_c$  baryons in the diquark model, *Eur. Phys. J. C* 78 (1) (2018) 29. [arXiv:1708.04650](#), [doi:10.1140/epjc/s10052-017-5501-6](#).
- [426] M. Cleven, F.-K. Guo, C. Hanhart, Q. Wang, Q. Zhao, Employing spin symmetry to disentangle different models for the  $XYZ$  states, *Phys. Rev. D* 92 (1) (2015) 014005. [arXiv:1505.01771](#), [doi:10.1103/PhysRevD.92.014005](#).
- [427] D. Ebert, R. N. Faustov, V. O. Galkin, Masses of heavy tetraquarks in the relativistic quark model, *Phys. Lett. B* 634 (2006) 214–219. [arXiv:hep-ph/0512230](#), [doi:10.1016/j.physletb.2006.01.026](#).
- [428] D. Ebert, R. N. Faustov, V. O. Galkin, Excited heavy tetraquarks with hidden charm, *Eur. Phys. J. C* 58 (2008) 399–405. [arXiv:0808.3912](#), [doi:10.1140/epjc/s10052-008-0754-8](#).
- [429] W. Chen, S.-L. Zhu, The Vector and Axial-Vector Charmonium-like States, *Phys. Rev. D* 83 (2011) 034010. [arXiv:1010.3397](#), [doi:10.1103/PhysRevD.83.034010](#).
- [430] S.-L. Zhu, Masses and decay widths of heavy hybrid mesons, *Phys. Rev. D* 60 (1999) 014008. [arXiv:hep-ph/9812405](#), [doi:10.1103/PhysRevD.60.014008](#).
- [431] S.-L. Zhu, Some decay modes of the  $1^{++}$  hybrid meson in QCD sum rules revisited, *Phys. Rev. D* 60 (1999) 097502. [arXiv:hep-ph/9903537](#), [doi:10.1103/PhysRevD.60.097502](#).
- [432] F. E. Close, P. R. Page, The Production and decay of hybrid mesons by flux tube breaking, *Nucl. Phys. B* 443 (1995) 233–254. [arXiv:hep-ph/9411301](#), [doi:10.1016/0550-3213\(95\)00085-7](#).
- [433] F. E. Close, S. Godfrey, Charmonium hybrid production in exclusive  $B$  meson decays, *Phys. Lett. B* 574 (2003) 210–216. [arXiv:hep-ph/0305285](#), [doi:10.1016/j.physletb.2003.09.011](#).
- [434] E. Kou, O. Pene, Suppressed decay into open charm for the  $Y(4260)$  being an hybrid, *Phys. Lett. B* 631 (2005) 164–169. [arXiv:hep-ph/0507119](#), [doi:10.1016/j.physletb.2005.09.013](#).
- [435] S.-L. Zhu, The Possible interpretations of  $Y(4260)$ , *Phys. Lett. B* 625 (2005) 212. [arXiv:hep-ph/0507025](#), [doi:10.1016/j.physletb.2005.08.068](#).
- [436] F. E. Close, P. R. Page, Gluonic charmonium resonances at BaBar and BELLE?, *Phys. Lett. B* 628 (2005) 215–222. [arXiv:hep-ph/0507199](#), [doi:10.1016/j.physletb.2005.09.016](#).
- [437] T. Barnes, F. E. Close, E. S. Swanson, Hybrid and conventional mesons in the flux tube model: Numerical studies and their phenomenological implications, *Phys. Rev. D* 52 (1995) 5242–5256. [arXiv:hep-ph/9501405](#), [doi:10.1103/PhysRevD.52.5242](#).
- [438] J. Merlin, J. E. Paton, Spin Interactions in the Flux Tube Model and Hybrid Meson Masses, *Phys. Rev. D* 35 (1987) 1668. [doi:10.1103/PhysRevD.35.1668](#).
- [439] P. Lacock, C. Michael, P. Boyle, P. Rowland, Hybrid mesons from quenched QCD, *Phys. Lett. B* 401 (1997) 308–312. [arXiv:hep-lat/9611011](#), [doi:10.1016/S0370-2693\(97\)00384-5](#).
- [440] T. Manke, I. T. Drummond, R. R. Horgan, H. P. Shanahan, Heavy hybrids from NRQCD, *Phys. Rev. D* 57 (1998) 3829–3832. [arXiv:hep-lat/9710083](#), [doi:10.1103/PhysRevD.57.R3829](#).
- [441] K. J. Juge, J. Kuti, C. J. Morningstar, The Heavy hybrid spectrum from NRQCD and the Born-Oppenheimer approximation, *Nucl. Phys. B Proc. Suppl.* 83 (2000) 304–306. [arXiv:hep-lat/9909165](#), [doi:10.1016/S0920-5632\(00\)91655-4](#).
- [442] I. T. Drummond, N. A. Goodman, R. R. Horgan, H. P. Shanahan, L. C. Stononi, Spin effects in heavy hybrid mesons on an anisotropic lattice, *Phys. Lett. B* 478 (2000) 151–160. [arXiv:hep-lat/9912041](#), [doi:10.1016/S0370-2693\(00\)00225-2](#).

- [443] T. Manke, Exotic quarkonia from anisotropic lattices, Nucl. Phys. B Proc. Suppl. 86 (2000) 397–400. [arXiv: hep-lat/9909038](#), [doi:10.1016/S0920-5632\(00\)00593-4](#).
- [444] L. Liu, G. Moir, M. Peardon, S. M. Ryan, C. E. Thomas, P. Vilaseca, J. J. Dudek, R. G. Edwards, B. Joo, D. G. Richards, Excited and exotic charmonium spectroscopy from lattice QCD, JHEP 07 (2012) 126. [arXiv: 1204.5425](#), [doi:10.1007/JHEP07\(2012\)126](#).
- [445] G. K. C. Cheung, C. O’Hara, G. Moir, M. Peardon, S. M. Ryan, C. E. Thomas, D. Tims, Excited and exotic charmonium,  $D_s$  and  $D$  meson spectra for two light quark masses from lattice QCD, JHEP 12 (2016) 089. [arXiv:1610.01073](#), [doi:10.1007/JHEP12\(2016\)089](#).
- [446] Y. Chen, W.-F. Chiu, M. Gong, L.-C. Gui, Z. Liu, Exotic vector charmonium and its leptonic decay width, Chin. Phys. C 40 (8) (2016) 081002. [arXiv:1604.03401](#), [doi:10.1088/1674-1137/40/8/081002](#).
- [447] M. Berwein, N. Brambilla, J. Tarrús Castellà, A. Vairo, Quarkonium Hybrids with Nonrelativistic Effective Field Theories, Phys. Rev. D 92 (11) (2015) 114019. [arXiv:1510.04299](#), [doi:10.1103/PhysRevD.92.114019](#).
- [448] B. Aubert, et al., Study of the exclusive initial-state radiation production of the  $D\bar{D}$  System, Phys. Rev. D 76 (2007) 111105. [arXiv:hep-ex/0607083](#), [doi:10.1103/PhysRevD.76.111105](#).
- [449] K. Abe, et al., Measurement of the near-threshold  $e^+e^- \rightarrow D^{(*)\pm}D^{(*)\mp}$  cross section using initial-state radiation, Phys. Rev. Lett. 98 (2007) 092001. [arXiv:hep-ex/0608018](#), [doi:10.1103/PhysRevLett.98.092001](#).
- [450] G. Pakhlova, et al., Observation of  $\psi(4415) \rightarrow D\bar{D}_2^*(2460)$  decay using initial-state radiation, Phys. Rev. Lett. 100 (2008) 062001. [arXiv:0708.3313](#), [doi:10.1103/PhysRevLett.100.062001](#).
- [451] G. Pakhlova, et al., Measurement of the  $e^+e^- \rightarrow D^0D^{*-}\pi^+$  cross section using initial-state radiation, Phys. Rev. D 80 (2009) 091101. [arXiv:0908.0231](#), [doi:10.1103/PhysRevD.80.091101](#).
- [452] D. Cronin-Hennessy, et al., Measurement of charm production cross sections in  $e^+e^-$  annihilation at energies between 3.97 and 4.26 GeV, Phys. Rev. D 80 (2009) 072001. [arXiv:0801.3418](#), [doi:10.1103/PhysRevD.80.072001](#).
- [453] B. Aubert, et al., Exclusive initial-state-radiation production of the  $D\bar{D}$ ,  $D^*\bar{D}$ , and  $D^*\bar{D}^*$  systems, Phys. Rev. D 79 (2009) 092001. [arXiv:0903.1597](#), [doi:10.1103/PhysRevD.79.092001](#).
- [454] P. del Amo Sanchez, et al., Exclusive production of  $D_s^+D_s^-$ ,  $D_s^{*+}D_s^-$ , and  $D_s^{*+}D_s^{*-}$  via  $e^+e^-$  annihilation with initial-state-radiation, Phys. Rev. D 82 (2010) 052004. [arXiv:1008.0338](#), [doi:10.1103/PhysRevD.82.052004](#).
- [455] G. Pakhlova, et al., Measurement of the near-threshold  $e^+e^- \rightarrow D\bar{D}$  cross section using initial-state radiation, Phys. Rev. D 77 (2008) 011103. [arXiv:0708.0082](#), [doi:10.1103/PhysRevD.77.011103](#).
- [456] K. A. Olive, et al., Review of particle physics, Chin. Phys. C 38 (2014) 090001. [doi:10.1088/1674-1137/38/9/090001](#).
- [457] J. Burmester, et al., The total hadronic cross-section for  $e^+e^-$  annihilation between 3.1 GeV and 4.8 GeV center-of-mass energy, Phys. Lett. B 66 (1977) 395–400. [doi:10.1016/0370-2693\(77\)90023-5](#).
- [458] R. Brandelik, et al., Total cross-section for hadron production by  $e^+e^-$  annihilation at center-of-mass energies between 3.6 and 5.2 GeV, Phys. Lett. B 76 (1978) 361. [doi:10.1016/0370-2693\(78\)90807-9](#).
- [459] J. Siegrist, et al., Hadron production by  $e^+e^-$  annihilation at center-of-mass energies between 2.6 GeV and 7.8 GeV: Part 1. total cross section, multiplicities and inclusive momentum distributions, Phys. Rev. D 26 (1982) 969. [doi:10.1103/PhysRevD.26.969](#).

- [460] J. Z. Bai, et al., Measurement of the total cross-section for hadronic production by  $e^+e^-$  annihilation at energies between 2.6–5 GeV, Phys. Rev. Lett. 84 (2000) 594–597. [arXiv:hep-ex/9908046](#), [doi:10.1103/PhysRevLett.84.594](#).
- [461] M. Ablikim, et al.,  $R$  value measurements for  $e^+e^-$  annihilation at 2.60 GeV, 3.07 GeV and 3.65 GeV, Phys. Lett. B 677 (2009) 239–245. [arXiv:0903.0900](#), [doi:10.1016/j.physletb.2009.05.055](#).
- [462] G. S. Abrams, et al., The discovery of a second narrow resonance in  $e^+e^-$  annihilation, Phys. Rev. Lett. 33 (1974) 1453–1455. [doi:10.1103/PhysRevLett.33.1453](#).
- [463] W. M. Tanenbaum, et al., Observation of an intermediate state in  $\psi'(3684)$  radiative cascade decay, Phys. Rev. Lett. 35 (1975) 1323. [doi:10.1103/PhysRevLett.35.1323](#).
- [464] J. S. Whitaker, et al., Radiative Decays of  $\psi(3095)$  and  $\psi'(3684)$ , Phys. Rev. Lett. 37 (1976) 1596. [doi:10.1103/PhysRevLett.37.1596](#).
- [465] J. Siegrist, et al., Observation of a Resonance at 4.4 GeV and Additional Structure Near 4.1 GeV in  $e^+e^-$  Annihilation, Phys. Rev. Lett. 36 (1976) 700. [doi:10.1103/PhysRevLett.36.700](#).
- [466] P. A. Rapidis, et al., Observation of a resonance in  $e^+e^-$  annihilation just above charm threshold, Phys. Rev. Lett. 39 (1977) 526, [Erratum: Phys.Rev.Lett. 39, 974 (1977)]. [doi:10.1103/PhysRevLett.39.526](#).
- [467] C. J. Biddick, et al., Inclusive gamma-ray spectra from  $\psi(3095)$  and  $\psi'(3684)$ , Phys. Rev. Lett. 38 (1977) 1324. [doi:10.1103/PhysRevLett.38.1324](#).
- [468] G. Goldhaber, et al.,  $D$  and  $D^*$  Meson production near 4 GeV in  $e^+e^-$  annihilation, Phys. Lett. B 69 (1977) 503–507. [doi:10.1016/0370-2693\(77\)90855-3](#).
- [469] S. W. Herb, et al., Observation of a dimuon resonance at 9.5 GeV in 400 GeV proton-nucleus collisions, Phys. Rev. Lett. 39 (1977) 252–255. [doi:10.1103/PhysRevLett.39.252](#).
- [470] R. Partridge, et al., Observation of an  $\eta_c$  candidate state with mass 2978 MeV  $\pm$  9 MeV, Phys. Rev. Lett. 45 (1980) 1150–1153. [doi:10.1103/PhysRevLett.45.1150](#).
- [471] C. Edwards, et al., Observation of an  $\eta'_c$  candidate state with mass 3592 MeV  $\pm$  5 MeV, Phys. Rev. Lett. 48 (1982) 70. [doi:10.1103/PhysRevLett.48.70](#).
- [472] C. Baglin, et al., Search for the  $p$  wave singlet charmonium state in  $\bar{p}p$  annihilations at the CERN intersecting storage rings, Phys. Lett. B 171 (1986) 135–141. [doi:10.1016/0370-2693\(86\)91013-0](#).
- [473] T. A. Armstrong, et al., Observation of the  $p$  wave singlet state of charmonium, Phys. Rev. Lett. 69 (1992) 2337–2340. [doi:10.1103/PhysRevLett.69.2337](#).
- [474] E. Laermann, F. Langhammer, I. Schmitt, P. M. Zerwas, The interquark potential: SU(2) color gauge theory with fermions, Phys. Lett. B 173 (1986) 437–442. [doi:10.1016/0370-2693\(86\)90411-9](#).
- [475] K. D. Born, E. Laermann, N. Pirch, T. F. Walsh, P. M. Zerwas, Hadron properties in lattice QCD with dynamical fermions, Phys. Rev. D 40 (1989) 1653–1663. [doi:10.1103/PhysRevD.40.1653](#).
- [476] Y.-B. Dong, Y.-W. Yu, Z.-Y. Zhang, P.-N. Shen, Leptonic decay of charmonium, Phys. Rev. D 49 (1994) 1642–1644. [doi:10.1103/PhysRevD.49.1642](#).
- [477] Q.-T. Song, D.-Y. Chen, X. Liu, T. Matsuki, Higher radial and orbital excitations in the charmed meson family, Phys. Rev. D 92 (7) (2015) 074011. [arXiv:1503.05728](#), [doi:10.1103/PhysRevD.92.074011](#).
- [478] J.-Z. Wang, L.-M. Wang, X. Liu, T. Matsuki, Deciphering the light vector meson contribution to the cross sections of  $e^+e^-$  annihilations into the open-strange channels through a combined analysis, Phys. Rev. D 104 (5) (2021) 054045. [arXiv:2106.14582](#), [doi:10.1103/PhysRevD.104.054045](#).

- [479] L.-P. He, D.-Y. Chen, X. Liu, T. Matsuki, Prediction of a missing higher charmonium around 4.26 GeV in  $J/\psi$  family, *Eur. Phys. J. C* 74 (12) (2014) 3208. [arXiv:1405.3831](#), [doi:10.1140/epjc/s10052-014-3208-5](#).
- [480] C.-Z. Yuan, Evidence for resonant structures in  $e^+e^- \rightarrow \pi^+\pi^-h_c$ , *Chin. Phys. C* 38 (2014) 043001. [arXiv:1312.6399](#), [doi:10.1088/1674-1137/38/4/043001](#).
- [481] M. Ablikim, et al., Study of  $e^+e^- \rightarrow \omega\chi_{cJ}$  at center-of-mass energies from 4.21 to 4.42 GeV, *Phys. Rev. Lett.* 114 (9) (2015) 092003. [arXiv:1410.6538](#), [doi:10.1103/PhysRevLett.114.092003](#).
- [482] M. Ablikim, et al., Observation of  $e^+e^- \rightarrow \pi^+\pi^-\psi(3770)$  and  $D_1(2420)^0\bar{D}^0 + \text{c.c.}$ , *Phys. Rev. D* 100 (3) (2019) 032005. [arXiv:1903.08126](#), [doi:10.1103/PhysRevD.100.032005](#).
- [483] M. Ablikim, et al., Search for the reaction  $e^+e^- \rightarrow \chi_{cJ}\pi^+\pi^-$  and a charmonium-like structure decaying to  $\chi_{cJ}\pi^\pm$  between 4.18 and 4.60 GeV, *Phys. Rev. D* 103 (5) (2021) 052010. [arXiv:2012.02682](#), [doi:10.1103/PhysRevD.103.052010](#).
- [484] M. Ablikim, et al., Observation of  $e^+e^- \rightarrow \eta\psi(2S)$  at center-of-mass energies from 4.236 to 4.600 GeV, *JHEP* 10 (2021) 177. [arXiv:2103.01480](#), [doi:10.1007/JHEP10\(2021\)177](#).
- [485] M. Ablikim, et al., Cross section measurement of  $e^+e^- \rightarrow \eta\psi(2S)$  and search for  $e^+e^- \rightarrow \eta\tilde{X}(3872)$ , *Phys. Rev. D* 109 (11) (2024) 112004. [arXiv:2403.16811](#), [doi:10.1103/PhysRevD.109.112004](#).
- [486] M. Ablikim, et al., Measurement of  $e^+e^- \rightarrow \pi^+\pi^-D^+D^-$  cross sections at center-of-mass energies from 4.190 to 4.946 GeV, *Phys. Rev. D* 106 (5) (2022) 052012. [arXiv:2208.00099](#), [doi:10.1103/PhysRevD.106.052012](#).
- [487] M. Ablikim, et al., Study of  $e^+e^- \rightarrow 2(p\bar{p})$  at center-of-mass energies between 4.0 and 4.6 GeV, *Phys. Rev. D* 103 (5) (2021) 052003. [arXiv:2012.11079](#), [doi:10.1103/PhysRevD.103.052003](#).
- [488] M. Ablikim, et al., Measurement of the cross section of  $e^+e^- \rightarrow \eta\pi^+\pi^-$  at center-of-mass energies from 3.872 GeV to 4.700 GeV, *JHEP* 12 (2022) 153. [arXiv:2202.12748](#), [doi:10.1007/JHEP12\(2022\)153](#).
- [489] M. Ablikim, et al., Study of the  $e^+e^- \rightarrow \pi^+\pi^-\omega$  process at center-of-mass energies between 4.0 and 4.6 GeV, *JHEP* 08 (2023) 159. [arXiv:2303.09718](#), [doi:10.1007/JHEP08\(2023\)159](#).
- [490] M. Ablikim, et al., Measurement of born cross section of  $e^+e^- \rightarrow \Sigma^+\bar{\Sigma}^-$  at center-of-mass energies between 3.510 and 4.951 GeV, *JHEP* 05 (2024) 022. [arXiv:2401.09468](#), [doi:10.1007/JHEP05\(2024\)022](#).
- [491] M. Ablikim, et al., Measurement of Born cross sections of  $e^+e^- \rightarrow \Xi^0\bar{\Xi}^0$  and search for charmonium(-like) states at  $\sqrt{s} = 3.51\text{--}4.95$  GeV, *JHEP* 11 (2024) 062. [arXiv:2409.00427](#), [doi:10.1007/JHEP11\(2024\)062](#).
- [492] M. Ablikim, et al., Measurement of the cross section of  $e^+e^- \rightarrow \Xi^-\bar{\Xi}^+$  at center-of-mass energies between 3.510 and 4.843 GeV, *JHEP* 11 (2023) 228. [arXiv:2309.04215](#), [doi:10.1007/JHEP11\(2023\)228](#).
- [493] M. Ablikim, et al., Measurement of Born cross sections and effective form factors of  $e^+e^- \rightarrow \Omega^-\bar{\Omega}^+$  from  $\sqrt{s} = 3.7$  to 4.7 GeV (8 2025). [arXiv:2508.01359](#).
- [494] M. Ablikim, et al., Measurements of  $e^+e^- \rightarrow K_S^0 K^\pm\pi^\mp\pi^0$  and  $K_S^0 K^\pm\pi^\mp\eta$  at center-of-mass energies from 3.90 to 4.60 GeV, *Phys. Rev. D* 99 (1) (2019) 012003. [arXiv:1810.09395](#), [doi:10.1103/PhysRevD.99.012003](#).
- [495] M. Ablikim, et al., Measurement of the cross section for  $e^+e^- \rightarrow \Xi^-\bar{\Xi}^+$  and observation of an excited  $\Xi$  baryon, *Phys. Rev. Lett.* 124 (3) (2020) 032002. [arXiv:1910.04921](#), [doi:10.1103/PhysRevLett.124.032002](#).
- [496] M. Ablikim, et al., Cross section measurement of  $e^+e^- \rightarrow p\bar{p}\eta$  and  $e^+e^- \rightarrow p\bar{p}\omega$  at center-of-mass energies between 3.773 GeV and 4.6 GeV, *Phys. Rev. D* 104 (9) (2021) 092008. [arXiv:2102.04268](#), [doi:10.1103/PhysRevD.104.092008](#).

- [497] M. Ablikim, et al., Observation of a near-threshold enhancement in the  $\Lambda\bar{\Lambda}$  mass spectrum from  $e^+e^- \rightarrow \phi\Lambda\bar{\Lambda}$  at  $\sqrt{s}$  from 3.51 to 4.60 GeV, Phys. Rev. D 104 (5) (2021) 052006. [arXiv:2104.08754](#), [doi:10.1103/PhysRevD.104.052006](#).
- [498] M. Ablikim, et al., Cross sections for the reactions  $e^+e^- \rightarrow K^+K^-\pi^+\pi^-(\pi^0)$ ,  $K^+K^-K^+K^-(\pi^0)$ ,  $\pi^+\pi^-\pi^+\pi^-(\pi^0)$ ,  $p\bar{p}\pi^+\pi^-(\pi^0)$  in the energy region between 3.773 and 4.600 GeV, Phys. Rev. D 104 (11) (2021) 112009. [arXiv:2109.12751](#), [doi:10.1103/PhysRevD.104.112009](#).
- [499] M. Ablikim, et al., Cross section measurements of the processes  $e^+e^- \rightarrow \omega\pi^0$  and  $\omega\eta$  at center-of-mass energies between 3.773 and 4.701 GeV, JHEP 07 (2022) 064. [arXiv:2203.02682](#), [doi:10.1007/JHEP07\(2022\)064](#).
- [500] M. Ablikim, et al., Measurement of  $e^+e^- \rightarrow \phi\eta'$  cross sections at center-of-mass energies between 3.508 and 4.600 GeV, Phys. Rev. D 107 (7) (2023) 072003. [arXiv:2210.06988](#), [doi:10.1103/PhysRevD.107.072003](#).
- [501] M. Ablikim, et al., Measurement of  $e^+e^- \rightarrow \Lambda\bar{\Lambda}\eta$  from 3.5106 to 4.6988 GeV and study of  $\Lambda\bar{\Lambda}$  mass threshold enhancement, Phys. Rev. D 107 (11) (2023) 112001. [arXiv:2211.10755](#), [doi:10.1103/PhysRevD.107.112001](#).
- [502] M. Ablikim, et al., Measurement of  $e^+e^- \rightarrow pK^-\bar{\Lambda} + c.c.$  cross sections between 4.009 GeV and 4.951 GeV, JHEP 12 (2023) 027. [arXiv:2307.02328](#), [doi:10.1007/JHEP12\(2023\)027](#).
- [503] M. Ablikim, et al., Measurement of  $e^+e^- \rightarrow \phi\eta'$  cross sections at center-of-mass energies from 3.508 to 4.951 GeV and search for the decay  $\psi(3770) \rightarrow \phi\eta'$ , Phys. Rev. D 108 (5) (2023) 052015. [arXiv:2307.12736](#), [doi:10.1103/PhysRevD.108.052015](#).
- [504] M. Ablikim, et al., Study of  $e^+e^- \rightarrow \eta\phi$  at center-of-mass energies from 3.773 to 4.600 GeV, Phys. Rev. D 108 (11) (2023) 112011. [arXiv:2308.08161](#), [doi:10.1103/PhysRevD.108.112011](#).
- [505] M. Ablikim, et al., Measurement of the cross sections of  $e^+e^- \rightarrow K^-\bar{\Xi}^+\Lambda/\Sigma^0$  at center-of-mass energies between 3.510 and 4.914 GeV, JHEP 07 (2024) 258. [arXiv:2406.18183](#), [doi:10.1007/JHEP07\(2024\)258](#).
- [506] M. Ablikim, et al., Measurement of Born cross section of  $e^+e^- \rightarrow \Sigma^0\bar{\Sigma}^0$  at  $\sqrt{s}=3.50-4.95$  GeV, Phys. Rev. D 111 (5) (2025) L051502. [arXiv:2412.20305](#), [doi:10.1103/PhysRevD.111.L051502](#).
- [507] M. Ablikim, et al., Cross section measurement of  $e^+e^- \rightarrow f_1(1285)\pi^+\pi^-$  at center-of-mass energies between 3.808 and 4.951 GeV (1 2025). [arXiv:2501.14206](#).
- [508] M. Ablikim, et al., Measurement of the Born cross section for  $e^+e^- \rightarrow pK^-K^-\bar{\Sigma}^+$  at  $\sqrt{s} = 3.5-4.9$  GeV (8 2025). [arXiv:2508.11276](#).
- [509] M. Ablikim, et al., Measurement of the cross section for  $e^+e^- \rightarrow \Lambda\bar{\Lambda}$  and evidence of the decay  $\psi(3770) \rightarrow \Lambda\bar{\Lambda}$ , Phys. Rev. D 104 (9) (2021) L091104. [arXiv:2108.02410](#), [doi:10.1103/PhysRevD.104.L091104](#).
- [510] M. Ablikim, et al., Cross sections measurement of  $e^+e^- \rightarrow \Xi(1530)^0\bar{\Xi}^0 + c.c.$  and search for  $\psi(3770) \rightarrow \Xi(1530)^0\bar{\Xi}^0 + c.c.$  (12 2025). [arXiv:2512.17275](#).
- [511] S. Jia, et al., Observation of a vector charmoniumlike state in  $e^+e^- \rightarrow D_s^+D_{s1}(2536)^- + c.c.$ , Phys. Rev. D 100 (11) (2019) 111103. [arXiv:1911.00671](#), [doi:10.1103/PhysRevD.100.111103](#).
- [512] D.-Y. Chen, X. Liu, X.-Q. Li, H.-W. Ke, Unified Fano-like interference picture for charmoniumlike states  $Y(4008)$ ,  $Y(4260)$  and  $Y(4360)$ , Phys. Rev. D 93 (2016) 014011. [arXiv:1512.04157](#), [doi:10.1103/PhysRevD.93.014011](#).
- [513] D.-Y. Chen, X. Liu, T. Matsuki, Interference effect as resonance killer of newly observed charmoniumlike states  $Y(4320)$  and  $Y(4390)$ , Eur. Phys. J. C 78 (2) (2018) 136. [arXiv:1708.01954](#), [doi:10.1140/epjc/s10052-018-5635-1](#).

- [514] M. Ablikim, et al., Observation of a charged charmoniumlike structure  $Z_c(4020)$  and search for the  $Z_c(3900)$  in  $e^+e^- \rightarrow \pi^+\pi^-h_c$ , Phys. Rev. Lett. 111 (24) (2013) 242001. [arXiv:1309.1896](#), [doi:10.1103/PhysRevLett.111.242001](#).
- [515] M. Ablikim, et al., Determination of the  $\psi(3770)$ ,  $\psi(4040)$ ,  $\psi(4160)$  and  $\psi(4415)$  resonance parameters, eConf C070805 (2007) 02. [arXiv:0705.4500](#), [doi:10.1016/j.physletb.2007.11.100](#).
- [516] J.-Z. Wang, X. Liu, Identifying a characterized energy level structure of higher charmonium well matched to the peak structures in  $e^+e^- \rightarrow \pi^+D^0D^{*-}$ , Phys. Lett. B 849 (2024) 138456. [arXiv:2306.14695](#), [doi:10.1016/j.physletb.2024.138456](#).
- [517] G. Cotugno, R. Faccini, A. D. Polosa, C. Sabelli, Charmed baryonium, Phys. Rev. Lett. 104 (2010) 132005. [arXiv:0911.2178](#), [doi:10.1103/PhysRevLett.104.132005](#).
- [518] F.-K. Guo, J. Haidenbauer, C. Hanhart, U.-G. Meissner, Reconciling the  $X(4630)$  with the  $Y(4660)$ , Phys. Rev. D 82 (2010) 094008. [arXiv:1005.2055](#), [doi:10.1103/PhysRevD.82.094008](#).
- [519] D. V. Bugg, An alternative fit to Belle mass spectra for  $D\bar{D}$ ,  $D^*\bar{D}^*$  and  $\Lambda_c\bar{\Lambda}_c$ , J. Phys. G 36 (2009) 075002. [arXiv:0811.2559](#), [doi:10.1088/0954-3899/36/7/075002](#).
- [520] M. Ablikim, et al., Precision measurement of the  $e^+e^- \rightarrow \Lambda_c^+\bar{\Lambda}_c^-$  cross section near threshold, Phys. Rev. Lett. 120 (13) (2018) 132001. [arXiv:1710.00150](#), [doi:10.1103/PhysRevLett.120.132001](#).
- [521] X. L. Wang, et al., Measurement of  $e^+e^- \rightarrow \pi^+\pi^-\psi(2S)$  via Initial State Radiation at Belle, Phys. Rev. D 91 (2015) 112007. [arXiv:1410.7641](#), [doi:10.1103/PhysRevD.91.112007](#).
- [522] G. Pakhlova, et al., Measurement of  $e^+e^- \rightarrow D_s^{(*)+}D_s^{(*)-}$  cross sections near threshold using initial-state radiation, Phys. Rev. D 83 (2011) 011101. [arXiv:1011.4397](#), [doi:10.1103/PhysRevD.83.011101](#).
- [523] R. Aaij, et al., Observation of a resonance in  $B^+ \rightarrow K^+\mu^+\mu^-$  decays at low recoil, Phys. Rev. Lett. 111 (11) (2013) 112003. [arXiv:1307.7595](#), [doi:10.1103/PhysRevLett.111.112003](#).
- [524] T.-C. Peng, Z.-Y. Bai, J.-Z. Wang, X. Liu, Reevaluating the  $\psi(4160)$  resonance parameter using  $B^+ \rightarrow K^+\mu^+\mu^-$  data in the context of unquenched charmonium spectroscopy, Phys. Rev. D 111 (5) (2025) 054023. [arXiv:2412.11096](#), [doi:10.1103/PhysRevD.111.054023](#).
- [525] A. M. Badalian, B. L. G. Bakker, I. V. Danilkin, Dielectron widths of the  $S$ -,  $D$ -vector bottomonium states, Phys. Atom. Nucl. 73 (2010) 138–149. [arXiv:0903.3643](#), [doi:10.1134/S1063778810010163](#).
- [526] H.-F. Fu, L. Jiang, Coupled-channel-induced  $S$ - $D$  mixing of Charmonia and testing possible assignments for  $Y(4260)$  and  $Y(4360)$ , Eur. Phys. J. C 79 (6) (2019) 460. [arXiv:1812.00179](#), [doi:10.1140/epjc/s10052-019-6976-0](#).
- [527] Z.-L. Man, C.-R. Shu, Y.-R. Liu, H. Chen, Charmonium states in a coupled-channel model, Eur. Phys. J. C 84 (8) (2024) 810. [arXiv:2402.02765](#), [doi:10.1140/epjc/s10052-024-13132-7](#).
- [528] K. K. Seth, Alternative analysis of the  $R$  measurements: Resonance parameters of the higher vector states of charmonium, Phys. Rev. D 72 (2005) 017501. [arXiv:hep-ex/0405007](#), [doi:10.1103/PhysRevD.72.017501](#).
- [529] K.-T. Chao, Interpretations for the  $X(4160)$  observed in the double charm production at  $B$  factories, Phys. Lett. B 661 (2008) 348–353. [arXiv:0707.3982](#), [doi:10.1016/j.physletb.2008.02.039](#).
- [530] A. M. Badalian, B. L. G. Bakker, I. V. Danilkin, The  $S$ - $D$  mixing and di-electron widths of higher charmonium  $1^{--}$  states, Phys. Atom. Nucl. 72 (2009) 638–646. [arXiv:0805.2291](#), [doi:10.1134/S1063778809040085](#).
- [531] C. A. Bokade, Bhaghyesh, Conventional and XYZ charmonium states in a relativistic screened potential model, Phys. Rev. D 111 (1) (2025) 014030. [arXiv:2408.06759](#), [doi:10.1103/PhysRevD.111.014030](#).

- [532] M. N. Anwar, Y. Lu, B.-S. Zou, Modeling charmonium- $\eta$  decays of  $J^{PC} = 1^{--}$  Higher charmonia, Phys. Rev. D 95 (11) (2017) 114031. [arXiv:1612.05396](#), [doi:10.1103/PhysRevD.95.114031](#).
- [533] Y. Yang, Y. Guo, J. Sun, N. Wang, Q. Chang, G. Lu,  $B_u \rightarrow \psi M$  decays and  $S$ - $D$  wave mixing effects, Chin. Phys. C 42 (11) (2018) 113102. [arXiv:1808.07605](#), [doi:10.1088/1674-1137/42/11/113102](#).
- [534] X. H. Mo, C. Z. Yuan, P. Wang, On the leptonic partial widths of the excited  $\psi$  states, Phys. Rev. D 82 (2010) 077501. [arXiv:1007.0084](#), [doi:10.1103/PhysRevD.82.077501](#).
- [535] I. Balossino, F. Cossio, R. Farinelli, L. Lavezzi, The CGEM-IT: An upgrade for the BESIII experiment, Symmetry 14 (5) (2022) 905. [doi:10.3390/sym14050905](#).
- [536] M. Ablikim, et al., Anomalous line shape of the cross section for  $e^+e^- \rightarrow$  hadrons in the center-of-mass energy region between 3.650 and 3.872 GeV, Phys. Rev. Lett. 101 (2008) 102004. [doi:10.1103/PhysRevLett.101.102004](#).
- [537] M. Ablikim, et al.,  $\mathcal{R}(3780)$  resonance interpreted as the  $1^3D_1$ -wave dominant state of charmonium from precise measurements of the cross section of  $e^+e^- \rightarrow$  hadrons, Phys. Rev. Lett. 133 (24) (2024) 241902. [arXiv:2401.00878](#), [doi:10.1103/PhysRevLett.133.241902](#).
- [538] M. Ablikim, et al., First observation of a three-resonance structure in  $e^+e^- \rightarrow$  nonopen charm hadrons, Phys. Rev. Lett. 132 (19) (2024) 191902. [arXiv:2307.10948](#), [doi:10.1103/PhysRevLett.132.191902](#).
- [539] M. Ablikim, et al., Precise measurement of Born cross sections for  $e^+e^- \rightarrow D\bar{D}$  at  $\sqrt{s} = 3.80\text{--}4.95$  GeV, Phys. Rev. Lett. 133 (8) (2024) 081901. [arXiv:2402.03829](#), [doi:10.1103/PhysRevLett.133.081901](#).
- [540] B. Aubert, et al., Study of the Exclusive Initial-State-Radiation Production of the  $D\bar{D}$  System (2 2008). [arXiv:0710.1371](#).
- [541] Z.-Y. Lin, J.-Z. Wang, J.-B. Cheng, L. Meng, S.-L. Zhu, Identification of the  $G(3900)$  as the  $P$ -wave  $D\bar{D}^*/\bar{D}D^*$  resonance, Phys. Rev. Lett. 133 (24) (2024) 241903. [arXiv:2403.01727](#), [doi:10.1103/PhysRevLett.133.241903](#).
- [542] X. Cao, H. Lenske, The nature and line shapes of charmonium in the  $e^+e^- \rightarrow D\bar{D}$  reactions (10 2014). [arXiv:1410.1375](#).
- [543] M.-L. Du, U.-G. Meißner, Q. Wang,  $P$ -wave coupled channel effects in electron-positron annihilation, Phys. Rev. D 94 (9) (2016) 096006. [arXiv:1608.02537](#), [doi:10.1103/PhysRevD.94.096006](#).
- [544] T. V. Uglov, Y. S. Kalashnikova, A. V. Nefediev, G. V. Pakhlova, P. N. Pakhlov, Exclusive open-charm near-threshold cross sections in a coupled-channel approach, JETP Lett. 105 (1) (2017) 1–7. [arXiv:1611.07582](#), [doi:10.1134/S0021364017010064](#).
- [545] N. Hüsken, R. F. Lebed, R. E. Mitchell, E. S. Swanson, Y.-Q. Wang, C.-Z. Yuan, Poles and poltergeists in  $e^+e^- \rightarrow D\bar{D}$  data, Phys. Rev. D 109 (11) (2024) 114010. [arXiv:2404.03896](#), [doi:10.1103/PhysRevD.109.114010](#).
- [546] Q. Ye, Z. Zhang, M.-L. Du, U.-G. Meißner, P.-Y. Niu, Q. Wang, Resonance parameters of the vector charmoniumlike state  $G(3900)$ , Phys. Rev. D 112 (1) (2025) 016015. [arXiv:2504.17431](#), [doi:10.1103/qq61-ncln](#).
- [547] S. X. Nakamura, X. H. Li, H. P. Peng, Z. T. Sun, X. R. Zhou, Global coupled-channel analysis of  $e^+e^- \rightarrow c\bar{c}$  processes in  $\sqrt{s} = 3.75 - 4.7$  GeV (12 2023). [arXiv:2312.17658](#).
- [548] R.-Q. Qian, X. Liu, Unified coupled-channel description for the five near-threshold structures  $\psi(3770)$ ,  $G(3900)$ ,  $R(3760)$ ,  $R(3780)$  and  $R(3810)$  from  $e^+e^-$  annihilation, Phys. Rev. D 112 (9) (2025) L091502. [arXiv:2509.17679](#), [doi:10.1103/c5vs-211k](#).

- [549] K. F. Chen, et al., Observation of an enhancement in  $e^+e^- \rightarrow \Upsilon(1S)\pi^+\pi^-$ ,  $\Upsilon(2S)\pi^+\pi^-$ , and  $\Upsilon(3S)\pi^+\pi^-$  production around  $\sqrt{s} = 10.89$  GeV at Belle, Phys. Rev. D 82 (2010) 091106. [arXiv:0810.3829](#), [doi:10.1103/PhysRevD.82.091106](#).
- [550] M. Ablikim, et al., Observation of a charged charmoniumlike structure in  $e^+e^- \rightarrow \pi^+\pi^-J/\psi$  at  $\sqrt{s}=4.26$  GeV, Phys. Rev. Lett. 110 (2013) 252001. [arXiv:1303.5949](#), [doi:10.1103/PhysRevLett.110.252001](#).
- [551] Z. Q. Liu, et al., Study of  $e^+e^- \rightarrow \pi^+\pi^-J/\psi$  and Observation of a charged charmoniumlike state at Belle, Phys. Rev. Lett. 110 (2013) 252002, [Erratum: Phys.Rev.Lett. 111, 019901 (2013)]. [arXiv:1304.0121](#), [doi:10.1103/PhysRevLett.110.252002](#).
- [552] M. Ablikim, et al., Observation of a charged charmoniumlike structure in  $e^+e^- \rightarrow (D^*\bar{D}^*)^\pm\pi^\mp$  at  $\sqrt{s} = 4.26$ GeV, Phys. Rev. Lett. 112 (13) (2014) 132001. [arXiv:1308.2760](#), [doi:10.1103/PhysRevLett.112.132001](#).
- [553] M. Ablikim, et al., Observation of a neutral charmoniumlike state  $Z_c(4025)^0$  in  $e^+e^- \rightarrow (D^*\bar{D}^*)^0\pi^0$ , Phys. Rev. Lett. 115 (18) (2015) 182002. [arXiv:1507.02404](#), [doi:10.1103/PhysRevLett.115.182002](#).
- [554] M. Ablikim, et al., Measurement of  $e^+e^- \rightarrow \pi^0\pi^0\psi(3686)$  at  $\sqrt{s}$  from 4.009 to 4.600 GeV and observation of a neutral charmoniumlike structure, Phys. Rev. D 97 (5) (2018) 052001. [arXiv:1710.10740](#), [doi:10.1103/PhysRevD.97.052001](#).
- [555] T. Xiao, S. Dobbs, A. Tomaradze, K. K. Seth, Observation of the charged hadron  $Z_c^\pm(3900)$  and evidence for the neutral  $Z_c^0(3900)$  in  $e^+e^- \rightarrow \pi\pi J/\psi$  at  $\sqrt{s} = 4170$  MeV, Phys. Lett. B 727 (2013) 366–370. [arXiv:1304.3036](#), [doi:10.1016/j.physletb.2013.10.041](#).
- [556] M. Ablikim, et al., Confirmation of a charged charmoniumlike state  $Z_c(3885)^\mp$  in  $e^+e^- \rightarrow \pi^\pm(D\bar{D}^*)^\mp$  with double  $D$  tag, Phys. Rev. D 92 (9) (2015) 092006. [arXiv:1509.01398](#), [doi:10.1103/PhysRevD.92.092006](#).
- [557] M. Ablikim, et al., Observation of  $Z_c(3900)^0$  in  $e^+e^- \rightarrow \pi^0\pi^0J/\psi$ , Phys. Rev. Lett. 115 (11) (2015) 112003. [arXiv:1506.06018](#), [doi:10.1103/PhysRevLett.115.112003](#).
- [558] M. Ablikim, et al., Determination of the Spin and Parity of the  $Z_c(3900)$ , Phys. Rev. Lett. 119 (7) (2017) 072001. [arXiv:1706.04100](#), [doi:10.1103/PhysRevLett.119.072001](#).
- [559] M. Ablikim, et al., Observation of a Neutral Structure near the  $D\bar{D}^*$  Mass Threshold in  $e^+e^- \rightarrow (D\bar{D}^*)^0\pi^0$  at  $\sqrt{s} = 4.226$  and 4.257 GeV, Phys. Rev. Lett. 115 (22) (2015) 222002. [arXiv:1509.05620](#), [doi:10.1103/PhysRevLett.115.222002](#).
- [560] M. Ablikim, et al., Observation of  $e^+e^- \rightarrow \pi^0\pi^0h_c$  and a Neutral Charmoniumlike Structure  $Z_c(4020)^0$ , Phys. Rev. Lett. 113 (21) (2014) 212002. [arXiv:1409.6577](#), [doi:10.1103/PhysRevLett.113.212002](#).
- [561] D.-Y. Chen, X. Liu, T. Matsuki, Predictions of charged charmoniumlike structures with hidden-charm and open-strange channels, Phys. Rev. Lett. 110 (23) (2013) 232001. [arXiv:1303.6842](#), [doi:10.1103/PhysRevLett.110.232001](#).
- [562] D. M. J. Lovelock, et al., Masses, widths, and leptonic widths of the higher upsilon resonances, Phys. Rev. Lett. 54 (1985) 377–380. [doi:10.1103/PhysRevLett.54.377](#).
- [563] D. Besson, et al., Observation of new structure in the  $e^+e^-$  annihilation cross-section above  $B\bar{B}$  threshold, Phys. Rev. Lett. 54 (1985) 381. [doi:10.1103/PhysRevLett.54.381](#).
- [564] B. Aubert, et al., Measurement of the  $e^+e^- \rightarrow b\bar{b}$  cross section between  $\sqrt{s} = 10.54$ -GeV and 11.20-GeV, Phys. Rev. Lett. 102 (2009) 012001. [arXiv:0809.4120](#), [doi:10.1103/PhysRevLett.102.012001](#).
- [565] D. Santel, et al., Measurements of the  $\Upsilon(10860)$  and  $\Upsilon(11020)$  resonances via  $\sigma(e^+e^- \rightarrow \Upsilon(nS)\pi^+\pi^-)$ , Phys. Rev. D 93 (1) (2016) 011101. [arXiv:1501.01137](#), [doi:10.1103/PhysRevD.93.011101](#).

- [566] R. Mizuk, et al., Observation of a new structure near 10.75 GeV in the energy dependence of the  $e^+e^- \rightarrow \Upsilon(nS)\pi^+\pi^-$  ( $n = 1, 2, 3$ ) cross sections, JHEP 10 (2019) 220. [arXiv:1905.05521](#), [doi:10.1007/JHEP10\(2019\)220](#).
- [567] B. Aubert, et al., Study of hadronic transitions between  $\Upsilon$  states and observation of  $\Upsilon(4S) \rightarrow \eta\Upsilon(1S)$  decay, Phys. Rev. D 78 (2008) 112002. [arXiv:0807.2014](#), [doi:10.1103/PhysRevD.78.112002](#).
- [568] C. Meng, K.-T. Chao, Peak shifts due to  $B^{(*)} - \bar{B}^{(*)}$  rescattering in  $\Upsilon(5S)$  dipion transitions, Phys. Rev. D 78 (2008) 034022. [arXiv:0805.0143](#), [doi:10.1103/PhysRevD.78.034022](#).
- [569] Y. A. Simonov, Di-pion emission in heavy quarkonia decays, JETP Lett. 87 (2008) 121–123. [arXiv:0712.2197](#), [doi:10.1007/s11448-008-3001-5](#).
- [570] A. Ali, C. Hambrock, I. Ahmed, M. J. Aslam, A case for hidden  $b\bar{b}$  tetraquarks based on  $e^+e^- \rightarrow b\bar{b}$  cross section between  $\sqrt{s} = 10.54$  and 11.20 GeV, Phys. Lett. B 684 (2010) 28–39. [arXiv:0911.2787](#), [doi:10.1016/j.physletb.2009.12.053](#).
- [571] A. Ali, C. Hambrock, M. J. Aslam, Tetraquark interpretation of the BELLE data on the anomalous  $\Upsilon(1S)\pi^+\pi^-$  and  $\Upsilon(2S)\pi^+\pi^-$  production near the  $\Upsilon(5S)$  resonance, Phys. Rev. Lett. 104 (2010) 162001, [Erratum: Phys.Rev.Lett. 107, 049903 (2011)]. [arXiv:0912.5016](#), [doi:10.1103/PhysRevLett.104.162001](#).
- [572] A. Ali, C. Hambrock, S. Mishima, Tetraquark-based analysis and predictions of the cross sections and distributions for the processes  $e^+e^- \rightarrow \Upsilon(1S)(\pi^+\pi^-, K^+K^-, \eta\pi^0)$  near  $\Upsilon(5S)$ , Phys. Rev. Lett. 106 (2011) 092002. [arXiv:1011.4856](#), [doi:10.1103/PhysRevLett.106.092002](#).
- [573] J. Sonnenschein, D. Weissman, A tetraquark or not a tetraquark? A holography inspired stringy hadron (HISH) perspective, Nucl. Phys. B 920 (2017) 319–344. [arXiv:1606.02732](#), [doi:10.1016/j.nuclphysb.2017.04.016](#).
- [574] S. Patel, P. C. Vinodkumar, Tetraquark states in the bottom sector and the status of the  $Y_b$  (10890) state, Eur. Phys. J. C 76 (7) (2016) 356. [arXiv:1606.01047](#), [doi:10.1140/epjc/s10052-016-4186-6](#).
- [575] J.-R. Zhang, M.-Q. Huang, Could  $Y_b(10890)$  be the  $P$ -wave  $[bq][\bar{b}\bar{q}]$  tetraquark state?, JHEP 11 (2010) 057. [arXiv:1011.2815](#), [doi:10.1007/JHEP11\(2010\)057](#).
- [576] D.-Y. Chen, J. He, X.-Q. Li, X. Liu, Dipion invariant mass distribution of the anomalous  $\Upsilon(1S)\pi^+\pi^-$  and  $\Upsilon(2S)\pi^+\pi^-$  production near the peak of  $\Upsilon(10860)$ , Phys. Rev. D 84 (2011) 074006. [arXiv:1105.1672](#), [doi:10.1103/PhysRevD.84.074006](#).
- [577] V. A. Novikov, M. A. Shifman, Comment on the  $\psi' \rightarrow J/\psi\pi\pi$  decay, Z. Phys. C 8 (1981) 43. [doi:10.1007/BF01429829](#).
- [578] Y.-s. Oh, T. Song, S. H. Lee,  $J/\psi$  absorption by  $\pi$  and  $\rho$  mesons in meson exchange model with anomalous parity interactions, Phys. Rev. C 63 (2001) 034901. [arXiv:nucl-th/0010064](#), [doi:10.1103/PhysRevC.63.034901](#).
- [579] R. Casalbuoni, A. Deandrea, N. Di Bartolomeo, R. Gatto, F. Feruglio, G. Nardulli, Phenomenology of heavy meson chiral Lagrangians, Phys. Rept. 281 (1997) 145–238. [arXiv:hep-ph/9605342](#), [doi:10.1016/S0370-1573\(96\)00027-0](#).
- [580] A. Garmash, et al., Observation of  $Z_b(10610)$  and  $Z_b(10650)$  decaying to  $B$  mesons, Phys. Rev. Lett. 116 (21) (2016) 212001. [arXiv:1512.07419](#), [doi:10.1103/PhysRevLett.116.212001](#).
- [581] I. Adachi, Observation of two charged bottomonium-like resonances, in: 9th Conference on Flavor Physics and CP Violation, 2011. [arXiv:1105.4583](#).
- [582] A. Garmash, et al., Amplitude analysis of  $e^+e^- \rightarrow \Upsilon(nS)\pi^+\pi^-$  at  $\sqrt{s} = 10.865$  GeV, Phys. Rev. D 91 (7) (2015) 072003. [arXiv:1403.0992](#), [doi:10.1103/PhysRevD.91.072003](#).

- [583] I. Adachi, et al., Evidence for a  $Z_b^0(10610)$  in Dalitz analysis of  $\Upsilon(5S) \rightarrow \Upsilon(nS)\pi^0\pi^0$  (7 2012). [arXiv:1207.4345](#).
- [584] P. Krokovny, et al., First observation of the  $Z_b^0(10610)$  in a Dalitz analysis of  $\Upsilon(10860) \rightarrow \Upsilon(nS)\pi^0\pi^0$ , Phys. Rev. D 88 (5) (2013) 052016. [arXiv:1308.2646](#), [doi:10.1103/PhysRevD.88.052016](#).
- [585] I. Adachi, et al., Study of three-body  $\Upsilon(10860)$  decays, 2012. [arXiv:1209.6450](#).
- [586] D.-Y. Chen, X. Liu, S.-L. Zhu, Charged bottomonium-like states  $Z_b(10610)$  and  $Z_b(10650)$  and the  $\Upsilon(5S) \rightarrow \Upsilon(2S)\pi^+\pi^-$  decay, Phys. Rev. D 84 (2011) 074016. [arXiv:1105.5193](#), [doi:10.1103/PhysRevD.84.074016](#).
- [587] S. Prelovsek, H. Bahtiyar, J. Petkovic,  $Z_b$  tetraquark channel from lattice QCD and Born-Oppenheimer approximation, Phys. Lett. B 805 (2020) 135467. [arXiv:1912.02656](#), [doi:10.1016/j.physletb.2020.135467](#).
- [588] J.-R. Zhang, M. Zhong, M.-Q. Huang, Could  $Z_b(10610)$  be a  $B^*\bar{B}$  molecular state?, Phys. Lett. B 704 (2011) 312–315. [arXiv:1105.5472](#), [doi:10.1016/j.physletb.2011.09.039](#).
- [589] Y. Yang, J. Ping, C. Deng, H.-S. Zong, Possible interpretation of the  $Z_b(10610)$  and  $Z_b(10650)$  in a chiral quark model, J. Phys. G 39 (2012) 105001. [arXiv:1105.5935](#), [doi:10.1088/0954-3899/39/10/105001](#).
- [590] J. Nieves, M. P. Valderrama, Deriving the existence of  $B\bar{B}^*$  bound states from the  $X(3872)$  and heavy quark symmetry, Phys. Rev. D 84 (2011) 056015. [arXiv:1106.0600](#), [doi:10.1103/PhysRevD.84.056015](#).
- [591] Z.-F. Sun, J. He, X. Liu, Z.-G. Luo, S.-L. Zhu,  $Z_b(10610)^\pm$  and  $Z_b(10650)^\pm$  as the  $B^*\bar{B}$  and  $B^*\bar{B}^*$  molecular states, Phys. Rev. D 84 (2011) 054002. [arXiv:1106.2968](#), [doi:10.1103/PhysRevD.84.054002](#).
- [592] M. Cleven, F.-K. Guo, C. Hanhart, U.-G. Meissner, Bound state nature of the exotic  $Z_b$  states, Eur. Phys. J. A 47 (2011) 120. [arXiv:1107.0254](#), [doi:10.1140/epja/i2011-11120-6](#).
- [593] T. Mehen, J. W. Powell, Heavy quark symmetry predictions for weakly bound  $B$ -meson molecules, Phys. Rev. D 84 (2011) 114013. [arXiv:1109.3479](#), [doi:10.1103/PhysRevD.84.114013](#).
- [594] S. Ohkoda, Y. Yamaguchi, S. Yasui, K. Sudoh, A. Hosaka, Exotic mesons with hidden bottom near thresholds, Phys. Rev. D 86 (2012) 014004. [arXiv:1111.2921](#), [doi:10.1103/PhysRevD.86.014004](#).
- [595] M. T. Li, W. L. Wang, Y. B. Dong, Z. Y. Zhang,  $Z_b(10650)$  and  $Z_b(10610)$  states in a chiral quark model, J. Phys. G 40 (2013) 015003. [arXiv:1204.3959](#), [doi:10.1088/0954-3899/40/1/015003](#).
- [596] M.-Z. Liu, D.-J. Jia, D.-Y. Chen, Possible hadronic molecular states composed of  $S$ -wave heavy-light mesons, Chin. Phys. C 41 (5) (2017) 053105. [arXiv:1702.04440](#), [doi:10.1088/1674-1137/41/5/053105](#).
- [597] L. Zhao, L. Ma, S.-L. Zhu, Spin-orbit force, recoil corrections, and possible  $B\bar{B}^*$  and  $D\bar{D}^*$  molecular states, Phys. Rev. D 89 (9) (2014) 094026. [arXiv:1403.4043](#), [doi:10.1103/PhysRevD.89.094026](#).
- [598] W. Chen, T. G. Steele, H.-X. Chen, S.-L. Zhu, Mass spectra of  $Z_c$  and  $Z_b$  exotic states as hadron molecules, Phys. Rev. D 92 (5) (2015) 054002. [arXiv:1505.05619](#), [doi:10.1103/PhysRevD.92.054002](#).
- [599] Q. Wang, V. Baru, A. A. Filin, C. Hanhart, A. V. Nefediev, J. L. Wintern, Line shapes of the  $Z_b(10610)$  and  $Z_b(10650)$  in the elastic and inelastic channels revisited, Phys. Rev. D 98 (7) (2018) 074023. [arXiv:1805.07453](#), [doi:10.1103/PhysRevD.98.074023](#).
- [600] A. E. Bondar, A. Garmash, A. I. Milstein, R. Mizuk, M. B. Voloshin, Heavy quark spin structure in  $Z_b$  resonances, Phys. Rev. D 84 (2011) 054010. [arXiv:1105.4473](#), [doi:10.1103/PhysRevD.84.054010](#).
- [601] Y. Dong, A. Faessler, T. Gutsche, V. E. Lyubovitskij, Decays of  $Z_b^+$  and  $Z_b'^+$  as hadronic molecules, J. Phys. G 40 (2013) 015002. [arXiv:1203.1894](#), [doi:10.1088/0954-3899/40/1/015002](#).

- [602] X. Li, M. B. Voloshin,  $Z_b(10610)$  and  $Z_b(10650)$  decays to bottomonium plus pion, Phys. Rev. D 86 (2012) 077502. [arXiv:1207.2425](#), [doi:10.1103/PhysRevD.86.077502](#).
- [603] Q. Wu, D.-Y. Chen, T. Matsuki,  $D$  wave bottomonia production from  $Z_b^{(\prime)}$  decay, Phys. Rev. D 102 (2020) 114037. [arXiv:2012.02940](#), [doi:10.1103/PhysRevD.102.114037](#).
- [604] C.-J. Xiao, D.-Y. Chen, Analysis of the hidden bottom decays of  $Z_b(10610)$  and  $Z_b(10650)$  via final state interaction, Phys. Rev. D 96 (1) (2017) 014035. [doi:10.1103/PhysRevD.96.014035](#).
- [605] Q. Wu, Y. Zheng, S. Liu, G. Li, Investigations on the light hadron decays of  $Z_b(10610)$  and  $Z_b(10650)$ , Phys. Rev. D 107 (3) (2023) 034028. [arXiv:2211.02896](#), [doi:10.1103/PhysRevD.107.034028](#).
- [606] Q. Wu, D.-Y. Chen, F.-K. Guo, Production of the  $Z_b^{(\prime)}$  states from the  $\Upsilon(5S, 6S)$  decays, Phys. Rev. D 99 (3) (2019) 034022. [arXiv:1810.09696](#), [doi:10.1103/PhysRevD.99.034022](#).
- [607] Z.-G. Wang, T. Huang, The  $Z_b(10610)$  and  $Z_b(10650)$  as axial-vector tetraquark states in the QCD sum rules, Nucl. Phys. A 930 (2014) 63–85. [arXiv:1312.2652](#), [doi:10.1016/j.nuclphysa.2014.08.084](#).
- [608] Z.-G. Wang, Analysis of the hidden-bottom tetraquark mass spectrum with the QCD sum rules, Eur. Phys. J. C 79 (6) (2019) 489. [arXiv:1903.10895](#), [doi:10.1140/epjc/s10052-019-7019-6](#).
- [609] H.-W. Ke, X.-Q. Li, Y.-L. Shi, G.-L. Wang, X.-H. Yuan, Is  $Z_b(10610)$  a molecular state?, JHEP 04 (2012) 056. [arXiv:1202.2178](#), [doi:10.1007/JHEP04\(2012\)056](#).
- [610] Z.-G. Wang, T. Huang, Possible assignments of the  $X(3872)$ ,  $Z_c(3900)$  and  $Z_b(10610)$  as axial-vector molecular states, Eur. Phys. J. C 74 (5) (2014) 2891. [arXiv:1312.7489](#), [doi:10.1140/epjc/s10052-014-2891-6](#).
- [611] V. Gupta, G. Sanchez-Colon, S. Rajpoot, Sum rules for tetraquark decay coupling constants with broken SU(3) symmetry, Mod. Phys. Lett. A 27 (2012) 1250165. [arXiv:1304.1177](#), [doi:10.1142/S0217732312501659](#).
- [612] A. Ali, C. Hambrock, W. Wang, Tetraquark interpretation of the charged bottomonium-like states  $Z_b^{+-}(10610)$  and  $Z_b^{+-}(10650)$  and implications, Phys. Rev. D 85 (2012) 054011. [arXiv:1110.1333](#), [doi:10.1103/PhysRevD.85.054011](#).
- [613] D. V. Bugg, An Explanation of Belle states  $Z_b(10610)$  and  $Z_b(10650)$ , EPL 96 (1) (2011) 11002. [arXiv:1105.5492](#), [doi:10.1209/0295-5075/96/11002](#).
- [614] E. S. Swanson,  $Z_b$  and  $Z_c$  exotic states as coupled channel cusps, Phys. Rev. D 91 (3) (2015) 034009. [arXiv:1409.3291](#), [doi:10.1103/PhysRevD.91.034009](#).
- [615] D.-Y. Chen, X. Liu, T. Matsuki, Charged bottomonium-like structures in the hidden-bottom dipion decays of  $\Upsilon(11020)$ , Phys. Rev. D 84 (2011) 074032. [arXiv:1108.4458](#), [doi:10.1103/PhysRevD.84.074032](#).
- [616] D.-Y. Chen, X. Liu, T. Matsuki, Interpretation of  $Z_b(10610)$  and  $Z_b(10650)$  in the ISPE mechanism and the charmonium counterpart, Chin. Phys. C 38 (2014) 053102. [arXiv:1208.2411](#), [doi:10.1088/1674-1137/38/5/053102](#).
- [617] T. K. Pedlar, et al., Observation of the  $h_c(1P)$  using  $e^+e^-$  collisions above  $D\bar{D}$  threshold, Phys. Rev. Lett. 107 (2011) 041803. [arXiv:1104.2025](#), [doi:10.1103/PhysRevLett.107.041803](#).
- [618] C.-Z. Yuan, Talk given in Hadron Structure and Interactions in 2011, held by Research Center for Nuclear Physics of Osaka University (2011).
- [619] D.-Y. Chen, X. Liu, T. Matsuki, Novel charged charmoniumlike structures in the hidden-charm dipion decays of  $Y(4360)$ , Phys. Rev. D 88 (1) (2013) 014034. [arXiv:1306.2080](#), [doi:10.1103/PhysRevD.88.014034](#).
- [620] J. P. Lees, et al., Study of the reaction  $e^+e^- \rightarrow J/\psi\pi^+\pi^-$  via initial-state radiation at BaBar, Phys. Rev. D 86 (2012) 051102. [arXiv:1204.2158](#), [doi:10.1103/PhysRevD.86.051102](#).

- [621] K. Chilikin, et al., Observation of a new charged charmoniumlike state in  $\bar{B}^0 \rightarrow J/\psi K^- \pi^+$  decays, Phys. Rev. D 90 (11) (2014) 112009. [arXiv:1408.6457](#), [doi:10.1103/PhysRevD.90.112009](#).
- [622] V. M. Abazov, et al., Evidence for  $Z_c^\pm(3900)$  in semi-inclusive decays of  $b$ -flavored hadrons, Phys. Rev. D 98 (5) (2018) 052010. [arXiv:1807.00183](#), [doi:10.1103/PhysRevD.98.052010](#).
- [623] D.-Y. Chen, X. Liu, T. Matsuki, Reproducing the  $Z_c(3900)$  structure through the initial-single-pion-emission mechanism, Phys. Rev. D 88 (3) (2013) 036008. [arXiv:1304.5845](#), [doi:10.1103/PhysRevD.88.036008](#).
- [624] J. P. Lees, et al., Study of the reaction  $e^+e^- \rightarrow \psi(2S)\pi^+\pi^-$  via initial-state radiation at BaBar, Phys. Rev. D 89 (11) (2014) 111103. [arXiv:1211.6271](#), [doi:10.1103/PhysRevD.89.111103](#).
- [625] Q. Huang, D.-Y. Chen, X. Liu, T. Matsuki, Charged charmoniumlike structures in the  $e^+e^- \rightarrow \psi(3686)\pi^+\pi^-$  process based on the ISPE mechanism, Eur. Phys. J. C 79 (7) (2019) 613. [arXiv:1905.05650](#), [doi:10.1140/epjc/s10052-019-7121-9](#).
- [626] Z.-G. Wang, Analysis of the  $Z_c(4020)$ ,  $Z_c(4025)$ ,  $Y(4360)$  and  $Y(4660)$  as vector tetraquark states with QCD sum rules, Eur. Phys. J. C 74 (5) (2014) 2874. [arXiv:1311.1046](#), [doi:10.1140/epjc/s10052-014-2874-7](#).
- [627] Z.-G. Wang, T. Huang, Analysis of the  $X(3872)$ ,  $Z_c(3900)$  and  $Z_c(3885)$  as axial-vector tetraquark states with QCD sum rules, Phys. Rev. D 89 (5) (2014) 054019. [arXiv:1310.2422](#), [doi:10.1103/PhysRevD.89.054019](#).
- [628] C.-F. Qiao, L. Tang, Interpretation of  $Z_c(4025)$  as the hidden charm tetraquark states via QCD Sum Rules, Eur. Phys. J. C 74 (2014) 2810. [arXiv:1308.3439](#), [doi:10.1140/epjc/s10052-014-2810-x](#).
- [629] E. Braaten, How the  $Z_c(3900)$  Reveals the Spectra of Quarkonium Hybrid and Tetraquark Mesons, Phys. Rev. Lett. 111 (2013) 162003. [arXiv:1305.6905](#), [doi:10.1103/PhysRevLett.111.162003](#).
- [630] J. M. Dias, F. S. Navarra, M. Nielsen, C. M. Zanetti,  $Z_c^+(3900)$  decay width in QCD sum rules, Phys. Rev. D 88 (1) (2013) 016004. [arXiv:1304.6433](#), [doi:10.1103/PhysRevD.88.016004](#).
- [631] L. Maiani, V. Riquer, R. Faccini, F. Piccinini, A. Pilloni, A. D. Polosa, A  $J^{PG} = 1^{++}$  Charged Resonance in the  $Y(4260) \rightarrow \pi^+\pi^- J/\psi$  Decay?, Phys. Rev. D 87 (11) (2013) 111102. [arXiv:1303.6857](#), [doi:10.1103/PhysRevD.87.111102](#).
- [632] K. P. Khemchandani, A. Martinez Torres, M. Nielsen, F. S. Navarra, Relating  $D^*\bar{D}^*$  currents with  $J^\pi = 0^+, 1^+$  and  $2^+$  to  $Z_c$  states, Phys. Rev. D 89 (1) (2014) 014029. [arXiv:1310.0862](#), [doi:10.1103/PhysRevD.89.014029](#).
- [633] W. Chen, T. G. Steele, M.-L. Du, S.-L. Zhu,  $D^*\bar{D}^*$  molecule interpretation of  $Z_c(4025)$ , Eur. Phys. J. C 74 (2) (2014) 2773. [arXiv:1308.5060](#), [doi:10.1140/epjc/s10052-014-2773-y](#).
- [634] C.-Y. Cui, Y.-L. Liu, M.-Q. Huang, Could  $Z_c(4025)$  be a  $J^P = 1^+ D^*\bar{D}^*$  molecular state?, Eur. Phys. J. C 73 (12) (2013) 2661. [arXiv:1308.3625](#), [doi:10.1140/epjc/s10052-013-2661-x](#).
- [635] J. He, X. Liu, Z.-F. Sun, S.-L. Zhu,  $Z_c(4025)$  as the hadronic molecule with hidden charm, Eur. Phys. J. C 73 (11) (2013) 2635. [arXiv:1308.2999](#), [doi:10.1140/epjc/s10052-013-2635-z](#).
- [636] H.-W. Ke, Z.-T. Wei, X.-Q. Li, Is  $Z_c(3900)$  a molecular state, Eur. Phys. J. C 73 (10) (2013) 2561. [arXiv:1307.2414](#), [doi:10.1140/epjc/s10052-013-2561-0](#).
- [637] Y. Dong, A. Faessler, T. Gutsche, V. E. Lyubovitskij, Strong decays of molecular states  $Z_c^+$  and  $Z_c'^+$ , Phys. Rev. D 88 (1) (2013) 014030. [arXiv:1306.0824](#), [doi:10.1103/PhysRevD.88.014030](#).
- [638] J.-R. Zhang, Improved QCD sum rule study of  $Z_c(3900)$  as a  $\bar{D}D^*$  molecular state, Phys. Rev. D 87 (11) (2013) 116004. [arXiv:1304.5748](#), [doi:10.1103/PhysRevD.87.116004](#).

- [639] E. Wilbring, H. W. Hammer, U. G. Meißner, Electromagnetic structure of the  $Z_c(3900)$ , Phys. Lett. B 726 (2013) 326–329. [arXiv:1304.2882](#), [doi:10.1016/j.physletb.2013.08.059](#).
- [640] C.-Y. Cui, Y.-L. Liu, W.-B. Chen, M.-Q. Huang, Could  $Z_c(3900)$  be a  $I^G J^P = 1^+ 1^+ D^* \bar{D}$  molecular state?, J. Phys. G 41 (2014) 075003. [arXiv:1304.1850](#), [doi:10.1088/0954-3899/41/7/075003](#).
- [641] F.-K. Guo, C. Hidalgo-Duque, J. Nieves, M. P. Valderrama, Consequences of heavy quark symmetries for hadronic molecules, Phys. Rev. D 88 (2013) 054007. [arXiv:1303.6608](#), [doi:10.1103/PhysRevD.88.054007](#).
- [642] Y. Zhang, A. Hosaka, Q. Wang, S. Yasui,  $Z_c(3900)$  in a hadronic molecule and a triangle singularity approach at finite temperature, Phys. Rev. D 112 (1) (2025) 016014. [arXiv:2503.19374](#), [doi:10.1103/5nlp-vwrc](#).
- [643] Z.-W. Liu, J.-X. Lu, M.-Z. Liu, L.-S. Geng, Femtoscopy can tell whether  $Z_c(3900)$  and  $Z_{cs}(3985)$  are resonances, virtual states, or bound states, Sci. Bull. 70 (2025) 3515–3521. [arXiv:2404.18607](#), [doi:10.1016/j.scib.2025.09.022](#).
- [644] M.-Z. Liu, X.-Z. Ling, L.-S. Geng, Productions of  $X(3872)/Z_c(3900)$  and  $X_2(4013)/Z_c(4020)$  in  $Y(4220)$  and  $Y(4360)$  decays, Phys. Rev. D 110 (5) (2024) 054035. [arXiv:2404.07681](#), [doi:10.1103/PhysRevD.110.054035](#).
- [645] Q. Wu, M.-Z. Liu, L.-S. Geng, Productions of  $X(3872)$ ,  $Z_c(3900)$ ,  $X_2(4013)$ , and  $Z_c(4020)$  in  $B_{(s)}$  decays offer strong clues on their molecular nature, Eur. Phys. J. C 84 (2) (2024) 147. [arXiv:2304.05269](#), [doi:10.1140/epjc/s10052-024-12501-6](#).
- [646] X.-Y. Qi, Q. Wu, D.-Y. Chen, Pionic transitions from  $Z_c(4020)$  to  $D$  wave charmonia, Eur. Phys. J. C 83 (11) (2023) 1006. [arXiv:2302.10050](#), [doi:10.1140/epjc/s10052-023-12151-0](#).
- [647] X.-Y. Wang, G. Li, C.-S. An, J.-J. Xie, Radiative decays of the neutral  $Z_c(3900)$  and  $Z_c(4020)$ , Phys. Rev. D 106 (7) (2022) 074026. [arXiv:2210.06783](#), [doi:10.1103/PhysRevD.106.074026](#).
- [648] T. Ji, X.-K. Dong, M. Albaladejo, M.-L. Du, F.-K. Guo, J. Nieves, Establishing the heavy quark spin and light flavor molecular multiplets of the  $X(3872)$ ,  $Z_c(3900)$ , and  $X(3960)$ , Phys. Rev. D 106 (9) (2022) 094002. [arXiv:2207.08563](#), [doi:10.1103/PhysRevD.106.094002](#).
- [649] Q. Wu, D.-Y. Chen, X.-J. Fan, G. Li, Production of  $Z_c(3900)$  and  $Z_c(4020)$  in  $B_c$  decay, Eur. Phys. J. C 79 (3) (2019) 265. [arXiv:1902.05737](#), [doi:10.1140/epjc/s10052-019-6784-6](#).
- [650] C.-J. Xiao, D.-Y. Chen, Y.-B. Dong, W. Zuo, T. Matsuki, Understanding the  $\eta_c \rho$  decay mode of  $Z_c^{(\prime)}$  via the triangle loop mechanism, Phys. Rev. D 99 (7) (2019) 074003. [arXiv:1811.04688](#), [doi:10.1103/PhysRevD.99.074003](#).
- [651] J. He, D.-Y. Chen,  $Z_c(3900)/Z_c(3885)$  as a virtual state from  $\pi J/\psi - \bar{D}^* D$  interaction, Eur. Phys. J. C 78 (2) (2018) 94. [arXiv:1712.05653](#), [doi:10.1140/epjc/s10052-018-5580-z](#).
- [652] D.-Y. Chen, C.-J. Xiao, J. He, Hidden-charm decays of  $Y(4390)$  in a hadronic molecular scenario, Phys. Rev. D 96 (5) (2017) 054017. [doi:10.1103/PhysRevD.96.054017](#).
- [653] X.-H. Liu, G. Li, Exploring the threshold behavior and implications on the nature of  $Y(4260)$  and  $Z_c(3900)$ , Phys. Rev. D 88 (2013) 014013. [arXiv:1306.1384](#), [doi:10.1103/PhysRevD.88.014013](#).
- [654] Q. Wang, C. Hanhart, Q. Zhao, Systematic study of the singularity mechanism in heavy quarkonium decays, Phys. Lett. B 725 (1-3) (2013) 106–110. [arXiv:1305.1997](#), [doi:10.1016/j.physletb.2013.06.049](#).
- [655] K. Yu, G.-J. Wang, J.-J. Wu, Z. Yang, Three-coupled-channel analysis of  $Z_c(3900)$  involving  $D\bar{D}^*$ ,  $\pi J/\psi$ , and  $\rho\eta_c$ , Phys. Rev. D 110 (11) (2024) 114029. [arXiv:2409.10865](#), [doi:10.1103/PhysRevD.110.114029](#).

- [656] S. Prelovsek, L. Leskovec, Search for  $Z_c^+(3900)$  in the  $1^{+-}$  channel on the lattice, Phys. Lett. B 727 (2013) 172–176. [arXiv:1308.2097](#), [doi:10.1016/j.physletb.2013.10.009](#).
- [657] S. Prelovsek, C. B. Lang, L. Leskovec, D. Mohler, Study of the  $Z_c^+$  channel using lattice QCD, Phys. Rev. D 91 (1) (2015) 014504. [arXiv:1405.7623](#), [doi:10.1103/PhysRevD.91.014504](#).
- [658] Y. Ikeda, S. Aoki, T. Doi, S. Gongyo, T. Hatsuda, T. Inoue, T. Iritani, N. Ishii, K. Murano, K. Sasaki, Fate of the tetraquark candidate  $Z_c(3900)$  from lattice QCD, Phys. Rev. Lett. 117 (24) (2016) 242001. [arXiv:1602.03465](#), [doi:10.1103/PhysRevLett.117.242001](#).
- [659] Y. Ikeda, The tetraquark candidate  $Z_c(3900)$  from dynamical lattice QCD simulations, J. Phys. G 45 (2) (2018) 024002. [arXiv:1706.07300](#), [doi:10.1088/1361-6471/aa9afd](#).
- [660] T. Chen, Y. Chen, M. Gong, C. Liu, L. Liu, Y.-B. Liu, Z. Liu, J.-P. Ma, M. Werner, J.-B. Zhang, A coupled-channel lattice study on the resonance-like structure  $Z_c(3900)$ , Chin. Phys. C 43 (10) (2019) 103103. [arXiv:1907.03371](#), [doi:10.1088/1674-1137/43/10/103103](#).
- [661] D.-Y. Chen, X. Liu, T. Matsuki, Prediction of isoscalar charmoniumlike structures in the hidden-charm dieta decays of higher charmonia, J. Phys. G 42 (1) (2015) 015002. [arXiv:1309.4528](#), [doi:10.1088/0954-3889/42/1/015002](#).
- [662] M. Ablikim, et al., Search for the reaction channel  $e^+e^- \rightarrow \eta\eta J/\psi$  and the isospin partner of the  $Z_c(3900)$  at center-of-mass energies  $\sqrt{s} = 4.226 - 4.950$  GeV (1 2026). [arXiv:2601.15882](#).
- [663] S. H. Lee, M. Nielsen, U. Wiedner,  $D_s D^*$  molecule as an axial meson, J. Korean Phys. Soc. 55 (2009) 424. [arXiv:0803.1168](#), [doi:10.3938/jkps.55.424](#).
- [664] J. M. Dias, X. Liu, M. Nielsen, Prediction for the decay width of a charged state near the  $D_s \bar{D}^*/D_s^* \bar{D}$  threshold, Phys. Rev. D 88 (9) (2013) 096014. [arXiv:1307.7100](#), [doi:10.1103/PhysRevD.88.096014](#).
- [665] C. P. Shen, et al., Updated cross section measurement of  $e^+e^- \rightarrow K^+K^-J/\psi$  and  $K_S^0 K_S^0 J/\psi$  via initial state radiation at Belle, Phys. Rev. D 89 (7) (2014) 072015. [arXiv:1402.6578](#), [doi:10.1103/PhysRevD.89.072015](#).
- [666] M. Ablikim, et al., Observation of a near-threshold structure in the  $K^+$  recoil-mass spectra in  $e^+e^- \rightarrow K^+(D_s^- D^{*0} + D_s^{*-} D^0)$ , Phys. Rev. Lett. 126 (10) (2021) 102001. [arXiv:2011.07855](#), [doi:10.1103/PhysRevLett.126.102001](#).
- [667] M. Ablikim, et al., Evidence for a neutral near-threshold structure in the  $K_S^0$  recoil-mass spectra in  $e^+e^- \rightarrow K_S^0 D_s^+ D^{*-}$  and  $e^+e^- \rightarrow K_S^0 D_s^{*+} D^-$ , Phys. Rev. Lett. 129 (11) (2022) 112003. [arXiv:2204.13703](#), [doi:10.1103/PhysRevLett.129.112003](#).
- [668] M. Ablikim, et al., Observation of a vector charmoniumlike state at 4.7 GeV/ $c^2$  and search for  $Z_{cs}$  in  $e^+e^- \rightarrow K^+K^-J/\psi$ , Phys. Rev. Lett. 131 (21) (2023) 211902. [arXiv:2308.15362](#), [doi:10.1103/PhysRevLett.131.211902](#).
- [669] M. Ablikim, et al., Measurement of the  $e^+e^- \rightarrow K^+K^-\psi(2S)$  cross section at center-of-mass energies from 4.699 to 4.951 GeV and search for  $Z_{cs}^\pm$  in the  $Z_{cs}^\pm \rightarrow K^\pm\psi(2S)$  decay (7 2024). [arXiv:2407.20009](#).
- [670] M. Ablikim, et al., Measurement of cross sections of  $e^+e^- \rightarrow K_S^0 K_S^0 \psi(3686)$  from  $\sqrt{s} = 4.682$  to 4.951 GeV, JHEP 02 (2025) 120. [arXiv:2411.15752](#), [doi:10.1007/JHEP02\(2025\)120](#).
- [671] R. Aaij, et al., Observation of new resonances decaying to  $J/\psi K^+$  and  $J/\psi \phi$ , Phys. Rev. Lett. 127 (8) (2021) 082001. [arXiv:2103.01803](#), [doi:10.1103/PhysRevLett.127.082001](#).
- [672] R. Aaij, et al., Evidence of a  $J/\psi K_S^0$  structure in  $B^0 \rightarrow J/\psi \phi K_S^0$  decays, Phys. Rev. Lett. 131 (13) (2023) 131901. [arXiv:2301.04899](#), [doi:10.1103/PhysRevLett.131.131901](#).

- [673] Z.-H. Guo, J. A. Oller, Unified description of the hidden-charm tetraquark states  $Z_{cs}(3985)$ ,  $Z_c(3900)$ , and  $X(4020)$ , Phys. Rev. D 103 (5) (2021) 054021. [arXiv:2012.11904](#), [doi:10.1103/PhysRevD.103.054021](#).
- [674] Z.-G. Wang, Analysis of  $Z_{cs}(3985)$  as the axialvector tetraquark state, Chin. Phys. C 45 (7) (2021) 073107. [arXiv:2011.10959](#), [doi:10.1088/1674-1137/abfa83](#).
- [675] B.-D. Wan, C.-F. Qiao, About the exotic structure of  $Z_{cs}$ , Nucl. Phys. B 968 (2021) 115450. [arXiv:2011.08747](#), [doi:10.1016/j.nuclphysb.2021.115450](#).
- [676] Z.-H. Cao, W. He, Z.-F. Sun,  $Z_{cs}$  states and the mixture of hadronic molecule and diquark-anti-diquark components within effective field theory, Phys. Rev. D 107 (1) (2023) 014017. [arXiv:2205.11150](#), [doi:10.1103/PhysRevD.107.014017](#).
- [677] G. Yang, J. Ping, J. Segovia, Hidden-charm tetraquarks with strangeness in the chiral quark model, Phys. Rev. D 104 (9) (2021) 094035. [arXiv:2109.04311](#), [doi:10.1103/PhysRevD.104.094035](#).
- [678] M. Karliner, J. L. Rosner, Configuration mixing in strange tetraquarks  $Z_{cs}$ , Phys. Rev. D 104 (3) (2021) 034033. [arXiv:2107.04915](#), [doi:10.1103/PhysRevD.104.034033](#).
- [679] J. F. Giron, R. F. Lebed, S. R. Martinez, Spectrum of hidden-charm, open-strange exotics in the dynamical diquark model, Phys. Rev. D 104 (5) (2021) 054001. [arXiv:2106.05883](#), [doi:10.1103/PhysRevD.104.054001](#).
- [680] P.-P. Shi, F. Huang, W.-L. Wang, Hidden charm tetraquark states in a diquark model, Phys. Rev. D 103 (9) (2021) 094038. [arXiv:2105.02397](#), [doi:10.1103/PhysRevD.103.094038](#).
- [681] L. Maiani, A. D. Polosa, V. Riquer, The new resonances  $Z_{cs}(3985)$  and  $Z_{cs}(4003)$  (almost) fill two tetraquark nonets of broken  $SU(3)_f$ , Sci. Bull. 66 (2021) 1616–1619. [arXiv:2103.08331](#), [doi:10.1016/j.scib.2021.04.040](#).
- [682] Y.-J. Xu, Y.-L. Liu, C.-Y. Cui, M.-Q. Huang,  $\bar{D}_s^{(*)}D^{(*)}$  molecular state with  $J^P = 1^+$ , Phys. Rev. D 104 (9) (2021) 094028. [arXiv:2011.14313](#), [doi:10.1103/PhysRevD.104.094028](#).
- [683] M.-C. Du, Q. Wang, Q. Zhao, The nature of charged charmonium-like states  $Z_c(3900)$  and its strange partner  $Z_{cs}(3982)$  (11 2020). [arXiv:2011.09225](#).
- [684] L. Meng, B. Wang, S.-L. Zhu,  $Z_{cs}(3985)^-$  as the  $U$ -spin partner of  $Z_c(3900)^-$  and implication of other states in the  $SU(3)_F$  symmetry and heavy quark symmetry, Phys. Rev. D 102 (11) (2020) 111502. [arXiv:2011.08656](#), [doi:10.1103/PhysRevD.102.111502](#).
- [685] Z. Yang, X. Cao, F.-K. Guo, J. Nieves, M. P. Valderrama, Strange molecular partners of the  $Z_c(3900)$  and  $Z_c(4020)$ , Phys. Rev. D 103 (7) (2021) 074029. [arXiv:2011.08725](#), [doi:10.1103/PhysRevD.103.074029](#).
- [686] R. Chen, Q. Huang,  $Z_{cs}(3985)^-$ : A strange hidden-charm tetraquark resonance or not?, Phys. Rev. D 103 (3) (2021) 034008. [arXiv:2011.09156](#), [doi:10.1103/PhysRevD.103.034008](#).
- [687] B. Wang, L. Meng, S.-L. Zhu, Decoding the nature of  $Z_{cs}(3985)$  and establishing the spectrum of charged heavy quarkoniumlike states in chiral effective field theory, Phys. Rev. D 103 (2) (2021) L021501. [arXiv:2011.10922](#), [doi:10.1103/PhysRevD.103.L021501](#).
- [688] S. Han, L.-Y. Xiao, Aspects of  $Z_{cs}(3985)$  and  $Z_{cs}(4000)$ , Phys. Rev. D 105 (5) (2022) 054008. [arXiv:2203.00168](#), [doi:10.1103/PhysRevD.105.054008](#).
- [689] Q.-Y. Zhai, M.-Z. Liu, J.-X. Lu, L.-S. Geng,  $Z_{cs}(3985)$  in next-to-leading-order chiral effective field theory: The first truncation uncertainty analysis, Phys. Rev. D 106 (3) (2022) 034026. [arXiv:2205.03878](#), [doi:10.1103/PhysRevD.106.034026](#).

- [690] M.-L. Du, M. Albaladejo, F.-K. Guo, J. Nieves, Combined analysis of the  $Z_c(3900)$  and the  $Z_{cs}(3985)$  exotic states, Phys. Rev. D 105 (7) (2022) 074018. [arXiv:2201.08253](#), [doi:10.1103/PhysRevD.105.074018](#).
- [691] Q. Wu, D.-Y. Chen, W.-H. Qin, G. Li, Production of  $Z_{cs}$  in  $B$  and  $B_s$  decays, Eur. Phys. J. C 82 (6) (2022) 520. [arXiv:2111.13347](#), [doi:10.1140/epjc/s10052-022-10465-z](#).
- [692] X. Cao, Z. Yang, Hunting for the heavy quark spin symmetry partner of  $Z_{cs}$ , Eur. Phys. J. C 82 (2) (2022) 161. [arXiv:2110.09760](#), [doi:10.1140/epjc/s10052-022-10055-z](#).
- [693] V. Baru, E. Epelbaum, A. A. Filin, C. Hanhart, A. V. Nefediev, Is  $Z_{cs}(3982)$  a molecular partner of  $Z_c(3900)$  and  $Z_c(4020)$  states?, Phys. Rev. D 105 (3) (2022) 034014. [arXiv:2110.00398](#), [doi:10.1103/PhysRevD.105.034014](#).
- [694] Q. Wu, D.-Y. Chen, Exploration of the hidden charm decays of  $Z_{cs}(3985)$ , Phys. Rev. D 104 (7) (2021) 074011. [arXiv:2108.06700](#), [doi:10.1103/PhysRevD.104.074011](#).
- [695] J. Liu, D.-Y. Chen, J. He, Double exotic state productions in pion and kaon induced reactions, Eur. Phys. J. C 81 (11) (2021) 965. [arXiv:2108.00148](#), [doi:10.1140/epjc/s10052-021-09766-6](#).
- [696] M.-J. Yan, F.-Z. Peng, M. Sánchez Sánchez, M. Pavon Valderrama, Axial meson exchange and the  $Z_c(3900)$  and  $Z_{cs}(3985)$  resonances as heavy hadron molecules, Phys. Rev. D 104 (11) (2021) 114025. [arXiv:2102.13058](#), [doi:10.1103/PhysRevD.104.114025](#).
- [697] Z. Yu, Q. Wu, D.-Y. Chen,  $Z_{cs}^+$  production in  $B^+$  decays, Phys. Rev. D 112 (9) (2025) 094054. [arXiv:2506.06702](#), [doi:10.1103/fjjsv-fxpm](#).
- [698] Q. Wu, Y.-K. Chen, G. Li, S.-D. Liu, D.-Y. Chen, Hunting for the hidden-charm molecular states with strange quarks in  $B$  and  $B_s$  decays, Phys. Rev. D 107 (5) (2023) 054044. [arXiv:2302.01696](#), [doi:10.1103/PhysRevD.107.054044](#).
- [699] N. Ikeno, R. Molina, E. Oset, The  $Z_{cs}(3985)$  as a threshold effect from the  $\bar{D}_s^*D + \bar{D}_sD^*$  interaction, Phys. Lett. B 814 (2021) 136120. [arXiv:2011.13425](#), [doi:10.1016/j.physletb.2021.136120](#).
- [700] J.-Z. Wang, Q.-S. Zhou, X. Liu, T. Matsuki, Toward charged  $Z_{cs}(3985)$  structure under a reflection mechanism, Eur. Phys. J. C 81 (1) (2021) 51. [arXiv:2011.08628](#), [doi:10.1140/epjc/s10052-021-08877-4](#).
- [701] Y.-H. Ge, X.-H. Liu, H.-W. Ke, Threshold effects as the origin of  $Z_{cs}(4000)$ ,  $Z_{cs}(4220)$  and  $X(4700)$  observed in  $B^+ \rightarrow J/\psi\phi K^+$ , Eur. Phys. J. C 81 (9) (2021) 854. [arXiv:2103.05282](#), [doi:10.1140/epjc/s10052-021-09590-y](#).
- [702] J.-Z. Wang, D.-Y. Chen, X. Liu, T. Matsuki, Universal non-resonant explanation to charmoniumlike structures  $Z_c(3885)$  and  $Z_c(4025)$ , Eur. Phys. J. C 80 (11) (2020) 1040. [arXiv:2007.02263](#), [doi:10.1140/epjc/s10052-020-08621-4](#).
- [703] Y. Iwasaki, A possible model for new resonances-exotics and hidden charm, Prog. Theor. Phys. 54 (1975) 492. [doi:10.1143/PTP.54.492](#).
- [704] Y. Iwasaki, Is a state  $c\bar{c}c\bar{c}$  found at 6.0 GeV?, Phys. Rev. Lett. 36 (1976) 1266. [doi:10.1103/PhysRevLett.36.1266](#).
- [705] K.-T. Chao, The  $(cc) - (\bar{c}\bar{c})$  (diquark-anti-diquark) states in  $e^+e^-$  annihilation, Z. Phys. C 7 (1981) 317. [doi:10.1007/BF01431564](#).
- [706] A. M. Badalian, B. L. Ioffe, A. V. Smilga, Four quark states in the heavy quark system, Nucl. Phys. B 281 (1987) 85. [doi:10.1016/0550-3213\(87\)90248-3](#).
- [707] J. P. Ader, J. M. Richard, P. Taxil, Do narrow heavy heavy multi-quark state exist?, Phys. Rev. D 25 (1982) 2370. [doi:10.1103/PhysRevD.25.2370](#).

- [708] B.-A. Li, K.-F. Liu,  $J/\psi$  pair production in hadronic collisions, Phys. Rev. D 29 (1984) 426. doi:10.1103/PhysRevD.29.426.
- [709] R. J. Lloyd, J. P. Vary, All charm tetraquarks, Phys. Rev. D 70 (2004) 014009. arXiv:hep-ph/0311179, doi:10.1103/PhysRevD.70.014009.
- [710] M.-S. Liu, Q.-F. Lü, X.-H. Zhong, Q. Zhao, All-heavy tetraquarks, Phys. Rev. D 100 (1) (2019) 016006. arXiv:1901.02564, doi:10.1103/PhysRevD.100.016006.
- [711] G.-J. Wang, L. Meng, S.-L. Zhu, Spectrum of the fully-heavy tetraquark state  $QQ\bar{Q}'\bar{Q}'$ , Phys. Rev. D 100 (9) (2019) 096013. arXiv:1907.05177, doi:10.1103/PhysRevD.100.096013.
- [712] X. Chen, Fully-charm tetraquarks:  $cc\bar{c}\bar{c}$  (1 2020). arXiv:2001.06755.
- [713] V. R. Debastiani, F. S. Navarra, A non-relativistic model for the  $[cc][\bar{c}\bar{c}]$  tetraquark, Chin. Phys. C 43 (1) (2019) 013105. arXiv:1706.07553, doi:10.1088/1674-1137/43/1/013105.
- [714] M. A. Bedolla, J. Ferretti, C. D. Roberts, E. Santopinto, Spectrum of fully-heavy tetraquarks from a diquark+antidiquark perspective, Eur. Phys. J. C 80 (11) (2020) 1004. arXiv:1911.00960, doi:10.1140/epjc/s10052-020-08579-3.
- [715] J.-M. Richard, A. Valcarce, J. Vijande, String dynamics and metastability of all-heavy tetraquarks, Phys. Rev. D 95 (5) (2017) 054019. arXiv:1703.00783, doi:10.1103/PhysRevD.95.054019.
- [716] A. V. Berezhnoy, A. V. Luchinsky, A. A. Novoselov, Tetraquarks composed of 4 heavy quarks, Phys. Rev. D 86 (2012) 034004. arXiv:1111.1867, doi:10.1103/PhysRevD.86.034004.
- [717] J. Wu, Y.-R. Liu, K. Chen, X. Liu, S.-L. Zhu, Heavy-flavored tetraquark states with the  $QQ\bar{Q}\bar{Q}$  configuration, Phys. Rev. D 97 (9) (2018) 094015. arXiv:1605.01134, doi:10.1103/PhysRevD.97.094015.
- [718] M. Karliner, S. Nussinov, J. L. Rosner,  $QQ\bar{Q}\bar{Q}$  states: masses, production, and decays, Phys. Rev. D 95 (3) (2017) 034011. arXiv:1611.00348, doi:10.1103/PhysRevD.95.034011.
- [719] W. Chen, H.-X. Chen, X. Liu, T. G. Steele, S.-L. Zhu, Hunting for exotic doubly hidden-charm/bottom tetraquark states, Phys. Lett. B 773 (2017) 247–251. arXiv:1605.01647, doi:10.1016/j.physletb.2017.08.034.
- [720] Z.-G. Wang, Z.-Y. Di, Analysis of the vector and axialvector  $QQ\bar{Q}\bar{Q}$  tetraquark states with QCD sum rules, Acta Phys. Polon. B 50 (2019) 1335. arXiv:1807.08520, doi:10.5506/APhysPolB.50.1335.
- [721] M. N. Anwar, J. Ferretti, F.-K. Guo, E. Santopinto, B.-S. Zou, Spectroscopy and decays of the fully-heavy tetraquarks, Eur. Phys. J. C 78 (8) (2018) 647. arXiv:1710.02540, doi:10.1140/epjc/s10052-018-6073-9.
- [722] Y. Bai, S. Lu, J. Osborne, Beauty-full Tetraquarks, Phys. Lett. B 798 (2019) 134930. arXiv:1612.00012, doi:10.1016/j.physletb.2019.134930.
- [723] V. R. Debastiani, F. S. Navarra, Spectroscopy of the All-Charm Tetraquark, PoS Hadron2017 (2018) 238. arXiv:1711.11495, doi:10.22323/1.310.0238.
- [724] L. Heller, J. A. Tjon, On Bound States of Heavy  $Q^2\bar{Q}^2$  Systems, Phys. Rev. D 32 (1985) 755. doi:10.1103/PhysRevD.32.755.
- [725] S. Zouzou, B. Silvestre-Brac, C. Gignoux, J. M. Richard, Four quark bound states, Z. Phys. C 30 (1986) 457. doi:10.1007/BF01557611.
- [726] V. Khachatryan, et al., Observation of  $\Upsilon(1S)$  pair production in proton-proton collisions at  $\sqrt{s} = 8$  TeV, JHEP 05 (2017) 013. arXiv:1610.07095, doi:10.1007/JHEP05(2017)013.

- [727] A. M. Sirunyan, et al., Measurement of the  $\Upsilon(1S)$  pair production cross section and search for resonances decaying to  $\Upsilon(1S)\mu^+\mu^-$  in proton-proton collisions at  $\sqrt{s} = 13$  TeV, Phys. Lett. B 808 (2020) 135578. [arXiv:2002.06393](#), [doi:10.1016/j.physletb.2020.135578](#).
- [728] R. Aaij, et al., Search for beautiful tetraquarks in the  $\Upsilon(1S)\mu^+\mu^-$  invariant-mass spectrum, JHEP 10 (2018) 086. [arXiv:1806.09707](#), [doi:10.1007/JHEP10\(2018\)086](#).
- [729] Y. Xu, ATLAS results on exotic hadronic resonances, Acta Phys. Polon. Supp. 16 (3) (2023) 21. [arXiv:2209.12173](#), [doi:10.21468/SciPostPhysProc.15.013](#).
- [730] J. Zhang, K. Yi, Recent CMS results on exotic resonances, PoS ICHEP2022 (2022) 775. [arXiv:2212.00504](#), [doi:10.22323/1.414.0775](#).
- [731] J. Zhao, S. Shi, P. Zhuang, Fully-heavy tetraquarks in a strongly interacting medium, Phys. Rev. D 102 (11) (2020) 114001. [arXiv:2009.10319](#), [doi:10.1103/PhysRevD.102.114001](#).
- [732] Q.-F. Lü, D.-Y. Chen, Y.-B. Dong, Masses of fully heavy tetraquarks  $QQ\bar{Q}\bar{Q}$  in an extended relativized quark model, Eur. Phys. J. C 80 (9) (2020) 871. [arXiv:2006.14445](#), [doi:10.1140/epjc/s10052-020-08454-1](#).
- [733] M.-S. Liu, F.-X. Liu, X.-H. Zhong, Q. Zhao, Fully heavy tetraquark states and their evidences in LHC observations, Phys. Rev. D 109 (7) (2024) 076017. [arXiv:2006.11952](#), [doi:10.1103/PhysRevD.109.076017](#).
- [734] H.-X. Chen, W. Chen, X. Liu, S.-L. Zhu, Strong decays of fully-charm tetraquarks into di-charmonia, Sci. Bull. 65 (2020) 1994–2000. [arXiv:2006.16027](#), [doi:10.1016/j.scib.2020.08.038](#).
- [735] F.-X. Liu, M.-S. Liu, X.-H. Zhong, Q. Zhao, Higher mass spectra of the fully-charmed and fully-bottom tetraquarks, Phys. Rev. D 104 (11) (2021) 116029. [arXiv:2110.09052](#), [doi:10.1103/PhysRevD.104.116029](#).
- [736] R. N. Faustov, V. O. Galkin, E. M. Savchenko, Masses of the  $QQ\bar{Q}\bar{Q}$  tetraquarks in the relativistic diquark–antidiquark picture, Phys. Rev. D 102 (11) (2020) 114030. [arXiv:2009.13237](#), [doi:10.1103/PhysRevD.102.114030](#).
- [737] M. Karliner, J. L. Rosner, Interpretation of structure in the di-  $J/\psi$  spectrum, Phys. Rev. D 102 (11) (2020) 114039. [arXiv:2009.04429](#), [doi:10.1103/PhysRevD.102.114039](#).
- [738] H.-W. Ke, X. Han, X.-H. Liu, Y.-L. Shi, Tetraquark state  $X(6900)$  and the interaction between diquark and antidiquark, Eur. Phys. J. C 81 (5) (2021) 427. [arXiv:2103.13140](#), [doi:10.1140/epjc/s10052-021-09229-y](#).
- [739] B.-D. Wan, C.-F. Qiao, Gluonic tetracharm configuration of  $X(6900)$ , Phys. Lett. B 817 (2021) 136339. [arXiv:2012.00454](#), [doi:10.1016/j.physletb.2021.136339](#).
- [740] C. Gong, M.-C. Du, Q. Zhao, X.-H. Zhong, B. Zhou, Nature of  $X(6900)$  and its production mechanism at LHCb, Phys. Lett. B 824 (2022) 136794. [arXiv:2011.11374](#), [doi:10.1016/j.physletb.2021.136794](#).
- [741] J.-W. Zhu, X.-D. Guo, R.-Y. Zhang, W.-G. Ma, X.-Q. Li, A possible interpretation for  $X(6900)$  observed in four-muon final state by LHCb – A light Higgs-like boson? (11 2020). [arXiv:2011.07799](#).
- [742] J.-Z. Wang, D.-Y. Chen, X. Liu, T. Matsuki, Producing fully charm structures in the  $J/\psi$  -pair invariant mass spectrum, Phys. Rev. D 103 (7) (2021) 071503. [arXiv:2008.07430](#), [doi:10.1103/PhysRevD.103.L071503](#).
- [743] J.-Z. Wang, X. Liu, Improved understanding of the peaking phenomenon existing in the new di- $J/\psi$  invariant mass spectrum from the CMS Collaboration, Phys. Rev. D 106 (5) (2022) 054015. [arXiv:2207.04893](#), [doi:10.1103/PhysRevD.106.054015](#).

- [744] N. Santowsky, C. S. Fischer, Four-quark states with charm quarks in a two-body Bethe–Salpeter approach, *Eur. Phys. J. C* 82 (4) (2022) 313. [arXiv:2111.15310](#), [doi:10.1140/epjc/s10052-022-10272-6](#).
- [745] Z. Zhuang, Y. Zhang, Y. Ma, Q. Wang, Lineshape of the compact fully heavy tetraquark, *Phys. Rev. D* 105 (5) (2022) 054026. [arXiv:2111.14028](#), [doi:10.1103/PhysRevD.105.054026](#).
- [746] C. Deng, H. Chen, J. Ping, Towards the understanding of fully-heavy tetraquark states from various models, *Phys. Rev. D* 103 (1) (2021) 014001. [arXiv:2003.05154](#), [doi:10.1103/PhysRevD.103.014001](#).
- [747] Z.-G. Wang, Tetraquark candidates in the LHCb’s di- $J/\psi$  mass spectrum, *Chin. Phys. C* 44 (11) (2020) 113106. [arXiv:2006.13028](#), [doi:10.1088/1674-1137/abb080](#).
- [748] J. Sonnenschein, D. Weissman, Deciphering the recently discovered tetraquark candidates around 6.9 GeV, *Eur. Phys. J. C* 81 (1) (2021) 25. [arXiv:2008.01095](#), [doi:10.1140/epjc/s10052-020-08818-7](#).
- [749] J. F. Giron, R. F. Lebed, Simple spectrum of  $c\bar{c}c\bar{c}$  states in the dynamical diquark model, *Phys. Rev. D* 102 (7) (2020) 074003. [arXiv:2008.01631](#), [doi:10.1103/PhysRevD.102.074003](#).
- [750] Z.-G. Wang, Revisit the tetraquark candidates in the  $J/\psi J/\psi$  mass spectrum, *Int. J. Mod. Phys. A* 36 (02) (2021) 2150014. [arXiv:2009.05371](#), [doi:10.1142/S0217751X21500147](#).
- [751] R. Zhu, Fully-heavy tetraquark spectra and production at hadron colliders, *Nucl. Phys. B* 966 (2021) 115393. [arXiv:2010.09082](#), [doi:10.1016/j.nuclphysb.2021.115393](#).
- [752] Z. Zhao, K. Xu, A. Kaewsnod, X. Liu, A. Limphirat, Y. Yan, Study of charmoniumlike and fully-charm tetraquark spectroscopy, *Phys. Rev. D* 103 (11) (2021) 116027. [arXiv:2012.15554](#), [doi:10.1103/PhysRevD.103.116027](#).
- [753] H. Mutuk, Nonrelativistic treatment of fully-heavy tetraquarks as diquark-antidiquark states, *Eur. Phys. J. C* 81 (4) (2021) 367. [arXiv:2104.11823](#), [doi:10.1140/epjc/s10052-021-09176-8](#).
- [754] Q. Li, C.-H. Chang, G.-L. Wang, T. Wang, Mass spectra and wave functions of  $T_{QQ\bar{Q}\bar{Q}}$  tetraquarks, *Phys. Rev. D* 104 (1) (2021) 014018. [arXiv:2104.12372](#), [doi:10.1103/PhysRevD.104.014018](#).
- [755] G.-J. Wang, L. Meng, M. Oka, S.-L. Zhu, Higher fully charmed tetraquarks: Radial excitations and  $P$ -wave states, *Phys. Rev. D* 104 (3) (2021) 036016. [arXiv:2105.13109](#), [doi:10.1103/PhysRevD.104.036016](#).
- [756] Q.-N. Wang, Z.-Y. Yang, W. Chen, Exotic fully-heavy  $Q\bar{Q}Q\bar{Q}$  tetraquark states in  $\mathbf{8}_{[Q\bar{Q}]} \otimes \mathbf{8}_{[Q\bar{Q}]}$  color configuration, *Phys. Rev. D* 104 (11) (2021) 114037. [arXiv:2109.08091](#), [doi:10.1103/PhysRevD.104.114037](#).
- [757] Z.-G. Wang, Analysis of the  $X(6600)$ ,  $X(6900)$ ,  $X(7300)$  and related tetraquark states with the QCD sum rules, *Nucl. Phys. B* 985 (2022) 115983. [arXiv:2207.08059](#), [doi:10.1016/j.nuclphysb.2022.115983](#).
- [758] H.-T. An, S.-Q. Luo, Z.-W. Liu, X. Liu, Spectroscopic behavior of fully heavy tetraquarks, *Eur. Phys. J. C* 83 (8) (2023) 740. [arXiv:2208.03899](#), [doi:10.1140/epjc/s10052-023-11847-7](#).
- [759] J. Zhang, J.-B. Wang, G. Li, C.-S. An, C.-R. Deng, J.-J. Xie, Spectrum of the  $S$ -wave fully-heavy tetraquark states, *Eur. Phys. J. C* 82 (12) (2022) 1126. [arXiv:2209.13856](#), [doi:10.1140/epjc/s10052-022-11111-4](#).
- [760] R. N. Faustov, V. O. Galkin, E. M. Savchenko, Fully Heavy Tetraquark Spectroscopy in the Relativistic Quark Model, *Symmetry* 14 (12) (2022) 2504. [arXiv:2210.16015](#), [doi:10.3390/sym14122504](#).
- [761] W.-C. Dong, Z.-G. Wang, Going in quest of potential tetraquark interpretations for the newly observed  $T_{\psi\psi}$  states in light of the diquark-antidiquark scenarios, *Phys. Rev. D* 107 (7) (2023) 074010. [arXiv:2211.11989](#), [doi:10.1103/PhysRevD.107.074010](#).

- [762] G.-L. Yu, Z.-Y. Li, Z.-G. Wang, J. Lu, M. Yan, The  $S$ - and  $P$ -wave fully charmed tetraquark states and their radial excitations, *Eur. Phys. J. C* 83 (5) (2023) 416. [arXiv:2212.14339](#), [doi:10.1140/epjc/s10052-023-11445-7](#).
- [763] S. S. Agaev, K. Azizi, B. Barsbay, H. Sundu, Exploring fully heavy scalar tetraquarks  $QQ\bar{Q}\bar{Q}$ , *Phys. Lett. B* 844 (2023) 138089. [arXiv:2304.03244](#), [doi:10.1016/j.physletb.2023.138089](#).
- [764] Z.-Z. Chen, X.-L. Chen, P.-F. Yang, W. Chen,  $P$ -wave fully charm and fully bottom tetraquark states, *Phys. Rev. D* 109 (9) (2024) 094011. [arXiv:2402.03117](#), [doi:10.1103/PhysRevD.109.094011](#).
- [765] Y.-Y. Lin, J.-Y. Wang, A. Zhang, Mass spectrum of fully charmed  $[cc][\bar{c}\bar{c}]$  tetraquarks, *Eur. Phys. J. Plus* 139 (8) (2024) 707. [arXiv:2404.08971](#), [doi:10.1140/epjp/s13360-024-05480-w](#).
- [766] D. Nga Ongodo, A. A. Atangana Likéné, J. M. Ema'a Ema'a, P. Ele Abiama, G. H. Ben-Bolie, Hyperfine mass splittings in ground and radially excited states of heavy-flavored  $QQ\bar{Q}\bar{Q}$  tetraquarks: PGM defect and fractional order effects, *Nucl. Phys. A* 1063 (2025) 123215. [doi:10.1016/j.nuclphysa.2025.123215](#).
- [767] P. G. Ortega, D. R. Entem, F. Fernández, Exploring  $T_{\psi\psi}$  tetraquark candidates in a coupled-channels formalism, *Phys. Rev. D* 108 (9) (2023) 094023. [arXiv:2307.00532](#), [doi:10.1103/PhysRevD.108.094023](#).
- [768] X. Jin, Y. Xue, H. Huang, J. Ping, Full-heavy tetraquarks in constituent quark models, *Eur. Phys. J. C* 80 (11) (2020) 1083. [arXiv:2006.13745](#), [doi:10.1140/epjc/s10052-020-08650-z](#).
- [769] B.-C. Yang, L. Tang, C.-F. Qiao, Scalar fully-heavy tetraquark states  $QQ'\bar{Q}\bar{Q}'$  in QCD sum rules, *Eur. Phys. J. C* 81 (4) (2021) 324. [arXiv:2012.04463](#), [doi:10.1140/epjc/s10052-021-09096-7](#).
- [770] G. Yang, J. Ping, J. Segovia, Exotic resonances of fully-heavy tetraquarks in a lattice-QCD inspired quark model, *Phys. Rev. D* 104 (1) (2021) 014006. [arXiv:2104.08814](#), [doi:10.1103/PhysRevD.104.014006](#).
- [771] G.-J. Wang, Q. Meng, M. Oka,  $S$ -wave fully charmed tetraquark resonant states, *Phys. Rev. D* 106 (9) (2022) 096005. [arXiv:2208.07292](#), [doi:10.1103/PhysRevD.106.096005](#).
- [772] G.-J. Wang, M. Oka, D. Jido, Quark confinement for multiquark systems: Application to fully charmed tetraquarks, *Phys. Rev. D* 108 (7) (2023) L071501. [arXiv:2307.04310](#), [doi:10.1103/PhysRevD.108.L071501](#).
- [773] W.-L. Wu, Y.-K. Chen, L. Meng, S.-L. Zhu, Benchmark calculations of fully heavy compact and molecular tetraquark states, *Phys. Rev. D* 109 (5) (2024) 054034. [arXiv:2401.14899](#), [doi:10.1103/PhysRevD.109.054034](#).
- [774] Y. Wu, X. Liu, J. Ping, H. Huang, Y. Tan, Further study of  $c\bar{c}c\bar{c}$  system within a chiral quark model, *Eur. Phys. J. C* 85 (2) (2025) 147. [arXiv:2403.10375](#), [doi:10.1140/epjc/s10052-025-13822-w](#).
- [775] Q. Meng, G.-J. Wang, M. Oka, Mass spectra of full-heavy and double-heavy tetraquark states in the conventional quark model, *Phys. Rev. D* 111 (1) (2025) 014018. [arXiv:2404.01238](#), [doi:10.1103/PhysRevD.111.014018](#).
- [776] C.-M. Tang, C.-G. Duan, L. Tang, Fully charmed tetraquark states in  $8_{[c\bar{c}]} \otimes 8_{[c\bar{c}]}$  color structure via QCD sum rules, *Eur. Phys. J. C* 84 (7) (2024) 743. [arXiv:2405.05042](#), [doi:10.1140/epjc/s10052-024-13102-z](#).
- [777] A. V. Nefediev,  $X(6200)$  as a compact tetraquark in the QCD string model, *Eur. Phys. J. C* 81 (8) (2021) 692. [arXiv:2107.14182](#), [doi:10.1140/epjc/s10052-021-09511-z](#).
- [778] Z. Asadi, G. R. Boroun, Masses of fully heavy tetraquark states from a four-quark static potential model, *Phys. Rev. D* 105 (1) (2022) 014006. [arXiv:2112.11028](#), [doi:10.1103/PhysRevD.105.014006](#).

- [779] X.-K. Dong, V. Baru, F.-K. Guo, C. Hanhart, A. Nefediev, Coupled-Channel Interpretation of the LHCb Double- $J/\psi$  Spectrum and Hints of a New State Near the  $J/\psi J/\psi$  Threshold, Phys. Rev. Lett. 126 (13) (2021) 132001, [Erratum: Phys.Rev.Lett. 127, 119901 (2021)]. [arXiv:2009.07795](#), [doi:10.1103/PhysRevLett.127.119901](#).
- [780] Z.-R. Liang, X.-Y. Wu, D.-L. Yao, Hunting for states in the recent LHCb di- $J/\psi$  invariant mass spectrum, Phys. Rev. D 104 (3) (2021) 034034. [arXiv:2104.08589](#), [doi:10.1103/PhysRevD.104.034034](#).
- [781] Q. Zhou, D. Guo, S.-Q. Kuang, Q.-H. Yang, L.-Y. Dai, Nature of the  $X(6900)$  in partial wave decomposition of  $J/\psi J/\psi$  scattering, Phys. Rev. D 106 (11) (2022) L111502. [arXiv:2207.07537](#), [doi:10.1103/PhysRevD.106.L111502](#).
- [782] P. Niu, Z. Zhang, Q. Wang, M.-L. Du, The third peak structure in the double  $J/\psi$  spectrum, Sci. Bull. 68 (2023) 800–803. [arXiv:2212.06535](#), [doi:10.1016/j.scib.2023.03.025](#).
- [783] S.-Q. Kuang, Q. Zhou, D. Guo, Q.-H. Yang, L.-Y. Dai, Study of  $X(6900)$  with unitarized coupled channel scattering amplitudes, Eur. Phys. J. C 83 (5) (2023) 383. [arXiv:2302.03968](#), [doi:10.1140/epjc/s10052-023-11473-3](#).
- [784] Y.-L. Song, Y. Zhang, V. Baru, F.-K. Guo, C. Hanhart, A. Nefediev, Toward a precision determination of the  $X(6200)$  parameters from data, Phys. Rev. D 111 (3) (2025) 034038. [arXiv:2411.12062](#), [doi:10.1103/PhysRevD.111.034038](#).
- [785] Z.-H. Guo, J. A. Oller, Insights into the inner structures of the fully charmed tetraquark state  $X(6900)$ , Phys. Rev. D 103 (3) (2021) 034024. [arXiv:2011.00978](#), [doi:10.1103/PhysRevD.103.034024](#).
- [786] Q.-F. Cao, H. Chen, H.-R. Qi, H.-Q. Zheng, Some remarks on  $X(6900)$ , Chin. Phys. C 45 (10) (2021) 103102. [arXiv:2011.04347](#), [doi:10.1088/1674-1137/ac0ee5](#).
- [787] Y. Lu, C. Chen, K.-G. Kang, G.-y. Qin, H.-Q. Zheng,  $X(6900)$  peak could be a molecular state, Phys. Rev. D 107 (9) (2023) 094006. [arXiv:2302.04150](#), [doi:10.1103/PhysRevD.107.094006](#).
- [788] X.-K. Dong, V. Baru, F.-K. Guo, C. Hanhart, A. Nefediev, B.-S. Zou, Is the existence of a  $J/\psi J/\psi$  bound state plausible?, Sci. Bull. 66 (24) (2021) 2462–2470. [arXiv:2107.03946](#), [doi:10.1016/j.scib.2021.09.009](#).
- [789] M.-Z. Liu, L.-S. Geng, Is  $X(7200)$  the heavy anti-quark diquark symmetry partner of  $X(3872)$ ?, Eur. Phys. J. C 81 (2) (2021) 179. [arXiv:2012.05096](#), [doi:10.1140/epjc/s10052-021-08980-6](#).
- [790] Y. Lu, C. Chen, G.-y. Qin, H.-Q. Zheng, A discussion on the anomalous threshold enhancement of  $J/\psi$ - $\psi(3770)$  couplings and  $X(6900)$  peak, Chin. Phys. C 48 (4) (2024) 041001. [arXiv:2312.10711](#), [doi:10.1088/1674-1137/ad2361](#).
- [791] W.-Y. Liu, H.-X. Chen, Hadronic Molecules with Four Charm or Beauty Quarks, Universe 11 (2) (2025) 36. [arXiv:2405.14404](#), [doi:10.3390/universe11020036](#).
- [792] V. Patel, J. Oudichhya, A. K. Rai, Spectroscopy of  $cc\bar{c}\bar{c}$  and  $ss\bar{c}\bar{c}$  Tetraquarks within the Framework of Regge Phenomenology, Few Body Syst. 66 (4) (2025) 39. [arXiv:2511.02279](#), [doi:10.1007/s00601-025-02011-w](#).
- [793] J.-R. Zhang,  $0^+$  fully-charmed tetraquark states, Phys. Rev. D 103 (1) (2021) 014018. [arXiv:2010.07719](#), [doi:10.1103/PhysRevD.103.014018](#).
- [794] G. Huang, J. Zhao, P. Zhuang, Pair structure of heavy tetraquark systems, Phys. Rev. D 103 (5) (2021) 054014. [arXiv:2012.14845](#), [doi:10.1103/PhysRevD.103.054014](#).
- [795] A. J. Majarshin, Y.-A. Luo, F. Pan, J. Segovia, Bosonic algebraic approach applied to the  $[QQ][\bar{Q}\bar{Q}]$  tetraquarks, Phys. Rev. D 105 (5) (2022) 054024. [arXiv:2106.01179](#), [doi:10.1103/PhysRevD.105.054024](#).

- [796] R. Tiwari, D. P. Rathaud, A. K. Rai, Spectroscopy of all charm tetraquark states, *Indian J. Phys.* 97 (3) (2023) 943–954. [arXiv:2108.04017](#), [doi:10.1007/s12648-022-02427-8](#).
- [797] R. F. Lebed, All Heavy Tetraquarks: The Dynamical Diquark Model and Other Approaches, *Moscow Univ. Phys. Bull.* 77 (2) (2022) 458–461. [arXiv:2201.01721](#), [doi:10.3103/S002713492202059X](#).
- [798] W. Chen, Q.-N. Wang, Z.-Y. Yang, H.-X. Chen, X. Liu, T. G. Steele, S.-L. Zhu, Searching for fully-heavy tetraquark states in QCD moment sum rules, *Nucl. Part. Phys. Proc.* 318-323 (2022) 73–77. [arXiv:2212.03689](#), [doi:10.1016/j.nuclphysbps.2022.09.016](#).
- [799] R. Mistry, A. Majethiya, Spectroscopic study of exotic fully-heavy tetraquark states  $QQ\bar{Q}\bar{Q}$  ( $Q \in \{c, b\}$ ), *Chin. J. Phys.* 91 (2024) 932–946. [doi:10.1016/j.cjph.2024.08.040](#).
- [800] M. Malekhosseini, S. Rostami, A. R. Olamaei, K. Azizi, Exploring fully-heavy tetraquarks through the CGAN framework: Mass and width, *Nucl. Phys. B* 1018 (2025) 116977. [arXiv:2503.00993](#), [doi:10.1016/j.nuclphysb.2025.116977](#).
- [801] W.-C. Dong, Z.-G. Wang, J.-W. Zhou, Exploring the Interpretations of Charmonia and  $cc\bar{c}\bar{c}$  Tetraquarks in the Relativistic Flux Tube Model, *Symmetry* 17 (6) (2025) 931. [doi:10.3390/sym17060931](#).
- [802] C.-M. Tang, C.-G. Duan, L. Tang, C.-F. Qiao, QCD sum rule predictions on gluonic tetraquark states with  $J^{PC} = 0^{+-}, 0^{-+}$  and  $1^{\pm\pm}$  (11 2025). [arXiv:2511.18807](#).
- [803] V. O. Galkin, E. M. Savchenko, Relativistic description of asymmetric fully heavy tetraquarks in the diquark–antidiquark model, *Eur. Phys. J. A* 60 (5) (2024) 96. [arXiv:2310.20247](#), [doi:10.1140/epja/s10050-024-01311-9](#).
- [804] C.-M. Tang, C.-G. Duan, L. Tang, C.-F. Qiao, A novel configuration of gluonic tetraquark state, *Eur. Phys. J. C* 85 (4) (2025) 396. [arXiv:2411.11433](#), [doi:10.1140/epjc/s10052-025-14106-z](#).
- [805] X.-Z. Weng, X.-L. Chen, W.-Z. Deng, S.-L. Zhu, Systematics of fully heavy tetraquarks, *Phys. Rev. D* 103 (3) (2021) 034001. [arXiv:2010.05163](#), [doi:10.1103/PhysRevD.103.034001](#).
- [806] C. Hughes, E. Eichten, C. T. H. Davies, Searching for beauty-fully bound tetraquarks using lattice nonrelativistic QCD, *Phys. Rev. D* 97 (5) (2018) 054505. [arXiv:1710.03236](#), [doi:10.1103/PhysRevD.97.054505](#).
- [807] J.-M. Richard, A. Valcarce, J. Vijande, Few-body quark dynamics for doubly heavy baryons and tetraquarks, *Phys. Rev. C* 97 (3) (2018) 035211. [arXiv:1803.06155](#), [doi:10.1103/PhysRevC.97.035211](#).
- [808] W.-L. Wu, Y. Ma, Y.-K. Chen, L. Meng, S.-L. Zhu, Fully heavy tetraquark resonant states with different flavors, *Phys. Rev. D* 110 (3) (2024) 034030. [arXiv:2406.17824](#), [doi:10.1103/PhysRevD.110.034030](#).
- [809] W.-L. Wu, S.-L. Zhu, Fully charmed  $P$ -wave tetraquark resonant states in the quark model, *Phys. Rev. D* 111 (3) (2025) 034044. [arXiv:2411.17962](#), [doi:10.1103/PhysRevD.111.034044](#).
- [810] Z.-Y. Wang, J.-J. Qi, Z.-H. Zhang, X.-H. Guo, Spectra of  $bc\bar{b}\bar{c}$  tetraquark states from a diquark-antidiquark perspective, *Phys. Rev. D* 112 (7) (2025) 074038. [arXiv:2508.12366](#), [doi:10.1103/skdp-g4q1](#).
- [811] H. Yukawa, On the Interaction of Elementary Particles I, *Proc. Phys. Math. Soc. Jap.* 17 (1935) 48–57. [doi:10.1143/PTPS.1.1](#).
- [812] Q. Huang, R. Chen, J. He, X. Liu, Discovering a Novel Dynamics Mechanism for Charmonium Scattering (7 2024). [arXiv:2407.16316](#).
- [813] Y. Meng, C. Liu, X.-Y. Tuo, H. Yan, Z. Zhang, Lattice calculation of the  $\eta_c\eta_c$  and  $J/\psi J/\psi$   $s$ -wave scattering length, *Eur. Phys. J. C* 85 (4) (2025) 458. [arXiv:2411.11533](#), [doi:10.1140/epjc/s10052-025-14192-z](#).
- [814] G. Li, C. Shi, Y. Chen, W. Sun,  $\eta_c\eta_c$  and  $J/\psi J/\psi$  scatterings from lattice QCD (5 2025). [arXiv:2505.23220](#).

- [815] G. Li, C. Shi, Y. Chen, W. Sun, Tensor Resonance in  $J/\psi J/\psi$  Scattering from Lattice QCD (5 2025). [arXiv:2505.24213](#).
- [816] L. Zhang, T. Doi, Y. Lyu, T. Hatsuda, Y.-G. Ma, Probing nucleon- $\bar{\Omega}_{ccc}$  interaction via lattice QCD at physical quark masses, *Phys. Lett. B* 871 (2025) 139998. [arXiv:2508.10388](#), [doi:10.1016/j.physletb.2025.139998](#).
- [817] N. Mathur, M. Padmanath, D. Chakraborty, Strongly Bound Dibaryon with Maximal Beauty Flavor from Lattice QCD, *Phys. Rev. Lett.* 130 (11) (2023) 111901. [arXiv:2205.02862](#), [doi:10.1103/PhysRevLett.130.111901](#).
- [818] N. S. Dhindsa, D. Chakraborty, A. Radhakrishnan, N. Mathur, M. Padmanath, Precisely determining the ground state mass of Spin-3/2  $\Omega_{ccc}$  baryon from Lattice QCD, 2025. [arXiv:2512.23417](#).
- [819] C. M. G. Lattes, H. Muirhead, G. P. S. Occhialini, C. F. Powell, Processes involving charged mesons, *Nature* 159 (1947) 694–697. [doi:10.1038/159694a0](#).
- [820] N. Hoshizaki, S. Otsuki, W. Watari, M. Yonezawa, Nuclear forces and bosons: The sakata model and one-boson-exchange-potentials, *Progress of Theoretical Physics* 27 (6) (1962) 1199–1220. [arXiv:https://academic.oup.com/ptp/article-pdf/27/6/1199/5382274/27-6-1199.pdf](#), [doi:10.1143/PTP.27.1199](#).  
URL <https://doi.org/10.1143/PTP.27.1199>
- [821] P. A. Zyla, et al., Review of particle physics, *PTEP* 2020 (8) (2020) 083C01. [doi:10.1093/ptep/ptaa104](#).
- [822] C. P. Shen, et al., Observation of the  $\phi(1680)$  and the  $Y(2175)$  in  $e^+e^- \rightarrow \phi\pi^+\pi^-$ , *Phys. Rev. D* 80 (2009) 031101. [arXiv:0808.0006](#), [doi:10.1103/PhysRevD.80.031101](#).
- [823] H.-X. Chen, A. Hosaka, S.-L. Zhu, The  $I^G J^{PC} = 1^- 1^{-+}$  tetraquark states, *Phys. Rev. D* 78 (2008) 054017. [arXiv:0806.1998](#), [doi:10.1103/PhysRevD.78.054017](#).
- [824] G.-J. Ding, J.-F. Liu, M.-L. Yan, Dynamics of hadronic molecule in one-boson exchange approach and possible heavy flavor molecules, *Phys. Rev. D* 79 (2009) 054005. [arXiv:0901.0426](#), [doi:10.1103/PhysRevD.79.054005](#).
- [825] P. Guo, One spatial dimensional finite volume three-body interaction for a short-range potential, *Phys. Rev. D* 95 (5) (2017) 054508. [arXiv:1607.03184](#), [doi:10.1103/PhysRevD.95.054508](#).
- [826] W. R. Innes, et al., Observation of structure in the  $\Upsilon$  region, *Phys. Rev. Lett.* 39 (1977) 1240–1242, [Erratum: *Phys.Rev.Lett.* 39, 1640 (1977)]. [doi:10.1103/PhysRevLett.39.1240](#).
- [827] C. Klopfenstein, et al., Observation of the lowest  $P$  wave  $b\bar{b}$  bound states, *Phys. Rev. Lett.* 51 (1983) 160. [doi:10.1103/PhysRevLett.51.160](#).
- [828] F. Pauss, et al., Observation of  $\chi_b$  production in the exclusive reaction  $\Upsilon' \rightarrow \gamma\chi_b \rightarrow \gamma\gamma\Upsilon \rightarrow \gamma\gamma (e^+e^- \text{ or } \mu^+\mu^-)$ , *Phys. Lett. B* 130 (1983) 439. [doi:10.1016/0370-2693\(83\)91539-3](#).
- [829] K. Han, et al., Observation of  $P$ -wave  $b\bar{b}$  bound states, *Phys. Rev. Lett.* 49 (1982) 1612–1616. [doi:10.1103/PhysRevLett.49.1612](#).
- [830] G. Eigen, et al., Evidence for  $\chi'_b$  production in the exclusive reaction  $\Upsilon'' \rightarrow \gamma\chi'_b \rightarrow (\gamma\gamma\Upsilon' \text{ or } \gamma\gamma\Upsilon)$ , *Phys. Rev. Lett.* 49 (1982) 1616–1619. [doi:10.1103/PhysRevLett.49.1616](#).
- [831] B. Aubert, et al., Observation of the bottomonium ground state in the decay  $\Upsilon(3S) \rightarrow \gamma\eta_b$ , *Phys. Rev. Lett.* 101 (2008) 071801, [Erratum: *Phys.Rev.Lett.* 102, 029901 (2009)]. [arXiv:0807.1086](#), [doi:10.1103/PhysRevLett.101.071801](#).

- [832] G. Bonvicini, et al., Measurement of the  $\eta_b(1S)$  mass and the branching fraction for  $\Upsilon(3S) \rightarrow \gamma\eta_b(1S)$ , Phys. Rev. D 81 (2010) 031104. [arXiv:0909.5474](#), [doi:10.1103/PhysRevD.81.031104](#).
- [833] S. Dobbs, Z. Metreveli, K. K. Seth, A. Tomaradze, T. Xiao, Observation of the  $\eta_b(2S)$  meson in  $\Upsilon(2S) \rightarrow \gamma\eta_b(2S)$ ,  $\eta_b(2S) \rightarrow$  hadrons, and confirmation of  $\eta_b(1S)$  meson, Phys. Rev. Lett. 109 (2012) 082001. [arXiv:1204.4205](#), [doi:10.1103/PhysRevLett.109.082001](#).
- [834] J. P. Lees, et al., Study of radiative bottomonium transitions using converted photons, Phys. Rev. D 84 (2011) 072002. [arXiv:1104.5254](#), [doi:10.1103/PhysRevD.84.072002](#).
- [835] V. M. Abazov, et al., Observation of a narrow mass state decaying into  $\Upsilon(1S) + \gamma$  in  $p\bar{p}$  collisions at  $\sqrt{s} = 1.96$  TeV, Phys. Rev. D 86 (2012) 031103. [arXiv:1203.6034](#), [doi:10.1103/PhysRevD.86.031103](#).
- [836] J. P. Lees, et al., Evidence for the  $h_b(1P)$  meson in the decay  $\Upsilon(3S) \rightarrow \pi^0 h_b(1P)$ , Phys. Rev. D 84 (2011) 091101. [arXiv:1102.4565](#), [doi:10.1103/PhysRevD.84.091101](#).
- [837] I. Adachi, et al., First observation of the  $P$ -wave spin-singlet bottomonium states  $h_b(1P)$  and  $h_b(2P)$ , Phys. Rev. Lett. 108 (2012) 032001. [arXiv:1103.3419](#), [doi:10.1103/PhysRevLett.108.032001](#).
- [838] G. Bonvicini, et al., First observation of a  $\Upsilon(1D)$  state, Phys. Rev. D 70 (2004) 032001. [arXiv:hep-ex/0404021](#), [doi:10.1103/PhysRevD.70.032001](#).
- [839] P. del Amo Sanchez, et al., Observation of the  $\Upsilon(1^3D_J)$  bottomonium state through decays to  $\pi^+\pi^-\Upsilon(1S)$ , Phys. Rev. D 82 (2010) 111102. [arXiv:1004.0175](#), [doi:10.1103/PhysRevD.82.111102](#).
- [840] J. L. Richardson, The heavy quark potential and the  $\Upsilon$ ,  $J/\psi$  systems, Phys. Lett. B 82 (1979) 272–274. [doi:10.1016/0370-2693\(79\)90753-6](#).
- [841] W. Buchmuller, S. H. H. Tye, Quarkonia and quantum chromodynamics, Phys. Rev. D 24 (1981) 132. [doi:10.1103/PhysRevD.24.132](#).
- [842] A. Martin, A fit of upsilon and charmonium spectra, Phys. Lett. B 93 (1980) 338–342. [doi:10.1016/0370-2693\(80\)90527-4](#).
- [843] S. N. Gupta, S. F. Radford, W. W. Repko, Semirelativistic potential model for heavy quarkonia, Phys. Rev. D 34 (1986) 201–206. [doi:10.1103/PhysRevD.34.201](#).
- [844] M. Beyer, U. Bohn, M. G. Huber, B. C. Metsch, J. Resag, Relativistic effects and the constituent quark model of heavy quarkonia, Z. Phys. C 55 (1992) 307–315. [doi:10.1007/BF01482594](#).
- [845] L. Motyka, K. Zalewski, Mass spectra and leptonic decay widths of heavy quarkonia, Eur. Phys. J. C 4 (1998) 107–114. [arXiv:hep-ph/9709254](#), [doi:10.1007/s100520050190](#).
- [846] D. Ebert, R. N. Faustov, V. O. Galkin, Properties of heavy quarkonia and  $B_c$  mesons in the relativistic quark model, Phys. Rev. D 67 (2003) 014027. [arXiv:hep-ph/0210381](#), [doi:10.1103/PhysRevD.67.014027](#).
- [847] P. Gonzalez, A. Valcarce, H. Garcilazo, J. Vijande, Heavy meson description with a screened potential, Phys. Rev. D 68 (2003) 034007. [arXiv:hep-ph/0307310](#), [doi:10.1103/PhysRevD.68.034007](#).
- [848] J. Vijande, F. Fernandez, A. Valcarce, Constituent quark model study of the meson spectra, J. Phys. G 31 (2005) 481. [arXiv:hep-ph/0411299](#), [doi:10.1088/0954-3899/31/5/017](#).
- [849] S. F. Radford, W. W. Repko, Potential model calculations and predictions for heavy quarkonium, Phys. Rev. D 75 (2007) 074031. [arXiv:hep-ph/0701117](#), [doi:10.1103/PhysRevD.75.074031](#).
- [850] B.-Q. Li, K.-T. Chao, Bottomonium spectrum with screened potential, Commun. Theor. Phys. 52 (2009) 653–661. [arXiv:0909.1369](#), [doi:10.1088/0253-6102/52/4/20](#).

- [851] T. Wei-Zhao, C. Lu, Y. You-Chang, C. Hong, Bottomonium states versus recent experimental observations in the QCD-inspired potential model, *Chin. Phys. C* 37 (2013) 083101. [arXiv:1308.0960](#), [doi:10.1088/1674-1137/37/8/083101](#).
- [852] P. Gonzalez, Generalized screened potential model, *J. Phys. G* 41 (2014) 095001. [arXiv:1406.5025](#), [doi:10.1088/0954-3899/41/9/095001](#).
- [853] Y. Li, P. Maris, X. Zhao, J. P. Vary, Heavy quarkonium in a holographic basis, *Phys. Lett. B* 758 (2016) 118–124. [arXiv:1509.07212](#), [doi:10.1016/j.physletb.2016.04.065](#).
- [854] S. Godfrey, K. Moats, Bottomonium mesons and strategies for their observation, *Phys. Rev. D* 92 (5) (2015) 054034. [arXiv:1507.00024](#), [doi:10.1103/PhysRevD.92.054034](#).
- [855] J. Segovia, P. G. Ortega, D. R. Entem, F. Fernández, Bottomonium spectrum revisited, *Phys. Rev. D* 93 (7) (2016) 074027. [arXiv:1601.05093](#), [doi:10.1103/PhysRevD.93.074027](#).
- [856] W.-J. Deng, H. Liu, L.-C. Gui, X.-H. Zhong, Spectrum and electromagnetic transitions of bottomonium, *Phys. Rev. D* 95 (7) (2017) 074002. [arXiv:1607.04696](#), [doi:10.1103/PhysRevD.95.074002](#).
- [857] R. Kaushal, Bhaghyesh, Beauty hadron spectrum in a screened potential model, *Eur. Phys. J. C* 85 (7) (2025) 814. [arXiv:2505.13987](#), [doi:10.1140/epjc/s10052-025-14538-7](#).
- [858] C. A. Bokade, A. Bhaghyesh, Predictions for bottomonium from a relativistic screened potential model, *Chin. Phys.* 49 (7) (2025) 073102. [arXiv:2501.03147](#), [doi:10.1088/1674-1137/adc084](#).
- [859] C. Patrignani, et al., Review of particle physics, *Chin. Phys. C* 40 (10) (2016) 100001. [doi:10.1088/1674-1137/40/10/100001](#).
- [860] K. Gottfried, Hadronic transitions between quark-antiquark bound states, *Phys. Rev. Lett.* 40 (1978) 598. [doi:10.1103/PhysRevLett.40.598](#).
- [861] G. Bhanot, W. Fischler, S. Rudaz, A multipole expansion and the Casimir-Polder effect in quantum chromodynamics, *Nucl. Phys. B* 155 (1979) 208–236. [doi:10.1016/0550-3213\(79\)90363-8](#).
- [862] M. E. Peskin, Short distance analysis for heavy quark systems. 1. Diagrammatics, *Nucl. Phys. B* 156 (1979) 365–390. [doi:10.1016/0550-3213\(79\)90199-8](#).
- [863] G. Bhanot, M. E. Peskin, Short distance analysis for heavy quark systems. 2. Applications, *Nucl. Phys. B* 156 (1979) 391–416. [doi:10.1016/0550-3213\(79\)90200-1](#).
- [864] M. B. Voloshin, On dynamics of heavy quarks in nonperturbative QCD vacuum, *Nucl. Phys. B* 154 (1979) 365–380. [doi:10.1016/0550-3213\(79\)90037-3](#).
- [865] T.-M. Yan, Hadronic transitions between heavy quark states in quantum chromodynamics, *Phys. Rev. D* 22 (1980) 1652. [doi:10.1103/PhysRevD.22.1652](#).
- [866] Y.-P. Kuang, S. F. Tuan, T.-M. Yan, Hadronic transitions and  $P$  wave singlet states of heavy quarkonia, *Phys. Rev. D* 37 (1988) 1210–1219. [doi:10.1103/PhysRevD.37.1210](#).
- [867] Y.-P. Kuang, QCD multipole expansion and hadronic transitions in heavy quarkonium systems, *Front. Phys. China* 1 (2006) 19–37. [arXiv:hep-ph/0601044](#), [doi:10.1007/s11467-005-0012-6](#).
- [868] U. Tamponi, et al., First observation of the hadronic transition  $\Upsilon(4S) \rightarrow \eta h_b(1P)$  and new measurement of the  $h_b(1P)$  and  $\eta_b(1S)$  parameters, *Phys. Rev. Lett.* 115 (14) (2015) 142001. [arXiv:1506.08914](#), [doi:10.1103/PhysRevLett.115.142001](#).
- [869] M. B. Voloshin, Charmonium, *Prog. Part. Nucl. Phys.* 61 (2008) 455–511. [arXiv:0711.4556](#), [doi:10.1016/j.pnpnp.2008.02.001](#).

- [870] J. P. Lees, et al., Study of di-pion bottomonium transitions and search for the  $h_b(1P)$  state, Phys. Rev. D 84 (2011) 011104. [arXiv:1105.4234](#), [doi:10.1103/PhysRevD.84.011104](#).
- [871] X. H. He, et al., Observation of  $e^+e^- \rightarrow \pi^+\pi^-\pi^0\chi_{bJ}$  and Search for  $X_b \rightarrow \omega\Upsilon(1S)$  at  $\sqrt{s} = 10.867$  GeV, Phys. Rev. Lett. 113 (14) (2014) 142001. [arXiv:1408.0504](#), [doi:10.1103/PhysRevLett.113.142001](#).
- [872] F.-K. Guo, P.-N. Shen, H.-C. Chiang, R.-G. Ping, On the structure of the  $\pi\pi$  invariant mass spectra of the  $\Upsilon(4S) \rightarrow \Upsilon(1S, 2S)\pi^+\pi^-$ , Phys. Lett. B 658 (2007) 27–32. [arXiv:hep-ph/0601120](#), [doi:10.1016/j.physletb.2007.10.021](#).
- [873] Y. A. Simonov, A. I. Veselov, Bottomonium dipion transitions, Phys. Rev. D 79 (2009) 034024. [arXiv:0804.4635](#), [doi:10.1103/PhysRevD.79.034024](#).
- [874] Y. A. Simonov, A. I. Veselov, Strong decays and dipion transitions of  $\Upsilon(5S)$ , Phys. Lett. B 671 (2009) 55–59. [arXiv:0805.4499](#), [doi:10.1016/j.physletb.2008.12.001](#).
- [875] E. Kovalenko, et al., Study of  $e^+e^- \rightarrow \Upsilon(1S, 2S)\eta$  and  $e^+e^- \rightarrow \Upsilon(1S)\eta'$  at  $\sqrt{s} = 10.866$  GeV with the Belle detector, Phys. Rev. D 104 (11) (2021) 112006. [arXiv:2108.04426](#), [doi:10.1103/PhysRevD.104.112006](#).
- [876] Q. He, et al., Observation of  $\Upsilon(2S) \rightarrow \eta\Upsilon(1S)$  and search for related transitions, Phys. Rev. Lett. 101 (2008) 192001. [arXiv:0806.3027](#), [doi:10.1103/PhysRevLett.101.192001](#).
- [877] Y. Zhang, G. Li, Exploring the  $\Upsilon(4S, 5S, 6S) \rightarrow h_b(1P)\eta$  hidden-bottom hadronic transitions, Phys. Rev. D 97 (1) (2018) 014018. [arXiv:1801.03582](#), [doi:10.1103/PhysRevD.97.014018](#).
- [878] B. Wang, X. Liu, D.-Y. Chen, Prediction of anomalous  $\Upsilon(5S) \rightarrow \Upsilon(1^3D_J)\eta$  transitions, Phys. Rev. D 94 (9) (2016) 094039. [arXiv:1611.02369](#), [doi:10.1103/PhysRevD.94.094039](#).
- [879] U. Tamponi, et al., Inclusive study of bottomonium production in association with an  $\eta$  meson in  $e^+e^-$  annihilations near  $\Upsilon(5S)$ , Eur. Phys. J. C 78 (8) (2018) 633. [arXiv:1803.03225](#), [doi:10.1140/epjc/s10052-018-6086-4](#).
- [880] D.-Y. Chen, X. Liu, T. Matsuki, Explaining the anomalous  $\Upsilon(5S) \rightarrow \chi_{bJ}\omega$  decays through the hadronic loop effect, Phys. Rev. D 90 (3) (2014) 034019. [arXiv:1406.6763](#), [doi:10.1103/PhysRevD.90.034019](#).
- [881] Q. Huang, X. Liu, T. Matsuki, Proposal of searching for the  $\Upsilon(6S)$  hadronic decays into  $\Upsilon(nS)$  plus  $\eta^{(\prime)}$ , Phys. Rev. D 98 (5) (2018) 054008. [arXiv:1807.09137](#), [doi:10.1103/PhysRevD.98.054008](#).
- [882] Q. Huang, H. Xu, X. Liu, T. Matsuki, Potential observation of the  $\Upsilon(6S) \rightarrow \Upsilon(1^3D_J)\eta$  transitions at Belle II, Phys. Rev. D 97 (9) (2018) 094018. [arXiv:1804.01017](#), [doi:10.1103/PhysRevD.97.094018](#).
- [883] Q. Huang, B. Wang, X. Liu, D.-Y. Chen, T. Matsuki, Exploring the  $\Upsilon(6S) \rightarrow \chi_{bJ}\phi$  and  $\Upsilon(6S) \rightarrow \chi_{bJ}\omega$  hidden-bottom hadronic transitions, Eur. Phys. J. C 77 (3) (2017) 165. [arXiv:1701.00894](#), [doi:10.1140/epjc/s10052-017-4726-8](#).
- [884] B. Chen, A. Zhang, J. He, Bottomonium spectrum in the relativistic flux tube model, Phys. Rev. D 101 (1) (2020) 014020. [arXiv:1910.06065](#), [doi:10.1103/PhysRevD.101.014020](#).
- [885] Q. Li, M.-S. Liu, Q.-F. Lü, L.-C. Gui, X.-H. Zhong, Canonical interpretation of  $Y(10750)$  and  $Y(10860)$  in the  $Y$  family, Eur. Phys. J. C 80 (1) (2020) 59. [arXiv:1905.10344](#), [doi:10.1140/epjc/s10052-020-7626-2](#).
- [886] V. Kher, R. Chaturvedi, N. Devlani, A. K. Rai, Bottomonium spectroscopy using Coulomb plus linear (Cornell) potential, Eur. Phys. J. Plus 137 (3) (2022) 357. [arXiv:2201.08317](#), [doi:10.1140/epjp/s13360-022-02538-5](#).
- [887] Y.-S. Li, Z.-Y. Bai, Q. Huang, X. Liu, Hidden-bottom hadronic decays of  $\Upsilon(10753)$  with a  $\eta^{(\prime)}$  or  $\omega$  emission, Phys. Rev. D 104 (3) (2021) 034036. [arXiv:2106.14123](#), [doi:10.1103/PhysRevD.104.034036](#).

- [888] Z.-L. Luo, Y.-L. Song, F.-K. Guo, Decays of  $\Upsilon(10860)$  and  $\Upsilon(10753)$  into  $\omega\chi_{bJ}$ , Phys. Lett. B 870 (2025) 139960. [arXiv:2508.18720](#), [doi:10.1016/j.physletb.2025.139960](#).
- [889] Z.-G. Wang, Vector hidden-bottom tetraquark candidate:  $Y(10750)$ , Chin. Phys. C 43 (12) (2019) 123102. [arXiv:1905.06610](#), [doi:10.1088/1674-1137/43/12/123102](#).
- [890] A. Ali, L. Maiani, A. Y. Parkhomenko, W. Wang, Interpretation of  $Y_b(10753)$  as a tetraquark and its production mechanism, Phys. Lett. B 802 (2020) 135217. [arXiv:1910.07671](#), [doi:10.1016/j.physletb.2020.135217](#).
- [891] Z. Zhao, A. Kaewsnod, K. Xu, N. Tagsinsit, X. Liu, A. Limphirat, Y. Yan, Study of  $1^{--} P$  wave charmoniumlike and bottomoniumlike tetraquark spectroscopy (3 2025). [arXiv:2503.00552](#).
- [892] J. Tarrús Castellà, Spin structure of heavy-quark hybrids, AIP Conf. Proc. 2249 (1) (2020) 020008. [arXiv:1908.05179](#), [doi:10.1063/5.0008570](#).
- [893] J. Tarrús Castellà, E. Passemar, Exotic to standard bottomonium transitions, Phys. Rev. D 104 (3) (2021) 034019. [arXiv:2104.03975](#), [doi:10.1103/PhysRevD.104.034019](#).
- [894] P. G. Ortega, D. R. Entem, F. Fernández, J. Segovia, Assessment of  $\Upsilon$ -states above  $B\bar{B}$ -threshold using a constituent-quark-model based meson-meson coupled-channels framework, Phys. Rev. D 109 (11) (2024) 114007. [arXiv:2403.03770](#), [doi:10.1103/PhysRevD.109.114007](#).
- [895] P. Bicudo, M. Cardoso, N. Cardoso, M. Wagner, Bottomonium resonances with  $I = 0$  from lattice QCD correlation functions with static and light quarks, Phys. Rev. D 101 (3) (2020) 034503. [arXiv:1910.04827](#), [doi:10.1103/PhysRevD.101.034503](#).
- [896] P. Bicudo, N. Cardoso, L. Mueller, M. Wagner, Computation of the quarkonium and meson-meson composition of the  $\Upsilon(nS)$  states and of the new  $\Upsilon(10753)$  Belle resonance from lattice QCD static potentials, Phys. Rev. D 103 (7) (2021) 074507. [arXiv:2008.05605](#), [doi:10.1103/PhysRevD.103.074507](#).
- [897] A. M. Badalian, B. L. G. Bakker, I. V. Danilkin, On the possibility to observe higher  $n^3D_1$  bottomonium states in the  $e^+e^-$  processes, Phys. Rev. D 79 (2009) 037505. [arXiv:0812.2136](#), [doi:10.1103/PhysRevD.79.037505](#).
- [898] Z.-Y. Bai, Y.-S. Li, Q. Huang, X. Liu, T. Matsuki,  $\Upsilon(10753) \rightarrow \Upsilon(nS)\pi^+\pi^-$  decays induced by hadronic loop mechanism, Phys. Rev. D 105 (7) (2022) 074007. [arXiv:2201.12715](#), [doi:10.1103/PhysRevD.105.074007](#).
- [899] I. Adachi, et al., Study of  $\Upsilon(10753)$  decays to  $\pi^+\pi^-\Upsilon(nS)$  final states at Belle II, JHEP 07 (2024) 116. [arXiv:2401.12021](#), [doi:10.1007/JHEP07\(2024\)116](#).
- [900] Y.-S. Li, Z.-Y. Bai, X. Liu, Investigating the  $\Upsilon(10753) \rightarrow \Upsilon(1^3D_J)\eta$  transitions, Phys. Rev. D 105 (11) (2022) 114041. [arXiv:2205.04049](#), [doi:10.1103/PhysRevD.105.114041](#).
- [901] S.-D. Liu, Z.-X. Cai, Z.-S. Jia, G. Li, J.-J. Xie, Hidden-bottom hadronic transitions of  $\Upsilon(10753)$ , Phys. Rev. D 109 (1) (2024) 014039. [arXiv:2312.02761](#), [doi:10.1103/PhysRevD.109.014039](#).
- [902] I. Adachi, et al., Search for the  $e^+e^- \rightarrow \eta_b(1S)\omega$  and  $e^+e^- \rightarrow \chi_{b0}(1P)\omega$  processes at  $\sqrt{s} = 10.745$  GeV, Phys. Rev. D 109 (7) (2024) 072013. [arXiv:2312.13043](#), [doi:10.1103/PhysRevD.109.072013](#).
- [903] I. Adachi, et al., Observation of  $e^+e^- \rightarrow \omega\chi_{bJ}(1P)$  and search for  $X_b \rightarrow \omega\Upsilon(1S)$  at  $\sqrt{s}$  near 10.75 GeV, Phys. Rev. Lett. 130 (9) (2023) 091902. [arXiv:2208.13189](#), [doi:10.1103/PhysRevLett.130.091902](#).
- [904] I. Adachi, et al., Improved measurement of Born cross sections for  $\chi_{bJ}\omega$  and  $\chi_{bJ}(\pi^+\pi^-\pi^0)_{\text{non-}\omega}$  at Belle and Belle II (10 2025). [arXiv:2510.25461](#).

- [905] S.-D. Liu, H.-D. Cai, Z.-X. Cai, H.-S. Gao, G. Li, F. Wang, J.-J. Xie, Production of  $X_b$  via radiative transition of  $Y(10753)$ , Phys. Rev. D 109 (9) (2024) 094045. [arXiv:2403.01676](#), [doi:10.1103/PhysRevD.109.094045](#).
- [906] A. V. Anisovich, V. V. Anisovich, A. V. Sarantsev, Systematics of  $q\bar{q}$  states in the  $(n, M^2)$  and  $(J, M^2)$  planes, Phys. Rev. D 62 (2000) 051502. [arXiv:hep-ph/0003113](#), [doi:10.1103/PhysRevD.62.051502](#).
- [907] J.-S. Yu, Z.-F. Sun, X. Liu, Q. Zhao, Categorizing resonances  $X(1835)$ ,  $X(2120)$  and  $X(2370)$  in the pseudoscalar meson family, Phys. Rev. D 83 (2011) 114007. [arXiv:1104.3064](#), [doi:10.1103/PhysRevD.83.114007](#).
- [908] X. Wang, Z.-F. Sun, D.-Y. Chen, X. Liu, T. Matsuki, Non-strange partner of strangeonium-like state  $Y(2175)$ , Phys. Rev. D 85 (2012) 074024. [arXiv:1202.4139](#), [doi:10.1103/PhysRevD.85.074024](#).
- [909] Z.-C. Ye, X. Wang, X. Liu, Q. Zhao, The mass spectrum and strong decays of isoscalar tensor mesons, Phys. Rev. D 86 (2012) 054025. [arXiv:1206.0097](#), [doi:10.1103/PhysRevD.86.054025](#).
- [910] L.-P. He, X. Wang, X. Liu, Towards two-body strong decay behavior of higher  $\rho$  and  $\rho_3$  mesons, Phys. Rev. D 88 (3) (2013) 034008. [arXiv:1306.5562](#), [doi:10.1103/PhysRevD.88.034008](#).
- [911] C.-Q. Pang, L.-P. He, X. Liu, T. Matsuki, Phenomenological study of the isovector tensor meson family, Phys. Rev. D 90 (1) (2014) 014001. [arXiv:1405.3189](#), [doi:10.1103/PhysRevD.90.014001](#).
- [912] B. Wang, C.-Q. Pang, X. Liu, T. Matsuki, Pseudotensor meson family, Phys. Rev. D 91 (1) (2015) 014025. [arXiv:1410.3930](#), [doi:10.1103/PhysRevD.91.014025](#).
- [913] K. Chen, C.-Q. Pang, X. Liu, T. Matsuki, Light axial vector mesons, Phys. Rev. D 91 (7) (2015) 074025. [arXiv:1501.07766](#), [doi:10.1103/PhysRevD.91.074025](#).
- [914] C.-Q. Pang, B. Wang, X. Liu, T. Matsuki, High-spin mesons below 3 GeV, Phys. Rev. D 92 (1) (2015) 014012. [arXiv:1505.04105](#), [doi:10.1103/PhysRevD.92.014012](#).
- [915] C.-Q. Pang, Y.-R. Wang, J.-F. Hu, T.-J. Zhang, X. Liu, Study of the  $\omega$  meson family and newly observed  $\omega$ -like state  $X(2240)$ , Phys. Rev. D 101 (7) (2020) 074022. [arXiv:1910.12408](#), [doi:10.1103/PhysRevD.101.074022](#).
- [916] Q.-S. Zhou, J.-Z. Wang, X. Liu, T. Matsuki, Identifying the contribution of higher  $\rho$  mesons around 2 GeV in the  $e^+e^- \rightarrow \omega\pi^0$  and  $e^+e^- \rightarrow \rho\eta'$  processes, Phys. Rev. D 105 (7) (2022) 074035. [arXiv:2201.06393](#), [doi:10.1103/PhysRevD.105.074035](#).
- [917] B. Aubert, et al., A structure at 2175 MeV in  $e^+e^- \rightarrow \phi f_0(980)$  observed via initial-state radiation, Phys. Rev. D 74 (2006) 091103. [arXiv:hep-ex/0610018](#), [doi:10.1103/PhysRevD.74.091103](#).
- [918] B. Aubert, et al., The  $e^+e^- \rightarrow K^+K^-\pi^+\pi^-$ ,  $K^+K^-\pi^0\pi^0$  and  $K^+K^-K^+K^-$  cross sections measured with initial-state radiation, Phys. Rev. D 76 (2007) 012008. [arXiv:0704.0630](#), [doi:10.1103/PhysRevD.76.012008](#).
- [919] J. P. Lees, et al., Cross sections for the reactions  $e^+e^- \rightarrow K^+K^-\pi^+\pi^-$ ,  $K^+K^-\pi^0\pi^0$ , and  $K^+K^-K^+K^-$  measured using initial-state radiation events, Phys. Rev. D 86 (2012) 012008. [arXiv:1103.3001](#), [doi:10.1103/PhysRevD.86.012008](#).
- [920] M. Ablikim, et al., Measurement of  $e^+e^- \rightarrow \phi\pi^+\pi^-$  cross sections at center-of-mass energies from 2.00 to 3.08 GeV, Phys. Rev. D 108 (3) (2023) 032011. [arXiv:2112.13219](#), [doi:10.1103/PhysRevD.108.032011](#).
- [921] M. Ablikim, et al., Observation of  $Y(2175)$  in  $J/\psi \rightarrow \eta\phi f_0(980)$ , Phys. Rev. Lett. 100 (2008) 102003. [arXiv:0712.1143](#), [doi:10.1103/PhysRevLett.100.102003](#).

- [922] M. Ablikim, et al., Study of  $J/\psi \rightarrow \eta\phi\pi^+\pi^-$  at BESIII, Phys. Rev. D 91 (5) (2015) 052017. [arXiv:1412.5258](#), [doi:10.1103/PhysRevD.91.052017](#).
- [923] M. Ablikim, et al., Observation of  $e^+e^- \rightarrow \eta Y(2175)$  at center-of-mass energies above 3.7 GeV, Phys. Rev. D 99 (1) (2019) 012014. [arXiv:1709.04323](#), [doi:10.1103/PhysRevD.99.012014](#).
- [924] M. Ablikim, et al., Observation of a structure in  $e^+e^- \rightarrow \phi\eta'$  at  $\sqrt{s}$  from 2.05 to 3.08 GeV, Phys. Rev. D 102 (1) (2020) 012008. [arXiv:2003.13064](#), [doi:10.1103/PhysRevD.102.012008](#).
- [925] M. Ablikim, et al., Study of the process  $e^+e^- \rightarrow \phi\eta$  at center-of-mass energies between 2.00 and 3.08 GeV, Phys. Rev. D 104 (3) (2021) 032007. [arXiv:2104.05549](#), [doi:10.1103/PhysRevD.104.032007](#).
- [926] G.-J. Ding, M.-L. Yan,  $Y(2175)$ : Distinguish hybrid state from higher quarkonium, Phys. Lett. B 657 (2007) 49–54. [arXiv:hep-ph/0701047](#), [doi:10.1016/j.physletb.2007.10.020](#).
- [927] Q. Li, L.-C. Gui, M.-S. Liu, Q.-F. Lü, X.-H. Zhong, Mass spectrum and strong decays of strangeonium in a constituent quark model, Chin. Phys. C 45 (2) (2021) 023116. [arXiv:2004.05786](#), [doi:10.1088/1674-1137/abcf22](#).
- [928] C.-Q. Pang, Excited states of  $\phi$  meson, Phys. Rev. D 99 (7) (2019) 074015. [arXiv:1902.02206](#), [doi:10.1103/PhysRevD.99.074015](#).
- [929] T. Barnes, N. Black, P. R. Page, Strong decays of strange quarkonia, Phys. Rev. D 68 (2003) 054014. [arXiv:nucl-th/0208072](#), [doi:10.1103/PhysRevD.68.054014](#).
- [930] S. S. Afonin, I. V. Pusenkov, Universal description of radially excited heavy and light vector mesons, Phys. Rev. D 90 (9) (2014) 094020. [arXiv:1411.2390](#), [doi:10.1103/PhysRevD.90.094020](#).
- [931] G.-J. Ding, M.-L. Yan, A Candidate for  $1^{--}$  strangeonium hybrid, Phys. Lett. B 650 (2007) 390–400. [arXiv:hep-ph/0611319](#), [doi:10.1016/j.physletb.2007.05.026](#).
- [932] J. Ho, R. Berg, T. G. Steele, W. Chen, D. Harnett, Is the  $Y(2175)$  a strangeonium hybrid meson?, Phys. Rev. D 100 (3) (2019) 034012. [arXiv:1905.12779](#), [doi:10.1103/PhysRevD.100.034012](#).
- [933] Z.-G. Wang, Analysis of the  $Y(2175)$  as a tetraquark state with QCD sum rules, Nucl. Phys. A 791 (2007) 106–116. [arXiv:hep-ph/0610171](#), [doi:10.1016/j.nuclphysa.2007.04.012](#).
- [934] H.-X. Chen, X. Liu, A. Hosaka, S.-L. Zhu, The  $Y(2175)$  state in the QCD sum rule, Phys. Rev. D 78 (2008) 034012. [arXiv:0801.4603](#), [doi:10.1103/PhysRevD.78.034012](#).
- [935] N. V. Drenska, R. Faccini, A. D. Polosa, Higher tetraquark particles, Phys. Lett. B 669 (2008) 160–166. [arXiv:0807.0593](#), [doi:10.1016/j.physletb.2008.09.038](#).
- [936] H.-W. Ke, X.-Q. Li, Study of the strong decays of  $\phi(2170)$  and the future charm-tau factory, Phys. Rev. D 99 (3) (2019) 036014. [arXiv:1810.07912](#), [doi:10.1103/PhysRevD.99.036014](#).
- [937] S. S. Agaev, K. Azizi, H. Sundu, Nature of the vector resonance  $Y(2175)$ , Phys. Rev. D 101 (7) (2020) 074012. [arXiv:1911.09743](#), [doi:10.1103/PhysRevD.101.074012](#).
- [938] F.-X. Liu, M.-S. Liu, X.-H. Zhong, Q. Zhao, Fully-strange tetraquark  $ss\bar{s}\bar{s}$  spectrum and possible experimental evidence, Phys. Rev. D 103 (1) (2021) 016016. [arXiv:2008.01372](#), [doi:10.1103/PhysRevD.103.016016](#).
- [939] L. Zhao, N. Li, S.-L. Zhu, B.-S. Zou, Meson-exchange model for the  $\Lambda\bar{\Lambda}$  interaction, Phys. Rev. D 87 (5) (2013) 054034. [arXiv:1302.1770](#), [doi:10.1103/PhysRevD.87.054034](#).
- [940] C. Deng, J. Ping, Y. Yang, F. Wang, Baryonia and near-threshold enhancements, Phys. Rev. D 88 (7) (2013) 074007. [arXiv:1306.6725](#), [doi:10.1103/PhysRevD.88.074007](#).

- [941] Y. Dong, A. Faessler, T. Gutsche, Q. Lü, V. E. Lyubovitskij, Selected strong decays of  $\eta(2225)$  and  $\phi(2170)$  as  $\Lambda\bar{\Lambda}$  bound states, Phys. Rev. D 96 (7) (2017) 074027. [arXiv:1705.09631](#), [doi:10.1103/PhysRevD.96.074027](#).
- [942] S.-L. Zhu, New hadron states, Int. J. Mod. Phys. E 17 (2008) 283–322. [arXiv:hep-ph/0703225](#), [doi:10.1142/S0218301308009446](#).
- [943] A. Martínez Torres, K. P. Khemchandani, L. S. Geng, M. Napsuciale, E. Oset, The  $X(2175)$  as a resonant state of the  $\phi K\bar{K}$  system, Phys. Rev. D 78 (2008) 074031. [arXiv:0801.3635](#), [doi:10.1103/PhysRevD.78.074031](#).
- [944] S. Gomez-Avila, M. Napsuciale, E. Oset,  $\phi K^+ K^-$  production in electron-positron annihilation, Phys. Rev. D 79 (2009) 034018. [arXiv:0711.4147](#), [doi:10.1103/PhysRevD.79.034018](#).
- [945] B. B. Malabarba, X.-L. Ren, K. P. Khemchandani, A. Martínez Torres, Partial decay widths of  $\phi(2170)$  to kaonic resonances, Phys. Rev. D 103 (1) (2021) 016018. [arXiv:2011.03448](#), [doi:10.1103/PhysRevD.103.016018](#).
- [946] X. Wei, Q.-H. Shen, X.-H. Liu, J.-J. Xie, Shedding light on the nature of the  $\phi(2170)$  state in the  $e^+e^- \rightarrow \phi\pi^+\pi^-$  reaction, Phys. Rev. D 113 (1) (2026) 014022. [arXiv:2509.12552](#), [doi:10.1103/frs3-zpt2](#).
- [947] L.-M. Wang, J.-Z. Wang, X. Liu, Toward  $e^+e^- \rightarrow \pi^+\pi^-$  annihilation inspired by higher  $\rho$  mesonic states around 2.2 GeV, Phys. Rev. D 102 (3) (2020) 034037. [arXiv:2007.03118](#), [doi:10.1103/PhysRevD.102.034037](#).
- [948] M. Ablikim, et al., Measurement of  $e^+e^- \rightarrow K^+K^-$  cross section at  $\sqrt{s} = 2.00 - 3.08$  GeV, Phys. Rev. D 99 (3) (2019) 032001. [arXiv:1811.08742](#), [doi:10.1103/PhysRevD.99.032001](#).
- [949] M. Ablikim, et al., Observation of a Resonant Structure in  $e^+e^- \rightarrow K^+K^-\pi^0\pi^0$ , Phys. Rev. Lett. 124 (11) (2020) 112001. [arXiv:2001.04131](#), [doi:10.1103/PhysRevLett.124.112001](#).
- [950] A. V. Anisovich, C. A. Baker, C. J. Batty, D. V. Bugg, V. A. Nikonov, A. V. Sarantsev, V. V. Sarantsev, B. S. Zou, Partial wave analysis of  $\bar{p}p$  annihilation channels in flight with  $I = 1, C = +1$ , Phys. Lett. B 517 (2001) 261–272. [arXiv:1110.0278](#), [doi:10.1016/S0370-2693\(01\)01017-6](#).
- [951] A. V. Anisovich, C. J. Batty, D. V. Bugg, V. A. Nikonov, A. V. Sarantsev, A fresh look at  $\eta_2(1645), \eta_2(1870), \eta_2(2030)$  and  $f_2(1910)$  in  $\bar{p}p \rightarrow \eta_3\pi^0$ , Eur. Phys. J. C 71 (2011) 1511. [arXiv:1009.1781](#), [doi:10.1140/epjc/s10052-010-1511-3](#).
- [952] A. V. Anisovich, C. A. Baker, C. J. Batty, D. V. Bugg, L. Montanet, V. A. Nikonov, A. V. Sarantsev, V. V. Sarantsev, B. S. Zou, Combined analysis of meson channels with  $I = 1, C = -1$  from 1940 to 2410 MeV, Phys. Lett. B 542 (2002) 8–18. [arXiv:1109.5247](#), [doi:10.1016/S0370-2693\(02\)02302-X](#).
- [953] D. V. Amelin, et al., Natural parity resonances in  $\eta\pi^+\pi^-$ , Nucl. Phys. A 668 (2000) 83–96. [doi:10.1016/S0375-9474\(99\)00370-X](#).
- [954] L.-M. Wang, S.-Q. Luo, X. Liu, Light unflavored vector meson spectroscopy around the mass range of 2.4 ~ 3 GeV and possible experimental evidence, Phys. Rev. D 105 (3) (2022) 034011. [arXiv:2109.06617](#), [doi:10.1103/PhysRevD.105.034011](#).
- [955] M. Ablikim, et al., Measurement of the  $e^+e^- \rightarrow \Lambda\bar{\Lambda}$  cross section from threshold to 3.00 GeV using events with initial-state radiation, Phys. Rev. D 107 (7) (2023) 072005. [arXiv:2303.07629](#), [doi:10.1103/PhysRevD.107.072005](#).
- [956] B. Aubert, et al., Study of  $e^+e^- \rightarrow \Lambda\bar{\Lambda}, \Lambda\bar{\Sigma}^0, \Sigma^0\bar{\Sigma}^0$  using initial state radiation with BABAR, Phys. Rev. D 76 (2007) 092006. [arXiv:0709.1988](#), [doi:10.1103/PhysRevD.76.092006](#).
- [957] M. Ablikim, et al., Observation of a cross-section enhancement near mass threshold in  $e^+e^- \rightarrow \Lambda\bar{\Lambda}$ , Phys. Rev. D 97 (3) (2018) 032013. [arXiv:1709.10236](#), [doi:10.1103/PhysRevD.97.032013](#).

- [958] M. Ablikim, et al., Complete measurement of the  $\Lambda$  electromagnetic form factors, Phys. Rev. Lett. 123 (12) (2019) 122003. [arXiv:1903.09421](#), [doi:10.1103/PhysRevLett.123.122003](#).
- [959] D. Bisello, et al., Baryon pair production in  $e^+e^-$  annihilation at  $\sqrt{s} = 2.4$  GeV, Z. Phys. C 48 (1990) 23–28. [doi:10.1007/BF01565602](#).
- [960] Z.-Y. Bai, Q.-S. Zhou, X. Liu, Higher strangeonium decays into light flavor baryon pairs like  $\Lambda\bar{\Lambda}$ ,  $\Sigma\bar{\Sigma}$ , and  $\Xi\bar{\Xi}$ , Phys. Rev. D 108 (9) (2023) 094036. [arXiv:2307.16255](#), [doi:10.1103/PhysRevD.108.094036](#).
- [961] M. Ablikim, et al., Observation of a resonant structure in  $e^+e^- \rightarrow \omega\eta$  and another in  $e^+e^- \rightarrow \omega\pi^0$  at center-of-mass energies between 2.00 and 3.08 GeV, Phys. Lett. B 813 (2021) 136059. [arXiv:2009.08099](#), [doi:10.1016/j.physletb.2020.136059](#).
- [962] M. Ablikim, et al., Measurement of the  $e^+e^- \rightarrow \omega\pi^0\pi^0$  cross section at center-of-mass energies from 2.0 to 3.08 GeV, Phys. Rev. D 105 (3) (2022) 032005. [arXiv:2112.15076](#), [doi:10.1103/PhysRevD.105.032005](#).
- [963] Q.-S. Zhou, J.-Z. Wang, X. Liu, Role of the  $\omega(4S)$  and  $\omega(3D)$  states in mediating the  $e^+e^- \rightarrow \omega\eta$  and  $e^+e^- \rightarrow \omega\pi^0\pi^0$  processes, Phys. Rev. D 106 (3) (2022) 034010. [arXiv:2207.00276](#), [doi:10.1103/PhysRevD.106.034010](#).
- [964] M. Ablikim, et al., Study of  $e^+e^- \rightarrow \pi^+\pi^-\pi^0$  at  $\sqrt{s}$  from 2.00 to 3.08 GeV at BESIII, Phys. Rev. D 110 (3) (2024) 032005. [arXiv:2401.14711](#), [doi:10.1103/PhysRevD.110.032005](#).
- [965] Z.-Y. Bai, Q.-S. Zhou, X. Liu, Role of  $4S$ - $3D$  mixing in explaining the  $\omega$ -like  $Y(2119)$  observed in  $e^+e^- \rightarrow \rho\pi$  and  $e^+e^- \rightarrow \rho(1450)\pi$ , Phys. Rev. D 111 (5) (2025) 054013. [arXiv:2502.05754](#), [doi:10.1103/PhysRevD.111.054013](#).
- [966] J. P. Lees, et al., Precise measurement of the  $e^+e^- \rightarrow \pi^+\pi^-(\gamma)$  cross section with the initial-state radiation method at *BABAR*, Phys. Rev. D 86 (2012) 032013. [arXiv:1205.2228](#), [doi:10.1103/PhysRevD.86.032013](#).
- [967] J. P. Lees, et al., Resonances in  $e^+e^-$  annihilation near 2.2 GeV, Phys. Rev. D 101 (1) (2020) 012011. [arXiv:1912.04512](#), [doi:10.1103/PhysRevD.101.012011](#).
- [968] B. Aubert, et al., The  $e^+e^- \rightarrow 2(\pi^+\pi^-)\pi^0$ ,  $2(\pi^+\pi^-)\eta$ ,  $K^+K^-\pi^+\pi^-\pi^0$  and  $K^+K^-\pi^+\pi^-\eta$  cross sections measured with initial-state radiation, Phys. Rev. D 76 (2007) 092005, [Erratum: Phys.Rev.D 77, 119902 (2008)]. [arXiv:0708.2461](#), [doi:10.1103/PhysRevD.76.092005](#).
- [969] J. P. Lees, et al., Study of the reactions  $e^+e^- \rightarrow K^+K^-\pi^0\pi^0\pi^0$ ,  $e^+e^- \rightarrow K_S^0K^\pm\pi^\pm\pi^0\pi^0$ , and  $e^+e^- \rightarrow K_S^0K^\pm\pi^\pm\pi^+\pi^-$  at center-of-mass energies from threshold to 4.5 GeV using initial-state radiation, Phys. Rev. D 107 (7) (2023) 072001. [arXiv:2207.10340](#), [doi:10.1103/PhysRevD.107.072001](#).
- [970] M. N. Achasov, et al., Updated measurement of the  $e^+e^- \rightarrow \omega\pi^0 \rightarrow \pi^0\pi^0\gamma$  cross section with the SND detector, Phys. Rev. D 94 (11) (2016) 112001. [arXiv:1610.00235](#), [doi:10.1103/PhysRevD.94.112001](#).
- [971] M. Ablikim, et al., Measurement of the Born cross sections for  $e^+e^- \rightarrow \eta'\pi^+\pi^-$  at center-of-mass energies between 2.00 and 3.08 GeV, Phys. Rev. D 103 (7) (2021) 072007. [arXiv:2012.07360](#), [doi:10.1103/PhysRevD.103.072007](#).
- [972] M. Ablikim, et al., Measurement of the cross sections for  $e^+e^- \rightarrow \eta\pi^+\pi^-$  at center-of-mass energies between 2.00 and 3.08 GeV, Phys. Rev. D 108 (11) (2023) L111101. [arXiv:2310.10452](#), [doi:10.1103/PhysRevD.108.L111101](#).
- [973] X. Liu, Q.-S. Zhou, L.-M. Wang, Broad resonance structure in  $e^+e^- \rightarrow f_1(1285)\pi^+\pi^-$  and higher  $\rho$ -meson excitations, Phys. Rev. D 106 (9) (2022) 094012. [arXiv:2209.11525](#), [doi:10.1103/PhysRevD.106.094012](#).

- [974] Q.-S. Zhou, Z.-Y. Bai, J.-Z. Wang, H. Xu, X. Liu, Decoding the role of  $\rho$  mesonic states for elucidating the  $e^+e^- \rightarrow a_2(1320)\pi$  data and other reactions, Phys. Rev. D 112 (7) (2025) 074021. [arXiv:2507.21554](#), [doi:10.1103/pdfh-mk79](#).